NASA Contractor Report 191109

Effects of Buoyancy on Gas Jet Diffusion Flames

M. Yousef Bahadori and Raymond B. Edelman
Science Applications International Corporation
Torrance, California

April 1993

Prepared for
Lewis Research Center
Under Contract NAS3–22822

National Aeronautics and
Space Administration

TABLE OF CONTENTS

Section

TABLE OF CONTENTS (Cont.)

Section

Section 1

Introduction and Background

Introduction and Background

This final report documents the research findings of Contract NAS3-22822 performed by Science Applications International Corporation, entitled "Effects of Buoyancy on Gas Jet Diffusion Flames". The work was performed in two phases, as follows:

(a) Phase I, from October 1981 through October 1987; this phase consisted of a modest effort involving only a fundamental investigation of combustion in gas jet diffusion flames, a feasibility study for a space experiment and preparation of the associated Science Requirements Document (SRD) and Conceptual Design Review (CoDR);

(b) Phase II, from October 1987 through April 1992; this phase consisted of a comprehensive effort involving experiments in the 2.2-Second Drop Tower and the 5.18-Second Zero-Gravity Facility of NASA Lewis Research center, and preliminary tests in the KC-135 research aircraft, in addition to the associated theoretical modeling and data analyses.

The principal objective of the effort was to gain a better understanding of the fundamental phenomena involved in laminar gas jet diffusion flames in the absence of buoyancy by studying the transient phenomena of ignition and flame development, steady-state flame characteristics, soot effects, radiation, and , if any, extinction phenomena. This involved measurements of the flame size and development, as well as temperature, radiation, and (the originally planned) species concentration. Additionally, flame behavior, color, and luminosity were observed and recorded. The test quantified the effects of Reynolds number, nozzle size, fuel reactivity and type, oxygen concentration, pressure, and jet momentum on flame characteristics. Analytical and numerical modeling efforts were also performed.

During Phase I (in 1986) a space experiment was proposed and presented to NASA Headquarters at a Conceptual Design Review (CoDR). In 1987, NASA

Headquarters recommended that a comprehensive series of ground-based tests in the drop towers and tests using a research aircraft be conducted prior to a second CoDR. This led to the initiation of the second phase of the effort. In December 1991, the Phase II results were presented at a CoDR. NASA Headquarters recommended that a space experiment be re-proposed following the 1993 NASA Research Announcement (NRA).

This final report contains the 1986/87 Science Requirements and Conceptual Design documents, journal publications and meetings presentations resulting from the second phase of the effort, and the 1991 SRD/CoDR documents. It should be noted that the data and associated modeling results (only a representative set is presented in this document) are currently in the final phase of compilation, reduction and documentation. This will result in a substantial number of publications (a few preliminary versions of which are presented in this report) to be submitted to archival journals during the remaining months of 1992. This effort will be carried out while a new effort (Contract NAS3-25982), entitled "Effects of Buoyancy on Transitional and Turbulent Gas Jet Diffusion Flames" is underway. This new effort was initiated in November 1991. Due to the overlap between the two programs, the last meeting presentation of this report contains some preliminary results from the new effort.

The remainder of this section contains an overview of the major findings of the 2.2-second tests, the 5.18-second tests, the (preliminary) KC-135 tests, and the theoretical modeling effort.

(a) The 2.2-Second Drop-Tower Tests

These tests were conducted in order to characterize the behavior of flames, and to define the matrix for the 5.18-Second tests. Methane and propane flames were tested in quiescent oxidizing environments using different nozzle sizes (0.051 to 0.0825 cm in radius) and fuel flow rates (0.3 to 1.5 cc/sec for propane and 1.0 to 5.0 cc/sec for methane). In these experiments, the Reynolds number was varied from approximately 20 to 200, pressure from 0.5 to 1.5 atm, and oxygen volume fraction from 18% to 50% (using nitrogen as diluent). The flames were also ignited in microgravity, which demonstrated for the first time the ability to ignite and sustain a gas jet diffusion flame in a low-gravity environment.

The results showed that the 2.2 seconds of microgravity testing was not sufficient for the flame development to approach its near-steady state behavior. In addition, propane flames in high-oxygen-concentration/high-pressure environments showed significant soot formation resulting in flame-tip opening with a column of soot emerging from the tip of the flame. Low-pressure/low-oxygen-concentration flames were found to be extremely weak, blue in color with no visible soot emission, and had an open tip. The results also showed that microgravity flames are taller, wider, more diffuse, and have no flicker compared to the corresponding normal-gravity flames. These microgravity flames take much longer time to reach a near-steady state. The tests also quantified the effects of pressure, oxygen concentration, nozzle size, Reynolds number, and fuel type on the characteristics of microgravity hydrocarbon diffusion flames.

The observations and associated measurements on global flame characteristics provided a database for the 2.2-second microgravity flames, and were used to develop the test matrix for the longer-duration microgravity experiments described below.

(b) The 5.18-Second Microgravity tests

These tests were conducted to study the behavior of flames under longer-duration microgravity conditions, and to quantify both flame temperature and flame radiation. Global flame radiation was measured using a thermopile detector, which was the first demonstration of the ability to measure radiation from a flame in a microgravity environment. Temperatures were measured simultaneously at nine different locations (using a 3x3 rake of thermocouples) which provided time-resolved temperature data both inside and outside the flame. The results showed significant effects of microgravity on radiative losses and temperature field outside the flame, in addition to the global characteristics of the flame such as tip-opening in propane flames, and flame size, color and luminosity for the 5-second period. In addition, it was shown that although the flames appear to reach their near-steady state behavior towards the end of the drop, quantitative measurements point to a transient behavior, and that flames need to be tested at times longer than 5 seconds to fully quantify their steady-state characteristics.

Methane and propane flames were studied with one nozzle size (0.0825 cm in radius), with flow rates of 1.0 and 3.0 cc/sec for methane and 0.5 and 1.5 cc/sec for propane (when converted to the standard conditions). Oxygen concentration in a nitrogen diluent was also varied from 18% to 30%, while the environmental pressure was varied from 0.5 to 1.5 atm.

The results showed, for example, that flame far field experiences noticeable temperature rise in the absence of buoyancy; this rise in temperature dose not reach its steady state value at the end of the drop. In addition, continuous change in the color and luminosity of the flame was observed due to the transient response of the field surrounding the flame. Also, radiation measurements showed that microgravity flames can have radiative losses of up to an order of magnitude higher than their normal-gravity counterparts. This has a significant implication on radiative losses and radiative ignition in a microgravity environment. Two flames were studied at 1 atm (for propane) and 0.5 atm (for methane) with 15% oxygen concentration in a nitrogen environment. These flames were found to be entirely blue, extremely diffuse, and open-tipped. Yet the radiation levels were quiet significant compared to those in normal-gravity. This indicates that although soot formation and subsequent emission were reduced, contributions from the gas-phase species were quiet significant due to the absence of buoyancy; radiation, although lower, was of the same order of magnitude in blue flames compared to the luminous flames in microgravity.

The test matrix was not completed due to the closure of the Zero-Gravity Facility for renovation. However, a major part of the matrix was completed (except the intermediate flow rates of 2 cc/sec for methane and 1 cc/sec for propane). The original plan was to conduct gas-sampling measurements at mirror-image locations of the thermocouples with respect to the flame centerline. The experimental chamber had provisions for performing this task. However, this effort was not conducted due to the shut-down of the facility.

A substantial amount of data on flame size, color, tip characteristics, development, radiation, and temperature as a function of fuel type, Reynolds number, pressure, and oxygen concentration were obtained. Representative data are presented in different parts of this report. Data reduction and associated

documentation are currently in progress, and the results will be published in the open literature, in the near future.

(c) The KC-135 Tests

These preliminary flight tests were conducted to study the effects of longer durations of low-gravity environment on flame behavior. The intent was to conduct measurements to quantify flame radiation, temperature, species, and global characteristics, and to determine the effects of acceleration and g-gitter. Tests were conducted for methane and propane flames with one nozzle size. Observations on flame behavior were not conclusive, but showed that the overall characteristics of flames can be obtained for the attached (10^{-2}g) and free-float (10^{-3}g) configurations of the test package, that flames are strongly influenced by the g-level and g-jitter, and that an average time in the order of 5 seconds in the free-float case and 10 seconds in the bolted-down case may be obtained, although g-jitter affects the flame. No quantitative measurements were performed in these tests.

(d) Theoretical Modeling

During the course of the second phase of the program, various analytical models were developed. These included a transient model for the laminar diffusion flames, a model for the transient filling process in an evacuated or partially evacuated gas sampling bottle, and a model for the effects of g-jitter and partial gravity on the flame response.

A comprehensive numerical model which incorporates the effects of gravity, diffusion, inertia, viscosity, and combustion was modified to include gas-phase and soot radiation and multi-component diffusion. Work was also completed on the formulation of soot processes, thermophoresis, and finite-rate quasi-global kinetics. These submodels were not incorporated into the model by the end of the contract. The developed model is two-dimensional (cylindrical or rectangular) and solves the conservation equations for mass, momentum, energy, and species in their boundary-layer form. An explicit finite-difference scheme is used to solve these governing equations, using the von Mises transformation.

Selected predictions from the analytical and numerical models are presented in various sections of this report, and the findings are currently in the process of being submitted for journal publications.

The following sections present the SRD/CoDR documents, and associated publications and meeting presentations of the entire effort in a chronological order.

Section 2

"Effects of Buoyancy on Gas-Jet Diffusion Flames"

- Science Requirements Document-

R. B. Edelman and M. Y. Bahadori

January 1987

EFFECTS OF BUOYANCY ON GAS JET DIFFUSION FLAMES

- Science Requirements Document -

Submitted by:

Raymond B. Edelman (Principal Investigator)
M. Yousef Bahadori (Assistant Investigator)

SCIENCE APPLICATIONS INTERNATIONAL CORPORATION (SAIC)

Combustion Science and Advanced Technology Department
9760 Owensmouth Avenue
Chatsworth, California 91311

Submitted to:
NASA-LEWIS RESEARCH CENTER
21000 Brookpark Road
Cleveland, OH 44135

January 1987

TABLE OF CONTENTS

I. Introduction

Although diffusion flames have been the subject of research for many years they are not well understood and, while the effects of gravity on the burning process have been observed, the basic mechanisms responsible for these changes have yet to be determined. The goal of this research is to develop an improved understanding of gas jet diffusion flames. The laminar gas jet diffusion flame was selected for study because it embodies mechanisms important in all diffusion flames such as occur in fires and practical combustion systems. Furthermore, due to its relative simplicity and ease of control, it lends itself to direct theoretical and experimental studies. However, existing theoretical models are deficient and improved models are required because they are essential to the interpretation of data, providing a means of theoretically isolating mechanisms influencing the observed behavior. The complexity of these mechanisms and their coupling establish the requirement for data with which to verify assumptions inherent in the theoretical analyses. If gravity is eliminated, then its effect can be isolated and the complication of buoyancy-induced convection would be removed from the problem. The combination of zero-gravity and normal-gravity data would provide the information, both theoretical and experimental, to improve our understanding of diffusion flames in general and the effects of gravity on the burning process in particular. Although earthbound experiments under reduced-g conditions have shown significant differences in flame behavior relative to normal-g conditions, the data is severely limited and incomplete. The existing data is confined to semi-quantitative visual observations on flames, many of which were in a state of transient adjustment at the end of the 2.2-sec. drop-tower test time.

This document describes the requirements of an experiment that if performed in other low-gravity environments, would help to eliminate current deficiencies in our understanding of gas jet diffusion flames.

II. Background

The problem of fire safety has received the attention of researchers for many years which has resulted in a continuous effort to under-

stand the complicated processes occuring in fires. Recently, interest in the fire problem has been expanded to include aerospace applications due to the concern over fires aboard spacecraft. The primary conclusion drawn from the existing base of information on fires is that a more fundamental understanding of diffusion flames is needed in order to predict their behavior and to control them. Although the effects of gravity on a specific burning process have been observed, the mechanisms responsible for these changes have yet to be determined. A critical limitation of the existing earthbound experimental data obtained in the 2.2-sec. drop tower is that only limited elapsed time is available to fully characterize the flame behavior under reduced-gravity conditions.

Diffusion flames involve convective and diffusive effects and fires are a complicated type of this class of combustion process. Regardless of the type of fuel involved (i.e., liquid, solid or gaseous), the basic mechanisms which control the fires are the same. These include the processes of mixing, radiation, chemical kinetics, soot formation, diffusion, and buoyancy-induced convection. The laminar gas jet diffusion flame embodies these mechanisms while representing a basic element of more complex, convectively induced turbulent flames.

In order to understand the mechanisms controlling a fire, laboratory-scale turbulent gas jet diffusion flames have been extensively studied. These small-scale flames provide important information in relation to the processes occuring in practical combustion systems as well. However, turbulent flames are not fully understood and their understanding would benefit from more fundamental studies of laminar diffusion flames in which, under normal-g conditions, the complication of convection-induced turbulence is eliminated and the interplay of transport phenomena and chemical kinetics becomes more tractable. But even this basic flame is not completely characterized in relation to soot formation, radiation, diffusion, and kinetics. Therefore, gaining an understanding of laminar flames is essential to the understanding of fires in which the same basic pheonomena occur. By working under microgravity conditions, the effects of buoyancy can be isolated and the results would form a basis to address, in logical order, the fundamental processes occuring in diffusion flames (see Edelman and Bahadori, 1986).

In the remainder of this section, we describe a cross-section of past experimental and theoretical efforts in relation to laminar diffusion flames under both normal-gravity and reduced-g conditions.

Laminar gas jet diffusion flames (Fig. 1) have been a subject of extensive analytical, numerical and experimental research since the appearance of the classical work of Burke and Schumann (1928). Most of the analytical studies to date deal with the mathematical representations of flame shapes based on the Burke-Schumann methodology which neglects almost all of the phenomena critical to understanding the structure of these flames. These include transient effects, soot formation, non-uniform flow parameters, variable transport properties, coupling between the conservation equations, and finite-rate chemical kinetics. In all of the analytical approaches, the effect of buoyancy had to be neglected (i.e., high-momentum flows) in order to enable one to obtain a closed-form mathematical representation of flame shape, mass-fraction distribution and temperature distribution. In addition, the assumptions cited above render the theory of little value in understanding the structure of diffusion flames. Applications of this theory to laboratory-scale gas jet diffusion flames (Burke and Schumann, 1928; Astavin and Ryazantsev, 1979; Penner, Bahadori and Kennedy, 1984) and to the flamelets of composite solid propellants (Beckstead, 1981) have shown only qualitative agreement between the theoretical and experimental flame shapes. Table 1(a) describes a selected number of analytical works performed on laminar gas jet diffusion flames. Few numerical investigations of these types of flames under normal-g and microgravity conditions have been attempted. The results of numerical calculations of the set of conservation equations for normal-g (Mitchell, Sarofim and Clomburg, 1980) and zero-g flames (Edelman et al. 1973) have shown that improved understanding is needed in relation to the mechanisms occuring under these conditions. The mechanisms include radiation, soot formation, chemical kinetics and transient phenomena. Table 1(b) shows a selected number of numerical modeling approaches. Experimental investigations of normal-g flames have provided a large amount of information which is not obtainable from the theoretical studies cited above, i.e., flame structure, soot mass fraction and number density, and temperature, species and velocity distributions (see, for example, Mitchell, Sarofim and Clomburg, 1980, and Flower and

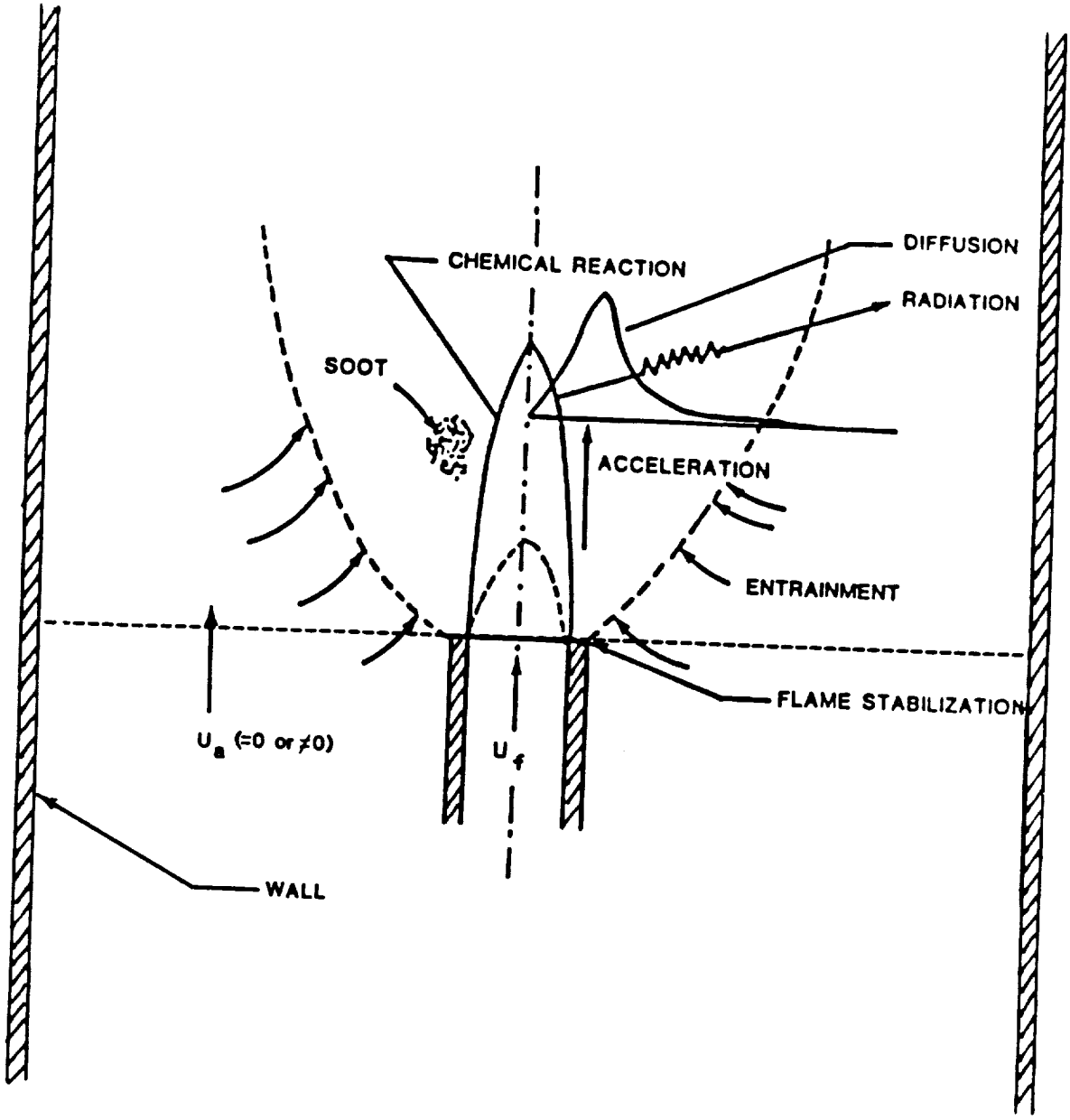

Fig. 1. Schematic diagram of a confined laminar gas jet diffusion flame.

Table 1(a). Selected Analytical Studies on Laminar Gas Jet Diffusion Flames.

AUTHOR(s)	METHOD	CHARACTERISTICS	DATA USED	DEFICIENCIES	COMMENTS
Burke and Schumann (1928)	Analytical representations of the shapes of laminar, cylindrically-symmetric, co-axial gas-jet diffusion flames under steady-state conditions.	Assumptions of equal and constant velocities, transport coefficients, and physical properties of the two gas streams; flame-sheet approximation; Lewis number of unity (which decouples the energy and species-conservation equations); constant pressure (which eliminates the momentum equation); absence of buoyancy; no axial diffusion.	Methane, city gas, and CO flames are used. Air flow rate=6-42 ft^3/hr, fuel flow rate= 2-25 ft^3/hr. Inside radius= 1/4-5/16 in. Outside radius= 1/2-5/8 in.	No account of the formation of products of combustion; lack of finite-rate kinetics and soot-formation mechanism; no effects of radiation; no axial diffusion; assumption of decoupled conservation equations; no transient effects.	Theoretical flame heights are compared with the experimental results under normal-g; qualitative agreement is obtained between experiment and theory.
Astavin and Ryazantsev (1979)	Same as Burke and Schmann (1928) but for fuel and oxidizer separated by a flow of an inert gas (a) from each other and (b) from the wall for both cylindrical and rectangular burners.	Same as Burke and Schumann (1928).	Parametric values of velocities, diffusion coefficients and tube diameters are used for methane/air flames.	Same as Burke and Schumann (1928).	Families of flame shapes and temperature contours are obtained. No comparison with data.
Penner, Bahadori and Kennedy (1984)	Same as Burke and Schumann (1928).	Same as Burke and Schumann (1928) but for constant arbitrary flow velocities, transport parameters and physical properties in the presence of axial diffusion with unimolecular decomposition reactions of fuel and oxidizer.	The data of Burke and Schumann (1928) and Mitchell et al (1980) are used.	Same as Burke and Schumann (1928) except for the effect of axial diffusion.	The results are in qualitative agreement with experimental data.
Beckstead (1981)	Analytical representation of the heights of laminar, cylindrically-symmetric flamelets of composite solid propellants under steady-state conditions.	Same as Burke and Schumann (1928) but in the presence of axial diffusion.	Typical coefficients of diffusion and velocities for evaporating solid propellant species are used.	Same as Burke and Schumann (1928) except for the effects of axial diffusion.	Flame stand-off distances are obtained. No data available.
Edelman and Bahadori (see the present document)	Analytical representation of the shapes of laminar, cylindrically-symmetric, transient, co-axial gas-jet diffusion flames.	Same as Burke and Schumann (1928) but in the presence of axial diffusion.	The data of Cochran (1972) and Cochran and Masica (1970) are used, e.g., nozzle radius=0.186 cm, methane velocity=25.8 cm/sec, etc.	Same as Burke and Schumann (1928) except for the effects of axial diffusion and transient phenomena.	Flame development with time is obtained. The results indicate that times greater than 2.2 sec are needed for flame to reach steady state under zero-g conditions.

Table 1(b). Selected Numerical Studies on Laminar Gas Jet Diffusion Flames.

AUTHOR(s)	METHOD	CHARACTERISTICS	DATA USED	DEFICIENCIES	COMMENTS
Mitchell, Sarofim and Clomburg (1980)	Numerical solution of governing conservation equations for mass, momentum, species, and energy, using a global chemical reaction at the flame boundary with infinite rate. A steady-state normal-g methane/air flame was studied which was laminar, confined, and axisymmetric.	Flame-sheet concept for locating the stoichiometric fuel-oxygen interface and hence, the points of heat release. Natural convection effects and variable thermodynamic and transport properties are allowed. Both axial and radial convection and diffusion are included.	Inner tube diameter=1.27 cm; outer tube diameter=5.18 cm, methane flow rate= 5.7 cm^3/sec; air flow rate=187.7 cm^3/sec.	No detailed chemical kinetics, soot formation or radiation.	Temperatures, species concentrations and velocities are obtained. The results show the important effect of buoyancy, by which, the velocity increases by a factor of 40 inside an overventilated CH_4-air flame. Good comparison with experimental data is obtained.
Klajn and Oppenheim (1982)	The numerical model treats the effects of exothermicity on the contours of gaseous, unconfined jet diffusion flames with negligible buoyancy effects.	Simplifying assumptions of flame-sheet approximation, Schmidt and Prandtl numbers of unity and constant specific heats. Solutions are obtained in closed algebraic form. Axial diffusion is not included.	Nondimensionalized values of diameters, stoichiometric ratios, velocities, etc. are used in a parametric form.	Lewis and Prandtl numbers of unity; infinite-rate global chemical reaction; no radiation or soot formation.	Fair agreement when compared with the experimental data under zero-g conditions of Cochran (1972) and Haggard and Cochran (1973).
Edelman, Fortune, Weilerstein, Cochran, and Haggard (1973)	Numerical solution of conservation equations. It is shown that kinetic effects are of primary importance in flames under reduced gravity. Other controlling factors are axial diffusion, radiation and transient effects.	The model includes the coupled effects of inertia, viscosity, diffusion, gravity, and combustion in a boundary-layer type formulation. Axial and radial convection and axial diffusion are considered.	Comparison with drop-tower data of Cochran and Masica (1970) and Cochran (1972); see Table 1(c).	No detailed kinetics, soot formation, axial diffusion, and radiation.	Good agreement for normal-g flames and fair agreement for steady-state, low-Re, zero-g flames of NASA-Lewis drop-tower experiments.

Bowman, 1983). Efforts to isolate the buoyancy effects in laminar flames have so far been limited to the 2.2-sec. NASA-Lewis Research Center drop-tower (gravity levels $\sim 10^{-5}$g) experiments (Cochran and Masica, 1970; Cochran, 1972; Haggard and Cochran, 1973; Haggard, 1981) and accompanying numerical modeling (Edelman, Fortune and Weilerstein, 1973; Edelman et al. 1973). The drop-tower experiments comprise of a self-contained gas jet diffusion flame apparatus which is allowed to fall inside a falling drag shield. Once establishing and recording the steady-state normal-g flame, the apparatus is dropped and the flame is observed throughout the duration of the fall, providing time-resolved data on the development of the flame shape for the near-zero-g condition achieved during the drop. Attempts have also been made to study the gas jet diffusion flames under elevated gravity conditions achieved in a centrifuge (Altenkirch et al. 1976) and under negative-g conditions by inverting the flame using a downward-flow configuration (Kimura and Ukawa, 1961; Haggard, 1981; SAIC's recent inverted flame data). Studies have been conducted on soot formation from laminar diffusion flames under normal-g conditions in the pressure range of 1.0-2.5 atm (Flower and Bowman, 1983); there is no study to date which quantitatively determines the effect of pressure on soot formation in the absence of buoyancy. Results of selected experimental works on laminar flames are presented in Table 1(c). We see that while the effects of buoyancy are apparent in all of the studies presented in Tables 1(a)-1(c), it has not been strictly isolated (except for the flames of drop-tower experiments), and a large gap in the data base exists in this context.

On the basis of the research cited above, we have identified those mechanisms in diffusion flames which are in need of further understanding from both theoretical and experimental points of view. These mechanisms include chemical kinetics, radiation, transient effects, soot formation, and axial diffusion.

Kinetic effects are probably the most complicated phenomena when combined with soot generation. Hydrocarbon diffusion flames show significant amounts of soot formation and agglomeration under normal-g conditions and atmospheric pressure. Increase in soot yield has been observed (Flower and Bowman, 1983) under elevated pressures. In the

Table 1(c). Selected Experimental Studies on Laminar Gas Jet Diffusion Flames.

AUTHOR(s)	METHOD	CHARACTERISTICS	DATA USED	DEFICIENCIES	COMMENTS
Mitchell, Sarofim and Clomburg (1980)	Confined, axisymmetric, laminar methane-air diffusion flames.	Distributions of temperature, velocity and species were measured. The effects of buoyancy have not been isolated.	Inner tube dia.= 1.27 cm; outer tube dia.=5.18 cm; methane flow rate= 5.7 cm^3/sec, air flow rate=187.7 cm^3/sec.	No kinetics, soot formation or radiation effects.	Importance of buoyancy is demonstrated, by which, the velocity increases by a factor of 40 inside an overventilated CH_4-air flame. The data are in good agreement with the results of modeling.
Flower and Bowman (1983)	Structures of 2-D, laminar ethylene-air flames under normal-g and elevated-pressure conditions are studied.	Soot mass fraction and number density is obtained. No significant effect of pressure on the size of soot particles is observed.	Pressure range= 1.0 - 2.5 atm. A rectangular burner was used with air velocity = 22 cm/sec and fuel velocity= 7 cm/sec.	Only gas temperature and soot data are obtained.	Increase in soot yield (mass of soot/mass of fuel) as the pressure to the power 0.5 - 1.0 was observed. Maximum and integrated soot volume fractions increased as the pressure to a power between 1.5 - 2.0.
Cochran and Masica (1970)	NASA/Lewis drop-tower experiments (see the text for details).	Flame behavior is observed during the 2.2-sec drop of the test chamber. Quiescent air for all of the drop-tower experiments except those of Haggard (1981) which were studied for inverted flames (under normal-g conditions) and zero-g flames in the presence of forced-air velocities; see the text for details.	CH_4/air flames; nozzle radius= 0.186 - 0.442 cm; methane flow rate= 1.2 - 5.3 cm^3/sec.	Only flame lengths and behaviors are observed. No measurements on quantitative data was possible due to the short periods of drop.	Sudden increase in gravity level resulted in immediate reduction in flame length followed by flame expanding away from the burner and final extinguishment.
Cochran (1972)			CH_4/air flames; nozzle radius= 0.051 - 0.113 cm; fuel flow rate=0.7 - 12.2 cm^3/sec.		Steady-state, transient and extinguished flames existed in zero gravity. Flames were ~50% longer and wider in zero-g than in normal-g.

Table 1(c). Continued.

AUTHOR(s)	METHOD	CHARACTERISTICS	DATA USED	DEFICIENCIES	COMMENTS
Haggard and Cochran (1972)			Ethylene and propylene diffusion flames; nozzle radius=0.051 - 0.083 cm; fuel flow rate=0.4 - 3.6 cm^3/sec.		Flame length is described in terms of flow parameters and fuel properties. Stable zero-g lengths were observed.
Haggard (1981)			CH_4/air flames; fuel-nozzle radius= 0.05 - 0.30 cm; coaxial, convergent air-nozzle radius= 1.4 cm at exit plane; fuel flow rate=1.55 - 10.3 cm^3/sec; air flow rate=0-597 cm^3/sec.		Experimental and computed flame lengths for normal-g have shown good agreement. Flame extinguishment upon entry into zero-g was studied. Relatively low forced-air velocities (<10cm/sec) were sufficient to sustain combustion in zero gravity.
Altenkrich, Eichhorn, Hsu, Brancic, and Cerallos (1976)	Gas-jet diffusion flames under elevated gravity conditions achieved in a centrifuge.	Hydrogen, methane, ethane and propane are used.	1.83-m diameter centrifuge; burner inside diameter= 0.05 - 0.21 cm; rotational speed= 200 rpm.	Only photographs are obtained and flame lengths are measured.	The results indicate that flame length and carbon luminosity decrease with increasing buoyancy. Also, flame lift-off and extinguishment were observed as the g-level increased.
Kimura and Ukawa (1961)	Gas-jet diffusion flames under negative-g conditions by inverting the flame using a downward-flow configuration.	Data are obtained for both normal-g and inverted flames.	City gas flames are used. Fuel nozzle dia.=1.5, 3 and 6 mm; air duct dia.=52 and 98 mm; air flow rate ≤ 10 m/sec, fuel flow rate ≤ 40 m/sec.	Only flame lengths are observed.	Flame length is proportional to the fuel flow rate and inversely proportional to the diffusion coefficient.

Table 1(c). Continued.

AUTHOR(s)	METHOD	CHARACTERISTICS	DATA USED	DEFICIENCIES	COMMENTS
SAIC's inverted flame	A downward-flow configuration is used to study coaxial gas-jet diffusion flames.	Temperature, flame shape, etc. are obtained. Stagnation points are predicted indicating that unattached recirculation zones exist above the centerline downstream of these flames.	Air inlet velocity =6.4 ft/sec; methane injection velocity=0.17 - 1.2 ft/sec; fuel-tube diameter=0.19 in.; duct diameter=6.0 in.	No quantitative information on soot, velocity, species, radiation etc.	Importance of recirculation in inverted flames is demonstrated. The tip of the flame spread out and the flame was capped with a concave upward surface, see Fig. 2.
Bonne (1971)	Two-dimensional hydrocarbon-air diffusion flames at normal gravity.	Strong convective effects were present, complicating the data interpretation.	Methane and propane were used. Rectangular burners were employed.	The study did not reveal quantitative understanding of the phenomena of extinguishment from the point of view of the coupling between kinetics, soot formation, and radiation.	The results show that radiative extinguishment occurs prior to depletion of the available fuel and oxidizer. Radiative transfer was responsible for cooling these flames to the point of visible flame disappearance.

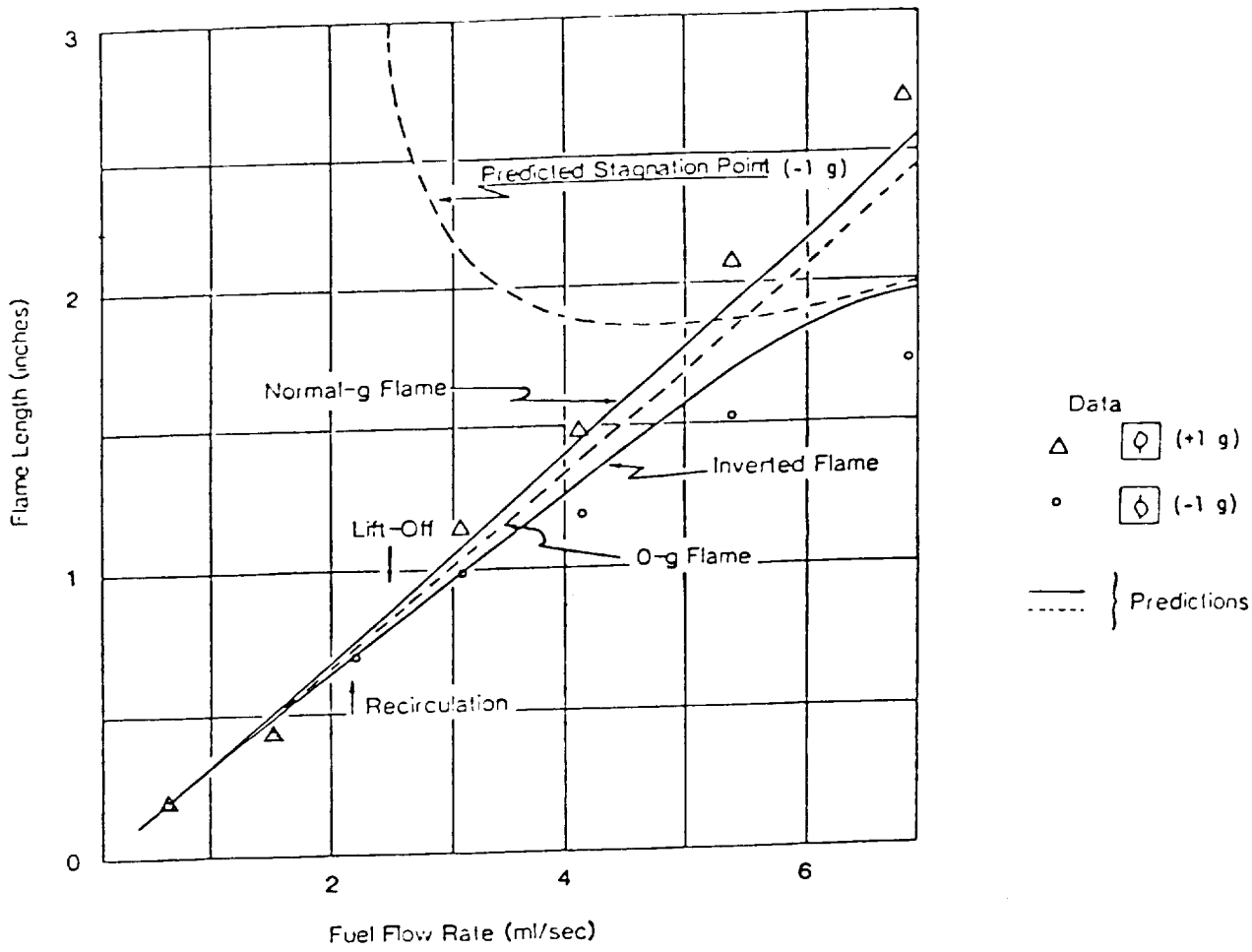

Fig. 2. Flame height vs. fuel flow rate for a confined gas jet diffusion flame. Air inlet velocity = 6.4 ft/sec, methane injection velocity = 0.17 - 1.2 ft/sec, fuel tube diameter = 0.19 in, and duct diameter = 6 in; from SAIC's results. The results show the predicted characteristics of normal-g, zero-g and negative-g flames along with the experimental data, recirculation, and lift-off.

presence of buoyancy, the coupling between combustion kinetics and soot formation is strong and the present models are not quite capable of predicting the effect of buoyancy on the formation of particulates. Flame radiation is mainly due to the presence of soot particles and the interaction between kinetics and radiation is directly influenced by their generation. These mechanisms are accentuated in the absence of buoyancy. The orange-reddish appearance of the near-zero-g flames is an indication of pyrolysis in the hot fuel-rich portions of the flame which results in appreciable amounts of solid carbon (Cochran and Masica, 1970; Cochran, 1972; Edelman et al. 1973). These studies have shown that flame temperature is reduced due to the large globular flame surface and continuum radiation from soot. Thermal radiation can result in an energy loss of up to 40% of the heat input which augments the kinetic effects that can contribute to flame extinguishment. The studies also suggest that pyrolysis and soot formation are of potential importance in terms of their effect upon the local molecular weight (buoyant force). Experimental results have revealed the non-uniform heat-release mechanism throughout the flow field; partial combustion and soot formation dominate in the near-jet region, while the soot burn-off process is facilitated downstream due to the increased residence time and continued heating. The kinetics of the combustion process under microgravity conditions significantly influence the accuracy of the predictions as can be seen in Fig. 3, which shows the effect of heat release on flame shape and its comparison with the experimental data. The partial oxidation analysis shows smaller flame radii and shorter flame lengths, a behavior observed even for the steady-state predictions of flames that were actually quenched during the drop-test sequence. Further results using the partial oxidation analysis models (Edelman et al. 1973) are compared with the experimental data of Cochran (1972) in Fig. 4; they show substantially improved agreement with respect to the results obtained assuming complete combustion model. This tends to confirm the potential role of chemical kinetics in microgravity flames.

Ignition, flame stabilization and flame propagation are directly related to kinetic effects and are transient in nature. Existing data

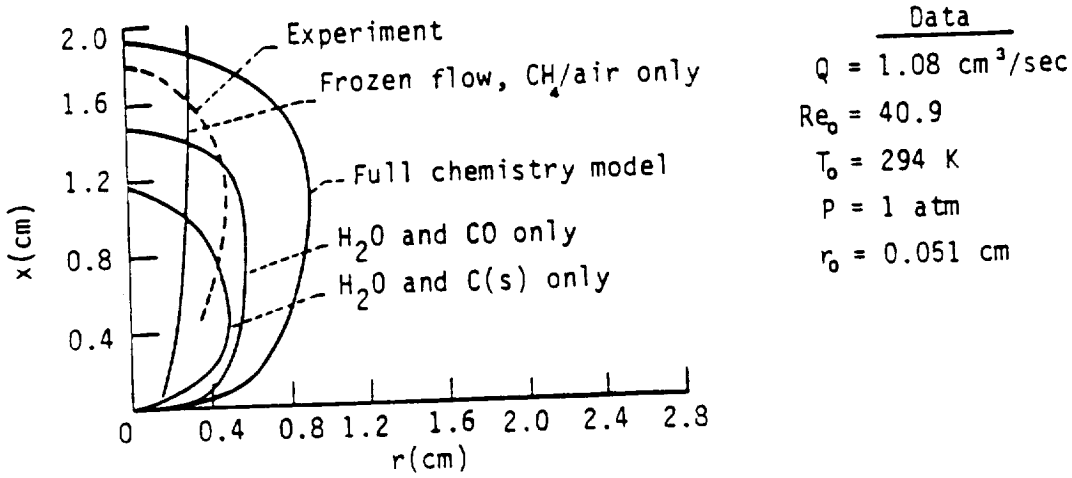

Fig. 3. Effect of chemistry model upon analytical prediction of a steady-state zero-gravity methane-air flame; reproduced from Edelman et al. (1973). The experimental data were obtained from Cochran (1972).

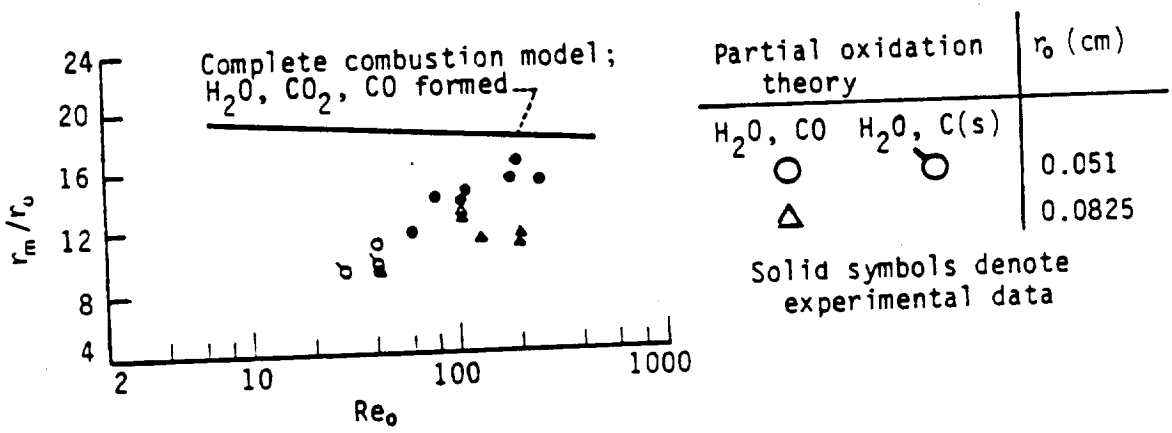

Fig. 4. Comparison of theoretical model with experimental zero-gravity flame widths in ambient methane-air flames, as a function of fuel Reynolds number; reproduced from Edelman et al. (1973). The experimental data were obtained from Cochran (1972).

is insufficient to determine how the combined effects of chemical kinetics, soot formation and radiation affect these phenomena under both normal-g and near-zero-g conditions. As a matter of fact, most of the steady, normal-gravity flames of the drop-tower experiments were extinguished during the drop (Cochran and Masica, 1970; Cochran, 1972), suggesting that a combination of chemical kinetics, radiation and transient phenomena are responsible for extinction. The major role of transient effects is demonstrated in Table 2. There exists a certain range of fuel velocity in which a transient period occurs between steady state and flame extinguishment. It can be seen that extinguished, transient and steady-state flames contribute equally to the construction of this table. The parameter characterizing the relative importance of transient effects is the Strouhal number $(r_m/u_m\tau_c)$, i.e., the ratio of the residence time to the time associated with the drop sequence (see Edelman et al. 1973). Here, r_m = maximum flame radius, u_m = axial velocity at maximum flame width and τ_c = time required for the flame to attain its minimum length upon the release of the test cell. Comparisons between zero-g and normal-g flames have shown that the residence times are 5 to 10 times longer under zero-g condition. Also, for residence times of the order of 100 msec, sustained combustion under zero-g conditions has not been observed. The methane-air flame data show that when quenching occurs it is generally preceded by the attainment of a minimum flame length in times on the order of 50-100 msec, which is a characteristic time associated with the drop sequence, i.e., the Strouhal number is of the order of unity or greater. The hot products of normal-g combustion are retained within the zero-g flames because of the reduction in convective transport. The flame zone is then shielded from fresh oxygen due to the retention of the hot combustion gases. This promotes pyrolysis of the constantly flowing fresh fuel through the flame. A critical reduction in temperature due to radiation occurs before the flame is given enough time to adjust to a steady-state configuration with convective transport matching diffusive transport. The result is a reduced heat release rate probably due to the change in the oxidation kinetics which ultimately results in flame quenching. Figure 5 shows an extinguished flame under

Table 2. Methane-Air Flame Data of the Drop-Tower Experiments; Reproduced from Cochran (1972).

Run	Burner radius, R_0, cm	Average normal-gravity length, L_1, cm	Maximum normal-gravity radius, $R_{max_{1G}}$, cm	Flow rate, cm^3/sec	Average axial velocity, U_∞, cm/sec	Zero-gravity minimum length, L_0, cm	Extinguishment length, cm	Steady state zero-gravity length, L_s, cm	Steady state zero-gravity maximum radius, $R_{max_{0G}}$, cm
1	0.051	9.30	0.46	6.65	813.8	7.51	----	(a)	0.77
2		3.42	.37	2.80	342.6	2.96	----	5.02	.70
3		2.48	.37	2.10	291.2	2.10	----	3.80	.72
4		6.95	.51	5.15	630.2	5.91	----	9.78	.83
5		3.51	.42	2.90	354.9	3.08	----	5.38	.74
6		6.54	.51	4.90	599.6	5.59	----	9.76	.78
7		.72	.24	.75	91.8	.68	0.88	-----	----
8		1.08	.32	1.08	132.2	1.04	----	1.80	.48
9		1.76	.44	1.60	195.8	1.63	----	2.76	.60
10	.113	.94	.35	.94	23.4	.78	1.10	-----	----
11		1.88	.40	1.70	42.4	1.46	2.15	-----	----
12		2.22	.41	1.98	49.2	1.60	(b)	-----	----
13		1.08	.36	1.08	26.9	1.01	1.24	-----	----
14		1.22	.33	1.18	29.3	1.01	1.36	-----	----
15		1.92	.38	1.72	42.9	1.48	2.12	-----	----
16		2.46	.38	2.16	53.8	1.81	2.61	-----	----
17		5.92	.55	4.95	123.4	4.50	(b)	-----	----
18		4.20	.51	3.55	88.5	2.65	4.66	-----	----
19		5.13	.58	4.30	107.3	3.36	5.78	-----	----
20		5.80	.60	4.85	120.9	3.76	7.55	-----	----
21		11.43	.69	9.65	240.5	8.91	(b)	-----	----
22		14.13	.73	12.20	304.1	8.96	(a)	-----	----
23	.0825	11.20	.63	8.55	399.8	8.17	----	16.62	.91
24		8.31	.58	6.42	300.2	7.20	----	12.70	.95
25		5.78	.58	4.55	212.9	3.68	----	8.97	1.04
26		3.52	.36	2.90	135.6	2.51	(b)	-----	----
27		2.31	.34	2.00	93.5	1.81	(b)	-----	----
28		.95	.31	1.00	46.8	.82	1.22	-----	----
29		1.65	.35	1.50	70.2	1.42	(b)	-----	----
30		7.06	.48	5.50	257.2	5.21	----	10.86	.92

[a]Out of camera field of view.

[b]Transient flame.

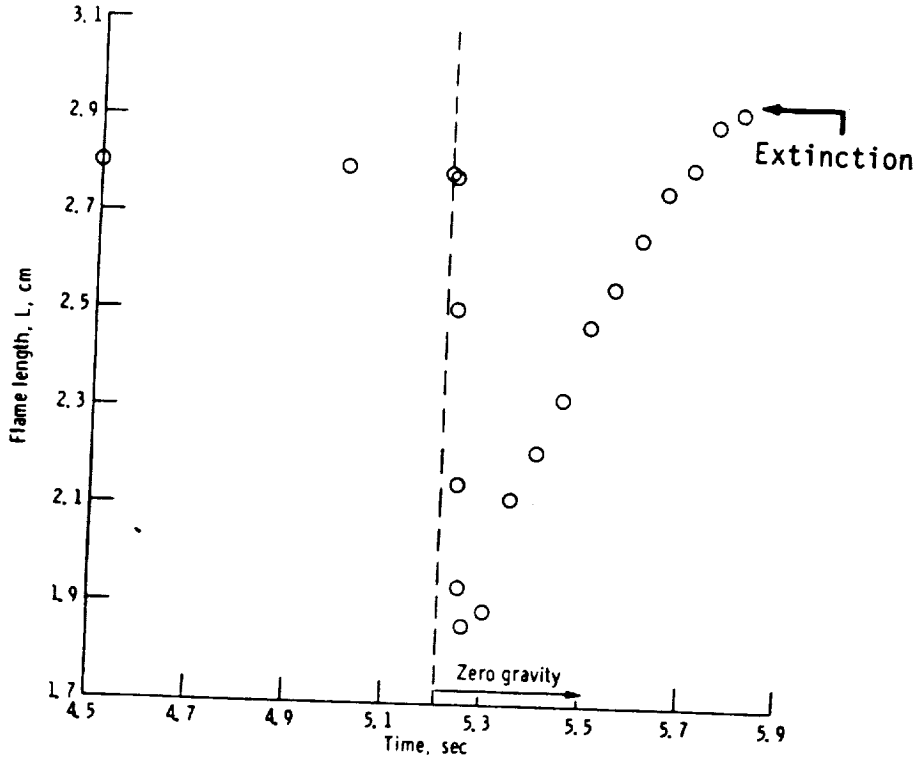

Fig. 5. Flame length as a function of time for CH_4/air flames under zero gravity. Normal-gravity length = 2.78 cm, methane flow rate = 2.8 cm^3/sec, nozzle radius = 0.186 cm, velocity = 25.44 cm/sec, zero-gravity minimum length = 1.86 cm, and extinguishment length = 2.93 cm; reproduced from Cochran and Masica (1970).

zero-g conditions (Cochran and Masica, 1970). A flame which (apparently) reaches steady state in the 2.2-sec. drop-tower experiment is shown in Fig. 6 (Cochran, 1972); whether the oscillations persist given sufficient time is unknown. The reported steady-state flames may, in fact, be in transition from a transient state to extinguishment. However, Haggard (1981) has shown that relatively low forced-air velocities ($\simeq$ 10 cm/sec) are sufficient to sustain methane flame combustion in zero gravity. This experimental result shows the sensitivity of the extinguishment process to convective transport in these low-momentum diffusion flames.

We have recently developed an analytical model for the shapes and heights of zero-g, laminar, cylindrically symmetric, transient diffusion flames which incorporates the effects of axial diffusion (see Sec. IV). The assumptions are: (i) flame-sheet approximation, (ii) equal and constant properties, flow velocities and diffusion coefficients in the two gas streams, and (iii) negligible buoyancy effects, i.e., zero gravity. The only adjustable parameter in this analysis is the diffusion coefficient. The results of the mathematical representation of flame height as a function of time are in good agreement with those of the drop-tower experiments for the early portion of extinguished flames and steady-state zero-gravity flames (see Sec. IV). This analysis shows that the theoretical steady-state flame lengths are approached slowly. Since the theory does not include the effects of radiation and chemical kinetics, quenching can not be predicted by this analysis and the predicted approach to steady state may, in fact, be faster than would be the case if these effects were taken into account.

The importance of axial diffusion for short flames has been realized since 1928 (Burke and Schumann). It has been included in the analytical solutions for laboratory-scale diffusion flames (Penner, Bahadori and Kennedy, 1984) and in the flame height calculations of composite solid propellants (Beckstead, 1981) because of the comparable sizes of physical dimensions and flame heights. Observations in the drop-tower experiments have shown the existence of much more globular-flames compared with those at normal-g with flame height/

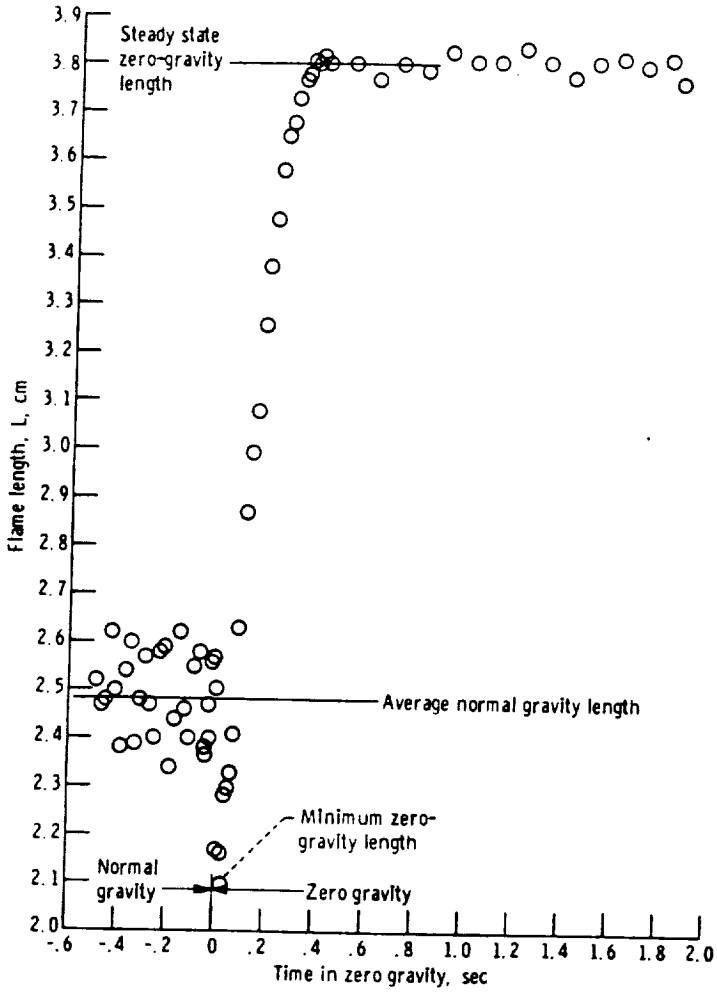

Fig. 6. Flame length as a function of time in zero gravity for Run 3 of Table 2; reproduced from Cochran (1972). For this CH_4/air flame, average normal-gravity length = 2.48 cm, nozzle radius = 0.051 cm, zero-gravity minimum length = 2.1 cm, steady-state zero-gravity length = 3.8 cm, fuel velocity = 291.2 cm/sec, maximum normal-gravity radius = 0.37 cm, flow rate = 2.1 cm^3/sec, and steady-state zero-gravity maximum radius = 0.72 cm.

maximum flame radius ~ 1 (see Edelman et al. 1973). In addition, significant deviation between theory and experiment is reported for low-Reynolds number flames (i.e., fuel-jet Re ~ 100) in the drop-tower experiments. These results suggest that axial diffusion in flames under microgravity conditions is as significant as radial diffusion especially during the transient development of the flame toward a possible steady state and in late-time flame extinguishment. Figure 7 shows the effect of axial diffusion on both transient and steady-state behavior of a methane-air diffusion flame obtained from the analytical derivation for unsteady, laminar diffusion flames with cylindrical symmetry in the presence of axial diffusion (see Sec. IV). This result shows that axial diffusion has a significant effect on the development of the flame under zero-g conditions.

III. Objectives

The overall objective of the experiment is to gain a better fundamental understanding of laminar gas jet diffusion flames in general, and the effect of buoyancy in particular.

This overall objective will be achieved by meeting a set of specific objectives that involve obtaining new data for elimination of the inadequacies in the existing data and theory. This will be accomplished by studying the following phenomena:

a) Unsteady phenomena associated with ignition and flame development;
b) Steady-state structure;
c) Soot generation and radiation;
d) Quenching phenomena.

Specific collateral objectives involve measurements that include:

1) Flame shape development and flame extinction;
2) Color and luminosity;
3) Temperature distributions;
4) Species concentrations;
5) Radiation measurements.

Thus, by eliminating buoyancy-induced convective effects, this microgravity experiment will clarify the existing fundamental uncertainties by:

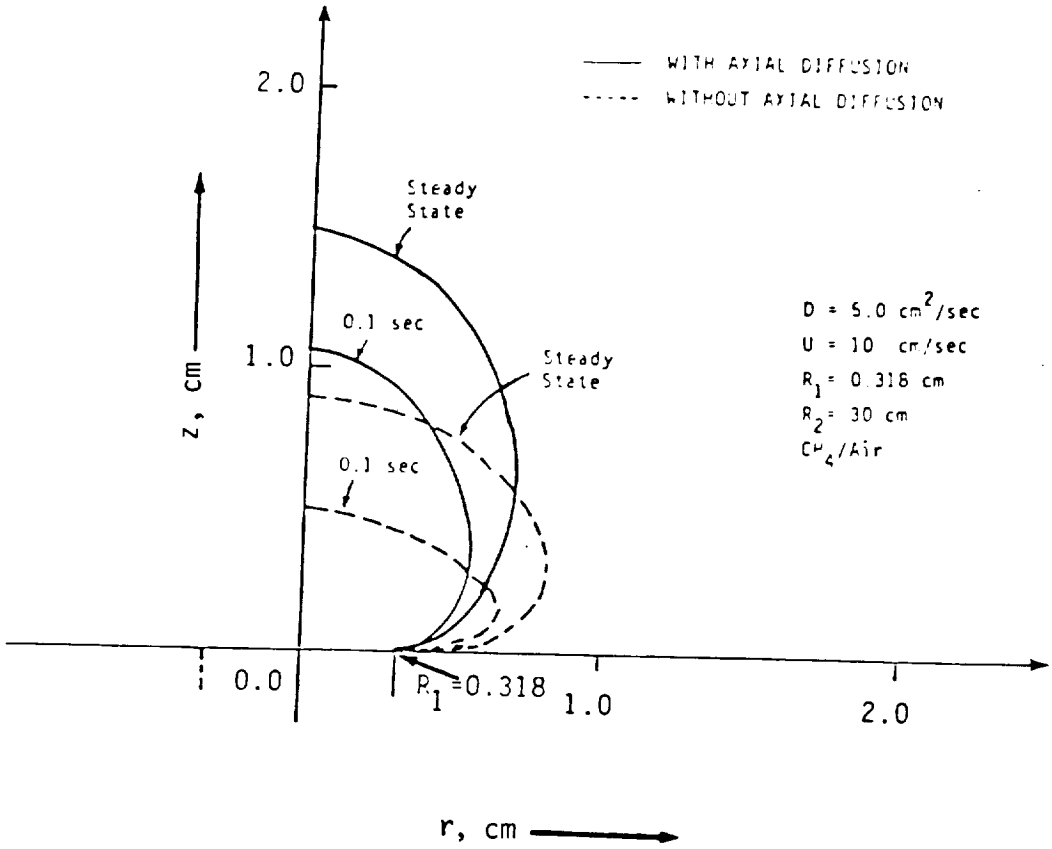

Fig. 7. Comparison between the shapes of laminar diffusion flames in both absence and presence of axial diffusion using the analytical solution for transient flames (see Sec. IV); D = binary diffusion coefficient of CH_4 in N_2 (evaluated at T = 1800 K), U = equal and constant velocities of the two streams, $R_1(R_2)$ = inner(outer) tube radius, r = radial coordinate and z = axial coordinate.

i) Obtaining as much data as possible from reduced-gravity earthbound experiments;

ii) Contributing to the development and validation of reliable theoretical analyses that form a basis for encapsulating and, thereby, interpreting the experimental observations;

iii) Providing insight into the unsteady phenomena of ignition, flame propagation and extinction under microgravity conditions with direct applications to fires in space;

iv) Obtaining required data for future microgravity studies of laminar flames, transition from laminar to turbulent flames and, consequently, the behavior of fully developed turbulent flames by eliminating the complex phenomena of buoyancy-generated turbulence.

IV. Current Modeling Status

In this section, we present results of the application of two theoretical analyses, each developed to examine certain aspects of the mechanisms controlling diffusion flame behavior. The first analysis accounts for inertia, diffusion, viscosity, thermal conductivity, and arbitrary g-levels for fuel jets issuing into a coaxial air stream of arbitrary velocity under steady flow conditions. The second analysis accounts for transient and axial diffusion effects under the specialized conditions of constant and uniform velocity and physical properties. In addition, an advanced transient, two-dimensional analysis and finite-difference methodology which would be adopted for application in the future work is described.

1.. Steady Flow Jet Diffusion Flame Analysis

The mathematical model of Edelman et al. (1973) has been used, with modifications, to obtain solutions for laminar jet diffusion flames. The approach involves a finite-difference solution of the partial differential equations for mass, momentum, elements, and energy, which are in their boundary-layer form. The effects included are diffusion, viscosity, inertia, combustion, gravity, and radiation. The chemistry assumed is that of shifting equilibrium.

Figure 8 shows the flow field of an axisymmetric, steady-state, vertical laminar jet. The fuel is injected at a finite velocity into

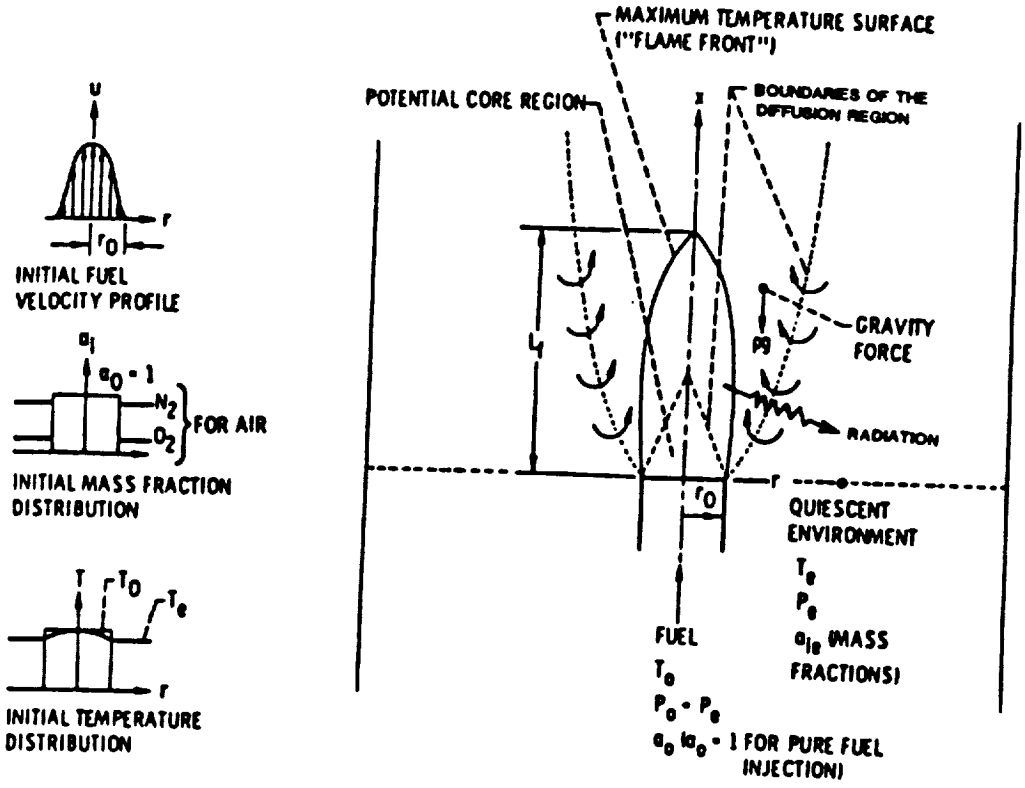

Fig. 8. Schematic of vertical laminar jet; reproduced, with modifications, from Edelman et al. (1973).

the quiescent surroundings. The effects upon the velocity field are shear or molecular diffusion of momentum, pressure gradient and gravity. The buoyant force is a combination of gravity and pressure gradient. In the vertical jet problem, convection of energy, heat release rate, heat conduction, and the energy transported due to diffusion of species affect the temperature field through the velocity field and the concentration field. The concentration field is, in turn, affected by the convection of species through the flow and therefore by the velocity field. Chemical production rate and diffusion are the mechanisms which directly cause changes in the species field. The diffusional gradients produce an air/fuel ratio distribution ranging from fuel rich to fuel lean in the mixing region (see Fig. 8). The surface upon which the equivalence ratio is unity is referred to as the "flame front" which corresponds to the maximum temperature. The assumptions made are: (a) diffusive processes are important only in the radial direction, (b) combustion is diffusion controlled, and (c) flow is steady and axisymmetric. The equations of continuity, momentum, diffusion of elements, and energy are nondimensionalized with respect to the state of the flow at the maximum flame width point (see Edelman et al., 1973). The equations of state are used to complete the set of equations. Multicomponent diffusion has been employed in the analysis and radiation is currently accounted for in terms of water and CO_2 radiation in the simple form:

$$q \propto \sigma(\epsilon_{H_2O} X_{H_2O} + \epsilon_{CO_2} X_{CO_2}) T^4 , \qquad (1)$$

where q = radiative heat loss, σ = Stefan-Boltzmann constant, ϵ = emissivity, X = mole fraction, and T = gas temperature.

The governing flow field conservation equations are transformed, into the von Mises plane, and then solved numerically by employing an explicit finite-difference technique. The details of the flow field, i.e., velicity, temperature and species fields along with the gross characteristics including combustion lengths and flow deflections have been obtained by the solution of the system of conservation equations. The global continuity equation has been eliminated from the system of differential equations by introducing the von Mises coordinates as the

independent variables, i.e., the transformation $x, r \rightarrow x, \psi$ is defined according to the relations

$$\rho u r^N = \psi^N \psi_r,$$
$$-\rho v r^N = \psi^N \psi_x, \tag{2}$$

where N = 0 (for plane 2-D flow) or 1 (for axisymmetric flow), ρ = density, u = axial velocity, v = radial velocity, r = radial coordinate, and subscripts r and x denote differentiation with respect to these variables. Figure 9 shows a generic point (n+1,M) in the $x - \psi$ grid network. The finite-difference formulation for the calculation of the flow at the point (n+1,M) is obtained by using the following explicit difference relations where P is only one of the three pertinent variables axial velocity, element mass fraction or mixture stagnation enthalpy:

$$\frac{\partial P}{\partial x} = \frac{P_{n+1,M} - P_{n,M}}{\Delta x}, \tag{3}$$

$$\frac{\partial P}{\partial \psi} = \frac{1}{2} \frac{P_{n,M+1} - P_{n,M-1}}{\Delta \psi}, \tag{4}$$

$$\frac{\partial}{\partial \psi}\left[b \frac{\partial P}{\partial \psi}\right] = \frac{b_{n,M+\frac{1}{2}} [P_{n,M+1} - P_{n,M}] - b_{n,M-\frac{1}{2}} [P_{n,M-1}]}{\Delta \psi^2}, \tag{5}$$

where

$$b = \rho u r^{2N} \mu / \psi^N, \tag{6}$$

$$b_{n,M\pm\frac{1}{2}} = \frac{1}{2} [b_{n,M} + b_{n,M\pm1}], \tag{7}$$

$$\psi = M(\Delta \psi), \tag{8}$$

and μ is the viscosity. Thus, for example, the momentum equation at an arbitrary point in the field takes on the following form:

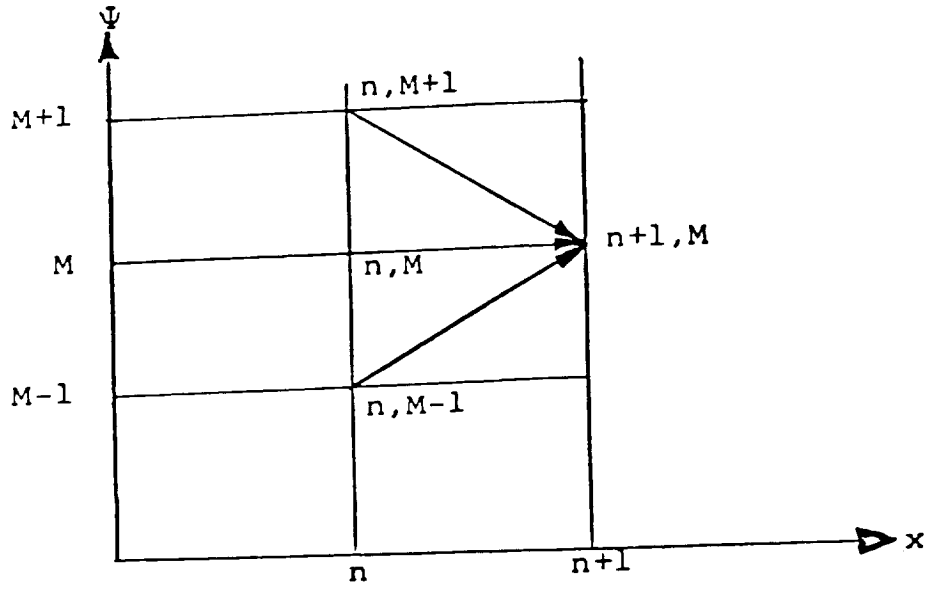

Fig. 9. Schematic of the grid network used in the explicit finite-difference technique. The arrows indicate the calculation of the flow field at point (n+1, M) from data at station n; reproduced from Edelman, Fortune and Weilerstein (1972).

$$U_{n+1,M} = U_{n,M} + \frac{\Delta x}{M^N(\Delta\psi)^{2+N}} \left\{ (b)_{n,M+\frac{1}{2}} U_{n,M+1} - [b_{n,M+\frac{1}{2}} \right.$$

$$\left. + b_{n,M-\frac{1}{2}}] U_{n,M} + b_{n,M+\frac{1}{2}} U_{n,M-1} \right\} + (\rho_e - \rho)g \frac{\Delta x}{(\rho u)_{n,M}} \quad (9)$$

The remaining conservation equations are described in a similar manner in Edelman, Fortune and Weilerstein (1972). However, the inclusion of radiation and modified boundary conditions represent modifications of the original formulation. Radiation is included via the approximation of optically thin medium. The modified boundary conditions provide for the presence of confinement to account for pressure field that develops in the case of the ducted flow. The effect of flow confinement has been included by using (a) skin friction coefficient for shear stress calculations at the wall, (b) displacement thickness for effective area variations in the viscous layer, and (c) inviscid flow calculations for the region bounded by the mixing region and the boundary layer which provides the effects of pressure variation due to confinement.

The present model incorporates the effect of radiation, which is an improvement over the previous models. However, other modifications (e.g., soot radiation, detailed kinetics and elliptic effects) still need to be included. An interesting result of the model is presented in Fig. 10 which shows that in order to eliminate the take-over of convective effects under reduced-g conditions, the gravitational acceleration must be less than 10^{-3}g.

2. Analytical Solution for Transient Jet Diffusion Flames

In this section, we present analytical solutions for the shapes of laminar, transient diffusion flames with cylindrical symmetry in the presence of axial diffusion. The solution is based on, and is an extension of, the previous steady-state analyses (see Burke and Schumann, 1928, Penner, Bahadori and Kennedy, 1985, and Bahadori, Li and Penner, 1986).

The assumptions used in the formulation of the problem are: (i) constant pressure, which eliminates the momentum-conservation equation, (ii) Lewis number of unity, which decouples the energy- and species-

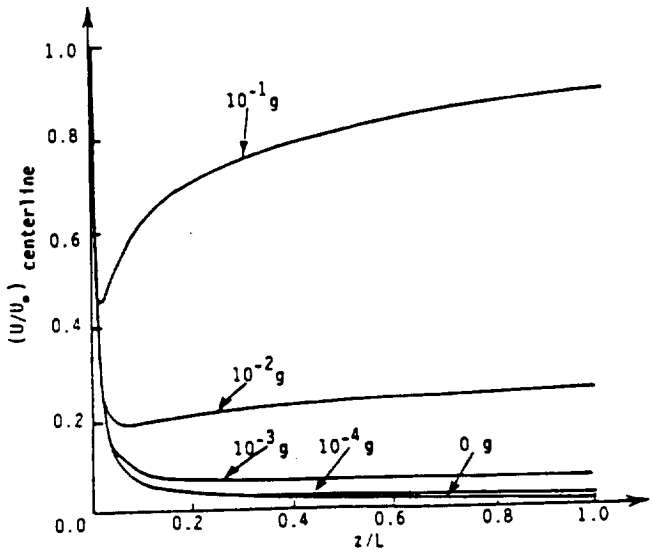

Fig. 10. Results of the numerical calculations (using the modified model of Edelman and co-workers, 1973) for normalized velocity along the jet centerline vs. normalized vertical distance for different g-levels. These calculations are carried out for a steady-state methane-air flame. The jet velocity is U_o = 93.5 cm/sec and the nozzle radius is 0.0825 cm. The axial distance is normalized using a value of L = 50 cm. Note the increase in velocity beyond the axial location of z = 4 cm for 10^{-2}g (which is a result of the the take-over of convective effects).

conservation equations, and thereby, reduces the problem to one governing equation, (iii) equal and constant flow velocities, transport parameters and physical properties in the two gas streams, (iv) flame-sheet approximation, which defines the flame location as a boundary at which the fuel and oxidizer have vanishingly small mass fractions and arrive in stoichiometric mass flux ratios, (v) no buoyancy effects, and (vi) inclusion of both axial and radial diffusion. The assumption of equal (and constant) velocities might seem to be the most limiting one. This assumption greatly simplifies the analysis because of the elimination of the momentum equation. But the effect of velocity on shape is relatively small as shown in the previous numerical calculations; in fact, the velocity drops to the ambient velocity in distances (from the centerline) of approximately 2-3 radii of the inner cylinder under normal-g conditions. This implies the domination of diffusion in regions where the flame is present. The assumption of constant diffusion coefficient is more restrictive. However, application of the present model in a parametric way has allowed us to extrapolate the transient drop-tower data of Cochran and Masica (1970) and Cochran (1972), and obtain estimates of the time to reach an apparent steady state. The drop-tower data have shown that upon the release of the test cell and removal of the convective velocity due to the drop in the g-level, the flame height drops to a minimum which is an indication of a tendency to quench. But since the fuel is constantly flowing into the products of combustion, the flame starts to develop from the new position and (in some cases) reaches an apparent steady state. The analysis approximates this event by characterizing the turning on of the fuel valve and igniting the flame at the same time and recording the flame development.

For the cylindrically symmetric flow of gases, we consider the model of Fig. 11 with an inert gas entering along the inner of two concentric cylinders (with radius d/2) for times $t<0$. The oxidizer flows in the outer cylindrical shell (bounded by the radii d/2 and d'/2) at all times. The flow of the inert gas is replaced by the fuel flow of the same velocity at times $t>0$, i.e., the interface between the fuel and the inert gas arrives at the port at $t = 0$, and ignition occurs when this interface is at the burner port. This model enables us to mathematically formulate

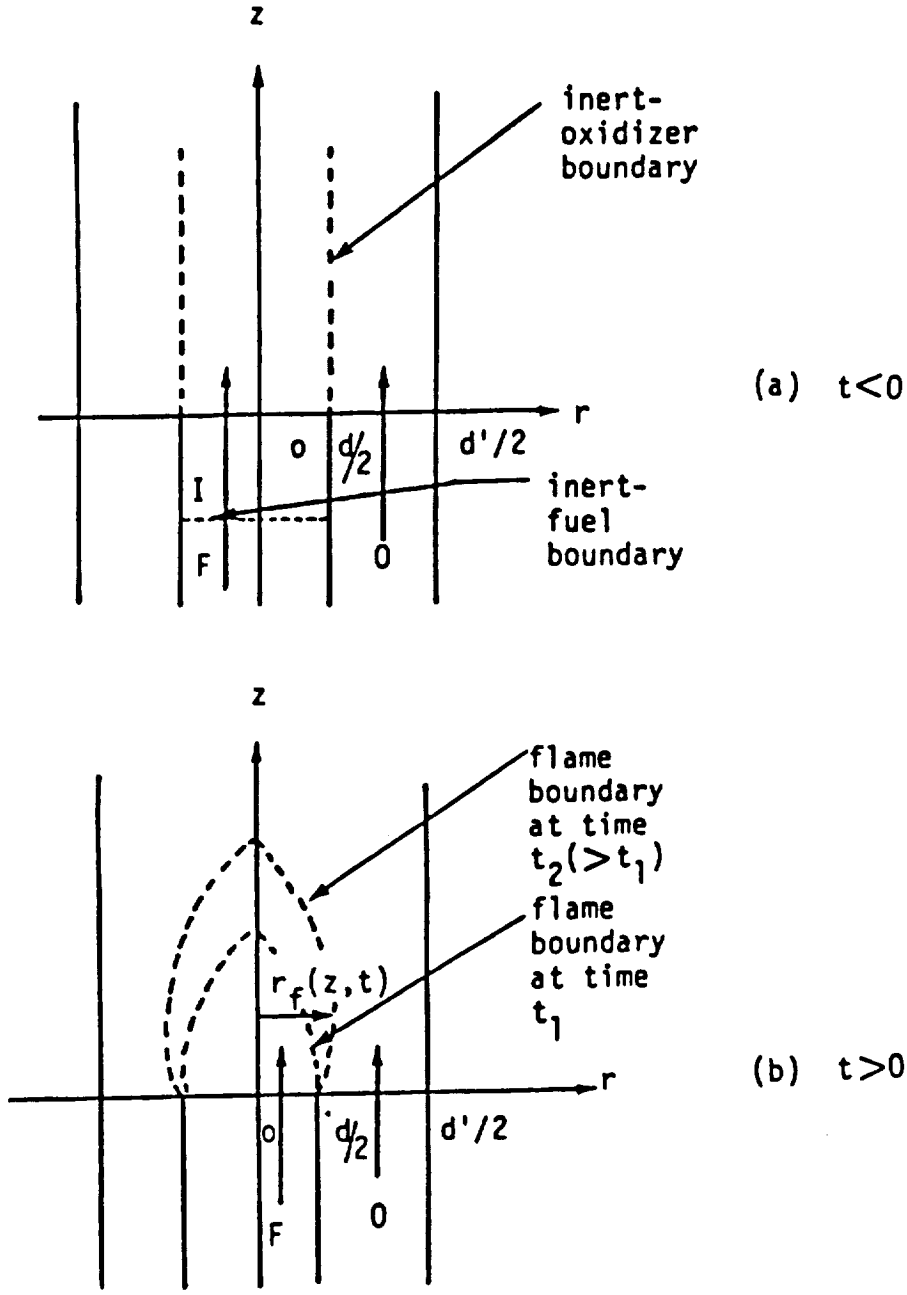

Fig. 11. Schematic diagram of concentric cylinders with inert I entering at z = 0 for 0<r<d/2 during the times t<0 [see (a)] which is replaced by fuel F during the times t>0 at the burner port. The oxidizer 0 is entering at z = 0 for d/2<r<d'/2 at all times [(a) and (b)]. The flame development is shown in (b) for two different times. Here, d/2 is the radius of the inner cylinder, d'/2 is the radius of the outer cylindrical shell, z is the axial coordinate, r is the radial coordinate, and $r_f(z,t)$ is the flame radius.

the problem and obtain an analytical representation of flame-shape development as a function of time.

The species-conservation equations with both radial and axial diffusion (and no radial or tangential velocity components) for fuel and oxidizer above the burner port at times t>0 become, respectively,

$$\frac{\partial Y_F}{\partial t} + u_F \frac{\partial Y_F}{\partial z} = D_F\left(\frac{1}{r}\frac{\partial Y_F}{\partial r} + \frac{\partial^2 Y_F}{\partial r^2} + \frac{\partial^2 Y_F}{\partial z^2}\right) \text{ for } 0 \le r < r_f,\ z > 0,\ t > 0, \tag{10}$$

$$\frac{\partial Y_O}{\partial t} + u_O \frac{\partial Y_O}{\partial z} = D_O\left(\frac{1}{r}\frac{\partial Y_O}{\partial r} + \frac{\partial^2 Y_O}{\partial r^2} + \frac{\partial^2 Y_O}{\partial z^2}\right) \text{ for } r_f < r < d'/2,\ z > 0,\ t > 0, \tag{11}$$

where Y = mass fraction, u = velocity, D = diffusion coefficient, t = time, z = axial coordinate, r = radial coordinate, r_f = flame radius, and subscripts F and O denote the fuel and oxidizer, respectively. Equations (10) and (11) reduce to a single differential equation

$$\frac{\partial Y}{\partial t} + u\frac{\partial Y}{\partial z} = D\left(\frac{1}{r}\frac{\partial Y}{\partial r} + \frac{\partial^2 Y}{\partial r^2} + \frac{\partial^2 Y}{\partial z^2}\right) \text{ for } 0 \le r < d'/2,\ z > 0, t > 0, \tag{12}$$

which is valid over the entire region $0 \le r < d'/2$ once we impose the conditions of $u_O = u_F = u$ = constant and $D_O = D_F = D$ = constant and introduce the single variable

$$Y(r,z,t) = \begin{cases} Y_F & \text{for } 0 \le r < r_f,\ z > 0,\ t > 0, \\ -\nu Y_O & \text{for } r_f < r < d'/2,\ z > 0,\ t > 0, \end{cases} \tag{13}$$

where ν is the stoichiometric ratio of grams of fuel consumed per gram of oxidizer at a flame front. In view of Eq. (13), the initial conditions are

$$Y(r,z,0) = \begin{cases} 0 & \text{for } 0 \le r < d/2,\ z > 0,\ t = 0, \\ -\nu Y_{O,o} & \text{for } d/2 < r < d'/2,\ z > 0,\ t = 0, \end{cases} \tag{14}$$

$$Y(r,0,t) = \begin{cases} Y_{F,o} & \text{for } 0 \le r < d/2,\ z = 0,\ t > 0, \\ -\nu Y_{O,o} & \text{for } d/2 < r < d'/2,\ z = 0,\ t > 0, \end{cases} \tag{15}$$

where the subscript o denotes the initial conditions. The symmetry condition is

$$\partial Y(0,z,t)/\partial r = 0, \tag{16}$$

and the boundary condition is

$$\partial Y(d'/2,z,t)/\partial r = 0, \tag{17}$$

which corresponds to the absence of oxidizer flow through the wall. The flame-sheet approximation then defines the location of the flame boundary using

$$Y(r_f,z,t) = 0 \tag{18}$$

which then gives an analytical experssion for flame shape in the form $r_f(z,t) = 0$.

The method of separation of variables when applied to Eqs. (12)-(18) gives the flame location at any time t as

$$\sum_{j=2}^{\infty} \frac{2\left(Y_{F,o} + \nu Y_{0,o}\right)\left(\frac{d}{2}\right) J_1\left(\lambda_j \frac{d}{2}\right) J_o\left(\lambda_j r_f\right)}{\lambda_j \left(\frac{d'}{2}\right)^2 J_o^{\,2}\left(\lambda_j \frac{d'}{2}\right)}$$

$$\times \exp\left\{\frac{u\left(t+\frac{z}{u}\right)}{2Dt}\left[1 - \sqrt{1 + \frac{4Dt\left[D\lambda_j^2 t + \ell n\left(\frac{Y_{F,o} + \nu Y_{0,o}}{\nu Y_{0,o}}\right)\right]}{u^2\left(t+\frac{z}{u}\right)^2}}\right] z\right\}$$

$$= -\left[\left(Y_{F,o} + \nu Y_{0,o}\right)\left(\frac{d}{d'}\right)^2 - \nu Y_{0,o}\right]$$

$$\times \exp\left\{\frac{u\left(t+\frac{z}{u}\right)}{2Dt}\left[1 - \sqrt{1 + \frac{4Dt\ \ell n\left[1 - \frac{Y_{F,o}\,(d/d')^2}{\nu_{0,o}\left[1-(d/d')^2\right]}\right]}{u^2\left(t+\frac{z}{u}\right)^2}}\right] z\right\}, \tag{19}$$

where J_0 and J_1 are Bessel functions of the first kind of orders zero and one, respectively, and the eigenvalues λ_j are the roots of $J_1(\lambda_j d'/2) = 0$ with $\lambda_j \neq 0$. For large times (i.e., $t \to \infty$), Eq. (19) reduces to the following solution for steady-state flame shape:

$$\sum_{j=2}^{\infty} \frac{2\left(Y_{F,o} + \nu Y_{0,o}\right)\left(\frac{d}{2}\right) J_1\left(\lambda_j \frac{d}{2}\right) J_o\left(\lambda_j r_f\right)}{\lambda_j \left(\frac{d'}{2}\right)^2 J_o^{\,2}\left(\lambda_j \frac{d'}{2}\right)} \cdot \exp\left[\frac{u}{2D}\left(1 - \sqrt{1 + \frac{4D^2\lambda_j^2}{u^2}}\right) z\right]$$

$$= -\left[\left(Y_{F,o} + \nu Y_{0,o}\right)\left(\frac{d}{d'}\right)^2 - \nu Y_{0,o}\right]. \qquad (20)$$

In the absence of axial diffusion, Eq. (20) reduces to the classical solution of Burke and Schumann (1928) for steady-state, cylindrically symmetric laminar diffusion flames with no buoyancy (see Penner, Bahadori and Kennedy, 1986), viz.

$$2\left(\frac{d}{d'}\right)\sum_{j=2}^{\infty} \frac{J_1\left(\lambda_j \frac{d}{2}\right) J_o\left(\lambda_j r_f\right) \exp\left(-D\lambda_j^2 z/u\right)}{\left(\lambda_j \frac{d'}{2}\right) J_o^{\,2}\left(\lambda_j \frac{d'}{2}\right)} = \frac{\nu Y_{0,o}}{Y_{F,o} + \nu Y_{0,o}} - \left(\frac{d}{d'}\right)^2. \qquad (21)$$

Equation (19) was solved numerically by using polynomial expressions for Bessel functions. The input to the problem consists of the values for $Y_{F,o}$, ν, $Y_{0,o}$, $d/2$, $d'/2$, u, D, and a selected number of times ranging from 0.05 sec. to 100 sec. The radial distance $d'/2$ was divided into 40 intervals which were not necessarily equal due to the steep variations in mass fractions. The number of eigenvalues calculated in the program was 2000; these were obtained by finding the roots of $J_1(\lambda_j d'/2) = 0$. A large number of eigenvalues were needed (especially at smaller times) due to the slow decay of the exponential terms. Calculation of the terms in the summations were stopped once the exponential terms became smaller than 10^{-6} since the coefficients in front of the exponentials are always of the order of 1 or smaller. Once all the λ_j were calculated, $J_o(\lambda_j d'/2)$ and $J_1(\lambda_j d/2)$ were obtained. Provisions were made to calculate $J_o(\lambda_j r)$ at the beginning of the program for any selected radial distance r. The steady-state flame height calculations were performed by setting $r = 0$ in Eq. (20) and obtaining a value of z for

which this equation was satisfied (using marching in the axial direction from the burner port for specified step sizes.) The steady-state flame height served as an upper limit for the axial locations along the flame boundary in the calculation of steady-state flame shape, transient flame heights and transient flame shapes. For each selected axial location, one point in the radial direction was obtained at which a sign change in mass fraction occured; this is an indication of going from fuel region to oxidizer region, i.e., location of the flame. The time-dependent flame heights and shapes were then obtained by following the procedure for calculating the steady-state flame shapes but using Eq. (19) for any selected time.

The results of the present model are compared with the data obtained from the drop-tower tests in Figs. 12 and 13. Although the assumptions used in the development of the model are somewhat extensive, the results are a useful tool for extrapolating the drop-tower data and helping us to estimate the time required to reach steady state under reduced-g conditions.

3. Transient, Navier-Stokes Based Model

The model which will be used in the future work consists of the modification of an existing SAIC transient, axisymmetric Navier-Stokes based model and code that will predict flame ignition and development to steady state, include both axial and radial diffusion, include soot formation and disposition chemistry, account for radiation from soot, CO_2 and H_2O, predict flame extinction, and obtain temperature, velocity and species fields. The modified model will be in transient, axisymmetric, full Navier-Stokes form, which includes two-dimensional conservation equations for mass, momentum, energy, and species, with arbitrary g-levels and both Fickian and multicomponent diffusion. A radiation model such as the discrete ordinates model will properly take into account the effect of soot, CO_2 and H_2O, and sub-global kinetics with finite reaction rates will be included. Postulated detailed reactions involving many active species are available. However, to try to understand the essential features of diffusion flames, simpler chemistry is more appropriate, e.g., two-, three- or four-step global models which

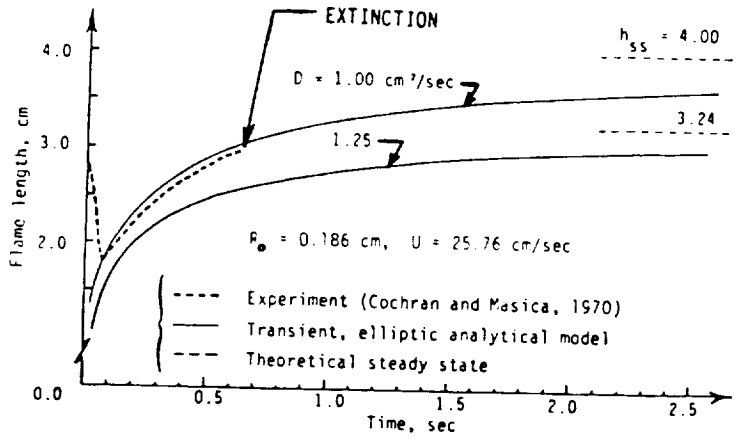

Fig. 12. Comparison between the analytical and experimental flame height-time variations under micro-gravity conditions. Here, D = binary diffusion coefficient of methane in nitrogen, U = fuel velocity, R_0 = nozzle radius, and h_{ss} = steady-state flame height. The value of D = 1 cm^2/sec corresponds to a temperature of 750 K. The experimental results show the flame extinguishment at approximately 0.6 sec (see Fig. 5).

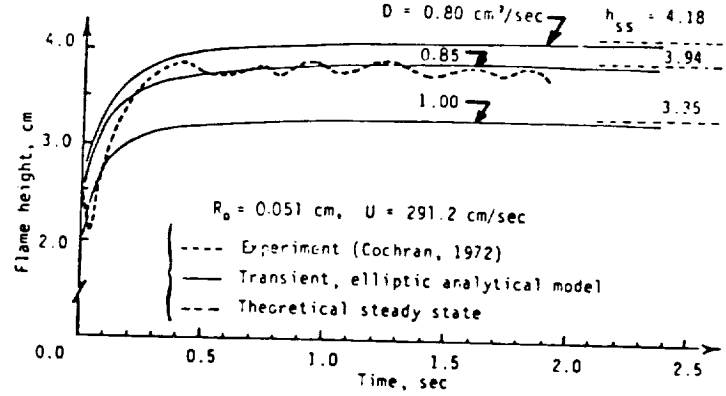

Fig. 13. Comparison between the analytical and experimental flame height-time variations under micro-gravity conditions. The symbols are defined in Fig. 12. The value of D = 0.85 cm^2/sec corresponds to a temperature of 650 K. The experimental result was reported as having reached steady state in 0.4 sec (see Fig. 6). However, note the oscillatory behavior in the data and the theory that shows steady state has not been reached.

are capable of delineating the major regions of the reaction process, and also lend themselves to the prediction of ignition and stabilization characteristics in detailed numerical computations.

The numerical technique involves a control volume differencing scheme, i.e., the governing equations are expressed in integral form for a finite-difference grid element. A generalized coordinate system is used to resolve irregular and moving boundaries. This consists of general quadrilateral cells which allows grid points to move with the fluid (Lagrangian), be held fixed (Eulerian) or be moved in any prescribed manner. An acoustically implicit solution for pressure is employed to relax the Courant condition on the time step (i.e., a semi-implicit method); this is especially suitable for low-speed flows which are indeed of interest in the present problem. The staggered grid system consists of cell-centered scalar quantities and node-centered flow velocities. The stress terms in the governing equations are obtained through explicit time differencing and centered spatial differencing. For all but the pure Lagrangian solution, the spatial advective derivatives are written such that a purely centered to full donor cell differencing may be employed. This allows the use of numerical stabilization without the addition of an explicit artificial viscosity.

Within the framework of this model, phenomena including ignition, flame stabilization, flame development as a fuction of gravitational acceleration, radiation, and environmental conditions can be analyzed. Specific attention will be given to the modeling of finite-rate oxidation, soot formation and combustion processes utilizing global reactions. The results of this analysis will provide fundamental information on conditions relevant to flame development and flame extinction phenomena for which no comprehensive theoretical analysis of the type described here currently exists.

V. Data Necessary to Validate/Improve Model(s)

The reduced gravity data that is required to validate and improve the existing theoretical models consists of temperature distribution, species concentrations, velocity distribution, flame development from ignition, flame spread, luminosity, color, soot formation, and radiation.

In Sec. II the current understanding of diffusion flames was shown to be incomplete. The strong convective effects induced by buoyancy under normal-g conditions complicate achieving the basic understanding needed to predict the behavior of diffusion flames under arbitrary g-levels.

The NASA-Lewis drop-tower observations show that significant changes in flame structure occur during the drop. In many cases, the transient associated with the transition from a normal-g flame to the near-zero-g condition persists throughout the available test time of 2.2 secs. In some cases, the flame quenches during the drop. This may be due to the sudden loss of the buoyancy-driven convective flow followed by the accumulation of hot products of combustion which results in enhanced soot formation, radiation cooling and the onset of a chemical kinetic limitation on the heat release process. Such an occurence could lead to quenching or possibly a slow readjustment to an "apparent" steady-state zero-g flame as construed from the drop-tower observations. Longer test times than 2.2 sec. would eliminate the uncertainty as to whether, in fact, a steady state is achievable under microgravity conditions. Igniting the gas jet once it is in a microgravity environment would not only address the limitation of the available drop-tower data but would also provide a new fundamental information on ignition under microgravity conditions.

The results of measurements of temperature, species concentrations and flame behavior, shape and luminosity when compared with the numerical models will enable us to obtain the velocity field, kinetics information, radiation and soot formation. As we will discuss later, new data on ignition is more than desirable; preliminary studies on flame ignition after the release of the test cell in the 2.2-sec. drop tower must be conducted before studying laminar diffusion flames for longer test times. These experiments will also provide information on post-ignition flame behavior that will be used to finalize the test matrix and measurement program for the low-gravity experiments, as discussed in the next section. Quantitative data (e.g., temperature and species) will be obtained as part of these experiments. If test time limitations still remain a problem in meeting the critical science requirements, a plan for a space experiment will be developed to obtain these

data.

In general, the data obtained from the experiments will be used in the development and validation of the theoretical analyses. Table 3 and Fig. 14 show the relationship between the various data obtained from the experiments and the theoretical modeling.

VI. Identification of Experiments

A total program of experiments for laminar gas jet diffusion flames is given in Tables 4 and 5. The experimental techniques that may be applied are cinematography, sampling, temperature and pressure measurements, accelerometry (if accelerometers are available), and radiometry. The parameters that can be varied during the entire program are: chamber pressure, type of fuel, nozzle diameter, fuel-flow rate, and chamber oxidizer (i.e., O_2/N_2 ratio). The fundamental effects that can be studied are: transient behavior, igniton, chemistry, soot yield, radiation, fuel reactivity, and diffusivities.

A matrix of tests has been selected based on the requirements summarized in Table 4. This matrix consists of 48 flames which include three flow rates, two nozzle radii, two fuels, two chamber oxidizers, and two chamber pressures. Three flow rates are selected because the flow rate is an important parameter governing the structure of the gas jet diffusion flames. Two nozzle diameters are selected to provide independent variation in Reynolds number for a given flow rate where the Reynolds number is shown to be important with respect to the degree of the transient behavior observed in the flame. The combination of two pressure levels and two environmental compositions is sufficient to define the effect of oxygen partial pressure on flame chemistry. Methane is selected to be the primary fuel because of the available background data and theory. Velocities will be determined from the theoretical analyses while radiation measurements will provide an indirect measure of soot formation.

Upon completion of preliminary testing including ignitor development in the 2.2-sec. drop tower, the complete matrix outlined above will be carried out utilizing both the 5-sec. drop tower and the specially outfitted KC-135.

Table 3. Relationship Between Data and Modeling.

COUPLED EFFECTS: INERTIA, CONVECTION, DIFFUSION, VISCOSITY, CONDUCTIVITY, RADIATION, CHEMISTRY, GRAVITY

FUNDAMENTAL UNCERTAINTIES	KEY MECHANISMS	DATA*	MODELING*
EXTINCTION	KINETICS, RADIATION	SPECIES, TEMPERATURE, VISUAL, RADIATION	TRANSIENT, 2-D NAVIER-STOKES INCLUDING CHEMICAL KINETICS AND RADIATION
IGNITION	KINETICS, CONDUCTION	VISUAL	
FLAME DEVELOPMENT	KINETICS, DIFFUSION, CONVECTION	TEMPERATURE, SPECIES VISUAL, RADIATION	
OSCILLATORY BEHAVIOR	TRANSIENT, INERTIA	VISUAL	
SOOT FORMATION AND DISPOSITION**	KINETICS	TEMPERATURE, SPECIES, SOOT, VISUAL, RADIATION	

*CONNECTION BETWEEN DATA AND MODELING: PREDICT TEMPERATURE, SPECIES, VELOCITY, FLAME-SHAPE DEVELOPMENT, ETC. AND COMPARE WITH MEASURED RESULTS (EXCLUDING VELOCITY) TO VALIDATE AND IMPROVE MODELING.

USE SIMPLISTIC MODELING, ADD RESULTS TO THE DATA BASE.

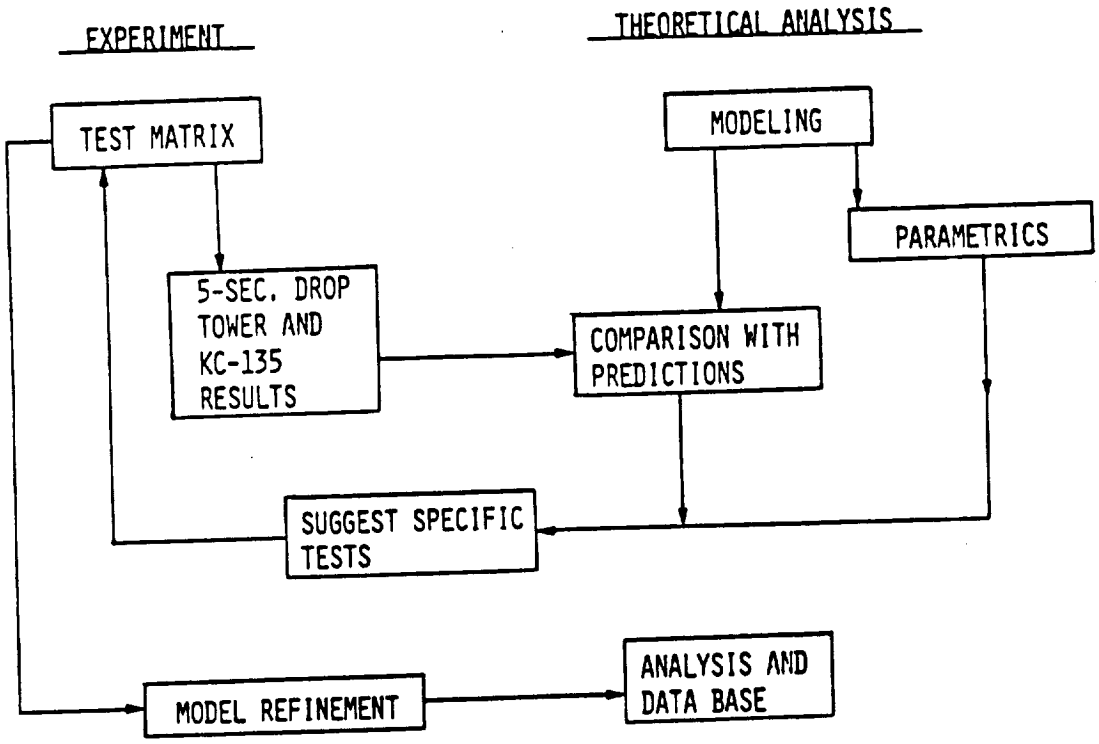

Fig. 14. Relationship between data and modeling.

Table 4. Operating Conditions, Ranges of Variables and Applications to Model Development for Defining the Total Program of Experiments.

OPERATING CONDITIONS	RANGES OR TYPES	APPLICATIONS TO MODEL DEVELOPMENT	DISCUSSION	NUMBER OF EXPERIMENTS FOR TOTAL PROGRAM
Fuel Flow Rate	$\dot{Q}_{CH_4}$ = 1.0, 2.0 and 3.0 cc/sec $\dot{Q}_{C_3H_8}$ = 0.5, 1.0 and 1.5 cc/sec	Effect of injection velocity on flame characteristics (for a given nozzle radius) to help sort out the effects of diffusion processes.	Effect of Reynolds number on steady state, transient and quenching phenomena can be studied.	3
Nozzle Radius	R_o = 0.051 and 0.0825 cm	Effect of nozzle size on flame characteristics (for a given fuel-flow rate) to help sort out the effects of diffusion processes.		2
Fuel	Methane; Propane	Effect of fuel reactivity, stoichiometry and diffusivity on flame structure and behavior, kinetics, and soot formation.	CH_4 is selected because of the base of data that already exists. C_3H_8 is selected to examine a heavier-than-air fuel, and because it is representative of a wide range of higher-molecular weight hydrocarbons.	2
Chamber Pressure	P_o = ½ atm and 1 atm	Effects of pressure on soot formation, quenching, radiation, kinetics, and ignition.	Reduced pressure is used to enhance kinetic effects. It indirectly clarifies the effects of lower O_2/N_2 ratio (compared to air) via partial pressure.	2
Chamber Oxidizer	(O_2/N_2)=0.21/0.79 and an oxygen-deficient O_2/N_2 mixture (compared to air)	Effects on the kinetics, soot formation and ignition behavior.	To study ambient compositional effects on flame structure. Air $(O_2/N_2$=0.21/0.79) is selected as a baseline. Reduced levels of O_2 are selected to enhance kinetics.	2
				Σ = 48

Table 5. Measurement Techniques, their Rationale and Applications to Model Development.

MEASUREMENTS	RATIONALE/APPLICATIONS TO MODEL DEVELOPMENT
Cinematography (using High-speed movie cameras)	Obtaining time-resolved visualization data on ignition, flame development, color, luminosity, and quenching. Flame shapes can be compared directly with model predictions.
Thermocouples (using rakes)	Obtaining temperature distributions in the flow field above the flame. These temperature distributions can be compared directly with the model predictions of thermal field.
Sampling probes (using sampling bottles)	Obtaining species distributions above the flame which can be compared with the model predictions of species field.
Pressure Transducer	Measurement of the increase in chamber pressure due to the burning process yields estimates of the overall heat release rate.
Velocity Measurement	Measurements for the scale of this experiment require a laser-based diagnostics, which is not feasible at this time. This requires a compromise in which predictions and other measurements will be used to provide the velocity.
Radiometery	Isolation of thermal radiation, and as a result, determination of the effect of radiation on reduction in temperature within the flame. Potential exists for determination of soot concentration and generation. Evidence shows that radiation from soot is not dominated by CO_2 and H_2O. Therefore, calculations for CO_2 and H_2O combined with measured radiation yield the contribution from soot, and hence, soot concentration.
Accelerometer (if available)	Measurements of the gravitational acceleration enables us to interpret the data that could be affected by gravitational levels greater than 10^{-3}g.

The present program focuses on laminar flames. Turbulent diffusion flames will be deferred for the future.

VII. Apparatus and Conditions

Experimental conditions, components of apparatus, ranges, requirements, and specifications are presented in Table 6. A generic chamber design is shown in Fig. 15.

Ground-based testing of the experimental chamber, camera, ignition system, thermocouples, pressure transducers, fuel tank, linings, valves, radiometer, sampling probes, and sampling bottles should be conducted in order to ensure that:

a) The equipment operates reliably;
b) Reproducible results can be obtained;
c) Calibration of the flow system is accurate
d) The ignitor functions properly, that flames can indeed be ignited and ignition duration is defined (using the drop-tower facility);
e) Tubes, valves, fuel tank, camera, thermocouples, sampling probes, sampling bottles, radiometer, and the experimental chamber can withstand the impact in the zero-gravity facility and KC-135 flight conditions;
f) There is no leakage from the experimental chamber, tubes, valves, and fuel;
g) Stress analysis on the chamber, tubes, and fuel tank have been done, especially for the chamber to withstand the highest temperatures and pressures reached.

VIII. Data Analysis

The films will be developed and analyzed using a motion picture analyzer to observe and measure the flame development and other processes. The thermocouples' output is analyzed along with the records of the chamber pressure. Acceleration records (if available) during the experiment will be analyzed, and observations related to microgravity pertrubations will be explained in the analysis and interpretation of data and flame behavior. The gas environment in the chamber

Table 6, Apparatus and Conditions.

COMPONENT	REQUIREMENTS	SPECIFICATIONS AND DISCUSSION
Fuel	$\dot{Q}$ = 1 - 3 cm^3/sec for methane; $\dot{Q}$ = 0.5 - 1.5 cm^3/sec for propane; pure, high quality fules.	The amount of fuel required for a single test is based on the fuel flow rate and an estimated time of the experiment for each flame.
Experimental Chamber	Closed, sealed, either cylindrical or rectangular. Minimum height/diameter = 1.5. Must withstand pressures of up to 3 atm, gas temperatures of up to 400K and metal temperatures up to 310K.	The chamber must be able to withstand the specified conditions for the required period of time. Provisions for thermocouples, ignitors, transducers and viewing ports must be made in the chamber. Fig. 15 shows a generic chamber design.
Chamber Environment	Two compositions [21% O_2 - 79% N_2 (air) and oxygen-deficient O_2/N_2 mixtures (compared to air)] and two pressures [1 atm (14.7 psia) and 0.5 atm] for different flames. Before each test, the gas temperature should be 295 ± 5K. Pressure tolerance (± 0.1 psia); O_2 tolerance (±0.1 mole % at the beginning of the test set). Specifics will be determined from the final design of the experiment including the input from 5-sec drop-tower studies.	Flames are going to be selected in such a way that the maximum amount of oxygen burned at the end of the flight does not exceed 10% of the original number of moles of oxygen. Chamber pressure should be recorded before, during and after the experiment. Chamber temperature must be monitored over the entire experiment.
Nozzles	Radius = 0.051 and 0.0825 cm; distance from the tip to the chamber ceiling ≥30 cm; distance between nozzles = 5 - 10 cm (if more than one nozzle per chamber), equally distant from the centerline of the chamber and in line with the camera(s) with the smaller-size nozzle closer to the camera; minimum distance from wall for nozzle positioning = 10 cm.	This nozzle arrangement ensures that temperatures <350K and negligible gas velocities exist at the top of the chamber, which prevents both extensive heating of the chamber ceiling and significant recirculation which would otherwise be a source of flame disturbance. Since the maximum flame radii is ~0.5 - 1.0 cm, proximity of the nozzles will not cause flame disturbance. Nozzles must be secured inside the chamber to avoid misalignment or loosening due to vibrations in KC-135 or impact in drop tower.
Ignition	Each nozzle (if more than one nozzle is used in the chamber) needs one ignitor. Spark ignition is preferred. The details of the ignition system will be worked out after the test results of the 2.2-sec drop tower become available.	Ignition is the most crucial factor in the experiment. Tests should be conducted in the 2.2-sec drop tower for all of the flames to be studied to ensure that reliable and reproducible ignition occurs for each flame. The procedure is to drop the test cell, and then simultaneously open the fuel valve and ignite the flow under the near-zero-g condition.
Fuel Tank	Internal pressure: TBD for drop tower and KC-135.	The tank must contain enough fuel in order to avoid large pressure drops at the end of a series of tests per flight in the KC-135.

Table 6 (Cont.).

COMPONENT	REQUIREMENTS	SPECIFICATIONS AND DISCUSSION
Viewing	The field of view must be 5-cm horizontal by 8-cm vertical at the plane passing through the flame centerline and perpendicular to the axis of the camera. Besides viewing port for camera, a viewing section must be provided for the radiometer and the experimenter.	Two viewing ports might be required.
Fuel-Tubing System	The tubes can be made from stainless steel. The accuracy of flow control should be within $\pm$ 0.01 cm^3/sec. Flow valves, explosion-proof solenoid valves, and regulators should be provided and tested. Pre-calibrated precision valves might be required to maintain specific flow rates.	Flow recording during the tests will be helpful in ensuring that the required flow rates are maintained.
Chamber Cooling	Times of up to 5-10 minutes are required for the chamber environment to cool down to the ambient temperature after each flame measurement. The maximum gas-temperature rise inside the chamber will be less than 80°C (assuming no heat transfer to the container) during each test. This maximum gas-temperature rise will raise the temperature of the container by <2°C if all of the heat release is transferred to the metal.	Cooling can be facilitated by providing an internal fan for forced convection inside the chamber.
Acceleration	The acceleration should be recorded at intervals during the KC-135 flights if the capability exists. The acceptable g-levels are in the range 10^{-3}g - 10^{-6}g. The results of the g-jitter analysis show that frequencies >1 Hz are acceptable.	The acceleration should not be greater than 10^{-3}g, because (a) the velocity of the burned gas starts to increase downstream after reaching a minimum (see Fig. 10) for gravitational accelerations greater than 10^{-3}g, and (b) the gas temperature decays more slowly for gravitational accelerations greater than 10^{-3}g (see Fig. 16). Burning will be affected by g-level (Figs. 10 and 16) but measurements will not be adversely affected by various g-levels.
Camera	Since the flame development at the early stages of ignition is quite rapid, the movie camera should be capable of operating at a framing rate of approximately 400 frames per second. Color, 16mm film will be adequate for the experiment. A timing system should be provided to record accurate time intervals (of the order of 0.1 sec) on the film.	Filming begins prior to the opening of the fuel valve and the ignition process which are synchronized.

Table 6 (Cont.).

COMPONENT	REQUIREMENTS	SPECIFICATIONS AND DISCUSSION
Sampling	Quenching quartz microprobes may be used for sampling. They are inserted at 5-10 cm above the burner port, and at a specified time during the test will remove gas samples from the flow field by suction into a vacuum teflon-lined sampling tank of ~30-cm^3 volume and final pressure of ~ 5-7 psia.	Perturbations due to sample removal do not cause major flame disturbances as long as suction is controlled over a short period of time and is not sudden.
Scaling	A scale should be located inside the chamber and be recorded on the film for flame height measurements.	———
Thermocouples	A rake of thermocouples will be used to measure temperature distributions in the flow field. The thermocouples can be type "S" Pt/Pt-10%Rh (1650 °C upper limit, 1760 °C melting point), with wire diameter=0.13 mm and bead size=0.4 mm. The output voltages (16 ± 0.1 mV) should provide temperature measurements with ± 10K. A sampling rate of 10-100 sec^{-1} (depending on the capabilities of the data collection system) will be adequate. The beads can be exposed.	Gas-temperature measurements will be conducted at fixed locations above the flame at 5-15 cm above the nozzle(s). Since corrections for heat conduction, radiation, etc. are available for large probes, accuracy will not pose a major problem. The rake with 6-9 thermocouples will provide temperature distributions
Recording	The data collection will be comprised of film (color, 16 mm) history of the combustion process (see the discussion on camera), thermocouple(s) output at a rate of once every 10-100 msec, chamber pressure (once every 10 msec), and acceleration (if the capability exists).	Other specifics are described in the individual sections in this table.
Radiometer	A radiometer will be designed to record flame radiation.	Specifics will be determined from final design of the experiment, complexity of the experimental package and test requirements.

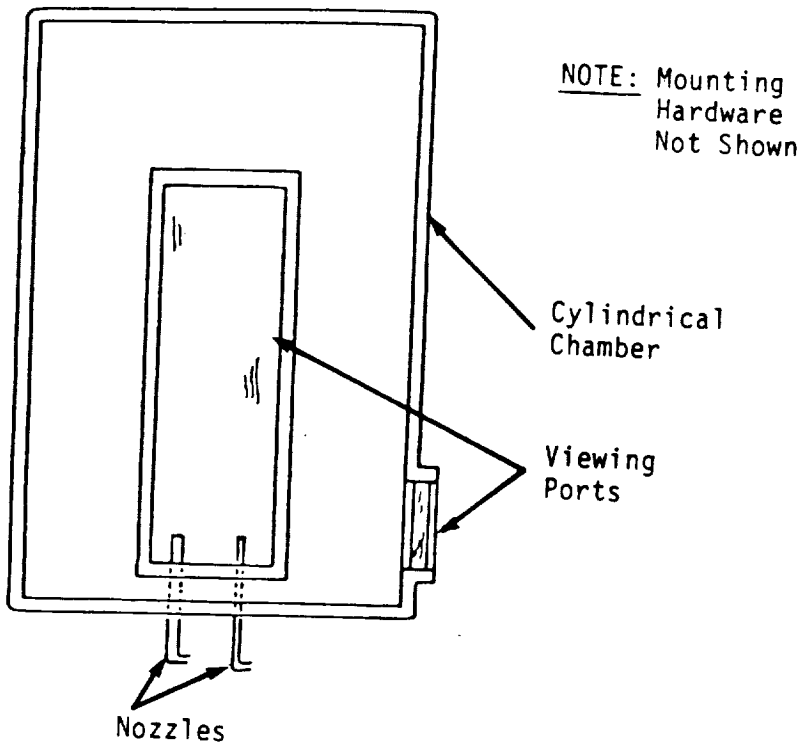

Fig. 15. Generic experimental chamber design for gas jet diffusion-flame experiment. The chamber can be either cylindrical or rectangular.

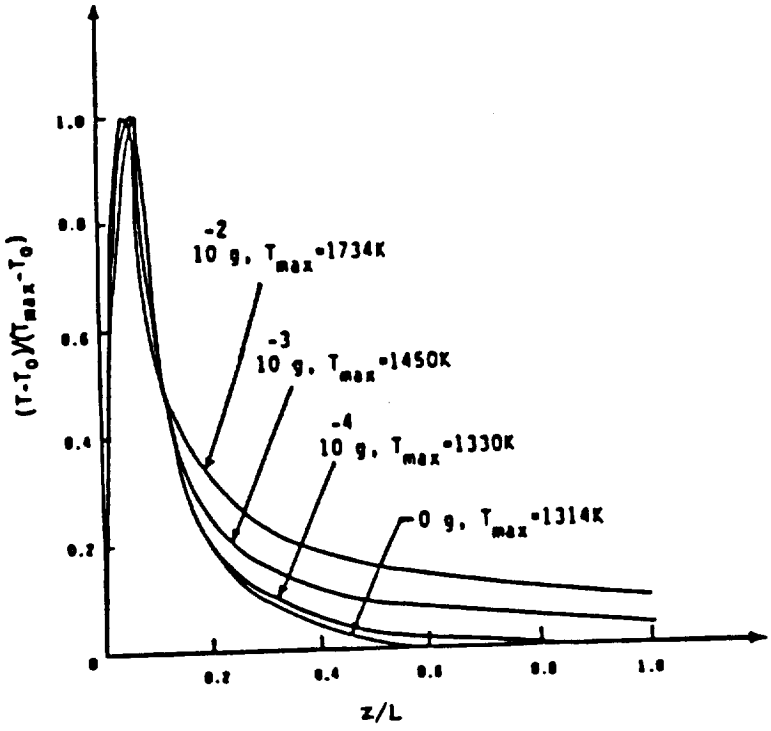

Fig. 16. Results of numerical calculations for normalized temperatures along the jet centerline vs. normalized vertical distance for different g-levels. Here, T_{max} is the maximum temperature reached at the centerline and T_o = 300 K is the initial gas temperature. Other symbols and conditions are defined in Fig. 10.

will be analyzed to obtain information in relation to H_2O, O_2, CO, CO_2, H_2, formaldehyde, and hydrocarbon concentrations.

Theoretical predictions will be used to support the analysis and interpretation of the data base developed from these experiments. The results of temperature and species measurements combined with the global characteristics of the flame (e.g., shape and luminosity) provide both quantitative and qualitative information for improving the theoretical models. The information on thermal and chemical fields will help to gain insight into the chemistry and fluid dynamics of the process. When experimental data is used in conjunction with the predictions, model validation is facilitated in relation to ignition, flame propagation, kinetics, and radiation effects. Also flame-scaling criteria will be put on a firmer fundamental basis.

IX. References

Altenkirch, R.A., Eichhorn, R., Hsu, N.N., Brancic, A.B., and Cerallos, N.E. (1976) Characteristics of laminar gas jet diffusion flames under the influence of elevated gravity. Sixteenth Symposium (International) on Combustion, pp. 1165-1174. The Combustion Institute, Pittsburgh, PA.

Astavin, V.S. and Ryazantsev, Yu. S. (1979) Temperature and concentration distribution in the reaction region of parallel flows of unmixed reactants. Fluid Dynamics 14, 274-279; Translated from Izvestiya Akademii Nauk SSSR - Mekhanika Zhidkosti i Gaza 14, 139-146.

Bahadori, M.Y., Li, C-P., and Penner, S.S. (1986) Two adjacent, coupled laminar diffusion flames with cylindrical symmetry. Progress in Astronautics and Aeronautics, Vol. 105 - Dynamics of Reactive Systems, Part I: Flames and Configurations (J.R. Bowen, J.-C. Leyer and R.I. Soloukhin, Eds.). pp. 192-207. American Institute of Aeronautics and Astronautics, New York.

Beckstead, M.W. (1981) A model for solid propellant combustion. Eighteenth Symposium (International) on Combustion, pp. 175-185. The Combustion Institute, Pittsburgh, PA; see also Derr, R.L., Beckstead, M.W., and Cohen, N.S. (1969) Combustion tailoring criteria for solid propellants. AFRPL-TR-69-190 (835-F), Redlands, CA.

Bonne, U. (1971) Radiative extinguishment of diffusion flames at zero gravity. Combust. Flame 16, 147-159.

Burke, S.P. and Schumann, T.E.W. (1928) Diffusion flames. Ind. Eng. Chem. 20, 998-1004.

Cochran, T.H. (1972) Experimental investigation of laminar gas jet diffusion flames in zero gravity. NASA TN D-6523, 26 pp.

Cochran, T.H. and Masica, W.J. (1970) Effects of gravity on laminar gas jet diffusion flames. NASA TN D-5872.

Edelman, R.B. and Bahadori, M.Y. (1986) Effects of buoyancy on gas jet diffusion flames: Experiment and theory. Acta Astronautia (in press).

Edelman, R.B., Fortune, O., and Weilerstein, G. (1973) Analytical study of gravity effects on laminar diffusion flames. NASA CR-120921, 136 pp.

Edelman R.B., Fortune, O.F., Weilerstein, G., Cochran, T.H., and Haggard, JR., J.B. (1973) An analytical and experimental investigation of gravity effects upon laminar gas jet diffusion flames. Fourteenth Symposium (International) on Combustion, pp. 399-412. The Combustion Institute, Pittsburgh, PA.

Flower, W.L. and Bowman, C.T. (1983) Measurements of the structure of sooting laminar diffusion flames at variable pressure. Report SAND83-8776, Sandia National Laboratories, Livermore, CA 94550; paper Western States Section of the Combustion Institute, WSS/CI 83-56.

Haggard, J.B. (1981) Forced and natural convection in laminar jet diffusion flames. NASA Technical Paper No. 1841. 21 pp.

Haggard, J.B. and Cochran, T.H. (1973) Hydrogen and hydrocarbon diffusion flames in a weightless environment. NASA TN D-7165, 28 pp.

Kimura, I. and Ukawa, H. (1961) A study of the combustion of laminar fuel jets. Japan Society of Mechanical Engineers 27, 736-746; translated as NASA Technical Translation, NASA TT F-13, 459, February 1971.

Klajn, M. and Oppenheim, A.K. (1982) Influence of exothermicity on the shape of a diffusion flame. Nineteenth Symposium (International) on Combustion, pp. 223-235. The Combustion Institute, Pittsburgh, PA.

Mitchell, R.E., Sarofim, A.F., and Clomburg, L.A. (1980) Experimental and numerical investigation of confined laminar diffusion flames. Combust. Flame 37, 227-244.

Penner, S.S., Bahadori, M.Y., and Kennedy, E.M. (1984) Laminar diffusion flames with cylindrical symmetry, arbitrary values of diffusion coefficients and inlet velocities, and chemical reactions in the approach streams. Progress in Astronautics and Aeronautics, Vol. 95 - Dynamics of Flames and Reactive Systems (J.R. Bowen, N. Manson, A.K. Oppenheim, and R.I. Soloukhin, Eds.). pp. 261-292. American Institute of Aeronautics and Astronautics, New York.

Section 3

"Effects of Buoyancy on Gas-Jet Diffusion Flames"

- Conceptual Design Review-

R. B. Edelman and M. Y. Bahadori

June 1986

CONCEPTUAL DESIGN REVIEW

EFFECTS OF BUOYANCY ON GAS JET DIFFUSION FLAMES

Raymond B. Edelman (Principal Investigator)
M. Yousef Bahadori (Assistant Investigator)

SCIENCE APPLICATIONS INTERNATIONAL CORPORATION
Chatsworth, California

Sponsor:
NASA - Lewis Research Center
Cleveland, Ohio
Contract NAS3-22822

Sandra L. Olson (Project Monitor)

JUNE 1986

Science Applications International Corporation

BACKGROUND

WHY THE LAMINAR GAS JET DIFFUSION FLAME?

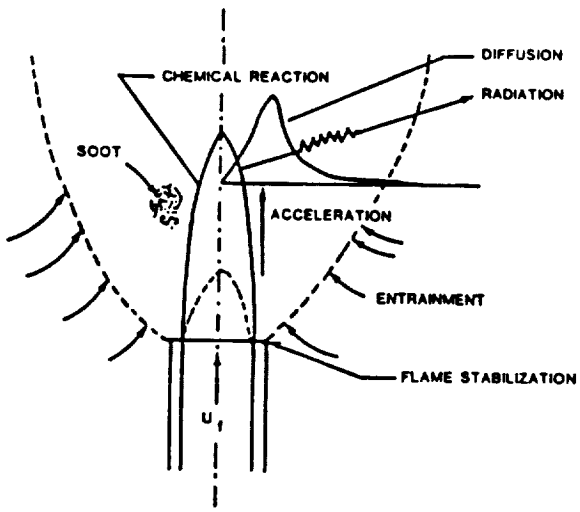

- EMBODIES MECHANISMS FOUND IN NATURAL FIRES AND CONTROLLED COMBUSTION PROCESSES
- SIMPLE AND BASIC
- EASY TO CONTROL
- LAMINAR FLAME NEEDS BETTER UNDERSTANDING AND IS A STEP TOWARD UNDERSTANDING THE MORE COMPLEX TURBULENT DIFFUSION FLAME

Science Applications International Corporation

APPROACH

- ISOLATE THE EFFECTS OF BUOYANCY BY ELIMINATING GRAVITY
- EXPERIMENTAL
- THEORETICAL

RESULTS APPLICABLE TO FIRES ON EARTH AND IN SPACE

OBSERVATIONS FROM DROP-TOWER EXPERIMENTS

- UNDER REDUCED-GRAVITY CONDITIONS FLAMES EXHIBIT DISTINCTIVE CHARACTERISTICS RELATIVE TO NORMAL-g CONDITIONS
  - BECOME GLOBULAR
  - MORE SOOTY
  - TEND TO QUENCH
- DROP-TOWER RESULTS HAVE SHOWN THAT
  - SOME FLAMES EXTINGUISH
  - SOME ARE IN TRANSITION BETWEEN EXTINGUISHMENT AND STEADY STATE (LACK OF ENOUGH TIME)
  - OTHERS REACH (AN APPARENT) STEADY STATE WITH FLAME-HEIGHT FLUCTUATIONS

SAIC

2.2-SEC. DROP-TOWER EXPERIMENTS

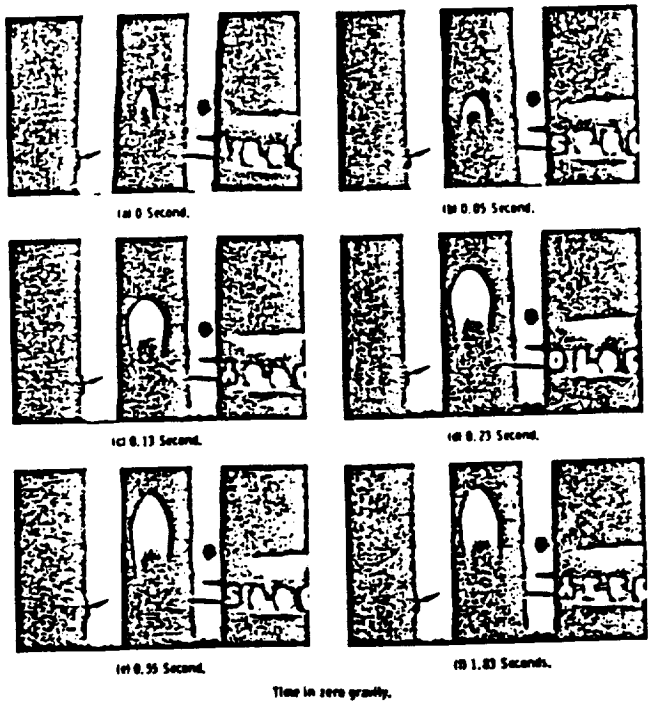

Burner radius = 0.051 cm,
Average normal-g length = 2.48 cm,
Maximum normal-g radius = 0.37 cm,
Methane flow rate = 2.1 cm^3/sec,
Axial velocity = 291.2 cm/sec,
Zero-g minimum length = 2.1 cm,
Steady-state zero-g length = 3.8 cm,
Steady-state zero-g maximum radius = 0.72 cm,
Reynolds no. = 79.5 .

Steady state zero-gravity jet diffusion flame (Cochran, 1972)

SAIC

2.2-SEC. DROP-TOWER EXPERIMENTS (CONT.)

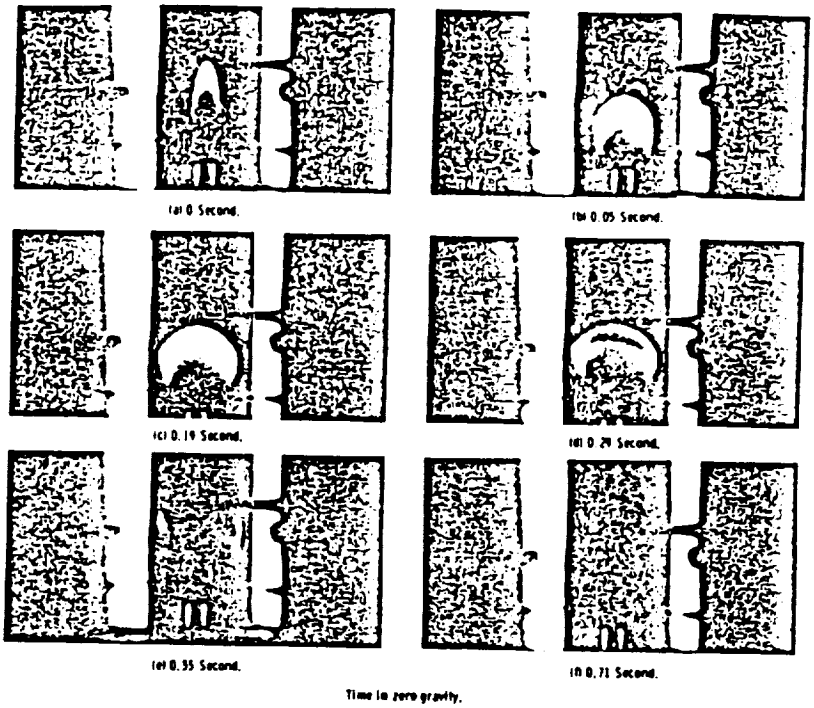

Nozzle radius = 0.186 cm,
Normal-g length = 2.78 cm,
Methane flow rate = 2.8 cm^3/sec,
Flow velocity = 25.44 cm/sec,
Zero-g minimum length = 1.86 cm,
Extinguishment length = 2.93 cm.
Reynolds no. = 28.4

Extinguished zero-gravity jet diffusion flame
(Cochran and Masica, 1970)

Science Applications International Corporation

2.2-SEC. DROP-TOWER EXPERIMENTS (CONT.)

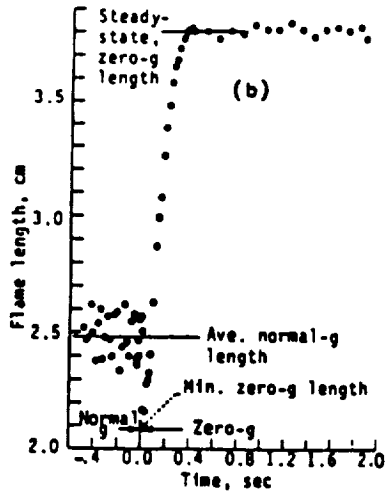

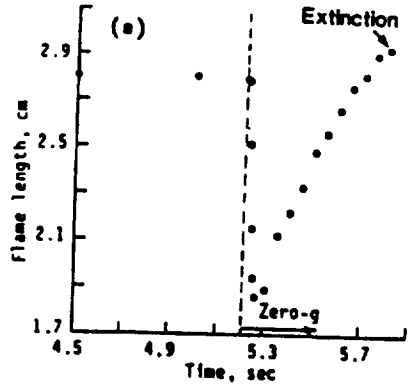

Cochran (1972)

Methane flow rate = 2.1 cm^3/sec
Nozzle radius = 0.051 cm
Nozzle velocity = 291.2 cm/sec
Reynolds no. = 79.5

Cochran and Masica (1970)

Methane flow rate = 2.8 cm^3/sec
Nozzle radius = 0.186 cm
Nozzle velocity = 25.44 cm/sec
Reynolds no. = 28.4

DROP-TOWER RESULTS

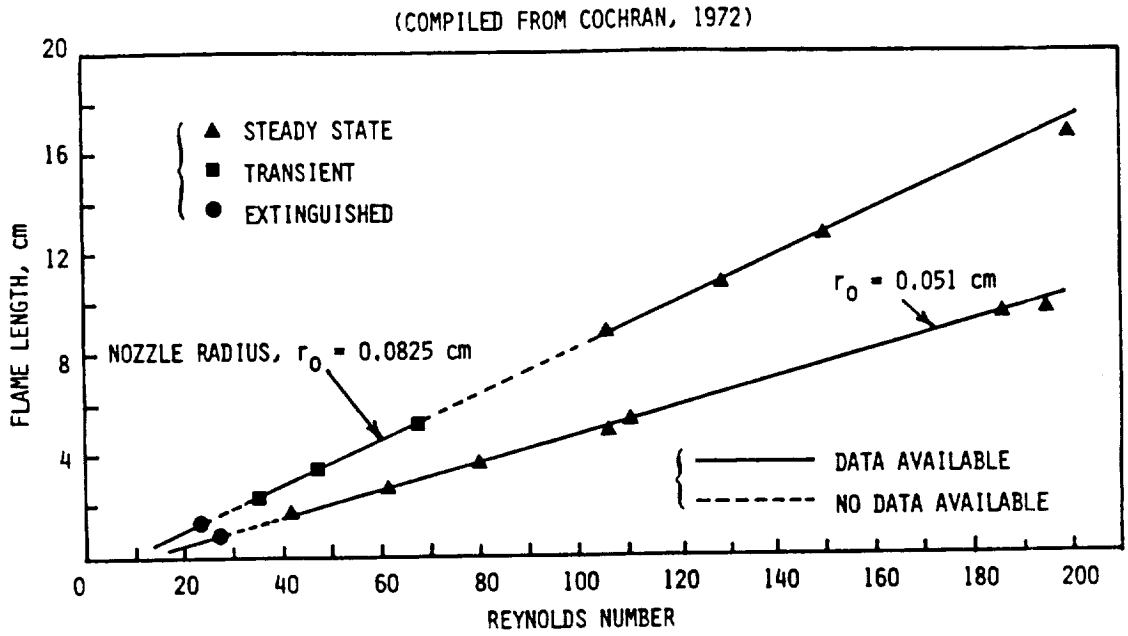

Science Applications International Corporation

THEORETICAL ANALYSES

- STEADY FLOW
- TRANSIENT
- g-JITTER ANALYSIS (DISCUSSED UNDER "RESEARCH REQUIREMENTS" SECTION)

STEADY FLOW ANALYSIS

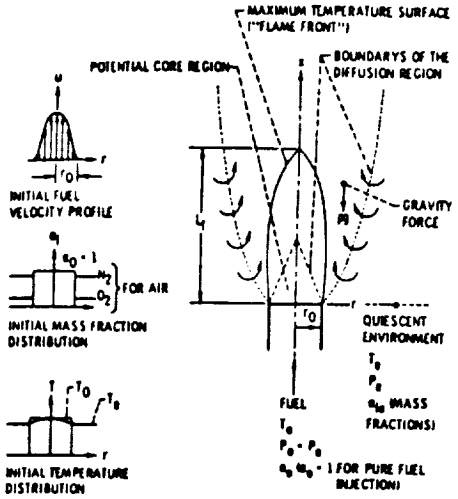

Schematic of vertical laminar jet.

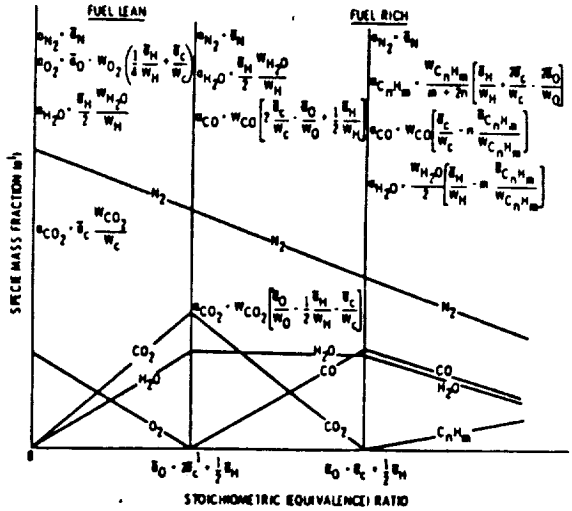

Schematic of "complete combustion" equilibrium chemistry model.

- STEADY, AXISYMMETRIC FLOW
- 2-D CONSERVATION EQUATIONS FOR MASS, SPECIES, MOMENTUM, AND ENERGY
- PARABOLIC FORM
- MULTICOMPONENT DIFFUSION
- INFINITELY FAST REACTIONS
- RADIATION

STEADY FLOW ANALYSIS (CONT.)

Continuity

$$\frac{\partial(\bar{\rho}\bar{u}\bar{r})}{\partial\bar{x}} + \frac{\partial(\bar{\rho}\bar{v}\bar{r})}{\partial\bar{r}} = 0$$

Momentum

$$\bar{\rho}\bar{u}\frac{\partial\bar{u}}{\partial\bar{x}} + \bar{\rho}\bar{v}\frac{\partial\bar{u}}{\partial\bar{r}} = \left(\frac{1}{Re}\right)\frac{1}{\bar{r}}\frac{\partial(\bar{\mu}\bar{r}\partial\bar{u}/\partial\bar{r})}{\partial\bar{r}} + \left(\frac{Gr}{Re^2}\right)\bar{\Delta\rho}$$

Diffusion of Elements

$$\bar{\rho}\bar{u}\frac{\partial\tilde{\alpha}^{\ell}}{\partial\bar{x}} + \bar{\rho}\bar{v}\frac{\partial\tilde{\alpha}^{\ell}}{\partial\bar{r}} = -\left(\frac{1}{Re}\right)\frac{1}{\bar{r}}\frac{\partial(\bar{r}\bar{j}^{\ell})}{\partial r}$$

Energy

$$\bar{\rho}\bar{u}\frac{\partial\bar{H}}{\partial\bar{x}} + \bar{\rho}\bar{v}\frac{\partial\bar{H}}{\partial\bar{r}} = \left(\frac{1}{Re}\right)\frac{1}{\bar{r}}\frac{\partial}{\partial\bar{r}}\left\{\frac{\bar{\mu}\bar{r}}{Pr}\frac{\partial\bar{h}}{\partial\bar{r}} - \bar{r}\sum_{k}(\bar{h}^{k}\bar{j}^{k})\right\} + \dot{q}_{r}$$

STEADY FLOW ANALYSIS (CONT.)

Equations of State

$$\rho = \frac{p}{RT \sum_i \alpha^i / w^i} \quad ; \quad i = \text{all gaseous species} \qquad h = \sum_k \alpha^k h^k$$

where

$$h = H - u^2/2$$

$$\bar{u} = u/u^* \qquad \bar{x} = x/r^*$$

$$\bar{r} = r/r^* \qquad \bar{\mu} = \mu/\mu^*$$

$$\bar{\rho} = \rho/\rho^* \qquad \Delta\rho = \frac{\bar{\rho}_e - \bar{\rho}}{\bar{\rho}_e - 1} = \frac{\rho_e - \rho}{\rho_e - \rho^*} = \Delta\overline{\rho}$$

$$\bar{H} = H/H^*$$

$$\bar{v} = v/u^*$$

$$Gr = \frac{\rho^{*2} r^{*3} g}{\mu^{*2}} \left(\frac{\rho_e - \rho^*}{\rho^*}\right)$$

$$Re = \frac{\rho^* u^* r^*}{\mu^*}$$

$$\bar{j}^k = -\frac{1}{Sc}\,\bar{\mu}\,\frac{\partial \alpha^k}{\partial \bar{r}} \qquad \tilde{\alpha}^\ell = \sum_k \nu^{k\ell}\,\frac{w^\ell}{w^k}\,\alpha^k \qquad \tilde{j}^\ell = \sum_k \nu^{k\ell}\,\frac{w^\ell}{w^k}\,j^k$$

$$\therefore \quad \bar{\rho}\bar{u}\,\frac{\partial \tilde{\alpha}^\ell}{\partial \bar{x}} + \bar{\rho}\bar{v}\,\frac{\partial \tilde{\alpha}^\ell}{\partial \bar{r}} = \frac{1}{ReSc}\,\frac{1}{\bar{r}}\,\frac{\partial}{\partial \bar{r}}\left(\bar{r}\bar{\mu}\,\frac{\partial \tilde{\alpha}^\ell}{\partial \bar{r}}\right)$$

and

$$\bar{\rho}\bar{u}\,\frac{\partial \bar{H}}{\partial \bar{x}} + \bar{\rho}\bar{v}\,\frac{\partial \bar{H}}{\partial \bar{r}} = \frac{1}{Re}\,\frac{1}{\bar{r}}\,\frac{\partial}{\partial \bar{r}}\left\{\bar{r}\bar{\mu}\left[\frac{1}{Pr}\,\frac{\partial \bar{h}}{\partial \bar{r}} + \frac{1}{Sc}\sum_k \bar{h}^k\,\frac{\partial \alpha^k}{\partial \bar{r}}\right]\right\} + \dot{q}_r$$

SAIC

STEADY FLOW ANALYSIS (CONT.)

Boundary Conditions

$0 \le r \le r_j$ @ $x = 0$:

- $H = H_o(r)$
- $u = u_o(r)$
- $\alpha_i = \alpha_{io}(r)$ = 1 for pure fuel
- $v = 0$

Note: Arbitrary initial profiles may be specified including parabolic for the velocity.

$r > r_j$:

- $H = H_e$
- $u = u_e$ [$u_e = 0$ for the quiescent environment
- $\alpha_i = \alpha_{ie}$

@ $x \ge 0$:

$r = \infty$:

- $u = 0$
- $H = H_e$
- $\alpha_i = \alpha_{ie}$

$r = 0$:

- $\frac{\partial u}{\partial r} = \frac{\partial H}{\partial r} = \frac{\partial \alpha_i}{\partial r} = 0$ (symmetry)
- $v = 0$

where

$$H = \frac{u^2}{2} + \sum_i \alpha_i h_i \qquad \frac{dp_e}{dx} = -\rho_e g$$

SAIC

STEADY FLOW ANALYSIS (CONT.)

Multicomponent Diffusion

$$\frac{1}{\rho}\sum_{j=1}^{N}\frac{1}{w_j \mathcal{D}_{kj}}\left(\alpha^k j^j - \alpha^j j^k\right) = \sum_{j=1}^{N}\frac{1}{w_j}\left(\alpha_j \frac{\partial \alpha^k}{\partial r} - \alpha^k \frac{\partial \alpha^j}{\partial r}\right)$$

$$\sum_{j=1}^{N} j^j = 0 \quad ; \qquad \tilde{j}^\ell = \sum_k \nu^{k\ell}\frac{w^\ell}{w^k} j^k \qquad \mathcal{D}_{kj} = \frac{2.663 \times 10^{-2}\, T^{1.5}}{P\,\Omega_{kj}^{(1,1)}}\,\Gamma_{kj}\ \left(\frac{m^2}{sec}\right)$$

Where [T] = $^\circ$K, and [P] = $\frac{N}{m^2}$

In addition,

$$\Gamma_{kj} = \frac{1}{\sigma_{kj}^2}\sqrt{\frac{W_k + W_j}{2W_kW_j}}$$

with the collision cross-section given by:

$$\sigma_{kj} = \frac{\sigma_k + \sigma_j}{2}$$

$$\Omega_{kj}^{(1,1)} = 1.5146 - 0.62499\,\tau_{kj} + 0.10023\,\tau_{kj}^2$$

$$\tau_{kj} = \ell n\,(T/\epsilon_{kj}) \qquad \epsilon_{kj} = \sqrt{\epsilon_k \epsilon_j} \quad (^\circ K)$$

Science Applications International Corporation

STEADY FLOW ANALYSIS (CONT.)

Thermal Conductivity

The mixture rules for the thermal conductivity are given by:

$$\lambda = \sum_{k=1}^{N\ gases}\left[\frac{a_k\lambda_k'}{a_k + \sum_{\substack{j=1\\ j\neq k}}^{N} a^j \eta_{kj}\zeta_{kj}} + \frac{a_k\lambda_k''}{a_k + \sum_{\substack{j=1\\ j\neq k}}^{N} a^j \eta_{kj}}\right]\ \frac{Joule}{(m\text{-}sec\text{-}^\circ K)}$$

$$\lambda_k' = 3.75\,\frac{\tilde{R}}{W_k}\mu_k \qquad \lambda_k'' = \lambda_k'\,\frac{[0.352\,c_p^k\,W^k - 0.88]}{\tilde{R}} \qquad \tilde{R} = 8.3143 \times 10^3\ \frac{(J)}{kgm\text{-}mole}\ ^\circ K$$

$$\zeta_{kj} = 1 + \frac{2.41\,(W_k - W_j)\,(W_k - 0.142\,W_j)}{(W_k + W_j)^2} \qquad \eta_{kj} = \frac{\left[1 + \sqrt{\frac{\lambda_k'}{\lambda_j'}}\,\beta_{kj}\right]^2}{\gamma_{kj}}$$

Note that

$$\mathcal{J}^k = \sum_k \nu^{k\ell}\frac{W^\ell}{W^k} J_k$$

STEADY FLOW ANALYSIS (CONT.)

Viscosity

$$\mu = \sum_{k=1}^{N\ \text{gases}} \frac{\alpha_k \mu_k}{\alpha_k + \sum_{\substack{j=1 \\ j \neq k}}^{N} \frac{\left[1+\beta_{kj}\sqrt{\frac{\mu_k}{\mu_j}}\right]^2}{\gamma_{kj}} \alpha_j}$$

where

$$\beta_{kj} = \left(\frac{W_j}{W_k}\right)^{\frac{1}{4}}$$

and

$$\gamma_{kj} = \frac{W_j}{W_k}\sqrt{8\left(1+\frac{W_k}{W_j}\right)}$$

with

$$\mu_k = \frac{2.6693 \times 10^{-6}\sqrt{TW^k}}{\sigma_k^2 \Omega_k(2,2)} \quad \left(\frac{kg}{m\text{-}sec}\right)$$

and,

$$\Omega_k^{(2,2)} = 1.6507 - 0.6688\,\tau_k + 0.10725\,\tau_k^2$$

ANALYTICAL PREDICTIONS VS. EXPERIMENTAL RESULTS*

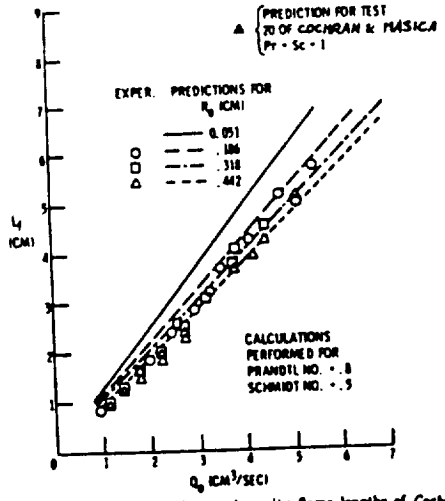

Comparison of experimental normal-gravity flame lengths of Cochran and Masica (1970) with theoretical prediction.

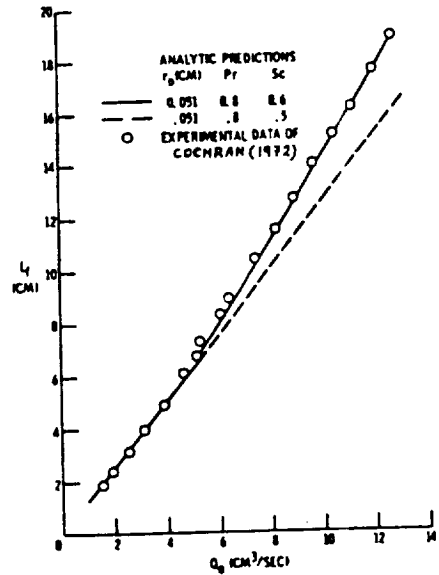

Influence of Schmidt Number upon analytical prediction of normal-gravity flame lengths.

★ Reproduced from Edelman et al. (1973).

ANALYTICAL PREDICTIONS VS. EXPERIMENTAL RESULTS (CONT.)

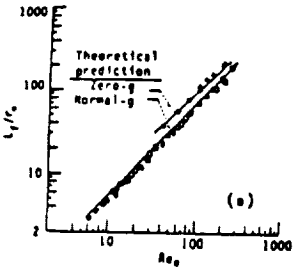

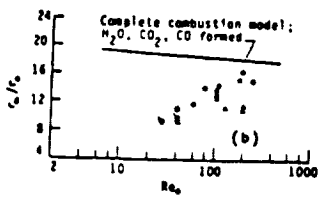

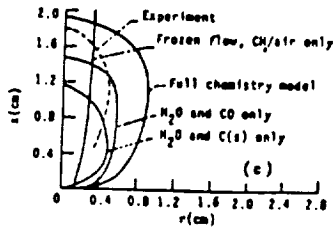

Experimental data*, †

Normal-g	r_o (cm)
○	0.051
△	0.0825
□	0.113
◇	0.186
◈	0.318
▽	0.442

Solid symbols denote zero-g

Partial oxidation theory		r_o (cm)
H_2O, CO	H_2O, C(s)	
○	◔	0.051
△		0.0825

Solid symbols denote experimental data*

Data*

Q = 1.08 cm³/sec

Re_o = 40.9

T_o = 294 K

P = 1 atm

r_o = 0.051 cm

(Reproduced from Edelman et al 1973)

* Cochran (1972)
† Cochran and Masica (1970)

ANALYTICAL PREDICTIONS VS. EXPERIMENTAL RESULTS (CONT.)

EFFECTS OF NEGATIVE-G (INVERTED FLAME)

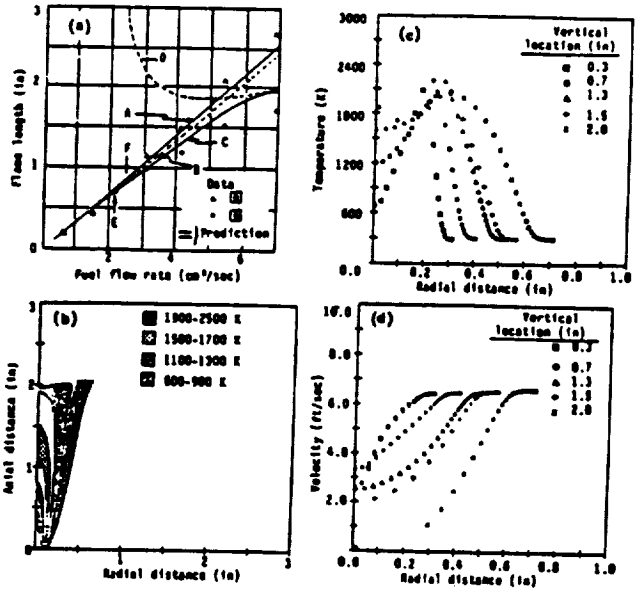

Methane injection velocity = 0.17 – 1.2 ft/sec in Fig. (a), where characteristics of normal-g (A), zero-g (B), negative-g (C), stagnation points (D), recirculation (E), and lift-off (F) are shown.

In all of the figures, air inlet velocity = 6.4 ft/sec, fuel-tube diameter = 0.19 in., and duct diameter = 6 in.

Fuel injection velocity = 1.2 ft/sec in (b), (c) and (d).

PHOTOGRAPH OF THE INVERTED FLAME

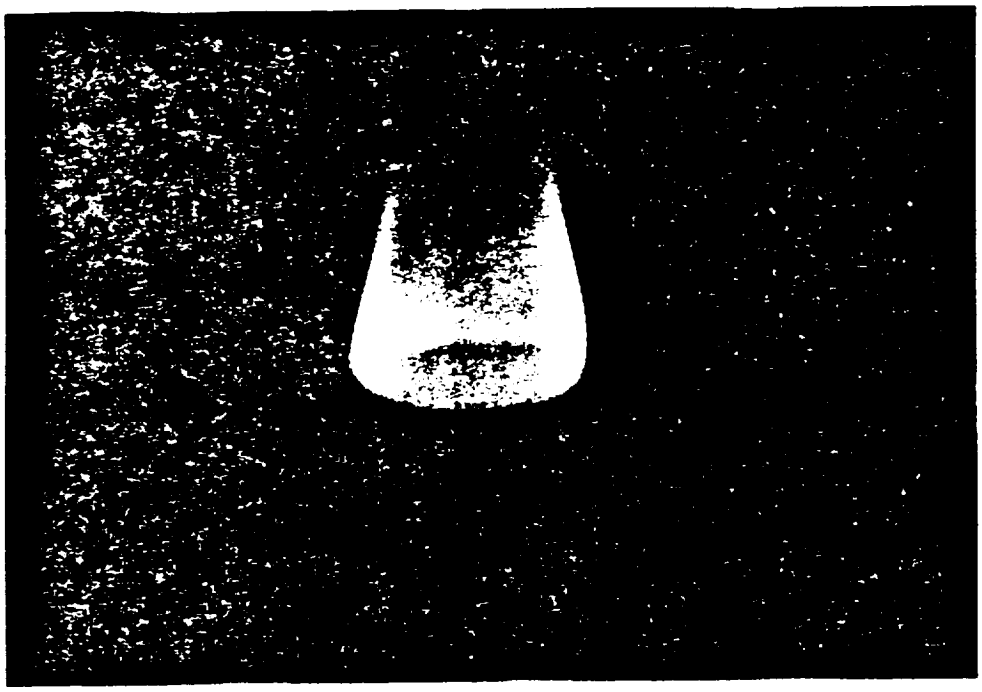

TRANSIENT ANALYSIS

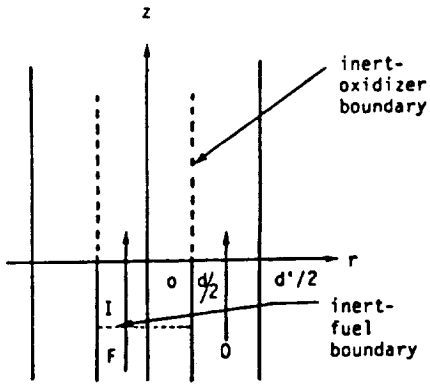

(a) $t<0$

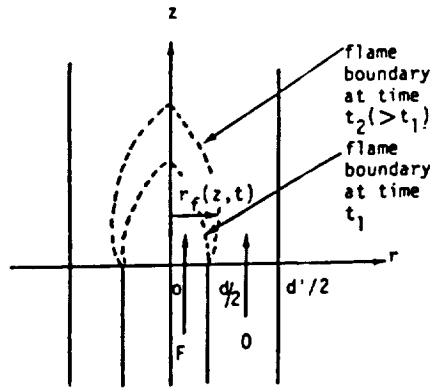

(b) $t>0$

- CONSTANT PRESSURE
- LEWIS NUMBER OF UNITY
- EQUAL AND CONSTANT FLOW VELOCITIES, TRANSPORT PARAMETERS, AND PHYSICAL PROPERTIES
- FLAME SHEET APPROXIMATION
- NO BUOYANCY EFFECTS
- BOTH AXIAL AND RADIAL DIFFUSION INCLUDED

TRANSIENT ANALYSIS (CONT.)

GOVERNING EQUATION:

$$\begin{cases} \dfrac{\partial Y_F}{\partial t} + u_F \dfrac{\partial Y_F}{\partial z} = D_F\left(\dfrac{1}{r}\dfrac{\partial Y_F}{\partial r} + \dfrac{\partial^2 Y_F}{\partial r^2} + \dfrac{\partial^2 Y_F}{\partial z^2}\right) \\ \qquad\qquad 0 < r < r_f\,,\ z>0,\ t>0\,, \\ \dfrac{\partial Y_O}{\partial t} + u_O \dfrac{\partial Y_O}{\partial z} = D_O\left(\dfrac{1}{r}\dfrac{\partial Y_O}{\partial r} + \dfrac{\partial^2 Y_O}{\partial r^2} + \dfrac{\partial^2 Y_O}{\partial z^2}\right) \\ \qquad\qquad r_f < r < d'/2\,,\ z>0,\ t>0\,, \end{cases}$$

$$\therefore\quad \frac{\partial Y}{\partial t} + u\frac{\partial Y}{\partial z} = D\left(\frac{1}{r}\frac{\partial Y}{\partial r} + \frac{\partial^2 Y}{\partial r^2} + \frac{\partial^2 Y}{\partial z^2}\right)$$
$$0 < r < d'/2\,,\ z>0,\ t>0\,,$$

WHERE $u_O = u_F = u = \text{CONST.}$, $D_O = D_F = D = \text{CONST.}$,

$$Y(r,z,t) = \begin{cases} Y_F & 0<r<r_f\,,\ z>0,\ t>0, \\ -\nu Y_O & r_f<r<d'/2\,,\ z>0,\ t>0, \end{cases}$$

$$\nu = \left(\text{GRAM OF F/GRAM OF O}\right)_{\text{STOICH.}}$$

Science Applications International Corporation

TRANSIENT ANALYSIS (CONT.)

INITIAL CONDITIONS:

$$Y(r,z,0) = \begin{cases} 0 & 0<r<d/2\,,\ z>0,\ t=0, \\ -\nu Y_{O,\infty} & d/2<r<d'/2\,,\ z>0,\ t=0, \end{cases}$$

$$Y(r,0,t) = \begin{cases} Y_{F,\infty} & 0<r<d/2\,,\ z=0,\ t>0, \\ -\nu Y_{O,\infty} & d/2<r<d'/2\,,\ z=0,\ t>0. \end{cases}$$

SYMMETRY CONDITION:

$$\partial Y(0,z,t)/\partial r = 0\,.$$

BOUNDARY CONDITION:

$$\partial Y(d'/2,\,z,\,t)/\partial r = 0\,.$$

FLAME LOCATION:

$$Y(r_f\,,\,z,\,t) = 0\,.$$

TRANSIENT ANALYSIS (CONT.)

TRANSIENT FLAME SHAPE:

$$\sum_{j=2}^{\infty} \frac{2(Y_{F,\infty}+\nu Y_{O,\infty})(\frac{d}{2})J_1(\lambda_j\frac{d}{2})J_o(\lambda_j r_f)}{\lambda_j(\frac{d'}{2})^2 J_o^2(\lambda_j\frac{d'}{2})}$$

$$\times \exp\left\{\frac{u(t+\frac{z}{u})}{2Dt}\left[1-\sqrt{1+\frac{4Dt\left[D\lambda_j^2 t+\ln\left(\frac{Y_{F,\infty}+\nu Y_{O,\infty}}{\nu Y_{O,\infty}}\right)\right]}{u^2(t+\frac{z}{u})^2}}\right]z\right\}$$

$$= -\left[(Y_{F,\infty}+\nu Y_{O,\infty})(\frac{d}{d'})^2-\nu Y_{O,\infty}\right]$$

$$\times \exp\left\{\frac{u(t+\frac{z}{u})}{2Dt}\left[1-\sqrt{1+\frac{4Dt\ln\left[1-\frac{Y_{F,\infty}(d/d')^2}{\nu Y_{O,\infty}[1-(d/d')^2]}\right]}{u^2(t+\frac{z}{u})^2}}\right]z\right\},$$

WHERE λ_j $(j>1)$ ARE THE ROOTS OF $J_1(\lambda_j d'/2)=0$.

STEADY-STATE FLAME SHAPE $(t\to\infty)$

$$\sum_{j=2}^{\infty} \frac{2(Y_{F,\infty}+\nu Y_{O,\infty})(\frac{d}{2})J_1(\lambda_j\frac{d}{2})J_o(\lambda_j r_f)}{\lambda_j(\frac{d'}{2})^2 J_o^2(\lambda_j\frac{d'}{2})}\cdot\exp\left[\frac{u}{2D}\left(1-\sqrt{1+\frac{4D^2\lambda_j^2}{u^2}}\right)z\right]$$

$$= -\left[(Y_{F,\infty}+\nu Y_{O,\infty})(\frac{d}{d'})^2-\nu Y_{O,\infty}\right].$$

SAIC

COMPARISON BETWEEN TRANSIENT ANALYSIS AND DROP-TOWER RESULTS

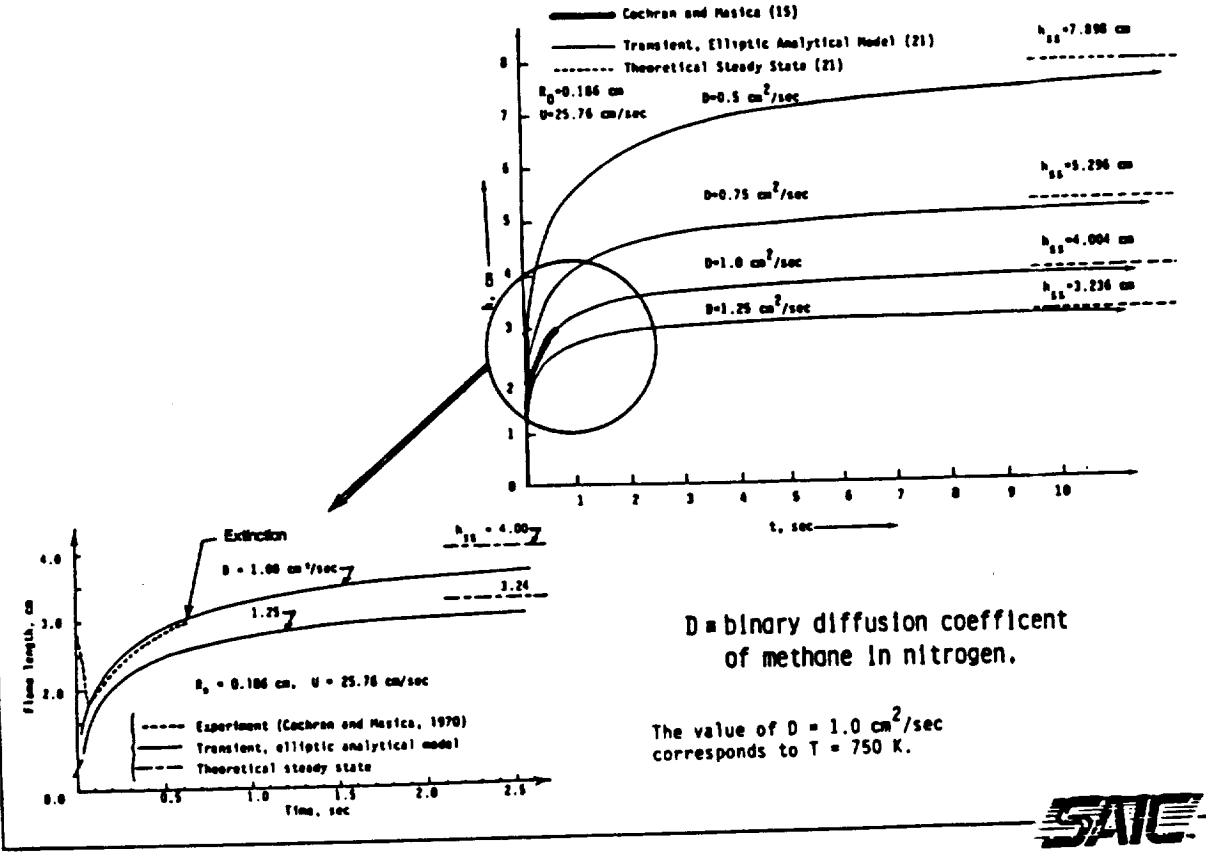

D = binary diffusion coefficent of methane in nitrogen.

The value of D = 1.0 cm^2/sec corresponds to T = 750 K.

SAIC

COMPARISON BETWEEN TRANSIENT ANALYSIS AND DROP-TOWER RESULTS

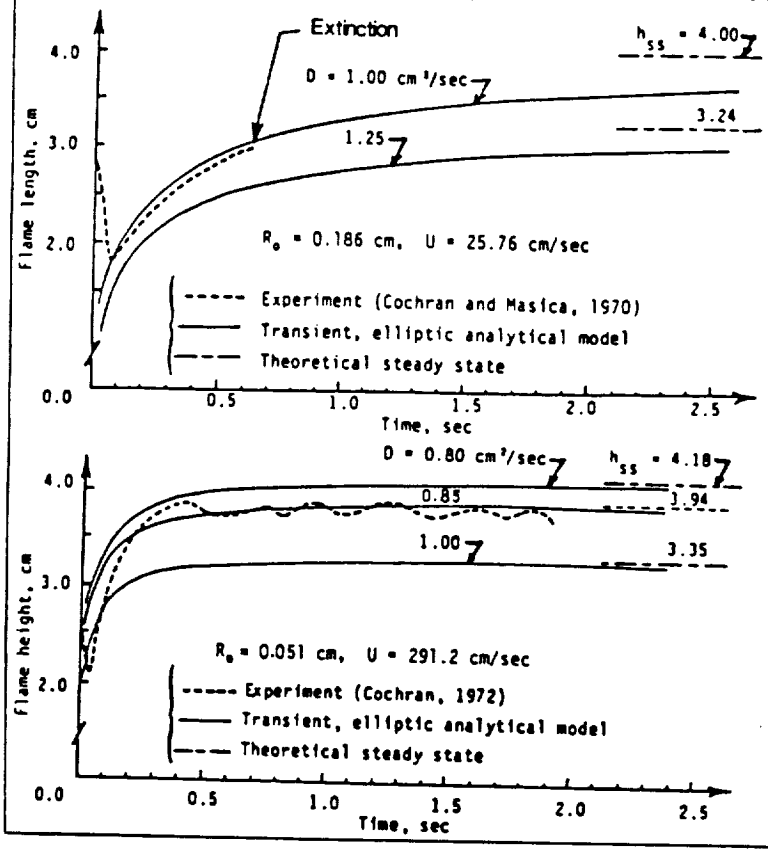

D = binary diffusion coefficent of methane in nitrogen.

The values of D=1.0 and 0.85 cm^2/sec correspond to T=750 and 650k, respectively.

EFFECT OF AXIAL DIFFUSION (TRANSIENT ANALYSIS)

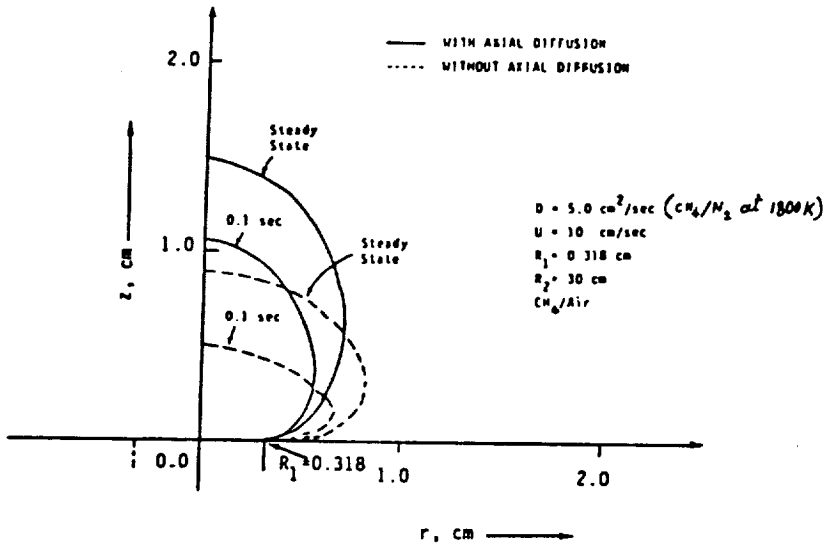

BACKGROUND SUMMARY

LAMINAR GAS JET DIFFUSION FLAMES :

- BUOYANCY SIGNIFICANTLY ALTERS FLAME STRUCTURE
- CHEMICAL KINETICS-RADIATION-TRANSIENT INTERACTIONS ARE IMPORTANT UNDER REDUCED-GRAVITY ENVIRONMENT
- ADDITIONAL MICROGRAVITY DATA IS REQUIRED TO OBTAIN SUFFICIENT QUANTITATIVE UNDERSTANDING OF LAMINAR GAS JET DIFFUSION FLAMES

Science Applications International Corporation

PROPOSED PROGRAM

PROGRAM OBJECTIVES

- OVERALL:

  GAIN A BETTER FUNDAMENTAL UNDERSTANDING OF LAMINAR GAS-JET DIFFUSION FLAMES IN GENERAL, AND EFFECT OF BUOYANCY IN PARTICULAR.

- SPECIFIC:

  OBTAIN NEW DATA FOR ELIMINATION OF INADEQUACIES IN THE EXISTING DATA AND THEORY. THIS WILL BE ACCOMPLISHED BY STUDYING:

  - UNSTEADY PHENOMENA OF IGNITION AND FLAME DEVELOPMENT
  - STEADY-STATE FLAME STRUCTURE
  - RADIATION AND KINETICS
  - QUENCHING PHENOMENA

Science Applications International Corporation

SUMMARY OF RESEARCH REQUIREMENTS*

*The research requirements are detailed in the Science Requirements Document

TOTAL PROGRAM AND MINIMUM MATRIX OF TESTS

OPERATING CONDITONS AND RANGES	NUMBER OF EXPERIMENTS FOR TOTAL PROGRAM	MINIMUM MATRIX OF TESTS
FUEL FLOW RATE : ≤ 15 CM^3/SEC	3	3
NOZZLE RADIUS = 0.05-0.45 CM	2	2
FUEL: METHANE, PROPANE	2	1 (METHANE)
CHAMBER PRESSURE = 1/2 AND 1 ATM	2	2
CHAMBER OXIDIZER: AIR (O_2/N_2 = 0.21/0.79), AND AN OXYGEN - DEFICIENT O_2/N_2 MIXTURE (O_2/N_2 = 0.10/0.90)	2	1 (AIR)
TOTAL NO. OF FLAMES:	48	12

Science Applications International Corporation

RATIONALE FOR TEST MATRIX SELECTION

- COMBINATION OF THE EFFECTS OF INJECTION VELOCITY AND NOZZLE SIZE ON FLAME CHARACTERISTICS HELP SORT OUT THE EFFECTS OF DIFFUSION PROCESSES.
- EFFECT OF REYNOLDS NUMBER ON STEADY-STATE, TRANSIENT AND QUENCHING PHENOMENA CAN BE STUDIED.
- EFFECT OF FUEL REACTIVITY, STOICHIOMETRY AND DIFFUSIVITY ON FLAME STRUCTURE AND BEHAVIOR CAN BE STUDIED USING DIFFERENT FUELS.
- CH_4 IS SELECTED BECAUSE OF THE BASE OF DATA THAT ALREADY EXISTS. C_3H_8 IS SELECTED TO EXAMINE A HEAVIER-THAN-AIR FUEL, AND BECAUSE IT IS REPRESENTATIVE OF A WIDE RANGE OF HIGHER-MOLECULAR-WEIGHT HYDROCARBONS.
- EFFECTS OF PRESSURE ON SOOT FORMATION, QUENCHING, RADIATION, KINETICS, AND IGNITION CAN BE STUDIED. REDUCED PRESSURE IS USED TO ENHANCE KINETIC EFFECTS.
- AMBIENT COMPOSITIONAL EFFECTS ON FLAME STRUCTURE, KINETICS, SOOT FORMATION, AND IGNITION CAN BE STUDIED USING DIFFERENT CHAMBER OXIDIZERS. REDUCED LEVELS OF O_2 ARE SELECTED TO ENHANCE KINETICS.

RESEARCH REQUIREMENTS

FUEL	PURE, HIGH-QUALITY METHANE; PROPANE WILL BE CONSIDERED FOR LATER FLIGHTS; METHANE VOLUME FLOW RATE = 0-15 CM^3/SEC; PROPANE VOLUME FLOW RATE = 0-5 CM^3/SEC.
EXPERIMENT TIME	UP TO 40 SEC FOR EACH FLAME.
FUEL TANK	INTERNAL PRESSURE = TBD (BASED ON THE NUMBER AND CHARACTERISTICS OF FLAMES STUDIED DURING EACH TEST); 5-15 ATM.
EXPERIMENTAL CHAMBER	EITHER CYLINDRICAL OR RECTANGULAR; MIN.HEIGHT/DIA.(OR WIDTH) = 1.5. VOLUME (IF IN MID-DECK) = 0.04 M^3 (MUST FIT INTO TWO LOCKERS); VOLUME (IF IN MSL) > 0.04 M^3 (TBD BASED ON THE NUMBER OF FLAMES PER FLIGHT; LESS SEVERE RESTRICTION ON OCCUPIED SPACE COMPARED TO MID-DECK); VOLUME (IF IN SPACELAB) > 0.04 M^3.
INITIAL CHAMBER PRESSURE	1/2 ATM AND 1 ATM.
CHAMBER ENVIRONMENT	STD. AIR (21% O_2 ,79% N_2). ALSO. 10% O_2. 90% N_2 FOR LATER FLIGHTS.

Science Applications International Corporation

RESEARCH REQUIREMENTS (CONT.)

O_2 CONSUMED	≤10% AT THE END OF THE FLIGHT; PREFERABLY 1% - 3% AT THE END OF EACH FLAME MEASUREMENT.
NOZZLES	RADIUS = 0.05 - 0.45 CM. LENGTH = 15 CM.
FLOW CONTROL ACCURACY	= 0.01 CM^3/SEC.
ACCELERATION ENVIRONMENT	$<10^{-3}G$.
OPERATOR INVOLVEMENT	• FLAME IGNITION • MOTION PICTURE PHOTOGRAPHY OF FLAME • VISUAL OBSERVATION • TEMPERATURE, PRESSURE AND ACCELERATION MEASUREMENTS • SAMPLE REMOVAL • RADIATION MEASUREMENTS.
TOLERANCES	GAS ΔT BEFORE EACH TEST = ± 5K (2%); GAS ΔP BEFORE EACH TEST = ± 0.3 PSIA (2%); ΔO_2 AT THE BEGINNING OF THE TEST SET = ± 0.1MOLE%.

RESEARCH REQUIREMENTS (CONT.)

IGNITION	EITHER SPARK OR HEATED WIRE (SPARK PREFERRED); POWER SUPPLIED BY SHUTTLE; FINAL DETAILS OF SUBSYSTEM TBD FROM THE 5-sec DROP-TOWER TESTS.
CAMERA FRAMING RATE	400 FRAMES/SEC FOR THE FIRST 5 SEC. OF MEASUREMENTS (TO STUDY IGNITION) AND 100 FRAMES/SEC FOR THE REST OF THE PERIOD; I.E., TWO-SPEED CAMERA IS PREFERRED.
VIEWING (RESOLUTION)	FIELD OF VIEW MUST BE 5-cm HORIZONTAL BY 10-cm VERTICAL AT THE PLANE PASSING THROUGH THE FLAME CENTERLINE AND PERPENDICULAR TO THE AXIS OF THE CAMERA.
DATA RECORDING RATES	THERMOCOUPLE SAMPLING RATE = 20/SEC AND TRANSDUCER SAMPLING RATE = 20/SEC (PREFERRED).

Science Applications International Corporation

ACCELERATION

- ACCELERATIONS GREATER THAN 10^{-3}g RESULT IN (a) INCREASE IN VELOCITY OF THE BURNED GAS AFTER REACHING A MINIMUM AT DOWNSTREAM (TAKE-OVER OF CONVECTIVE EFFECTS), AND (b) SLOWER DECAY OF GAS TEMPERATURE DOWNSTREAM OF THE NOZZLE.
- BURNING WILL BE AFFECTED BY g-LEVEL, BUT MEASUREMENTS WILL NOT BE ADVERSELY AFFECTED BY VARIOUS g-LEVELS.
- SEE THE FOLLOWING ANALYSIS FOR THE EFFECT OF RESIDUAL ACCELERATIONS (g-JITTER).

EFFECTS OF GRAVITATIONAL ACCELERATION

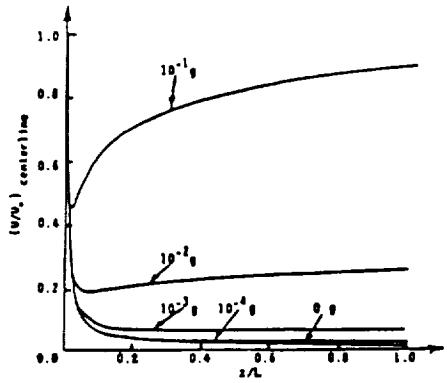

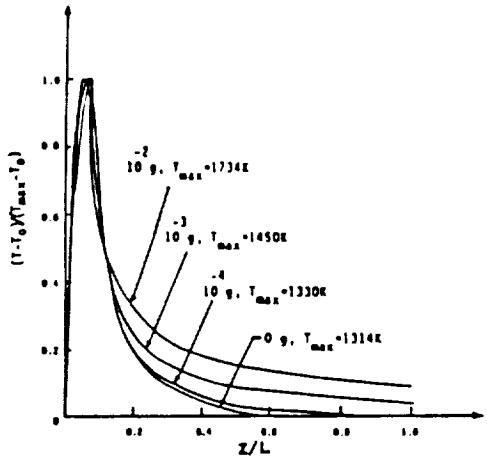

U_0 = jet velocity, 93.5 cm/sec

Nozzle radius = 0.0825 cm

L = 50 cm

T_{max} = maximum temperature reached at the centerline

T_0 = initial gas temperature, 300K

EFFECT OF RESIDUAL ACCELERATIONS
ORDER-OF-MAGNITUDE ANALYSIS

CONTINUITY: $$\frac{\partial \rho}{\partial t} + \frac{\partial(\rho u)}{\partial x} + \frac{\rho v}{r} + \frac{\partial(\rho v)}{\partial r} = 0 \qquad (1)$$

ASSUMPTIONS: $\rho = \tilde{\rho}$, $u = \tilde{u} + \hat{u}\, e^{i\omega t}$, $v = \tilde{v} + \hat{v}\, e^{i\omega t}$.

SUBSTITTUION IN THE CONTINUITY EQUATION YIELDS THE FOLLOWING TWO EQUATIONS FOR THE STEADY-STATE AND TIME-DEPENDENT COMPONENTS:

$$\tilde{u}\frac{\partial \tilde{\rho}}{\partial x} + \tilde{\rho}\frac{\partial \tilde{u}}{\partial x} + \frac{\tilde{\rho}\tilde{v}}{r} + \tilde{\rho}\frac{\partial \tilde{v}}{\partial r} + \tilde{v}\frac{\partial \tilde{\rho}}{\partial r} = 0 \qquad (2)$$

$$\hat{u}\frac{\partial \tilde{\rho}}{\partial x} + \tilde{\rho}\frac{\partial \hat{u}}{\partial x} + \frac{\tilde{\rho}\hat{v}}{r} + \tilde{\rho}\frac{\partial \hat{v}}{\partial r} + \hat{v}\frac{\partial \tilde{\rho}}{\partial r} = 0 \qquad (3)$$

USING $\left[\frac{\partial}{\partial x}\right] \equiv \frac{1}{L}$, $\left[\frac{\partial}{\partial r}\right] \equiv \frac{1}{R}$ AND $\left[\frac{1}{r}\right] \equiv \frac{1}{R}$, WHERE L = FLAME LENGTH AND R = MAXIMUM FLAME RADIUS, WE THEN OBTAIN

$$\frac{\tilde{v}}{R} \sim -\frac{2\tilde{u}}{3L} \qquad \frac{\hat{v}}{R} \sim -\frac{2\hat{u}}{3L} \qquad (4)$$

EFFECT OF RESIDUAL ACCELERATIONS (CONTINUED)

MOMENTUM: $$\rho \frac{\partial u}{\partial t} + \rho u \frac{\partial u}{\partial x} + \rho v \frac{\partial u}{\partial r} = \frac{1}{r}\frac{\partial}{\partial r}\left(\mu r \frac{\partial u}{\partial r}\right) + g(\rho_e - \rho) \quad (5)$$

ASSUMPTIONS: $\rho = \tilde{\rho}$, $g = \tilde{g} + \hat{g} e^{i\omega t}$, $u = \tilde{u} + \hat{u} e^{i\omega t}$, $v = \tilde{v} + \hat{v} e^{i\omega t}$,

CONSTANT VISCOSITY, AND NEGLIGIBLE HIGHER-ORDER PERTURBATION TERMS, I.E., $e^{2i\omega t}$ TERMS.

SUBSTITUTION IN THE MOMENTUM EQUATION YIELDS

$$\tilde{\rho}\tilde{u}\frac{\partial \tilde{u}}{\partial x} + \tilde{\rho}\tilde{v}\frac{\partial \tilde{u}}{\partial r} = \mu\left(\frac{1}{r}\frac{\partial \tilde{u}}{\partial r} + \frac{\partial^2 \tilde{u}}{\partial r^2}\right) + \tilde{g}(\rho_e - \tilde{\rho}) \quad (6)$$

$$\tilde{\rho} i\omega \hat{u} + \tilde{\rho}\frac{\partial \tilde{u}}{\partial x}\hat{u} + \tilde{\rho}\tilde{u}\frac{\partial \hat{u}}{\partial x} + \tilde{\rho}\tilde{v}\frac{\partial \hat{u}}{\partial r} + \tilde{\rho}\hat{v}\frac{\partial \tilde{u}}{\partial r} = \mu\left(\frac{1}{r}\frac{\partial \hat{u}}{\partial r} + \frac{\partial^2 \hat{u}}{\partial r^2}\right) + \hat{g}(\rho_e - \tilde{\rho}) \quad (7)$$

USING $\left[\frac{\partial}{\partial x}\right] = \frac{1}{L}$, $\left[\frac{\partial}{\partial r}\right] = \frac{1}{R}$, $\left[\frac{1}{r}\right] = \frac{1}{R}$, AND $\left[\frac{\partial^2}{\partial r^2}\right] = \frac{1}{R^2}$, EQS. (6) AND (7) YIELD, RESPECTIVELY

$$\tilde{u} \sim \frac{3\nu L}{R^2}\left[1 + \sqrt{1 + \frac{R^4 \tilde{g}\left(\frac{\rho_e}{\tilde{\rho}} - 1\right)}{3\nu^2 L}}\right], \qquad \boxed{|\hat{u}| \sim \frac{\hat{g}\left(\frac{\rho_e}{\tilde{\rho}} - 1\right)}{\left[\omega^2 + \left(\frac{2\tilde{u}}{3L} - \frac{2\nu}{R^2}\right)^2\right]^{1/2}}} \quad (8)$$

WHERE WE HAVE USED EQS. (4), ν IS THE KINEMATIC VISCOSITY.

SAIC

EFFECT OF RESIDUAL ACCELERATIONS (CONTINUED)

ENERGY:

ASSUMPTIONS: $\rho = \tilde{\rho}$, $u = \tilde{u} + \hat{u} e^{i\omega t}$, $v = \tilde{v} + \hat{v} e^{i\omega t}$, $h = \tilde{h} + \hat{h} e^{i\omega t}$,

Le = 1 (I.E., $\rho D = \lambda / C_p$ = CONST.), NEGLIGIBLE KINETIC ENERGY, AND NEGLIGIBLE SECOND-ORDER PERTURBATION TERMS. THE ASSUMPTION OF Le = 1 DECOUPLES THE ENERGY-AND ELEMENT-CONSERVATION EQUATIONS.

$$\rho\frac{\partial h}{\partial t} + \rho u\frac{\partial h}{\partial x} + \rho v\frac{\partial h}{\partial r} = \frac{\lambda}{C_p}\left(\frac{1}{r}\frac{\partial h}{\partial r} + \frac{\partial^2 h}{\partial r^2}\right) \quad (9)$$

THE FOLLOWING EQUATIONS ARE THEN OBTAINED FROM EQ. (9):

$$\tilde{\rho}\tilde{u}\frac{\partial \tilde{h}}{\partial x} + \tilde{\rho}\tilde{v}\frac{\partial \tilde{h}}{\partial r} = \frac{\lambda}{C_p}\left(\frac{1}{r}\frac{\partial \tilde{h}}{\partial r} + \frac{\partial^2 \tilde{h}}{\partial r^2}\right) \quad (10)$$

$$\tilde{\rho} i\omega \hat{h} + \tilde{\rho}\tilde{u}\frac{\partial \hat{h}}{\partial x} + \tilde{\rho}\hat{u}\frac{\partial \tilde{h}}{\partial x} + \tilde{\rho}\tilde{v}\frac{\partial \hat{h}}{\partial r} + \tilde{\rho}\hat{v}\frac{\partial \tilde{h}}{\partial r} = \frac{\lambda}{C_p}\left(\frac{1}{r}\frac{\partial \hat{h}}{\partial r} + \frac{\partial^2 \hat{h}}{\partial r^2}\right) \quad (11)$$

USING $\left[\frac{\partial}{\partial x}\right] = \frac{1}{L}$, $\left[\frac{\partial}{\partial r}\right] = \frac{1}{R}$, $\left[\frac{1}{r}\right] = \frac{1}{R}$, AND $\left[\frac{\partial^2}{\partial r^2}\right] = \frac{1}{R^2}$,

EQS. (10) AND (11) YIELD

$$\boxed{|\hat{h}| \sim \frac{|\hat{u}|\,\tilde{h}/3L}{\left[\omega^2 + \left(\frac{\tilde{u}}{3L} - \frac{2D}{R^2}\right)^2\right]^{1/2}}} \quad (12)$$

WHERE WE HAVE USED EQS. (4), SUBSTITUTION OF EQ. (8) IN (12) YIELDS

$$\boxed{\frac{\hat{g}}{g_0} \sim \frac{3L\left[\omega^2 + \left(\frac{\tilde{u}}{3L} - \frac{2D}{R^2}\right)^2\right]^{1/2}\left[\omega^2 + \left(\frac{2\tilde{u}}{3L} - \frac{2\nu}{R^2}\right)^2\right]^{1/2}\left(\frac{|\hat{h}|}{\tilde{h}}\right)}{g_0\left(\frac{\rho_e}{\tilde{\rho}} - 1\right)}} \quad (13)$$

SAIC

EFFECT OF RESIDUAL ACCELERATIONS (CONT.)

CALCULATIONS FOR FLAME A

CH_4/AIR FLAME, u_0=291.2 cm/s, r_0=0.051 cm. NUMERICAL SOLUTION BASED ON Le=Pr=1 HAVE SHOWN THAT FOR 0-G: L_f=0.209 ft=6.37 cm, R_{max}=0.033 ft=1 cm, AND $T_{flame\ tip}$=1620K. SINCE Sc=1, D=ν=4.0 cm^2/sec AT T=1620K FOR DIFFUSION OF CH_4 IN AIR. THE FOLLOWING PLOT OF h vs. L_f FOR DIFFERENT RADIATION COEFFICIENTS (RF) SHOWS THAT $\Delta h = 2.3\times10^4\,\Delta L_f$ (WITH ΔL_f IN ft.). ALSO, NUMERICAL RESULTS SHOW THE TAKE-OVER OF CONVECTIVE EFFECTS FOR ACCELERATIONS GREATER THAN 10^{-3}G (SEE BELOW). AT 10^{-3}G, L_f=0.206 ft=6.28 cm. WE DO NOT ALLOW MORE THAN 33% VARIATION IN DIFFERENCE IN FLAME HEIGHTS BETWEEN 0-G AND 10^{-3}G. THEREFORE $\Delta h = (2.3\times10^4)\times0.33(0.209-0.206)=23$. NUMERICAL RESULTS SHOW THAT h=550 AT THE FLAME TIP. HENCE $|\hat{h}|/\tilde{h}=23/550=0.042$.

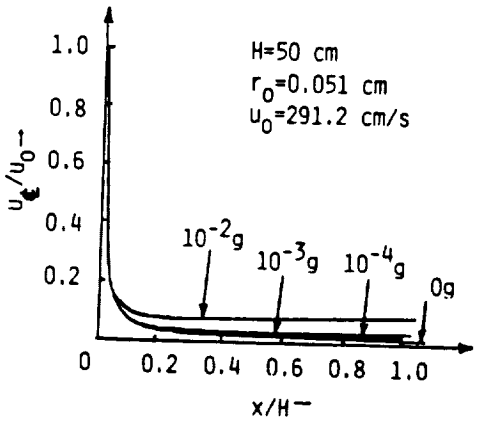

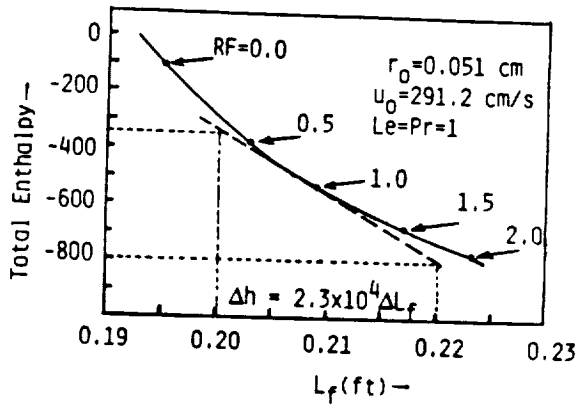

EFFECT OF RESIDUAL ACCELERATIONS (CONTINUED)

CALCULATIONS FOR FLAME A (CONTD)

SUBSTITUTION OF L_f=6.37 cm, R_{max}=1 cm, $\tilde{u}$=1/2 u_0 ≃ 145 cm/sec, D=ν=4.0 cm^2/sec, g_0=980 cm/sec^2, $(\rho_e/\tilde{\rho})=(\tilde{T}/T_e)$=1620/300=5.4 (ASSUMING AIR), AND $|\hat{h}|/\tilde{h}$ = 0.042 IN THE EXPRESSION FOR $\hat{g}/g_0$ GIVES

$$\hat{g}/g_0 = 0.000185\sqrt{(\omega^2 + 0.17)(\omega^2 + 51.5)}.$$

THE FOLLOWING DIAGRAM SHOWS THE ALLOWABLE FREQUENCIES.

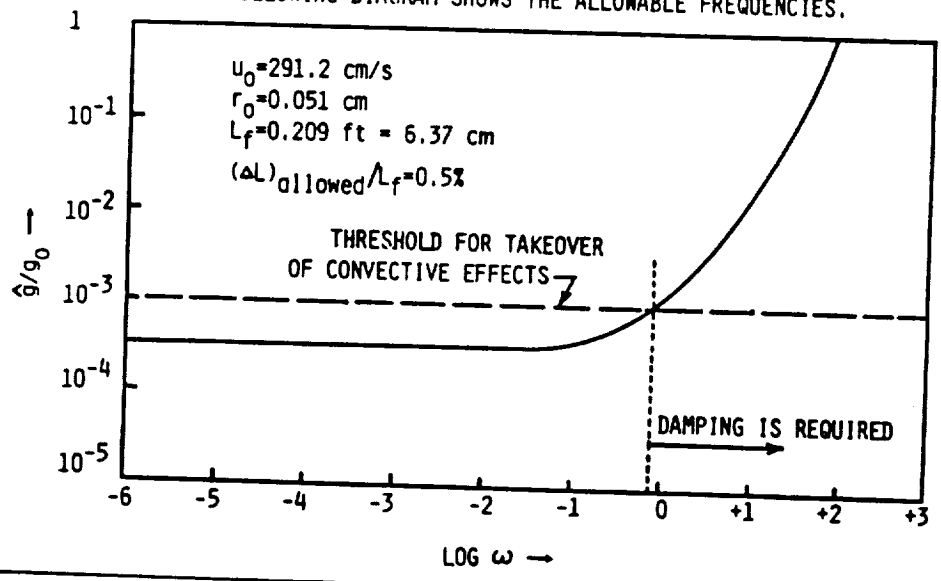

EFFECT OF RESIDUAL ACCELERATIONS (CONT.)

CALCULATIONS FOR FLAME B

CH_4/AIR FLAME, u_0=93.5 cm/sec, r_0=0.0825 cm. NUMERICAL SOLUTIONS BASED ON Le=Pr=1 HAVE SHOWN THAT FOR 0-G: L_f=0.191 ft=5.82 cm, R_{max}=0.04 ft=1.22 cm, AND $T_{flame\ tip}$≃1120K. SINCE Sc=1, D=ν=2.0 cm^2/s AT T=1120 K FOR DIFFUSION OF CH_4 IN AIR. THE FOLLOWING PLOT OF h vs. L_f FOR DIFFERENT RADIATION COEFFICIENTS (RF) SHOWS THAT $\Delta h = 1\times10^4\ \Delta L_f$ (WITH ΔL_f IN ft). ALSO, NUMERICAL RESULTS SHOW THE TAKE-OVER OF CONVECTIVE EFFECTS FOR ACCELERATIONS GREATER THAN 10^{-3}G (SEE BELOW) AT 10^{-3}G, L_f=0.173 ft=5.27 cm. WE DO NOT ALLOW MORE THAN 33% VARIATION IN DIFFERENCE IN FLAME HEIGHTS BETWEEN 0-G AND 10^{-3}G. THEREFORE $\Delta h = (1\times10^4)\times0.33\times(0.191-0.173)=60$. NUMERICAL RESULTS SHOW THAT h=850 AT THE FLAME TIP. HENCE $|\hat{h}|/\bar{h}$ = 60/850=0.07.

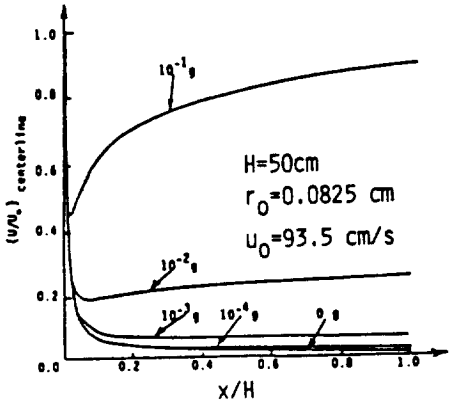

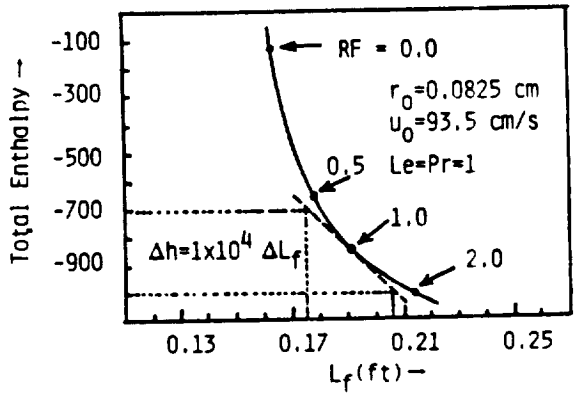

SAIC

EFFECT OF RESIDUAL ACCELERATIONS (CONT.)

CALCULATIONS FOR FLAME B (CONTD)

SUBSTITUTION OF L_f = 5.82 cm, $\bar{u}$ = 1/2 u_0 ≃ 45 cm/sec, R_{max} = 1.22 cm, D = ν = 2.0 cm^2/sec, g_0 = 980 cm/sec^2, $(\rho_e/\bar{\rho}) = (\bar{T}/T_e)$ = 1120/300 = 3.73 (ASSUMING AIR), AND $|\hat{h}|/\bar{h}$ = 0.07 IN THE EXPRESSION FOR $\hat{g}/g_0$ GIVES

$$\hat{g}/g_0 = 0.00046\sqrt{(\omega^2 + 0.01)\ (\omega^2 + 6.09)}.$$

THE FOLLOWING DIAGRAM SHOWS THE ALLOWABLE FREQUENCIES.

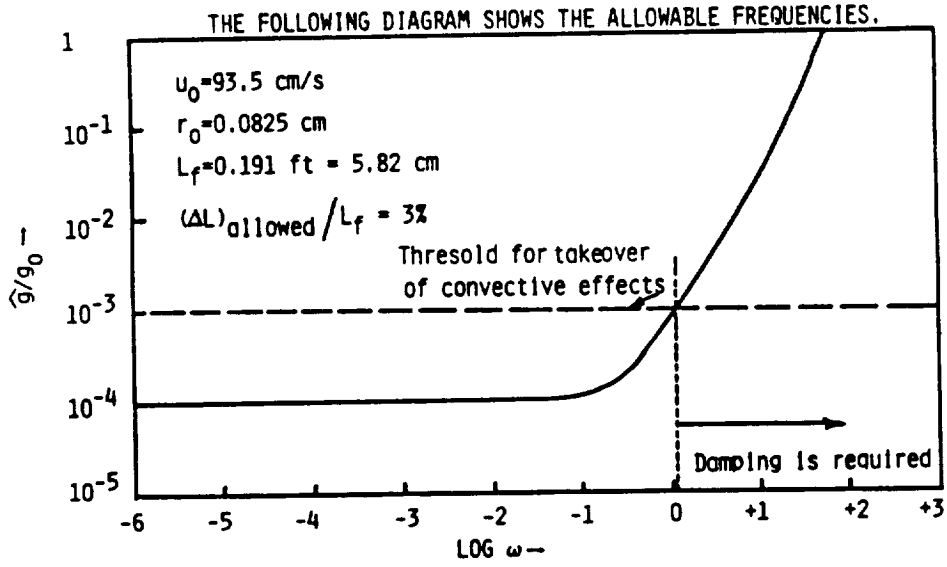

SAIC

DATA ACQUISITION

- RECORD FLAME IGNITION AND DEVELOPMENT DURING COMBUSTION
- RECORD GAS TEMPERATURES AT DIFFERENT LOCATIONS ABOVE THE FLAME
- CONTINUOUSLY RECORD CHAMBER PRESSURE AND TEMPERATURE
- RECORD ACCELERATION
- GAS-SAMPLE REMOVAL
- RADIATION MEASUREMENTS

Science Applications International Corporation

MEASUREMENT TECHNIQUES AND APPLICATIONS TO MODEL DEVELOPMENT

MEASUREMENTS	RATIONALE/APPLICATIONS TO MODEL DEVELOPMENT	TOTAL PROGRAM	MINIMUM MATRIX OF TEST
CINEMATOGRAPHY (USING HIGH-SPEED MOVIE CAMERAS)	OBTAINING TIME-RESOLVED VISUALIZATION DATA ON IGNITION, FLAME DEVELOPMENT, COLOR, LUMINOSITY, AND QUENCHING. FLAME SHAPES CAN BE COMPARED DIRECTLY WITH MODEL PREDICTIONS.	YES	YES
THERMOCOUPLES (USING RAKES)	OBTAINING TEMPERATURE DISTRIBUTIONS IN THE FLOW FIELD ABOVE THE FLAME. THESE TEMPERATURE DISTRIBUTIONS CAN BE COMPARED DIRECTLY WITH THE MODEL PREDICTIONS OF THERMAL FIELD.	YES	YES
SAMPLING PROBES (USING SAMPLING BOTTLES)	OBTAINING SPECIES DISTRIBUTION ABOVE THE FLAME WHICH CAN BE COMPARED WITH THE MODEL PREDICTIONS OF SPECIES FIELD.	YES	YES
PRESSURE TRANSDUCER	MEASUREMENT OF THE INCREASE IN CHAMBER PRESSURE DUE TO THE BURNING PROCESS YIELDS ESTIMATES OF THE OVERALL HEAT RELEASE RATE.	YES	YES

MEASUREMENT TECHNIQUES AND APPLICATIONS TO MODEL DEVELOPMENT (CONT.)

MEASUREMENTS	RATIONALE/APPLICATIONS TO MODEL DEVELOPMENT	TOTAL PROGRAM	MINIMUM MATRIX OF TESTS
VELOCITY MEASUREMENT	MEASUREMENTS FOR THE SCALE OF THIS EXPERIMENT REQUIRE A LASER-BASED DIAGNOSTICS, WHICH IS NOT FEASIBLE AT THIS TIME. THIS REQUIRES A COMPROMISE IN WHICH PREDICTIONS AND OTHER MEASUREMENTS WILL BE USED TO PROVIDE THE VELOCITY.	NO	NO
RADIOMETRY (TBD)	ISOLATION OF THERMAL RADIATION, AND AS A RESULT, DETERMINATION OF THE EFFECT OF RADIATION ON REDUCTION IN TEMPERATURE WITHIN THE FLAME. POTENTIAL EXISTS FOR DETERMINATION OF SOOT CONCENTRATION AND GENERATION. EVIDENCE SHOWS THAT RADIATION FROM SOOT IS NOT DOMINATED BY CO_2 AND H_2O. THEREFORE, CALCULATIONS FOR CO_2 AND H_2O COMBINED WITH MEASURED RADIATION YIELD THE CONTRIBUTION FROM SOOT, AND HENCE, SOOT CONCENTRATION.	YES*	YES*

*IF EARTHBOUND EXPERIMENTS SHOW THAT RADIATION MEASUREMENTS ARE REDUNDANT, COMBINATION OF THEORETICAL ANALYSES AND EARTHBOUND RESULTS WILL BE USED TO DELETE THOSE MEASUREMENTS FROM THE SPACE PROGRAM.

Science Applications International Corporation

MEASUREMENT TECHNIQUES AND APPLICATIONS TO MODEL DEVELOPMENT (CONT.)

MEASUREMENTS	RATIONALE/APPLICATIONS TO MODEL DEVELOPMENT	TOTAL PROGRAM	MINIMUM MATRIX OF TESTS
ACCELEROMETER (IF AVAILABLE)	MEASUREMENTS OF THE GRAVITATIONAL ACCELERATION ENABLES US TO INTERPRET THE DATA THAT COULD BE AFFECTED BY GRAVITATIONAL LEVELS GREATER THAN 10^{-3} G.	YES	YES (IF AVAILABLE)

RATIONALE FOR OBSERVING THE COLOR OF FLAMES

THE WOLFHARD-PARKER SLOT-BURNER HAS CLEARLY IDENTIFIED DIFFERENT REGIONS AND COLORS IN A DIFFUSION FLAME.

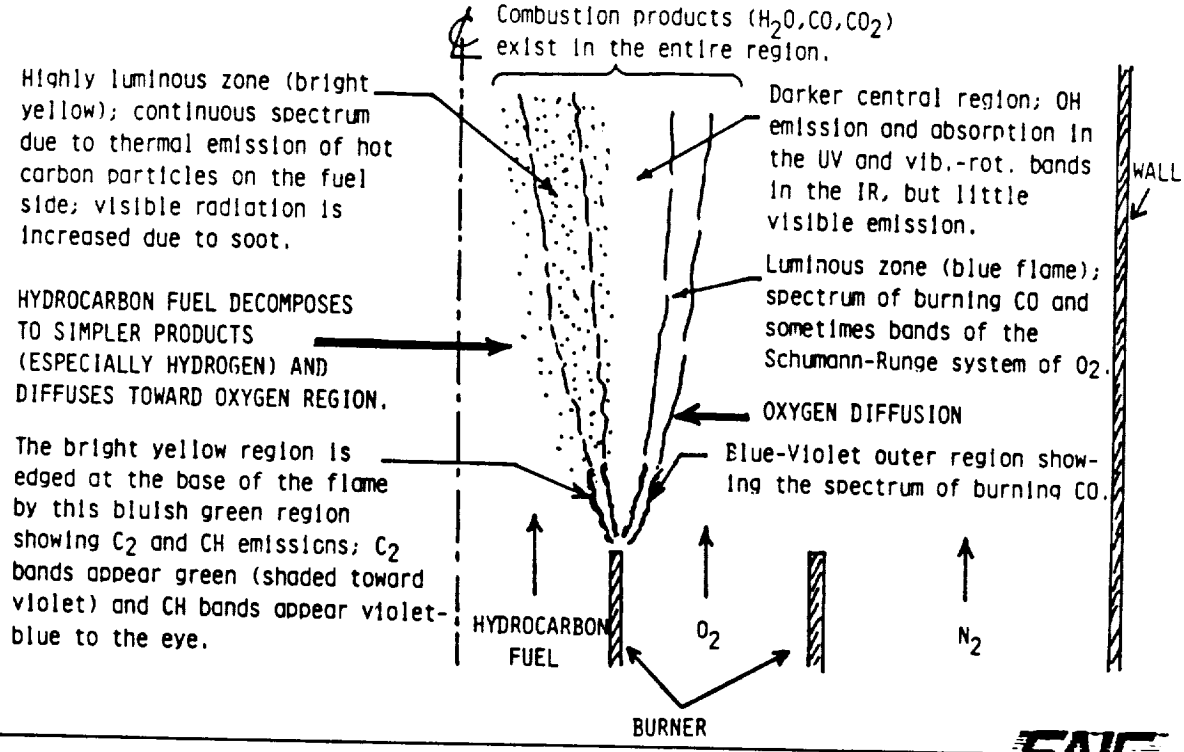

SAIC

Science Applications International Corporation

RATIONALE FOR OBSERVING THE COLOR OF FLAMES (CONTD)

- FLAMES EMIT DISCRETE BAND SPECTRA.
- SPECTRA IN VISIBLE AND UV REGIONS ARE DUE TO CHANGES OF ELECTRONIC ENERGY, IN NEAR IR ARE DUE TO CHANGES OF VIBRATIONAL AND ROTATIONAL ENERGY, AND IN EXTREME IR ARE DUE TO CHANGES IN ROTATIONAL ENERGY ONLY.
- NONE OF THE STABLE PRODUCTS OF COMBUSTION (I.E., H_2O, CO_2, CO, O_2 OR N_2) GIVE SPECTRA OF APPRECIABLE STRENGTH IN THE VISIBLE OR UV REGIONS.
- ONLY OH GIVES A BAND SYSTEM IN THE UV.
- FOR HOT FLAMES, THE BULK OF THE ENERGY IS RADIATED IN THE CO_2 BANDS AT 2.7 AND 4.4μ AND FOR WATER VAPOR AT 2.8μ .
- OTHER VIBRATIONAL BANDS OF INTEREST ARE CO AT 2.3 AND 4.5μ , NO AT 2.6 AND 5.2μ , AND THE OH VIBRATIONAL BANDS THAT COVER THE NEAR IR AREA TO ABOUT 4μ .
- AT FLAME TEMPERATURES, THE MAXIMUM EMISSION TENDS TO BE IN THE NEAR IR BETWEEN ABOUT 2μ AND 1μ ACCORDING TO THE TEMPERATURE OF THE FLAME.
- FOR CLEAR FLAMES, THE RADIATION IN THE VISIBLE AND UV ACCOUNTS FOR LESS THAN 0.4% OF THE HEAT OF COMBUSTION. THIS VISIBLE RADIATION COMES MAINLY FROM THE INNER CONE, WHILE THE IR RADIATION COMES FROM THE MAIN BODY OF THE GASES, BOTH THE INTERCONAL GASES AND THE BURNT PRODUCTS.
- USING BLUE, GREEN OR YELLOW LIGHT, THE PHOTOGRAPHS OF BUNSEN FLAMES HAVE SHOWN ONLY THE INNER CONE CLEARLY, BUT USING INFRARED LIGHT OF WAVELENGTH 8,500 OR 10,050 °A, THE INNER CONE IS INVISIBLE BUT THE INTERCONAL GASES SHOW UP.
- FOR LUMINOUS FLAMES, RADIATION FROM SOOT PARTICLES INCREASES THE RADIATION IN THE VISIBLE.

SAIC

JUSTIFICATION FOR A SPACE EXPERIMENT

- $< 10^{-3}$ g is required
- g-jitter at $f < 1$ Hz is required
- Test times ≈ 40 sec

SAIC

ROLE OF ADDITIONAL GROUND-BASED EXPERIMENTS

- OPTIMIZE THE FINAL SPACE EXPERIMENT TEST MATRIX
- MINIMIZE THE SPACE EXPERIMENT COMPLEXITY BY REDUCING THE MEASUREMENT REQUIREMENTS
- ASSIST IN THE DEVELOPMENT OF TECHNOLOGY FOR THE SPACE EXPERIMENT

SAIC

OVERALL PROGRAM APPROACH

OVERALL PROGRAM

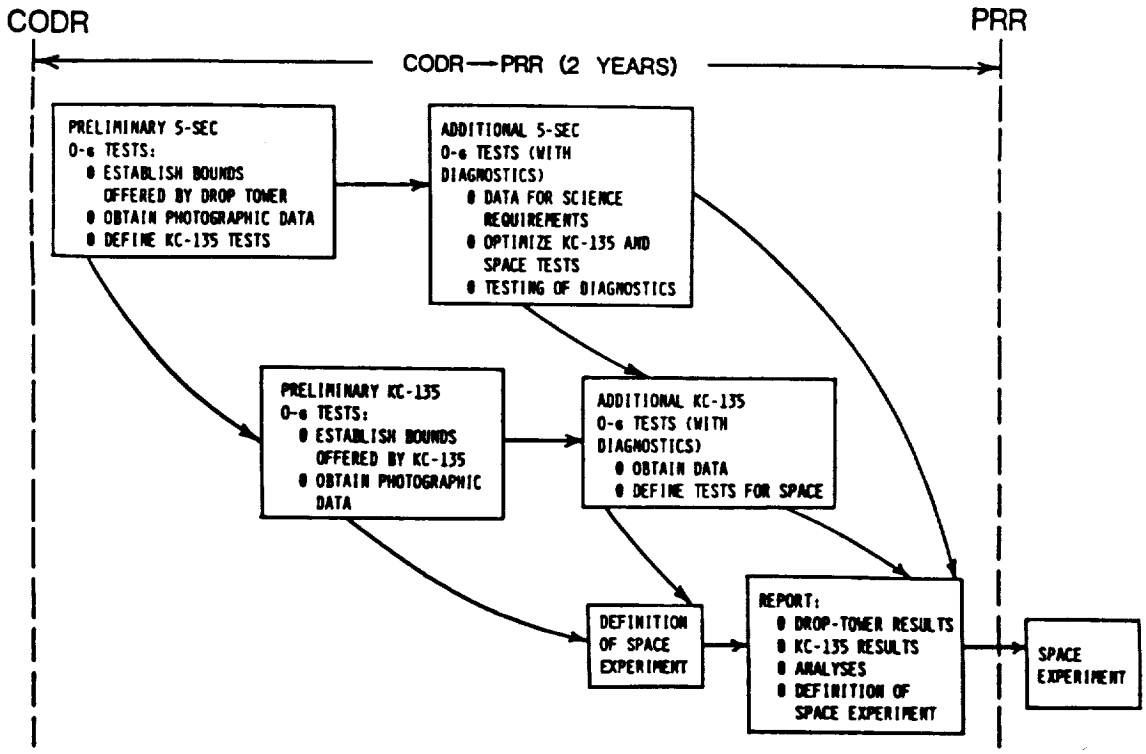

ACTIVITIES AFTER CODR AND BEFORE PRR

- INITIATE THE DETAILED PLAN FOR EXPERIMENTS IN THE 5-SEC. DROP-TOWER FACILITY, DESIGN THE EXPERIMENTAL CHAMBER AND IGNITOR, AND CONDUCT DROP-TOWER EXPERIMENTS TO DEVELOP THE IGNITOR, VERIFY IGNITION, AND OBTAIN INITIALLY ONLY PHOTOGRAPHIC AND THEN COMPLETE DATA.
- INITIATE THE DETAILED PLAN FOR KC-135 TESTING, DESIGN THE EXPERIMENTAL CHAMBER AND CONDUCT KC-135 AIRCRAFT FLIGHT TESTING FOR NOMINAL 0-G TEST TIMES OF 10-15 SECONDS, ASSESS THE PERFORMANCE OF THE EXPERIMENTAL HARDWARE AND ANALYZE THE TEST DATA RESULTS.
- FINALIZE THE SPACE EXPERIMENT TEST MATRIX BASED ON THE RESULTS OF GROUND-BASED EXPERIMENTS.
- INITIATE THE NUMERICAL ANALYSIS FOR TRANSIENT IGNITION AND STEADY-STATE COMBUSTION UNDER MICRO-GRAVITY CONDITIONS WHICH DIRECTLY SIMULATES THE CONDITIONS UNDER WHICH THE EXPERIMENTS ARE GOING TO BE CONDUCTED BY USING ELLIPITIC EQUATIONS IN CONJUNCTION WITH FINITE-RATE KINETICS, SOOT FORMATION AND RADIATION.

SAIC

Science Applications International Corporation

GROUND-BASED EXPERIMENTS

SAIC

GROUND-BASED EXPERIMENT COMPONENTS

- EXPERIMENTAL CHAMBER
- CAMERA
- IGNITION SYSTEM
- THERMOCOUPLES
- PRESSURE TRANSDUCER
- FUEL TANK
- FUEL LINES
- VALVES AND FITTINGS
- RADIOMETER
- SAMPLING PROBES
- SAMPLING BOTTLES

Science Applications International Corporation

RESULTS OF GROUND-BASED TESTING

- Improve theoretical model
- Develop experimental technique
- Optimize space experiment

EARTHBOUND AND SPACE PROGRAMS

REQUIREMENTS: $<10^{-3}$G; G-JITTER AT F < 1Hz; TEST TIMES = 40 SEC.

	EARTHBOUND PROGRAM		SPACE PROGRAM
	DROP TOWER: T=5 SEC, G=0(10^{-5}), G-JITTER NEGL.	KC-135: T=10-15 SEC, G ~ 10^{-2} IF FREE FLOATING, CABLE MAY CAUSE JITTER.	SHUTTLE: T > 40 SEC, G= $<10^{-3}$ AVAILABLE, TEST DURING "QUIET TIMES".
EXPERIMENTS WILL STUDY:	• IGNITION • TRANSIENT FLAME DEVELOPMENT • STEADY-STATE FLAMES		• IGNITION • TRANSIENT FLAME DEVELOPMENT • STEADY-STATE FLAMES
MEASUREMENT TECHNIQUES TO BE USED:	• PHOTOGRAPHY • TEMPERATURE MEASUREMENTS • RADIOMETRY • COMBUSTION PRODUCTS SAMPLING		• PHOTOGRAPHY • TEMPERATURE MEASUREMENTS • RADIOMETRY* • COMBUSTION PRODUCTS SAMPLING

*IF EARTHBOUND EXPERIMENTS SHOW THAT RADIATION MEASUREMENTS ARE REDUNDANT, COMBINATION OF THEORETICAL ANALYSES AND EARTHBOUND RESULTS WILL BE USED TO DELETE THOSE MEASUREMENTS FROM THE SPACE PROGRAM.

SAIC

Science Applications International Corporation

CONCEPT DESIGN

SAIC

PROCEDURE FOR PRELIMINARY STUDIES IN THE 5-SEC DROP TOWER

- START THE CAMERA AND DROP THE TEST CELL
- START THE FUEL FLOW AND IGNITION SYSTEM FROM 1/2 TO 1 SEC AFTER RELEASE OF THE TEST CELL
- DURATION OF SPARK IGNITION TO BE OPTIMIZED WITH TESTING
- SEQUENCE OF OPERATIONS CONTROLLED BY BATTERY-POWERED TIMER SWITCH
- MOVIE CAMERA RECORDS BOTH THE IGNITION PROCESS AND FLAME DEVELOPMENT
- THESE RESULTS WILL BE USED IN FINALIZING THE KC-135 FLIGHT TESTS

SAIC

Science Applications International Corporation

PROGRAM SUMMARY

SAIC

Science Applications International Corporation

COMPARISONS BETWEEN MID-DECK, SPACELAB AND MATERIALS SCIENCE LAB FOR CONDUCTING THE EXPERIMENT

- MID-DECK
  - VOLUME AND WEIGHT CONSTRAINTS (-)
  - DIRECT ASTRONAUT INVOLVEMENT (+)
  - LESS COMPLEXITY (+)
  - LESS AUTOMATION (+)
  - VENTING (-)
- SPACELAB
  - MORE AVAILABLE VOLUME (+)
  - DIRECT ASTRONAUT INVOLVEMENT (+)
  - LESS COMPLEXITY (+)
  - LESS AUTOMATION (+)
  - VENTING (+)
- MATERIALS SCIENCE LAB
  - MORE AVAILABLE VOLUME (+)
  - INDIRECT ASTRONAUT INVOLVEMENT (-)
  - MORE COMPLEXITY DUE TO FULL AUTOMATION (-)
  - EXPOSURE OR LACK OF EXPOSURE TO SUN MAY CAUSE PROBLEMS IN RELATION TO COOLING OR HEATING OF THE CHAMBER (-)
  - VENTING (+)

SAIC

Science Applications International Corporation

COMPARISONS BETWEEN MID-DECK, SPACELAB AND MATERIALS SCIENCE LAB FOR CONDUCTING THE EXPERIMENT

	MSL	MID-DECK	SPACELAB
VOLUME CONSTRAINT	+1	0	+1
WEIGHT CONSTRAINT	+1	0	+1
DIRECT ASTRONAUT INVOLVEMENT	-1	+1	+1
COMPLEXITY DUE TO AUTOMATION	0	+1	+1
COMPLEXITY DUE TO DESIGN	-1	+1	+1
VENTING	+1	-1	+1
Σ:	+1	+2	+6

SAIC

EXPERIMENT DESCRIPTION

- COMPONENTS:
  NOZZLES, EXPERIMENTAL CHAMBER, FUEL TANK, FUEL VALVES, THERMOCOUPLES, TRANSDUCER, SAMPLING PROBES, SAMPLING BOTTLES, IGNITOR, HEAT MANAGEMENT SYSTEM, CAMERA(S), DATA ACQUISITION SYSTEM.

- FUEL:
  METHANE; PROPANE

EXPERIMENTAL CHAMBER

- SEALED CHAMBER, EITHER CYLINDRICAL OR RECTANGULAR, ALUMINUM
- MUST BE ABLE TO WITHSTAND THE SPECIFIED CONDITIONS FOR THE REQUIRED PERIOD OF TIME FROM COMPLETION OF ASSEMBLY TO POST-FLIGHT DATA ANALYSIS
- MINIMUM HEIGHT/DIAMETER (OR WIDTH) = 1.5
- VOLUME ($> 0.04\ m^3$)
- TWO WINDOWS (ONE FOR CAMERA, ONE FOR OBSERVATION)
- PORT(S) FOR THERMOCOUPLES, SAMPLING PROBES, IGNITORS, AND TRANSDUCER
- NUMBER OF NOZZLES ENTERING THE CHAMBER: TWO
- CHAMBER MUST WITHSTAND PRESSURES OF UP TO 3 ATM, GAS TEMPERATURES OF UP TO 495K, AND METAL TEMPERATURES OF UP TO 310K (CONSERVATIVE ESTIMATES FOR UPPER LIMITS)

VIEWING

- THE FIELD OF VIEW MUST BE 5 - CM HORIZONTAL BY 10 - CM VERTICAL AT THE PLANE PASSING THROUGH THE FLAME CENTERLINE AND PERPENDICULAR TO THE AXIS OF THE CAMERA
- BESIDES VIEWING PORT FOR CAMERA, A VERTICAL VIEWING SECTION MUST BE PROVIDED FOR OBSERVATION (EITHER DIRECT OR VIA A TV CAMERA)

Science Applications International Corporation

WINDOWS

	EXPERIMENT IN SPACELAB
TOTAL NO. OF WINDOWS	2
VIEWING PORT(S)	1; USED FOR HIGH-SPEED CAMERA; SMALLER THAN OBSERVATION WINDOW.
OBSERVATION WINDOW	1; LARGER THAN (AND 90^{o} APART FROM) THE VIEWING PORT FOR HIGH-SPEED CAMERA; USED FOR ASTRONAUT'S OBSERVATION

GAS COMPOSITION IN THE EXPERIMENTAL CHAMBER

- STANDARD AIR (21% O_2, 79% N_2). ALSO, 10% O_2-90% N_2.
- OXYGEN DEPLETION: <10% AT THE END OF THE EXPERIMENT.
- USE PREFILLED CHAMBER MIXTURE.
- O_2 TOLERANCE AT THE BEGINNING OF THE TEST SET: ±0.1 MOLE %.
- INITIAL PRESSURES FOR EACH FLAME = 1 ATM AND 1/2 ATM.
- GAS TEMPERATURE BEFORE EACH TEST = 295 ± 5K.
- PRESSURE TOLERANCE = ±0.3 PSIA BEFORE EACH TEST.
- CHAMBER PRESSURE SHOULD BE RECORDED BEFORE, DURING AND AFTER THE EXPERIMENT (AT LEAST EVERY 50 MILLISEC., I.E., 20 SAMPLES/SEC.).
- CHAMBER TEMPERATURE MUST BE MONITORED DURING THE ENTIRE EXPERIMENT (AT LEAST EVERY 50 MILLISEC., I.E., 20 SAMPLES/SEC.).

Science Applications International Corporation

VENTING

- ADVANTAGES
  - MANY FLAMES CAN BE STUDIED IN ONE FLIGHT
  - SMALLER CHAMBER
  - WEIGHT REDUCTION
  - CONTROL OVER THE % O_2 BURNED
  - FLAMES WITH DIFFERENT CHAMBER PRESSURES CAN BE STUDIED
  - NO CHAMBER COOLING AFTER EACH FLAME
  - IF FUEL IS ACCIDENTALLY RELEASED IN THE CHAMBER, EVACUATION IS EASY
- DISADVANTAGES
  - AIR MUST BE CARRIED ABOARD
  - VALVES FOR EVACUATING AND RE-FILLING THE CHAMBER
  - ACCURATE CONTROL OVER CHAMBER PRESSURE
  - WEIGHT ADDITION DUE TO AIR TANK

FUEL-TUBING SYSTEM

- STAINLESS STEEL TUBES
- FLOW CONTROL ACCURACY = ± 0.01 CM^3/SEC
- FLOW VALVES, EXPLOSION — PROOF SOLENOID VALVES, AND REGULATORS
- PRE-CALIBRATED PRECISION VALVES

SAIC

NOZZLES

- RADIUS = 0.05 - 0.45 CM
- DISTANCE FROM PORT TO CHAMBER CEILING ≥30 CM
- DISTANCE BETWEEN NOZZLES (IF MORE THAN ONE NOZZLE PER CHAMBER) = 5-10 CM
- NOZZLE(S) EQUALLY DISTANT FROM CHAMBER CENTERLINE
- NOZZLE(S) IN LINE WITH THE CAMERA
- MINIMUM DISTANCE FROM WALL FOR NOZZLE POSITIONING = 10 CM
- THIS NOZZLE ARRANGEMENT ENSURES THAT TEMPERATURES ≤350K AND NEGLIGIBLE GAS VELOCITIES EXIST AT THE CHAMBER CEILING (I.E., PREVENTION OF EXTENSIVE HEATING OF CHAMBER CEILING AND SIGNIFICANT RECIRCULATION)
- PROXIMITY OF THE NOZZLES DOES NOT CAUSE FLAME DISTURBANCE BECAUSE MAXIMUM FLAME RADII ≃0.5 - 1.0 CM
- NOZZLES MUST BE SECURED INSIDE THE CHAMBER TO AVOID MISALIGNMENT OR LOOSENING DUE TO VIBRATIONS OR DURING LIFT-OFF
- MINIMUM NOZZLE LENGTH IN THE CHAMBER = 15 CM

SAIC

FUEL

- PURE, HIGH-QUALITY METHANE
- PROPANE WILL BE CONSIDERED FOR LATER FLIGHTS
- METHANE VOLUME FLOW RATE = 0 - 15 CM^3/SEC
- PROPANE VOLUME FLOW RATE = 0 - 5 CM^3/SEC
- AMOUNT OF FUEL CARRIED WILL BE SUFFICIENT TO PERFORM THE ENTIRE TEST MATRIX
- FUEL TANK VOLUME = TBD BASED ON
  - NUMBER OF FLAMES
  - VOLUME FLOW RATE OF EACH FLAME
  - 40-SEC BURNING TIME PER FLAME
  - PRESSURE IN THE FUEL TANK

SAIC

FUEL TANK(S)

- INITIAL PRESSURE = 5 - 15 ATM
- NO FUEL(S) LEFT AT THE END OF THE EXPERIMENT
- STAINLESS STEEL TANKS
- DUAL SYSTEM FOR PRESSURE CONTROL
- FUEL PRESSURE REMAINS FAIRLY CONSTANT THROUGHOUT THE EXPERIMENT
- ONE FUEL TANK IF ONLY CH_4: TWO FUEL TANKS IF BOTH CH_4 AND C_3H_8

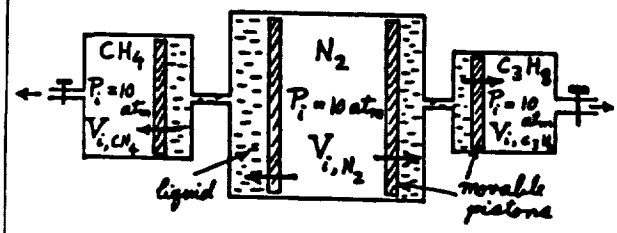

BEFORE EXPERIMENT

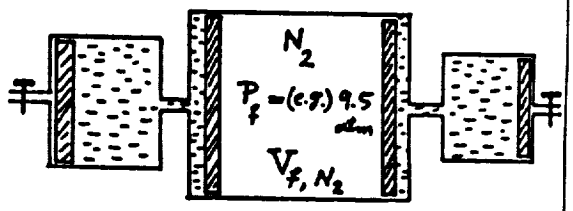

AFTER EXPERIMENT

$$(P_i V_i)_{N_2} = (P_f V_f)_{N_2} \Rightarrow \left(\frac{V_f - V_i}{V_i}\right)_{N_2} = \frac{P_i - P_f}{P_f} \Rightarrow \frac{V_{i,CH_4} + V_{i,C_3H_8}}{V_{i,N_2}} = \frac{P_i}{P_f} - 1$$

$$\therefore \quad V_{i,N_2} = \left[\hat{R}T\left(m_{CH_4}/M_{CH_4} + m_{C_3H_8}/M_{C_3H_8}\right)/P_i\right] \Big/ \left(P_i/P_f - 1\right)$$

SAIC

IGNITION

- MINIMUM DISTURBANCE TO FLAME
- EITHER SPARK OR HEATED-WIRE IGNITION (SPARK PREFERRED)
- POWER IS SUPPLIED BY SHUTTLE POWER
- IGNITION AND FUEL INJECTION MUST BE SYNCHRONIZED
- FINAL DETAILS OF THE IGNITION SUBSYSTEM TBD FROM THE 5-SEC DROP-TOWER TESTS

SAIC

IGNITION SYSTEM OPTIONS

SPARK IGNITION★	HEATED-WIRE IGNITION
• Nozzle is treated as an electrode. • Electrodes are fixed. • Power is supplied by shuttle 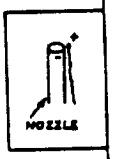 • Provisions must be made for appropriate coils to increase the spark voltage. • Interference with other Shuttle operations must be addressed.	• One ignitor is sufficient for both nozzles if the ignitor arm is rotatable. • Ignitor can have only two positions (i.e., vicinity of the two nozzles). 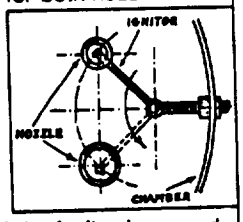 • Once ignition occurs, the arm is rotated and the ignitor is moved to the other nozzle location. • Ignitor is coiled 0.33-cm-diameter nichrome wire. • Power is supplied by shuttle
• Ignition and fuel injection must be synchronized. • Final details of ignition subsystem TBD from the drop tower tests.	

★Preferred

SAIC

HEAT RELEASE PER FLAME

$$CH_4 + 2O_2 \rightarrow CO_2 + 2H_2O \; ; \quad C_3H_8 + 5O_2 \rightarrow 3CO_2 + 4H_2O$$

$$Q_{release} = q_F m_F = q_F \left(\frac{P_o \dot{V}_F t}{R_F T_o}\right) = q_F \left(\frac{P_o M_F \dot{V}_F t}{\hat{R} T_o}\right)$$

WHERE q = ENTHALPY OF COMBUSTION OF FUEL AT 25°C WITH WATER VAPOR IN THE PRODUCTS, m_F = MASS OF FUEL, t = EXPERIMENT TIME, $\dot{V}_F$ = VOLUME FLOW RATE OF FUEL, T_o = INITIAL TEMPERATURE, P_o = INITIAL PRESSURE, M_F = FUEL MOLECULAR WEIGHT, AND $\hat{R}$ = UNIVERSAL GAS CONSTANT.

FOR CH_4: q = 50.010 kJ/kg, M = 16 kg/kgmole

FOR C_3H_8: q = 46.353 kJ/kg, M = 44 kg/kgmole

USING T_o = 300K, $\hat{R}$ = 8.3143 kJ/kgmole-K AND t = 40 sec, WE OBTAIN THE FOLLOWING DIAGRAM:

Science Applications International Corporation

HEAT RELEASE PER FLAME (CONT.)

$(Q_{release})_{CH_4} = 0.0128\, P\dot{V}_F$, $(Q_{release})_{C_3H_8} = 0.0326\, P\dot{V}_F$ with $Q_{release}$ in kJ, P in kPa and $\dot{V}_F$ in cm^3/sec.

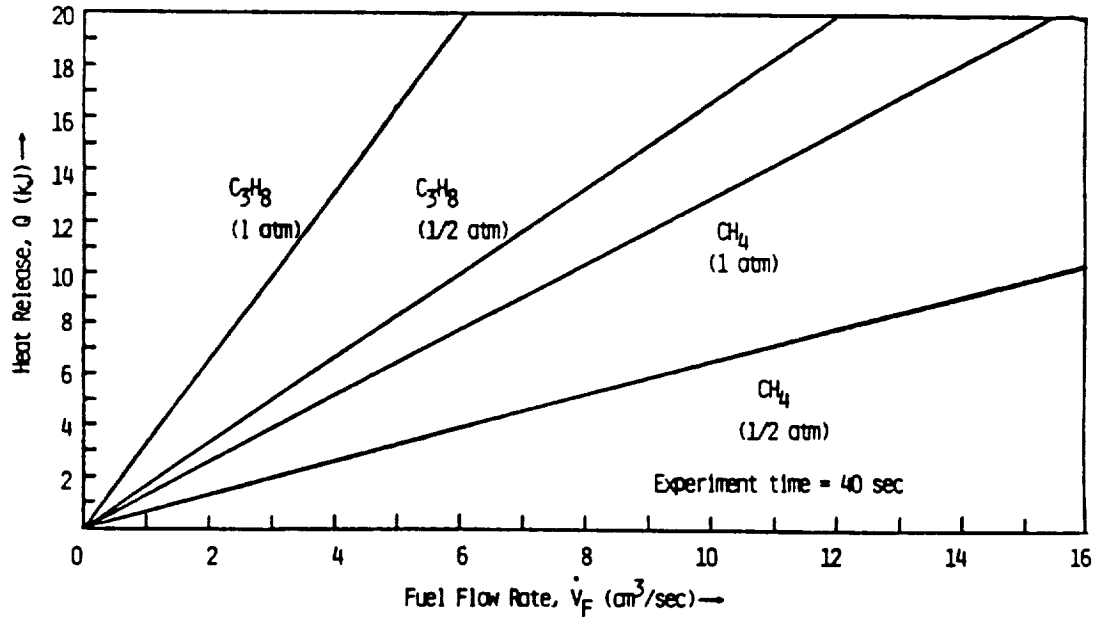

CHAMBER TEMPERATURE

- TEST CELL TEMPERATURE SET POINT FOR EACH FLAME = 295 ± 5K
- TEMPERATURE RISE AT THE END OF EACH FLAME MEASUREMENT = TBD (TYPICAL 20 - 200K MAXIMUM) *
- COOLING BY FAN (IN SPACELAB)

---

* GAS TEMPERATURE WITH ADIABATIC WALLS

TEMPERATURE RISE IN THE EXPERIMENTAL CHAMBER

ASSUMPTIONS: Ideal gas
All of the heat release is absorbed by the gas only
No heat loss
Constant specific heat
Burning has negligible effect on no. of moles of air

From the 1st law of thermodynamics,

$$Q = m_{air}(u - u_o) = n_{air} M_{air} c_v (T - T_o)$$

$$n_{air} = P_o V_{ch.} / \hat{R} T_o = P_o (\phi + 1) i \dot{V}_F t / \hat{R} T_o \chi$$

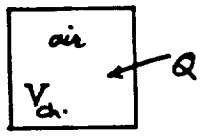

where we have used the previously-derived expression for $V_{ch.}$ (see Appendix).

$$\therefore \quad Q = P_o (\phi + 1) i \dot{V}_F t M_{air} c_v (T - T_o) / \hat{R} T_o \chi$$

Equating this relation with the previously-derived expression (see Appendix)

$$Q = g_F P_o M_F \dot{V}_F t / \hat{R} T_o$$

yields

$$\boxed{\Delta T = T - T_o = g_F M_F \chi / c_v (\phi + 1) i M_{air}}$$

In this derivation, u = specific internal energy and c_v = constant-volume specific heat.

TEMPERATURE RISE IN THE EXPERIMENTAL CHAMBER (CONT.)

Using $(c_v)_{air} = 0.718$ kJ/kg - K, $(c_v)_{90\% N_2,\ 10\% O_2} = 0.732$ kJ/kg - K,

$M_{air} = 28.84$ kg/kg mole, $M_{90\% N_2,\ 10\% O_2} = 28.40$ kg/kg mole,

and also

for CH_4: $M_F = 16$ kg/kg mole, $l = 2$, $q_F = 50{,}010$ kJ/kg,

for C_3H_8: $M_F = 44$ kg/kg mole, $l = 5$, $q_F = 46{,}353$ kJ/kg,

we obtain the gas-temperature rise as a function of % oxygen burned.

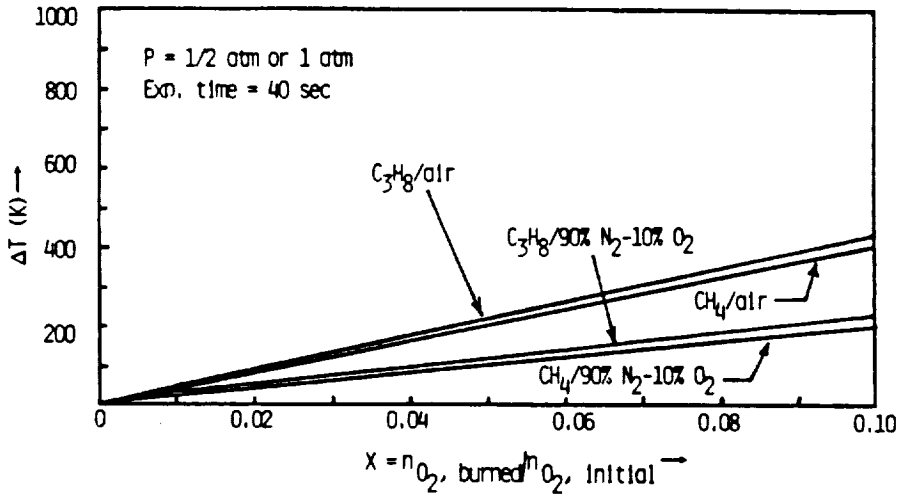

Science Applications International Corporation

CHAMBER PRESSURE

- TEST CELL PRESSURE SET POINT FOR EACH FLAME = 14.7 ± 0.3 PSIA = 101 ± 2 KPA = 1 ± 0.02 ATM; ALSO, 0.5 ± 0.01 ATM FOR SOME FLAMES
- FOR ALL TESTS, TOLERANCE ON PRESSURE SET POINT IS ± 2%, WHETHER P = 0.5 ATM OR 1.0 ATM
- PRESSURE RISE DURING COMBUSTION:
  - STRONGLY DEPENDENT ON CHAMBER VOLUME
  - TBD
  - TYPICAL: 5% (MIN.) TO 80% (MAX.)
- TRANSDUCER MEASUREMENT PRECISION = ± 0.15 PSIA (I.E., 1%)

PRESSURE RISE IN THE EXPERIMENTAL CHAMBER

$$PV = n\hat{R}T \Rightarrow \frac{P}{P_o} = \frac{T}{T_o} \Rightarrow \Delta P = \frac{P_o}{T_o}\Delta T$$

USING THE RELATION DERIVED FOR ΔT,

$$\Delta P \equiv P - P_o = P_o f_F M_F x / T_o c_v (\phi + 1) i M_{air}$$

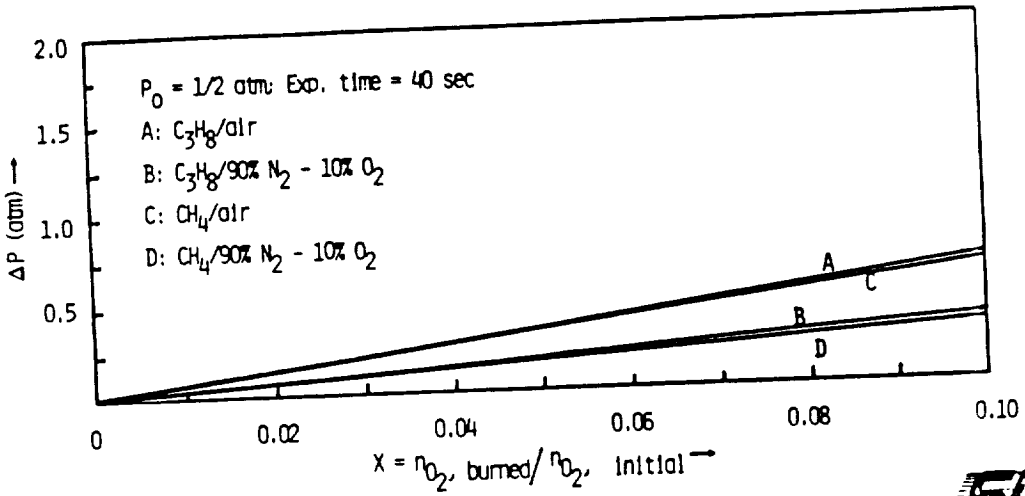

PRESSURE RISE IN THE EXPERIMENTAL CHAMBER (CONT.)

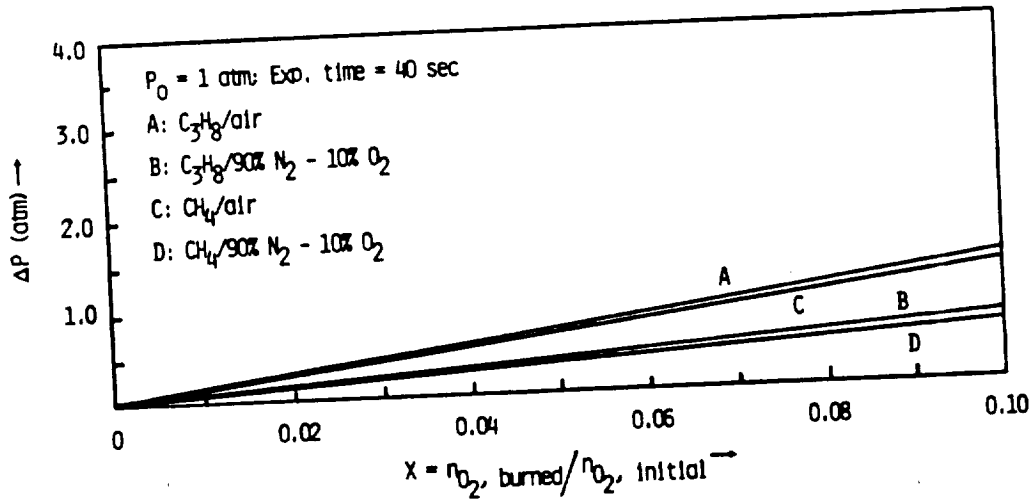

COOLING OF THE CHAMBER

- TIMES OF THE ORDER OF 5 MIN. ARE REQUIRED FOR THE CHAMBER ENVIRONMENT TO COOL DOWN TO THE AMBIENT TEMPERATURE AFTER EACH FLAME MEASUREMENT (IF IN MIDDECK OR SPACELAB).
- THE MAXIMUM GAS-TEMPERATURE RISE IN THE CHAMBER WILL BE ≈100 K FOR THE CASE OF 2% O_2 DEPLETION AND C_3H_8/AIR FLAME, ASSUMING NO HEAT TRANSFER TO THE ALUMINUM VESSEL.
- THIS MAXIMUM GAS-TEMPERATURE RISE WILL RAISE THE CONTAINER TEMPERATURE BY <1K IF ALL OF THE HEAT RELEASE IS TRANSFERRED TO METAL.
- COOLING CAN BE FACILITATED BY PROVIDING AN INTERNAL FAN FOR FORCED CONVECTION INSIDE THE CHAMBER.
- SPECIFICS OF COOLING: TBD.

SAIC

WATER - VAPOR CONDENSATION

- We are solving for an amount of fuel that when converted into CO_2 and H_2O, results in condensation (relative humidity, $\phi = p_w/p_g = 1$) at a chamber pressure of 1 atm and the lowest allowable chamber temperature of 290K.

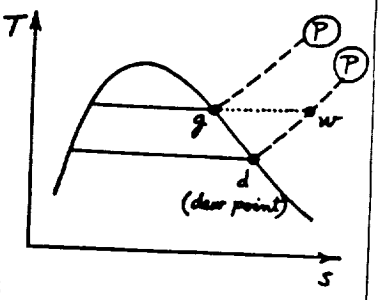

- $CH_4 + 2O_2 \rightarrow CO_2 + 2H_2O$; $C_3H_8 + 5O_2 \rightarrow 3CO_2 + 4H_2O$.
- At the end of the experiment, assuming that m_{CH_4} and $m_{C_3H_8}$ grams of fuels are burned, the total number of moles in the chamber is

$$n_{t,f} = n_{N_2,i} + (n_{O_2,i} - \Sigma n_{O_2,b}) + \Sigma n_{CO_2} + \Sigma n_{H_2O}$$

$$= n_{N_2,i} + (n_{O_2,i} - 2n_{CH_4} - 5n_{C_3H_8}) + (n_{CH_4} + 3n_{C_3H_8}) + (2n_{CH_4} + 4n_{C_3H_8})$$

$$= n_{air,i} + n_{CH_4} + 2n_{C_3H_8}$$

where subscripts t = total, f = final, i = initial, and b = burned.

- But

$$\frac{p_{H_2O}}{P} = \frac{n_{H_2O}}{n_{t,f}} = \frac{2n_{CH_4} + 4n_{C_3H_8}}{n_{air,i} + n_{CH_4} + 2n_{C_3H_8}}$$

$$\therefore \; n_{air,i}/P = (2/p_{H_2O} - 1/P)(n_{CH_4} + 2n_{C_3H_8})$$

SAIC

WATER-VAPOR CONDENSATION (CONTINUED)

- Therefore

$$V_{ch.} = \hat{R}\, T\, (2/p_{H_2O} - 1/P)\, (m_{CH_4}/M_{CH_4} + 2m_{C_3H_8}/M_{C_3H_8})$$

- Using $T = 290K$, $P = 101.325$ kPa, $p_{H_2O} \equiv p_g = 2.0855$ kPa (from saturated H_2O tables for $T = 290$ K), $M_{CH_4} = 16$, $M_{C_3H_8} = 44$ kg/kgmole, and $\hat{R} = 8.3143$ kJ/kgmole-K, we obtain

$$V_{ch.} = 143\, m_{CH_4} + 104\, m_{C_3H_8} \qquad (\text{m in kg, V in } m^3)$$

- This equation gives the maximum allowable masses of fuels burned as a function of the chamber volume that result in no condensation on the windows of the chamber for a chamber environment of $P = 1$ atm and $T = 290$ K.

Science Applications International Corporation

MEASUREMENTS

- Flame Shape Development and Flame Extinction
- Color and Luminosity
- Temperature Profiles
- Species Concentrations
- Radiation Measurements
- Chamber Pressure
- Acceleration Environment

FLAME-DIMENSION MEASUREMENT

- A SCALE FACTOR FOR THE FLAME-LENGTH MEASUREMENTS CAN BE OBTAINED FROM THE BURNER DIAMETER.

SAIC

PHOTOGRAPHY

- ONE CAMERA PREFERRED*
- COLOR, 16mm FILM
- MUST HOLD ENOUGH FILM FOR UP TO 40 SEC
- FRAMING RATE = 400 FRAMES/SEC FOR THE FIRST 5 SEC. OF MEASUREMENTS (TO STUDY IGNITION) AND 100 FRAMES/SEC FOR THE REST OF THE PERIOD
- A TWO-SPEED CAMERA IS PREFERRED
- CAMERA STARTS BEFORE FUEL STARTUP AND IGNITION
- LENS-TO-NOZZLE DISTANCE = TBD
- IF TWO NOZZLES ARE USED, LENS-TO-NOZZLE DISTANCE MUST BE ADJUSTED
- FILM CHANGE AFTER EACH FLAME MEASUREMENT
- TIMING SYSTEM SHOULD BE PROVIDED TO RECORD ACCURATE TIME INTERVALS (~0.1 SEC) ON THE FILM

* TWO CAMERAS IF LIMITATION ON FILM LENGTH OR DIFFICULTIES WITH TWO-SPEED CAMERA.

SAIC

THERMOCOUPLES

- RAKE OF THERMOCOUPLES FOR MEASUREMENTS OF TEMPERATURE DISTRIBUTIONS; MINIMUM: 6 THERMOCOUPLES, PREFERRED: 9 THERMOCOUPLES PER NOZZLE.
- GAS TEMPERATURE MEASUREMENTS CONDUCTED AT FIXED LOCATIONS ABOVE THE FLAME (5-15 CM ABOVE THE NOZZLES).
- EXAMPLE: TYPE "S" P_T/P_T-10% R_H (1650°C UPPER LIMIT, 1760°C MELTING POINT). WIRE DIAMETER = 0.13 MM, BEAD SIZE = 0.44 MM; BEADS CAN BE EXPOSED. OUTPUT VOLTAGES (16 ± 0.1 MV) SHOULD PROVIDE TEMPERATURE MEASUREMENTS WITH ± 10K.
- MEASUREMENT ACCURACY WILL NOT POSE A MAJOR PROBLEM SINCE CORRECTIONS FOR HEAT CONDUCTION, RADIATION, ETC. ARE AVAILABLE.
- SAMPLING RATE = 20/SEC.

SAIC

THERMOCOUPLES (CASE A)

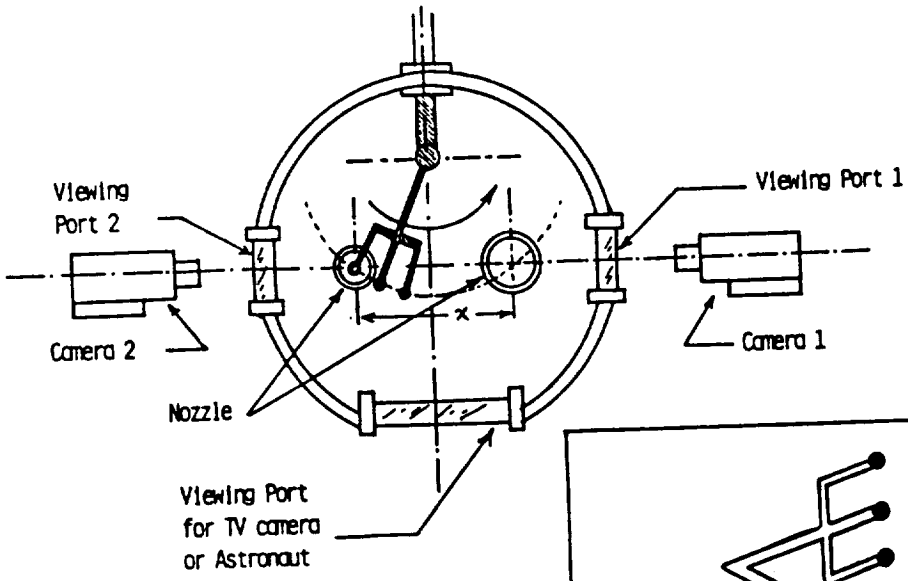

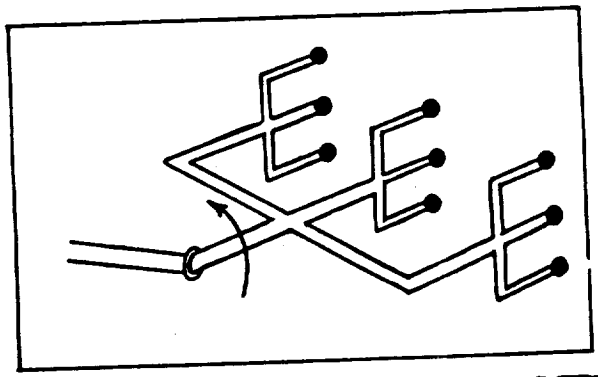

DIMENSION NOT TO SCALE;
SEPARATION DISTANCE x = TBD;
ONE CAMERA IS PREFERRED.

SAIC

THERMOCOUPLES (CASE B)*

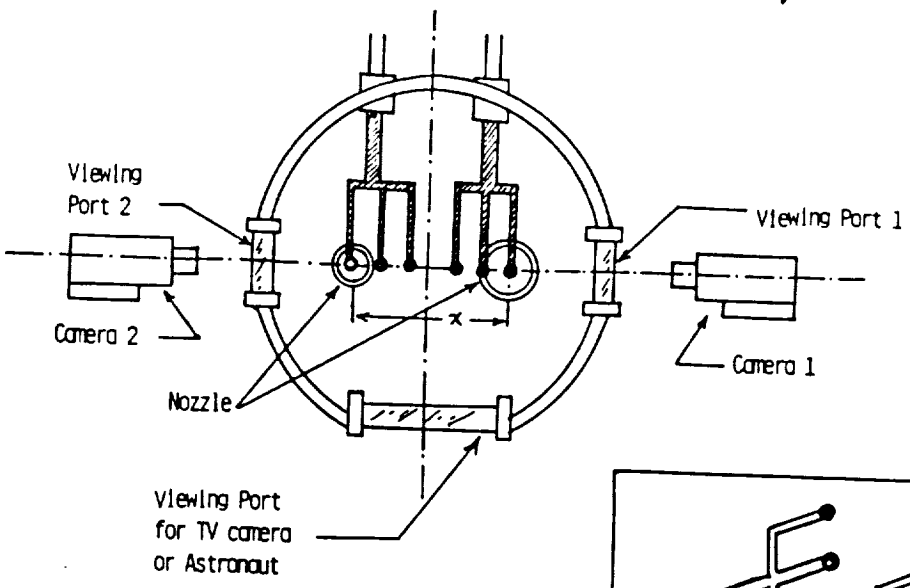

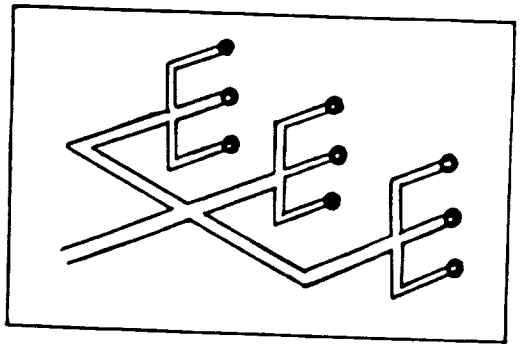

DIMENSION NOT TO SCALE;
SEPARATION DISTANCE x = TBD;
ONE CAMERA IS PREFERRED.

* Preferred

Science Applications International Corporation

GAS SAMPLING

- QUENCHING QUARTZ MICROPROBES
- 5-10 cm ABOVE THE BURNER PORT (~0-5 cm ABOVE THE FLAME TIP)
- SUCTION (CONTROLLED DURATION) AT A SPECIFIED TIME INTO SAMPLING TANKS (VACCUUM TEFLON-LINED)
- THREE PROBES FOR EACH BURNER (RAKE OF PROBES)
- ONE TANK PER PROBE PER FLAME (VOLUME OF TANK ~30 cm^3)
- SAMPLING BOTTLE INITIALLY EVACUATED
- FINAL PRESSURE IN THE SAMPLING TANK: ~5 – 7 PSIA
- DETAILS TBD
- SAMPLING CONDUCTED WHEN FLAME REACHES STEADY STATE
- PERTURBATIONS DUE TO SAMPLE REMOVAL DO NOT CAUSE FLAME DISTURBANCES AS LONG AS SUCTION IS NOT SUDDEN

RADIOMETER* (CONT.)

- RECTANGULAR APERTURE = 14.5 cm HEIGHT x 1 cm WIDTH
- BACKGROUND IS PROVIDED BY THE LIGHT TRAP (WEDGE ANGLE = 12^{o})
- THE INTERNAL APERTURES AND ADJUSTABLE EXTERNAL RECTANGULAR APERTURE PREVENT ERRONEOUS READINGS DUE TO INTERNAL REFLECTIONS OR UNWANTED STRAY RADIATION.
- THE SHUTTER PROVIDES ZERO-OFFSET READINGS THAT CAN BE SUBTRACTED FROM THE OPEN-SHUTTER OUTPUTS.
- THE TOTAL RADIANT POWER $\dot{Q}_{RAD}$ CAN BE COMPUTED FROM THE MEASURED IRRADIANCE H UNDER THE ASSUMPTION OF SPHERICALLY-ISOTROPIC EMISSION AS $\dot{Q}_{RAD} = 4\pi S^2 H$ WHERE S IS THE DISTANCE BETWEEN THE RADIOMETER SENSOR AND FLAME AXIS.
- DISTANCE FROM NOZZLE CENTERLINE TO THE SENSOR ~ 30 cm.
- THERMOPILE SENSOR: E.G. SENSORS INC. MODEL C1 WITH INTRAN 2 WINDOW, SENSITIVE AREA 1 mm DIA.
- A PROGRAMMABLE CALCULATOR CAN BE USED FOR DIGITAL RECORDING OF THE ELECTRICALLY-FILTERED RADIANCE OUTPUT.
- DETAILS TBD BASED ON FURTHER STUDIES, ANALYSES AND ENGINEERING CONSTRAINTS.

*BASED ON THE DESIGN OF MARKSTEIN; 20TH SYMPOSIUM (INT'L) ON COMBUSTION, PP. 1055-1061.

SAIC

POWER REQUIRED FOR EACH FLAME MEASUREMENT*

(CONSERVATIVE ESTIMATES)

SPACELAB AVAILABLE POWER: > POWER IN MSL.

	COMPONENT	POWER (WATTS)	TIME (SEC)	SOURCE
A	16mm CAMERA	60	40 SEC PER FLAME	ORBITER
B	IGNITOR: NICHROME WIRE (OR SPARK)	50 (OR NEGL.)	2-5 SEC TBD (OR NEGL.)	ORBITER
C	SOLENOID VALVE FOR FUEL	10	40 SEC	ORBITER
D	EXPERIMENT CONTROLLER	10	ALL THE TIME	ORBITER
E	6-9 DIGITIZED THERMOCOUPLES	20	> 40 SEC	ORBITER
F	FAN (CHAMBER)	30	TBD	ORBITER
G	CONTROL PANEL	10	ALL THE TIME	ORBITER
H	TEMP. & PRESSURE CONTROLLER	10	ALL THE TIME	ORBITER
I	3 VALVES FOR SAMPLE REMOVAL	15	<5 SEC; TBD	ORBITER
	Σ:	165-215	———	———

*RADIOMETER AND ACCELEROMETER POWER REQUIREMENTS NOT INCLUDED.

SAIC

GAS-SAMPLING CONFIGURATION

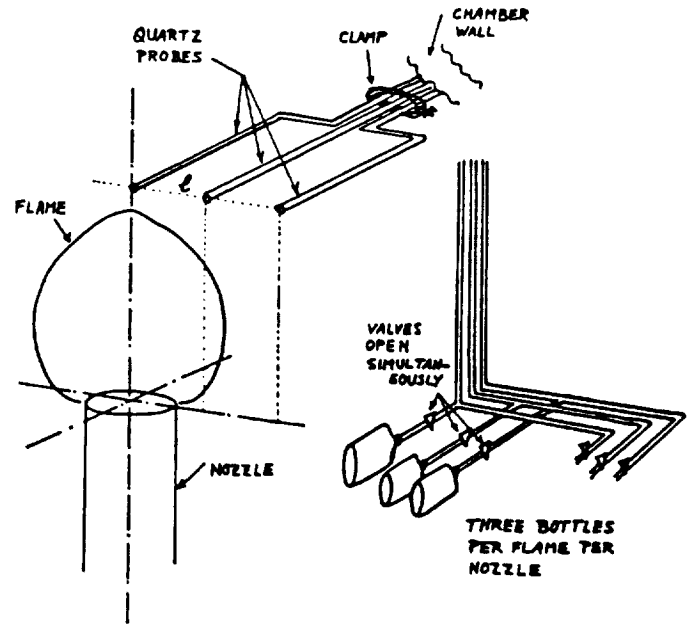

Separation distance (ℓ): TBD

SAIC

RADIOMETER*

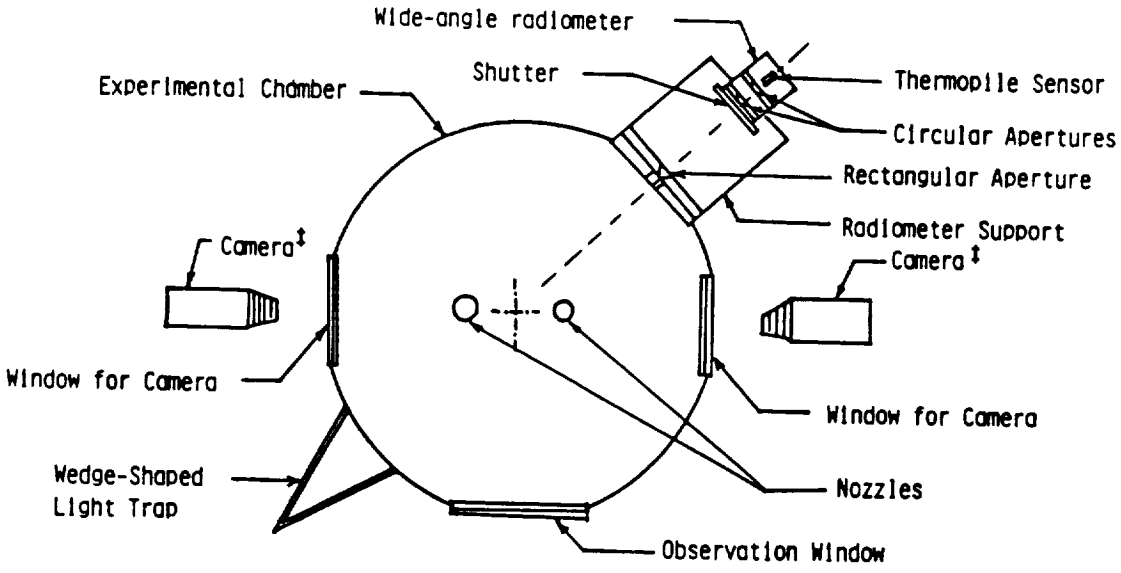

* BASED ON THE DESIGN OF MARKSTEIN; 20TH SYMPOSIUM (INT'L) ON COMBUSTION, PP.1055-1061.

‡ ONE CAMERA IS PREFERRED.

SAIC

POWER REQUIRED FOR EACH FLAME MEASUREMENT (CONT.)

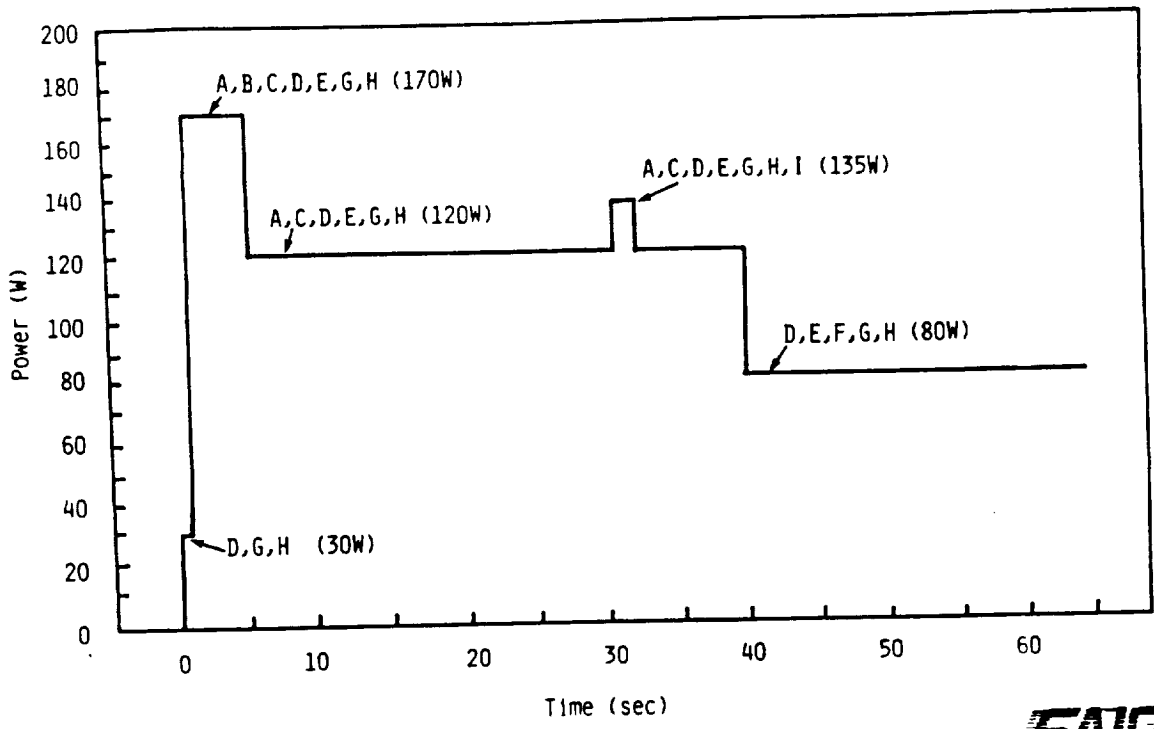

Science Applications International Corporation

ELECTRICAL SYSTEM REQUIREMENTS

- MEASUREMENT DEVICES:
  - ENVIRONMENTAL TEMPERATURE: 1 TEMPERATURE SENSOR OUTSIDE THE CHAMBER
  - COMBUSTION TEMPERATURE: 9 THERMOCOUPLES ABOVE EACH NOZZLE IS PREFERRED
  - CHAMBER TEMPERATURE: 1 TEMPERATURE SENSOR FASTENED TO THE CHAMBER
  - CHAMBER PRESSURE: 1 PRESSURE TRANSDUCER INSIDE THE CHAMBER
  - RADIOMETER: TBD AND ITS REQUIREMENTS TBD
- CONTROLS:
  - IGNITOR: TBD
  - ROTATING-ARM IGNITOR IF THE 2-NOZZLE CONFIGURATION IS USED WITH NICHROME-WIRE IGNITOR
  - ROTATING-ARM THERMOCOUPLES IF THIS OPTION IS USED
  - CAMERA(S): TURN POWER ON AND OFF
  - ALL VALVES, INCLUDING FUEL VALVES, SAMPLING-BOTTLE VALVES, AND VENTING VALVE (IF APPLICABLE)
  - INTERFACES: START, STOP, INDICATORS, ETC.
- DATA COLLECTION:
  - RECORDERS

EXPERIMENT TIMELINE AND SEQUENCE ★

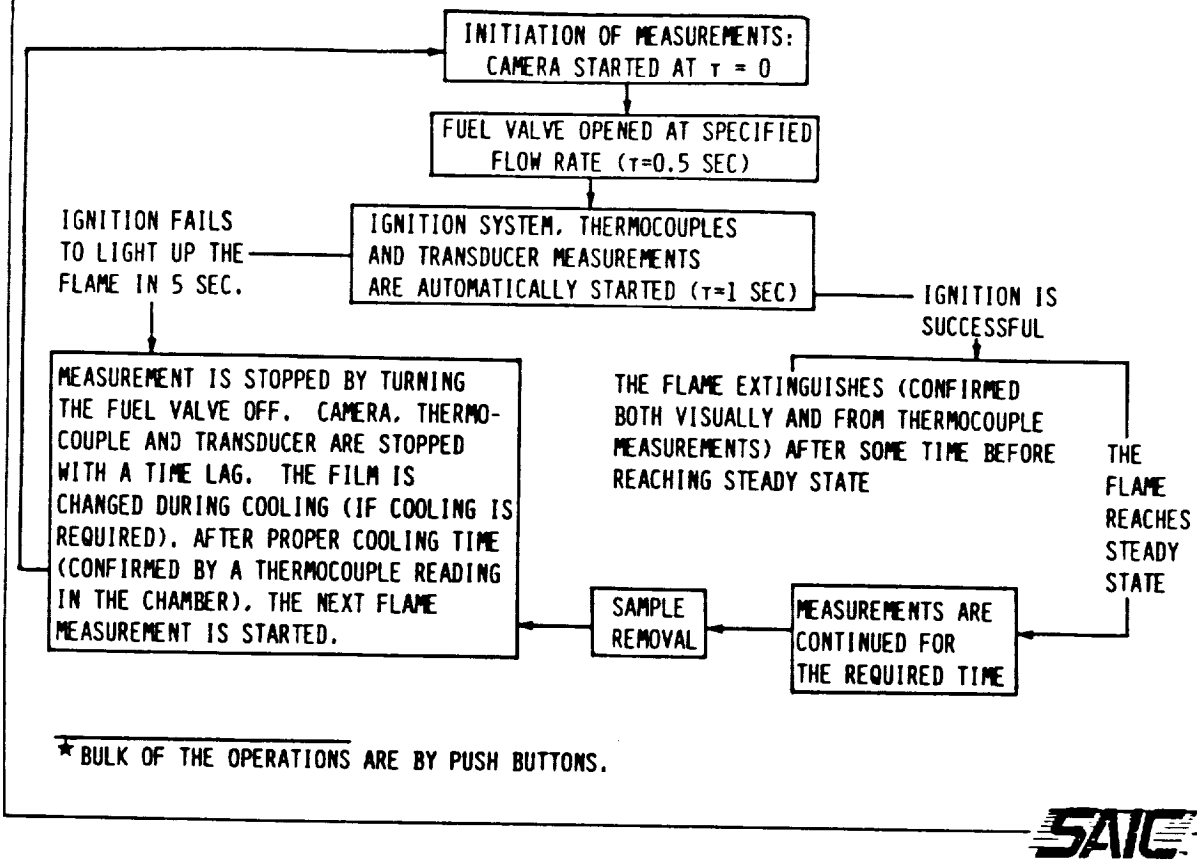

★ BULK OF THE OPERATIONS ARE BY PUSH BUTTONS.

SAIC

Science Applications International Corporation

ASTRONAUT INTERFACES

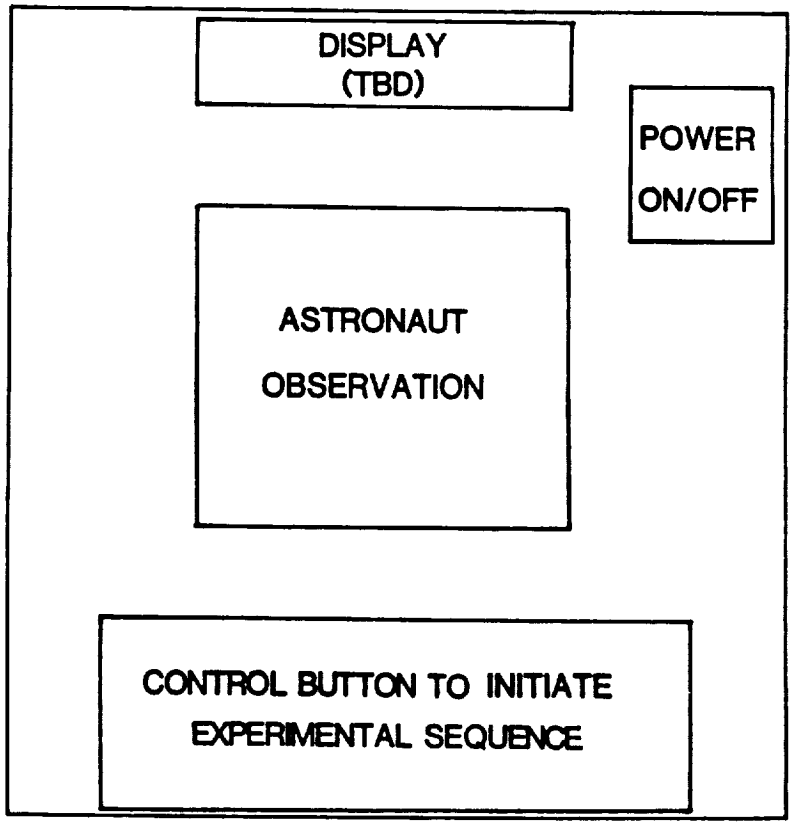

SAIC

SAFETY

SAFETY ISSUES

- FUEL CARRIED ON BOARD
  - TRIPLE CONTAINMENT IS REQUIRED (PRESSURE VESSELS)
  - AMOUNT CARRIED: TBD
  - IF RELEASED IN SPACELAB OR IN COMBUSTION CHAMBER, MUST BE BELOW LOWER FLAMMABILITY LIMIT EVEN UNDER EXTREME CONDITIONS OF HIGHEST TEMPERATURE, EMERGENCY LANDING, ETC.
- FLAME IN THE EXPERIMENT CHAMBER
  - EM INTERFERENCE WITH SHUTTLE OPERATION IF SPARK IGNITION
  - PORTS FOR THERMOCOUPLES, IGNITOR(S), PROBES
  - FUEL TUBING SYSTEM AND VALVES
    - DOUBLE CONTAINMENT
    - VIBRATION IS CRITICAL
  - OTHER FLAMMABLE MATERIALS (E.G., FILM)
  - MATERIALS OF CONSTRUCTION
  - SAMPLING BOTTLES (MUST BE EVACUATED BEFORE EXPERIMENT)

CREW OPERATIONS*

- EXPERIMENT IN SPACELAB
  - EXPERIMENT ON
  - FUEL FLOW, CAMERA(S), IGNITION, THERMOCOUPLES, TRANSDUCER ON
  - CONFIRM IGNITION
  - OBSERVE COMBUSTION
  - REMOVE SAMPLES
  - FUEL FLOW AND CAMERA OFF
  - EXPERIMENT OFF
  - CONTINUE TO RECORD TEMP. AND PRESSURE
  - APPLY COOLING (FAN)
  - EXCHANGE FILM CASSETTES
  - REPEAT FOR NEW FLAME

*BULK OF THESE OPERATIONS ARE BY PUSH BUTTON.

AUTOMATION

- THE FOLLOWING OPERATIONS CAN BE FULLY AUTOMATED IN SPACELAB:
  - EXPERIMENT ON
  - FUEL FLOW, CAMERA(S), IGNITION, THERMOCOUPLES, TRANSDUCER ON
  - OPEN AND SHUT SAMPLE-REMOVAL VALVES
  - FUEL FLOW AND CAMERA OFF
  - COOLING FAN ON AND OFF
- THE FOLLOWING NEED DIRECT ASTRONAUT INVOLVEMENT:
  - CONFIRM IGNITION
  - OBSERVE COMBUSTION DIRECTLY
  - CHANGE FILM CASSETTES

FUEL SAFETY CONSIDERATIONS

THE FOLLOWING REALISTIC AND HYPOTHETICAL SITUATIONS HAVE BEEN STUDIED IN DETAIL:

- PRESSURE RISE IN THE EXPERIMENTAL CHAMBER IF ALL OF THE FUEL IS RELEASED IN THE CHAMBER AND THE MIXTURE IS ACCIDENTALLY IGNITED.
- THE ABOVE SITUATION WILL NOT HAPPEN IF THE AMOUNT OF FUEL CARRIED IS NOT SUFFICIENT TO MAKE A FLAMMABLE MIXTURE IN THE EXPERIMENTAL CHAMBER (I.E., BELOW LOWER FLAMMABILITY LIMIT, BASED ON THE AMOUNT OF AIR IN CHAMBER).
- ASSUMING THAT INCOMPLETE COMBUSTION OF $CH_4 + 1.5O_2 \rightarrow CO + 2H_2O$ OCCURS DURING ALL OF THE FLAME EXPERIMENTS, THE MIXTURE OF N_2, CO AND H_2O REMAINED IN THE EXPERIMENTAL CHAMBER SHOULD NOT BE FLAMMABLE.
- ALL OF THE ABOVE SITUATIONS HAVE BEEN STUDIED ASSUMING THAT THE MIXTURE IS NOW RELEASED IN THE ENVIRONMENT FROM THE POINT OF VIEW OF CONTAMINATION. A TABLE OF CONTAMINANTS AND THEIR MAXIMUM ALLOWED CONCENTRATIONS IS FOLLOWING.

  - THE CONCLUSION OF THESE STUDIES IS THAT BASICALLY THE FLAMMABILITY IS NOT A PROBLEM UNDER THE UNLIKELY OCCURRENCE OF THE EVENTS OUTLINED ABOVE.

SAIC

CONTAMINATION

Maximum Allowable Concentrations (MACs) of Atmospheric Contaminants in Manned Spacecraft (both Spacelab and Mid-deck). Ref: NHB 8060.1 B and SPAH (APP.C)

MATERIAL	MOL. WT.	MACs/7-DAY	
		ppm	mg/m^3
CH_4	16.04	2700	1771
C_3H_8	44.09	500	901.4
CO	28.01	25	28.6
NO	30.01	5	6.1
NO_2	46.01	0.5	0.94

** For missions up to 7 days.

- The concentration of each contaminant in the spacecraft atmosphere must not exceed its MAC value.
- Group limit concept for a group of contaminants:

$$\sum_I c_I/MAC_I = T < 1$$

where c_I = concentration of contaminant I.

In addition, the interaction of contaminant groups that have potential additive effects must satisfy the relation

$$\sum_J T_J < 1.$$

SAIC

RELEASE OF CONTAMINANTS IN SPACELAB

IF THE EXPERIMENT IS CONDUCTED IN THE SPACELAB, THE FOLLOWING AMOUNT(S) OF FUEL(S) ARE THE ALLOWABLE MASSES TO BE CARRIED ABOARD THE SPACECRAFT BASED ON THE RELEASE IN ONLY 10-m^3 OF THE SPACECRAFT ENVIRONMENT* (ASSUMING 1 atm AND 298K) USING THE CONTAMINATION TABLE FOR MACs/7-DAY:

CH_4 ONLY: $m_{CH_4} = 17.71$ gr, % v/v = 0.27% (NOT FLAMMABLE)

C_3H_8 ONLY: $m_{C_3H_8} = 9.01$ gr, % v/v = 0.05% (NOT FLAMMABLE)

BOTH CH_4 AND C_3H_8 CARRIED ABOARD:

$$\frac{m_{CH_4}}{17.71} + \frac{m_{C_3H_8}}{9.01} = 1.$$

*PRESSURIZED VOLUMES IN SPACELAB: SHORT MODULE (WITH SHORTEST TUNNEL = 38.11 m^3, LONG MODULE (WITH LONGEST TUNNEL) = 77.82 m^3.

SAIC

Science Applications International Corporation

MAXIMUM CO PRODUCTION

ASSUMPTION:

$$CH_4 + 1.5\ O_2 \rightarrow CO + 2H_2O$$

$$C_3H_8 + 3.5\ O_2 \rightarrow 3CO + 4H_2O$$

$$n_{CH_4} = m_{CH_4}/M_{CH_4},\quad n_{C_3H_8} = m_{C_3H_8}/M_{C_3H_8}$$

$$n_{CO} = n_{CH_4} + 3n_{C_3H_8},\quad n_{H_2O} = 2n_{CH_4} + 4n_{C_3H_8}$$

$$n_{O_2,b} = 1.5n_{CH_4} + 3.5n_{C_3H_8}$$

$$n_{total,\,i} = n_{air},\quad n_{total,\,f} = n_{air} - n_{O_2,b} + n_{CO} + n_{H_2O}$$

$$\therefore\ n_{total,\,f} = n_{air} - (1.5n_{CH_4} + 3.5n_{C_3H_8}) + (n_{CH_4} + 3n_{C_3H_8}) + (2n_{CH_4} + 4n_{C_3H_8})$$

$$= n_{air} + 1.5n_{CH_4} + 3.5n_{C_3H_8}$$

$$\%\ v/v\ CO = \frac{V_{CO}}{V_{total}} = \frac{n_{CO}}{n_{total,\,f}} = \frac{(n_{CH_4} + 3n_{C_3H_8}) \times 100}{n_{air} + 1.5n_{CH_4} + 3.5n_{C_3H_8}}$$

SAIC

POST-FLIGHT DATA ANALYSIS

Science Applications International Corporation

POST-FLIGHT DATA ANALYSIS

- EXPERIMENTAL
  - FILMS WILL BE DEVELOPED AND ANALYZED TO MEASURE FLAME DEVELOPMENT AND OTHER PROCESSES
  - TEMPERATURES WILL BE DEDUCED FROM THERMOCOUPLE OUTPUT RECORDS
  - RECORDS OF CHAMBER PRESSURE WILL BE EVALUATED
  - SPACECRAFT ACCELERATION RECORDS AND G-JITTER DURING THE FLIGHT WILL BE STUDIED; PERTURBATIONS WILL BE EXPLAINED BY THE ANALYSIS AND INTERPRETATION OF FLIGHT DATA AND FLAME BEHAVIOR
  - REMOVED SAMPLES WILL BE ANALYZED TO OBTAIN INFORMATION IN RELATION TO DISTRIBUTIONS OF H_2O, O_2, CO, CO_2, N_2, HYDROCARBONS, ETC.
  - RESULTS OF RADIOMETRY WILL BE RELATED TO SOOT FORMATION AND FLAME TEMPERATURE

POST-FLIGHT DATA ANALYSIS (CONT.)

- THEORETICAL
  - THEORETICAL PREDICTIONS WILL BE USED TO SUPPORT THE ANALYSIS AND INTERPRETATION OF THE DATA BASE DEVELOPMENT FROM THESE EXPERIMENTS
  - THEORETICAL MODELS WILL BE IMPROVED USING THE RESULTS OF
    - TEMPERATURE MEASUREMENTS
    - SPECIES MEASUREMENTS
    - CHAMBER PRESSURE RECORDS
    - ACCELERATION RECORDS
    - GLOBAL CHARACTERISTICS (E.G., FLAME SHAPE AND LUMINOSITY)
  - CHEMISTRY AND FLUID DYNAMICS OF THE PROCESS WILL BENEFIT FROM THE INFORMATION ON THERMAL AND CHEMICAL FIELDS
  - COMBINATION OF EXPERIMENTAL DATA AND PREDICTIONS FACILITATES MODEL VALIDATION IN RELATION TO IGNITION, FLAME PROPAGATION, KINETICS, RADIATION, AND SCALING CRITERIA

Science Applications International Corporation

CODR APPENDIX

(CALCULATIONS)

VOLUME OF THE EXPERIMENTAL CHAMBER

$$n_F = m_F/M_F = \dot{m}_F t/M_F = \rho_F \dot{V}_F t/M_F = P_o \dot{V}_F t/\hat{R}T_o$$

$$F + iO \longrightarrow jP + kP'$$

$$n_{O,b} = i n_F = i P_o \dot{V}_F t/\hat{R}T_o \;, \quad n_{O,b} = n_{O,i} - n_{O,f}$$

$$x = n_{O,b}/n_{O,i} \;, \quad \phi = n_I/n_{O,i}$$

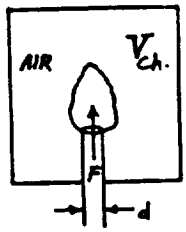

HERE, n = NO. OF MOLES, $\dot{m}$ = MASS FLOW RATE, m = MASS, t = EXPERIMENT TIME, M = MOLECULAR WEIGHT, ρ = DENSITY, $\dot{V}$ = VOLUME FLOW RATE, P = PRESSURE, $\hat{R}$ = UNIVERSAL GAS CONSTANT, T = TEMPERATURE, F = FUEL, O = OXIDIZER, P' = CO_2, P'' = H_2O, AND i,j, and k = STOICHIOMETRIC COEFFICINETS FOR COMPLETE COMBUSTION; SUBSCRIPTS: F = FUEL, O=OXIDIZER, o AND I = INITIAL CONDITION, f = FINAL CONDITION, b = BURNED, AND I = INERT (NITROGEN).

ASSUMPTIONS:

A) BURNING OF FUEL HAS NEGLIGIBLE EFFECT ON TOTAL NO. OF MOLES.
B) CONSTANT T AND P IN THE CHAMBER DURING BURNING.

$$\therefore \; V_{Ch.} = n_{air}\hat{R}T_o/P_o = (n_I + n_{O,i})\hat{R}T_o/P_o = (\phi+1)\, n_{O,i}\hat{R}T_o/P_o$$

$$= (\phi+1)(n_{O,b}/x)\hat{R}T_o/P_o = (\phi+1)\, i P_o \dot{V}_F t \hat{R}T_o/x\hat{R}T_o P_o$$

$$\boxed{V_{Ch.} = (\phi+1)\, i \dot{V}_F t/x}$$

Science Applications International Corporation

VOLUME OF THE EXPERIMENTAL CHAMBER (CONTD)

Chamber Environment: 90% N_2 and 10% O_2 (ϕ = 9), T = 298K,
P = 1/2 atm or 1 atm

X ≡ no. of moles of O_2 burned/initial no. of moles of O_2

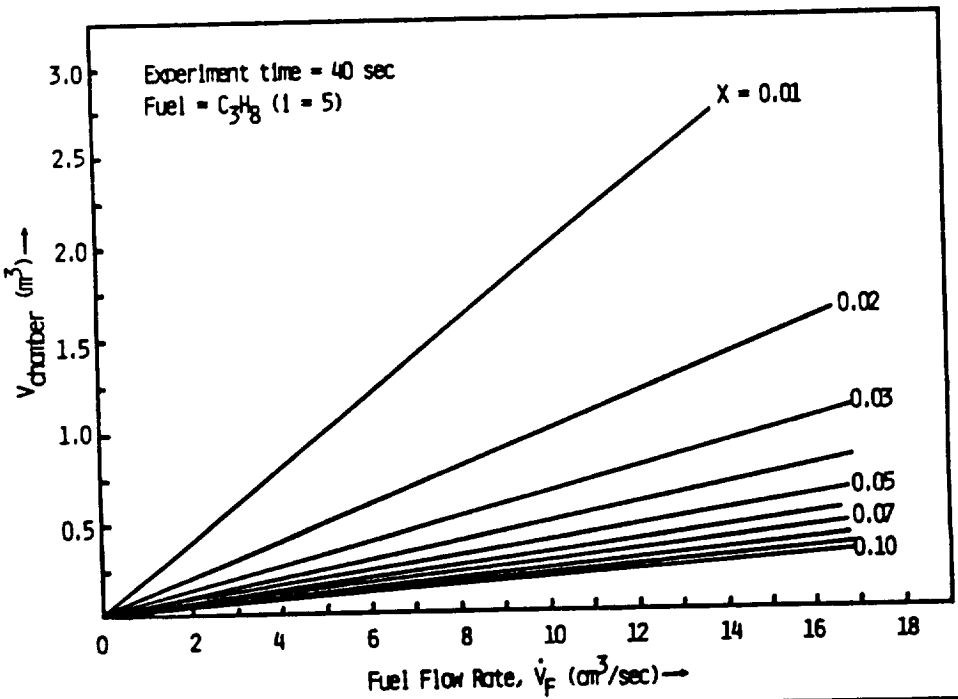

VOLUME OF THE EXPERIMENTAL CHAMBER (CONTD)

Chamber Environment = Air (79% N_2 and 21% O_2, $\phi = 3.76$), T = 298K,

P = 1/2 atm or 1 atm

X ≡ no. of moles of O_2 burned/initial no. of moles of O_2

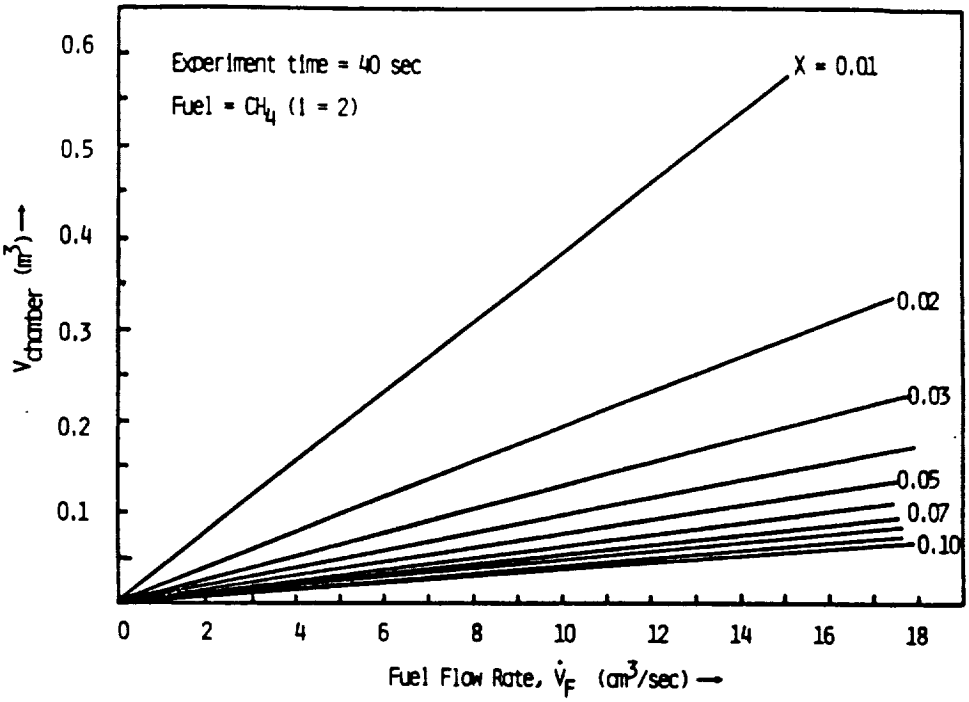

SAIC

Science Applications International Corporation

VOLUME OF THE EXPERIMENTAL CHAMBER (CONTD)

Chamber Environment: 90% N_2 and 10% O_2 ($\phi = 9$), T = 298K,

P = 1/2 atm or 1 atm

X ≡ no. of moles of O_2 burned/initial no. of moles of O_2

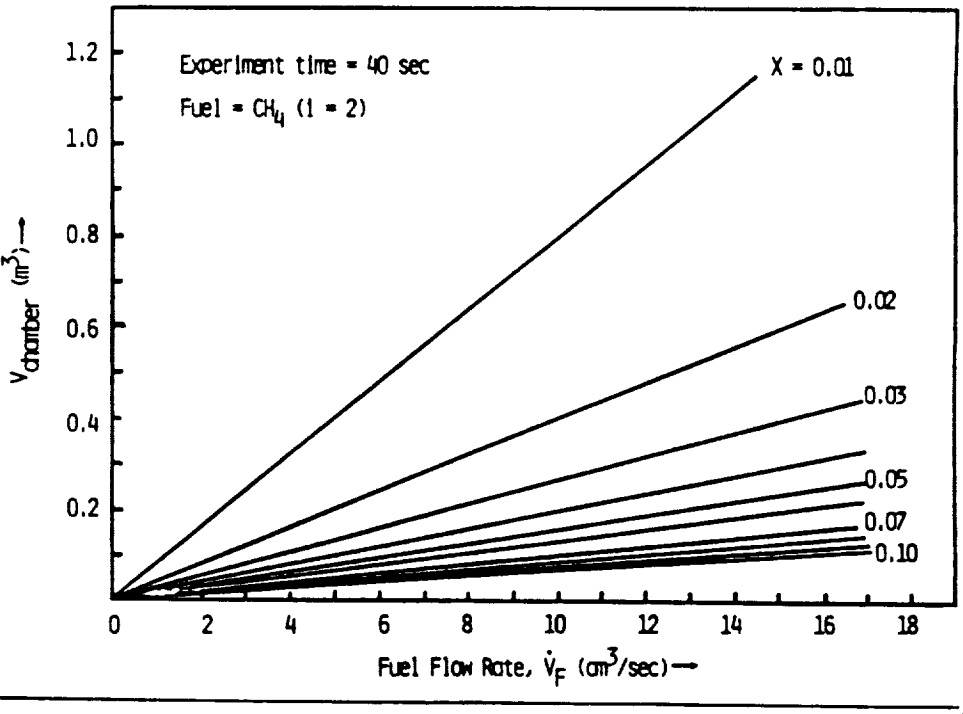

SAIC

VOLUME OF THE EXPERIMENTAL CHAMBER (CONTD)

Chamber Environment = Air (79% N_2 and 21% O_2, ϕ = 3.76), T = 298K

P = 1/2 atm or 1 atm

X ≡ no. of moles of O_2 burned/initial no. of moles of O_2

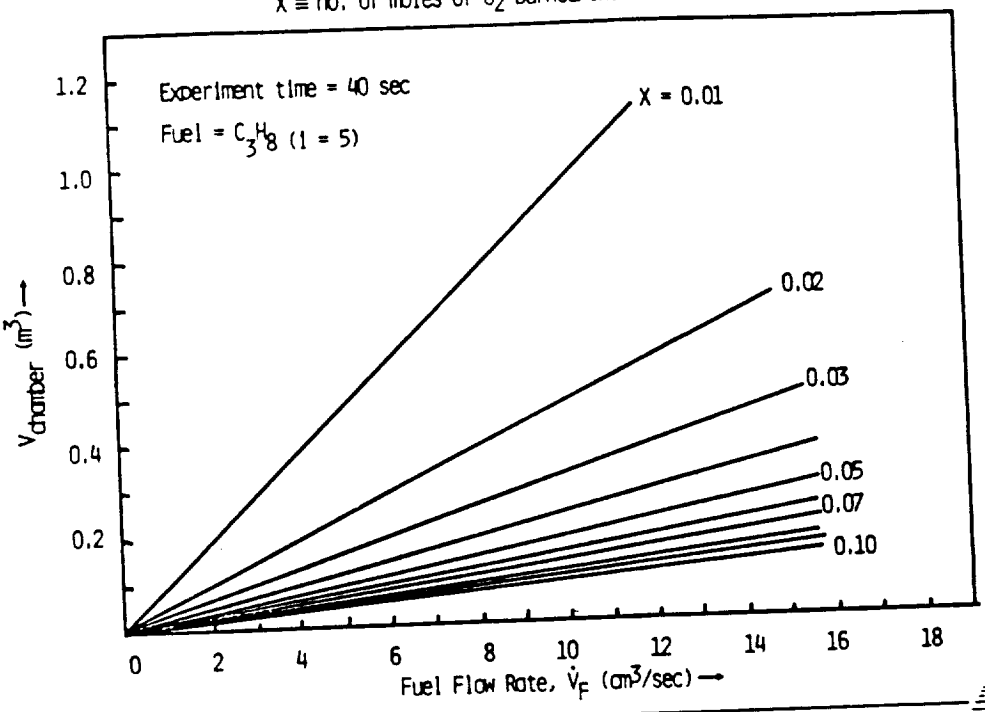

SAIC

FIRST FLIGHT

- SIX FLAMES.
- CHAMBER PRESSURE = 1 atm.
- CH_4/AIR FLAMES.
- TWO NOZZLES.
- 40 SECONDS PER FLAME EXPERIMENT TIME.
- EXPERIMENT CONDUCTED IN SPACELAB OR MSL.

SAIC

CONDITIONS; FIRST FLIGHT

	FLAMES A			FLAMES B			Σ	COMMENTS
	A1	A2	A3	B1	B2	B3		
FUEL	CH_4	CH_4	CH_4	CH_4	CH_4	CH_4	—	———
OXIDIZER	AIR	AIR	AIR	AIR	AIR	AIR	—	———
NOZZLE RADIUS (cm)	0.051	0.051	0.051	0.0825	0.0825	0.0825	—	———
INITIAL CHAMBER PRESSURE (atm)	1	1	1	1	1	1	—	———
INITIAL CHAMBER TEMPERATURE (K)	295	295	295	295	295	295	—	———
EXPERIMENT TIME (SEC)	40	40	40	40	40	40	—	———
FUEL FLOW RATE (cm^3/sec)	0.75	1.60	2.80	1.00	2.90	4.55	—	———
FUEL VELOCITY (cm/sec)	91.8	195.8	342.7	46.8	135.6	212.8	—	———
FUEL REYNOLDS NUMBER	28.4	60.6	106.0	23.4	67.9	106.5	—	———

SAIC

Science Applications International Corporation

CONDITIONS; FIRST FLIGHT (CONTD)

	FLAMES A			FLAMES B			Σ	COMMENTS
	A1	A2	A3	B1	B2	B3		
CHAMBER VOLUME (m^3)	0.058	0.058	0.058	0.058	0.058	0.058	—	SELECTED BASED ON = 10% O_2 CONSUMPTION AT THE END OF THE EXPERIMENT
% O_2 BURNED, X	0.5	1.1	1.9	0.7	2.0	3.0	-9.2	———
GAS-TEMPERATURE RISE, ΔT (K)	21	45	77	29	82	122	—	USING THE PREVIOUSLY-DERIVED EQUATION.
PRESSURE RISE, ΔP (atm)	0.07	0.15	0.26	0.10	0.28	0.42	—	USING THE PREVIOUSLY-DERIVED EQUATION.
HEAT RELEASE (kJ)	1.0	2.1	3.6	1.3	3.8	5.9	17.7	USING THE PREVIOUSLY-DERIVED EQUATION.

SAIC

Science Applications International Corporation

CONDITIONS; FIRST FLIGHT (CONTD)

	FLAMES A			FLAMES B			Σ	COMMENTS
	A1	A2	A3	B1	B2	B3		
MASS OF FUEL (gr)	0.020	0.043	0.074	0.027	0.077	0.121	0.362	———
MASS OF H_2O (gr)	0.045	0.097	0.167	0.061	0.173	0.272	0.815	BASED ON STOICHIOMETRIC COMBUSTION WITH CO_2 AND H_2O AS PRODUCTS
MASS OF ALUMINUM CHAMBER (kg), HEIGHT/ DIAMETER = 2	37.84	37.84	37.84	37.84	37.84	37.84	—	BASED ON A CYLINDRICAL CHAMBER WITH 1.5 cm THICK-NESS.
MAXIMUM ALUMINUM TEMPERATURE RISE (K)	0.03	0.07	0.11	0.04	0.12	0.18	—	ASSUMING THAT ALL OF THE HEAT RELEASE IS SUDDENLY TRANSFERRED TO THE METAL.

SAIC

Science Applications International Corporation

CONDITIONS; FIRST FLIGHT (CONTD)

	FLAMES A			FLAMES B			Σ	COMMENTS
	A1	A2	A3	B1	B2	B3		
MAX. CO PRODUCED(% $^{V}/v$)	0.05%	0.11%	0.19%	0.07%	0.20%	0.32%	0.94%	BASED ON $CH_4 + 1.5\ O_2 - CO + 2H_2O$. NOTE THAT LOWER FLAMMABILITY LIMIT OF CO + H_2O IN AIR = 12.5% $^{V}/v$.
CH_4 RELEASED IN THE CHAMBER (% $^{V}/v$)	0.05%	0.11%	0.19%	0.07%	0.20%	0.32%	0.94%	NOT FLAMMABLE BECAUSE LOWER FLAMMABILITY LIMIT IS 5.3% AT ATMOSPHERIC P AND T.
ORIGINAL MASS OF AIR IN CHAMBER (gr)	—	—	—	—	—	—	68.88	BASED ON 21% O_2, 79% N_2 AT 1 atm AND 295K

SAIC

CONDITIONS; FIRST FLIGHT (CONTD)

	FLAMES A			FLAMES B			Σ	COMMENTS
	A1	A2	A3	B1	B2	B3		
MINIMUM CHAMBER VOLUME IF ONE CHAMBER PER FLAME (m^3)	0.0029	0.0061	0.0107	0.0038	0.0110	0.0173	——	BASED ON 10% OXYGEN CONSUMPTION FOR EACH FLAME.
OCCUPIED VOLUME IN THE FUEL TANK (cm^3)	3.0	6.5	11.2	4.1	11.7	18.4	55	BASED ON THE SUGGESTED DESIGN OF FUEL TANK, P= 10 atm.

Science Applications International Corporation

MOTION INDUCED IN THE CHAMBER DUE TO JET MOMENTUM

$$u_{jet}\,\dot{m}_{jet}\,t_{test} = m_{air}\,u_{air}$$

$$u_{air} = m_{jet}\,u_{jet}/m_{air}$$

For $V_{chamber} = 0.058\ m^3$, $m_{air} = 68.88$ gr

	Flames A			Flames B		
	A1	A2	A3	B1	B2	B3
u_{jet}, cm/s	91.8	195.8	342.7	46.8	135.6	212.8
m_{jet}, gr	0.02	0.043	0.074	0.027	0.077	0.121
$u_{air,\ induced}$, cm/s	0.03	0.12	0.37	0.02	0.15	0.37

REFERENCE DOCUMENTS

- KHB 1700.7 (Nov. 1982) — "Space Transportation System: Payload Ground Safety Handbook"
- JSC-21000-PIP-SML (Basic, June 1985) — "Shuttle/Payload Standard Integration Plan for Small Payload Accomodation"
- LeRC/MSIS (Draft, Feb. 1984) — "Principal Investigator's Guide to STS Materials Science Experiments"
- NHB 1700.7A — "Safety Policy and Requirements for Payloads Using the Space Transporation System (STS)"
- HB-SI-09-84-1100 (Draft, Sep. 1984) — "MSL Users Handbook"
- NHB 8060.1B (Sep. 1981) — "Flammability, Odor, and Offgassing Requirements and Test Procedures for Materials in Environments that Support Combustion"
- JSC-11123 (Change 1, Sep.1978) — "Space Transportation System Payload Safety Guidelines Handbook"
- JSC-13830A (May 1983) — "Implementation Procedure for STS Payloads System Safety Requirements"
- JSC-18798 (Feb. 1983) — "Interpretation of STS Payload Safety Requirements"
- ICD 2-1 M001 (March 1984; Errata: Dec. 1984) — "Orbiter Middeck/Payload Standard Interfaces Control Document"
- JSC-14084 (Sep. 1983) — "Shuttle/Payload Standard Integration Plan for Middeck-Type Payloads"
- JSC-16536 (Rev. B: Sep. 1982) — "Orbiter Middeck Payload Provisions Handbook: Experiments and Operations-Support Division"

Science Applications International Corporation

REFERENCE DOCUMENTS (CONTINUED)

- JSC-20052 — "Space Shuttle Payload: Design and Development"
  - Vol. 1 (Rev. B, Feb. 1985): Executive Overview,
  - Vol. 2 (Rev. B, Feb. 1985): Avionics Interfaces and Requirements,
  - Vol. 3 (Rev. B, Feb. 1985): Flight Design Guidelines and Requirements,
  - Vol. 4 (Rev. 1, Sep. 1984): Kennedy Space Center Operations,
  - Vol. 5 (Rev. B, Feb. 1985): Management Documentation,
  - Vol. 6 (Rev. B, Feb. 1985): Mission Operations Interfaces,
  - Vol. 7 (Rev. B, Feb. 1985): Safety Guidelines and Requirements,
  - Vol. 8 (Rev. B, Feb. 1985): Structural/Mechanical Interfaces and Requirements,
  - Vol. 9 (Rev. 1, Sep. 1984): Thermal Interfaces and Requirements.
- JSC-14363 — "Shuttle/Payload Integration Activities Plan"
- JSC-SE-R-0006B — "General Specifications NASA/JSC Requirements for Materials and Processes"
- JSC-14095 — "Requirements for the Orbiter Crew Compartment"
- JSC-07700 — "Volume XIV Mission Integration Control Board Configuration"
- MSFC-SPEC-522 — "Design Criteria for Controlling Stress Corrosion Cracking"
- JSC-08962 — "Compilation of VCM Data of Nonmetallic Materials"

Section 4

"Effects of Buoyancy on Gas-Jet Diffusion Flames: Experiment and Theory"

R. B. Edelman and M. Y. Bahadori

Acta Astronautica, Vol. 13, No. 11/12, pp. 681-688, 1986

"Effects of Buoyancy on Gas-Jet Diffusion Flames: Experiment and Theory," by Edelman and Bahadori, could not be included in this report, but may be found in Acta Astronautica.

Section 5*

"LAMINAR DIFFUSION FLAMES UNDER MICRO-GRAVITY CONDITIONS"

R. B. Edelman, M. Y. Bahadori, S. L. Olson, and D. P. Stocker

Paper AIAA-88-0645, AIAA 26th Aerospace Sciences Meeting, Reno, Nevada, January 1988

* A revised version of this paper has been published in the AIAA Journal (see Section 9).

AIAA'88

AIAA-88-0645
Laminar Diffusion Flames Under Micro-gravity Conditions

R. B. Edelman and M. Y. Bahadori, Science Applications International Corp., Chatsworth, CA; and S. L. Olson and D. P. Stocker, National Aeronautics and Space Administration, Lewis Research Center, Cleveland, OH

AIAA 26th Aerospace Sciences Meeting

January 11-14, 1988/Reno, Nevada

Paper AIAA 88-0645

AIAA 26th Aerospace Sciences Meeting, January 12-15, 1988, Reno, Nevada

LAMINAR DIFFUSION FLAMES UNDER MICRO-GRAVITY CONDITIONS

Raymond B. Edelman* and M. Yousef Bahadori†
Science Applications International Corporation
Combustion Science and Advanced Technology Department
Chatsworth, California

and

Sandra L. Olson‡ and Dennis P. Stocker§
National Aeronautics and Space Administration
Lewis Research Center
Cleveland, Ohio

Abstract

This paper presents the results of an on-going experimental and theoretical effort for the study of laminar gas-jet diffusion flames under micro-gravity conditions. Preliminary results of ignition studies of methane and propane flames in the 2.2-second NASA-Lewis Drop Tower (gravity level $<10^{-5}$g) are presented. Also, theoretical analyses leading to the definition of experiments to be conducted in the NASA-Lewis 5.18-second Zero-Gravity Facility (gravity level $<10^{-5}$g) and the KC-135 airplane (free-floating) are described. Experimental and theoretical studies show that under reduced-gravity conditions, laminar diffusion flames are strongly affected by the combined effects of kinetics, radiation and transient phenomena (i.e., flame ignition, stabilization and extinction). The results of calculations for flames in zero-gravity are presented and ignition of a family of flames in micro-gravity which reach a near-steady state in the 2.2-second available time is reported and analyzed. Observations on the distinct nature of the flame color and luminosity in micro-gravity are described and the flame behavior under transient, high-deceleration rates is discussed. The design of the test hardware along with the description of the types of measurements and instrumentation being used in the continuation of this work are briefly discussed.

1. Introduction

Laminar gas-jet diffusion flames under micro-gravity conditions have shown distinct characteristics relative to the flames in normal gravity.[1-9] Aside from the primary goal of understanding the behavior of fires in spacecraft environments, isolation of the effects of buoyancy aids the analysis of the coupled physico-chemical phenomena of radiation, kinetics, convection, and diffusion for flames in normal-gravity conditions. As a result, the modeling efforts can benefit from the removal of one coupled constraint (i.e., buoyant force) from the formulation of the problem. Extensive studies of micro-gravity gas-jet diffusion flames in the past [1-9] have paved the way for a comprehensive, theoretical and experimental research effort, of which, the present paper is the preliminary outcome.

The background and results of the past efforts on laminar flames in micro-gravity environments are presented in Sec. 2. Section 3 gives a description of the apparatus. In Sec. 4, the experimental procedure is described. Section 5 presents the results and data comparisons, followed by the conclusions and description of the future efforts in Sec. 6.

2. Background

Experimental and theoretical efforts on the study of gas-jet diffusion flames in micro-gravity environments are described and analyzed in a recent publication. [9] Assessment of the existing data obtained under reduced-gravity conditions has shown that further research is required before reliable predictions of ignition, stabilization and propagation of the flames under micro-gravity conditions can be made. In this section, a brief description of the studies conducted toward the understanding of the behavior of laminar diffusion flames in reduced-gravity environments is presented.

Experimental Efforts

Studies of gas-jet diffusion flames under micro-gravity conditions have been conducted in the 2.2-second NASA-Lewis Drop Tower ($<10^{-5}$g). Methane, hydrogen, propylene, and ethylene flames have been extensively studied. [1-8] In these studies, the flames were ignited in normal gravity, allowed to reach steady state, and then the experiment package was dropped inside a falling drag shield. High-speed movies of the flames have shown that during the transitory period of adjustment from normal-gravity to micro-gravity, a sudden decrease in the flame height occurred within ~0.05 seconds. After the decrease of the flame height to a minimum, i.e., $0.6 < h_{min}/h_{1-g} < 1.0$ (depending on the jet Reynolds number), the flame height began to increase with time, resulting in extinction with $1.0 < h_{ex}/h_{1-g} < 1.3$, reaching an apparent steady state with $1.4 < h_{0-g}/h_{1-g} < 1.7$, or remaining in a transitory state by the time the package came to rest in a sand box at the bottom of the tower. Compared to the flames in normal-gravity, larger, rather globular flames are observed in micro-gravity which are due to the absence of buoyant force, making diffusion the major mechanism of transport. The orange-reddish appearance of these hydrocarbon flames [1-8] is due to the significant amounts of solid carbon formed by pyrolysis in the hot fuel-rich portion of the flames.

The observed flame behavior in micro-gravity, i.e., reaching an apparent steady state, being in a transient mode, or extinguishment, has been attributed to the influence of the jet Reynolds

*Assistant Vice President, Director; Member AIAA
†Senior Staff Scientist; Member AIAA
‡NASA Project Scientist
§NASA Experiment Manager

number, i.e., the combined effects of nozzle size, jet velocity and fuel type. Figure 1 shows the behavior of two methane-air flames [1,4] in micro-gravity, i.e., an extinguished flame [Fig. 1(a)] and a flame which apparently reached steady state [Fig. 1(b)] within the 2.2 seconds of the drop. The data suggest that for a certain range of fuel velocity, a transient period occurs between a near-steady state and flame extinguishment. However, the results of the present study (see the section on experimental results) have shown that a majority of the flames which were in a transitory state in the previous studies were indeed ignited and reached a near-steady state once the flame was ignited in micro-gravity. The source of the difference in the behavior of the flame is the method of ignition. If the flame is ignited in normal-gravity and then dropped, the transitional behavior is due to the accumulation of the hot products of combustion in the flame region which results from the sudden loss of the buoyancy-driven convective flow. This can enhance soot formation, radiation cooling and the onset of a chemical kinetic limitation on the heat release process. The combination of these effects leads to either quenching or a slow readjustment to a steady-state flame, depending on the jet momentum and the fuel mass-flow rate. Even a flame which reaches an apparent steady state [Fig. 1(b)] shows some oscillations at the final stages of the drop which suggests that the flame may be in transition from a transient state to extinguishment.

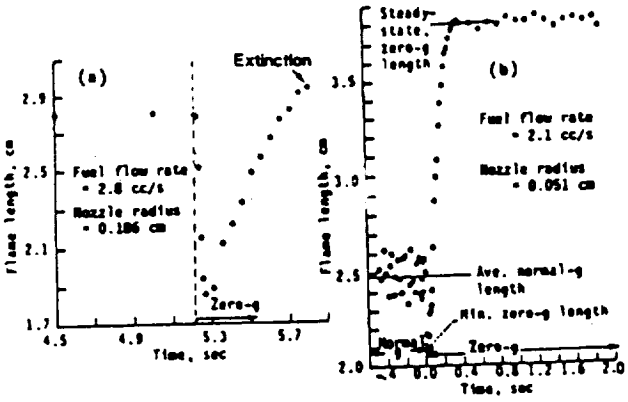

Fig. 1 Methane-air flame lengths as a function of time in micro-gravity for (a) an extinguished flame, [1] and (b) a flame which reached an apparent steady state at the end of the drop. [4]

The sensitivity of the extinguishment process to convective transport has been demonstrated; [8] low forced-air velocities ($\simeq$10 cm/s) in co-axial jets of methane-air diffusion flames in micro-gravity were sufficient to sustain combustion for methane flow rates that otherwise resulted in extinguished flames. The ignition approach, i.e., igniting the flame in normal-gravity and then dropping the apparatus, the test time limitation of 2.2 seconds, and the lack of quantitative data have so far been the weaknesses in achieving a more fundamental and quantitative understanding of gas-jet diffusion flames in micro-gravity environments. However, this past experimental and theoretical work [1-8] has provided the basis for the focused, quantitative approach described in this paper.

Theoretical Studies

A mathematical model has been developed [6,7] for the study of laminar gas-jet diffusion flames under arbitrary gravitational accelerations based on the parabolic form of the equations of motion. The model includes the effects of inertia, viscosity, diffusion, radiation, and chemical reactions. The differencing scheme is an explicit finite-difference technique. The chemistry assumed is that of shifting equilibrium, and both Fickian and multi-component diffusion are considered. Figure 2 shows a comparison between the predicted and measured flame heights under both normal-gravity and zero-gravity conditions. Excellent agreement was obtained for flame height predictions (Fig. 2). However, it was shown [6,7] that accurate flame shape predictions require an accurate prediction of the relative rates of the molecular transport of species, momentum and energy.

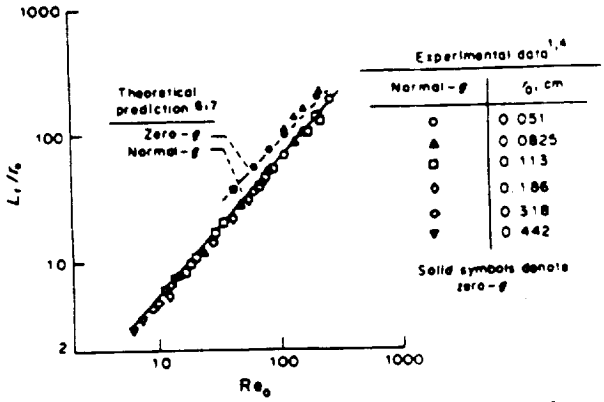

Fig. 2 Comparisons between the theoretical predictions and experimental results for non-dimensional flame heights vs. jet Reynolds numbers; methane-air flames. [6,7]

Flame ignition and development toward steady state in zero gravity requires a time-dependent analysis. An analytical model was developed [9] for the shapes and heights of zero-g, laminar, cylindrically symmetric, transient diffusion flames with the effects of axial diffusion included. The analysis shows that the theoretical steady-state flame lengths are approached slowly. However, the theory did not include the effects of radiation and kinetics. As a result, the predicted approach to steady state may be faster if these effects were taken into account. Figure 3 shows a comparison between the analytical and experimental flame heights under micro-gravity conditions, where D is the binary diffusion coefficient of methane in nitrogen, U is the fuel velocity, R_o is the nozzle radius, h_{ss} is the theoretical steady-state flame height, and a value of D = 1 cm^2/s corresponds to a temperature of 750 K.

Flames can be strongly affected by the level of gravitational acceleration acting upon them. The change in the flame behavior due to the convective effects can be seen in Fig. 4, where the centerline velocity as a function of axial distance for different gravitational levels is shown. [9] In Fig. 4, U_o = 93.5 cm/s is the velocity of the methane jet and L = 50 cm is the normalizing axial distance, with the nozzle radius = 0.0825 cm.

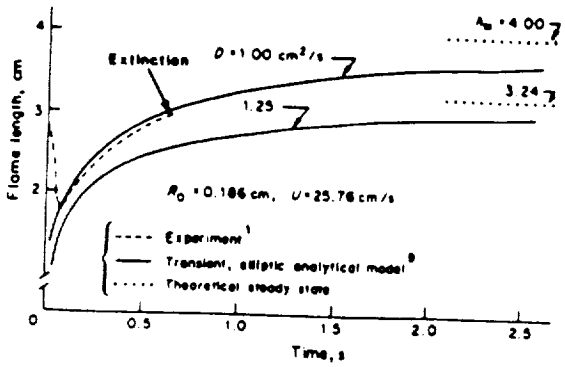

Fig. 3 Analytical and experimental variations of flame heights with time under micro-gravity conditions. 9

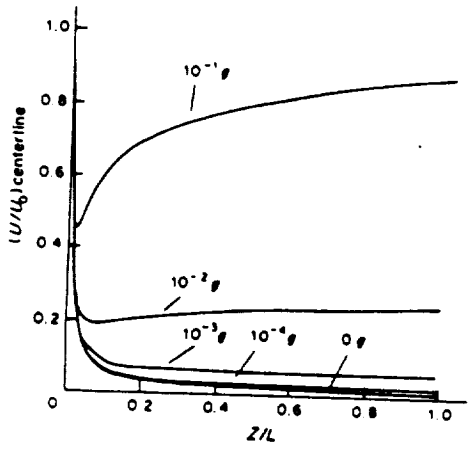

Fig. 4 Centerline velocity vs. axial distance along the jet for a methane-air flame as a function of gravitational level. 9

Residual accelerations (i.e., g-jitter) can cause fluctuations in flame height. These accelerations exist in the KC-135 airplane and in the spacecraft during maneuvering. Using an order-of-magnitude analysis for the governing equations and with the aid of the steady-state model 6,7 already described, an approximation for the effects of frequency of oscillations in the g-level on the flame height can be obtained. Figure 5 shows a result of such analysis. The calculation was performed for a methane-air flame with a jet velocity of 93.5 cm/s, nozzle radius of 0.0825 cm, gravity level of 10^{-3}g, and a 3% allowable fluctuation in flame height. In Fig. 5, any combination of amplitude ($\hat{g}$) and frequency (ω) of jitter which results in a point above the solid curve must be damped.

The steady-state model described previously is not only applicable to the description of the fundamental processes, but also to the design of the experiment described in the next section. For example, by injecting different fuel-flow rates in air, the flammable region which the spark must pass through for successful ignition of the flame in zero-gravity is identified. Figure 6 shows an example of such a calculation.

In Fig. 7, temperature distributions above a flame at different axial locations are shown. Results of this nature have aided in identifying the proper locations for the instrumentation (e.g., thermocouples and sampling probes).

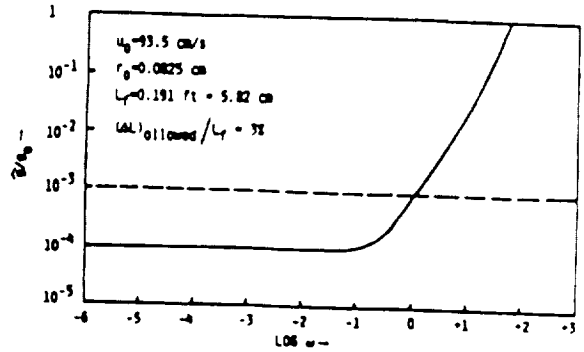

Fig. 5 Effect of residual accelerations and the dampening requirement.

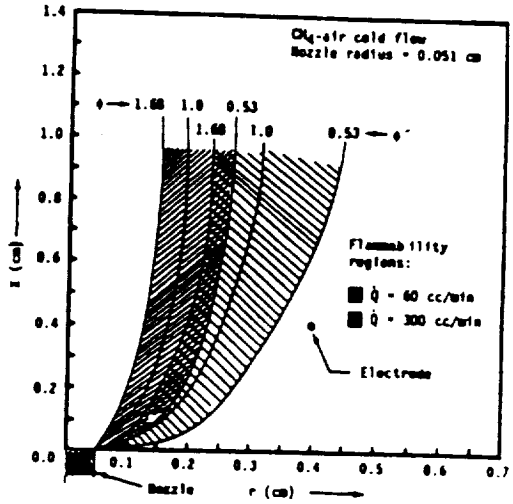

Fig. 6 Flammability regions for cold jets of methane in air.

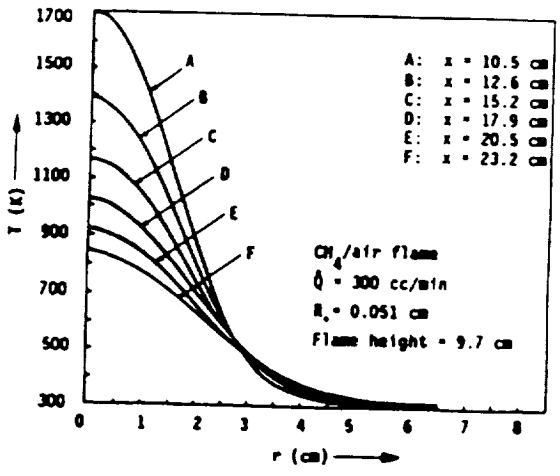

Fig. 7 Temperature distributions above a methane-air flame in micro-gravity.

The transient effects described in this section, i.e., ignition, flame development toward steady state, extinction, sensitivity to the effects of chemical kinetics, and the attended radiation as affected by these processes, cannot

be adequately analyzed without a more complete transient, multi-dimensional analysis of these flames. The intent of the experimental data, i.e., temperature, species and radiation measurements is largely to provide support in the formulation and validation of such a model that is under development in this research.

3. Apparatus

The experimental studies were conducted in the 2.2-second NASA-Lewis Drop Tower (Fig. 8). The tower consists of a building 6.4 x 6.4 x 30.5 m. The drop area in the building is 1.5 x 2.75 x 27 m. The 2.2-second period of micro-gravity was obtained by allowing the experiment package to free-fall from the eighth floor. The experiment was suspended from the ceiling by a highly stressed music wire, and then released by pressurization of an air cylinder that forced a knife edge into the support wire which rested against an anvil.

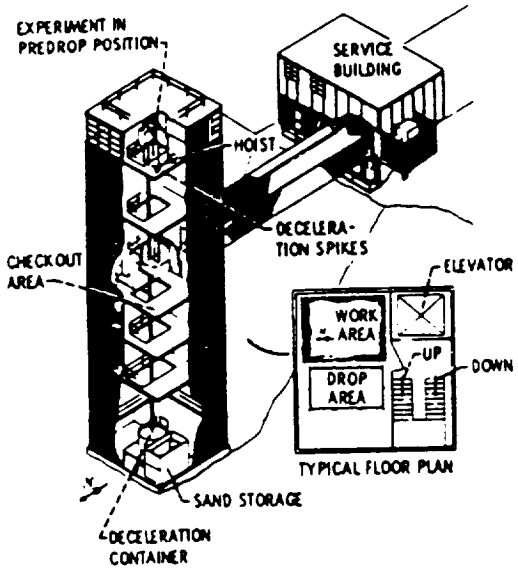

Fig. 8 2.2-second drop tower.

The experiment package was allowed to free-fall inside a protective air-drag shield (Fig. 9). The drag shield had a high ratio of weight to frontal area and a low drag coefficient, resulting in a gravity level of less than 10^{-5}g acting on the experiment package during the 23-m fall. The aluminum spikes of the drag shield decelerated the package in a sand container located at the bottom of the drop tower.

The experiment package and a schematic diagram of the flow system are shown in Figs. 10 and 11, respectively. The apparatus consists of a combustion chamber which contains a burner, the lighting system, a viewing port for the high-speed camera, the spark ignitor, and ports for filling the chamber with oxidizer and venting the burned gases. The other components of the system were a metering valve, solenoid valve, pressure gauge, pressure regulator, fuel bottle, hand valves, and vents. The volume of the combustion chamber was approximately 40,000 cm^3. Two fuel nozzles with inside radii of 0.051 cm and 0.0825 cm were used in the studies. The detailed sketch of the burner and dimensions of the tubes are shown in Fig. 12. The

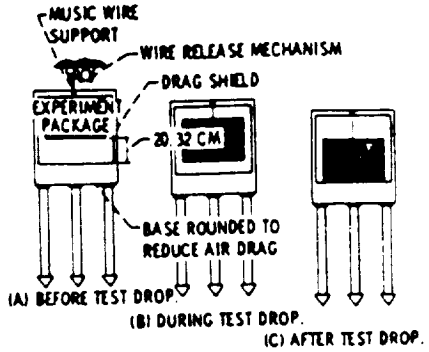

Fig. 9 Position of the experiment package relative to the drag shield.

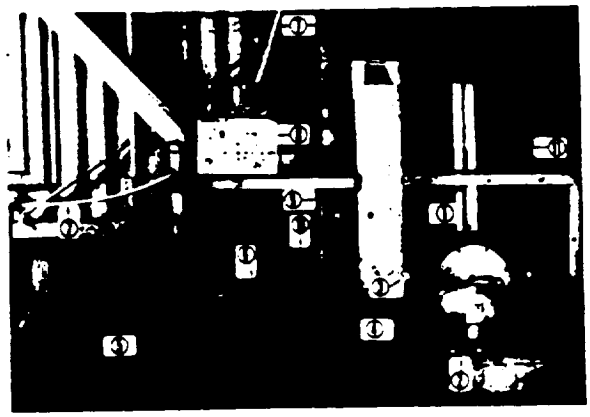

Fig. 10 Experiment package: ① Combustion chamber; ② Flowmeter; ③ Viewing window partially hidden by strut; ④ Solenoid valve hidden by strut; ⑤ Mixing system; ⑥ Pressure regulator; ⑦ Fill line; ⑧ Control panel; ⑨ Fuel bottle; ⑩ Camera partially hidden by regulator and fuel bottle; ⑪ to vent.

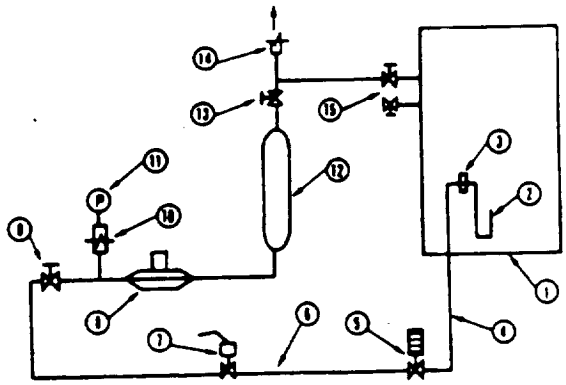

Fig. 11 Schematic diagram of the flow system: ① Experiment chamber; ② Burner nozzle; ③ Chamber bulkhead; ④ 1/8 in. o.d. tubing; ⑤ Metering valve with Vernier markings; ⑥ 1/4 in. o.d. tubing; ⑦ Solenoid valve; ⑧ Pressure regulator; ⑨ Hand valve; ⑩ Quick disconnect; ⑪ Pressure gauge; ⑫ Fuel bottle; ⑬ Hand valve; ⑭ Quick disconnect; ⑮ Vents.

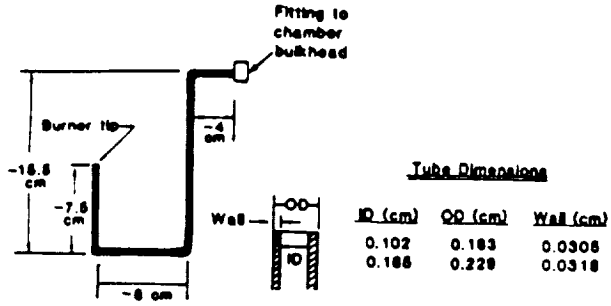

Fig. 12 Sketch of the burner and tube dimensions.

burner tips were cut off and were not machined to a sharp edge. The high-speed Milliken movie camera (16mm) was originally set for a rate of 40 frames per second. As a result, some of the low-flow rate flames were not quite visible in the processed (Tungsten Eastman Ektachrome Video News) films. Visibility was subsequently improved by reducing the framing rate to 20 frames/sec.

As previously cited, theoretical calculations were used to guide the location of the spark electrode at 4 mm above the nozzle tip and 4 mm away from the nozzle centerline. The electrode was positioned approximately 90° to the centerline of the camera. A ground wire was attached to the nozzle, making it the second electrode. A schematic diagram of the electrical system for the ignitor is shown in Fig. 13. The spark energy and frequency were approximately 18 mJ and 4.8 Hz, respectively. For all of the tests, the spark-ignition system was left on for the entire test time of 3.0 seconds, i.e., 2.2 seconds under micro-gravity condition and about 0.8 seconds after impact. The ignitor occasionally did not spark at the burner tip but shorted out elsewhere. However, this did not affect the flame behavior. A frame-by-frame study of the movies showed no disturbance of the flames by the spark during the 3.0 seconds of burning.

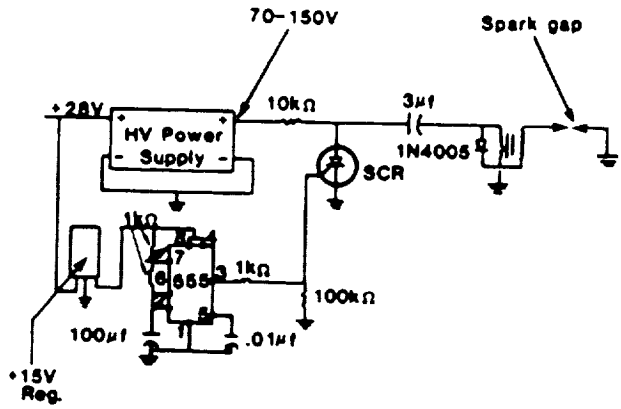

Fig. 13 Electrical system for the ignitor.

The metering valve (with Vernier markings) was calibrated for 1 psig upstream pressure, and the pressure regulator had a 0-5 psig capability. The fuel bottle was approximately 500 cm^3 in volume, filled with either methane or propane. The dry air in the combustion chamber was composed of 21% oxygen and 79% nitrogen, and had a pressure of 1.0 ± 0.01 atm in the chamber.

4. Experimental Procedure

Methane and propane flames were ignited under both normal-gravity and micro-gravity conditions and the flame behavior was recorded during the 3.0 seconds of burning. This section describes briefly the initial setup, test setup, normal-gravity test, drop-test preparation, drop-test procedure, post-drop procedure, and post-test procedure.

Initial Setup

The desired nozzle size was installed in the experimental chamber and the spark electrode was positioned. After sealing and evacuating the chamber, dry air was introduced in the chamber to raise the pressure to 1.0 ± 0.01 atm. The fuel bottle was then evacuated and filled with either methane or propane to approximately 2.0 atm. The fuel pressure regulator was set for a pressure difference of 1 psi, and the film was loaded in the high-speed camera.

Test Setup

The total test time and the desired duration for the spark generation were set. The filming rate was selected and the fuel flow rate was set using the calibrated metering valve.

Normal-Gravity Testing

Before conducting the particular normal-gravity test, several tests (not filmed) were conducted to verify ignition and fine-tune the pressure regulator. After successful ignitions, the normal-gravity test was filmed. The lights in the room were dimmed and the chamber window and camera were covered. This was not necessary in the drop tests because the experiment package was inside the drag shield. The master and camera jumpers were installed and the master switch was turned on. By turning on the ready switch, the chamber light was automatically turned on. The movie camera was started and given approximately 3.0 seconds for start-up, at which time the master and camera jumpers were quickly removed, causing the chamber light to go out, the fuel solenoid valve to open and the spark generator to start. After the test was completed, the camera stopped, the solenoid valve was closed and the spark ignitor stopped. The master, ready and camera switches were then turned off. The film was advanced (to leave a blank space) by installing the camera jumper and turning the camera switch on for a few seconds.

Drop-Test Preparation

The pressure gauge was removed to prevent unnecessary fatigue during the deceleration period. The experiment package was placed in the drag shield and hoisted to the top of the tower. The master and camera jumpers were then connected through the drag shield. A pre-drop burn (not filmed) was conducted while the package was at the top of the tower to ensure that there was enough fuel at the burner tip. The switches were then turned off and the master jumper was reconnected. The camera jumper was connected to a remote switch so that the connection could be made without disturbing the package.

Drop-Test Procedure

The master, ready and camera switches were turned on, resulting in the turning on of the chamber light. The camera did not start here as the jumper connection was open at the camera jumper switch. The drag shield was then closed and the package was steadied as it was connected to the music wire. The camera jumper switch was turned on, and after allowing approximately 3.0 seconds for the camera start-up, the drop was initiated. This was accomplished by cutting the wire via a hydraulically powered blade with the help of the weight of the package. The jumpers were pulled, resulting in the start of the experiment. Table 1 shows the drop sequence.

Post-Drop Procedure

The drop package was electrically grounded to dissipate any charge built up on penetration into the sand. The package was hoisted back up to the preparation area. The master, ready and camera switches were turned off. The package was removed from the drag shield. The film was advanced to leave a blank space on the film between two tests. The pressure gauge was reattached and checked for any changes in the fuel-bottle pressure. Then, the test set-up procedure was repeated for the next test.

Post-Test Procedure

The excess fuel in the fuel bottle was burned off and the bottle and experiment chamber were evacuated, exhausting the contents outdoors. The film was removed from the camera (if necessary) and the batteries were recharged (if necessary).

5. Results

Table 2 shows the experimental conditions and the average steady-state flame lengths, maximum flame radii, and approximate time to reach steady state for both normal-gravity and micro-gravity methane and propane flames. The normal-gravity flames were flickering in most cases and the steady-state flame heights and maximum radii are the averages. Figures 14 and 15 show the flame lengths as a function of time for methane and propane flames in micro-gravity, respectively. The methane flames at low volume-flow rates were very faint. However, they were sufficiently visible to identify the maximum radius, but beyond this height, visible radiation could not be observed and the flame appeared to be under-ventilated. This is shown by the truncated data given in Fig. 14. The planned longer-time experiments together with temperature and concentration measurements will help to clarify the structure of these flames. The higher-flow rate methane flames reached near-steady state with some fluctuations at the later times. These flames with a 0.0825-cm nozzle radius were in a transient state in the previous studies [4] where the flames were ignited in normal-gravity and then dropped. Figure 16 shows the corresponding comparisons.

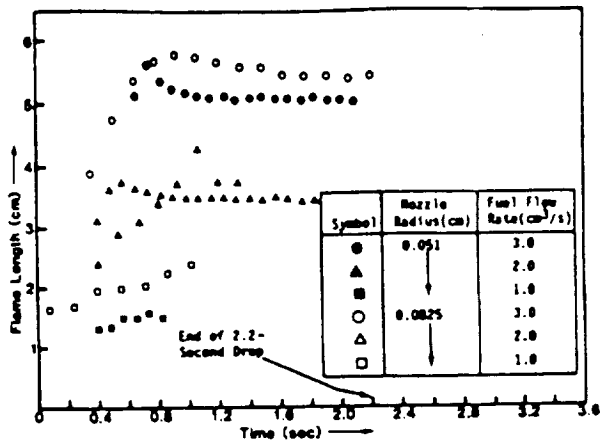

Fig. 14 Micro-gravity methane-flame heights.

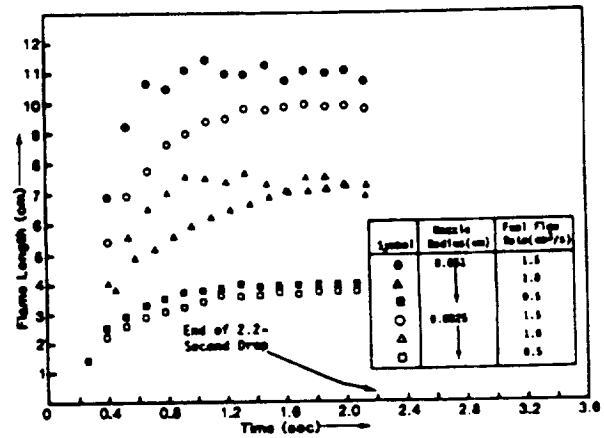

Fig. 15 Micro-gravity propane-flame heights.

The steady-state parabolic model [6,7] described previously was applied to the zero-gravity flames

Table 1. Drop Sequence

Time (sec)	Event
-3.0 (Approx.)	Camera (with timing light) starts operating. The chamber light is on.
0	Experiment package drops. Chamber light goes out. Fuel solenoid valve opens. Spark electrode is activated.
*	Fuel jet ignites.
2.2	Drop package impacts the sand box. Flame may extinguish on impact, then re-ignite from sparking.
3.0 (Approx.)	Experiment ends. Camera stops. Fuel solenoid valve closes. Spark generation stops.

*Test results have shown that ~0.2-0.5 seconds is needed for the flame to ignite due to the frequency of ~4.8 sparks/sec.

Table 2 Data obtained from micro-gravity and normal-gravity experiments[a]

Flame number	G	Nozzle radius, cm	Fuel	Fuel volume flow rate, cm^3/sec	Steady-state flame height, cm	S.S. Maximum flame radius, cm	Approx. time to reach S.S., sec	Reynolds number[b]
1	0	0.051	Methane	1.0	1.5[c]	0.67	~0.6	38
2				2.0	3.5	0.70	0.8	76
3				3.0	5.1	0.75	1.0	114
4		0.0825		1.0	2.4[c]	1.06	~1.0	24
5				2.0	3.7[c]	1.05	0.9	48
6				3.0	5.5	1.11	1.6	72
7		0.051	Propane	0.5	4.0	0.90	1.2	70
8				1.0	7.2	1.02	0.8	140
9				1.5	11.1	1.11	~0.8	210
10		0.0825		0.5	3.8	1.32	1.2	44
11				1.0	7.3	1.53	1.8	88
12				1.5	9.9	1.73	1.3	132
13	1	0.051	Methane	1.0	0.9	0.35	~0.8	38
14				2.0	2.0	0.43	1.3	76
15				3.0	4.0(?)	0.36	(?)	114
16		0.0825		1.0	0.9	0.38	0.6	24
17				2.0	2.5	0.60	0.4	48
18				3.0	3.6	0.61	~0.3	72
19		0.051	Propane	0.5	2.6	0.45	0.4	70
20				1.0	5.6	0.50	0.4	140
21				1.5	8.0	0.50	1.3	210
22		0.0825		0.5	3.0	0.57	0.4	44
23				1.0	7.8(?)	0.50	(?)	88
24				1.5	8.0	0.58	~0.4	132

[a]Experiments were conducted at 1 atm chamber pressure and 21% O_2 - 79% N_2 chamber environment. Question marks indicate uncertainties in the measurements due to the flame flicker.
[b]Reynolds number is based on the nozzle radius.
[c]These flames were diffuse, faint, and resembling an under-ventilated flame; it could not be concluded that they reached steady state (see Fig. 14).

studied in the present work. The results are shown in Fig. 17, where a satisfactory trend in the predicted behavior of the flames is demonstrated. However, the propane flames are slightly longer and the methane flames shorter than the predicted flames. Since soot is not explicitly accounted for in the model, the radiation loss is not accurately predicted. It appears that the slight over-prediction of the methane flame heights is due to the over-prediction of the gas radiation which results in slightly cooler, and hence, taller flames. On the other hand, propane is known to soot more prolifically than methane, leading to a substantially higher radiation loss than is predicted by the current model, even though the gas radiation may be somewhat over-predicted.

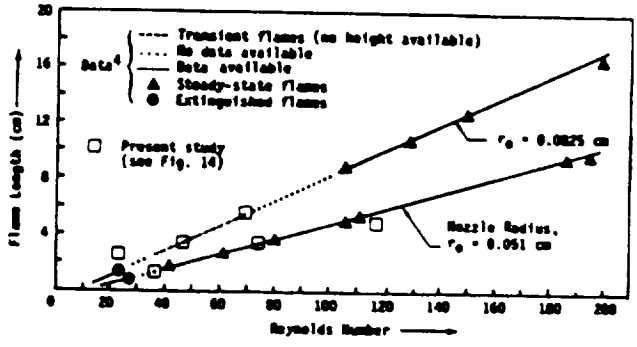

Fig. 16 Methane flame heights as a function of Reynolds number.

In micro-gravity flames, the heat release mechanism is not uniform throughout the flow field.[6] Pyrolysis (producing soot) and partially oxidized species dominate in the near-jet region, while the continued heating and increased residence time result in the tendency to burn off these species downstream of the flow. However, pyrolysis and soot formation reduce the temperature level in the flame, and with the aid of the increased residence time, sooting is enhanced, which, in turn,

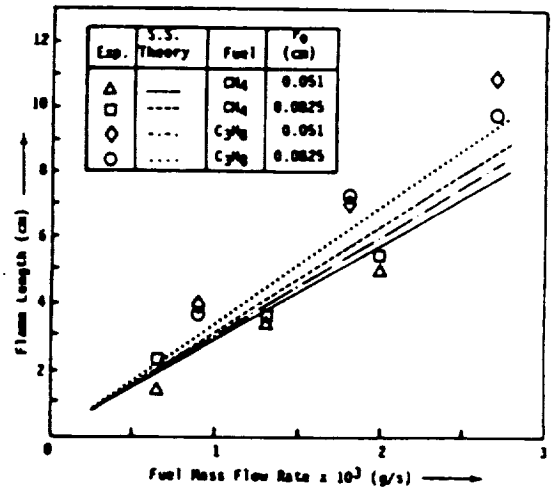

Fig. 17 Predicted and measured flame heights in micro-gravity.

results in enhanced radiation, more cooling, and delayed soot burn-off downstream of the flame.

The observed open tip of the propane flames and quenching at the tip (see Fig. 18), giving the appearance of an under-ventilated flame is due to the combined pyrolysis, cooling and soot-formation processes.

In Fig. 18, a frame-by-frame analysis of Flame No. 11 of Table 2 is presented, where the flame reaches steady state and remains fairly uniform throughout the drop. The orange-reddish color of the flame is due to the soot at cooler temperatures than would be expected for typical burn-off conditions. In addition, the other colors indicate the presence of particular species present in hydrocarbon flames, e.g., blue-violet (outer region at the base showing the spectrum of burning CO), bluish-green region (showing C_2 and CH emissions where C_2 bands appear green shaded toward violet and CH bands appearing violet-blue), and highly luminous zone (bright yellow due to the continuous spectrum of the thermal emission of burning carbon particles) which becomes yellow, then orange, and then red and dark red toward the boundary of the visible region as the temperature of the unburned soot decreases.

The general inverse relationship between wavelength and temperature is consistent with Wein's law which implies an increase in the wavelength with reduction in temperature. The burning soot particle is yellow, i.e., $\sim$0.58-μm wavelength (1370 K < T < 1670 K, where 1670 K is the temperature of a white hot body). As the temperature decreases, the soot particle becomes orange red ($\sim$1370 K, $\sim$0.6 μm), then cherry red ($\sim$1170 K, $\sim$0.6-0.65 μm), and finally dull red ($\sim$970 K, $\sim$0.65-0.70 μm). These effects are clearly shown in the results of Fig. 18, which show the cooling by pyrolysis and enhanced radiation due to increased soot formation.

As a consequence of the systematic study of flame color and luminosity, important species identification will become possible, and when combined with species and temperature measurements, a data base for the model development is anticipated.

Frame number 35 of Fig. 18 shows the moment at which the package is decelerating at some high rate. The induced convective effects transport the hot products of combustion away from the nozzle, causing flame extinction within <0.1 seconds. Re-ignition can be seen due to the spark at a later time, resulting in a behavior observed in normal-gravity, i.e., flickering. A study of the high-speed movies of this segment of the test will reveal the behavior of the flame in the transient state under rapid changes in gravity level, and when combined with the transient analysis, will serve as a by-product data base for further analysis.

6. Conclusions

A spark ignitor has been developed which successfully ignites methane and propane diffusion flames in micro-gravity environments.

In the prior research on gas-jet diffusion flames, ignition was accomplished in normal-gravity, and the established flame was then subjected to the micro-gravity condition. This gave rise to a transient behavior that was experiment-related, resulting in the questions of ignitability and flame development in micro-gravity. The present study shows that those transient flames, in most cases (i.e., higher flow rates), reached a near-steady state in the 2.2 seconds of the drop.

The lower-flow rate methane flames (1.0-2.0 cm^3/s) appeared faint, diffuse, and resembling an under-ventilated flame. This suggests that longer test times and quantitative measurements are needed to truly identify the behavior of the flames at very low flow rates, and possibly, obtain a limiting flow rate, below which, the flames extinguish.

The same argument is applicable to propane flames, where all of the flames reached a near-steady state with intense yellow to orange to red toward the boundary of the flame, and an open tip, showing under-ventilated behavior. This is attributed to the effects of radiation and cooling which stop the soot burn-off process and result in quenching at the flame tip. Although the propane flames (0.5-1.5 cm^3/s) did not quench, there should exist a lower limit on the flow rate, below which, the propane flames extinguish as well.

The predicted flame heights using a steady-state parabolic model were in good agreement with the measured steady-state flame heights. The slight over-prediction and under-prediction for methane and propane flames, respectively, is due to the over-predictation of gas-phase radiation for methane flames and under-prediction of total radiation (i.e., soot and gas-phase) for propane flames.

It is also apparent that the flame colors can aid in the identification of major species and regions of soot burn-off and quenching due to soot radiation.

The planned longer test times provided by the 5.18-second Zero-Gravity Facility ($<10^{-5}$g) and the KC-135 airplane (free-floating, 10-15 seconds) combined with flame visualization and temperature and concentration measurements will provide a more complete quantitative description of these flames, which will be used as a baseline for data comparisons and model development.

Acknowledgements

This work is supported by NASA-Lewis Research Center under the PACE (Physics and Chemistry Experiments in Space) program, contract NAS3-22822.

The authors would like to express their appreciation to Professor Irvin Glassman for a discussion on the interpretation of the colors observed in micro-gravity flames. They also wish to thank Mr. Matthew Hart of Purdue University for the assembly of the experiment package, Mr. Thomas Morrissey for conducting parts of the numerical calculations, and Ms. Angelica Ciraulo for the graphics and typing the manuscript.

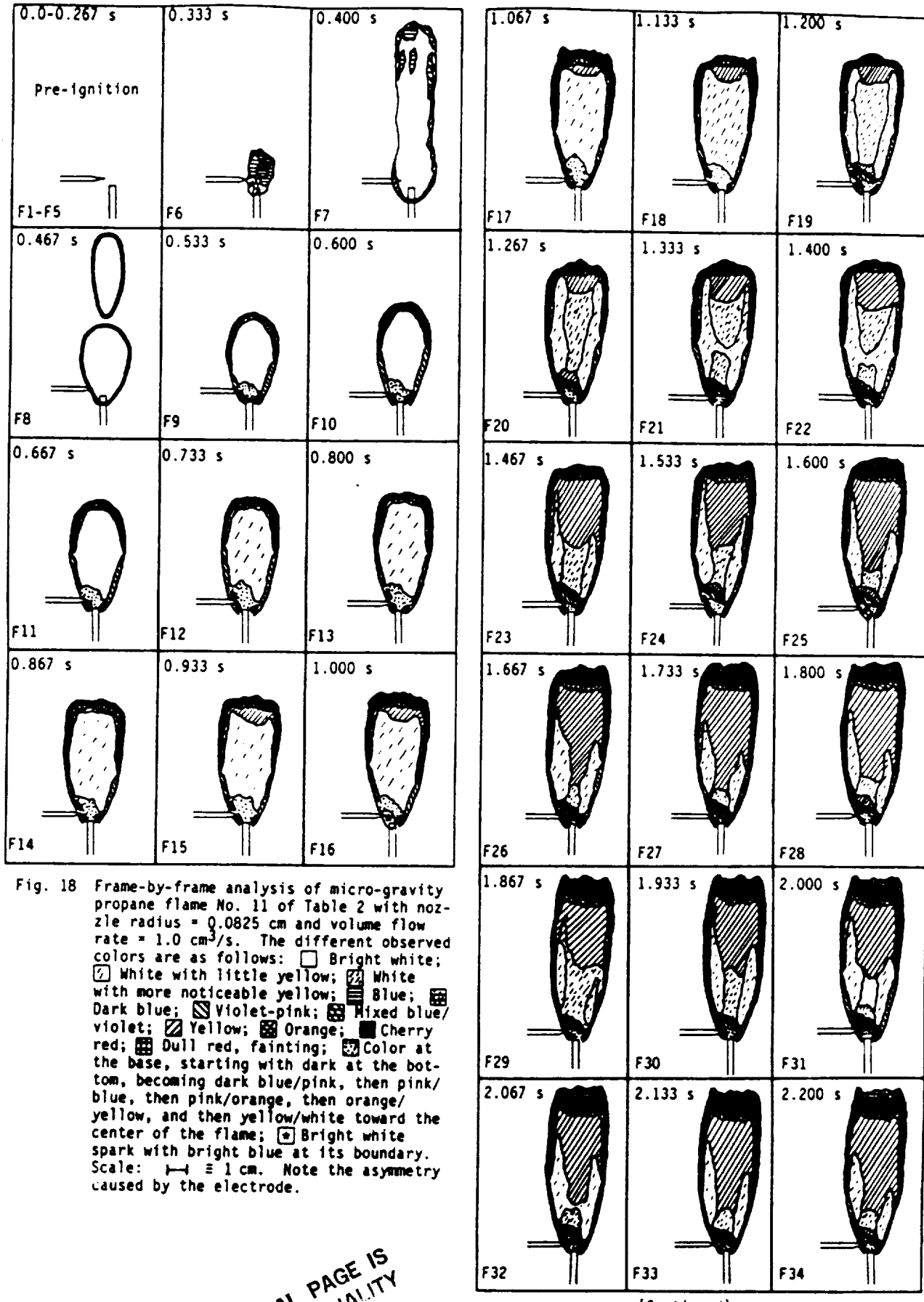

Fig. 18 Frame-by-frame analysis of micro-gravity propane flame No. 11 of Table 2 with nozzle radius = 0.0825 cm and volume flow rate = 1.0 cm^3/s. The different observed colors are as follows: ☐ Bright white; ▨ White with little yellow; ▨ White with more noticeable yellow; ▤ Blue; ▦ Dark blue; ▧ Violet-pink; ▦ Mixed blue/violet; ▨ Yellow; ▩ Orange; ■ Cherry red; ▦ Dull red, fainting; ▨ Color at the base, starting with dark at the bottom, becoming dark blue/pink, then pink/blue, then pink/orange, then orange/yellow, and then yellow/white toward the center of the flame; ▣ Bright white spark with bright blue at its boundary. Scale: ⊢⊣ ≡ 1 cm. Note the asymmetry caused by the electrode.

(Continued)

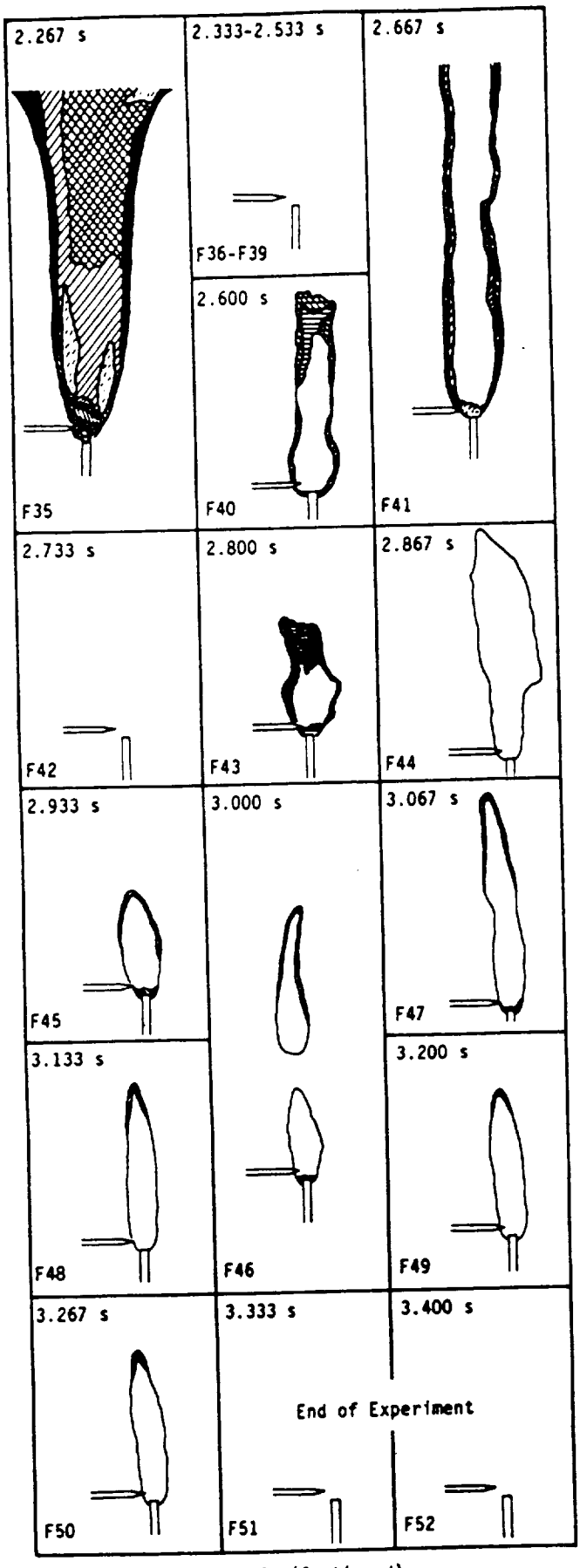

Fig. 18 (Continued)

References

1. Cochran, T.H. and Masica, W.J., "Effects of gravity on Laminar Gas Jet Diffusion Flames," NASA TN D-5872, 1970.

2. Cochran, T.H. and Masica, W.J., "An Investigation of Gravity Effects on Laminar Gas-Jet Diffusion Flames," Thirteenth Symposium (International) on Combustion, The Combustion Institute, Pittsburgh, PA, 1971, pp. 821-829.

3. Haggard, J.B., Jr. and Cochran, T.H., "Stable Hydrocarbon Diffusion Flames in a Weightless Environment," Combustion Science and Technology, Vol. 5, 1972, pp. 291-298.

4. Cochran, T.H., "Experimental Investigation of Laminar Gas Jet Diffusion Flames in Zero Gravity," NASA TN D-6523, 1972.

5. Haggard, J.B., Jr. and Cochran, T.H., "Hydrogen and Hydrocarbon Diffusion Flames in a Weightless Environment," NASA TN D-7165, 1973.

6. Edelman, R.B., Fortune, O.F., Weilerstein, G., Cochran, T.H., and Haggard, J.B., Jr. "An Analytical and Experimental Investigation of Gravity Effects Upon Laminar Gas Jet Diffusion Flames," Fourteenth Symposium (International) on Combustion, The Combustion Institute, Pittsburgh, PA, 1973, pp. 399-412.

7. Edelman, R.B., Fortune, O. and Weilerstein, G., "Analytical Study of Gravity Effects on Laminar Diffusion Flames," NASA CR-120921, 1973.

8. Haggard, J.B., Jr. "Forced and Natural Convection in Laminar-Jet Diffusion Flames," NASA TP 1841, 1981.

9. Edelman, R.B. and Bahadori, M.Y., "Effects of Buoyancy on Gas-Jet Diffusion Flames: Experiment and Theory," Acta Astronautica, Vol. 13, No. 11/12, 1986, pp. 681-688.

Section 6*

"GAS-JET DIFFUSION FLAMES UNDER REDUCED-GRAVITY CONDITIONS"

M. Y. Bahadori and R. B. Edelman

Paper LBS-88-014, presented at the Second Symposium on Lunar Bases and Space Activities in the 21st Century, Lunar and Planetary Institute, Houston, Texas April 1988

* A revised version of this paper is in press in the Proceedings of the Second Symposium on Lunar Bases (see Section 14).

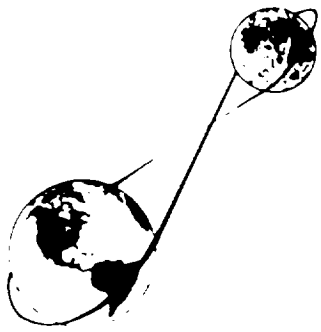

LUNAR BASES & SPACE ACTIVITIES IN THE 21st CENTURY

April 5 - 7, 1988
Westin Galleria Hotel
Houston, Texas

GAS-JET DIFFUSION FLAMES UNDER REDUCED-GRAVITY CONDITIONS

M. Yousef Bahadori and Raymond B. Edelman

Science Applications International Corporation
Combustion Science and Advanced Technology Department
9760 Owensmouth Avenue, Chatsworth, California 91311

Paper No. LBS-88-014

Symposium sponsored by NASA, AIAA, the Lunar & Planetary Institute, the American Geophysical Union, the American Nuclear Society, the American Society of Civil Engineers, the Space Studies Institute and the National Space Society.

GAS-JET DIFFUSION FLAMES UNDER REDUCED-GRAVITY CONDITIONS

M. Yousef Bahadori and Raymond B. Edelman
Science Applications International Corporation
Combustion Science and Advanced Technology Department
9760 Owensmouth Avenue, Chatsworth, CA 91311

Abstract - The need for an improved understanding of fires is becoming of critical importance with increased space travel and utilization. While the control of fires in space as well as on earth is not understood, it is known that both buoyancy-induced convection and buoyancy-induced turbulence affect ignition, stabilization, propagation, and extinction in low-momentum reactive flows. The objective of this research is to gain a more fundamental understanding of fires, and to quantify the flame behavior under reduced-gravity levels. Gas-jet diffusion flames are considered in an interactive theoretical and experimental project. Current research on laminar gas-jet diffusion flames has shown that under reduced-g levels, the flames become larger, globular in shape and more sooty affecting the radiation heat loss and, under some conditions, the flames tend toward extinction. In the case of turbulent flames, it has been found that both buoyancy-induced convection and buoyancy-induced turbulence affect the flowfield structure. This paper presents the results of theoretical and experimental studies of micro-gravity diffusion flames and the potential of Lunar- and Martian-based laboratories to obtain data at reduced-gravity levels.

INTRODUCTION

The problem of fire safety has been of equal concern both on earth and in space. The 21st Century has already started to show the signs of regular space travel, manned space stations, Lunar and Martian bases, and deep space exploration. All of these activities raise the question of fire prevention in space, and the use of low-gravity environments in order to further our knowledge of combustion on earth. Micro-gravity combustion research has been vigorously pursued in the last decade with the same question in mind in relation to safety as well as the fundamental understanding. Solid, liquid, and gaseous combustion studies have been conducted in the earthbound facilities which simulate the micro-gravity environment, and promising results have so far been obtained to warrant the continuation of this branch of combustion research all the way into the next century. In this paper, we present an overview of studies on gas-jet diffusion flames in micro-gravity environments, the results obtained for laminar diffusion flames, and the possibility of conducting turbulent-flame studies under reduced-gravity conditions in order to understand the behavior of fires not only in space but on earth as well.

LAMINAR DIFFUSION FLAMES

The term "diffusion flame" classifies those types of flames in which the fuel and oxidizer are not premixed, whether the reactants are in the solid, liquid or gaseous form. A schematic of a laminar gas-jet diffusion flame is shown in Fig. 1 with the different physico-chemical phenomena involved indicated. Coupling exists between chemical kinetics, fluid dynamics, radiation, diffusion, inertia, soot formation and disposition (in hydrocarbon flames), and buoyancy under non-zero-gravity conditions. In zero-gravity environments, the buoyant force is eliminated and the remaining phenomena are responsible for the rather different behavior of flames which is observed in micro-gravity ex-

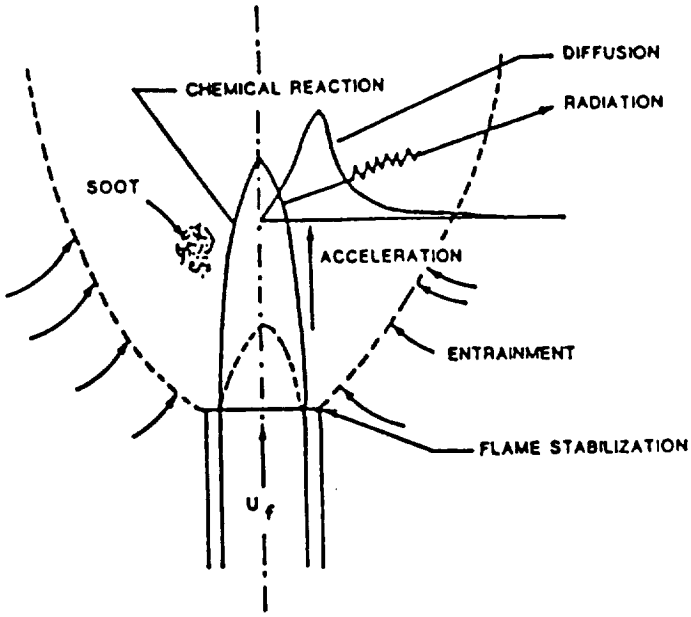

Fig. 1. Physical and chemical processes occurring in laminar gas-jet diffusion flames of hydrocarbons.

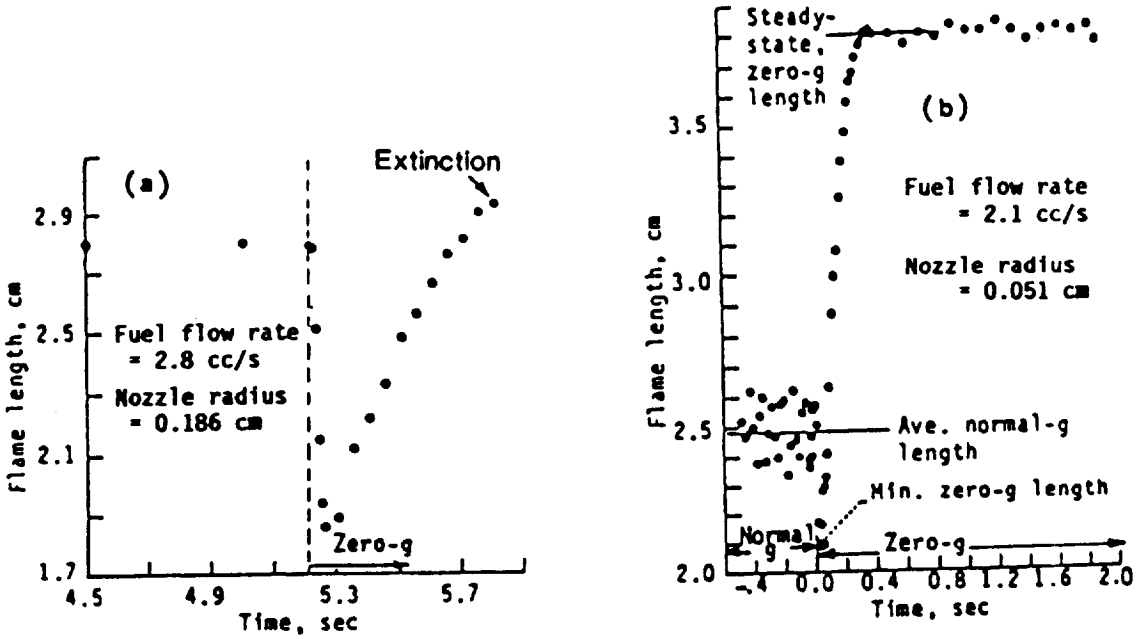

Fig. 2. Methane-air flame lengths as a function of time in microgravity for (a) an extinguished flame [1], and (b) a flame which reached an apparent steady state at the end of the drop [4].

periments conducted to-date. In this section, the combined theoretical and experimental efforts for gas-jet diffusion flames in the absence of buoyancy are described and theoretical results for flames under 2/5g (Mars) and 1/6g (Moon) conditions are presented.

Laminar diffusion flames have been studied in the 2.2-second NASA-Lewis drop tower facility (gravity level $<10^{-5}$g), in which hydrogen and various hydrocarbon flames were ignited and established in normal-g and then subjected to micro-gravity condition by allowing the experiment package to drop inside a falling drag shield [1-7]. Compared to the flames in normal gravity, larger, globular, and sootier flames (of hydrocarbons) are observed under micro-gravity conditions. This is due to the absence of buoyancy which makes diffusion the major mechanism of transport compared to the momentum of the burned gases. The orange-reddish appearance of these hydrocarbon flames is due to significant soot formation. This is caused by flame suffocation since the hot products of combustion are trapped in the vicinity of the flame due to the absence of the buoyant force, and the continued combustion depends on the slow diffusion of oxygen causing major pyrolysis of the hot fuel-rich portion of the flame. Figure 2 shows an extinguished flame [1] and a flame which reached a near-steady state during the 2.2 seconds of the drop [4]. During the transitory period of adjustment from normal-gravity to micro-gravity ($\sim$ 0.05 s), a sudden decrease in the flame height occurred, and then the flame height began to increase with time, resulting in extinction, reaching an apparent steady state, or remaining in a transitory state by the time the package came to rest at the end of the drop. This has been attributed to the influence of the jet Reynolds number, i.e., the combined effects of the nozzle size, jet velocity and fuel type. The method of ignition [1-7], i.e., igniting the flame in normal gravity and allowing it to reach steady state and then dropping the package is largely responsible for the different flame behaviors in addition to the lack of enough time for the adjustment of the flame to the micro-gravity condition. We have recently shown that hydrocarbon flames can be successfully ignited under micro-gravity conditions and most of the flames which were in a transient state or extinguished in the previous studies indeed reached a near-steady state [8]. Figure 3 shows a family of methane flame heights as a function of fuel Reynolds number for the two methods of ignition, and Fig. 4 shows the heights for methane and propane flames by igniting them in micro-gravity [8].

A mathematical model has been developed [6, 9] for the study of laminar gas-jet diffusion flames under arbitrary gravitational accelerations based on the parabolic form of the equations of motion, which includes the effects of inertia, viscosity, diffusion, radiation, and chemical reactions. Figure 5 shows the excellent agreement between the predicted and measured flame heights under both normal-gravity and zero-gravity conditions [6, 9]. We have recently applied this model to a family of methane flames under different gravitational levels. Figure 6 shows the non-dimensional centerline velocity vs. the axial distance. Clearly, the effect of convection plays a major and different role for different gravitational environments. The partial effect of convection compared to that in normal-g, and coupled with the effects of chemistry, soot formation and radiation, results in different flame behaviors under different gravitational levels. For example, Fig. 7 shows a propane flame under both normal-gravity and micro-gravity conditions. The shape, color, luminosity, products of combustion, and in general, the flame behavior cannot be truly understood unless experiments are conducted (along with appropriate diagnostics) under the g-level of interest, and then when combined with the theoretical

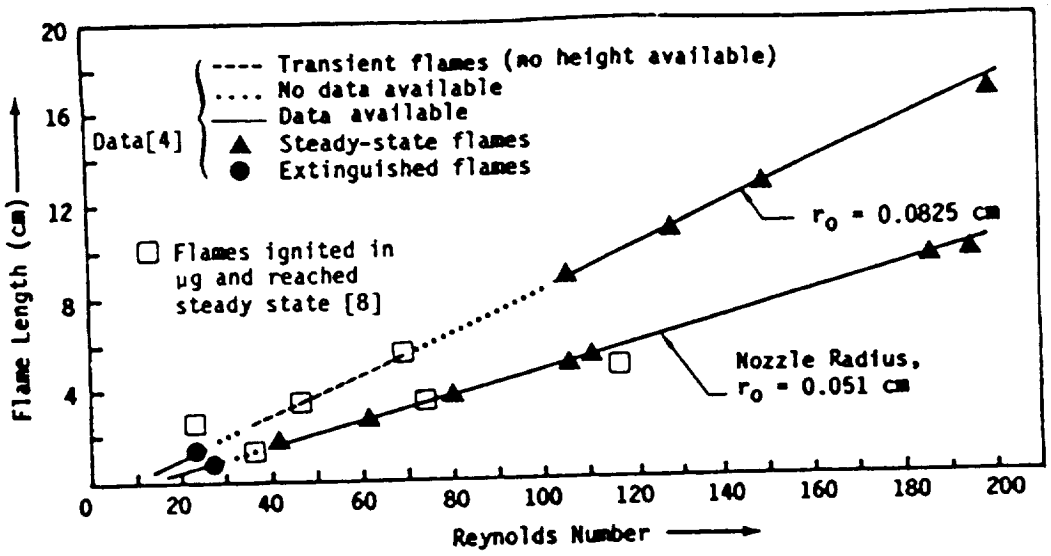

Fig. 3. Methane flame heights as a function of fuel Reynolds number [8].

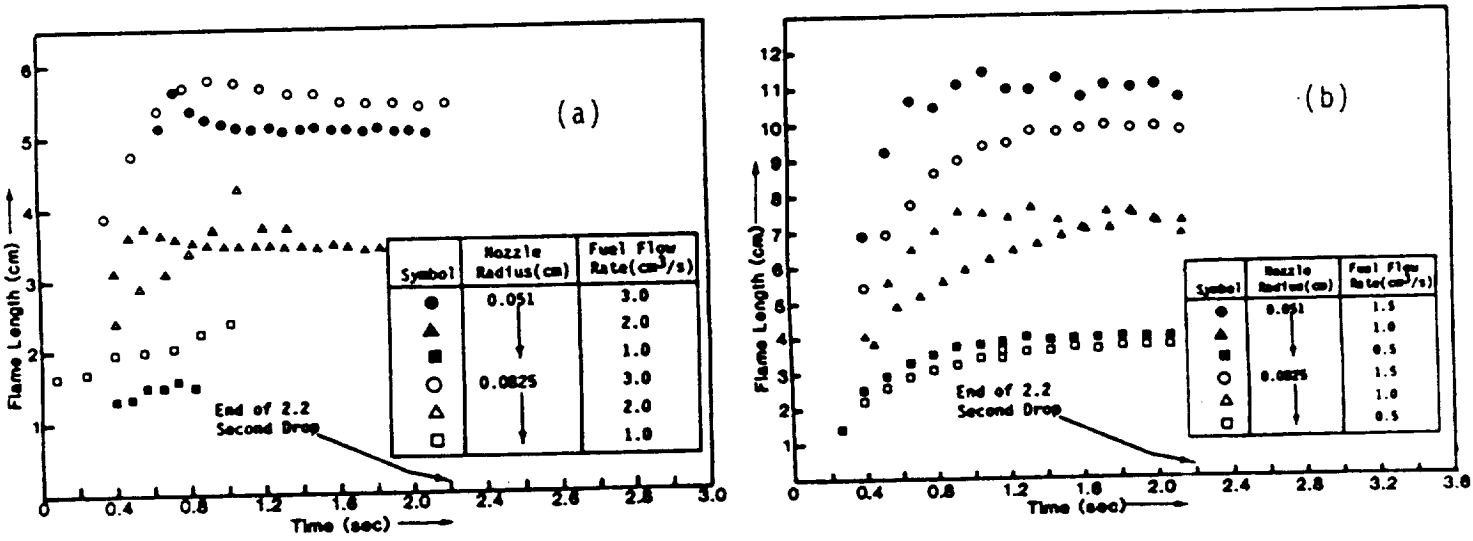

Fig. 4. Micro-gravity flames of (a) methane and (b) propane [8]. The low-volume flow rate flames of methane did not extinguish, but were extremely faint and difficult to observe.

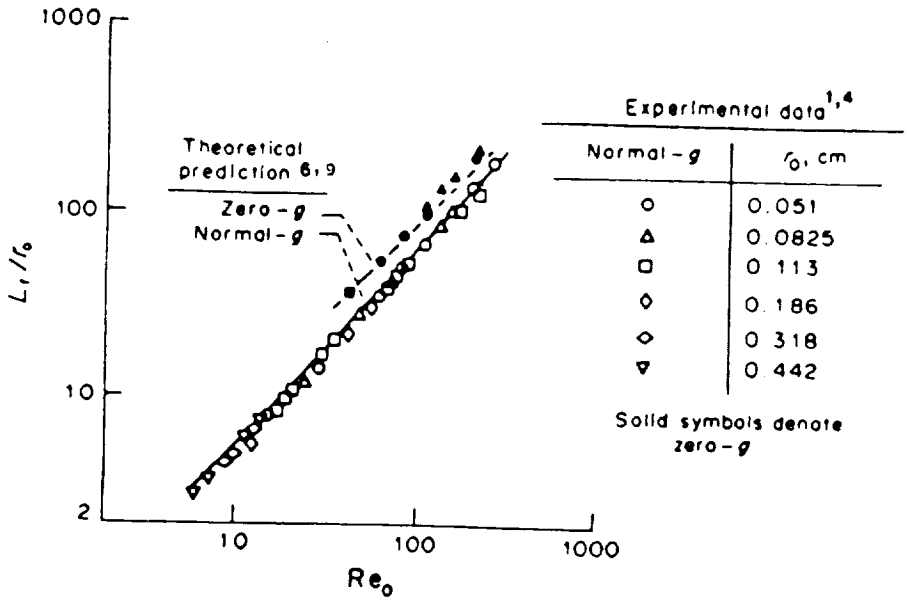

Fig. 5. Comparisons between the theoretical predictions and experimental results for non-dimensional flame heights vs. jet Reynolds numbers; methane-air flames [6].

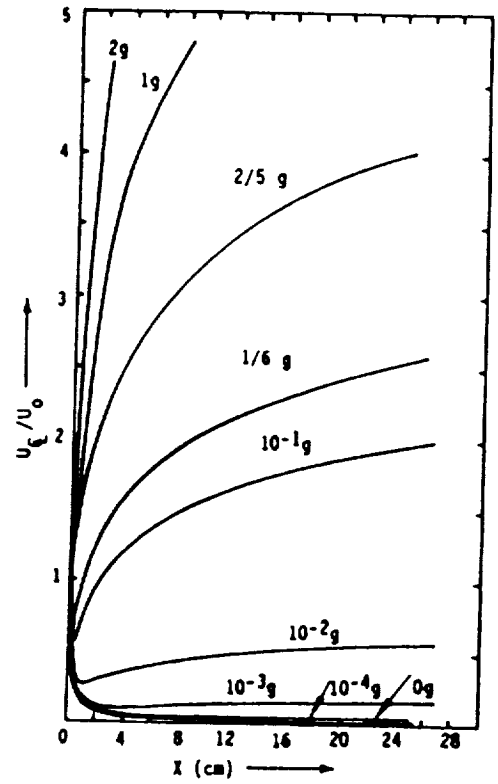

Fig. 6. Centerline velocity vs. axial distance along the jet for a methane-air flame as a function of gravitational level. Nozel radius = 0.0825 cm, volume flow rate = 1 cc/sec., pressure = 1 atm, U_o = 46.8 cm/s.

analyses, will provide a data base for the understanding of fires both on earth and under reduced-gravity conditions such as on the Moon, Mars, or in free space. In a recent publication [10], we have analyzed the past experimental and theoretical efforts on laminar gas-jet diffusion flames. The following section gives a brief account of the potential for conducting turbulent diffusion flames under reduced-gravity conditions.

TURBULENT DIFFUSION FLAMES

Turbulent gas-jet diffusion flames under normal-gravity conditions have been the subject of extensive theoretical and experimental studies for a number of decades. The classical behavior of a turbulent jet diffusion flame is shown in Fig. 8 for the dependence of length and structure of the flame on flow velocity for a tube of given size. As the jet velocity increases, the flame transists from laminar (where mixing is governed by molecular diffusion only) to fully developed turbulent behavior (where mixing is due, largely, to eddy diffusion or convection, with the final homogeneity being attained by molecular diffusion). For the tube size used in the flame study of Fig. 8, a velocity is reached where further increases in the jet velocity result in no change in flame height. It can be shown that this is a characteristic of momentum-dominated flames, i.e., flames in which buoyancy is not important. Although much progress has been made toward the characterization of momentum-dominated turbulent flames, i.e., flames with large Froude number ($Fr = V^2/gd$, where V is the flow velocity, g is the gravitational acceleration, and d is the nozzle diameter), this is not the case for low-momentum turbulent flames characteristic of unconfined fires. In this case, the fire research community depends primarily on empirical results which, having been obtained under normal-gravity conditions, have the buoyancy effect inherently embedded within these correlations. When buoyancy is important (i.e., low-momentum flames), unlike Fig. 8, a constant height as a function of velocity is not reached for fully developed turbulent region (see Fig. 9). Although there is an apparent dependency on Reynolds number ($Re = Vd/\nu$, where V is the flow velocity, d is the nozzle diameter, and ν is the kinematic viscosity) beyond the transition region, this is really not the case. The reason is that as the nozzle size gets sufficiently large for a given velocity level, the buoyant force becomes important; this is reflected through the Froude number, i.e., the ratio of momentum to buoyant force. In fact, normalization of the describing equations shows that in general, for fully developed turbulent flows, the flow should be independent of Reynolds number but not the Froude number. Although it appears that the buoyancy effects are indeed important as the momentum level decreases relative to the buoyancy effect (i.e., as Froude number decreases), the mechanisms responsible for this behavior are far from being fully understood. Thus, the need for more fundamental data and analysis is apparent because of the requirement to define the hazard and control of fires not only on earth but under reduced-gravity (e.g., Lunar and Martian bases) and micro-gravity (i.e., in space) conditions as well.

For low-momentum flames, strong interactions between buoyancy and turbulent-flame structure exist which affect the flame behavior and chemistry. There are two gravity-induced mechanisms responsible for the alteration of a low-momentum flowfield. The first arises directly from the buoyant force acting on the time-averaged or mean flowfield and appears as a gravity term in the mean momentum equation. The second mechanism arises out of the interaction between density and velocity fluctuations which manifest in a source of turbulent kinetic energy. Under normal-gravity conditions, it is not possible to separate these two effects in terms of their impact on mixing rate, and hence, flame structure. Clearly,

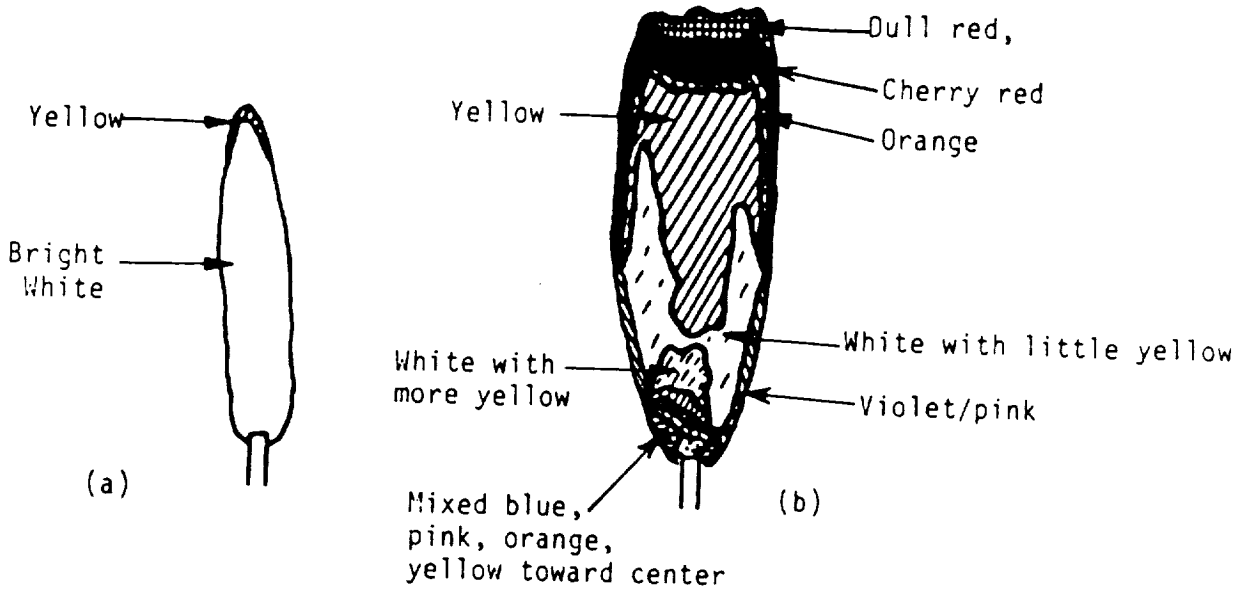

Fig. 7. (a) Normal-gravity and (b) micro-gravity propane-air diffusion flames at 1 atm. Nozzle radius = 0.0825 cm and volume flow rate = 1.0 cm^3/sec. Scale: ⟝⟞ ≡ 1 cm; reproduced from [8].

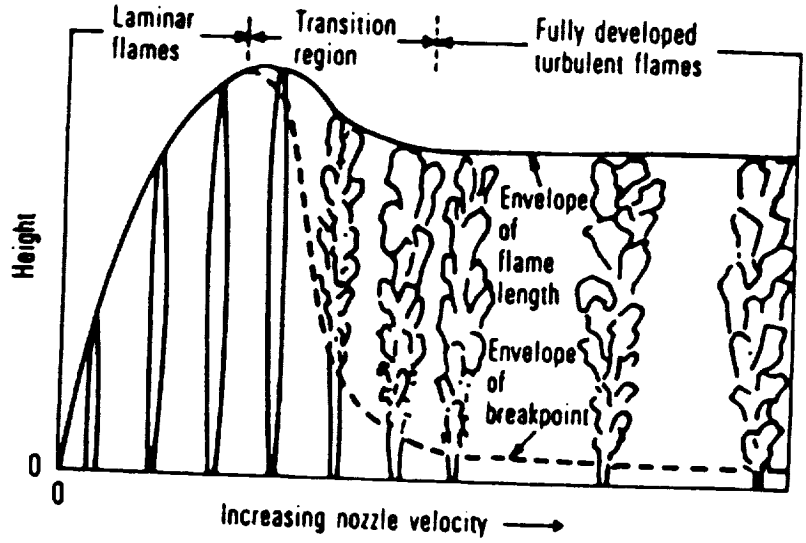

Fig. 8. Change in the flame height and behavior with increase in nozzle velocity for a typical gas-jet diffusion flame [11].

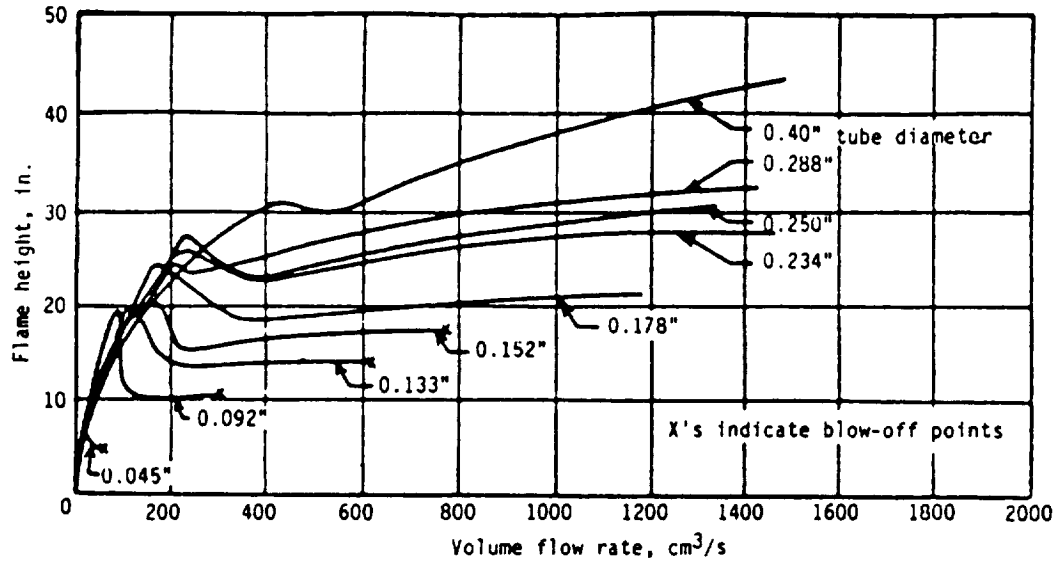

Fig. 9. Effects of volume flow rate and tube diameter on flame height for city gas diffusion flames [12].

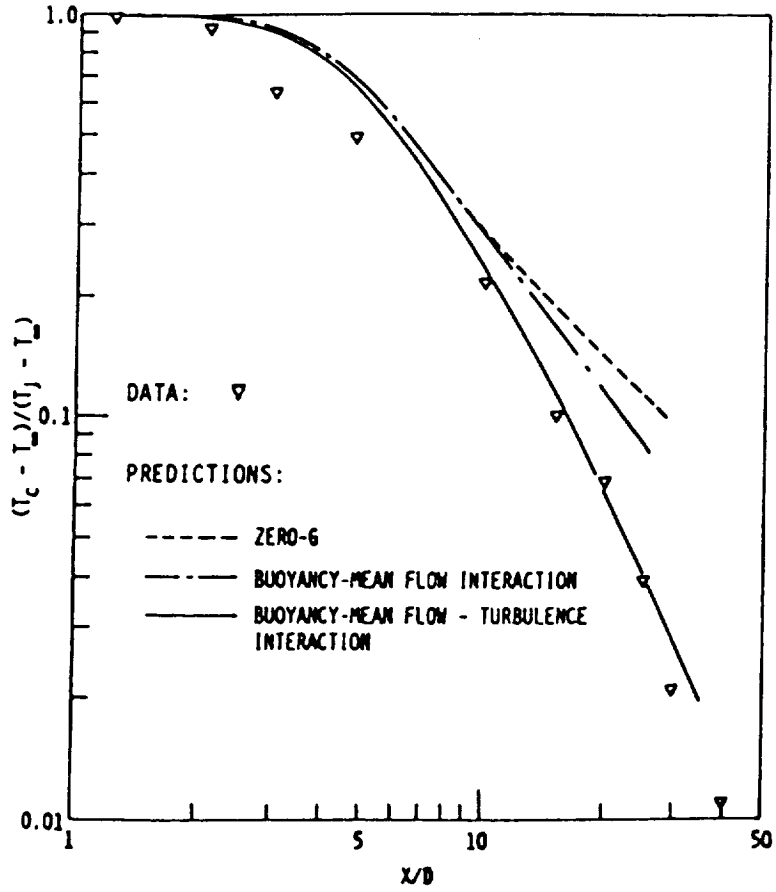

Fig. 10. Effect of modeling assumptions on the prediction of centerline temperature for a hot buoyant jet (U_j = 21.6 ft/sec); data from [13].

the advantage of operating in a low-gravity environment would be to provide a major significant base of new information isolating the combined effects of buoyancy. Then, with a theoretical model, the effects of buoyancy on the mean flow and on the generation of turbulent kinetic energy would be separable. With the aid of a theoretical model characterizing these two mechanisms, recent studies at SAIC have illustrated the importance of gaining a further understanding of both of these mechanisms. The model has been applied to a hot plume in which temperature measurements were made within the plume. The results are shown in Figs. 10-12. Figure 10 shows a comparison between the relative effects of the two buoyancy-related mechanisms (i.e., effects on the mean flow and on the generation of turbulent kinetic energy). The data points correspond to the normal-g condition [13]. The best agreement with the data is obtained when both mean flow and turbulent interactions with buoyancy are taken into account. Figure 11 shows the non-dimensional centerline distance as a function of Froude number for a particular value of non-dimensional centerline temperature. Comparison with data is again satisfactory, and the effect of Froude number on both normal-g and zero-g ($Fr = \infty$) cases is shown. Figure 12 shows the effect of Reynolds number for both normal-g and zero-g conditions. Comparisons with the data show good agreement and as the Reynolds number increases, the behavior approaches that of the zero-g case. (The data points close to the jet port show a poor agreement with the predictions which is believed to be due to the disturbances caused by the heating coil mounted inside the jet set up). As Figs. 10-12 show, the effects of buoyancy on both turbulent kinetic energy and on the mean flowfield are equally important. Numerical models would be capable of separating the effects of the two mechanisms, and when combined with the experimental results under both normal-g and arbitrary-g conditions, would elucidate the behavior of turbulent diffusion flames under a variety of reduced-gravity conditions such as Martian conditions (2/5g), Lunar bases (1/6g), and in space ($<10^{-6}$g).

The results presented in Figs. 10-12 are for an externally heated plume. What is required now is application of similar turbulent models to flames wherein we might expect the effects to be even greater than those in the hot plume because the distributed heat release in a flame results in the persistence of gravity-induced mean flow and turbulence under normal-g conditions. Thus, we would expect the difference between normal-g and reduced-g environments to produce noticeable and significant differences in the flame structure. Of course, an experimental data base under reduced-gravity conditions would be invaluable in furthering our understanding of these effects on the one hand, and the question of fire behavior and prevention on the other, in addition to the development and validation of the theoretical models accounting for the two mechanisms previously cited.

CLOSURE

Although the effects of buoyancy on low-momentum flames have been qualitatively observed, it is only recently that quantitative descriptions of the phenomena affected by gravity have been attempted. Understanding this phenomena is not only of fundamental interest but it is of critical importance to fire safety in space as well as on earth. Furthermore, for processing and manufacturing in space, controlled flames used as one form of heat source are likely to be employed. This paper has presented results that indicate significant effects of gravity on laminar and turbulent flame structures. More-

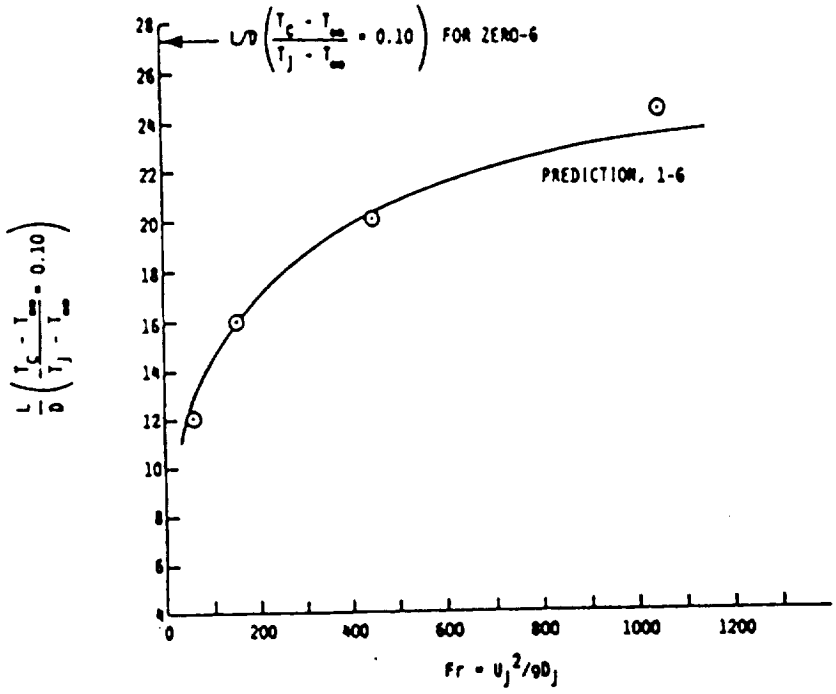

Fig. 11. Non-dimensional centerline distance as a function of Froude number for a particular value of non-dimensional centerline temperature in a hot buoyant jet (U_j = 21.6 ft/sec); data from [13].

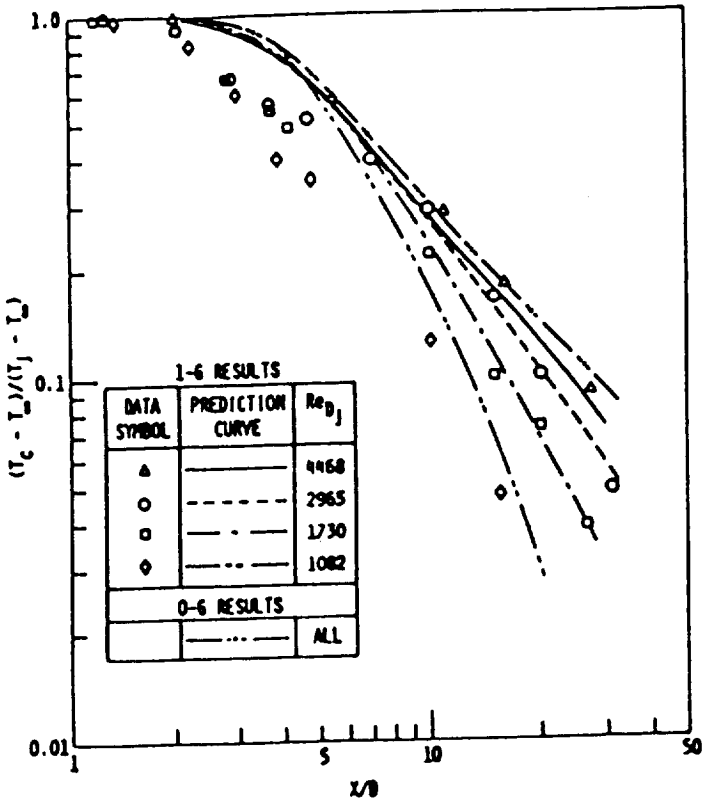

Fig. 12. Effect of modeling assumptions on the prediction of centerline temperature under both normal-g and zero-g conditions for a hot buoyant jet; data from [13].

over, it has been shown that to develop a more fundamental understanding of this phenomena and to develop reliable prediction capability, quantitative data obtained under reduced-gravity conditions uninhibited by test time and size limitations is needed. The potential to obtain data from experiments conducted on the Moon and Mars offers this opportunity, one which cannot be equalled in earthbound facilities including drop towers and aircrafts flying parabolic trajectories.

Acknowledgements - This work is supported, in part, by NASA-Lewis Research Center under the PACE (Physics and Chemistry Experiments in Space) program, Contract NAS3-22822, with Ms. Sandra L. Olson and Mr. Dennis P. Stocker as the NASA project scientists.

REFERENCES

1. Cochran, T.H. and Masica, W.J., "Effects of Gravity on Laminar Gas-Jet Diffusion Flames," NASA TN D-5872, 1970.

2. Cochran, T.H. and Masica, W.J., "An Investigation of Gravity Effects on Laminar Gas-Jet Diffusion Flames," Thirteenth Symposium (International) on Combustion, The Combustion Institute, Pittsburgh, PA, pp. 821-829, 1971.

3. Haggard, J.B., Jr. and Cochran, T.H., "Stable Hydrocarbon Diffusion Flames in a Weightless Environment," Combustion Science and Technology, Vol. 5, pp. 291-298, 1972.

4. Cochran, T.H., "Experimental Investigation of Laminar Gas-Jet Diffusion Flames in Zero Gravity," NASA TN D-6523, 1972.

5. Haggard, J.B., Jr. and Cochran, T.H., "Hydrogen and Hydrocarbon Diffusion Flames in a Weightless Environment," NASA TN D-7165, 1973.

6. Edelman, R.B., Fortune, O.F., Weilerstein, G., Cochran, T.H., and Haggard, J.B., Jr., "An Analytical and Experimental Investigation of Gravity Effects Upon Laminar Gas-Jet Diffusion Flames," Fourteenth Symposium (International) on Combustion, The Combustion Institute, Pittsburgh, PA, pp. 399-412, 1973.

7. Haggard, J.B., Jr., "Forced and Natural Convection in Laminar-Jet Diffusion Flames," NASA TP-1841, 1981.

8. Edelman, R.B., Bahadori, M.Y., Olson, S.L., and Stocker, D.P., "Laminar Diffusion Flames Under Micro-Gravity Conditions," Paper AIAA 88-0645, AIAA 26th Aerospace Sciences Meeting, Reno, Nevada, January 11-14, 1988; submitted to AIAA Journal.

9. Edelman, R.B., Fortune, O. and Weilerstein, G., "Analytical Study of Gravity Effects on Laminar Diffusion Flames," NASA CR-120921, 1973.

10. Edelman, R.B. and Bahadori, M.Y., "Effects of Buoyancy on Gas-Jet Diffusion Flames: Experiment and Theory," Acta Astronautica, Vol. 13, No. 11/12, pp. 681-688, 1986.

11. Hottel, H.C. and Hawthorne, W.R., "Diffusion in Laminar Flame Jets," Third Symposium on Combustion, pp. 254-266, Williams and Wilkins Co., Baltimore, 1949.

12. Wohl, K., Gazley, C. and Kapp, N., "Diffusion Flames," Third Symposium on Combustion, pp. 288-300, Williams and Wilkins Co., Baltimore, 1949.

13. Cleeves, V. and Boelter, L.M.K., "Isothermal and Nonisothermal Air-Jet Investigations," Chemical Engineering Progress, Vol. 43, No. 3, pp. 123-133, 1947.

Section 7

"OXYGEN-CONCENTRATION EFFECTS ON MICROGRAVITY LAMINAR METHANE AND PROPANE DIFFUSION FLAMES"

M. Y. Bahadori and D. P. Stocker

Paper presented at the Eastern States Meeting of The Combustion Institute, Albany, New York, October/November 1989

Oxygen-Concentration Effects on Microgravity Laminar Methane and Propane Diffusion Flames*

M. Yousef Bahadori†
Science Applications International Corporation, Torrance, California

and

Dennis P. Stocker
NASA-Lewis Research Center, Cleveland, Ohio

1. Introduction

Laminar diffusion flames of hydrocarbons under microgravity conditions have shown distinct characteristics relative to normal-gravity flames [1]. Compared to the flames in normal-gravity environments, larger, sootier, and somewhat globular flames are observed in microgravity. This is due to the significant reduction in the buoyant force, which makes diffusion the dominant mechanism of transport. As a result, increased residence time, enhanced soot formation, radiation cooling due to the larger flame size, and the possible onset of a chemical-kinetics limitation on the heat-release process become responsible for the very different characteristics of these flames compared to those in normal gravity.

In normal-gravity environments, laminar diffusion flames of hydrocarbons flicker and are yellow, whereas their microgravity counterparts are orange/red with practically no flicker. The colors observed in the previous studies [1] indicate that extensive soot formation enhanced by the increased residence time results in more cooling, and hence, delayed soot burn-off downstream of the flame. In addition, open tips are observed for propane flames [2], which indicates that unburned and pyrolyzed fuel species escape through the flame tip in microgravity; this tip-quenching combined with thermophoresis are responsible for the observed underventilated-type microgravity flames.

The previous studies [1, 2] have been limited to atmospheric flames burning in air. In this paper, we present the results of microgravity experiments conducted for methane and propane diffusion flames with oxygen-nitrogen mixtures containing 18% - 30% oxygen, and burning in quiescent environments at 1 atm pressure.

2. Apparatus and Experimental Procedure

The experiments were conducted in the 2.2-second NASA-Lewis Research Center Drop Tower. Schematics of the apparatus and a detailed description of the experimental procedure can be found elsewhere [2]. Two fuel nozzles were used in the studies. The tapered tips had a nozzle exit radius of approximately 0.048 cm and 0.074 cm, respectively. The flames were ignited in microgravity using a spark electrode located at 1.0 cm above the nozzle tip and 1.5 cm away from the nozzle centerline, with the nozzle acting as the second electrode. The spark ignitor, unlike the one in the previous study [2], was far enough from the flame boundary to cause no flame disturbance. As a result, a stronger spark than that of the previous system [2] was used to ensure that low-oxygen concentration flames indeed ignite. The spark-ignition system was set to 0.4 sec. to 1.0 sec., depending on the flame, following the release of the package.

Methane and propane diffusion flames were studied at 1 atm chamber pressure with O_2/N_2 mixtures of 18%, 19%, 21%, and 30% oxygen. The volume-flow rates were 1.75 and 5.25 cc/s for methane, and 0.64 and 0.96 cc/s for propane. The filming rate was 12-16 frames/sec., and the (tungsten Eastman Ektachrome Video News) films were force-processed 2-f stops for low-oxygen-concentration and 21%-O_2 flames. The slow filming rate and force-processing ensure that blue is discernable.

---

* Presented at the 1989 Fall Technical Meeting (Eastern Section) of the Combustion Institute, Albany, New York, October 30 - November 1, 1989.
This work is supported by NASA-Lewis Research Center under Contract NAS3-22822.

† Author to whom correspondence should be sent; on-site at the NASA-Lewis Research Center, MS 500-217, Cleveland, Ohio 44135.

3. Results and Discussion

Figures 1 and 2 show the flame height as a function of percent oxygen for different flow rates under both normal-gravity and microgravity conditions. The methane results (Fig. 1) are for the small nozzle only. The propane results (Fig. 2) correspond to both small and large nozzles. the flames are taller in microgravity compared to their normal-gravity counterparts; the reason being the entrapment of the combustion products in the vicinity of the flame due to the absence of the buoyant force, which makes diffusion the dominant mechanism of transport, and results in longer residence time for fuel to burn. The normal-gravity flame heights in Figs. 1 and 2 are the averages of minimum and maximum flickering-flame height.

In general, the higher the oxygen concentration, the shorter the flame, regardless of the gravity level. This is obvious since the residence time for burning the fuel is related to the level of oxygen in the environment. Figures 1 and 2 show that at some high-enough oxygen concentration, the normal-gravity and microgravity flame lengths may become equal. This indicates that oxygen may be so abundant that entrapment of the combustion products in microgravity flames may have no effect on the diffusion of oxygen toward the flame front. On the other hand, in high-oxygen-concentration normal-gravity flames buoyant removal of the products may have a negligible effect in promoting oxygen diffusion compared to the abundance of oxygen. However, this needs to be verified experimentally.

Figures 1 and 2 show that for a fixed nozzle size, the higher the flow rate, the bigger the difference between microgravity and normal-gravity flame heights. In addition, the smaller the nozzle, the taller the microgravity flame for a fixed flow rate; the same is true for normal-gravity flames, but not as strong an effect compared to microgravity (see Fig. 2), the reason being the dominant effect of buoyancy in normal-gravity flames of different nozzle sizes with same flow rates. Based on the jet Reynolds number, it can be seen that both increased flow rate for fixed nozzle size and decreased nozzle size for fixed flow rate result in a greater initial jet momentum, i.e., larger Reynolds number, and hence a taller flame.

Drastic changes in flame color and luminosity occur due to the absence of buoyancy. This can be seen in Fig. 3 where selected flame shapes are presented for various oxygen concentrations. In microgravity, the methane-flame heights are most affected by the oxygen concentration, whereas the color is more significantly changed for propane flames. In addition, reduced buoyancy makes the flames much wider compared to normal-gravity flames. This is due to the adjustment of the flame location, since in microgravity, diffusion becomes responsible for the transport of fuel and oxidizer toward the flame front. Hence, the buoyant force upon the removal of combustion products from the vicinity of the flames aids the arrival of oxygen to the flame front causing the flame to be pencil-like in normal gravity.

The various colors observed in microgravity have significant physical implications. In general, methane flames do not change drastically in color upon the removal of buoyancy, although they become dimmer due to the larger flame surface and have more radiation losses, resulting in cooler flames. However, the propane flames change remarkably in both color and characteristics. Referring to Fig. 3, the dim, large blue flame of propane (indicating the spectrum of burning CO) at 18% oxygen concentration is indicative of a very cool flame with probably no soot formation. In addition, the intense yellow/orange/red/dull red colors observed at higher oxygen concentrations show that extensive soot formation, burn-off and quenching occurs with flames being still underventilated even in the 30%-O_2 environment. However, the normal-gravity propane flames look more-or-less the same from the color point of view. The trends for propane flames show that at higher oxygen concentrations we may obtain a closed-tip flame in microgravity but the red (indicating soot at cooler temperatures) may still persist.

The unique underventilated behavior of microgravity propane flames shows that extensive soot formation due to pyrolysis, increased residence time and radiation cooling is a characteristic of microgravity flames. Indeed, the films show that soot escapes through the tip of the flame (see red and dull red regions). This tip quenching is believed to be due to limited oxygen-fuel mixing, radiative losses from the hot combustion products and soot particles, and extensive amount of unburned fuel escaping thorugh the flame tip. The low-oxygen-concentration flame of propane shows that near-limit extinction may be approaching. However, the extinction mechanism may be different compared to normal-gravity flames; in other words, at still lower oxygen concentrations we may observe a flame of the same size but so cool and dim that heat release due to reaction can no longer compete with heat loss, causing flame extinction.

The qualitative observations presented here are the preliminary results for this on-going program. Work is underway to quantify these findings using temperature, species, and radiation measurements in the 5.18-second Zero-Gravity Facility of NASA-Lewis.

4.0 Conclusions

Effects of various levels of oxygen in the environment have been studied for laminar methane and propane diffusion flames in microgravity. The flames show significant changes in color, luminosity, and characteristics compared to normal-gravity flames. Quenching at the tip, and hence an underventilated behavior, is observed for propane flames over a wide range of oxygen concentration due to extensive soot formation and radiation cooling. The observed colors indicate that radiative loss may be the most important cause of flame extinction for the near-limit flames.

References

1. Edelman, R.B., and Bahadori, M.Y., "Effects of Buoyancy on Gas-Jet Diffusion Flames: Experiment and Theory," Acta Astronautica, Vol. 13, No. 11/12, 1986, pp. 681-688; see also references cited in this work.

2. Bahadori, M.Y., Edelman, R.B., Stocker, D.P., and Olson, S.L., "Ignition and Behavior of Laminar Gas-Jet Diffusion Flames in Microgravity," in press, AIAA J., 1989.

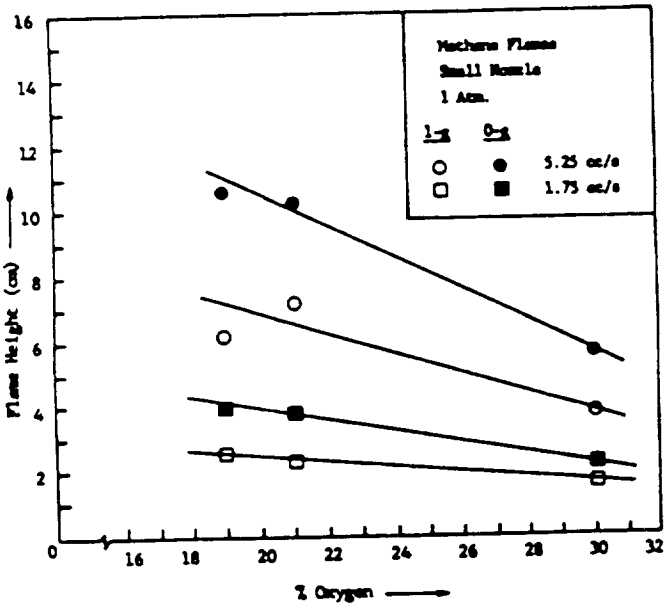

Fig. 1. Flame height vs. percent oxygen for both normal-gravity and microgravity methane diffusion flames.

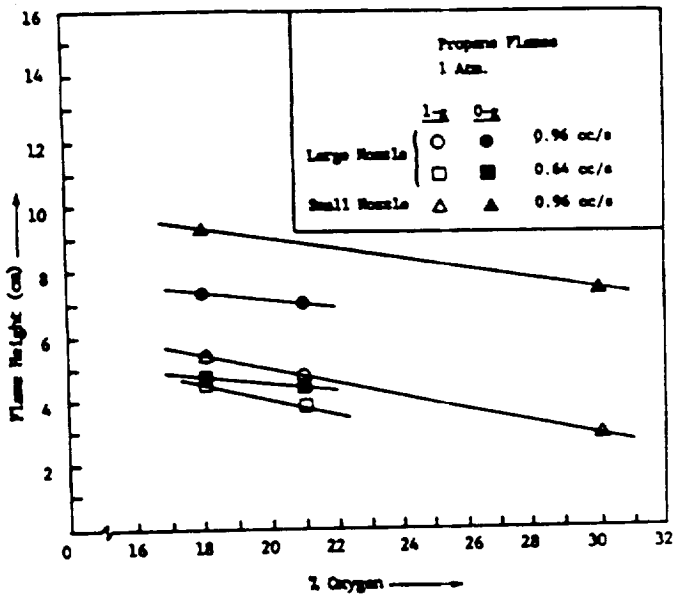

Fig. 2. Flame height vs. percent oxygen for both normal-gravity and microgravity propane diffusion flames.

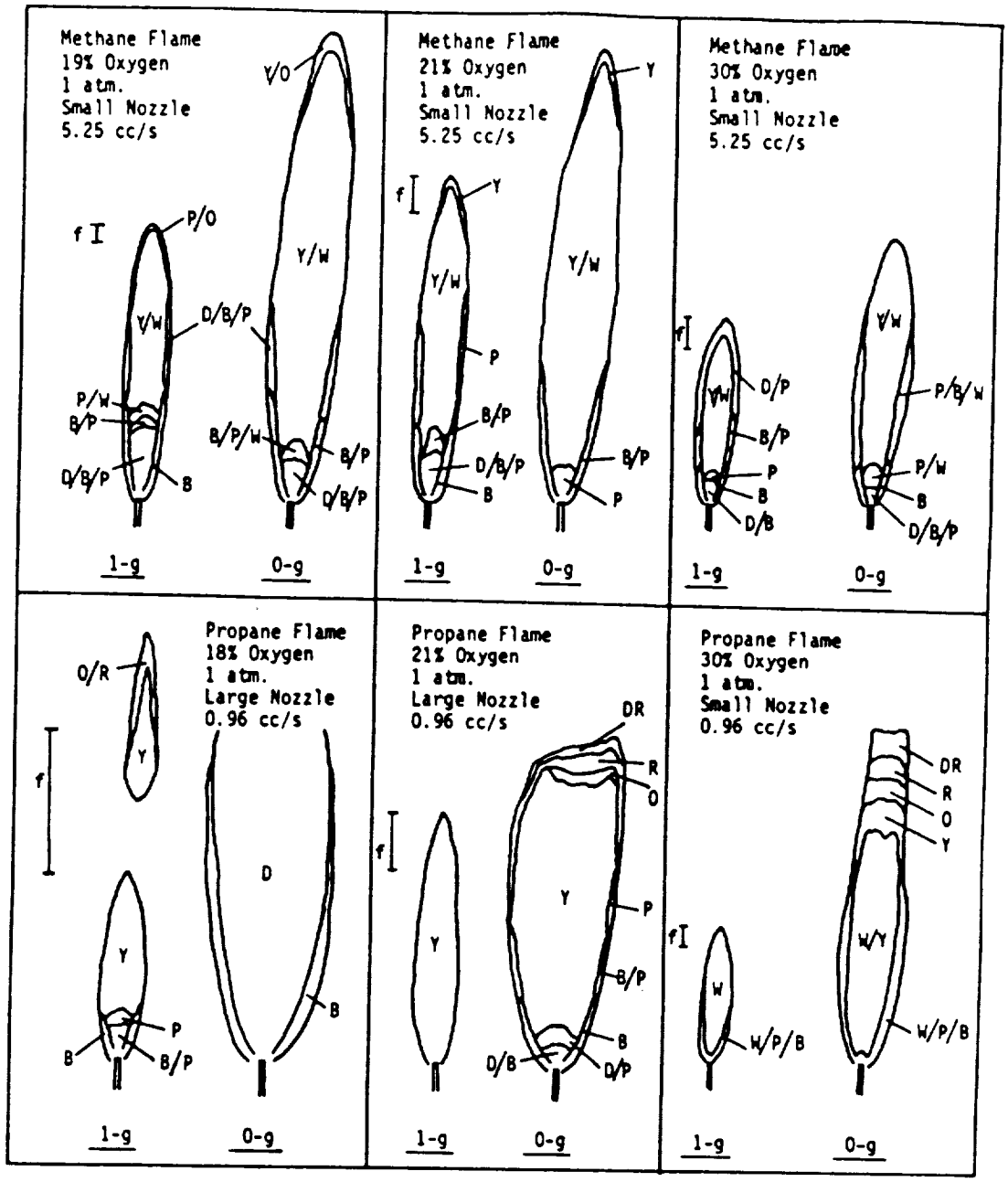

Fig. 3. Normal-gravity and microgravity laminar diffusion flames of methane and propane, burning in quiescent environments at 1 atm with different oxygen-nitrogen mixtures. The two nozzles have a tapered-tip radius of 0.048 and 0.074 cm. The various colors indicated in the diagram are as follows: B (blue), D (dark), O (orange), P (pink), R (red), W (white), Y (yellow), and DR (dull red). The bars show the range of normal-gravity flame flicker (f). The coloring may be slightly off due to the force-processing of films for low-oxygen and 21%-O_2 environments. The films for the flames in 30%-O_2 environments were not force-processed. The low-oxygen-concentration flame of propane in normal gravity shows pockets of flame leaving the flickering part. Scale: ⟷ = 1 cm.

Section 8

"MEASUREMENT OF TEMPERATURE IN MICROGRAVITY LAMINAR DIFFUSION FLAMES"

M. Y. Bahadori, R. B. Edelman, R. G. Sotos, and D. P. Stocker

Paper presented at the Eastern States Meeting of The Combustion Institute, Orlando, Florida, December 1990

Measurement of Temperature in Microgravity Laminar Diffusion Flames[1]

M.Y. Bahadori[2] and R.B. Edelman[3]
Science Applications International Corporation, Torrance, California
and
R.G. Sotos and D.P. Stocker
NASA Lewis Research Center, Cleveland, Ohio

1. Introduction

Laminar diffusion flames of hydrocarbons under microgravity conditions have been studied extensively [1-11]. It has been shown that compared to the flames in normal-gravity environments, larger, globular, and more sooty flames are observed in microgravity. This is due to the reduction of buoyancy, which makes diffusion a more dominant mechanism of transport. As a result, increased residence time, enhanced soot formation, radiative cooling due to the larger flame size, and the possible onset of a chemical kinetics limitation on the heat release process become responsible for the different characteristics observed between normal-gravity and microgravity flames.

In the previous studies [1-11], qualitative information and semiquantitative data have been obtained using visualization of flame characteristics and behavior by studying these flames in the 2.2-Second Drop Tower of NASA Lewis Research Center. However, the limitation of available time in microgravity and the lack of quantitative data have prompted the current investigation.

In the present work, laminar diffusion flames of propane burning in quiescent oxidizing environments of different pressure and oxygen concentration have been studied in the 5.18-Second Zero Gravity Facility of NASA Lewis Research Center. The first demonstration of the ability to map the thermal field in a microgravity combustion study is presented in this paper. A rake of nine thermocouples has provided temperature data. Cinematography along with this data has enabled us to compare the flames quantitatively and obtain information on their characteristics. For each microgravity flame, the normal-gravity counterpart was also studied.

2. Apparatus and Experimental Procedure

Figure 1 shows a schematic of the hardware. The volume of the sealed combustion chamber is 0.087 m^3. The tapered-tip nozzle inner radius is 0.0825 cm. Propane flames at a volume-flow rate of 1.5 cc/sec were studied. The cold-jet Reynolds number was 130 in all cases. The oxidizing environment was composed of 19%-O_2/81%-N_2 at 1.0 atm, 21%-O_2/79%-N_2 at 1.0 atm, and 21%-O_2/79%-N_2 at 0.5 atm, respectively.

The flames were ignited using a spark electrode, located 1.0 cm above the nozzle tip and 2.0 cm away from the nozzle centerline, with the nozzle acting as the ground electrode. The spark-ignition system was activated for approximately 1.0 sec for both the normal-gravity and microgravity flames. The microgravity flames were ignited after the release

---

1 Presented at the 1990 Fall Technical Meeting (Eastern Section) of The Combustion Institute, Orlando, Florida, December 3-5, 1990. This work is supported by NASA Lewis Research Center under Contract NAS3-22822.

2 Author to whom correspondence should be sent to the following address: SAIC/NASA LeRC, MS 500-217, Cleveland, Ohio 44135.

3 Present Address: Rockwell International Corporation, Rocketdyne Division, Canoga Park, California.

of the package in the evacuated drop tube.

Two movie cameras (filming rates = 12 and 30 frames/sec, respectively) using Kodak Ektachrome Video News films recorded the flame development and behavior. A rake of nine thermocouples (3x3) measured the temperature above the normal-gravity flame tip and both inside and outside the microgravity flames. These thermocouples were located in a plane passing through the nozzle centerline. The thermocouple columns were 2 cm apart, with the column closest to the nozzle centerline being 0.75 cm away from it. The rows of thermocouples were 3 cm apart. Although the thermocouples were fixed with respect to each other, the whole rake could be adjusted vertically with respect to the nozzle tip (prior to testing) to measure temperature at specified heights.

3. Results and Discussion

Figure 2 shows the size, shape, and color of the flames studied in addition to the position of the thermocouple rake with respect to the flame. The normal-gravity flames were typically established within 0.5 sec following ignition, and flickered throughout the experiment duration with the typical flicker frequency of laminar diffusion flames burning in quiescent environments. All of the normal-gravity flames were generally yellow/white, and the color was not strongly affected by either pressure or oxygen concentration. The results have shown that the lower the oxygen concentration or pressure, the wider the normal-gravity flame. This can be explained in terms of the availability of oxygen in the environment. The results presented in Fig. 2 also agree with previous observations that at a fixed Reynolds number, the lower the pressure, the smaller the flicker range [9], and the lower the oxygen concentration, the larger the flicker range [7] for normal-gravity propane flames.

Flames in microgravity were always taller and wider than their normal-gravity counterparts, and were flicker-free. Removal of buoyancy results in the dominance of diffusive processes which are responsible for these changes. In addition, the lack of buoyant force causes the flame to develop toward its steady state over a much longer time (of the order of seconds). The microgravity flames shown in Fig. 2 correspond to the shapes and colors observed just prior to the deceleration of the package, and were fairly uniform during the last second of the drop. However, unlike flames in normal gravity which were pencil-like and had closed tip, the microgravity flames of propane had an open tip, resembling underventilated behavior. This is believed to be caused by the combination of enhanced sooting, a significant drop in the gas velocity near the flame tip, extensive radiative loss, accumulation of the combustion products in the vicinity of the flame, and thermophoretic effects. These processes cause the flame tip to open due to the reduced transport of oxygen, and presumably result in fuel escape through the tip. The microgravity flames of Fig. 2 are dimmer, more sooty, and orange/red in color. Just like normal-gravity flames, the lower the oxygen concentration or pressure, the wider the flame. Using the criteria of red-to-dull red transition region for the location where burning ceases [9], it can be seen that the lower the oxygen concentration or pressure, the taller the microgravity flame [7,9].

Figure 3 shows a typical set of temperature data for the propane flame burning in 19%-O_2/81%-N_2 environment at 1 atm, under both normal-gravity and microgravity conditions. The lowest row of thermocouples is 10 cm above the nozzle tip. An initial overshoot in temperature is observed in both cases due to the presence of excess fuel at ignition.

Figure 3 presents some useful information not only in relation to the temperature field, but also for other flame characteristics and behavior. The normal-gravity data show that the temperature drops quickly to the ambient somewhere between the radial locations of 0.75 and 2.75 cm. This is due to the effect of buoyant force which carries and removes the combustion products in a narrow column determined by the maximum flame radius. In addition, the strong buoyancy-driven portion of the flame causes the three thermocouples near the centerline to show roughly equal temperatures, which essentially reach steady state approximately 3 seconds after the start of the experiment.

The data presented in Fig. 3 for microgravity flames show that far above and away from the flame, the gas is still experiencing a temperature rise due to the continuous release of the combustion products in the vicinity of the flame and their subsequent diffusion. This figure also shows that the gas temperature does not reach a steady value

anywhere in the field during the 5 seconds of microgravity, again due to the continuous dilution and heating of the environment caused by the combustion products. In addition, large temperature gradients exist in the axial direction for the microgravity flame, and the variation of temperature in the radial direction is significant all the way to the far field.

Figure 4 shows the temperature data at t = 5 seconds as a function of the axial location of the thermocouples for fixed radial locations. Both normal-gravity and microgravity data are shown in this figure. All of the normal-gravity data indicate that the second and third columns of thermocouples (see Fig. 2) register a temperature of 300 K. The first column (closest to the centerline) shows a constant and small decrease in temperature with an increase in height for flames A, B and C. Normal-gravity flame D does not show a fixed slope, probably because it is a taller, wider, and more diffuse flame due to the lower pressure. The microgravity flames A and B of Fig. 4 show almost identical temperature distributions but it needs to be determined whether flames in environments with less than 19% oxygen will show the same levels of temperature. Significant differences in temperature levels are observed between microgravity flames C and D, with the 0.5-atm flame being taller and wider. The combination of larger flame size and reduced pressure contribute to increased radiative loss, which raises the field temperature to higher levels.

Figure 5 shows the temperature data as a function of the radial location of the thermocouples for fixed axial locations in the microgravity flames. The normal-gravity data is not presented in this figure, since the temperature drops to ambient somewhere between the first two columns of thermocouples. Due to the uncertainty in the monotonic behavior of temperature between the first and second thermocouples of the lowest row, the plots have not been extended to the temperature at the first thermocouple. It is possible that there is a peak in temperature between the innermost thermocouples due to the presence of the flame zone, especially for flames C and D.

4. Conclusions

Mapping of the thermal field has been demonstrated for the first time in microgravity flames using a rake of nine thermocouples.

Normal-gravity and microgravity flames of propane burning under different environments of pressure and oxygen concentration show significant differences in height, width, color, and temperature distribution.

Low-pressure microgravity flames show significantly higher temperatures; this is apparently caused by both increased radiative loss and larger flame size due to reduced pressure.

Compared to microgravity flames under atmospheric conditions, the low-oxygen-concentration flames do not show as significant an effect as the low-pressure flames. However, these oxygen-deficient flames may show significant changes at low-enough oxygen concentrations.

Longer test durations appear to be required to reach steady state in microgravity.

References

1. Cochran, T.H. and Masica, W.J., "Effects of Gravity on Laminar Gas Jet Diffusion Flames," NASA TN D-5872 (1970).
2. Cochran, T.H., "Experimental Investigation of Laminar Gas Jet Diffusion Flames in Zero Gravity," NASA TN D-6523 (1972).
3. Haggard, J.B. and Cochran, T.H., "Hydrogen and Hydrocarbon Diffusion Flames in a Weightless Environment," NASA TN D-7165 (1973).
4. Edelman, R.B., Fortune, O.F., Weilerstein, G., Cochran, T.H., and Haggard, J.B., "An Analytical and Experimental Investigation of Gravity Effects Upon Laminar Gas Jet Diffusion Flames," Fourteenth Symposium (International) on Combustion, pp. 399-412, The Combustion Institute, Pittsburgh, Pa (1973).
5. Haggard, J.B., "Forced and Natural Convection in Laminar Jet Diffusion Flames," NASA TP-1841 (1981).
6. Edelman, R.B. and Bahadori, M.Y., "Effects of Buoyancy on Gas-Jet Diffusion Flames: Experiment and Theory," Acta Astronautica, 13, No. 11/12, pp. 681-688 (1986).
7. Bahadori, M.Y. and Stocker, D.P., "Oxygen-Concentration Effects on Microgravity Laminar Methane and Propane Diffusion Flames," Fall 1989 Eastern States Meeting of The Combustion Institute, Albany, New York, October/November 1989.
8. Bahadori, M.Y., Edelman, R.B., Stocker, D.P., and Olson, S.L., "Ignition and Behavior of Laminar Gas-Jet Diffusion Flames in Microgravity," AIAA J. 28, pp. 236-244 (1990).
9. Bahadori, M.Y., Stocker, D.P., and Edelman, R.B., "Effects of Pressure on Microgravity Hydrocarbon Diffusion Flames," Paper AIAA 90-0651, AIAA 28th Aerospace Sciences Meeting, Reno, Nevada, January 1990.
10. Stocker, D.P., "Size and Shape of Laminar Burke-Schumann Diffusion Flames in Microgravity," Spring 1990 Central States Meeting of The Combustion Institute, Cincinnati, Ohio, May 1990.
11. Bahadori, M.Y., "An Analytical Solution for Transient, Cylindrically Symmetric Laminar Diffusion Flames in the Absence of Buoyancy," Spring 1990 Central States Meeting of The Combustion Institute, Cincinnati, Ohio, May 1990.

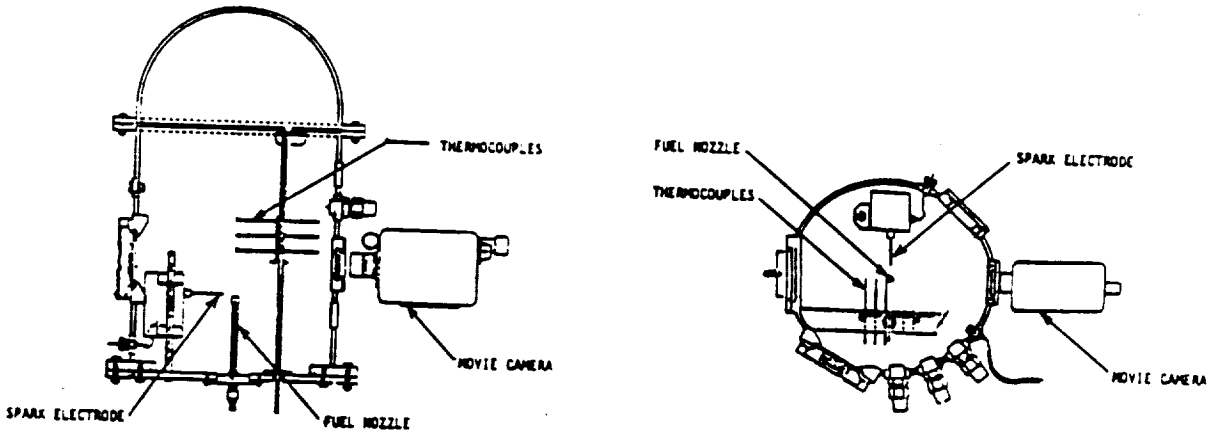

Figure 1. Experimental hardware for the 5.18-second tests.

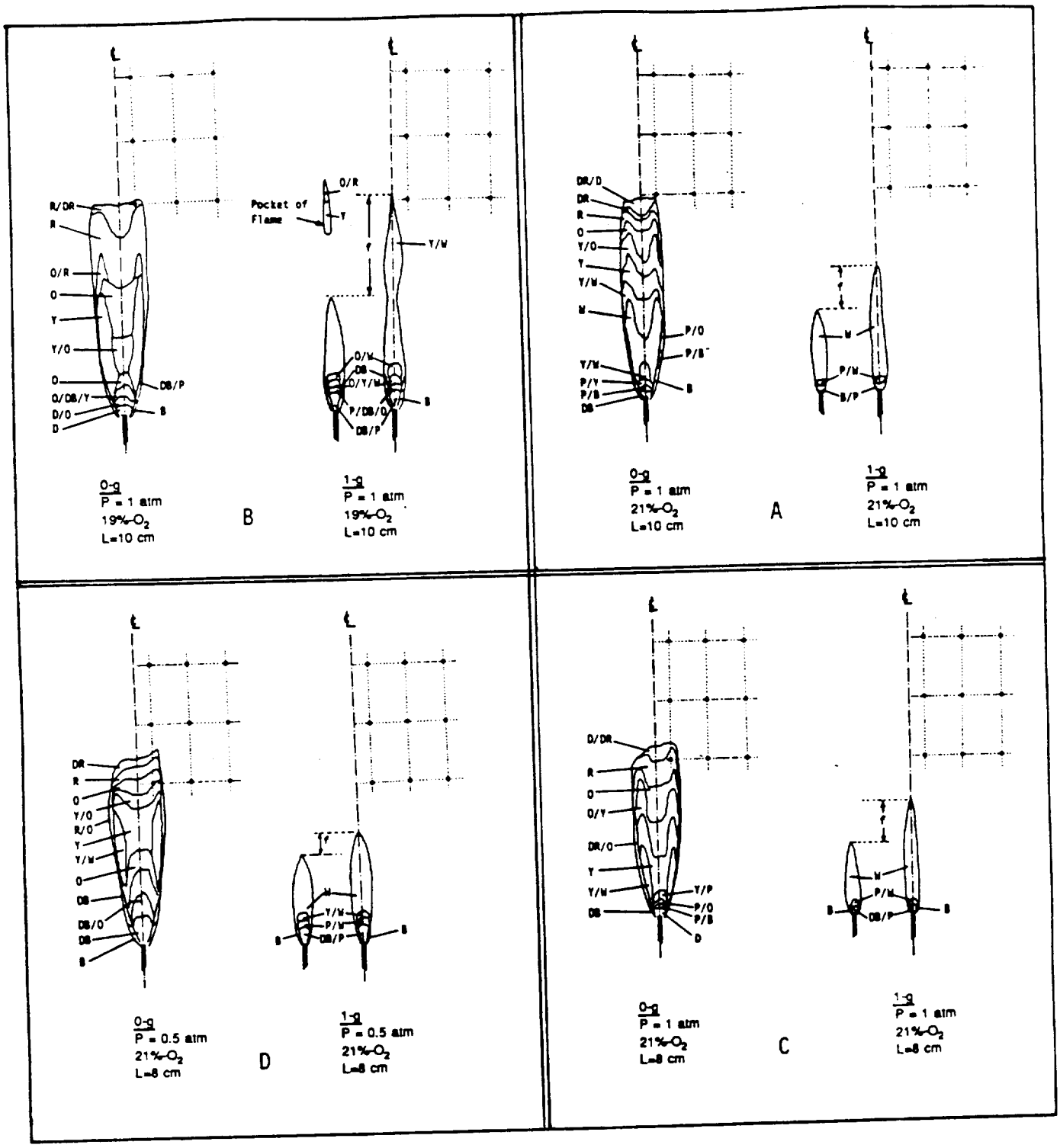

Figure 2. Flames of propane at 1.5 cm^3/sec for both normal-gravity and microgravity conditions. The colors are as follows: B (blue), D (dark), DB (dark blue), DR (dull red), O (orange), P (pink), R (red), W (white), Y (yellow). The flicker range, f, is shown for the normal-gravity flames. L is the distance between the nozzle tip and the lowest row of thermocouples. The columns of thermocouples are, respectively, 0.75 cm away from the centerline, and then 2 cm apart. The rows of thermocouples are 3 cm apart. These diagrams are to scale.

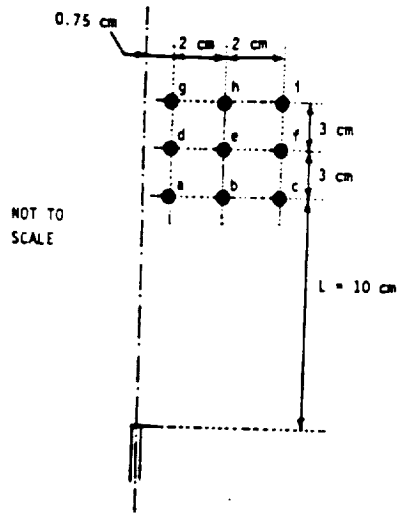

Propane - 19% O_2 Flame

Flow Rate = 1.5 cc/s

Nozzle Radius = 0.0825 cm

P = 1 atm

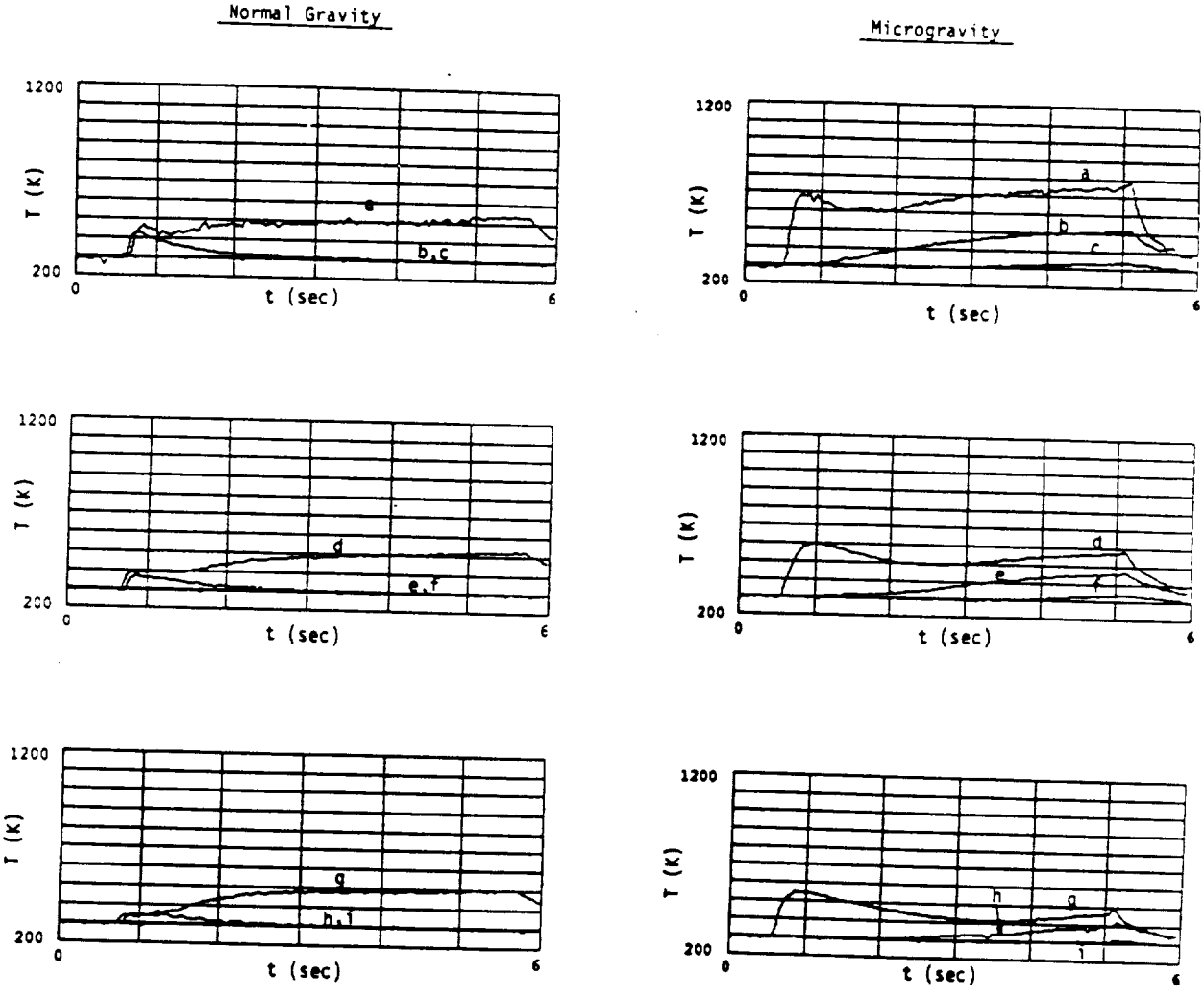

Figure 3. Typical temperature data for a normal-gravity and microgravity flame.

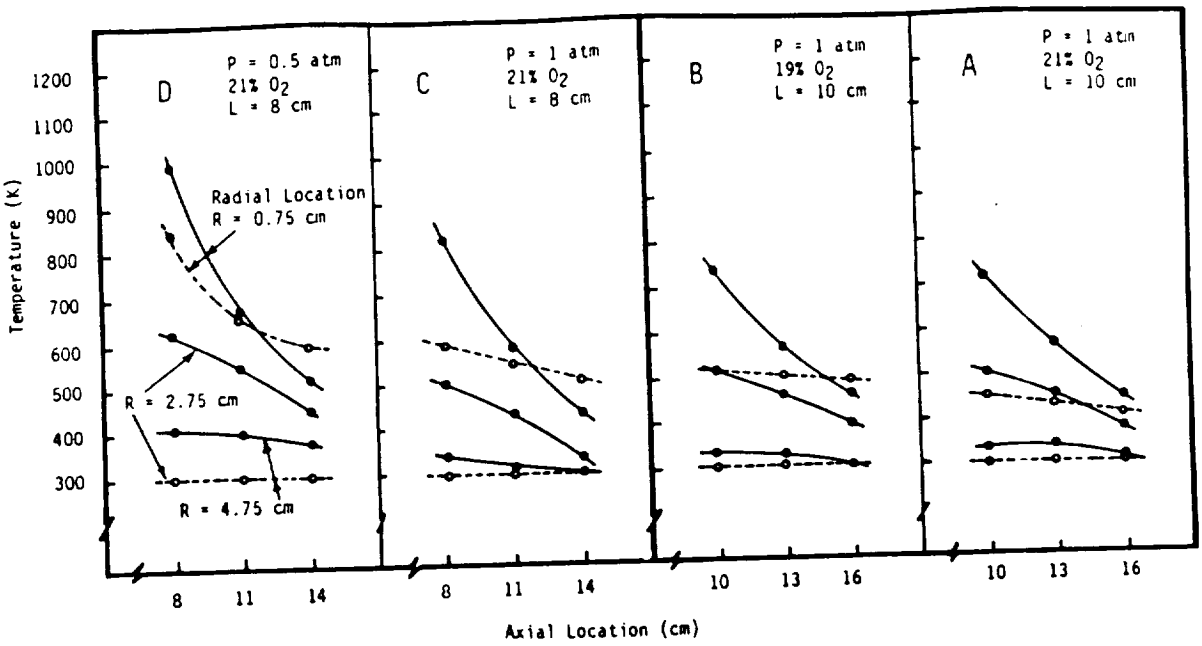

Figure 4. Temperature plots as a function of the axial location of thermocouples for both normal-gravity (open symbols and dashed lines) and microgravity (closed symbols and solid lines) flames of propane with a volume flow rate of 1.5 cm^3/sec. L is the distance between the nozzle tip and the lowest row of thermocouples. The radial locations indicated in the diagram are applicable to all plots.

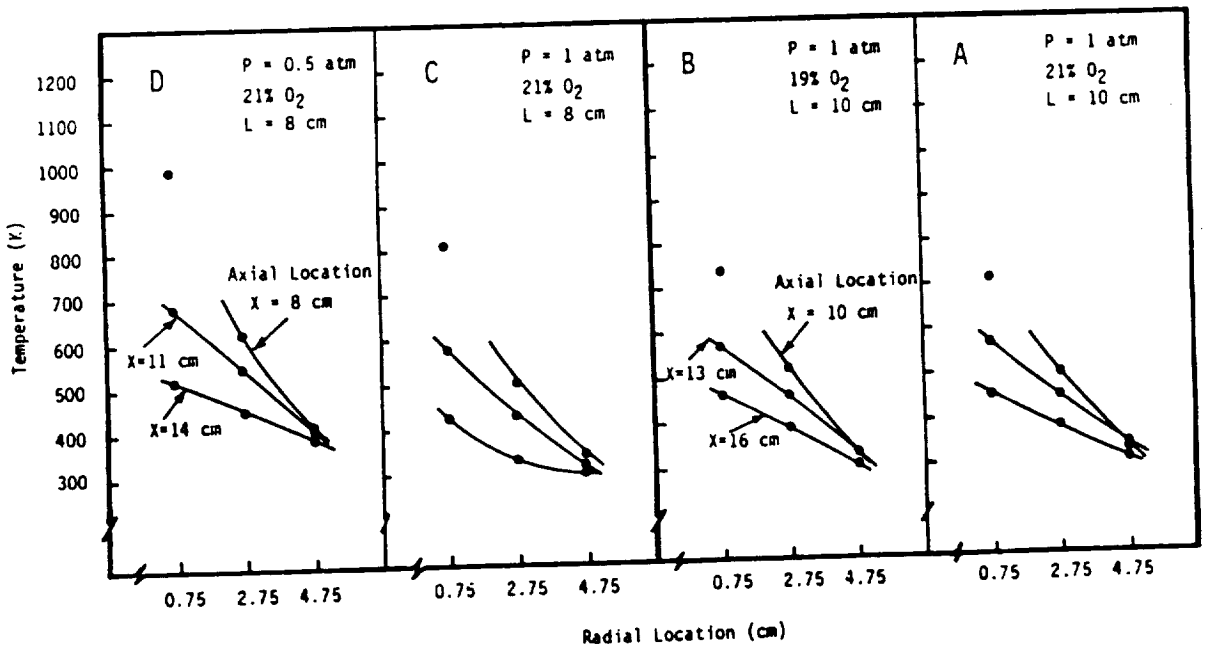

Figure 5. Temperature plots as a function of the radial location of thermocouples for microgravity flames of propane with a volume flow rate of 1.5 cm^3/sec. L is the distance between the nozzle tip and the lowest row of thermocouples. The axial locations indicated in the diagram are applicable to those of the same family (i.e. same L). The incomplete plots indicate the presence of flame between the two columns of thermocouples.

Section 9*

"IGNITION AND BEHAVIOR OF LAMINAR GAS-JET DIFFUSION FLAMES IN MICROGRAVITY"

M. Y. Bahadori, R. B. Edelman, D. P. Stocker, and S. L. Olson

AIAA Journal, Vol. 28, No. 2, pp. 236-244, 1990

* This paper is a revised journal publication of paper AIAA-88-0645 (see Section 5).

Ignition and Behavior of Laminar Gas-Jet Diffusion Flames in Microgravity

M. Y. Bahadori, R. B. Edelman, D. P. Stocker, S. L. Olson

Reprinted from

AIAA Journal

Volume 28, Number 2, February 1990, Pages 236–244
AMERICAN INSTITUTE OF AERONAUTICS AND ASTRONAUTICS, INC.
370 L'ENFANT PROMENADE, SW • WASHINGTON, DC 20024

Ignition and Behavior of Laminar Gas-Jet Diffusion Flames in Microgravity

M. Yousef Bahadori* and Raymond B. Edelmant
Science Applications International Corporation, Torrance, California
and
Dennis P. Stocker‡ and Sandra L. Olson‡
NASA Lewis Research Center, Cleveland, Ohio

This paper presents the results of studies on the ignition and behavior of cylindrically symmetric, laminar diffusion flames of methane and propane in quiescent air under microgravity conditions. The experiments were conducted in the 2.2 s NASA-Lewis Research Center Drop Tower. The characteristics of gas-jet diffusion flames ignited in microgravity environments have not been reported in the past. In prior research, similar flames were ignited in normal gravity and then subjected to the microgravity condition once the flame was established. The different ignition methods result in different flame behavior and conclusions in relation to extinction, transient adjustment, and approach toward steady state in microgravity. Specifically, some of the flames of the previous studies, which were in a transient state or reportedly extinguished, reach a near-steady state when ignited in microgravity. In addition, low-flow-rate methane flames in the present study (filmed at 15 frames/s) were entirely blue, whereas blue was not discernible in the microgravity flames of the previous works (filmed at 400 frames/s). Based on these findings, it is concluded that some of the previously reported "extinguished" flames may have been blue (and not visible on the high-speed film). In this paper, comparisons between the two methods of ignition and observations of the flame behavior and distinct nature of flame color and luminosity are presented. Application of a steady-state, parabolic model has shown satisfactory agreement between the predicted and observed flame heights for those flames that reached a near-steady state in the 2.2 s period of microgravity.

Introduction

THE term "diffusion flame" classifies those types of flames in which the fuel and the oxidizer are not premixed, and the combustion process is governed by the diffusion of reactants toward each other. Fires are a complicated type of this class of flames. Regardless of the nature of the fuel involved, (i.e., liquid, solid, or gaseous), the fundamental mechanisms that control the combustion process are the same. These include the coupled processes of mixing, chemical kinetics, flame radiation, diffusion, inertia, soot formation and disposition (in hydrocarbon flames), and, depending upon the Grashof or Froude number, buoyancy-induced convection.

Gas-jet diffusion flames are laminar or turbulent, depending on the relative effects of inertia and viscous forces, which can best be described in terms of the jet Reynolds number based on the fuel properties and nozzle size. Fundamental studies of laminar diffusion should lead to an improved understanding of turbulent diffusion flames, which are of practical interest, and are not fully understood.

The behavior of most fires on Earth is dominated by buoyancy-induced convection which masks the chemical-diffusional interactions that are fundamental to the understanding of combustion phenomena. In low-gravity environments, the buoyant force is suppressed and the remaining mechanisms of kinetics, radiation, diffusion, inertia, soot processes, and mixing become responsible for the very different observed behavior of laminar flames. As a result, aside from the primary goal of understanding the behavior of fires in spacecraft environments, microgravity combustion studies facilitate the study of the physico-chemical phenomena masked by buoyancy under normal-gravity conditions. In addition, numerical modeling of flames can benefit from the removal of one constraint (buoyant force) by focusing on the remaining phenomena, which are not separable and cannot be isolated.

Background

Laminar diffusion flames of hydrogen, methane, ethylene, and propylene have been studied[1-9] in the 2.2 s NASA Lewis Research Center Drop Tower. In these studies, the flames were ignited in normal gravity and allowed to reach steady state. The experiment package was then dropped, subjecting the flame to the microgravity condition. High-speed movies of the flames have shown that during a very short period of adjustment from normal gravity to microgravity, a sudden decrease in the flame height (h) occurred within 0.05 s. After the decrease of the flame height to a minimum with $0.6<(h_{min}/h_{1-g})<1.0$ (depending on the jet Reynolds number), the flame height increased with time. This resulted in either extinction with $1.0<(h_{ex}/h_{1-g})<1.3$, approach toward an apparent steady state with $1.4<(h_{\mu-g}/h_{1-g})<1.7$, or continual increase until the end of the test time. Here, the subscripts min, ex, $\mu-g$, and $1-g$ correspond, respectively, to minimum, extinguished, microgravity, and normal-gravity flame heights. Compared to laminar flames in normal gravity, those observed in microgravity are larger, diffuse, and rather globular. This is due to the absence of the buoyant convection, leaving diffusion a much more important mechanism of

Received November 1987; presented in part as Paper AIAA-88-0645 at the AIAA 26th Aerospace Sciences Meeting, Reno, NV, Jan. 11-14, 1988; revision received March 15, 1989. This paper is declared a work of the U.S. Government and is not subject to copyright protection in the United States.

*Senior Scientist, Thermal Hydraulics Division. Member AIAA. Author to whom correspondence should be sent. On-site at the NASA-Lewis Research Center, MS 500-217, Cleveland, OH 44135.

†Director of the Combustion Science and Advanced Technology Department, Chatsworth, CA. Currently at Rockwell International Corporation, Rocketdyne Division, Canoga Park, CA. Member AIAA.

‡NASA Project Scientist.

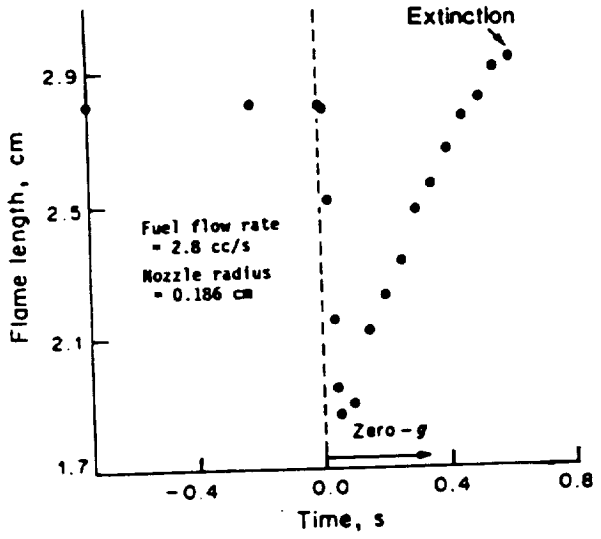

Fig. 1 Length as a function of time in microgravity for an extinguished methane-air diffusion flame.[1]

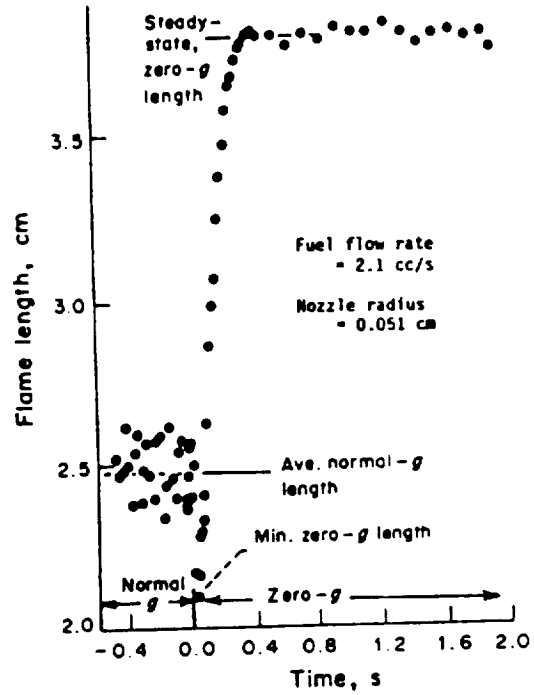

Fig. 2 Length as a function of time in microgravity for a methane-air diffusion flame that reached near-steady state.[4]

transport relative to the jet momentum. However, as will be seen later, jet momentum still affects the flame shape.

The observed flame behavior in microgravity, i.e., steady state, transient, or extinguished, has been attributed to the influence of the jet Reynolds number. Figures 1 and 2 show the behavior of two methane-air flames[1,4] in microgravity: an extinguished flame (Fig. 1) and a flame which apparently reached steady state (Fig. 2) during the drop. The data presented in the previous works[1,4] suggest that for a fixed tube size and variable fuel velocity, a certain range of the jet Reynolds number exists for which the 2.2 s available time is not sufficient to yield either flame extinction or steady state. However, it will be shown (see the Results and Discussion section) that a majority of these "transient" or even "extinguished" flames of the previous studies reached a near-steady state when the flame was ignited in microgravity.

The reported[1,4] microgravity flame behavior may best be described by the following mechanisms, based on the qualitative observations of the films. If the flame is ignited in normal gravity and then dropped, a rapid decrease in flame height occurs (see Figs. 1 and 2). This behavior is due to the sudden accumulation of the hot combustion products in the flame region, resulting from the loss of the buoyancy-driven convective flow. The flame zone then becomes shielded from the oxygen, which promotes pyrolysis of the constantly flowing fresh fuel. A critical reduction in temperature occurs, caused by a reduced heat-release rate probably due to the change in the oxidation kinetics. This enhances soot formation and radiation cooling, resulting in the onset of a chemical-kinetic limitation on the heat release process. The combination of these effects and the jet momentum leads to either extinction or a slow readjustment to a steady-state flame (with convective transport matching diffusive transport).

The sensitivity of the extinguishment process to convective transport in microgravity has been demonstrated.[8] Low forced-air velocities ($\simeq$ 10 cm/s) in coaxial jets of methane-air diffusion flames were sufficient to sustain combustion in microgravity, whereas similar microgravity flames in quiescent air reportedly extinguished. This indicates that relatively small forced-convection currents play a major role in combustion under microgravity conditions.

The ignition approach previously used in the drop tower experiments exposes an established normal-gravity flame to a sudden change in the gravity level. It is not clear whether the reported microgravity flame behavior is due to this step change in gravity level or the microgravity environment itself. In addition, it is conceivable that buoyant forces could induce

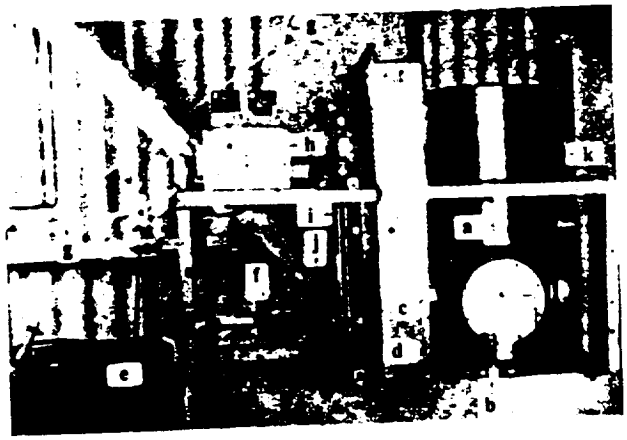

Fig. 3 Experiment package: a) combustion chamber; b) flow meter; c) viewing window partially hidden by strut; d) solenoid valve hidden by strut; e) mixing system; f) pressure regulator; g) fill line; h) control panel; i) fuel bottle; j) camera partially hidden by regulator and fuel bottle; k) to vent.

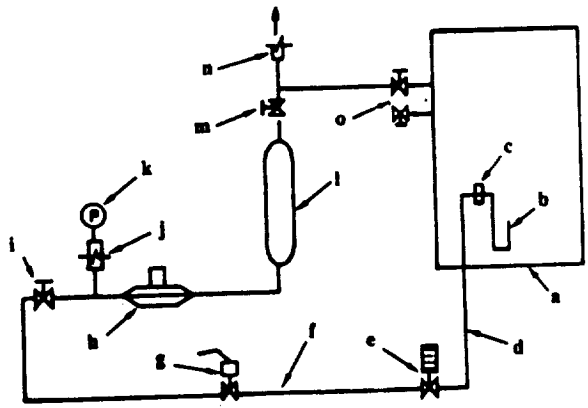

Fig. 4 Schematic diagram of the flow system: a) combustion chamber; b) burner nozzle; c) chamber bulkhead; d) 1/8 in. O.D. tubing; e) metering valve with Vernier markings; f) 1/4 in. O.D. tubing; g) solenoid valve; h) pressure regulator; i) hand valve; j) quick disconnect; k) pressure gauge; l) fuel bottle; m) hand valve; n) quick disconnect; o) vents.

Table 1 Data obtained from microgravity and normal-gravity experiments[a]

Flame number	G	Nozzle radius, cm	Fuel	Fuel volume flow rate, cm^3/s	Steady-state flame height, cm	S.S. maximum flame radius, cm	Approx. time to reach S.S., s	Reynolds number[b]
1	0	0.051	Methane	1.0	1.5[c]	0.67	0.6	38
2				2.0	3.5	0.70	0.8	76
3				3.0	5.1	0.75	1.0	114
4		0.0825		1.0	2.4[c]	1.06	1.0	24
5				2.0	3.7[c]	1.05	0.9	48
6				3.0	5.5	1.11	1.6	72
7		0.051	Propane	0.5	4.0	0.90	1.2	70
8				1.0	7.2	1.02	0.8	140
9				1.5	11.1	1.11	0.8	210
10		0.0825		0.5	3.8	1.32	1.2	44
11				1.0	7.3	1.53	1.8	88
12				1.5	9.9	1.73	1.3	132
13	1	0.051	Methane	1.0	0.9	0.35	0.8	38
14				2.0	2.0	0.43	1.3	76
15				3.0	4.0(?)	0.36	(?)	114
16		0.0825		1.0	0.9	0.38	0.6	24
17				2.0	2.5	0.60	0.4	48
18				3.0	3.6	0.61	0.3	72
19		0.051	Propane	0.5	2.6	0.45	0.4	70
20				1.0	5.6	0.50	0.4	140
21				1.5	8.0	0.50	1.3	210
22		0.0825		0.5	3.0	0.57	0.4	44
23				1.0	7.8(?)	0.50	(?)	88
24				1.5	8.0	0.58	0.4	132

[a]Question marks indicate uncertainties in the measurements due to the flame flicker.
[b]Reynolds number is based on the nozzle radius.
[c]These flames were diffuse, faint, and resembling an underventilated flame; it could not be concluded that they reached steady state.

enough momentum during the pretest normal-gravity period to persist throughout the 2.2 s test time. In order to study the true characteristics of microgravity flames, it seems logical to simplify the initial conditions by igniting the flames in microgravity. The focus of this paper is to study the behavior of flames ignited in microgravity in order to achieve a more fundamental understanding of diffusion flames.

Apparatus

Laminar methane and propane diffusion flames in quiescent air were studied in the 2.2 s NASA-Lewis Research Center Drop Tower (facility described elsewhere[6]). The experiment package and a schematic diagram of the flow system are shown in Figs. 3 and 4, respectively. The combustion chamber contains a burner, the lighting system, a viewing port for the camera, the spark ignitor, and ports for filling the chamber with oxidizer and for venting the burned gases. The other components of the system are shown in Fig. 4. The volume of the combustion chamber is approximately 0.04 m^3. Two fuel nozzles with inside radii of 0.051 cm and 0.0825 cm were used in the studies. The fuel system was calibrated, based on the standard conditions of 0°C and 1 atm. The fuel flow rates were 1.0, 2.0, and 3.0 cm^3/s for methane, and 0.5, 1.0, and 1.5 cm^3/s for propane. The 16 mm movie camera was originally set for a filming rate of 30 frames/s and the film (Tungsten Eastman Ektachrome Video News) was force-processed 2 f-stops. At this filming rate, the dim blue portion of the microgravity flames was not clearly visible in the processed films. Visibility was subsequently improved by reducing the framing rate to 15 frames/s.

A spark electrode was located 4 mm above the nozzle tip and 4 mm away from the nozzle centerline. The electrode was perpendicular to the centerline of the camera. The nozzle, electrically grounded, acted as the second electrode. The spark was pulsed at 4.8 Hz, with approximately 18 mJ/pulse. The flames were ignited during the first 0.2–0.4 s in microgravity. For all of the tests, the spark-ignition system was active for the entire 2.2 s test time and about 0.8 s after impact. The ignitor occasionally did not arc to the burner tip but shorted out elsewhere, however, this did not affect the flame behavior. A frame-by-frame study of the movies showed no disturbance of the flames by the spark during the 3.0 s of burning.

The 500-cm^3 fuel bottle contained either methane or propane filled to 2 atm. The dry air in the combustion chamber was composed of 21% oxygen and 79% nitrogen, and had a pressure of 1.0 atm in the chamber. Due to the short duration of each test, the amount of oxygen consumed was negligible, always less than 0.3% per flame. The air in the experiment chamber was changed after a number of tests were conducted, when $< 5\%$ of oxygen was depleted. Details of the experimental procedure can be found elsewhere.[10]

Results and Discussion

Table 1 shows the experimental conditions and the average steady-state flame lengths, maximum flame radii, and approximate time to reach steady state for both normal-gravity and microgravity flames of methane and propane. The normal-gravity flames flickered (except at low-flow rates), and the steady-state flame heights and maximum radii are averages. Figures 5 and 6 show the flame lengths as a function of time for methane and propane flames in microgravity, respectively. Unlike flames in normal gravity, those under the microgravity conditions are fairly steady and do not flicker. The methane flames at low volume-flow rates were very faint and appeared to have an open tip. They were sufficiently visible to identify the maximum radius, but beyond this height, visible radiation could not be observed and the flame appeared to be underventilated. This is shown by the truncated data given in Fig. 5. The higher flow-rate methane flames reached near-steady state with some fluctuations at the later times. Previous studies of these methane flames with the 0.0825 cm nozzle radius have shown a transient state at the completion of the drop.[4] In general, Table 1 shows the following relationships for flame heights (h) and maximum flame radii (r_m): $1.2 < (h_{\mu-g}/h_{1-g}) < 1.8$ for both nozzle sizes; $1.6 < (r_{m,\mu-g}/r_{m,1-g}) < 2.2$ for the smaller nozzle; $2.3 < (r_{m,\mu-g}/r_{m,1-g}) < 3.1$ for the larger nozzle. Here, the subscripts $\mu - g$ and $1 - g$ correspond to the microgravity and normal-gravity flame dimensions,

respectively. An overshoot in the methane flame heights can be seen in Fig. 5, whereas the propane flames in Fig. 6 do not show this behavior. This observation is currently under investigation.

Figure 7 shows a comparison between the two methods of ignition for a methane flame, with a fuel flow rate of 3.0 cm^3/s (2.9 cm^3/s for the normal-gravity ignition case[4]) and a nozzle radius of 0.051 cm. The trends in flame development are similar, and the steady-state flame heights are the same. Typical normal-gravity flame flicker is also shown in Fig. 7. The normal-gravity ignition method suggests that the microgravity flame behavior may be affected by the flickering normal-gravity flame height at the instant the package is subjected to the microgravity condition.

The flame heights observed in the previous[4] and present studies are compared in Fig. 8. The jet Reynolds number is selected as a common parameter because it represents the effects of nozzle size, fuel type, and jet momentum, which are shown to control the behavior of the flame as far as extinction and approach toward steady state are concerned. In Fig. 8, the triangles represent those flames which have reached a (near-) steady state.[4] The flames which are reported extinguished are also shown (circles); the heights correspond to those at extinction during the drop. To distinguish between the different regimes, lines are drawn to connect the different available data points. Thus, the solid lines cover both the steady-state and extinguished regimes for which reported data is available. The broken line for the larger nozzle shows the

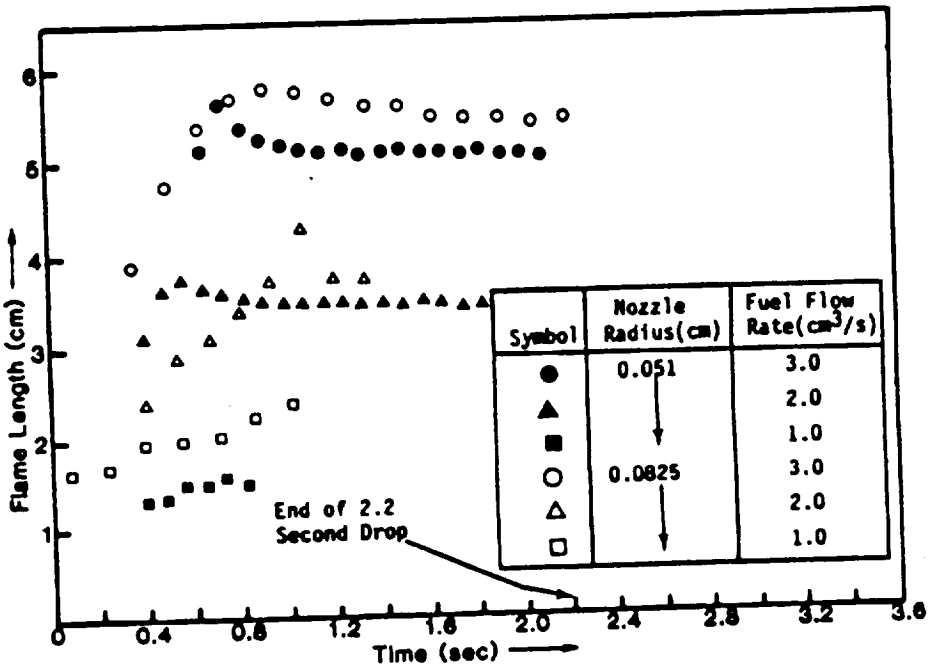

Fig. 5 Microgravity methane flame heights.

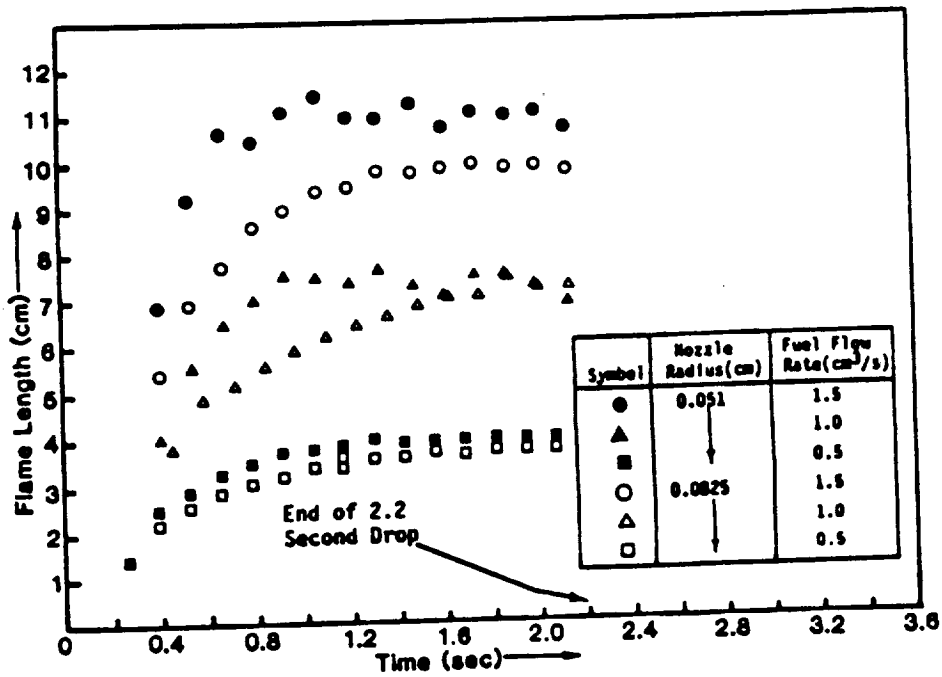

Fig. 6 Microgravity propane flame heights.

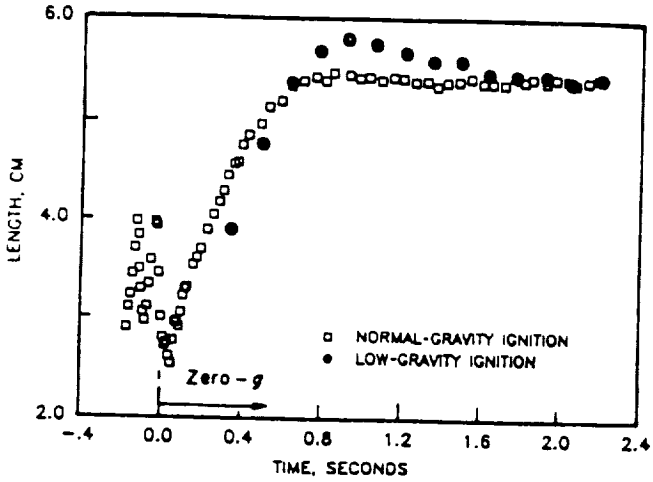

Fig. 7 Comparison between the normal-gravity[4] and microgravity ignition of flame No. 6 of Table 1.

range of Reynolds numbers for which the flames required longer than 2.2 s to establish their final state. This regime comprises the "transient" flames of the previous work,[4] for which no heights are available. In addition the dotted lines correspond to those regions for which no flames were studied. Therefore, the dotted and broken lines are not meant to indicate that flame heights can be deduced at intermediate Reynolds numbers from Fig. 8. Rather, they give the ranges of Reynolds numbers which cover this class of flames. The squares shown in Fig. 8 are the observed (near-) steady-state flame heights of the present study, obtained from Fig. 5. Although the truncated data in Fig. 5 for the lower flow rates may give the impression that the flames extinguished, these flames indeed existed throughout the drop. As mentioned before, they were very faint and appeared to have open tips with indeterminate length, resembling typical underventilated flame behavior.

It can be seen in Fig. 8, that the previously reported extinguished flames (circles) may not extinguish if the flame is ignited in microgravity. However, low-flow rate methane

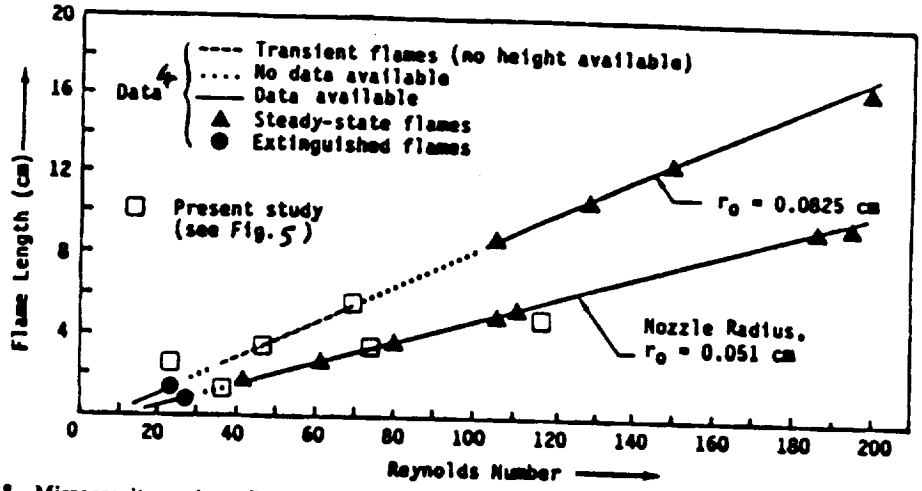

Fig. 8 Microgravity methane-flame heights as a function of jet Reynolds number (see the text for details).

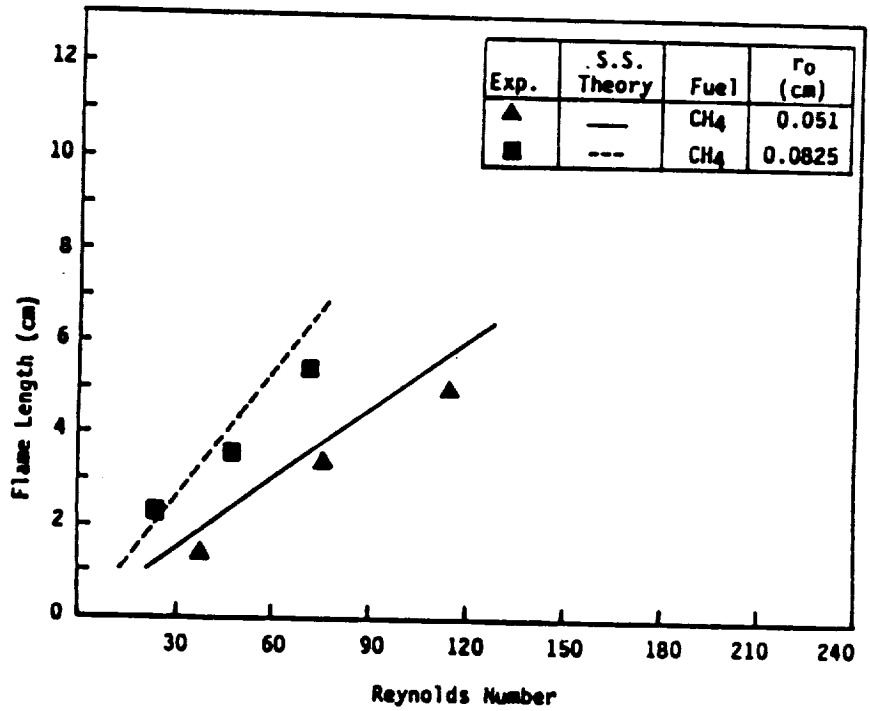

Fig. 9 Predicted and measured microgravity methane-flame heights vs jet Reynolds number.

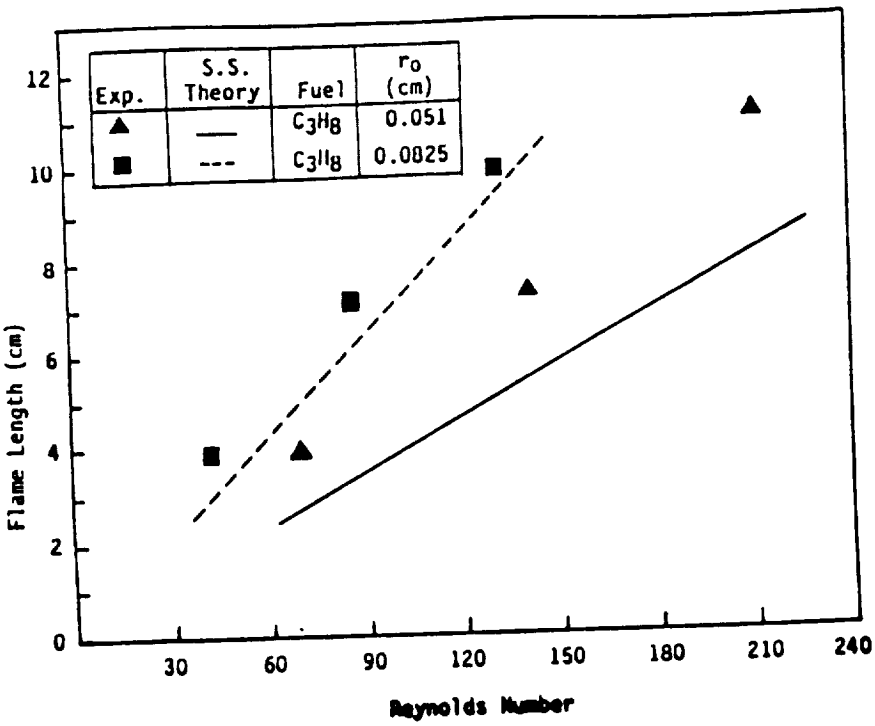

Fig. 10 Predicted and measured microgravity propane-flame heights vs jet Reynolds number.

flames in the present study (filmed at 15 frames/s) were entirely blue, whereas blue was not discernible in the microgravity flames of the previous works (filmed at 400 frames/s). Based on these findings, it is concluded that the previously reported "extinguished" flames may have been blue (and not visible on the high-speed films).

A previously developed computational model[6,7] is used to predict steady-state flame heights for comparison with the experimental data. The parabolic model for studying laminar gas-jet diffusion flames under arbitrary gravitational accelerations consists of the conservation equations for elements, mass, momentum, and energy. It includes the effects of inertia, viscosity, diffusion, and chemical reactions. The chemistry assumed is that of shifting equilibrium, and both Fickian and multicomponent diffusion are considered. The radiation model is a thin-gas approximation using carbon dioxide and water vapor. The differencing scheme is an explicit finite-difference technique. The results have shown a very good agreement with the earlier experimental data for both normal-gravity and microgravity conditions.[6,7] However, it was shown that accurate flame shape predictions require an accurate prediction of the relative rates of molecular transport of species, momentum, and energy. This steady-state, parabolic model has been applied to the microgravity flames of Figs. 5 and 6. The results are shown in Figs. 9 and 10, where a satisfactory trend in the predicted behavior of the flames is demonstrated. However, the propane flames are slightly longer and the methane flames shorter than the predicted flames. One possible explanation is the absence of soot and the associated radiation in the model in contrast to the high concentrations of soot observed in most of the microgravity flames. In addition, the absence of elliptic effects (axial diffusion) and the relatively simple predictions for the molecular transport rates (i.e., species, momentum, and energy) may contribute to the differences between the predicted and measured flame heights.

Figure 11 shows a comparison between different theoretical and experimental results. The data points correspond to the steady-state flame heights of the present study and previous work.[4] The predictions are those presented in Figs. 9 and

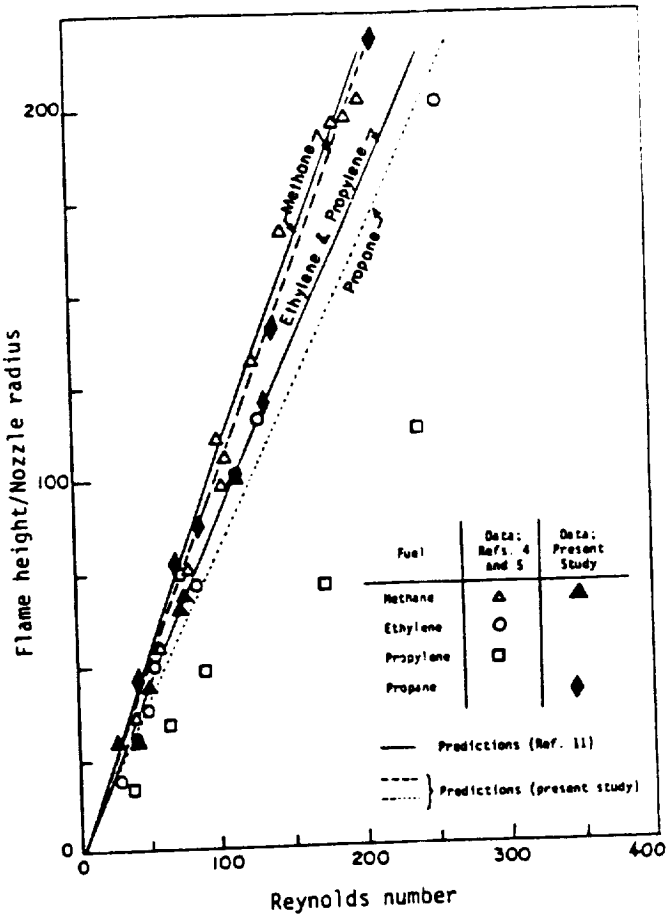

Fig. 11 Measured and predicted microgravity flame heights for different fuels; reproduced,[11] with modifications and additions.

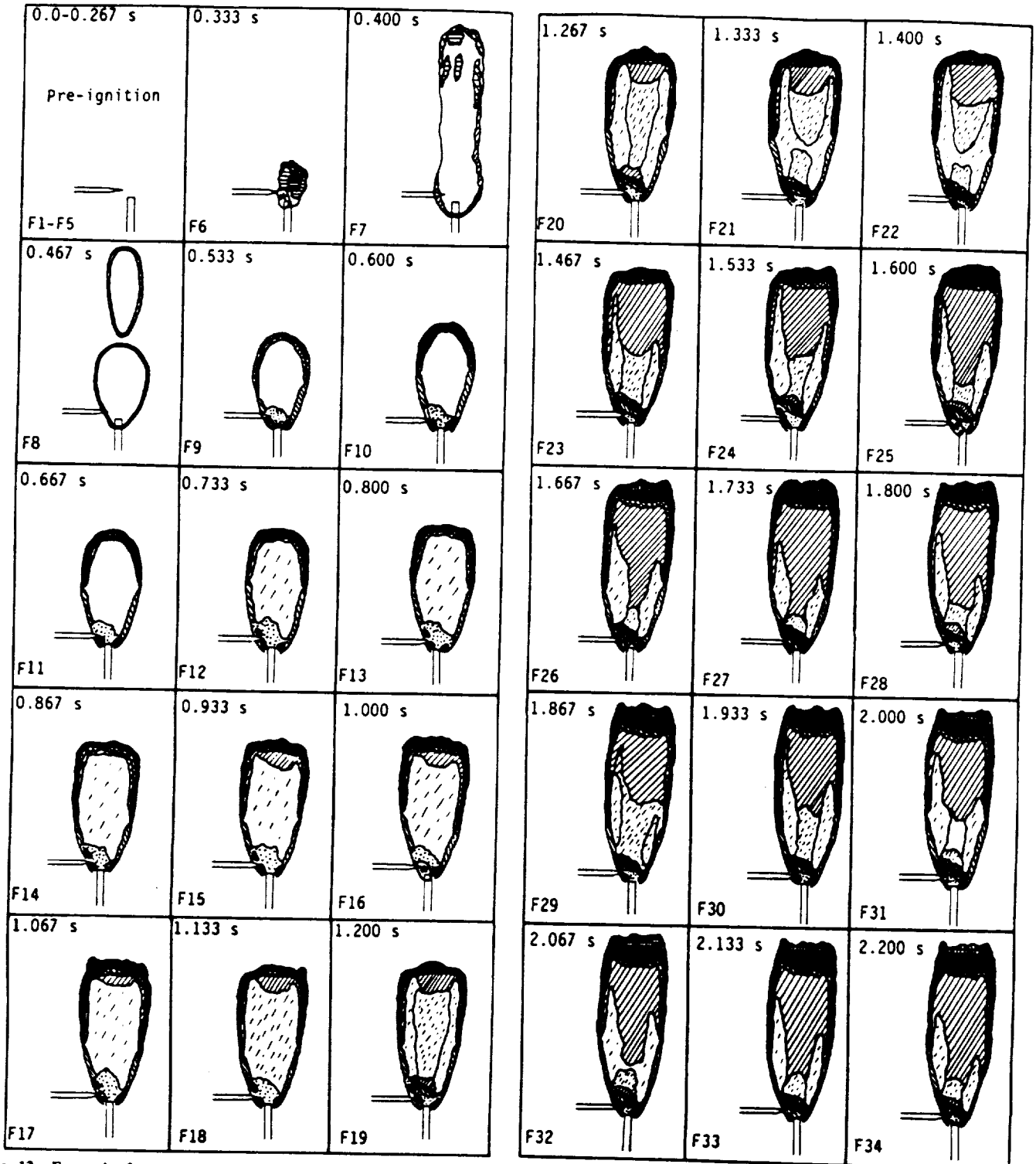

Fig. 12 Frame-by-frame analysis of microgravity propane flame No. 11 of Table 1 with nozzle radius = 0.0825 cm and volume-flow rate = 1.0 cm^3/s. The various observed colors are as follows: ☐ bright white; ▨ white with little yellow; ▨ white with more noticeable yellow; ▤ blue; ▤ dark blue; ▧ violet/pink; ▩ mixed blue/violet; ▨ yellow; ▩ orange; ■ cherry red; ▩ dull red, fainting; ☐ color at the base, starting with dark at the bottom, becoming dark blue/pink, then pink/blue, then pink/orange, then orange/yellow, and then yellow/white toward the center of the flame; ▣ bright white spark with bright blue at its boundary. Scale ⟼⟻ = 1 cm. Note the asymmetry caused by the electrode.

effort.[11] The two numerical models show a good agreement with each other and with the data. The propylene-flame heights of the previous studies[4] do not agree with the predictions.[11] This is surprising, since propylene and propane are very close in chemical structure and satisfactory agreement is obtained for methane, ethylene, and propane.

In gas-jet diffusion flames, the heat-release mechanism is not uniform throughout the flowfield. Pyrolysis, producing soot and partially oxidized species, dominates in the near-jet region, while the continued heating and increased residence time result in the tendency to burn off these species downstream in the vicinity of the flame tip. However, pyrolysis and soot formation reduce the temperature level in the flame and, with the aid of the increased residence time, sooting is enhanced. This, in turn, results in enhanced radiation, more cooling, and delayed soot burn-off downstream of the flame. This effect is much more pronounced in microgravity flames than those in normal gravity, due to the lack of buoyancy. As

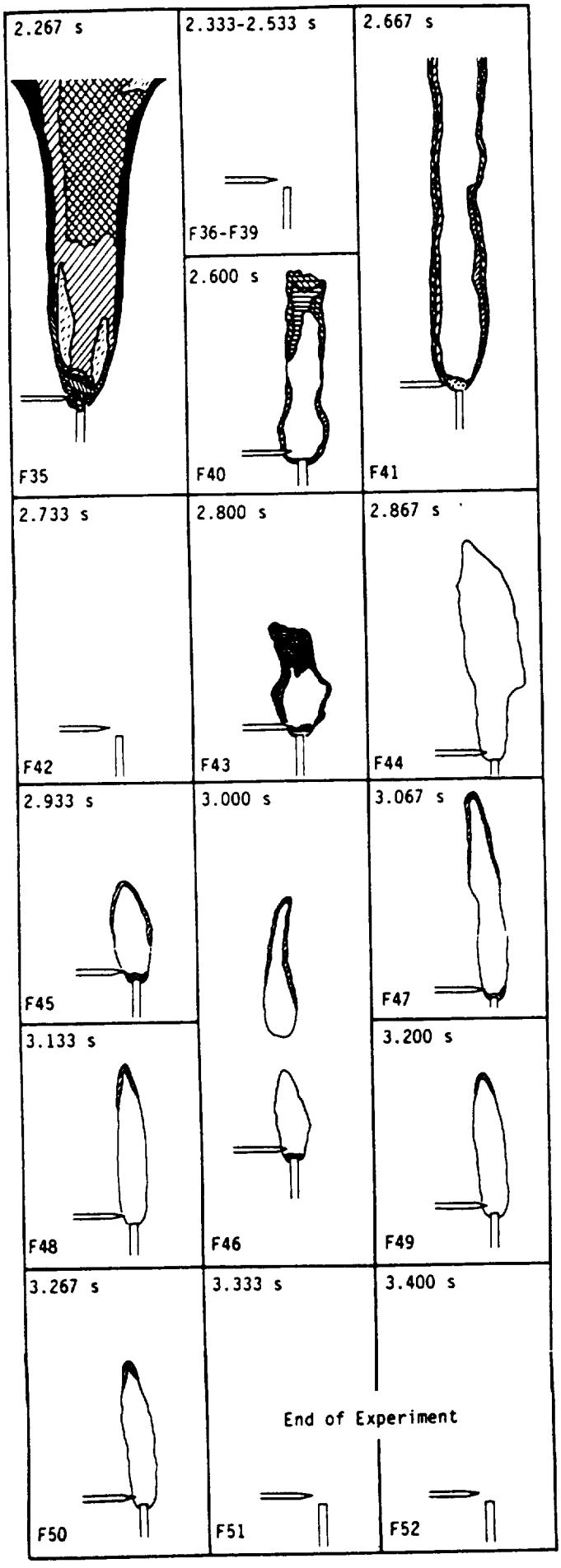

Fig. 12 Continued.

a result, thermophoretic effects may become an important factor in the regions of large temperature gradients with high soot concentrations. The observed open tip of the propane flames and quenching at the tip give the appearance of an underventilated flame (see Fig. 12).

In Fig. 12, a frame-by-frame analysis of flame No. 11 of Table 1 is presented. This propane flame reaches steady state and remains fairly uniform throughout the drop. The colors indicate the presence of particular species in hydrocarbon flames, e.g., blue-violet region (outer region at the base showing the spectrum of burning CO) and bluish-green region (showing C_2 and CH emissions, where C_2 bands appear green shaded toward violet and CH bands appear violet-blue). A highly luminous zone (bright yellow) indicates the thermal emission of burning carbon particles. This luminous zone becomes yellow, then orange, and then red and dark red toward the boundary of the visible region, as the temperature of the unburned soot decreases. The reddish-orange color of the flame is due to the soot at cooler temperatures than would be expected for typical burnoff conditions.

The color of the radiating soot, in conjunction with Wien's law, can be used as an indicator of the approximate local flame temperature. The cloud of burning soot particles is yellow, i.e., $\sim 0.58-\mu$m wavelength ($1370\ \text{K} < T < 1670\ \text{K}$, where 1670 K is the temperature of a white hot body). As the temperature decreases, the soot particles become orange red (~ 1370 K, $\sim 0.6\ \mu$m), then cherry red (~ 1170 K, 0.6–0.65 μm), and finally dull red (~ 970 K, 0.65–0.70 μm). These effects are shown clearly in the results of Fig. 12, which indicate cooling by pyrolysis and enhanced radiation due to increased soot formation.

Frame number 35 of Fig. 12 shows the flame during the rapid deceleration as the experiment package is brought to rest at the end of the drop. The high level of induced convection causes blowoff within <0.1 s. After the impact, reignition can be seen due to the spark pulses, resulting in normal-gravity behavior, i.e., flame flicker. Examination of high-speed movies for the deceleration period reveals the behavior of the flame in the transient state under rapid changes in gravity level, providing byproduct data for further analysis. A study of laminar diffusion flames under elevated gravitational conditions is reported elsewhere.[12]

Conclusions

Ignition of laminar methane and propane diffusion flames in microgravity environments has been demonstrated. The new ignition method combined with the refined photographic technique has shown that flames previously thought to have been extinguished were still burning during the entire 2.2 s of microgravity.

The low-flow rate methane flames are blue and very dim, prompting further studies to determine the extinction limits for laminar diffusion flames in microgravity environments.

Many flames (especially those of propane) have an open tip resembling an underventilated behavior. This is attributed to radiation, soot formation, and possibly thermophoretic effects, which appear to become more important in flames under microgravity conditions. However, a thorough analysis must be made to determine the relative importance of each.

The predicted flame heights, using a steady-state parabolic model, are in good agreement with the measured steady-state flame heights.

Longer test times are planned through the use of the 5.18 s Zero-Gravity Facility and the KC-135 aircraft (free-floating, 10–15 s). Flame visualization, and radiation, temperature, and concentration measurements at these longer test times are going to provide a more complete quantitative description of these flames.

Acknowledgments

This work is supported by NASA Lewis Research Center under Contract NAS3-22822. The authors would like to

express their appreciation to Professor Irvin Glassman for a discussion on the interpretation of the colors observed in microgravity flames. They also wish to thank Mr. Matthew Hart for conducting the design-feasibility drop tests, and Mr. Thomas Morrissey for conducting parts of the numerical calculations.

References

[1]Cochran, T. H. and Masica, W. J., "Effects of Gravity on Laminar Gas Jet Diffusion Flames," NASA TN D-5872, 1970.

[2]Cochran, T. H. and Masica, W. J., "An Investigation of Gravity Effects on Laminar Gas-Jet Diffusion Flames," *Thirteenth Symposium (International) on Combustion*, The Combustion Inst., Pittsburgh, PA, 1971, pp. 821-829.

[3]Haggard, J. B. Jr. and Cochran, T. H., "Stable Hydrocarbon Diffusion Flames in a Weightless Environment," *Combustion Science and Technology*, Vol. 5, Aug. 1972, pp. 291-298.

[4]Cochran, T. H., "Experimental Investigation of Laminar Gas Jet Diffusion Flames in Zero Gravity," NASA TN D-6523, 1972.

[5]Haggard, J. B. Jr. and Cochran, T. H., "Hydrogen and Hydrocarbon Diffusion Flames in a Weightless Environment," NASA TN D-7165, 1973.

[6]Edelman, R. B., Fortune, O. F., Weilerstein, G., Cochran, T. H., and Haggard, J. B. Jr. "An Analytical and Experimental Investigation of Gravity Effects Upon Laminar Gas Jet Diffusion Flames," *Fourteenth Symposium (International) on Combustion*, The Combustion Inst., Pittsburgh, PA, 1973, pp. 399-412.

[7]Edelman, R. B., Fortune, O., and Weilerstein, G., "Analytical Study of Gravity Effects on Laminar Diffusion Flames," NASA CR-120921, 1973.

[8]Haggard, J. B. Jr., "Forced and Natural Convection in Laminar-Jet Diffusion Flames," NASA TP 1841, 1981.

[9]Edelman, R. B. and Bahadori, M. Y., "Effects of Buoyancy on Gas-Jet Diffusion Flames: Experiment and Theory," *Acta Astronautica*, Vol. 13, No. 11/12, 1986, pp. 681-688.

[10]Edelman, R. B., Bahadori, M. Y., Olson, S. L., and Stocker, D. P., "Laminar Diffusion Flames Under Micro-Gravity Conditions," Paper AIAA 88-0645, AIAA 26th Aerospace Sciences Meeting, Reno, NV, Jan. 1988.

[11]Klajn, M. and Oppenheim, A. K., "Influence of Exothermicity on the Shape of a Diffusion Flame," *Nineteenth Symposium (International) on Combustion*, The Combustion Inst., Pittsburgh, PA, 1982, pp. 223-235.

[12]Altenkirch, R. A., Eichhorn, R., Hsu, N. N., Brancic, A. B., and Cevallos, N. E., "Characteristics of Laminar Gas Jet Diffusion Flames Under the Influence of Elevated Gravity," *Sixteenth Symposium (International) on Combustion*, The Combustion Inst., Pittsburgh, PA, 1976, pp. 1165-1174.

Section 10

"AN ANALYTICAL SOLUTION FOR TRANSIENT, CYLINDRICALLY SYMMETRIC LAMINAR DIFFUSION FLAMES IN THE ABSENCE OF BUOYANCY"

M. Y. Bahadori

Paper presented at the Central States Meeting of The Combustion Institute, Cincinnati, Ohio, May 1990

An Analytical Solution For Transient, Cylindrically Symmetric Laminar Diffusion Flames in the Absence of Buoyancy*

M. Yousef Bahadori†
Science Applications International Corporation
Torrance, California

Abstract - Analytical solutions are obtained, to the first approximation, for the transient shape and height of overventilated, cylindrically symmetric, laminar diffusion flames in the absence of gravity. Equal and constant flow speeds, transport parameters, and physical properties are assumed for the fuel and oxidizer streams. Axial and radial diffusion are accounted in the formulation. The solution yields the development of the flame boundary from ignition toward steady state, and reduces smoothly to the classical solution of laminar diffusion flames as, independently, axial diffusion becomes negligible, and steady state is approached. Comparisons with the results of microgravity experiments show a satisfactory agreement for the increase in flame height with time. The solution is useful in estimating the time required for the development of the flame toward steady state following ignition in microgravity environments.

1. Introduction

This analysis is based on, and is an extension of, studies on heat flow in composite cylinders [1], and on defining the boundaries of cylindrically symmetric laminar diffusion flames with equal flow velocities and diffusion coefficients in the absence of buoyancy [2]. Recently, analytical solutions have been developed for flame shapes with arbitrary values of diffusion coefficients and inlet velocities of the fuel and oxidizer [3]. Also, the Burke-Schumann model [2] has been extended for two competing laminar diffusion flames with cylindrical symmetry [4], and two and three flames with rectangular symmetry [5].

Efforts to study laminar diffusion flames under near-zero-gravity conditions have so far been limited to 2.2 seconds of microgravity in the NASA-Lewis Drop Tower. In these experiments, a self-contained gaseous diffusion-flame apparatus was allowed to fall inside a falling drag shield. The method provided time-resolved data on the development of flame shape for the near-zero-gravity condition achieved during the drop. Various hydrocarbon diffusion flames burning in quiescent air have been studied [6-13], and some of these works have been reviewed in a recent article [14]. Currently, preliminary studies of microgravity laminar diffusion flames with secondary air flows are underway [15], with the intent of comparing the results with Burke-Schumann type models [2,3].

*Presented at the Central States Section Meeting (Spring, 1990) of The Combustion Institute, Cincinnati, Ohio, May 20-22, 1990. This work is supported by NASA Lewis Research Center under Contract NAS3-22822.

†Senior Scientist; on-site at NASA Lewis Research Center, MS 500-217, Cleveland, Ohio 44135.

2. Formulation

In this section, a problem is formulated for overventilated, laminar, transient, cylindrically symmetric diffusion flames to obtain, to the first approximation, a closed-form mathematical representation for the development of the flame boundary with time following ignition in a zero-gravity environment. The assumptions used in the formulation are as follows: (a) constant pressure, (b) unity Lewis number, (c) equal and constant flow velocities, transport parameters, and physical properties in the fuel and oxidizer streams, (d) flame-sheet approximation, and (e) no buoyancy effects. Axial diffusion is included in the formulation.

For the cylindrically symmetric flow of gases, we consider the model of Fig. 1, where an inert gas flows in the inner of two concentric cylinders for times $t < 0$. The oxidizer flows in the outer cylindrical shell at all times. The flow of the inert gas is replaced by a fuel flow of the same velocity at $t = 0$, i.e., the interface between the fuel and inert gas arrives at the burner port at $t = 0$, and ignition occurs at this instant of time.

The species-conservation equations for the fuel and oxidizer above the burner port at times $t > 0$ reduce to a single differential equation

$$\frac{\partial Y}{\partial t} + u\frac{\partial Y}{\partial z} = D\left(\frac{1}{r}\frac{\partial Y}{\partial r} + \frac{\partial^2 Y}{\partial r^2} + \frac{\partial^2 Y}{\partial z^2}\right) \quad \text{for } 0 \leq r < d'/2, \quad z > 0, \quad t > 0, \tag{1}$$

once we impose the conditions $u_F = u_O = u = \text{const.}$ and $D_F = D_O = D = \text{const.}$, in addition to introducing a single variable

$$Y(r,z,t) = \begin{cases} Y_F & \text{for } 0 \leq r < r_f, \quad z > 0, \quad t > 0, \\ -\nu Y_O & \text{for } r_f < r < d'/2, \quad z > 0, \quad t > 0. \end{cases} \tag{2}$$

Here, Y is the mass fraction, u is the velocity, D is the diffusion coefficient, t is the time, z is the axial coordinate, r is the radial coordinate, $r_f(z,t)$ is the flame radius, ν is the stoichiometric ratio of grams of fuel consumed per gram of oxidizer at the flame front, and subscripts F and O denote the fuel and oxidizer, respectively.

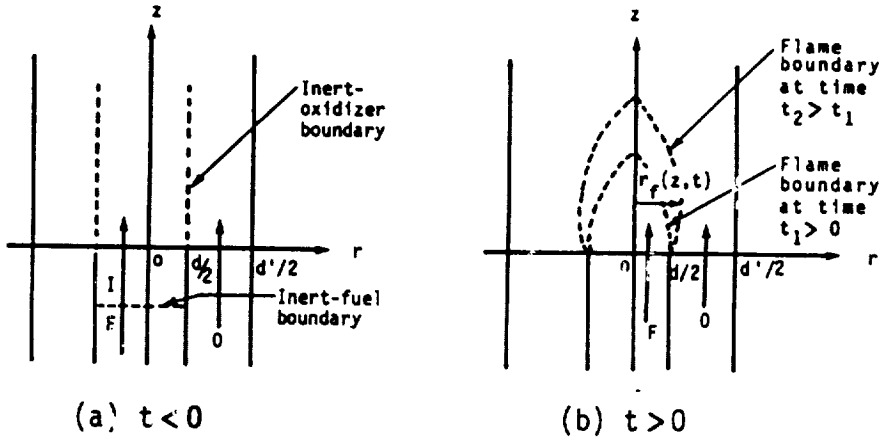

Fig. 1. Schematic diagram of concentric cylinders with inert I entering at $z=0$ for $0 \leq r < d/2$ during the times $t<0$ [see (a)], which is replaced by the flow of fuel F at $t \geq 0$ [see (b)]. The oxidizer O is entering at $z=0$ for $d/2 < r < d'/2$ at all times [(a) and (b)].

In view of Eq. (2), the initial conditions (denoted by subscript o) are

$$Y(r,z,0) = \begin{cases} 0 & \text{for } 0 \leq r < d/2, \quad z > 0, \quad t = 0, \\ -\nu Y_{0,o} & \text{for } d/2 < r < d'/2, \quad z > 0, \quad t = 0, \end{cases} \tag{3}$$

$$Y(r,0,t) = \begin{cases} Y_{F,o} & \text{for } 0 \leq r < d/2, \quad z = 0, \quad t > 0, \\ -\nu Y_{0,o} & \text{for } d/2 < r < d'/2, \quad z = 0, \quad t > 0. \end{cases} \tag{4}$$

The symmetry and boundary conditions are, respectively,

$$\partial Y(0,z,t)/\partial r = 0, \tag{5}$$

$$\partial Y(d'/2,z,t)/\partial r = 0. \tag{6}$$

The flame-sheet approximation defines the location of the flame boundary, viz.

$$Y(r_f,z,t) = 0. \tag{7}$$

We now derive an expression for the flame shape in the form $f(r_f,z,t) = 0$.

3. Method of Solution

Using separation of variables, the general solution becomes

$$Y(r,z,t) = \sum_{j=1}^{\infty} \sum_{k=1}^{\infty} E_{jk} J_0(\lambda_j r) \exp\left[-D(\lambda_j^2 - \beta_{jk}^2)t\right] \exp\left[\frac{u}{2D}\left(1 - \sqrt{1 + 4\beta_{jk}^2 D^2/u^2}\right)z\right] , \tag{8}$$

where the E_{jk} are constants, J_0 is the Bessel function of the first kind of order zero, and λ_j and β_{jk} are eigenvalues. In deriving Eq. (8), the symmetry condition has been used to show that Bessel functions of the second kind of order zero can not exist. In addition, the boundary condition yields

$$J_1(\lambda_j d'/2) = 0 , \tag{9}$$

which is the equation determining the eigenvalues λ_j. Here, J_1 is the Bessel function of the first kind of order one.

Using the initial conditions, the coefficients E_{jk} and eigenvalues β_{jk} can be evaluated. Substitution of Eqs. (3) and (4) in Eq. (8) yields

$$\sum_{j=1}^{\infty} J_0(\lambda_j r) \sum_{k=1}^{\infty} E_{jk} \exp\left[\frac{u}{2D}\left(1 - \sqrt{1 + 4\beta_{jk}^2 D^2/u^2}\right) z\right] = \begin{cases} 0 & \text{for } 0 \leq r < d/2, \quad z > 0, \quad t = 0, \\ -\nu Y_{0,o} & \text{for } d/2 < r < d'/2, \quad z > 0, \quad t = 0, \end{cases} \tag{10}$$

$$\sum_{j=1}^{\infty} J_0(\lambda_j r) \sum_{k=1}^{\infty} E_{jk} \exp\left[-D\left(\lambda_j^2 - \beta_{jk}^2\right) t\right] = \begin{cases} Y_{F,o} & \text{for } 0 \leq r < d/2, \quad z = 0, \quad t > 0, \\ -\nu Y_{0,o} & \text{for } d/2 < r < d'/2, \quad z = 0, \quad t > 0. \end{cases} \tag{11}$$

We hold z constant and vary r over the range of the problem in Eq. (10). The inner sum is therefore a constant depending on j, and denoted by $G_j(z)$. Hence,

$$\sum_{j=1}^{\infty} G_j(z) J_0(\lambda_j r) = \begin{cases} 0 & \text{for } 0 \leq r < d/2, \quad z > 0, \quad t = 0, \\ -\nu Y_{0,o} & \text{for } d/2 < r < d'/2, \quad z > 0, \quad t = 0. \end{cases} \tag{12}$$

Multiplying both sides of Eq. (12) by $rJ_0(\lambda_j r)dr$, integrating over the range

$0 \leq r < d'/2$, and using the orthogonality properties of Bessel functions, it can be shown that for $\lambda_j \neq 0$ (i.e., $j > 1$),

$$G_j(z) = \frac{2\nu Y_{0,o}(d/2)\, J_1(\lambda_j d/2)}{\lambda_j (d'/2)^2\, J_0^2(\lambda_j d'/2)} , \quad \text{for} \quad j > 1, \tag{13}$$

Eq. (9) has been used in the derivation of Eq. (13). The approach for $G_1(z)$ needs special treatment involving expansions of Bessel functions and taking the limits as $\lambda_1 \to 0$, which ultimately gives

$$G_1(z) = -\nu Y_{0,o} \left[1 - (d/d')^2\right] , \quad \text{for} \quad j = 1. \tag{14}$$

Hence, substitution of Eqs. (13) and (14) in Eq. (10) yields

$$\sum_{k=1}^{\infty} E_{1k} \exp\left[\frac{u}{2D}\left(1 - \sqrt{1 + 4\beta_{1k}^2 D^2/u^2}\right) z\right] = -\nu Y_{0,o} \left[1 - (d/d')^2\right] , \quad \text{for} \quad j = 1, \tag{15}$$

$$\sum_{k=1}^{\infty} E_{jk} \exp\left[\frac{u}{2D}\left(1 - \sqrt{1 + 4\beta_{jk}^2 D^2/u^2}\right) z\right] = \frac{2\nu Y_{0,o}(d/2) J_1(\lambda_j d/2)}{\lambda_j (d'/2)^2\, J_0^2(\lambda_j d'/2)} , \quad \text{for} \quad j > 1. \tag{16}$$

We now hold t constant and vary r over the range of the problem in Eq. (11). Again, the inner sum is a constant depending on j. Following the same approach in deriving Eqs. (15) and (16), it can be shown that

$$\sum_{k=1}^{\infty} E_{1k} \exp\left(D\beta_{1k}^2 t\right) = \left(Y_{F,o} + \nu Y_{0,o}\right)(d/d')^2 - \nu Y_{0,o} , \quad \text{for} \quad j = 1, \tag{17}$$

$$\sum_{k=1}^{\infty} E_{jk} \exp\left[-D(\lambda_j^2 - \beta_{jk}^2)t\right] = \frac{2\left(Y_{F,o} + \nu Y_{0,o}\right)(d/2)\, J_1(\lambda_j d/2)}{\lambda_j (d'/2)^2\, J_0^2(\lambda_j d'/2)} , \quad \text{for} \quad j > 1. \tag{18}$$

The flame location (where $Y = 0$) is obtained from Eq. (8), viz.

$$\sum_{j=2}^{\infty} J_0(\lambda_j r_f) \exp(-D\lambda_j^2 t) \sum_{k=1}^{\infty} E_{jk} \exp(D\beta_{jk}^2 t) \exp\left[\frac{u}{2D}\left(1 - \sqrt{1 + 4\beta_{jk}^2 D^2/u^2}\right) z\right]$$

$$= -\sum_{k=1}^{\infty} E_{1k} \exp(D\beta_{1k}^2 t) \exp\left[\frac{u}{2D}\left(1 - \sqrt{1 + 4\beta_{1k}^2 D^2/u^2}\right) z\right] . \tag{19}$$

Equations (15)-(18) give the coefficients E_{jk} and eigenvalues β_{jk} $(j \geq 1)$.

So far, we have not deviated from, or made approximations in the rigorous approach for obtaining the solution. However, Eqs. (15)-(18) show that for each λ_j, there may exist an infinite number of coefficients E_{jk} and eigenvalues β_{jk}. This makes the task of analytically examining the solution impossible. We therefore make the following assumption to obtain a first-order, approximate solution : <u>At any fixed z and t, there exist only one E_{jk} and one β_{jk} for each λ_j</u>. The assumption may be justified due to the fact that the classical solution [2], using only the first nonzero eigenvalue, has given satisfactory results for normal-gravity flame heights [16], especially in the light of the restrictive approximations made on the physical grounds to formulate the original problem. With this assumption, Eq. (19) reduces to

$$\sum_{j=2}^{\infty} E_j\, J_0(\lambda_j r_f) \exp\left[-D(\lambda_j^2 - \beta_j^2)t\right] \exp\left[\frac{u}{2D}\left(1 - \sqrt{1 + 4\beta_j^2 D^2/u^2}\right) z\right]$$

$$\doteq -E_1 \exp(D\beta_1^2 t) \exp\left[\frac{u}{2D}\left(1 - \sqrt{1 + 4\beta_1^2 D^2/u^2}\right) z\right] , \tag{20}$$

and Eqs. (15)-(18) yield

$$E_1 \exp\left[\frac{u}{2D}\left(1-\sqrt{1+4\beta_1^2D^2/u^2}\right)z\right] \doteq -\nu Y_{0,o}\left[1-(d/d')^2\right], \quad \text{for} \quad j=1, \tag{21}$$

$$E_j \exp\left[\frac{u}{2D}\left(1-\sqrt{1+4\beta_j^2D^2/u^2}\right)z\right] \doteq \frac{2\nu Y_{0,o}(d/2)\,J_1(\lambda_j d/2)}{\lambda_j(d'/2)^2\,J_0^2(\lambda_j d'/2)}, \quad \text{for} \quad j>1, \tag{22}$$

$$E_1 \exp(D\beta_1^2 t) \doteq \left(Y_{F,o}+\nu Y_{0,o}\right)(d/d')^2-\nu Y_{0,o}, \quad \text{for} \quad j=1, \tag{23}$$

$$E_j \exp\left[-D(\lambda_j^2-\beta_j^2)t\right] \doteq \frac{2\left(Y_{F,o}+\nu Y_{0,o}\right)(d/2)\,J_1(\lambda_j d/2)}{\lambda_j(d'/2)^2\,J_0^2(\lambda_j d'/2)}, \quad \text{for} \quad j>1. \tag{24}$$

Proper manipulation of Eqs. (21)-(24) for the four unknowns, and substitution in Eq. (20) yields, finally,

$$\sum_{j=2}^{\infty}\frac{2\left(Y_{F,o}+\nu Y_{0,o}\right)(d/2)\,J_1(\lambda_j d/2)}{\lambda_j(d'/2)^2\,J_0^2(\lambda_j d'/2)}\,J_0(\lambda_j r_f)\exp\left\{\frac{u(t+z/u)}{2Dt}\left\{1-\sqrt{1+\frac{4Dt\left[D\lambda_j^2 t+\ln\left(1+Y_{F,o}/\nu Y_{0,o}\right)\right]}{u^2(t+z/u)^2}}\right\}z\right\}$$

$$\doteq -\left[\left(Y_{F,o}+\nu Y_{0,o}\right)(d/d')^2-\nu Y_{0,o}\right]\exp\left\{\frac{u(t+z/u)}{2Dt}\left\{1-\sqrt{1+\frac{4Dt\ln\left[1-\frac{Y_{F,o}(d/d')^2}{\nu Y_{0,o}\left[1-(d/d')^2\right]}\right]}{u^2(t+z/u)^2}}\right\}z\right\}, \tag{25}$$

which is the equation for flame shape. The flame height can be obtaind by setting $r_f = 0$ in Eq. (25).

In the limit of $t\to\infty$, Eq. (25) yields the solution to the steady-state problem with axial diffusion [3], i.e.,

$$\sum_{j=2}^{\infty}\frac{2\left(Y_{F,o}+\nu Y_{0,o}\right)(d/2)\,J_1(\lambda_j d/2)}{\lambda_j(d'/2)^2\,J_0^2(\lambda_j d'/2)}\,J_0(\lambda_j r_f)\exp\left[\frac{u}{2D}\left(1-\sqrt{1+\frac{4D^2\lambda_j^2}{u^2}}\right)z\right]$$

$$= -\left[\left(Y_{F,o}+\nu Y_{0,o}\right)(d/d')^2-\nu Y_{0,o}\right], \tag{26}$$

In the limit of $(2D\lambda_j/u)^2 \ll 1$ (i.e., negligible axial diffusion), Eq. (26) reduces to the classical solution of Burke and Schumann [2,3], as follows:

$$\sum_{j=2}^{\infty}\frac{2\left(Y_{F,o}+\nu Y_{0,o}\right)(d/2)\,J_1(\lambda_j d/2)}{\lambda_j(d'/2)^2\,J_0^2(\lambda_j d'/2)}\,J_0(\lambda_j r_f)\exp\left(-\frac{D\lambda_j^2 z}{u}\right)$$

$$= -\left[\left(Y_{F,o}+\nu Y_{0,o}\right)(d/d')^2-\nu Y_{0,o}\right]. \tag{27}$$

It should be noted that Eq. (25) upon using

$$\frac{4Dt\left[D\lambda_j^2 t+\ln\left(1+Y_{F,o}/\nu Y_{0,o}\right)\right]}{u^2(t+z/u)^2}\ll 1 \quad \text{and} \quad \frac{4Dt\ln\left\{1-\frac{Y_{F,o}(d/d')^2}{\nu Y_{0,o}\left[1-(d/d')^2\right]}\right\}}{u^2(t+z/u)^2}\ll 1,$$

yields the transient solution in the absence of axial diffusion, viz.

$$\sum_{j=2}^{\infty} \frac{2\left(Y_{F,o} + \nu Y_{O,o}\right)(d/2)\, J_1(\lambda_j d/2)}{\lambda_j (d'/2)^2 J_0^2(\lambda_j d'/2)} J_0(\lambda_j r_f) \exp\left\{-\frac{\left[D\lambda_j^2 t + \ln\left(1 + Y_{F,o}/\nu Y_{O,o}\right)\right]}{u\,(t + z/u)} z\right\}$$

$$\doteq -\left[\left(Y_{F,o} + \nu Y_{O,o}\right)(d/d')^2 - \nu Y_{O,o}\right] \exp\left\{-\frac{\ln\left[1 - \dfrac{Y_{F,o}\,(d/d')^2}{\nu Y_{O,o}\left[1 - (d/d')^2\right]}\right]}{u\,(t + z/u)} z\right\} . \qquad (28)$$

This expression can also be obtained by formulating the problem posed in Sec. 2 without axial diffusion, and following the same method of solution outlined in the present section.

4. Results and Discussion

Equation (25) was solved numerically using polynomial expressions for Bessel functions. Up to 2000 eigenvalues were calculated in the program using Eq. (9). A large number of eigenvalues was needed (especially at earlier times) due to the slow decay of the exponential terms. The flame shape was solved for selected times. This is similar to solving the classical solution for the flame radial location at any fixed height.

Figure 2 shows the comparisons for two microgravity flames: an extinguished flame [6], and one which reached a near-steady state [7] in 2.2 seconds of microgravity. In these experiments, the flames have been ignited in normal gravity, and after attaining steady state, were subjected to a microgravity condition. As a result, the flame height drops to a minimum upon release of the package due to the consequent entrapment of the combustion products caused by the removal of buoyancy, and then starts to develop due to the continuous flow of fuel (see Fig. 2). The flame of Fig. 2(a) shows extinction, which the present model is not capable of predicting; however, recent studies [11] have shown that by igniting the flame in microgravity and improving the photographic technique, flames which were previously reported as extinguished [7] were probably burning during the entire 2.2 seconds. The intent in this paper is to investigate the behavior of the analytical solution, and make preliminary comparisons with some experimental results on flame development in general. Work is underway to apply the model to more recent data, e.g., those of Fig. 3 which show flame development following ignition in microgravity. It is anticipated that similar results will be obtained, especially since comparisons between normal-gravity and microgravity ignition (see Fig. 4) have shown that the trends in flame development are similar, and the flames reach the same steady-state height. Note that although the experimental results of Fig. 2 correspond to a quiescent oxidizing environment, the model which is formulated for co-flowing configurations can predict the flame-height development fairly accurately through selection of an appropriate diffusion coefficient, especially in the light of the restrictive assumptions made to formulate the problem (Sec. 2). Since the diffusion coefficient is the sole controlling parameter in the Burke-Schumann type solutions, Fig. 2 also shows the parametric effect of diffusion coefficient on flame-height behavior, confirming that the larger the diffusion coefficient, the shorter the flame height.

Figure 5 shows the predicted development of shape with time for a methane-air flame. Note that the predicted maximum-flame radii are smaller than the experimental results (not presented here) due to the presence of air

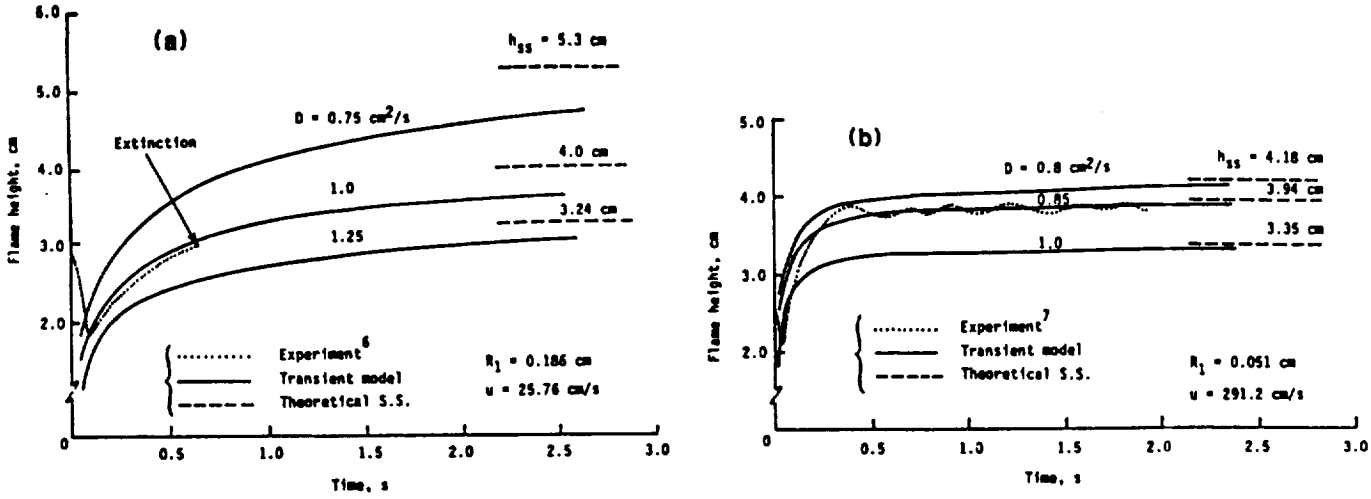

Fig. 2. Comparisons between the analytical and experimental variations of flame height with time. The experimental results show flame extinction at approximately 0.6 sec [Fig. 1(a)], and reaching an apparent steady state in 0.4 sec [Fig. 1(b)]. The binary diffusion coefficient of methane in nitrogen, D, has been used parametrically to show its effect. The values of 0.85 and 1.0 cm^2/s correspond, respectively, to temperatures of 650 and 750 K. Here, h_{ss} is the theoretical steady state-flame height, u is the gas velocity, and R_1 is the inner (nozzle) radius. Axial diffusion has been included in the analytical solution.

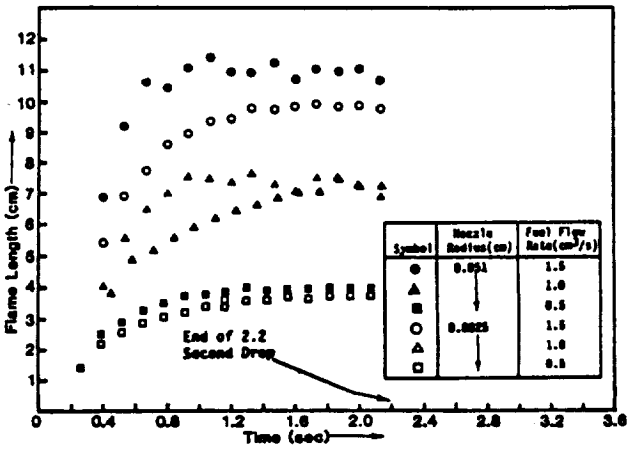

Fig. 3. Flame heights for propane following ignition in microgravity; reproduced from [11].

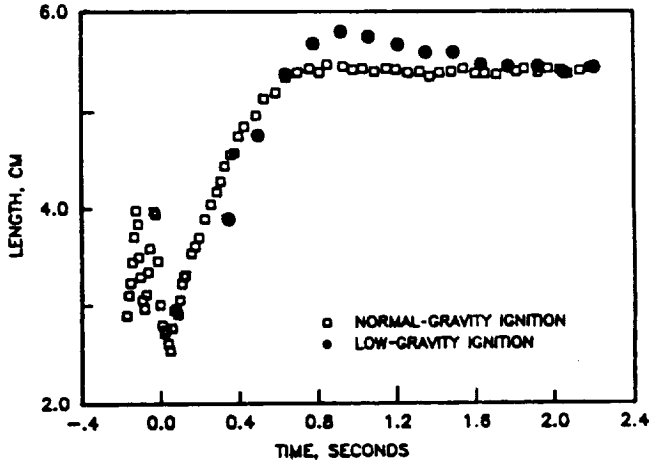

Fig. 4. Comparison between the normal-gravity [7] and microgravity ignition of a methane flame with nozzle radius = 0.0825 cm and fuel-flow rate = 3.0 cm^3/sec; reproduced from [11].

flow in the analytical model. In Fig. 6, the effects of diffusion coefficient and axial diffusion are shown for a transient methane-air flame. It can be seen that the choice of diffusion coefficient has a significant effect on both approach toward steady state and flame height. However, the flame maximum radius is hardly affected by diffusion coefficient. In addition, the effect of axial diffusion is more pronounced at larger diffusion coefficients, which also cause a faster approach toward steady state.

Figure 7 shows the effect of tube diameter-ratio on the theoretical flame behavior. As can be seen, the smaller the outer radius (i.e., the

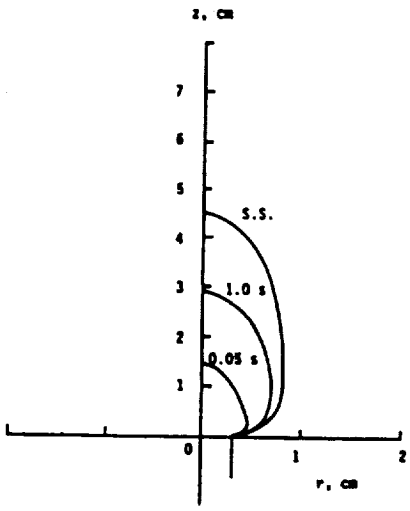

Fig. 5. Theoretical flame shape as a function of time for the solution with axial diffusion. The diffusion coefficient (CH_4 in N_2) is 1.0 cm^2/s (corresponding to 750 K). Methane and air have a velocity of 10 cm/s. The inner and outer radii are 0.318 and 30 cm, respectively. Compare the steady-state solution with those of Fig. 6.

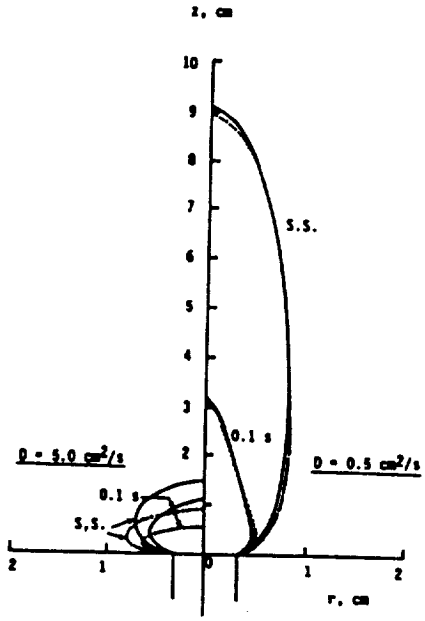

Fig. 6. Comparisons between the theoretical shapes of microgravity flames both with (solid lines) and without (dotted lines) axial diffusion. Flame shapes at 0.1 sec and at steady state are shown. The effect of diffusion coefficient (CH_4 in N_2) is illustrated using D = 0.5 and 5.0 cm^2/s (corresponding to T = 500 and 1800 K, respectively). Here, methane and air have a velocity of 10 cm/s. The inner and outer radii are 0.318 and 30 cm, respectively.

smaller the amount of available air), the taller the flame. Also, beyond a certain outer radius, the flame height becomes independent of the outer geometry. In Fig. 8, the effect of gas velocity on flame development is presented. The results are in agreement with the predictions from the classical solution that the steady-state flame height varies linearly with the gas velocity (i.e., volume flow rate). However, the present model shows that the same is true at any instant of time during flame development.

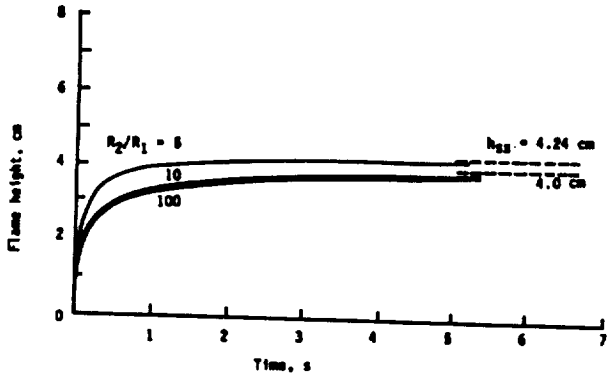

Fig. 7. Effect of outer-tube radius (R_2) on flame height. The model includes axial diffusion. Here, nozzle radius (R_1) = 0.186 cm, diffusion coefficient for CH_4 in N_2 = 1.0 cm^2/s, and h_{ss} is the theoretical steady-state flame height. Both fuel and air have a velocity of 25.76 cm/s.

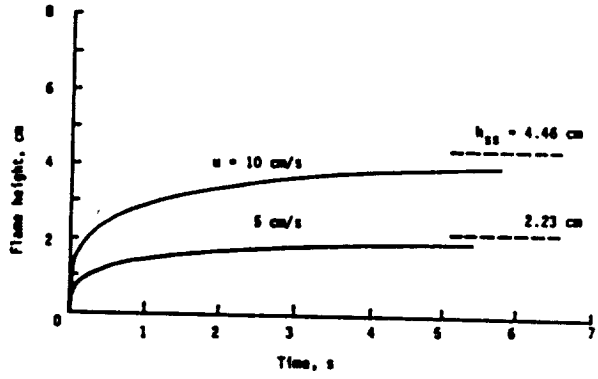

Fig. 8. Effects of gas velocity on predicted flame height with no axial diffusion. Here, methane and air have the same velocity; diffusion coefficient = 1.0 cm^2/s, inner radius = 0.318 cm, outer radius = 30 cm, and h_{ss} is the predicted steady-state flame height.

5. Conclusions

Analytical solutions are obtained, to the first approximation, for the development of diffusion-flame shape and height with time, following ignition in a zero-gravity environment. The solution reduces smoothly to the classical solution of laminar diffusion flames while, independently, axial diffusion becomes negligible, and steady state is approached. Quantitative agreement is obtained for the results of experiments conducted in quiescent air during 2.2 seconds of microgravity, when the diffusion coefficient is chosen appropriately. The model can predict the results obtained from the (steady state) classical solution, and extends these observations to arbitrary times during flame development. Times of the order of 2-5 seconds are predicted for approach toward steady state. Work is underway to apply the model to fuels other than methane, compare the results with those of the experiments conducted in quiescent air while igniting in microgravity [11-13], study the effect of secondary air flow on microgravity flames using the on-going experimental results [15], and extend the transient model to incorporate the effects of arbitrary diffusion coefficients and inlet velocities for the fuel and oxidizer streams.

References

1. Penner, S.S. and Sherman, S., J. Chem. Phys. 15, 569-574 (1947).
2. Burke, S.P. and Schumann, T.E.W., Ind. Eng. Chem. 20, 998-1004 (1928).
3. Penner, S.S., Bahadori, M.Y., and Kennedy, E.M., Progress in Astronautics and Aeronautics; Vol. 95: Dynamics of Flames and Reactive Systems, (J.R. Bowen, N. Manson, A.K. Oppenheim, and R.I. Soloukhin, Eds.), American Institute of Aeronautics and Astronautics, New York, 261-292 (1984).
4. Bahadori, M.Y., Li, C.P., and Penner, S.S., Progress in Astronautics and Aeronautics; Vol. 105, Part I: Flames and Configurations, (J.R. Bowen, J.C. Leyer, and R.I. Soloukhin, Eds.), American Institute of Aeronautics and Astronautics, New York, 192-207 (1986).
5. Li, C.P., Wiesenhahn, D., and Penner, S.S., Combust. Flame, 65, 215-225 (1986).
6. Cochran, T.H. and Masica, W.J., "Effects of Gravity on Laminar Gas Jet Diffusion Flames," NASA TN D-5872 (1970).
7. Cochran, T.H., "Experimental Investigation of Laminar Gas Jet Diffusion Flames in Zero Gravity," NASA TN D-6523 (1972).
8. Haggard, J.B., Jr. and Cochran, T.H., Combust. Sci. Tech. 5, 291-298 (1972); see also "Hydrogen and Hydrocarbon Flames in a Weightless Environment," NASA TN D-7165 (1973).
9. Haggard, J.B., Jr., "Forced and Natural Convection in Laminar-Jet Diffusion Flames," NASA TP 1841 (1981).
10. Edelman, R.B., Fortune, O.F., Weilerstein, G., Cochran, T.H., and Haggard, J.B., Jr., Fourteenth Symposium (International) on Combustion, The Combustion Institute, Pittsburgh, PA, 399-412 (1973).
11. Bahadori, M.Y., Edelman, R.B., Stocker, D.P., and Olson, S.L., AIAA J., 28, 236-244 (1990).
12. Bahadori, M.Y. and Stocker, D.P., "Oxygen-Concentration Effects on Microgravity Laminar Methane and Propane Diffusion Flames," Fall 1989 Eastern Section Meeting of The Combustion Institute, Albany, NY (1989).
13. Bahadori, M.Y., Stocker, D.P., and Edelman, R.B., "Effects of Pressure on Microgravity Hydrocarbon Diffusion Flames," Paper AIAA 90-0651, AIAA 28th Aerospace Sciences Meeting, Reno, NV (1990).
14. Edelman, R.B. and Bahadori, M.Y., Acta Astronautica, 13, 681-688 (1986).
15. Stocker, D.P., "Size and Shape of Laminar Burke-Schumann Diffusion Flames in Microgravity," Spring 1990 Central States Meeting of The Combustion Institute, Cincinnati, OH (1990).
16. Williams, F.A., Combustion Theory, 2nd Ed., The Benjamin/Cummings Publishing Company, Inc., Melno Park, CA (1985).

Section 11

"EFFECTS OF PRESSURE ON MICROGRAVITY HYDROCARBON DIFFUSION FLAMES"

M. Y. Bahadori, D.P. Stocker, and R. B. Edelman

Paper AIAA-90-0651, AIAA 28th Aerospace Sciences Meeting, Reno, Nevada, January 1990

AIAA-90-0651

Effects of Pressure on Microgravity Hydrocarbon Diffusion Flames

M. Yousef Bahadori
Science Applications International Corporation
Torrance, California

Dennis P. Stocker
NASA Lewis Research Center
Cleveland, Ohio

Raymond B. Edelman
Rockwell International Corporation
Canoga Park, California

28th Aerospace Sciences Meeting
January 8-11, 1990/Reno, Nevada

EFFECTS OF PRESSURE ON MICROGRAVITY HYDROCARBON DIFFUSION FLAMES*

M. Yousef Bahadori†
Science Applications International Corporation
Torrance, California

Dennis P. Stocker‡
NASA Lewis Research Center
Cleveland, Ohio

and

Raymond B. Edelman¶
Rockwell International Corporation, Rocketdyne Division
Canoga Park, California

ABSTRACT

Laminar diffusion flames of propane burning in quiescent air ($21\%O_2$-$79\%N_2$) are studied under both normal-gravity and microgravity conditions at pressures of 0.5, 1.0 and 1.5 atm. The effects of three fuel mass-flow rates (corresponding to 0.5, 1.0 and 1.5 cm^3/sec at standard conditions of 1 atm and 294 K) have been investigated for each pressure. A circular nozzle of 0.15-cm diameter was used for these experiments, which were conducted in the 2.2-Second Drop Tower of NASA Lewis Research Center. The microgravity tests have shown enhanced sooting, tip-opening and soot escape, combined with changes in color, size, and luminosity of the flames. The corresponding normal-gravity flames do not show these characteristics. The observed differences are attributed to the effects of buoyancy which, once removed, result in increased residence time, dominance of diffusive processes, and extensive radiative loss combined with cooler overall flame temperatures. The paper presents the results in terms of the sooting behavior, Reynolds-number effects, pressure effects, tip-opening, and overall flame characteristics for both normal-gravity and microgravity flames.

*Paper AIAA 90-0651, presented at the AIAA 28th Aerospace Sciences Meeting, Reno, Nevada, January 8-11, 1990.

†Senior Scientist; Member AIAA. Author to whom correspondence should be sent to the following address: NASA Lewis Research Center, MS 500-217, Cleveland, Ohio 44135.

‡ NASA Project Scientist.

¶Project Scientist; Member AIAA.

1. Introduction

Laminar diffusion flames of hydrogen and hydrocarbons burning in quiescent air[1-3] or with secondary air flows[4] have been studied in the 2.2-Second Drop Tower of NASA Lewis Research Center. In these studies, the flames were ignited in normal gravity, and after attaining steady state, were subjected to microgravity. It was shown that microgravity gas jet diffusion flames are wider, taller and sootier than their normal-gravity counterparts, and are flicker-free. A review of these works is presented elsewhere.[9] Recent studies[10,11] have shown that by igniting the flame in microgravity, improving the photographic technique, and reducing the filming rate, flames which were reported as extinguished,[4] reached a near-steady state during the 2.2 seconds of microgravity. Ignition in microgravity has the advantages of eliminating the residual buoyancy-induced momentum (from the pre-drop normal-gravity period) and not subjecting the flame to a step change in gravity.

The present investigation of the effects of pressure on microgravity laminar diffusion flames seeks to gain a better understanding of sooting, extinction, enhanced burning, and in general, the physico-chemical phenomena involved in the behavior and characteristics of these flames. This is important not only from the fundamental standpoint, but with potential applications to spacecraft fire safety and control of combustion in low-gravity environments.

2. Experimental

Laminar diffusion flames of propane were studied in quiescent oxidizing environments in the 2.2-Second Drop Tower of NASA Lewis Research Center. For each microgravity flame, the corresponding normal-gravity flame was also studied. Details of the experimental hardware and procedure can be found elsewhere.[10,11] A circular nozzle (0.15 cm in diameter) was used to burn propane in air (21% oxygen, 79% nitrogen). The

volume of the combustion chamber was approximately 0.04 m^3. The flames were studied at chamber pressures of 0.5, 1.0 and 1.5 atm. For each pressure, three fuel mass-flow rates were used which, at standard conditions of 1 atm and 294 K, correspond to 0.5, 1.0 and 1.5 cm^3/sec. Hence, the cold-jet Reynolds numbers based on the fuel properties and nozzle radius were 49, 98 and 147 for the three mass flow rates. Note that the cold-jet velocities are inversely proportional to pressure.

A 16-mm Milliken movie camera recorded ignition and flame development with filming rates of 16, 20 and 24 frames/sec for pressures of 0.5, 1.0 and 1.5 atm, respectively, using Tungsten Eastman Ecktachrome Video News films. The films for the dim, 0.5-atm flames were force-processed 1 f-stop; the rest were processed normally.

The flames were ignited in microgravity with a spark ignitor. The electrode was located approximately 1.0 cm above the nozzle tip and 1.5 cm away from the nozzle centerline, with the electrically grounded nozzle acting as the second electrode. The ignition system was active for 0.4 sec, and was synchronized with the release of the package and subsequent opening of the fuel solenoid valve. Unlike the previous studies,[10,11] the electrode was far enough from the nozzle to cause no local disturbance to the (wide) microgravity flames.

3. Results

Table 1 shows the data obtained for the nine microgravity flames studied at three pressures and three fuel mass-flow rates. The normal-gravity data are shown in Table 2, with the flame height being the average of maximum and minimum heights (i.e., flicker zone). Table 3 gives the ratios of visible soot length (due to emission, burn-off and soot quenching, as will be seen later) to flame height for microgravity flames, and ratios of microgravity to normal-gravity flame height and maximum flame diameter. Consistent with earlier studies, the microgravity flame is larger than its normal-gravity counterpart in all cases.

Table 1 Microgravity data for propane flames

Flame no.	Re*	P, atm	Volume flow, cc/s	Flame height, cm	Max. dia., cm	Height at max. dia., cm	Tip dia., cm	Red soot height, cm	Blue base height, cm	Total sooting height, cm
1	49	1.5	0.33	4.6	2.2	2.4	1.9	0.6	0.3	4.3
2	98	1.5	0.67	7.4	2.2	4.8	2.1	1.4	0.2	7.2
3	147	1.5	1.00	10.6	2.4	7.6	2.2	2.0	0.2	10.4
4	49	1.0	0.50	3.1	1.9	2.5	1.2	0.2	0.5	2.6
5	98	1.0	1.00	6.1	2.3	4.8	2.1	0.7	0.6	5.5
6	147	1.0	1.50	8.2	2.3	5.6	2.2	1.3	0.5	7.7
7	49	0.5	1.00	3.4	2.4	2.4	0.0	0.0	1.0	2.4
8	98	0.5	2.00	7.0	2.7	5.4	1.2	0.5	0.8	6.2
9	147	0.5	3.00	9.6	2.8	8.0	2.0	1.0	0.7	8.9

*Reynolds number is based on the nozzle radius and cold-fuel properties; similarly in Tables 2 and 3.

Table 2 Normal-gravity data for propane flames

Flame no.	Re	P, atm	Volume flow, cc/s	Max. flame height, cm	Min. flame height, cm	Ave. flame height, cm	Max. dia., cm	Blue base height, cm
10	49	1.5	0.33	5.6	3.0	4.3	0.8	0.3
11	98	1.5	0.67	8.6	5.4	7.0	1.0	0.3
12	147	1.5	1.00	10.8	8.4	9.6	1.0	0.3
13	49	1.0	0.50	2.6	2.2	2.4	0.7	0.4
14	98	1.0	1.00	6.0	3.6	4.8	0.9	0.4
15	147	1.0	1.50	8.2	4.2	6.2	1.0	0.5
16	49	0.5	1.00	2.9	2.9	2.9	1.1	0.8
17	98	0.5	2.00	5.2	4.6	4.9	1.4	0.8
18	147	0.5	3.00	7.8	5.8	6.8	1.4	0.7

Table 3 Ratios of heights and diameters for propane flames*

Re	P, atm	$h_{s,0\text{-}g}/h_{0\text{-}g}$	$h_{0\text{-}g}/h_{1\text{-}g}$	$d_{max,0\text{-}g}/d_{max,1\text{-}g}$
49	1.5	0.93	1.07	2.75
98	1.5	0.97	1.06	2.20
147	1.5	0.98	1.10	2.40
49	1.0	0.84	1.29	2.71
98	1.0	0.90	1.27	2.56
147	1.0	0.94	1.32	2.30
49	0.5	0.71	1.17	2.18
98	0.5	0.89	1.43	1.93
147	0.5	0.93	1.41	2.00

*Here, h is the flame height and d is the flame diameter. The subscripts s, max, 0-g, and 1-g correspond, respectively, to soot length, maximum, microgravity, and normal-gravity.

Figure 1 shows the flame shapes and colors in both normal gravity and microgravity, for the flow rate corresponding to Re=98, and the three different pressures. In addition, the flicker range is shown in this figure for the normal-gravity flames.

Figure 1 and Table 2 show that in general, for normal-gravity flames, as the pressure increases, the average flame height increases (with an exception for flames at 1.0 atm), flame radius decreases, height of the blue base decreases, the reaction zone becomes thinner, flicker distance increases, and the flame becomes brighter. However, microgravity flames do not flicker (see Fig. 1); they generally have open tips with soot escaping through the tip, are taller than average normal-gravity flames (see Table 1), much wider than their normal-gravity counterparts, and are dimmer and sootier. In addition, as the pressure increases, microgravity flames show more red and orange colors near the tip, their blue-base length decreases, and their maximum radius decreases.

Microgravity flame heights are plotted as a function of fuel Reynolds number in Fig. 2, for different pressures. Figure 3 shows the same data as a function of pressure for different Reynolds numbers. It appears from Figs. 2 and 3 that the flame height correlates linearly with the Reynolds number, but reaches an apparent minimum between 0.5 and 1.5 atm. The flame height in all of these microgravity tests was based on the location where red soot changes color into dull red, indicating local flame extinction (as can be seen in Fig. 1). Experimental studies have shown that soot ceases to burn near 1300K. The red to dull-red transition seems to roughly correspond to this temperature limit (as will be shown later). However, there are other definitions that could be adopted such as the separation point between orange and red, or yellow

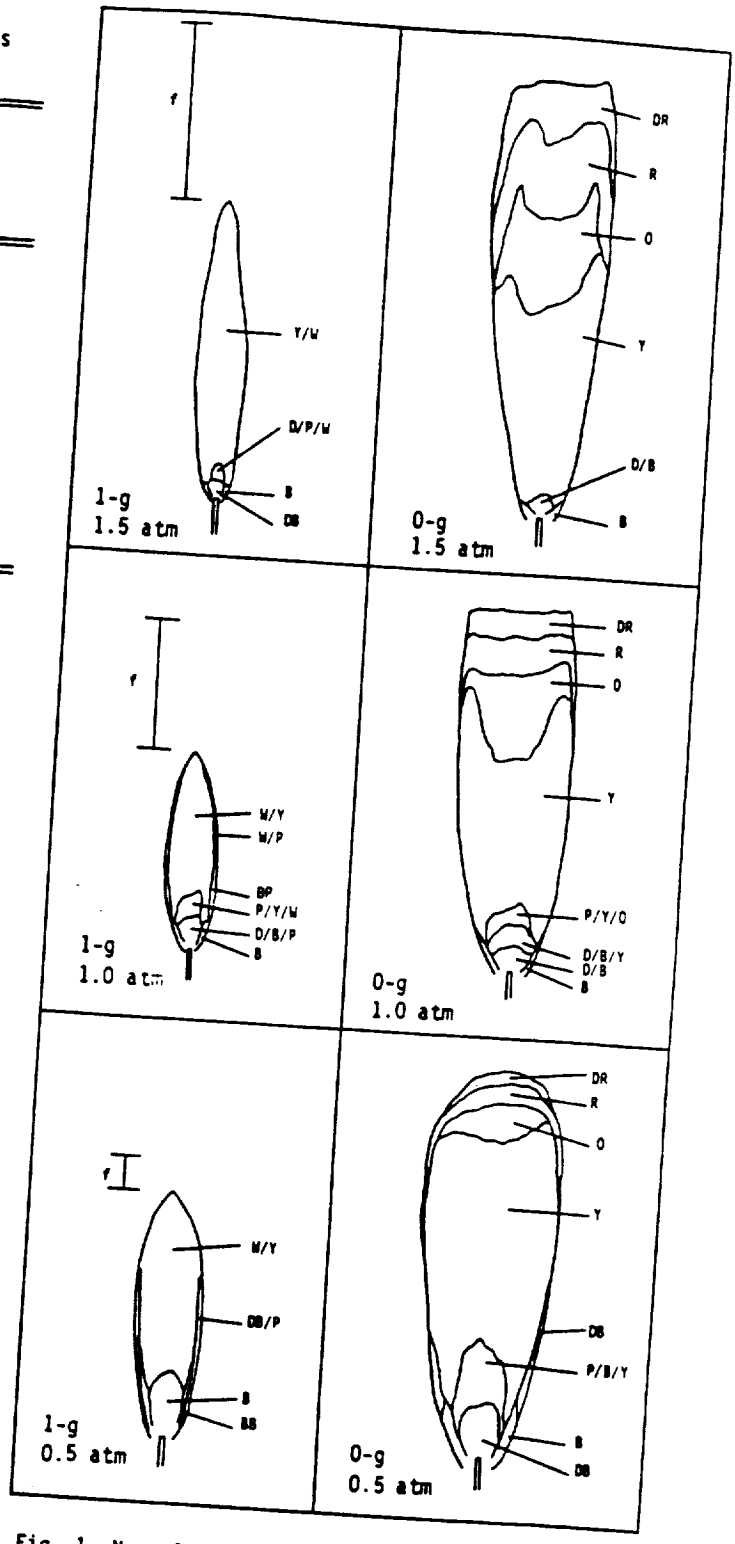

Fig. 1 Normal-gravity and microgravity flames of propane with nozzle diameter = 0.15 cm and fuel Reynolds number = 98 (based on the nozzle radius). The various colors observed are as follows: B (blue), BB (bright blue), D (dark), DB (dark blue), DP (dark pink), DR (dull red), O (orange), P (pink), R (red), W (white), and Y (yellow). The range of flicker (f) is also indicated for normal-gravity flames; scale: ——, = 1 cm.

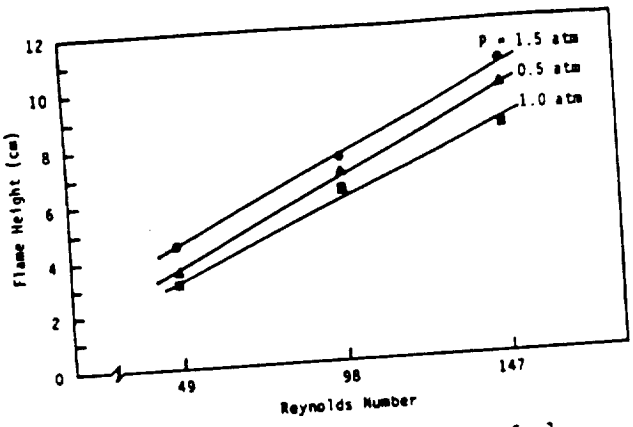

Fig. 2 Microgravity flame height vs. fuel Reynolds number for different pressures. The lines connect the data points. Note that the flame height is largest at 1.5 atm and smallest at 1.0 atm; compare with Fig. 3.

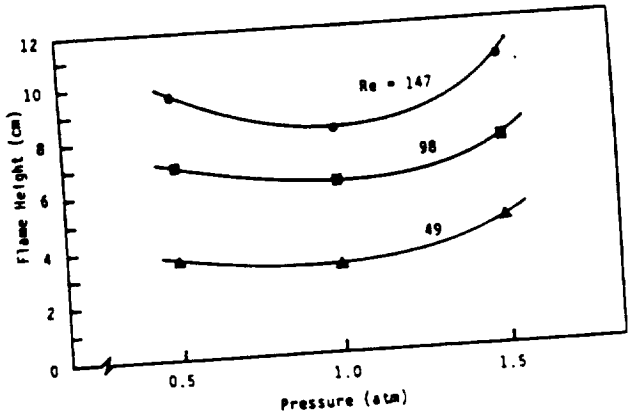

Fig. 3 Microgravity flame height vs. pressure for different fuel Reynolds number. The lines connect the data points. Note that at each Reynolds number, there exists a pressure betwween 0.5 and 1.0 atm at which the flame is shortest; compare with Fig. 2.

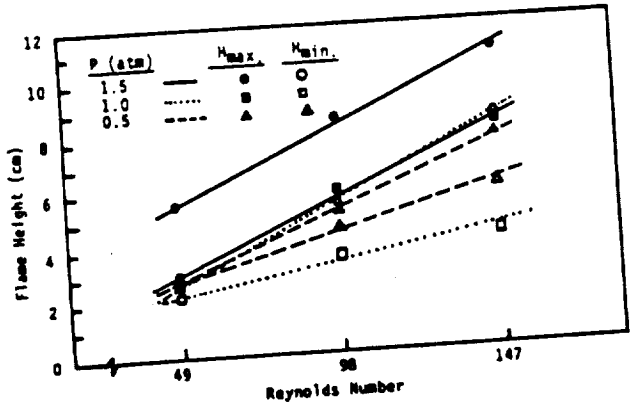

Fig. 4 Minimum (open symbols) and maximum (closed symbols) normal-gravity flame heights (flicker range) vs. fuel Reynolds number for different pressures. The lines connect the data points. Note that the 0.5-atm flame at the lowest Reynolds number does not flicker.

and orange. Of course, making this determination is difficult and other definitions might add some additional effects. Currently, other criteria are being looked at to define a flame height for open-tip microgravity flames and to sort out the effects of glowing particles in masking the actual flame location. This subject will be discussed in more detail in the next section.

Figure 4 shows the minimum and maximum heights for the (flickering) normal-gravity flames. The minimum and average normal-gravity heights (see Table 2) behave similar to the microgravity flames in relation to the effect of pressure. That is, again there exists a pressure in the range 0.5 atm $<P<1.5$ atm at which the minimum and average normal-gravity heights attain a minimum. This is consistent with the observations made in the microgravity flames. Note that the maximum height of the normal-gravity flames follows almost the same behavior with respect to pressure (see Fig. 4). It is interesting to note that in Fig. 4, the flame of lowest Reynolds number for 0.5 atm does not flicker in normal gravity (Table 2) and does not have an open tip in microgravity (Table 1).

Figure 5 shows the soot quench region (defined in this work as the length of the red zone at the flame tip), which increases with both pressure and fuel Reynolds number, indicating enhanced soot formation. In Fig. 6, the blue-base height (i.e., soot inception and agglomeration period prior to emission and burn-off) is plotted for both microgravity and normal-gravity flames as a function of fuel Reynolds number at different pressures. As the pressure increases, both normal-gravity and microgravity soot-inception regions decrease in length with little dependence on flow rate. Finally, Fig. 7 shows the microgravity flame-tip diameter vs. Reynolds number. Note that in Fig. 7, due to the uncertainty in the beginning of tip opening at 0.5 atm, no attempt has been made to connect the three data points.

4. Discussion

In general, for both normal-gravity and microgravity flames, the soot inception period and the region of burning CO (blue region at the base) decreases as the pressure increases. This indicates that formation, burn-off and emission of soot is facilitated by an increase in pressure. Recent normal-gravity studies of hydrocarbon flames[13] have shown that a pressure increase results in an increase in soot formation and a decrease in soot removal by oxidation. This agrees with the present observations of the normal-gravity flames, since brightness increases due to more soot, and hence, more emission in normal-gravity flames. In microgravity, as the pressure increases, the length of the yellow region decreases, but orange, red and dull red regions increase in length (see Fig. 1), indicating that more soot has been formed.

The complex processes of fuel pyrolysis and soot formation, coagulation and burn-off are all pressure-dependent. As the pressure increases, residence time increases because flow velocity decreases. In addition, a pressure increase results in an increase in collision frequency of the particles, and hence, growth in coagulation.

Also, collision frequency depends on the particle size, which is a determining factor in particle burn-off. But particle burn-off is oxygen-dependent, and as the pressure increases, the oxygen partial pressure increases. Therefore, there exist different, pressure-dependent, competitive rates of fuel pyrolysis and particle agglomeration and burn-off, which suggest the importance of the relative effects of these rate processes. The competition between these processes may be responsible for the non-monotonic behavior of the flame height with pressure in both normal-gravity and microgravity (see Figs. 2 and 3, and Table 2). It seems that there exists a pressure in the range 0.5 atm <P <1.5 atm for any Reynolds number, at which the flame attains its minimum height due to the most efficient burning caused by the competing effects of oxygen availability, pressure, and the rate processes mentioned earlier. This phenomena is exacerbated by increasing Reynolds number. Hence, at low-enough Reynolds number, the flame heights may become equal regardless of pressure (see Fig. 3).

The orange-reddish color of the microgravity flames indicates that soot may be at a cooler temperature than would be expected for typical burn-off conditions. In addition, the other colors in both normal-gravity and microgravity flames suggest the presence of particular species present in hydrocarbon flames, e.g., blue-violet (outer region at the base showing the spectrum of burning CO), bluish-green region (showing C_2 and CH emissions, where C_2 bands appear green shaded toward violet and CH bands appearing blue-violet), and a highly luminous zone (bright yellow due to the continuous spectrum of burning carbon particles). This luminous zone becomes yellow, then orange, then red and dull red toward the boundary of the visible region as the temperature of the soot decreases in microgravity flames. Assuming soot to be a black body, the burning particle is yellow, i.e., visible radiation of ~0.58-μm wavelength (1370K <T <1670K, where 1670K is the temperature of a white hot body), and as the temperature decreases, the soot particle becomes orange-red (~1370K, ~0.6 μm), then cherry red (~1170K, 0.6-0.65 μm), and finally dull red (~970K, 0.65-0.70 μm). These effects are shown in Fig. 2, which indicate cooling by pyrolysis and enhanced radiation due to increased soot formation.

Figure 5 shows that as the pressure increases, the quench length increases. This indicates that more soot has been formed, which then requires a longer residence time to quench. Again, the lowest Reynolds number at 0.5 atm shows no quench length since the flame tip is closed.

In Fig. 7, the microgravity flame-tip diameter is plotted as a function of Reynolds number. The 1.5-atm and 1.0-atm flames show an asymptotic type of convergence, indicating that beyond a certain Reynolds number, the flame tip has a fixed diameter. Therefore, regardless of pressure (and hence, availability of oxygen), jet-momentum and fuel mass-flow rate dominate the flame adjustment to the location of stoichiometry.

As can be seen in Table 3, the lower the pressure and Reynolds number, the shorter the non-dimensional soot length for microgravity flames.

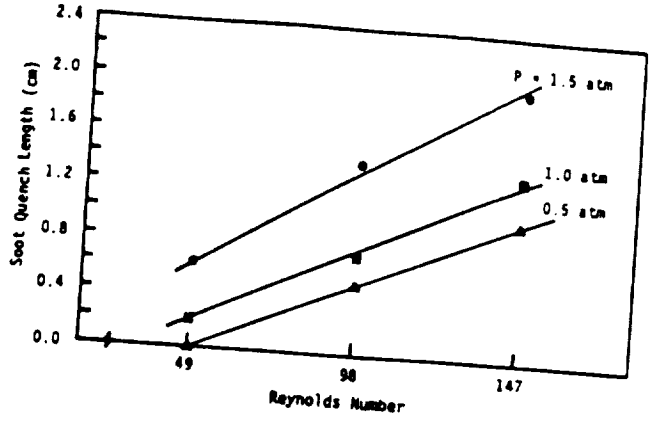

Fig. 5 Soot quench length (red region at the flame tip) vs. fuel Reynolds number as a function of pressure. The solid lines connect the data points.

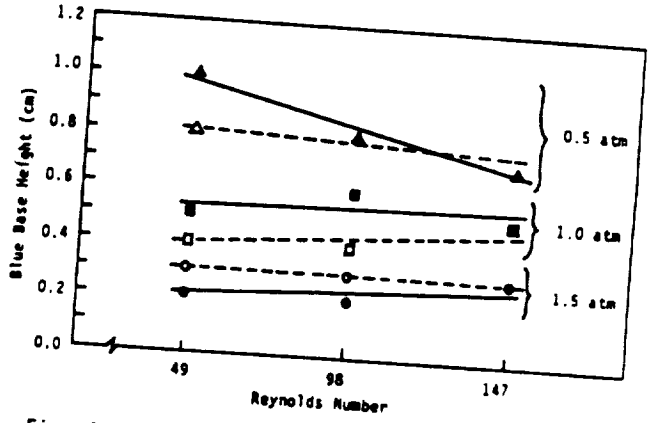

Fig. 6 Blue-base height vs. fuel Reynolds number at different pressures for normal-gravity flames (open symbols and dashed lines) and microgravity flames (closed symbols and solid lines). Whenever the normal-gravity and microgravity data coincide, only the microgravity symbol is used. The lines connect the data points.

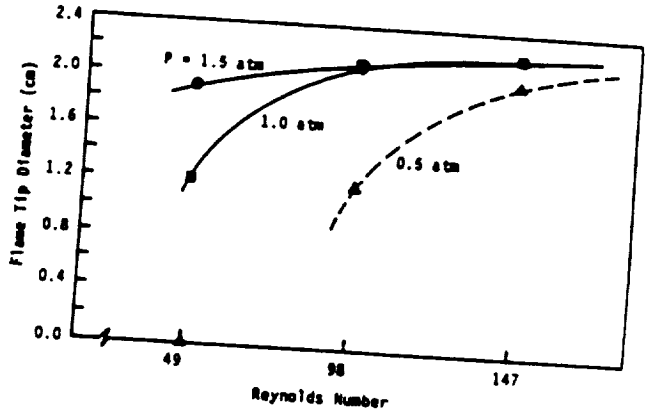

Fig. 7 Flame-tip diameter vs. fuel Reynolds Number at different pressures for microgravity flames. The broken line indicates uncertainty in connecting the data points due to the lack of information on the smallest Reynolds number for which the tip opens.

Since normal-gravity flames flicker, the soot length was not tabulated for these flames. The ratio of microgravity to (average) normal-gravity flame height increases with decrease in pressure, and is fairly uniform over the range of Reynolds numbers studied. This shows that as pressure is raised, microgravity and normal-gravity flame heights may become equal. However, the ratio of microgravity to normal-gravity maximum flame diameter does not yield sufficiently uniform behavior to draw a similar conclusion.

5. CONCLUSIONS

Laminar diffusion flames of propane burning in quiescent air have been studied under both normal-gravity and microgravity conditions at 0.5, 1.0 and 1.5 atm. For each pressure, three fuel-flow rates are used. The results show the following conclusions:

1. Normal-gravity flames flicker, and the flickering range is dampened as pressure decreases. Microgravity flames are steady and flicker-free, and are taller than their normal-gravity counterparts. The effect becomes more pronounced as the pressure decreases (i.e., jet velocity increases).

2. Microgravity propane flames generally have open tips with soot quenching and escape at the tip, and beyond a certain Reynolds number, the flame-tip diameter becomes independent of pressure. At each pressure, there may be a well-defined Reynolds number below which the microgravity flame can not have an open tip, corresponding to a non-flickering normal-gravity flame. Also, the smaller the normal-gravity flicker range, the smaller the tip diameter in microgravity.

3. The higher the pressure, the shorter the soot inception height, resulting in a faster approach toward sooting in both normal-gravity and microgravity flames. This causes more extensive sooting in microgravity with a larger soot-quench zone. Previous normal-gravity studies have shown that sooting is enhanced and burn-off is depressed by increase in pressure. Microgravity flames follow the same trend.

4. At low pressures, less-efficient burning and a broader flame zone exist due to the kinetics effects. At high pressures, more soot and longer soot-burning zones make the task of identifying the gas-phase flame front difficult. For the range of pressures studied, there exists a particular intermediate pressure at which both the microgravity and normal-gravity flame heights are minimized.

The type of data obtained in this study indicates that more testing is required at intermediate, lower, and higher pressures, in addition to a wider range of Reynolds numbers to more fully characterize the effects of pressure on microgravity diffusion flames. Data on soot formation and disposition need, in their own right, a separate study. Gathering these data will represent a unique source of information for unraveling the complex processes involved in sooting flames. Furthermore, additional analyses (beside the on-going theoretical effort) need to be performed for defining the test conditions. Although it is evident that the effects of buoyancy can be used beneficially to enhance the data base on soot formation and disposition processes, it is essential that tests involving non-sooting flames be conducted as well. Such tests are planned to sort out the effects of soot on the interpretation of data, in addition to providing a way for diagnosis of both sooting and non-sooting flames under different environmental conditions in microgravity environments.

Acknowledgements

This work is supported by NASA Lewis Research Center under Contract NAS3-22822. The authors would like to thank Dr. Howard Ross of NASA LeRC for many helpful discussions and suggestions.

References

1. Cochran, T.H. and Masica, W.J., "Effects of Gravity on Laminar Gas Jet Diffusion Flames," NASA TN D-5872, 1970.

2. Cochran, T.H. and Masica, W.J., Thirteenth Symposium (International) on Combustion, The Combustion Institute, Pittsburgh, PA, 1971, pp. 821-829.

3. Haggard, J.B. Jr. and Cochran, T.H., Combustion Science and Technology, 5, 1972, pp. 291-298.

4. Cochran, T.H. "Experimental Investigation of Laminar Gas Jet Diffusion Flames in Zero Gravity," NASA TN D-6523, 1972.

5. Haggard, J.B. Jr. and Cochran, T.H., "Hydrogen and Hydrocarbon Diffusion Flames in a Weightless Environment," NASA TN D-7165, 1973.

6. Edelman, R.B., Fortune, O.F., Weilerstein, G., Cochran, T.H., and Haggard, J.B., Jr., Fourteenth Symposium (International) on Combustion, The Combustion Institute, Pittsburgh, PA, 1973, pp. 399-412.

7. Edelman, R.B., Fortune, O., and Weilerstein, G., "Analytical Study of Gravity Effects on Laminar Diffusion Flames," NASA CR-120921, 1973.

8. Haggard, J.B. Jr., "Forced and Natural Convection in Laminar-Jet Diffusion Flames," NASA TP 1841, 1981.

9. Edelman, R.B. and Bahadori, M.Y., Acta Asronautica, 13, 1986, pp. 681-688.

10. Edelman, R.B., Bahadori, M.Y., Olson, S.L., and Stocker, D.P., "Laminar Diffusion Flames Under Microgravity Conditions," Paper AIAA 88-0645, AIAA 26th Aerospace Sciences Meeting, Reno, NV, 1988.

11. Bahadori, M.Y., Edelman, R.B., Stocker, D.P., and Olson, S.L., "Ignition and Behavior of Laminar Gas-Jet Diffusion Flames in Microgravity, AIAA J., 1990, in press.

12. Kent, J.H. and Wagner, H. Gg., Combust. Sci. Tech., 41, 1984, pp. 245-269.

13. Flower, W.L. and Bowman, C.T., Twenty-First Symposium (International) on Combustion, The Combustion Institute, Pittsburgh, PA, pp. 1115-1124, 1986.

Section 12

"RADIATION FROM GAS-JET DIFFUSION FLAMES IN MICROGRAVITY ENVIRONMENTS"

M. Y. Bahadori, R. B. Edelman, R. G. Sotos and D. P. Stocker

Paper AIAA-91-0719, AIAA 29th Aerospace Sciences Meeting,
Reno, Nevada, January 1991

AIAA-91-0719

Radiation from Gas-Jet Diffusion Flames in Microgravity Environments

M. Yousef Bahadori
Science Applications International Corporation
Torrance, California

Raymond B. Edelman
Rockwell International Corporation
Canoga Park, California

Raymond G. Sotos and Dennis P. Stocker
NASA Lewis Research Center
Cleveland, Ohio

29th Aerospace Sciences Meeting
January 7-10, 1991/Reno, Nevada

RADIATION FROM GAS-JET DIFFUSION FLAMES IN MICROGRAVITY ENVIRONMENTS*

M. Yousef Bahadori†
Science Applications International Corporation
Torrance, California

Raymond B. Edelman‡
Rockwell International Corporation, Rocketdyne Division
Canoga Park, California

and

Raymond G. Sotos§ and Dennis P. Stocker¶
NASA Lewis Research Center
Cleveland, Ohio

ABSTRACT

This paper presents the first demonstration of quantitative flame-radiation measurement in microgravity environments, with the objective of studying the influences and characteristics of radiative transfer on the behavior of gas-jet diffusion flames with possible application to spacecraft fire detection. Laminar diffusion flames of propane, burning in quiescent air at atmospheric pressure, are studied in the 5.18-Second Zero-Gravity Facility of NASA Lewis Research Center. Radiation from these flames is measured using a wide-view angle, thermopile-detector radiometer, and comparisons are made with normal-gravity flames. The results show that the radiation level is significantly higher in microgravity compared to normal-gravity environments due to larger flame size, enhanced soot formation, and entrapment of combustion products in the vicinity of the flame. These effects are the consequences of the removal of buoyancy which makes diffusion the dominant mechanism of transport. The results show that longer test times may be needed to reach steady state in microgravity environments.

*Paper AIAA-91-0719, presented at the AIAA 29th Aerospace Sciences Meeting, Reno, Nevada, January 7-10, 1991.

†Senior Scientist; Member AIAA. Author to whom correspondence should be sent to the following address: SAIC/NASA LeRC, MS 500-217, Cleveland, Ohio 44135.

‡Chief Scientist; Member AIAA.

§Manager, Zero-Gravity Facility.

¶NASA Project Scientist.

1. Introduction

The term "diffusion flame" classifies those types of flames in which the fuel and oxidizer are not premixed. The basic mechanisms which control these flames (and combustion in general) include the coupled processes of mixing, chemical kinetics including soot formation and disposition, flame radiation, and buoyancy-induced convection. A major problem impeding our understanding of flame behavior is the masking effect of buoyancy on flames that are studied in a normal-gravity environment. The behavior of fires on earth is determined by the combined convective and diffusive effects, where buoyancy-induced convection masks the processes of chemical-diffusional interaction that are fundamental to the understanding of combustion phenomena. In zero-gravity environments, the buoyant force is eliminated, and the remaining physico-chemical processes are responsible for the different behavior of flames observed in the microgravity experiments conducted to-date.[1]

Recent studies of microgravity laminar diffusion flames have shown some unique, and in most cases, unexpected phenomena.[2-7] For example, in order to study the effects of microgravity on flammability and extinction of flames in the near-limit regions, tests were conducted under reduced-oxygen[2] and/or reduced-pressure[3] conditions. The results show that flame characteristics, color, luminosity, and sooting behavior are strongly affected in microgravity compared to normal gravity.[2] Sooting was eliminated in microgravity propane flames at 18% oxygen, and the flames were entirely blue, whereas their normal-gravity counterparts were yellow, luminous, and very similar to flames under atmospheric conditions. This has an important implication, namely, reduced radiative heating and reduced hazard of flame spreading to the surrounding combustible materials by reducing the oxygen concentration in microgravity environments. In addition, flammability limits may be quite different in microgravity and normal-gravity flames under identical conditions of pressure and oxygen concentration. The present study was conducted to investigate the effects of radiative loss on flame behavior and characteristics.

2. Experimental

The experiments were conducted in the 5.18-Second Zero-Gravity Facility of NASA Lewis Research Center. Figure 1 shows a schematic of the hardware. The volume of the sealed combustion chamber was 0.087 m^3. The tapered-tip nozzle had an inner diameter of 0.17 cm. Both normal-gravity and microgravity flames of propane were studied in quiescent oxidizing environments of 21% oxygen-79% nitrogen at 1 atm. The fuel volume-flow rates were 0.5, 1.0 and 1.5 cm^3/sec, corresponding to a cold-jet Reynolds number of 45, 90, and 135, respectively.

The flames were ignited using a spark electrode located 1.0 cm above the nozzle tip and 2.0 cm away from the nozzle centerline, with the nozzle acting as the ground electrode. The ignition system was activated for approximately 1.0 sec for both the normal-gravity and microgravity flames. The microgravity flames were ignited after the release of the package in the evacuated drop tube. Two movie cameras (filming rates = 12 and 30 frames/sec, respectively) using Kodak Ektachrome Video News films recorded the flame development and behavior.

The wide-view-angle radiometer was comprised of a 1.5x1.5-mm, fast-response thermopile detector with a Calcium Fluoride (CaF_2) window (Oriel Corporation, Model 7106), with a time constant of 40 msec, field of view of 90-100°, and maximum irradiance of 0.2 W/cm^2. In addition, the experiment chamber was equipped with a CaF_2 window to allow maximum transmission of the infrared radiation. The window had a usable transmission range of 0.2-9.0 μm, with its absorptivity falling off above 1.0 μm to about 50% at 10.0 μm; its approximate transmission in the linear range was 94%. The inside of the chamber was painted black to avoid reflection from the wall.

The radiometer was calibrated using a black-body source (Barnes Engineering, Model 11-210), with an opening of 2.54 cm in diameter. A nanometer (Keithly Instrument, Model 181) was used to measure the radiometer response to various temperatures of the black-body source. The distance from the nozzle centerline (and for calibration, from the black-body source) to the radiometer sensor was 28.6 cm, and from the shutter iris to the sensor was 3.84 cm. The iris on the shutter had a diameter of 2.54 cm. The diameter of the Calcium Fluoride window was 4.45 cm. The nozzle/window/iris/sensor arrangement was such that the entire flame could be seen by the sensor.

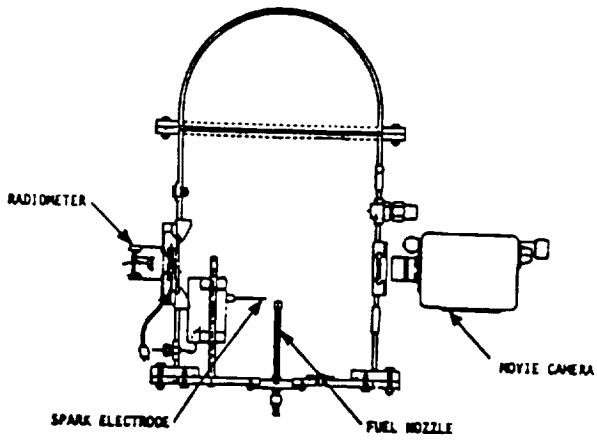

Fig. 1 Experiment package for the 5.18-second microgravity tests.

3. Results

Figure 2 shows the flame shapes and colors for the three flow rates under both normal-gravity and microgravity conditions. The normal-gravity flames were flickering with a typical flicker frequency of laminar diffusion flames in the absence of air flow. However, the microgravity flames developed continuously toward steady state during the 5 seconds of available time, and the shapes presented in Fig. 2 are for the last few fractions of a second.

Figure 3 shows the flame radiance as a function of time. The radiometer registers the data in terms of mV. Using the calibration chart and converting the mV to the equivalent black-body temperature of the calibration source, radiance ($\sigma T_b^4/\pi$) can be obtained, where σ is the Stefan-Boltzmann constant, and T_b is the black-body temperature.

In Table 1, the data obtained for both normal-gravity and microgravity flames are presented in terms of flame height, maximum flame diameter, radiance, and radiance/flame height. Data interpretation will be discussed in the next section. The radiance data are the average of the values during the last second of the experiment.

Figure 4 shows the radiance as a function of fuel-volume flow rate for both normal-gravity and microgravity flames.

Table 1 Normal-gravity and microgravity data for propane flames burning in quiescent air at 1.0 atmosphere

Volume flow rate, cm^3/sec	Normal-Gravity Flames				Microgravity Flames			
	Ave. flame height, cm	Max. flame diameter, cm	Flame radiance, W/cm^2-sr	Radiance / Ave. Ht.	Flame height, cm	Max. flame diameter, cm	Flame radiance, W/cm^2-sr	Radiance / Height
0.5	2.1	~0.6	0.18	0.09	3.5	2.3	1.29	0.37
1.0	4.1	~0.7	0.34	0.08	5.9	2.4	2.31	0.39
1.5	4.9	~0.7	0.54	0.11	10.3	2.3	4.68	0.45

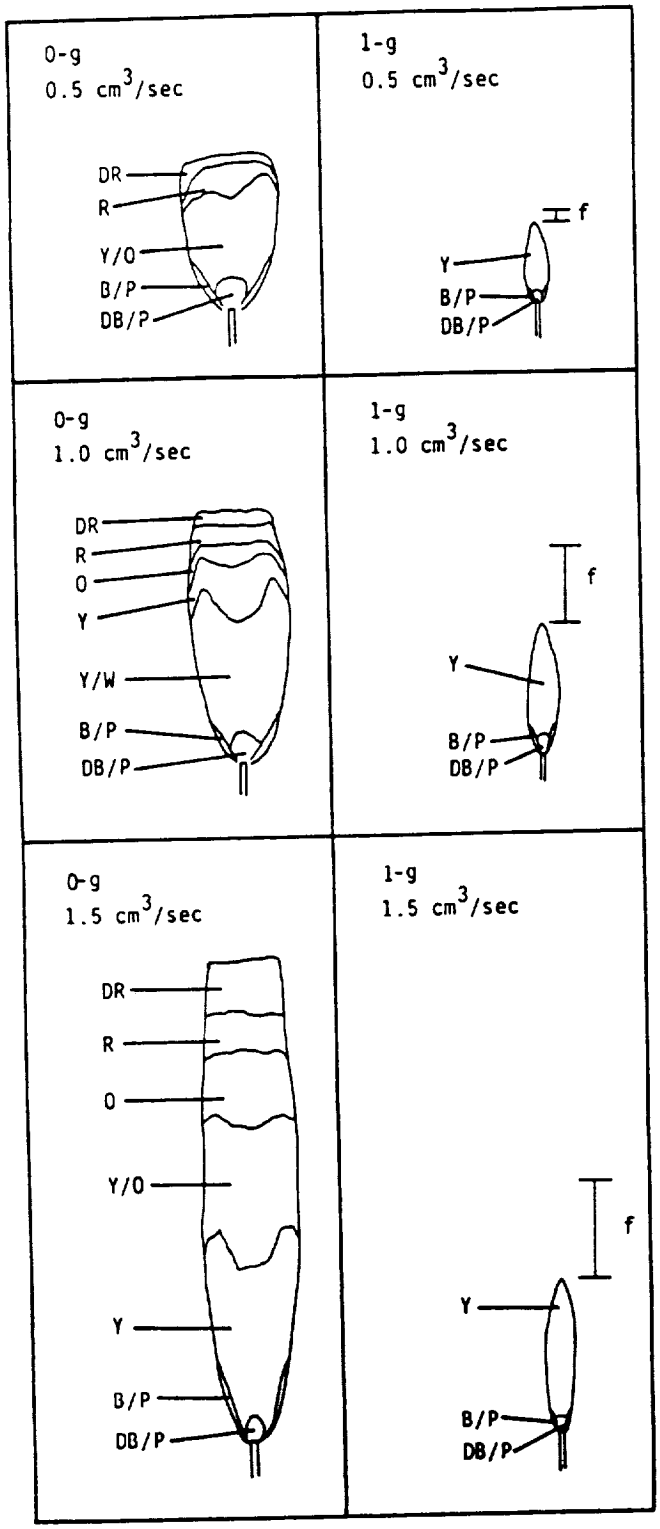

Fig. 2 Normal-gravity and microgravity flames of propane, at different volume flow rates, burning in quiescent air at 1.0 atm. The various colors observed are as follows: B (blue), DB (dark blue), DR (dull red), O (orange), P (pink), R (red), W (white), and Y (yellow). The range of flicker, f, is shown for the normal-gravity flames; scale: ⟷ = 1 cm.

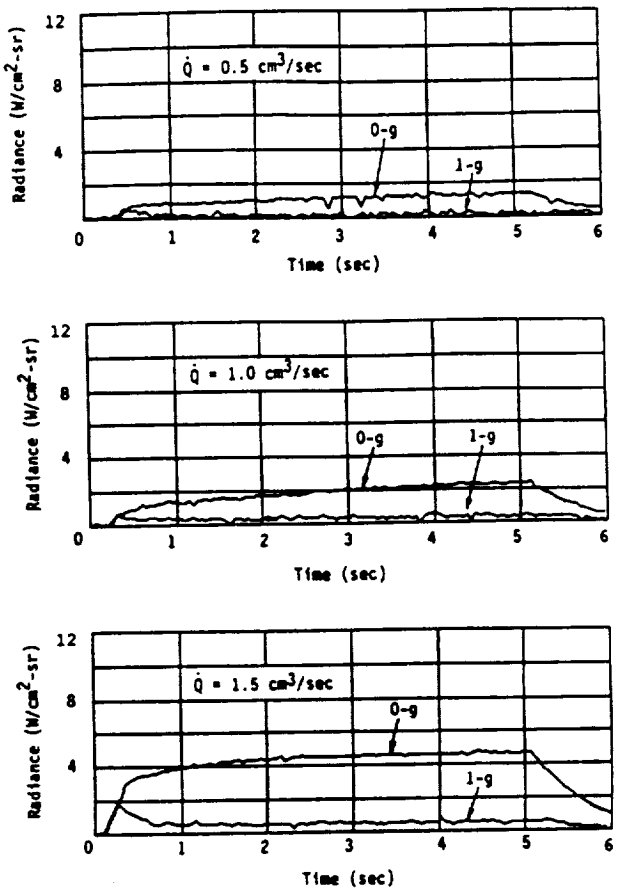

Fig. 3 Measured radiance vs. time for both normal-gravity and microgravity flames of propane burning in air at 1 atm.

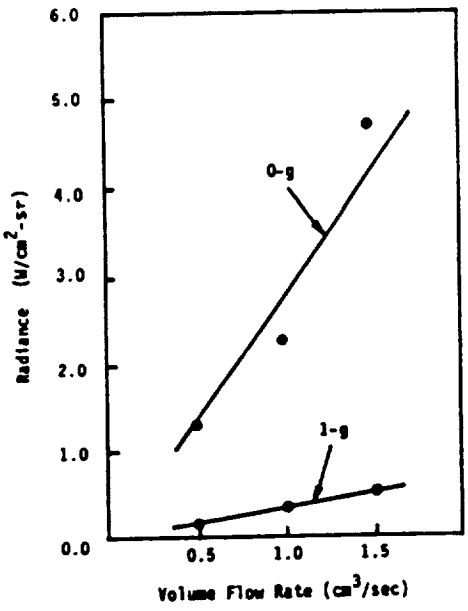

Fig. 4 Radiance as a function of fuel volume-flow rate for propane flames burning in air at 1 atm. The radiance data are the average values between 4.0 sec and 5.0 sec after ignition.

4. Discussion

The flame shapes presented in Fig. 2 show that microgravity flames are taller, wider, and sootier than their normal-gravity counterparts. The orange-reddish color of these flames is an indication of cooler temperatures than is expected for typical burn-off conditions. The yellow/orange/red/dull red regions in the flame show that the temperature of the soot decreases in microgravity flames, leading to local extinction at the flame tip. This tip-opening and underventilated-type behavior is a characteristic of sooty microgravity flames. Absence of buoyancy and dominance of diffusive processes result in longer residence times, enhanced soot formation, increased radiative loss and cooling by pyrolysis, which are responsible for the observed behavior and characteristics of microgravity flames. The data presented in Table 1 show that as the fuel flow rate increases, both microgravity and average normal-gravity flame heights increase, but the effect is more pronounced for microgravity flames. Although the maximum flame diameter is independent of fuel volume flow rate in both microgravity and normal gravity, the microgravity flames show a four-fold increase in diameter. This is due to the accumulation and slow transport of combustion products in the vicinity of the flame in microgravity. The microgravity flame heights presented in Table 1 are based on the location where red soot changes color into dull red, indicating local flame extinction. Experimental studies have shown that soot quenching occurs around 1300 K. Assuming soot to be a black body, orange-red ($\sim$1370 K), cherry red ($\sim$1170 K) and dull red ($\sim$970 K) clearly indicate that extinction occurs near the flame tip.

The data of Fig. 3 show that radiative loss is constant for normal-gravity flames throughout the duration of the test. This is largely due to the instantaneous removal of the hot combustion products under the influence of buoyancy. In addition, under normal-gravity condition, the flame immediately establishes following ignition, whereas in microgravity, a continuous development of the flame is observed (both visually by examining the films and through radiation data). Figures 3 and 4 show that fuel flow rate has a much more pronounced effect on the level of radiation from microgravity flames compared to those in normal gravity. The radiation data of Fig. 4 show that radiance varies linearly with fuel flow rate under normal-gravity condition, again, due to the dominance of buoyancy, which limits the radiative loss. However, in microgravity, radiance quickly starts to increase as the amount of injected fuel increases. This is not only due to the larger flame size and extensive soot formation, but also the accumulation and slow transport of the combustion products as mentioned before. The hot products of combustion (mostly CO_2 and H_2O) appear to contribute dramatically to radiative loss from the microgravity flames. The data of Table 1 and Fig. 4 show that radiative loss from the microgravity flames studied in this work is 6-9 times larger compared to the corresponding normal-gravity flames. In Table 1, radiance/flame height is also calculated. Since flame diameters are observed to be independent of flow rate for a given gravitational level, flame height is a good measure for obtaining radiance per unit volume of the flame. It can be seen that radiance/height is $\sim$0.1 for normal-gravity flames and $\sim$0.4 for microgravity flames. Whether these values change at higher flow rates needs to be determined.

The data presented in this study suggest that radiative ignition of nearby materials may be promoted in low-gravity environments due to the increased radiative loss from gas-jet diffusion flames. Examination of the data also show that radiation may not reach steady state in 5 seconds of microgravity. This is apparently due to the continuous accumulation and slow transport of combustion products in the vicinity of the flame. Sometimes the luminous region does not appear to increase in size. However, the diffusion of non-luminous hot gases in the surrounding causes the volume of the hot gas to increase, which is reflected through the continuous increase in radiation (and temperature of the field). This has a direct impact on the question of approach toward steady state in microgravity flames, indicating that the reduced-gravity earthbound facilities may not provide enough time to obtain the true steady-state data. Previous studies[1,6,7] have shown that transient effects become important for microgravity laminar diffusion flames. The data obtained in the present study seem to substantiate these observations.

5. Conclusions

Quantitative measurement of flame radiation has been obtained for the first time in a microgravity study. Laminar diffusion flames of propane, burning in quiescent air at atmospheric pressure, have been studied for flow rates of 0.5-1.5 cm^3/sec. The results show that flame radiation is 6-9 times larger in microgravity compared to normal gravity. Enhanced soot formation, larger flame size, and entrapment and slow transport of the hot combustion products in the vicinity of the microgravity flame are the contributing factors. The normal-gravity radiation data quickly reach steady state, whereas the corresponding microgravity data are in a transient state throughout the duration of the experiment. The results show that longer test times are needed in microgravity to reach steady state.

Acknowledgements - This work is supported by NASA Lewis Research Center under Contract NAS3-22822. The authors would like to thank Paul Tavernelli and John Kolacz of NASA LeRC, Engineering Directorate, for design of the data acquisition system and calibration of the radiometer.

References

[1]Edelman, R.B., and Bahadori, M.Y., Acta Astronautica, 13, pp. 681-688, 1986; see also references cited in this work.

[2]Bahadori, M.Y., and Stocker, D.P., "Oxygen-Concentration Effects on Microgravity Laminar Methane and Propane Diffusion Flames," 1989 Eastern States Meeting of The Combustion Institute, Albany, New York, October/November 1989.

[3]Bahadori, M.Y., Stocker, D.P., and Edelman, R.B., "Effects of Pressure on Microgravity Hydrocarbon Diffusion Flames," Paper AIAA-90-0651, AIAA 28th Aerospace Meeting, Reno, NV, Jan. 1990.

[4]Bahadori, M.Y., Edelman, R.B., Stocker, D.P., and Olson, S.L., AIAA J., 28, pp.236-244, 1990.

[5]Stocker, D.P., "Size and Shape of Laminar Burke-Schumann Diffusion Flames in Microgravity," 1990 Central States Meeting of The Combustion Institute, Cincinnati, Ohio, May 1990.

[6]Bahadori, M.Y., "An Analytical Solution for Transient, Cylindrically Symmetric Laminar Diffusion Flames in the Absence of Buoyancy," 1990 Central States Meeting of The Combustion Institute, Cincinnati, Ohio, May 1990.

[7]Bahadori, M.Y., Edelman, R.B., Sotos, R.G., and Stocker, D.P., "Measurement of Temperature in Microgravity Laminar Diffusion Flames," 1990 Eastern States Meeting of The Combustion Institute, Orlando, Florida, December 1990.

Section 13

"EFFECTS OF OXYGEN CONCENTRATION ON RADIATIVE LOSS FROM NORMAL-GRAVITY AND MICROGRAVITY METHANE DIFFUSION FLAMES"

M. Y. Bahadori, R. B. Edelman, D. P. Stocker, R. G. Sotos, and D. F. Vaughan

Paper AIAA-92-0243, AIAA 30th Aerospace Sciences Meeting,
Reno, Nevada, January 1992

AIAA-92-0243

Effects of Oxygen Concentration on Radiative Loss from Normal-Gravity and Microgravity Methane Diffusion Flames

M. Yousef Bahadori
Science Applications International Corporation
Torrance, California

Raymond B. Edelman
Rockwell International Corporation
Canoga Park, California

Dennis P. Stocker, Raymond G. Sotos, and David F. Vaughan
NASA Lewis Research Center
Cleveland, Ohio

30th Aerospace Sciences
Meeting & Exhibit
January 6-9, 1992 / Reno, NV

EFFECTS OF OXYGEN CONCENTRATION ON RADIATIVE LOSS FROM NORMAL-GRAVITY AND MICROGRAVITY METHANE DIFFUSION FLAMES*

M. Yousef Bahadori†
Science Applications International Corporation
Torrance, California

Raymond B. Edelman‡
Rockwell International Corporation, Rocketdyne Division
Canoga Park, California

and

Dennis P. Stocker,§ Raymond G. Sotos,¶ and David F. Vaughan•
NASA Lewis Research Center
Cleveland, Ohio

Abstract

Laminar diffusion flames of methane, burning in quiescent oxidizing environments at atmospheric pressure, have been studied under both normal-gravity and microgravity conditions. Radiation from these flames is measured using a wide-view-angle, thermopile detector radiometer. The oxidizer was 18%, 21%, and 30% oxygen in nitrogen. The results show that radiation levels are significantly higher in microgravity compared to normal-gravity environments. This is due to larger flame size, enhanced soot formation, and accumulation and slow transport of the combustion products in the vicinity of the flame, which are caused by the removal of buoyancy. For the normal-gravity flames, the effect of oxygen concentration on radiation is negligible, whereas in microgravity, the flame radiation is strongly affected by the amount of oxygen in the environment. This has direct applications to the problem of spacecraft fire detection and fire safety.

* Paper AIAA-92-0243, presented at the AIAA 30th Aerospace Sciences Meeting, Reno, Nevada, January 6-9, 1992.

† Senior Scientist; Senior Member AIAA. Author to whom correspondence should be sent to the following address: SAIC/NASA LeRC, MS 500-217, Cleveland, Ohio 44135.

‡ Chief Scientist, Member AIAA

¶ Manager, Zero-Gravity Facility.

§ NASA Project Scientist.

• Baldwin-Wallace College, Berea, Ohio.

1. Introduction

The fundamental understanding of flame characteristics under reduced-gravity conditions is essential to the problem of fire safety in spacecraft environments.[1] The behavior of fires on Earth is influenced by the combined convective and diffusive effects, where buoyancy-induced convection masks the processes of chemical-diffusional interaction. Under microgravity conditions, the buoyant force is nearly eliminated, and the coupled physico-chemical processes of diffusion, mixing, kinetics, radiation, and convection become more tractable. A major problem impeding our understanding of flame behavior is this masking effect of buoyancy, which results in some very significant

differences between the structure of normal-gravity and microgravity flames.[2]

"Diffusion" flames, as the name implies, are flames in which the fuel and oxidizer are initially "non-premixed", and the combustion process is governed by the diffusion of these reactants toward each other to form a reaction zone (i.e., the flame sheet). In "laminar" diffusion flames of gaseous fuels, as opposed to "turbulent" gas-jet diffusion flames, the flame height increases almost linearly with the increase in fuel-flow rate (or the Reynolds number). In recent studies of microgravity laminar diffusion flames, some unique and unexpected phenomena have been observed.[2-10] The results have shown that flame color, size, luminosity, sooting behavior, and approach toward steady state are significantly different in microgravity compared to normal gravity. In addition, these differences are exacerbated by the change in pressure and/or oxidizer composition for the microgravity flames.[3, 4, 10]

Radiative characteristics of flames is the focus of the present study. The total radiation from normal-gravity and microgravity flames of methane have been measured. This type of measurement has been used extensively by Markstein[11-16] to study radiation from a variety of laminar and turbulant diffusion flames in normal gravity environments.

2. Experimental

The experiments were conducted in the 5.18-Second Zero-Gravity Facility of NASA Lewis Research Center.[17] Figure 1 shows a schematic of the hardware. The volume of the combustion chamber was 0.087 m^3. The fuel nozzle (protruding 15 cm inside the chamber) had a tapered tip with inner radius of 0.0825 cm, and was positioned along the centerline of the cylindrical chamber. The nozzle was approximately 20 cm away from the chamber wall. The tip of the nozzle was approximately 50 cm away from the chamber top. The fuel was supplied from a stainless steel bottle of 75 cm^3 in volume at an initial pressure of 100 psig. Appropriate windows were mounted in the chamber wall for the movie cameras and the radiometer. A pressure transducer was used to record the chamber pressure during the test.

Both normal-gravity and microgravity flames of methane (99.9%-pure) were studied in quiescent oxidizing environments of 18%, 21% and 30% by volume of oxygen in nitrogen. The chamber pressure was 1.0 atm, and the fuel-volume flow rate was 3.0 cm^3/sec.

The flames were ignited using a spark electrode, which was located 1.0 cm above the nozzle tip and 2.0 cm away from the nozzle centerline, with the nozzle acting as the ground electrode. The ignition system was activated for 0.5-1.0 sec for the normal gravity and microgravity tests. The microgravity flames were ignited after the release of the package in the drop tube. Two movie cameras (filming rates = 12 and 30 frames/sec, respectively) using color Kodak Ektachrome Video News film recorded the flame development and behavior.

The wide-view angle radiometer was comprised of a 1.5 x 1.5-mm, fast-response thermopile detector with a Calcium Fluoride (CaF_2) window (Oriel Corporation, Model 7106), and a time constant of 40 msec, field of view of 90 - 100 degrees, and maximum irradiance of 0.2 W/cm^2. In addition, the experiment chamber was equipped with a CaF_2 window to allow maximum transmission of the infrared radiation. The window had a usable transmission range of 0.2 - 9.0 μm, with its absorptivity falling off above 1.0 μm to about 50% at 10.0 μm; its approximate transmission in the linear range was 94%. The radiometer was calibrated using a black-body source (Barnes Engineering, Model 11-210), with an opening of 2.54 cm in

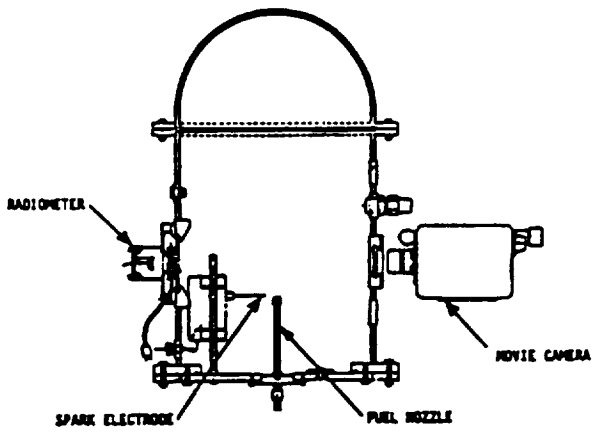

Fig. 1 Experiment package for the 5.18-second microgravity tests.

diameter. A nanometer (Keithly Instrument, Model 181) was used to measure the radiometer response to various temperatures of the black-body source. The distance from the nozzle centerline (and for calibration, from the black-body source) to the radiometer sensor was 28.6 cm, and from the shutter iris to the sensor was 3.84 cm. The iris on the shutter had an open diameter of 2.54 cm. The inner diameter of the Calcium Fluoride window was 4.45 cm. The nozzle/window/iris/sensor arrangement was such that the field of view on a plane passing through the centerline of the nozzle had a radius of 9.55 cm.

3. Results

Figure 2 shows the normal-gravity and microgravity flames of methane burning in quiescent oxidizing environments of 18%, 21%, and 30% by volume of oxygen in nitrogen. Following ignition, the normal-gravity flames establish quickly (in less than 0.5 sec), and show the typical flicker characteristics (with a frequency of 10 - 20 Hz) of laminar flames. The flicker range is also shown in Figure 2 for the normal-gravity flames. However, the microgravity flame heights continuously increase after ignition, and reach near-steady state after a few seconds following ignition. The microgravity flames shown in Figure 2 are for the last instant of the drop (just prior to the beginning of deceleration).

Figure 3 shows the flame radiance as a function of time for both normal-gravity and microgravity flames. Using the calibration chart, the data obtained from the radiometer reading (in mV) was converted to the equivalent black-body temperature (T_b) of the calibration source. The flame radiance ($\sigma T^4_b/\pi$) in W/cm^2-sr was then obtained as a function of time, where σ is the Stefan-Boltzmann constant.

Table 1 shows the data obtained in terms of flame height, flame maximum diameter, radiance, and radiance per unit projected flame area. This area was calculated by multiplying the flame height by the maximum flame diameter, to give a rough estimate of the relative values of radiance per unit flame area between the normal-gravity and microgravity flames. The radiance data are averages for the last second of each test. The

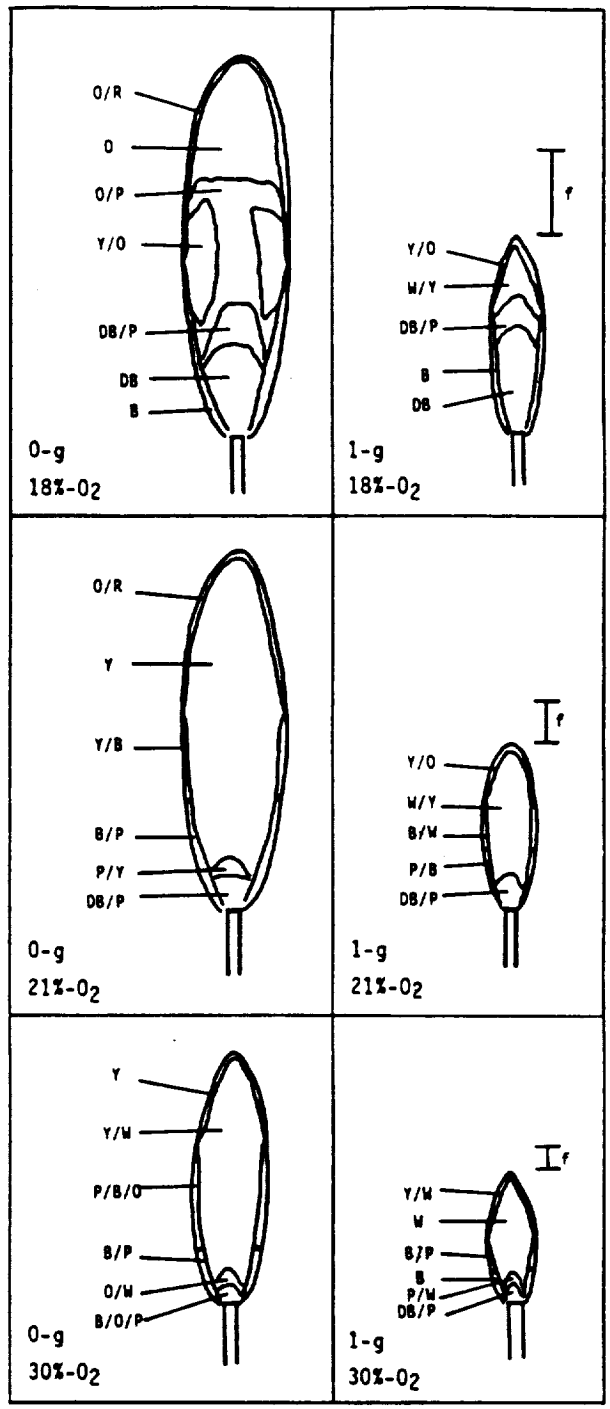

Fig. 2 Normal-gravity and microgravity flames of methane, burning in different oxygen-nitrogen environments at 1.0 atm. The various colors observed are as follows: B (blue), DB (dark blue), O (orange), P (pink), R (red), W (white), and Y (yellow). The range of flicker, f, is shown for the normal-gravity flames; scale: ⟷ = 1 cm.

heights for normal-gravity flames in Table 1 are the averages of minimum and maximum flickering-flame height.

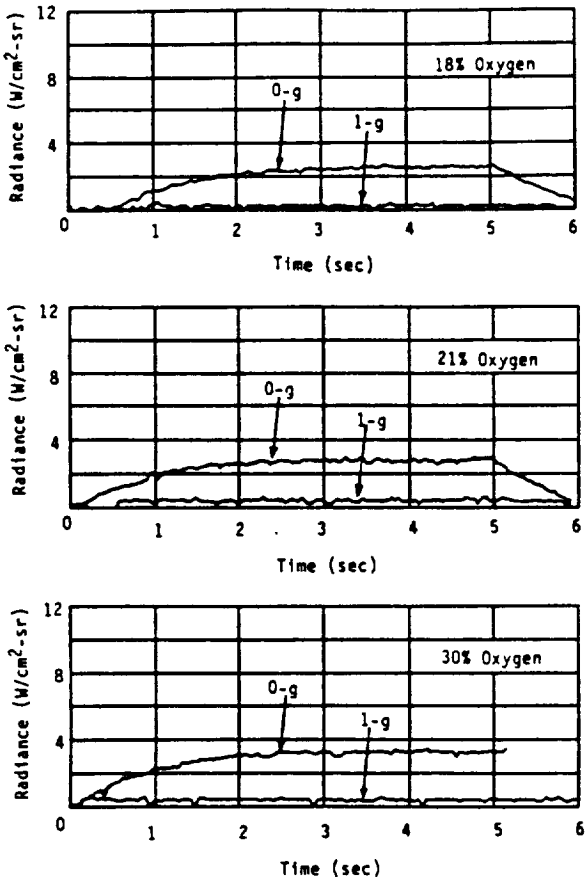

Fig. 3 Measured radiance vs. time for both normal-gravity and microgravity flames of methane burning in different oxidizing environments at 1 atm.

In Figure 4, flame radiance as a function of oxygen concentration is presented. Both normal-gravity and microgravity flames show an increase in radiance with increasing oxygen concentration. However, the effect is more significant for the microgravity flames.

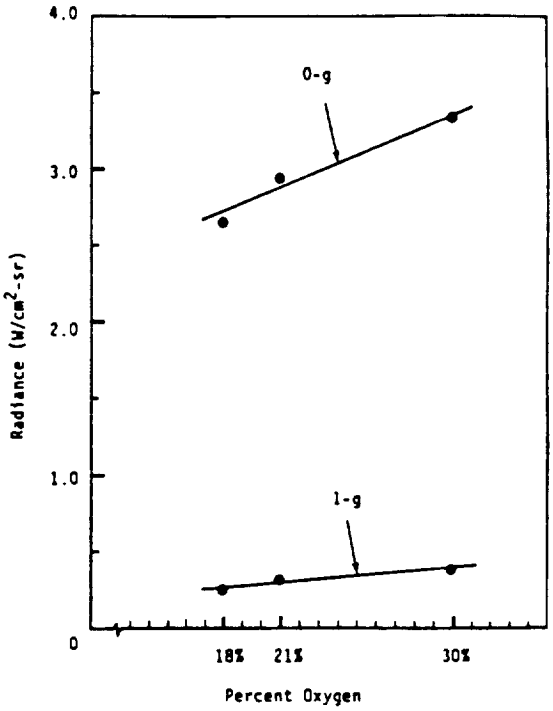

Fig. 4 Radiance as a function of percent oxygen for methane flames burning at 1 atm. The radiance data are the average values between 4.0 sec. and 5.0 sec. after ignition.

TABLE 1 NORMAL-GRAVITY AND MICROGRAVITY DATA FOR METHANE FLAMES BURNING IN QUIESCENT OXIDIZING ENVIRONMENTS AT 1.0 ATM

	Normal-Gravity Flames				Microgravity Flames			
Oxygen	Avg. flame height, cm	Max. flame diameter, cm	Flame radiance, W/cm²-sr	Radiance / Flame area	Flame height, cm	Max. flame diameter, cm	Flame radiance, W/cm²-sr	Radiance / Flame area
18%	5.2	1.3	0.24	0.04	8.2	2.4	2.65	0.13
21%	4.1	1.2	0.32	0.07	7.7	2.2	2.95	0.17
30%	3.1	1.1	0.38	0.11	5.4	1.7	3.33	0.36

4. Discussion

The flames of Figure 2 show the significant effects of buoyancy on size, shape and luminosity. The normal-gravity flames are generally yellow, flickering, and pencil-like, regardless of oxygen level in the environment. However, their flicker range decreases and their intensity appears to increase at higher oxygen concentrations. The microgravity flames, on the other hand, are taller, wider, and more diffuse than the normal-gravity flames. As the oxygen level increases, the flame becomes brighter due to higher gas-phase and particulate temperatures and faster soot burn-off.

The orange/reddish color of the microgravity flames is an indication of cooler temperatures than is expected for typical burn-off conditions. The yellow/orange/red regions in the flames show that the temperature of the soot decreases in microgravity flames. Absence of buoyancy and dominance of diffusive processes result in longer residence times, enhanced soot formation, increased radiative loss and additional cooling by pyrolysis, which are, in some combination, responsible for the observed characteristics of microgravity flames.

The data presented in Figure 3 show that radiative loss in normal-gravity flames is not only constant throughout the duration of the test, but that the level of radiation does not change significantly with increasing oxygen concentration. This is largely due to the rapid removal of the hot combustion products under the influence of buoyancy. In addition, the normal-gravity flames become established immediately following ignition, whereas in microgravity, the flame increases in height for a few seconds following ignition (both visually by examining the films and through radiation data).

Table 1 shows that for both normal-gravity and microgravity flames the radiation decreases with reduced ambient oxygen concentrations. It is interesting to note that the radiation from the normal gravity flames falls within a narrow range, as can be seen in Figure 4. Finally, Table 1 shows a linear variation of flame height with change in oxygen concentration for both the normal-gravity and microgravity flames. This is due to the availability of oxygen in the environment. The data presented in Table 1 also show that radiance per unit flame area is significantly different between normal-gravity and microgravity flames. This is attributed to the accumulation and slow transport of the hot combustion products in the vicinity of the microgravity flame.

5. Conclusion

Laminar diffusion flames of methane have been studied under both normal-gravity and microgravity conditions. The quiescent oxidizing environment was composed of 18%, 21%, and 30% oxygen in nitrogen at 1.0 atmosphere. A wide-view-angle, thermopile-detector radiometer was used to measure the overall radiative loss from these flames. The results show that flame radiation is an order of magnitude higher in microgravity compared to normal gravity for the flames studied in this work. Larger size of the microgravity flames caused by the removal of buoyancy and the accumulation and slow transport of the hot combustion products in the vicinity of the flame is largely responsible for this observation. The normal-gravity radiation data reach steady state in less than 1.0 second, whereas the microgravity data take up to 5.0 seconds to reach near-steady state. The normal-gravity flames do not show appreciable effects of oxygen concentration, whereas those in microgravity show significant increase in radiation with increasing oxygen concentration.

Acknowledgments

This work was supported by NASA Lewis Research Center under Contract NAS3-22822 with Science Applications International Corporation. D. F. Vaughan was supported by Grant NCC-3157 with Baldwin-Wallace College.

References

1. Sacksteder, K. R.: Twenty-Third Symposium (International) on Combustion, P. 1589, The Combustion Institute, 1990.

2. Edelman, R. B. and Bahadori, M. Y.: Acta Astronautica 13, 681 (1986); for previous studies of microgravity laminar diffusion flames, see references cited in this work.

3. Bahadori, M. Y. and Stocker, D. P.: Oxygen-Concentration Effects on Microgravity Laminar Methane and Propane Diffusion Flames, Eastern States Meeting of The Combustion Institute, Albany, New York, October/November 1989.

4. Bahadori, M. Y., Stocker, D. P., and Edelman, R. B.: Effects of Pressure on Microgravity Hydrocarbon Diffusion Flames, Paper AIAA-90-0651, AIAA 28th Aerospace Sciences Meeting, Reno, Nevada, January 1990.

5. Bahadori, M. Y., Edelman, R. B., Stocker, D. P., and Olson, S. L.: AIAA J. 28, 236 (1990).

6. Stocker, D. P.: Size and Shape of Laminar Burke-Schumann Diffusion Flames in Microgravity, Central States Meeting of The Combustion Institute, Cincinnati, Ohio, May 1990.

7. Bahadori, M. Y.: An Analytical Solution for Transient, Cylindrically Symmetric Laminar Diffusion Flames in the Absence of Buoyancy, Central States Meeting of The Combustion Institute, Cincinnati, Ohio, May 1990.

8. Bahadori, M. Y., Edelman, R. B., Sotos, R. G., and Stocker, D. P.: Measurement of Temperature in Microgravity Laminar Diffusion Flames, Eastern States Meeting of The Combustion Institute, Orlando, Florida, December 1990.

9. Bahadori, M. Y., Edelman, R. B., Sotos, R. G., and Stocker, D. P.: Radiation from Gas-Jet Diffusion Flames in Microgravity Environments, Paper AIAA-91-0719, AIAA 29th Aerospace Sciences Meeting, Reno, Nevada, January 1991.

10. Bahadori, M. Y., Edelman, R. B., Sotos, R. G., Stocker, D. P., and Vaughan, D. F.: Effects of Oxygen Concentration on Radiation From Microgravity Laminar Propane Diffusion Flames, submitted for presentation at the Twenty-Fourth Symposium (International) on Combustion, 1992.

11. Markstein, G. H.: Fifteenth Symposium (International) on Combustion, P. 1285, The Combustion Institute, 1974.

12. Markstein, G. H.: Combust. Flame 27, 51 (1976).

13. Markstein, G. H.: Sixteenth Symposium (International) on Combustion, P. 1407, The Combustion Institute, 1977.

14. Markstein, G. H. and deRis, J.: Twentieth Symposium (International) on Combustion, P. 1637, The Combustion Institute, 1984.

15. Markstein, G. H.: Twentieth Symposium (International) on Combustion, P. 1055, The Combustion Institute, 1984.

16. Markstein, G. H.: Radiant Emission and Smoke Points for Laminar Diffusion Flames of Fuel Mixtures, Report FMRC J.I. OMON4.BU, RC86-BT-4, Factory Mutual Research Corporation, Norwood, Massachusetts, June 1986.

17. Lekan, J.: Microgravity Research in NASA Ground-Based Facilities, NASA TM-10397, NASA Lewis Research Center, Cleveland, Ohio, 1989.

Section 14

"GRAVITATIONAL INFLUENCES ON THE BEHAVIOR OF CONFINED DIFFUSION FLAMES"

U. Hegde and M. Y. Bahadori

Paper AIAA-92-0334, AIAA 30th Aerospace Sciences Meeting,
Reno, Nevada, January 1992

AIAA 92-0334

Gravitational Influences on the Behavior of Confined Diffusion Flames

U. Hegde
Sverdrup Technology, Inc.
Lewis Research Center Group
Brook Park, OH
and
M. Y. Bahadori
Thermal Sciences Division
Science Applications International Corporation
Torrance, CA

30th Aerospace Sciences Meeting & Exhibit
January 6-9, 1992 / Reno, NV

AIAA-92-0334

GRAVITATIONAL INFLUENCES ON THE BEHAVIOR OF CONFINED DIFFUSION FLAMES

U. Hegde*
Sverdrup Technology, Inc.
NASA Lewis Research Center Group
Brook Park, Ohio 44142

M. Yousef Bahadori**
Science Applications International Corporation
Thermal Sciences Division
Torrance, California 90501

Abstract

Closed form, mathematical representations for the shapes of laminar diffusion flames stabilized on two-dimensional slot burners are derived for arbitrary gravitational levels. The solution technique employs the Schvab-Zeldovich conserved species variable. Effects of gravity on the velocity field are incorporated through the momentum equation; these effects, in turn, influence the species field. The results reduce smoothly to the classical Burke-Schumann solution as gravity approaches zero. It is shown that both flame height and width increase with decreasing gravity levels. Several interesting cases are considered explicitly; these include effects of negative and extremely high values of gravity. In the latter case it is shown that the flame collapses onto the burner surface. The analysis finds application in the modelling of steady and unsteady gas and solid propellant diffusion flames.

Nomenclature

a	one half of fuel slot width
b	one half of slot burner width
c	one half of burner chimney width
D	binary diffusion coefficient
g	gravitational acceleration
G	effective acceleration, defined by Eq. (21)
G_0	reference acceleration, defined by Eq. (22)
h	flame height
h_0	flame height at zero gravity
I	defined in Eq. (18)
M_F	mass injection rate of fuel
M	mass injection rate of (fuel + oxidizer)
N	total number of species present
p	pressure
Pe	Peclet number
u	x-component of velocity
v	y-component of velocity
W_F	molecular weight of fuel
W_{ox}	molecular weight of oxidizer
x	coordinate parallel to flame axis
y	coordinate normal to flame axis
y_l	line separating hot and cold flow regions
y_f	y-coordinate of flame surface
Y	Schvab-Zeldovich species variable
Y_F	mass fraction of fuel
Y_{ox}	mass fraction of oxidizer
ν	defined by Eq. (5)
ν_F	stoichiometric coefficient of fuel
ν_{ox}	stoichiometric coefficient of oxidizer
ρ	density
ψ	stream function
ψ_l	defined by Eq. (18)
$\sum$	summation from n = 1 to n = ∞

subscripts

0	reference quantity measured at y = 0
1	value in the hot flow region
2	value in the cold flow region

Introduction

This paper considers the effects of gravitational fields on laminar diffusion flames stabilized on two dimensional slot burners in a confined co-flow of fuel and oxidizer. This is a classical problem of interest and analytical solutions for flame shape and height in the absence of gravity are well known[1,2]. Due to the lack of available closed form solutions for buoyant flames, these results have

---

* Supervisor, Microgravity Science Section. Senior Member AIAA.

** Senior Scientist. Senior Member AIAA

been used in the past to describe flame shapes even in the presence of gravity. However, in recent years, it has come to be realized[3-5] that the ambient gravity level can significantly influence observable physical characteristics of such flames. It is only for momentum dominated laminar flames (i.e., flames for which the Froude number, u_0^2/gh, is much greater than unity) that the zero gravity solution has validity.

Numerical and experimental studies on laminar gas diffusion flames where buoyancy effects have explicitly been taken into account have found that gravitational fields significantly affect diffusion flame height and shape[3,6-8]. Based on these findings it is now recognized that there are two opposing aspects of gravity on diffusion flame heights. The increase in flow velocity caused by buoyancy tends to increase the flame height. However, conservation of mass demands that the streamlines of the flow converge. This results in an increase in species diffusion rates which contribute to a reduction in flame height. Following this line of reasoning, the effect of a gravitational field on flame height depends upon which factor is more important; sometimes this may be determined by burner geometry. For example, from analytical reasoning, Roper[4] has derived simplified expressions for flame height which show that buoyantly dominated flames are shorter than zero gravity flames for slot burners and of the same height for circular burners.

While the above noted expressions[4] are available for flame heights of burner stabilized buoyant flames, no closed form solutions are available for flame shapes and widths under arbitrary gravity levels. Such solutions are important for a variety of diffusion flame applications. For example, radiative and conductive heat transfer from diffusion flames depend upon the overall flame shape[9]. In addition, the behavior of unsteady diffusion flames can also, in many cases, be understood utilizing simplified expressions for the steady (time averaged) flame shape[10,11].

Diffusion flame investigations also find application in solid propellant combustion studies. Solid propellant flames are known to consist of intricate combinations of premixed and diffusion flames[12]. To simplify their investigations, researchers have often resorted to studying simplified flames which retain important characteristics of actual solid propellant flames. For example, slot burner flames[11,13], of the type considered in this paper, have been used to simulate the characteristics of sandwich type propellant flames[14]. However, buoyant effects on such flames have largely been neglected.

In this paper, analytical solutions for the shapes of laminar diffusion flames stabilized on slot burners are developed. Arbitrary gravitational fields directed along the axis of the flame are incorporated in the solution. The Schvab-Zeldovich conserved species formalism[2] is utilized. The conservation equations of mass, momentum and species are cast in stream function coordinates. Approximations on flame density and buoyant velocities, no more stringent than in previous analyses, are utilized to obtain closed form solutions for the conserved species variable. The flame shape is then obtained by the flame sheet approximation. These solutions reduce smoothly to the classical Burke-Schumann solution as the gravity level approaches zero. A variety of important cases are considered in the paper; these include cases with negative gravity (inverted flames), partial gravity and extremely high gravity levels.

Formulation

The configuration considered is shown in Fig. 1. Fuel flows through a slot of width 2a. There is a co-flow of oxidizer in the two outside slots. The width of an oxidizer slot is (b-a). The slot burner is placed in a chimney of width c through which there may be a secondary stabilizing flow. It is assumed that both fuel and oxidizer are injected at velocity u_{01}. These streams are heated by the presence of the established diffusion flame. The stabilizing (secondary) flow in the outer chimney is injected with an axial velocity u_{02} and is at the ambient (cold) density. Buoyancy causes the hotter stream above the burner to accelerate.

The equation for the line, $y_1(x)$, separating the hot and cold flows is first obtained from overall mass conservation assuming (a) the hot flow is at a constant density ρ_1 and (b) the secondary flow has constant density ρ_2 and axial velocity u_{02}. It will be shown later (see Eqns. (14) and (15)) that assumption (a) also implies that the u_1 is a function of x alone. This expression for y_1 is readily shown to be

$$y_1 = \frac{b[\rho_1 u_{01} - \rho_2 u_{02}]}{[\rho_1 u_1 - \rho_2 u_{02}]} \quad (1)$$

An one step reaction between fuel and oxidizer is assumed to take place

$$\nu_F F + \nu_{ox} Ox \rightarrow \nu_i M_i$$

The Schvab-Zeldovich conserved variable for chemical species is defined by

$$Y = \left[\frac{-Y_{ox}}{W_{ox}\nu_{ox}} + \frac{Y_F}{W_F \nu_F}\right] \frac{W_F \nu_F}{Y_{F,0}} \quad (2)$$

The equation for overall mass conservation may be written as

$$\frac{\partial \rho u}{\partial x} + \frac{\partial \rho v}{\partial y} = 0 \quad (3)$$

Using standard assumptions of perfect gas behavior, unity Lewis number and constant average molecular weight the conservation equation for Y is

$$\rho u \frac{\partial Y}{\partial x} + \rho v \frac{\partial Y}{\partial y} = \frac{\partial}{\partial y} \rho D \frac{\partial Y}{\partial y} \quad (4)$$

where, as in previous approaches[1-10], axial diffusion has been neglected.

Next, stream function coordinates are introduced by means of the two dimensional von Mises transformation

$$\rho u = \frac{\partial \psi}{\partial y} \quad (5)$$

$$-\rho v = \frac{\partial \psi}{\partial x} \quad (6)$$

The overall continuity equation is then satisfied and the species equation becomes

$$\frac{\partial Y}{\partial x} = \frac{\partial}{\partial \psi} (\rho u)(\rho D) \frac{\partial Y}{\partial \psi} \quad (7)$$

The line $y_1(x)$ from Eq. (1) transforms into the line

$$\psi_1 = \frac{b[\rho_1 u_{01} - \rho_2 u_{02}]}{\left[1 - \frac{\rho_2 u_{02}}{\rho_1 u_1}\right]} \quad (8)$$

It should be noted that ψ_1 is not, in general, a streamline of the flow. Furthermore, assuming that the diffusion coefficients in the hot and cold flows are separately constant the species equation can be written for the hot and cold flows as follows

$$\frac{\partial Y}{\partial x} = (\rho_1 u_1)(\rho_1 D_1) \frac{\partial^2 Y}{\partial \psi^2} \quad (9)$$

$$\frac{\partial Y}{\partial x} = (\rho_2 u_{02})(\rho_2 D_2) \frac{\partial^2 Y}{\partial \psi^2} \quad (10)$$

The above two equations are connected across the line ψ_1 by the conditions

$$(Y)_{\psi 1-} = (Y)_{\psi 1+} \quad (11)$$

and

$$(\rho_1 u_1)(\rho_1 D_1) \left[\frac{\partial Y}{\partial \psi}\right]_{\psi = \psi_{1-}} = (\rho_2 u_{02})(\rho_2 D_2) \left[\frac{\partial Y}{\partial \psi}\right]_{\psi = \psi_{1+}} \quad (12)$$

where the latter condition is obtained by integrating Eq.(7) across ψ_1.

Consideration is now given to the case where the secondary flow velocities are much smaller than the primary flow velocities; specifically, cases where

$$\frac{(\rho_2 u_{02})(\rho_2 D_2)}{(\rho_1 u_1)(\rho_1 D_1)} < 1$$

are considered so that it is appropriate to write

$$\left[\frac{\partial Y}{\partial \psi}\right]_{\psi=\psi_1-} = 0$$

and

$$\psi_1 = b\rho_1 u_{01} \qquad (13)$$

which is independent of x. In this case, ψ_1 becomes equal to the mass flow, M, exiting the burner and represents the streamline leaving the burner at y = b.

The problem is now reduced to solving Eq.(9) subject to the following conditions

at $\psi = 0$, M, for $x > 0$:

$$\frac{\partial Y}{\partial \psi} = 0$$

and at $x = 0$:

$0 < \psi < M_F$: $Y = 1$

$M_F < \psi < M$: $Y = -(Y_{ox,0}/Y_{F,0})(W_F\nu_F/W_{ox}\nu_{ox}) = -\nu$

The velocity u_1 is obtained from the axial momentum equation for the hot flow. Assuming that the pressure at any location x is imposed from the cold flow one obtains in stream function coordinates

$$\rho_1 u_1 \frac{\partial u_1}{\partial x} = (\rho_2 - \rho_1) g \qquad (14)$$

where the gravitational acceleration, g, is positive when directed along the negative x- axis. The solution for u_1 becomes

$$u_1 = \left[u_{01}^2 + \frac{2(\rho_2 - \rho_1) gx}{\rho_1}\right]^{\frac{1}{2}} \qquad (15)$$

which is a function of x alone.

$Y(x,\psi)$ may now be solved for in the region ($x > 0$, $0 < \psi < \psi_1$) using standard techniques. Upon transforming back into (x,y) coordinates the solution may be written as

$$Y = \frac{M_F}{M} - \nu\left[1 - \frac{M_F}{M}\right] + 2\sum \frac{(1+\nu)}{n\pi} \sin\left(n\pi \frac{M_F}{M}\right) \cos\left(\frac{n\pi\rho_1 u_1 y}{M}\right) e^{-\frac{n^2\pi^2 I}{PeM}} \qquad (16)$$

where

$$I = \int_0^x \rho_1 u_1 dx_0 \qquad (17)$$

and Pe is the Peclet number given by

$$Pe = \frac{u_{01} b}{D_1} \qquad (18)$$

The solution may be extended to the region $y_1 < y < c$ by solving Eq. (10) subject to the connection condition Eq.(11) and the impermeable wall condition

$$\frac{\partial Y}{\partial \psi} = 0$$

at $\psi = \psi_c$ (corresponding to y = c). However, in general, $Y(\psi_1)$ will be a function of x ; hence, a technique such as that of Penner et al[15] needs to be employed to obtain particular analytical solutions. The matter is not pursued further in this paper.

Results and Discussions

It is readily shown that in the limit of vanishing g, $u_1 = u_{01}$ and $I = \rho_1 u_{01} x$, so that Eq. (16) reduces to

$$Y = \frac{M_F}{M} - \nu\left(1 - \frac{M_F}{M}\right) + 2\sum \frac{(1+\nu)}{n\pi} \sin\left(n\pi \frac{M_F}{M}\right) \cos\left(n\pi \frac{y}{b}\right) e^{-\frac{n^2\pi^2 x}{Peb}} \qquad (19)$$

which agrees with the classical Burke-Schumann solution[1,2]. This solution is also obtained in the limit of ρ_2 approaching ρ_1.

The flame surface is obtained utilizing the flame sheet approximation ; that is, the condition Y = 0 at the flame surface. Thus, at any axial location x, the coordinate y_f of the flame surface is obtained from

$$0 = \frac{M_F}{M} - \nu\left[1 - \frac{M_F}{M}\right] + 2\sum \frac{(1+\nu)}{n\pi} \sin\left(n\pi \frac{M_F}{M}\right) \cos\left(\frac{n\pi \rho_1 u_1 y_f}{M}\right) e^{\frac{-n^2\pi^2 I}{PeM}} \qquad (20)$$

Furthermore, the flame height, x = h, is obtained when $y_f = 0$.

It is interesting to consider the variation of flame height with burner width for constant burner flow rates. Inspection of Eq.(20) reveals that I must then remain constant. For momentum dominated flames, for x = h, $I = u_{01}h$. For a constant flow rate bu_{01} remains constant so that in this case h varies linearly with b. However, for buoyancy dominated flames u_1 is, for practical purposes, independent of u_{01} so that I is independent of both u_{01} and b. Thus, for buoyancy dominated flames, the flame height is independent of the slot width. This recovers the results of Roper et al[8] for slot burners.

The variation of flame height with the gravitational level g, when the other parameters of the problem are kept constant may also be obtained from the condition that I for x = h remains unchanged. Define an effective acceleration

$$G = \frac{(\rho_2 - \rho_1)}{\rho_1} g \qquad (21)$$

and a reference acceleration

$$G_0 = u_{01}^2 / h_0 \qquad (22)$$

where h_0 is the flame height at zero gravity. Then, utilizing Eqns.(15), (17) and (20) it may be shown that

$$\frac{h}{h_0} = \frac{G_0}{2G}\left[\left[1 + 3\frac{G}{G_0}\right]^{2/3} - 1\right] \qquad (23)$$

The above equation is comparable to Eq. (5) of Ref. 8.

The behavior of h/h_0 for non-negative values of G is ploted in Fig. 2. It is seen that as G increases, the flame height decreases. In the limit of very high accelerations (as G -> ∞), h -> 0. Inspection of Eq. (16) and the initial conditions at x = 0 indicates that in this case, Y can be zero only at the location (x,y) = (0,a) so that the flame collapses onto the burner.

As G increases, the flame width, like the flame height, also decreases. This is shown in Fig. (3) where calculated flame shapes for G equal to u_{01}^2/b and $2u_{01}^2/b$ are plotted. The stoichiometric coefficients chosen for this calculation correspond to methane burning in oxygen so that $\nu = 0.25$. In addition, the physical parameters are a/b = 0.1, and Pe = 10.

Care must be taken in evaluating Eqns.(16) and (20) for negative values of G. In these cases, the streamlines above the burner surface diverge and a stagnation plane is obtained at

$$x_s = -\frac{u_{01}^2}{2G}$$

The developed theory is not valid in the neighborhood of the stagnation plane. A rough indication of the region of validity may be obtained from Eq. (13) which indicates that

$$y_1 = \frac{bu_{01}}{u_1}$$

Certainly, an upper limit to y_1 is the width c of the outer chimney so that the theory is not expected to be valid for

$$u_1 < \frac{bu_{01}}{c}$$

or equivalently for

$$x > \frac{u_{01}^2\left[\left(\frac{b}{c}\right)^2 - 1\right]}{2G}$$

For axial distances less than the above value of x, Eqns. (20) and (21) yield expressions for the flame shape and height. Note also that Eq. (23) indicates that the flame height will be less than x_* when $G/G_0 < -1/3$.

Calculated flame shapes for G equal to $-0.05\ u_{0i}^2/b$ and $-0.42u_{0i}^2/b$ are shown in Fig. (4). The other parameters of the calculation are the same as those for Fig. (3). Note that the flames are bigger and broader than those obtained when G is non-negative. Calculations also show that the flame surface tends to spread outward from the axis for negative values of G having magnitudes much larger than 1/3. This behavior agrees with observations of inverted flames under normal gravity conditions which exhibit tulip shapes[6].

Conclusions

The Burke-Schumann solution for slot burner stabilized diffusion flames has been extended to account for the effects of axially directed gravitational fields. It has been shown that both flame size and height decrease with increase in the gravity level. Predictions from the developed model are consistent with observed behavior of momentum and buoyancy dominated flames. These include the independence of buoyancy dominated flame height on burner width and lateral spreading of flames under negative accelerations. The analysis may be applied to steady and unsteady gas and solid propellant diffusion flame modelling.

Acknowledgements

This work was supported, in part, by NASA Lewis Research Center under Contracts NAS3-25266 (UH) and NAS3-22822 (MYB).

References

1. Burke, S. P., and Schumann, T. E. W., Industrial and Engineering Chemistry, Vol 20, pp. 998, 1928.
2. Williams, F. A., Combustion Theory, 2nd Ed., Benjamin/Cummings, CA, 1985.
3. Edelman, R. B., Fortune, O., and Weilerstein, G., Analytical Study of Gravity Effects on Laminar Diffusion Flames, NASA CR- 120921, 1973.
4. Roper, F. G., Combustion and Flame, Vol. 29, pp. 219-226, 1977.
5. Glassman, I., Combustion, 2nd Ed., Academic Press, Inc.,FL, 1987.
6. Edelman, R. B. and Bahadori, M. Y., Acta Astronautica, Vol. 13, No. 11/12, pp. 681-688, 1986.
7. Bahadori, M. Y., Edelman, R. B., Stocker, D. P., and Olson, S. L., AIAA Journal, Vol. 28, pp. 236-244, 1990.
8. Roper, F. G., Smith, C., and Cunningham, A. C., Combustion and Flame, Vol. 29, pp. 227-234, 1977.
9. Bahadori, M. Y., Edelman, R. B., Sotos, R. G., and Stocker, D. P., AIAA Paper No., 1991.
10. Hegde, U. G. and Zinn, B. T., AIAA Paper No. 89-2662, 1989.
11. Chen, T. Y., Hegde, U. G., Daniel, B. R. and Zinn, B. T., AIAA Paper No. 90-3929, 1990.
12. Beckstead, M. W., Derr, R. L., and Price, C. F., AIAA Journal, Vol. 8, No. 12, 1970.
13. Kumar, R. N., Strand, L. D., and McNamara, R. P., AIAA Paper No. 76-669, 1976.
14. Price, E. W., Sambamurthi, R. K., Sigman, R. K., and Panyam, R. R., Combustion and Flame, Vol. 63, pp. 381-413, 1986.
15. Penner, S. S., Bahadori, M. Y., and Kennedy, E. M., in Dynamics of Flames and Reactive Systems (Eds: J. R. Bowen, N. Manson , A. K. Oppenheim and R. I. Soloukhin), Vol. 95, Progress in Astronautics and Aeronautics, pp. 261-292, AIAA, Washington, DC, 1985.

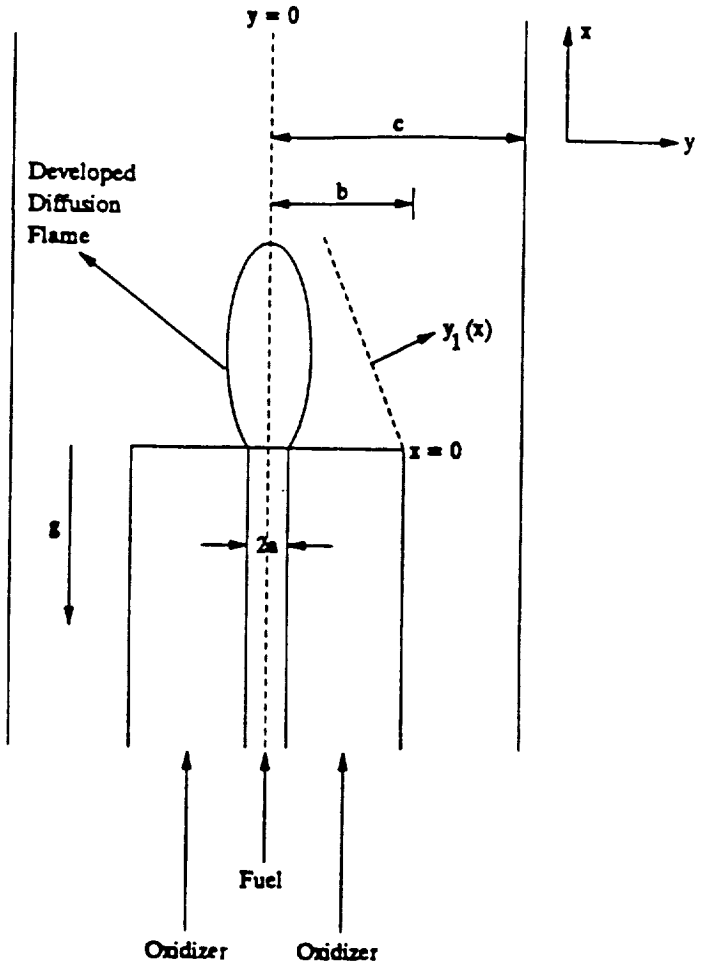

Figure 1. A Schematic of the Slot Burner Model Configuration.

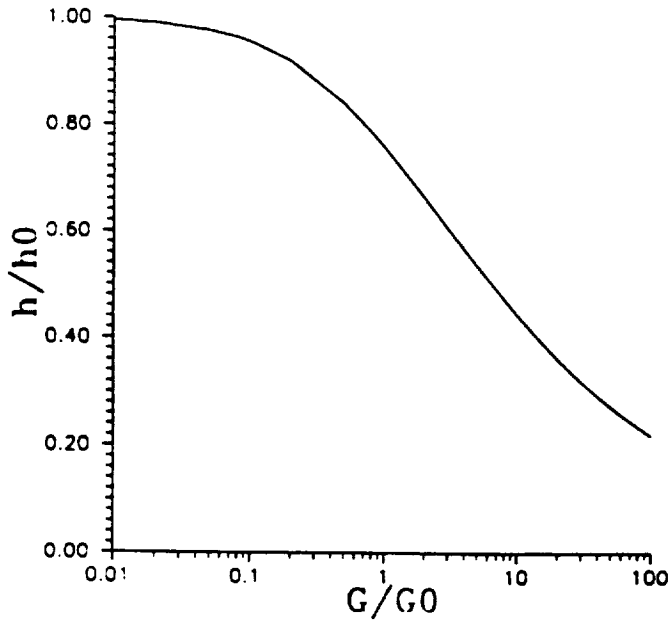

Figure 2. Diffusion Flame Height, h/h_0, as a Function of the Gravity Level G/G_0.

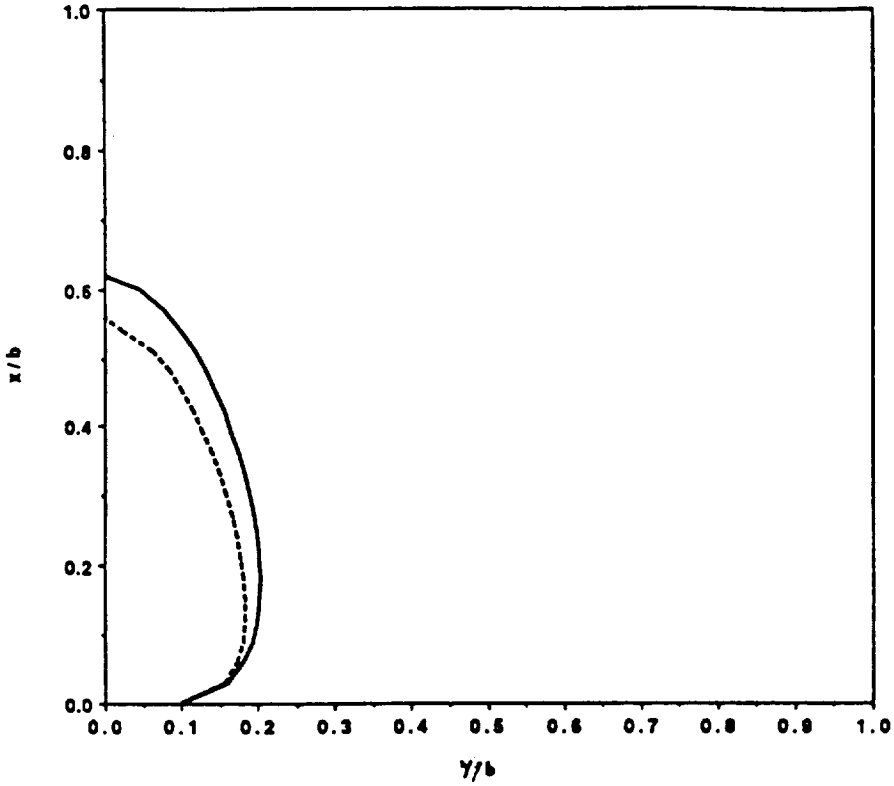

Figure 3. Diffusion Flame Shapes for G = u_{01}^2/b (—) and G = $2u_{01}^2/b$ (- - -).

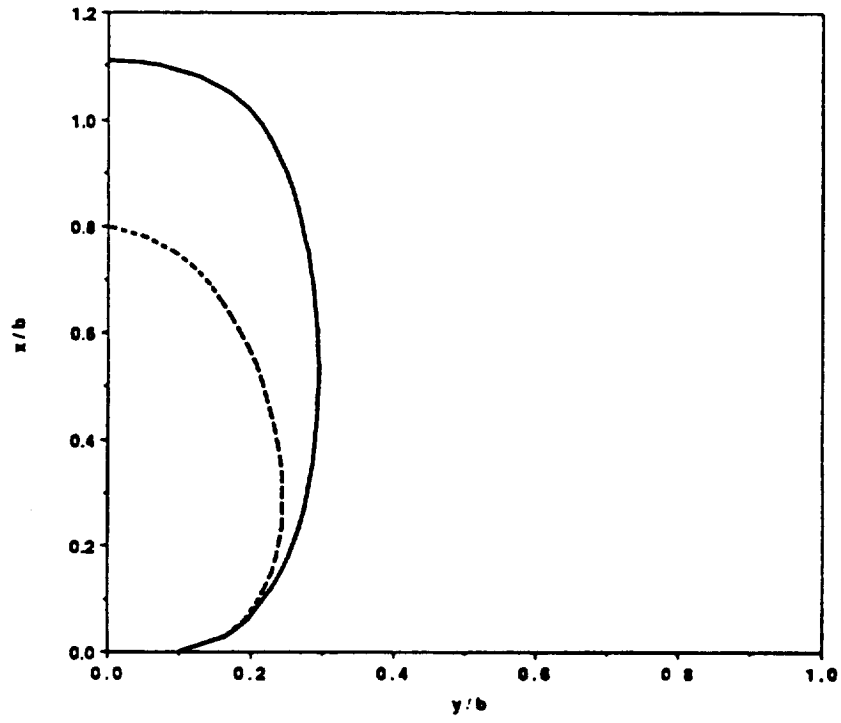

Figure 4. Diffusion Flame Shapes for G = -0.05 u_{01}^2/b (- - -) and G = -0.42 u_{01}^2/b (—).

Section 15*

"COMBUSTION OF GASEOUS FUELS UNDER REDUCED-GRAVITY CONDITIONS"

M. Y. Bahadori and E. B. Edelman

Paper LB-038, in press in Proceedings of the Second Symposium on Lunar Bases, Lunar and Planetary Institute, Houston, Texas, 1992

* This publication is a revised version of Paper LBS-88-014, Paper presented at the Second Symposium on Lunar Bases (see Section 6)

COMBUSTION OF GASEOUS FUELS UNDER REDUCED-GRAVITY CONDITIONS

M. Yousef Bahadori

Science Applications International Corporation, Thermal Sciences Division

21151 Western Avenue, Torrance, California 90501

Raymond B. Edelman

Rockwell International Corporation, Rocketdyne Division, WC-79

6633 Canoga Avenue, Canoga Park, California 91303

Abstract - The need for an improved understanding of fires is becoming critically important with increased space travel and utilization. While the control of fires in low-gravity environments is not well-understood, it is known that buoyancy significantly affects the flame behavior and characteristics. The objective of this research is to gain a more fundamental understanding of fires, and to quantify flame behavior under reduced-gravity levels. Non-premixed flames of gaseous fuels are considered in this study because they are relatively simple and easy to control, yet embody mechanisms found in all types of combustion processes ranging from uncontrolled fires to practical combustion systems. This paper presents some recent results from microgravity studies of these flames. In addition, the potential usefulness of Lunar- and Martian-based laboratories are discussed to understand the characteristics and behavior of fires in reduced-gravity environments.

INTRODUCTION

The problem of fire safety has been of equal concern both on Earth and in space. The 21st Century will begin a period of regular space travel, manned space stations, Lunar and Martian bases, and deep-space exploration. All of these activities raise the question of fire prevention in space, and the use of low-

gravity environments to further our knowledge of combustion on Earth.

Microgravity combustion research has been vigorously pursued in the last decade in relation to fire-safety issues as well as the fundamental understanding of combustion phenomena. Combustion studies of solid, liquid, and gaseous fuels have been conducted in earthbound facilities which provide short durations of microgravity. Promising results have so far been obtained to warrant the continuation of this branch of combustion science.

The objective of this research is to gain a more fundamental understanding of fires, and to quantify the flame behavior under reduced-gravity levels. Non-premixed flames of gaseous fuels are being investigated because they are relatively simple and easy to control, yet embody mechanisms found in all types of combustion processes.

In the following sections we present: (a) general characteristics of laminar and turbulent diffusion (i.e., non-premixed) flames, (b) available earthbound facilities for conducting reduced-gravity combustion studies, (c) some new results obtained from laminar diffusion-flame studies in microgravity, and (d) critical need for the understanding of low-gravity turbulent flames, all directed toward the goal of understanding the behavior of flames not only in space but on Earth as well.

LAMINAR AND TURBULENT DIFFUSION FLAMES

The term "diffusion flame" classifies those types of flames in which the fuel and oxidizer are not premixed, whether the reactants are in the solid (e.g., coal combustion), liquid (e.g., droplet combustion), or gaseous form (e.g., cigarette lighter flame). Unlike "premixed" flames, as in internal-combustion engines, the burning process in diffusion flames is governed by diffusion of the fuel gas and oxygen toward each other to form a thin flame sheet which separates the two reactants. The schematic diagram of a normal-

gravity gas-jet diffusion flame burning in a quiescent oxidizing environment is shown in Fig. 1, where the different physico-chemical phenomena governing the combustion process are indicated. The gaseous fuel (e.g., methane) is injected through a nozzle, the tip of which acts as a flame holder.

In combustion processes, coupling exists between chemical kinetics, fluid dynamics, diffusion of species, inertia, radiation, and soot formation and disposition. In addition, under non-zero-gravity condition, buoyancy is imposed on these processes (due to the density difference between the hot combustion products and the cold environment). The buoyant force causes the hot products to be removed from the flame in the direction opposite to the direction of the gravitational force. This complicates the understanding of the coupled processes involved in combustion.

In zero-gravity environments, the buoyant force is eliminated, and the remaining processes become more tractable. Isolation, or even reduction of buoyancy, makes it easier to understand the interplay between these chemical and physical processes which are not seperable regardless of the gravity level. These phenomena are responsible for the very different behavior of flames observed in microgravity compared to those in normal gravity (Edelman and Bahadori, 1986).

Gas-jet diffusion flames are selected in this study because they are a representative of a wide variety of combustion processes from the fundamental standpoint. These flames are laminar or turbulent, depending on the combination of jet momentum, nozzle diameter, and fuel properties. The classical behavior of a gas-jet diffusion flame in normal gravity (Hottel and Hawthorne, 1949) is shown in Fig. 2 which plots the dependence of length and structure of the flame on fuel velocity for a tube of given size. As the jet velocity increases, the flame transists from laminar (where mixing is governed by molecular diffusion) to fully developed turbulent behavior (where mixing is largely due to eddy diffusion or convection, with the final homogeneity being attained by molecular diffusion). It is this type of behavior which is anticipated to be strongly affected by the reduction in gravity level, as discussed later.

LOW-GRAVITY EARTHBOUND AND ORBITER FACILITIES

Figure 3 shows several earthbound and Space-Shuttle facilities which provide low-gravity environments for combustion research; for detailed description of these facilities, see Lekan (1989). To-date, most of the reduced-gravity combustion studies (including premixed flames, solid-surface combustion, laminar gas-jet diffusion flames, particle-cloud combustion, pool fires, and droplet combustion) have been conducted in the 2.2-Second Drop Tower (10^{-5}g), 5.18-Second Zero-Gravity Facility (10^{-5}g), and Model 25 Learjet (10^{-2}g for approximately 15 seconds, attached payloads) of NASA Lewis Research Center. In addition, studies are planned in the KC-135 aircraft of NASA Johnson Space Center (10^{-2}g, approximately 20 seconds for attached payloads; 10^{-3}g, approximately 8 seconds for free-floating payloads). For an overview of combustion studies in low-gravity environments, see Sacksteder (1991). The middeck and spacelab of the Space Shuttle (10^{-5}g) provide much longer test times and lower gravity levels, and also allow more detailed diagnostic measurements of flames.

In the 2.2-Second Drop Tower, the experiment package is enclosed in a drag shield which has a low drag coefficient. As the drag shield falls in this 27-m tower, the experiment package is released inside the shield. The air drag associated with the relative motion of the package within the shield is the only external force acting on the package. The shield comes to rest in a sand box at the bottom of the tower. The 5.18-Second Zero-Gravity Facility, which provides a 132-m free-fall distance, is a 6.1-m-diameter, 145-m-deep steel-walled vacuum chamber at 0.01 torr. The air-tight package is decelerated in a 6.1-m-deep container of polystyrene pellets. Aircraft flying parabolic (Keplerian) trajectories provide longer low-gravity test times, but at the cost of higher gravity levels. In the Learjet, the experiment is attached to the body of the aircraft. The KC-135 provides the same g-level as in the Learjet for bolted-down experiments, but because of its size, also permits free-float packages. Intermediate acceleration levels, especially Lunar (1/6g) and Martian (1/3g) gravities can also be achieved in the aircraft, providing opportunities to study combustion and fluid-physics phenomena under these specific reduced-gravity conditions.

MICROGRAVITY LAMINAR DIFFUSION FLAMES

Laminar diffusion flames of hydrogen and various hydrocarbons have been studied in the 2.2-Second Drop Tower (Cochran and Masica, 1970; Cochran, 1972; Haggard and Cochran, 1973; Edelman et al. 1973; Haggard, 1981; Bahadori and Stocker, 1989; Bahadori et al. 1990-a, 1990-b; for a review of earlier work, see Edelman and Bahadori, 1986) and the 5.18-Second Zero-Gravity Facility of NASA Lewis Research Center (Bahadori et al. 1990-c, 1991).

The normal-gravity flames of these fuels, when burned in quiescent oxidizing environments, generally flicker (due to hydrodynamic instabilities), are yellow (due to soot emission and burn-off), and are pencil-like in shape (due to the presence of buoyant force). In addition, the color of these flames is not strongly affected by changes in either pressure or oxygen concentration. This is a consequence of strong entrainment of oxidizer, again, due to the effect of buoyancy (see Fig. 1).

Figure 4 shows a normal-gravity and the corresponding microgravity flame of propane. Compared to laminar flames in normal gravity, those observed in microgravity are flicker-free, larger, diffuse, and rather globular. This is due to the absence of buoyant convection, leaving diffusion a much more dominant mechanism of transport. In addition, these flames are generally orange-reddish in color, which is a result of prolific sooting. Significant soot formation is caused by local flame suffocation, since the hot products of combustion accumulate in the vicinity of the flame due to the absence of buoyancy. As a result, continued combustion depends mainly on the diffusion of oxygen toward the flame front, causing major pyrolysis of the hot fuel-rich portion of the flame. As can be seen in Fig. 4, the microgravity flame appears to have a completely open tip. This suggests that extensive soot formation, radiative loss, cooler overall flame temperature, and a reduced oxygen supply contribute to extinction at the flame tip. It is quite possible that unburned and pyrolyzed hydrocarbons may escape through the flame tip in microgravity environments.

Pressure and oxygen concentration have a significant effect on flame characteristics, color, luminosity, and sooting behavior in microgravity compared to normal gravity (Bahadori and Stocker, 1989; Bahadori et al. 1990-b). Sooting was not visible in microgravity hydrocarbon flames at 18% oxygen in nitrogen, 0.5-atm environments, and the flames were entirely blue, whereas their normal-gravity counterparts were yellow, luminous, and very similar to flames under atmospheric conditions, or even high-pressure/high-oxygen-concentration flames. This has a very important implication, namely, there is reduced radiative heating and reduced hazard of flame spread to surrounding combustible materials in low-pressure/low-oxygen microgravity flames. Figure 5 shows the effects of oxygen concentration on normal-gravity and microgravity flames.

High-pressure and high-oxygen-concentration environments also affect the enhancement and intensity of burning in microgravity. Massive sooting, flame-tip opening, and extinction and soot breakthrough at the tip were observed even in 50%-oxygen environments. The tip-opening and soot-escape phenomena are unique characteristics of microgravity flames. Figure 6 shows the effects of pressure.

Recent tests (Bahadori et el. 1991) have shown that flame radiation is an order of magnitude higher in microgravity compared to normal gravity for laminar gas jet diffusion flames. Enhanced soot formation, larger flame size, and accumulation and slow transport of the hot combustion products are the contributing factors. Figure 7 shows the flame radiance as a function of fuel-volume-flow rate under both normal-gravity and microgravity conditions. The data suggest that radiative ignition of nearby materials may be promoted in low-gravity environments due to the increased radiative transfer.

A mathematical model has been developed (Edelman et al. 1973) for the study of laminar diffusion flames under arbitrary gravitational accelerations based on the parabolic form of the equations of motion, which includes the effects of inertia, viscosity, diffusion, and chemical reactions. Figure 8 shows the excellent agreement between the predicted and measured flame heights under both normal-gravity and

zero-gravity conditions. We have recently applied this model to a family of methane flames under different gravitational levels. Figure 9 shows the non-dimensional centerline velocity vs. axial distance. Clearly, convective effects play a major and different role for different gravitational environments.

The shape, color, luminosity, sooting, radiation, combustion products, and other characteristics of the flame can not be truly understood unless experiments are conducted (along with appropriate diagnostics) under the g-level of interest. Then, when combined with the theoretical analysis, these results provide a data base for the understanding of fires both on Earth and under reduced-gravity conditions such as those on the Moon and Mars, or in spacecraft environments.

TURBULENT DIFFUSION FLAMES

Turbulent gas-jet diffusion flames under normal-gravity conditions have been the subject of extensive theoretical and experimental studies for a number of decades. Figure 2 shows the classical behavior of a turbulent jet diffusion flame. As the jet velocity increases, the flame transists from laminar to fully developed turbulent behavior. For the tube size used in the flame study of Fig. 2, a velocity is reached where further increases in the jet velocity result in no change in flame height. This is a characteristic of momentum-dominated flames, i.e., flames in which buoyancy is not important.

Much progress has been made toward the characterization of momentum-dominated turbulent flames. However, this is not the case for low-momentum turbulent flames characteristic of unconfined fires. In this case, the fire research community depends primarily on empirical results which, having been obtained under normal-gravity conditions, have the buoyancy effect inherently embedded within these correlations. When buoyancy is important (i.e., low-momentum flames, unlike Fig. 2), a constant height as a function of velocity is not reached in the turbulent region (see Fig. 10; Wohl et al. 1949). The mechanisms responsible for this behavior are far from being fully understood. Thus, the need for more fundamental data

and analysis is apparent because of the requirement to define the hazard and control of fires not only on Earth but in space as well.

For low-momentum flames, strong interactions between buoyancy and turbulent-flame structure exist which affect the flame behavior and chemistry through two gravity-induced mechanisms. The first arises directly from the buoyant force acting on the time-averaged or mean flow field, and appears as a gravity term in the mean momentum equation. The second mechanism arises out of the interaction between density and velocity fluctuations which appears as a source of turbulent kinetic energy. Under normal-gravity conditions, it is not possible to separate these two effects in terms of their impact on mixing rate, and hence, flame structure. Clearly, the advantage of operating in a low-gravity environment would be to provide a significant base of new information by isolating the combined effects of buoyancy. Then, with a theoretical model, the effects of buoyancy on the mean flow and on the generation of turbulent kinetic energy would be separable.

CLOSURE

Although the effects of buoyancy on low-momentum flames have been qualitatively observed, it is only recently that quantitative descriptions of the phenomena affected by gravity have been attempted. Understanding this phenomena is not only of fundamental interest, but it is of critical importance to fire safety in space as well as on Earth. Furthermore, for processing and manufacturing in space, controlled flames used as one form of heat source are likely to be employed.

This paper has presented results that indicate significant effects of gravity on the flame structure. Moreover, it has been shown that to develop a more fundamental understanding of this phenomena along with a reliable prediction capability, quantitative data obtained under reduced-gravity conditions uninhibited by test time and size limitations are needed. The potential to obtain data from experiments conducted on

Moon and Mars offers this opportunity, one which can not be equalled in earthbound facilities .

Acknowledgements - This work is supported, in part, by NASA Lewis Research Center, under Contract NAS3-22822 with Science Applications International Corporation.

REFERENCES

Bahadori M. Y. and Stocker D. P. (1989) Oxygen-concentration effects on microgravity laminar methane and propane diffusion flames. Paper presented at the 1989 Fall Technical Meeting (Eastern Section) of The Combustion Institute, Albany, New York. The Combustion Institute, Pittsburgh. 4 pp.

Bahadori M. Y., Edelman R. B., Stocker D. P., and Olson S. L. (1990-a) Ignition and behavior of laminar gas-jet diffusion flames in microgravity. AIAA J. 28, 236-244.

Bahadori M. Y., Stocker D. P., and Edelman R. B. (1990-b) Effects of pressure on microgravity hydrocarbon diffusion flames. Paper AIAA-90-0651, AIAA 28th Aerospace Sciences Meeting, Reno, Nevada. American Institute of Aeronautics and Astronautics, New York. 6 pp.

Bahadori M. Y., Edelman R. B., Sotos R. G., and Stocker D. P. (1990-c) Temperature measurements for microgravity laminar diffusion flames. Paper presented at the 1990 Fall Technical Meeting (Eastern Section) of The Combustion Institute, Orlando, Florida. The Combustion Institute, Pittsburgh. 4 pp.

Bahadori M. Y., Edelman R. B., Sotos R. G., and Stocker D. P. (1991) Radiation from gas-jet diffusion flames in microgravity environments. Paper AIAA-91-0719, AIAA 29th Aerospace Sciences Meeting, Reno,

Nevada. American Institute of Aeronautics and Astronautics, New York. 4 pp.

Cochran T. H. (1972) Experimental Investigation of Laminar Gas Jet Diffusion Flames in Zero Gravity. NASA TN D-6523. NASA Lewis Research Center, Cleveland. 26 pp.

Cochran T. H. and Masica W. J. (1970) Effects of Gravity on Laminar Gas Jet Diffusion Flames. NASA TN D-5872. NASA Lewis Research Center, Cleveland. 25 pp.

Edelman R. B. and Bahadori M. Y. (1986) Effects of buoyancy on gas-jet diffusion flames: Experiment and theory. Acta Astronautica, 13, No. 11/12, 681-688.

Edelman R. B., Fortune O. F., Weilerstein G., Cochran T. H., and Haggard J. B. (1973) An analytical and experimental investigation of gravity effects upon laminar gas jet diffusion flames. Fourteenth Symposium (International) on Combustion, pp. 399-412. The Combustion Institute, Pittsburgh.

Haggard J. B. (1981) Forced and Natural Convection in Laminar Jet Diffusion Flames. NASA TP-1841. NASA Lewis Research Center, Cleveland. 21 pp.

Haggard J. B. and Cochran T. H. (1973) Hydrogen and Hydrocarbon Diffusion Flames in a Weightless Environment. NASA TN D-7165. NASA Lewis Research Center, Cleveland. 28 pp.

Hottel H. C. and Hawthorne W. R. (1949) Diffusion in laminar flame jets. Third Symposium on Combustion, pp. 254-266. Williams and Wilkins Co., Baltimore.

Lekan J. (1989) Microgravity research in NASA Ground-Based Facilities. NASA TM-101397. NASA Lewis Research Center, Cleveland. 16 pp.

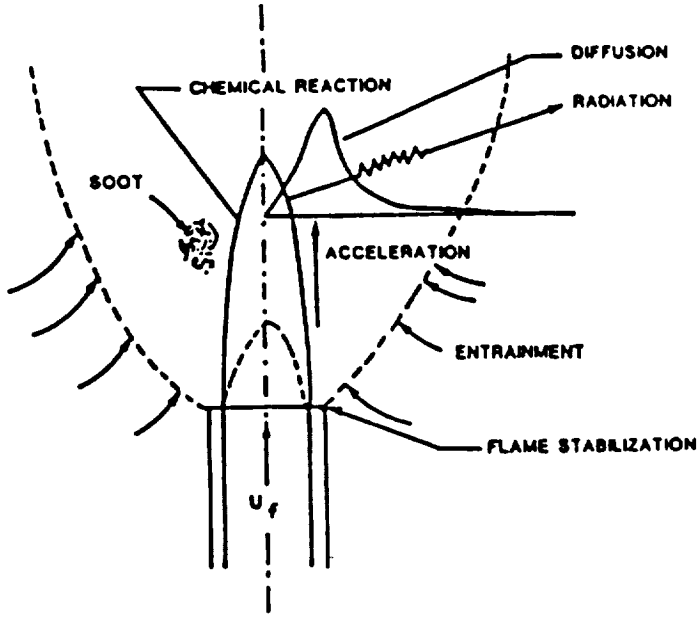

Figure 1. Physical and chemical processes occuring in laminar gas-jet diffusion flames of hydrocarbons in normal-gravity environments.

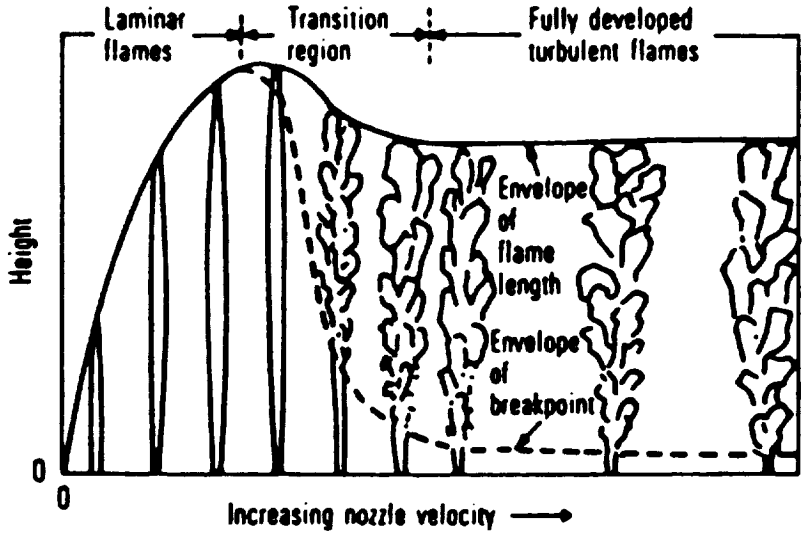

Figure 2. Change in the flame height and behavior with increase in nozzle velocity for a typical gas-jet diffusion flame; reproduced from Hottel and Hawthorne (1949).

Sacksteder K. R. (1991) The implications of experimentally controlled gravitational accelerations for combustion science. Twenty-Third Symposium (International) on Combustion, in press. The Combustion Institute, Pittsburgh. See also: NASA Lewis Research Center (1989) Microgravity Combustion Science: A Program Overview. NASA TM-101424. NASA Lewis Research Center, Cleveland. 18 pp.

Wohl K., Gazley C., and Kapp N. (1949) Diffusion flames. Third Symposium on Combustion, pp. 288-300. Williams ans Wilkins Co., Baltimore.

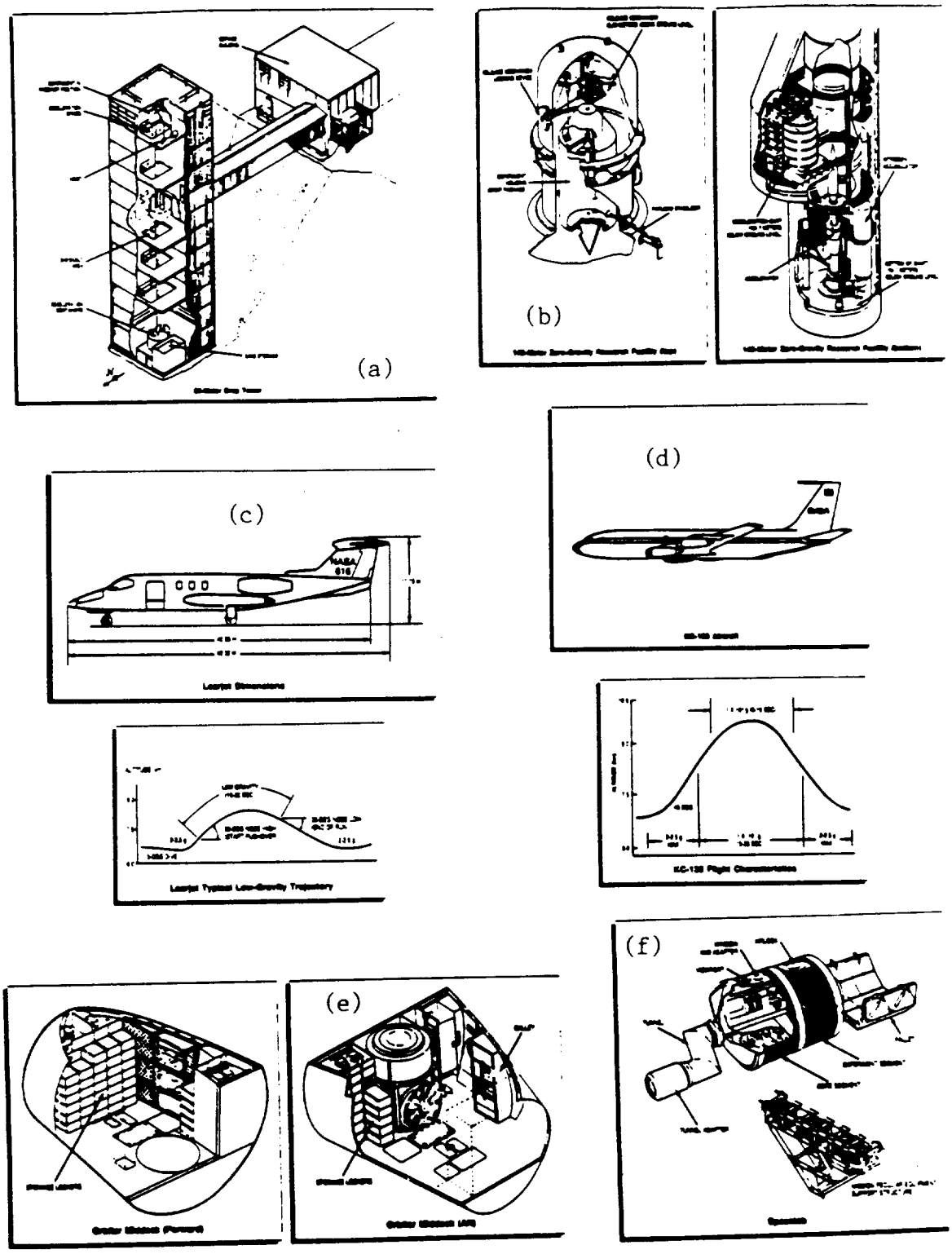

Figure 3. Earthbound and Shuttle orbiter facilities which provide low-gravity environments for combustion research; (a) 2.2-Second Drop Tower, (b) 5.18-Second Zero-Gravity Facility, (c) Learjet, (d) KC-135 aircraft, (e) Shuttle middeck, and (f) Spacelab.

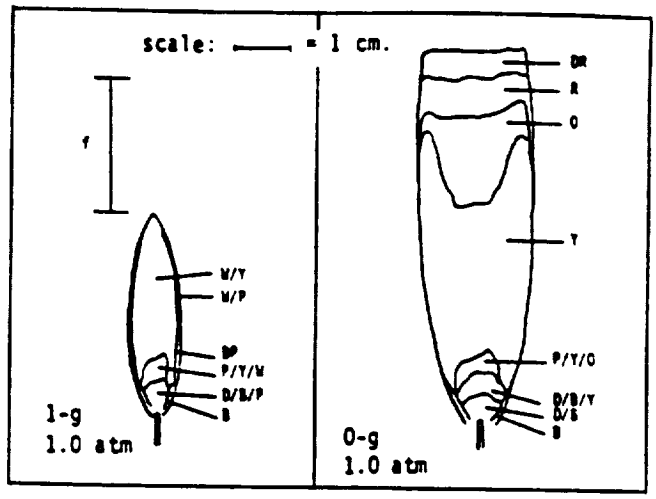

Figure 4. Normal-gravity and microgravity flames of propane burning in quiescent air at 1 atm; nozzle radius = 0.0825 cm and fuel-flow rate = 1.0 cc/sec. The various colors observed are as follows: B (blue), BB (bright blue), D (dark), DB (dark blue), DP (dark pink), DR (dull red), O (orange), P (pink), R (red), W (white), and Y (yellow). The range of flicker (f) is also shown for the normal-gravity flames; reproduced from Bahadori et al. (1990-b).

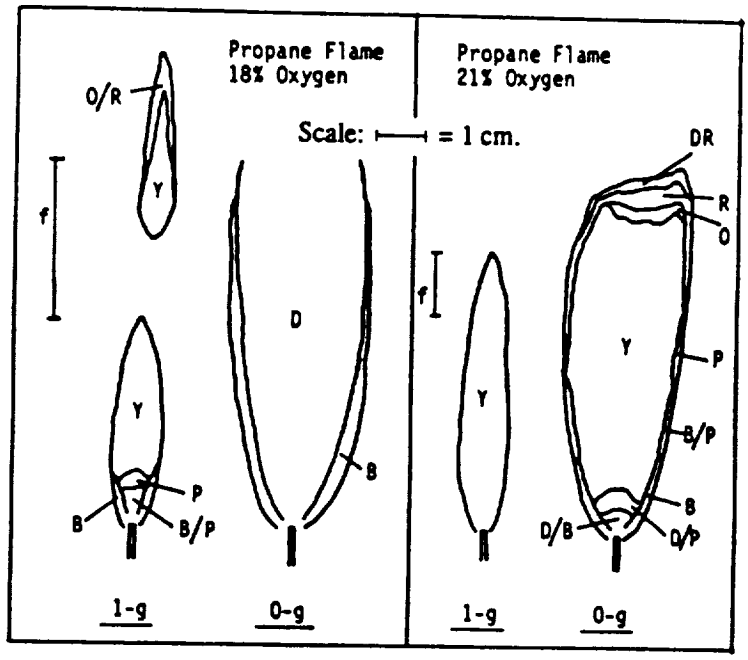

Figure 5. Effects of oxygen concentration on normal-gravity and microgravity flames of propane at 1 atm; nozzle radius = 0.074 cm and fuel-flow rate = 0.96 cc/sec. The various colors indicated in the diagram are as follows: B (blue), D (dark), DR (dull red), O (orange), P (pink), R (red), W (white), and Y (yellow). The bars show the range of normal-gravity flame flicker (f); reproduced from Bahadori and Stocker (1989).

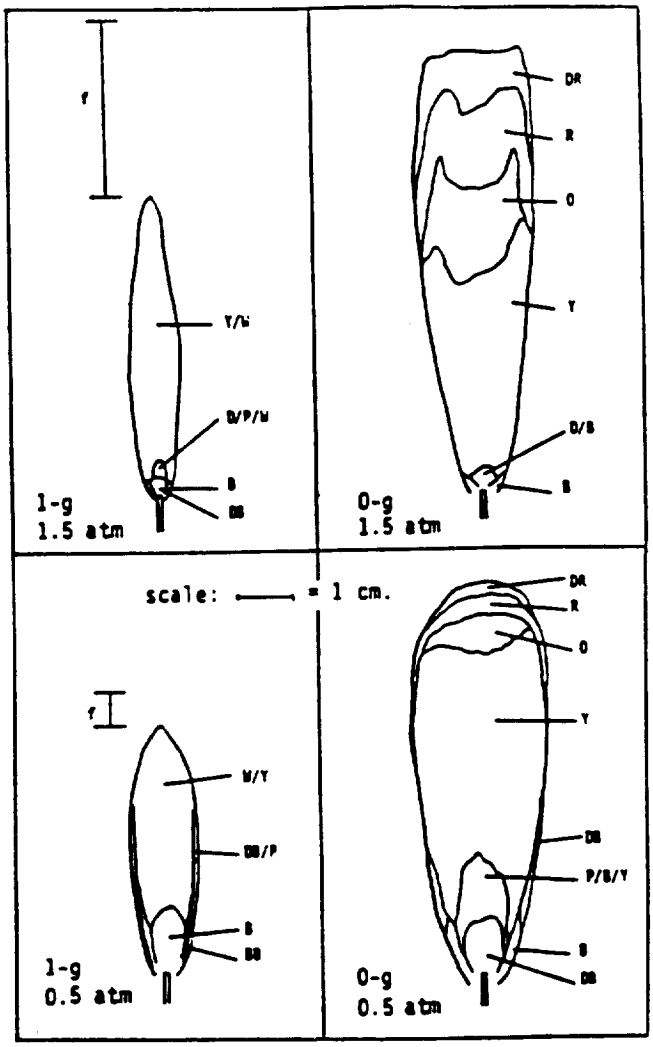

Figure 6. Effects of pressure on normal-gravity and microgravity flames of propane burning in quiescent air (21% oxygen in nitrogen). For details, see Fig. 4; reproduced from Bahadori et al. (1990-b).

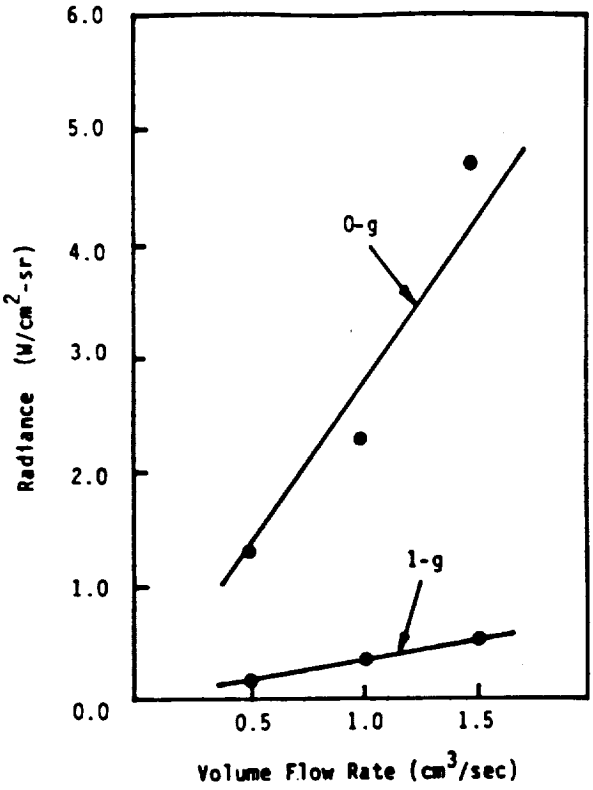

Figure 7. Radiance as a function of fuel volume-flow rate for propane flames burning in air at 1.0 atm; nozzle radius = 0.0825 cm; reproduced from Bahadori et al. (1991).

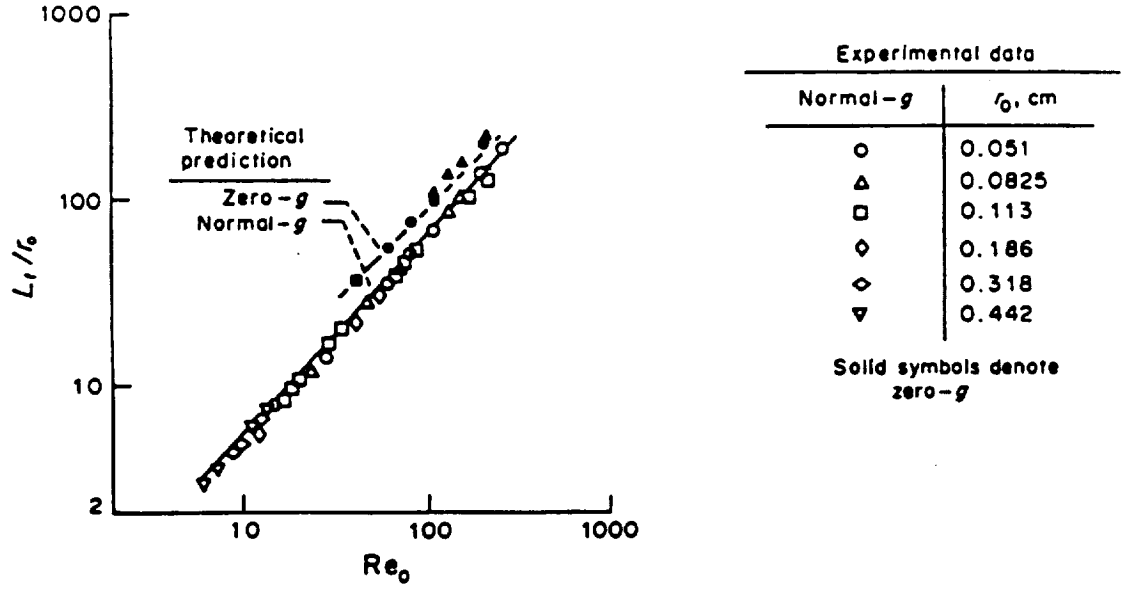

Figure 8. Comparisons between the theoretical predictions (Edelman et el. 1973) and experimental results (Cochran and Masica, 1970; Cochran, 1972) for non-dimensional flame height (height / nozzle radius) vs. jet Reynolds number (jet velocity x nozzle radius / fuel kinematic viscosity); methane-air flames at 1.0 atm; reproduced from Edelman et al. (1973).

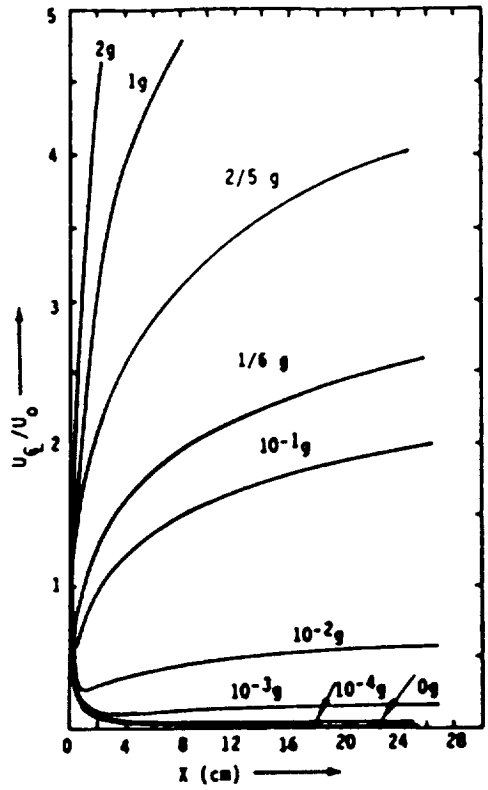

Figure 9. Predicted non-dimensional centerline velocity (with respect to jet exit velocity) vs. axial distance along the jet as a function of gravitational level; methane-air flames, nozzle radius = 0.0825 cm, fuel-flow rate = 1.0 cc/sec, pressure = 1.0 atm, and jet exit velocity = 46.8 cm/sec; reproduced from Edelman and Bahadori (1986).

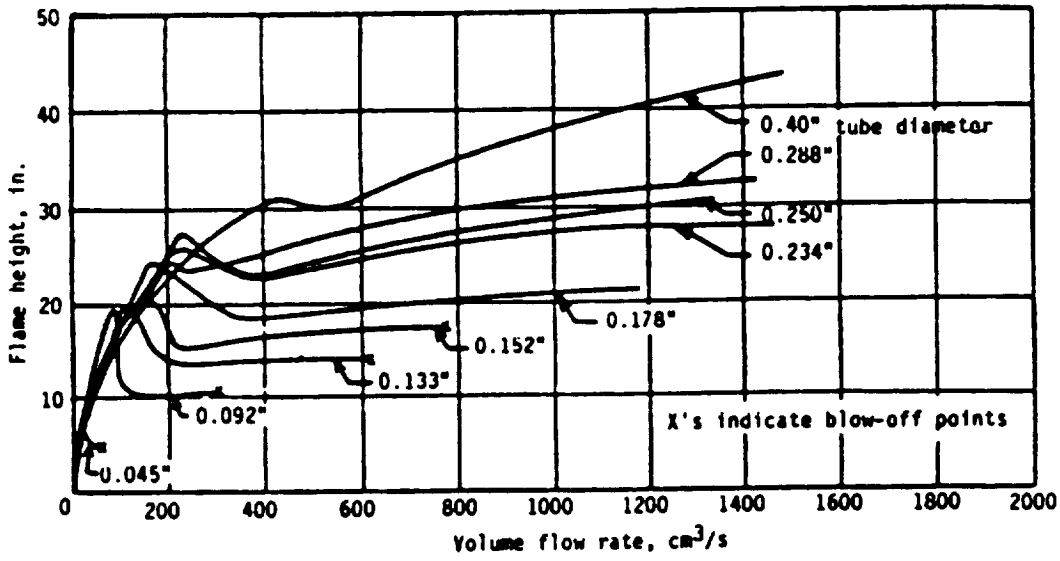

Figure 10. Effects of fuel-volume flow rate and tube diameter on flame height for city gas diffusion flames; reproduced from Wohl et al. (1949).

Section 16

"EFFECTS OF OXYGEN CONCENTRATION ON RADIATION FROM MICROGRAVITY LAMINAR PROPANE DIFFUSION FLAMES"

M. Y. Bahadori, R. B. Edelman, R. G. Sotos, D. P. Stocker, and D.F. Vaughan

1992

EFFECTS OF OXYGEN CONCENTRATION ON RADIATION FROM MICROGRAVITY LAMINAR PROPANE DIFFUSION FLAMES

M. Y. Bahadori† and R. B. Edelman††
Science Applications International Corporation
Thermal Sciences Division
Torrance, California 90501 USA
and
R. G. Sotos, D. P. Stocker, and D. F. Vaughan§
NASA Lewis Research Center
Space Experiments Division
Cleveland, Ohio 44135 USA

Abstract - Laminar diffusion flames of propane have been studied under both normal-gravity and (5.18-second) microgravity conditions. The quiescent oxidizing environment was at 1.0 atm pressure, and had 15% - 30% by volume of oxygen in nitrogen. Flame radiation was measured using a wide-view-angle, thermopile-detector radiometer. The results show that radiation levels are significantly higher in microgravity than in normal gravity. This is mainly due to the larger

† Author and address for correspondence: M. Yousef Bahadori, SAIC/NASA LeRC, MS 500-217, Cleveland, Ohio 44135.

†† Present address: Rockwell International Corporation, Rocketdyne Division, Canoga Park, California.

§ Baldwin-Wallace College, Berea, Ohio.

flame size and accumulation and slow transport of the combustion products in the vicinity of the flame, which are caused by the removal of buoyancy. In addition, it is shown that the sooting characteristics are different in microgravity compared to normal gravity. For the normal-gravity flames, the effects of oxygen concentration on radiation is shown to be negligible, whereas in microgravity environments, flame shape, color, luminosity, and radiation are strongly affected by the amount of oxygen in the environment. This has direct application to the problem of spacecraft fire detection and fire safety. The data suggest that longer test times are needed to reach steady state in microgravity environments.

1. Introduction

The problem of fire safety in spacecraft environments has been a major concern. In order to understand the behavior and characteristics of flames in low gravity, different programs have been underway to study the combustion processes of solid, liquid, and gaseous fuels in microgravity environments.[1-4] The focus of this research is on the fundamental understanding of the structure of laminar gas-jet diffusion flames under microgravity conditions. The basic mechanisms which control the diffusion flames include the coupled processes of mixing, chemical kinetics including soot formation and disposition, flame radiation, and buoyancy-induced convection. A major problem impeding our understanding of flame behavior is the masking effect of buoyancy on flames in normal-gravity environments. The buoyancy-induced convection masks the processes of chemical-diffusional interactions that are fundamental to the understanding of combustion phenomena. In microgravity environments, the buoyant force is nearly eliminated, and the remaining physico-chemical processes are responsible for the very different behavior of flames observed in the microgravity experiments conducted to-date.[5]

In recent studies of microgravity laminar diffusion flames,[6-12] some unique and, in most cases, unexpected phenomena have been observed. The results show that flame characteristics, color, luminosity, and sooting behavior are strongly affected in microgravity compared to normal gravity. In addition, it was shown that radiation can be up to an

order of magnitude higher in microgravity flames. Also, pressure and oxygen concentration have a more significant effect on microgravity flames than those in normal gravity.[7-8]

Radiation from laminar and turbulent gas-jet diffusion flames in normal-gravity environment has been measured by Markstein in an impressive and systematic way.[13-18] In this paper, we have followed his approach to measure the total radiation from microgravity flames of propane burning under different oxygen-containing environments, and have compared the results with their normal-gravity counterparts.

2. Experimental

The experiments were conducted in the 5.18-Second Zero-Gravity Facility of NASA Lewis Research Center.[19] Figure 1 shows a schematic of the hardware. The volume of the combustion chamber was 0.087 m^3. The fuel nozzle (protruding 15 cm inside the chamber) had a tapered tip with inner radius of 0.0825 cm, and was positioned along the centerline of the cylindrical chamber. The nozzle was approximately 20 cm away from the chamber wall. The tip of the nozzle was approximately 50 cm away from the chamber top. The fuel was supplied from a stainless steel bottle of 75 cm^3 in volume at an initial pressure of 100 psig. Appropriate windows were mounted in the chamber wall for the movie cameras and the radiometer. A pressure transducer was used to record the chamber pressure during the test.

Both normal-gravity and microgravity flames of propane (99.9%-pure) were studied in quiescent oxidizing environments of 15% to 30% by volume of oxygen in nitrogen. The chamber pressure was 1.0 atm, and the fuel-volume flow rate was 1.5 cm^3/sec, corresponding to a cold-jet Reynolds number of 90.

Most of the flames discussed here were ignited using a retracting, nichrome-wire, ignitor which was located 1.0 cm above the nozzle tip. It was removed from the flame area in 0.5 sec following ignition. Two of the flames discussed here were ignited using a spark ignition device which has since been replaced by the nichrome wire because of its

reliability. The ignition system was activated for 0.5-1.0 sec for the normal gravity and microgravity tests. The microgravity flames were ignited after the release of the package in the drop tube. Two movie cameras (filming rates = 12 and 30 frames/sec, respectively) using color Kodak Ektachrome Video News film recorded the flame development and behavior.

The wide-view angle radiometer was comprised of a 1.5 x 1.5-mm, fast-response thermopile detector with a Calcium Fluoride (CaF_2) window (Oriel Corporation, Model 7106), and a time constant of 40 msec, field of view of 90 - 100 degrees, and maximum irradiance of 0.2 W/cm^2. In addition, the experiment chamber was equipped with a CaF_2 window to allow maximum transmission of the infrared radiation. The window had a usable transmission range of 0.2 - 9.0 μm, with its absorptivity falling off above 1.0 μm to about 50% at 10.0 μm; its approximate transmission in the linear range was 94%. The radiometer was calibrated using a black-body source (Barnes Engineering, Model 11-210), with an opening of 2.54 cm in diameter. A nanometer (Keithly Instrument, Model 181) was used to measure the radiometer response to various temperatures of the black-body source. The distance from the nozzle centerline (and for calibration, from the black-body source) to the radiometer sensor was 28.6 cm, and from the shutter iris to the sensor was 3.84 cm. The iris on the shutter had an open diameter of 2.54 cm. The inner diameter of the Calcium Fluoride window was 4.45 cm. The nozzle/window/iris/sensor arrangement was

such that the field of view on a plane passing through the centerline of the nozzle had a radius of 9.55 cm.

3. Results

Figure 2 shows the normal-gravity and microgravity flames injecting propane into oxidizing environments of 15%, 18%, 21%, and 30% by volume of oxygen in nitrogen. Following ignition, the normal-gravity flames establish quickly (in less than 0.5 sec), and show the typical flicker characteristics (with a frequency of 10 - 20 Hz) of laminar flames burning in quiescent environments. Both minimum and maximum flame heights are shown in Figure 2 for the normal-gravity flames. However, the microgravity flame heights continuously increase after ignition, and the color of these flames constantly change, indicating that the flame needs longer time to reach a steady state. The microgravity flames shown in Figure 2 are for the last instant of the drop (just prior to the beginning of the deceleration period).

Figure 3 shows the flame radiance as a function of time for both normal-gravity and microgravity flames. Using the calibration chart, the data obtained from the radiometer reading (in mV) was converted to the equivalent black-body temperature (T_b) of the calibration source. The flame radiance ($\sigma T^4_b/\pi$) in W/cm^2-sr was then obtained as a function of time, where σ is the Stefan-Boltzmann constant.

Table 1 shows the data obtained in terms of flame height, flame maximum diameter, radiance, and radiance per unit projected flame area. This area was calculated by multiplying the flame height by the maximum flame diameter, to give a rough estimate of the relative

values of radiance per unit flame area between the normal-gravity and microgravity flames. The radiance data are for the last instant (at approximately 5 seconds) of the test. The heights for normal-gravity flames in Table 1 are the averages of minimum and maximum flickering-flame height. The heights for microgravity flames were measured as the points where blue was no longer visible on the film (for the 15%-O_2-flame), and where red could no longer be seen (for the other flames); see Figure 2. Table 1 also shows the rate of change of radiance with time during the last second of the experiment for both normal-gravity and microgravity flames.

In Figure 4, flame radiance as a function of oxygen concentration is presented. The normal-gravity flames show no significant changes in radiance with increasing oxygen percent. However, the microgravity flames show a linear variation of radiance with oxygen concentration.

4. Discussion

The flames of Figure 2 show the significant effects of buoyancy on shape, luminosity, and sooting characteristics. The normal-gravity flames are yellow, flickering, and pencil-like, regardless of oxygen level in the environment. However, their intensity appears to increase at higher oxygen concentrations. The microgravity flames are in general taller, wider, and sootier than the normal-gravity flames. The flame of 15% oxygen is entirely blue, indicating that sooting is reduced, and glowing and burning particles are not present. However, the continuous release and slow transport of the hot combustion products due to the absence of buoyancy may contribute to slow heating of the fuel rich region of the jet, and given enough time in microgravity, the blue flame may start to show an increase in sooting and subsequent change in the color of the flame. The flame in 18% oxygen shows a transition from non-sooting to the highly sooting condition. As the oxygen level increases, the tendency for sooting increases, which is accompanied by a brighter flame due to higher temperatures and increased sooting.

The orange/reddish color of the microgravity flames is an indication of cooler temperatures than is expected for typical burn-off conditions. The yellow/orange/red/dull red regions in the flames show that the temperature of the soot decreases in microgravity flames, leading to local extinction at the flame tip. This tip-opening and underventilated-type behavior is a characteristic of sooty microgravity flames. Absence of buoyancy and dominance of diffusive processes result in longer

residence times, enhanced soot formation, increased radiative loss and additional cooling by pyrolysis, which are, in some combination, responsible for the observed characteristics of microgravity flames.

The data presented in Figure 3 show that radiative loss in normal-gravity flames is not only constant throughout the duration of the test, but that the level of radiation does not change with increasing oxygen concentration. This is largely due to the instantaneous removal of the hot combustion products under the influence of buoyancy. In addition, the normal-gravity flames become established immediately following ignition, whereas in microgravity, a continuous development of the flame is observed (both visually by examining the films and through radiation data). The data of Figure 3 also show that at lower oxygen levels, radiation approaches a possible steady-state value more slowly compared to radiation from high-oxygen-concentration flames. This is due to the reduced temperature and concentration gradients and, hence, transport rates, at the reduced ambient oxygen levels. The rates of change of the radiation loss are shown in Table 1 where it is apparent that the microgravity flames have not reached a steady-state after 5 seconds. Table 1 also shows that for microgravity flames the radiation decreases with reduced ambient oxygen concentrations. The radiation from the normal gravity flames is affected by flickering and, consequently, shows no specific trend for the range of conditions tested. However, it is interesting to note that the radiation from these normal gravity flames falls within a relatively narrow band, as can be seen in Figure 4. Finally, Table 1 shows a non-monotonic flame length

dependence on oxygen concentration for both the normal gravity and microgravity flames. This may be due to the onset of chemical kinetic quenching caused by the lower oxygen concentrations and the attendant reduced temperatures. Concentration measurements, to be made in the future, will help to confirm the hypothesis that these flames involve incomplete combustion.

5. Conclusion

The effects of ambient oxygen concentration on radiation from normal-gravity and microgravity laminar propane diffusion flames have been measured using a wide-view-angle radiometer. The results show that while normal-gravity flames do not exhibit appreciable effects of oxygen concentration on radiation, microgravity flames show a continuous increase in radiation with increasing oxygen concentration. Although these flames had not reached steady-state, the level of radiation from the microgravity flames was up to an order of magnitude larger than that from normal-gravity flames. Further quantitative data and analysis is underway to more fully characterize and understand the behavior of gas-jet diffusion flames in microgravity environments.

Acknowledgments

This work was supported by NASA Lewis Research Center under Contract NAS3-22822.

References

1. Sacksteder, K. R.: Twenty-Third Symposium (International) on Combustion, P. 1589, The Combustion Institute, 1990.

2. Law, C. K.: Combustion in Microgravity: Opportunities, Challenges, and Progress, Paper AIAA-90-0120, AIAA 28th Aerospace Sciences Meeting, Reno, Nevada, January 1990.

3. Faeth, G. M.: Homogeneous Premixed and Non-premixed Flames in Microgravity: A Review, IKI/AIAA Microgravity Science Symposium, Moscow, May 1991.

4. Williams, F. A.: Microgravity Sci. Technol. III 3, 154 (1990).

5. Edelman, R. B. and Bahadori, M. Y.: Acta Astronautica 13, 681 (1986).

6. Bahadori, M. Y. and Stocker, D. P.: Oxygen-Concentration Effects on Microgravity Laminar Methane and Propane Diffusion Flames, Eastern States Meeting of The Combustion Institute, Albany, New York, October/November 1989.

7. Bahadori, M. Y., Stocker, D. P., and Edelman, R. B.: Effects of Pressure on Microgravity Hydrocarbon Diffusion Flames, Paper AIAA-90-0651, AIAA 28th Aerospace Sciences Meeting, Reno, Nevada, January 1990.

8. Bahadori, M. Y., Edelman, R. B., Stocker, D. P., and Olson, S. L.: AIAA J. 28, 236 (1990).

9. Stocker, D. P.: Size and Shape of Laminar Burke-Schumann Diffusion Flames in Microgravity, Central States Meeting of The Combustion Institute, Cincinnati, Ohio, May 1990.

10. Bahadori, M. Y.: An Analytical Solution for Transient, Cylindrically Symmetric Laminar Diffusion Flames in the Absence of Buoyancy, Central States Meeting of The Combustion Institute, Cincinnati, Ohio, May 1990.

11. Bahadori, M. Y., Edelman, R. B., Sotos, R. G., and Stocker, D. P.: Measurement of Temperature in Microgravity Laminar Diffusion Flames, Eastern States Meeting of The Combustion Institute, Orlando, Florida, December 1990.

12. Bahadori, M. Y., Edelman, R. B., Sotos, R. G., and Stocker, D. P.: Radiation from Gas-Jet Diffusion Flames in Microgravity Environments, Paper AIAA-91-0719, AIAA 29th Aerospace Sciences Meeting, Reno, Nevada, January 1991.

13. Markstein, G. H.: Fifteenth Symposium (International) on Combustion, P. 1285, The Combustion Institute, 1974.

14. Markstein, G. H.: Combust. Flame 27, 51 (1976).

15. Markstein, G. H.: Sixteenth Symposium (International) on Combustion, P. 1407, The Combustion Institute, 1977.

16. Markstein, G. H. and deRis, J.: Twentieth Symposium (International) on Combustion, P. 1637, The Combustion Institute, 1984.

17. Markstein, G. H.: Twentieth Symposium (International) on Combustion, P. 1055, The Combustion Institute, 1984.

18. Markstein, G. H.: Radiant Emission and Smoke Points for Laminar Diffusion Flames of Fuel Mixtures, Report FMRC J.I. OMON4.BU, RC86-BT-4, Factory Mutual Research Corporation, Norwood, Massachusetts, June 1986.

19. Lekan, J.: Microgravity Research in NASA Ground-Based Facilities, NASA TM-10397, NASA Lewis Research Center, Cleveland, Ohio, 1989.

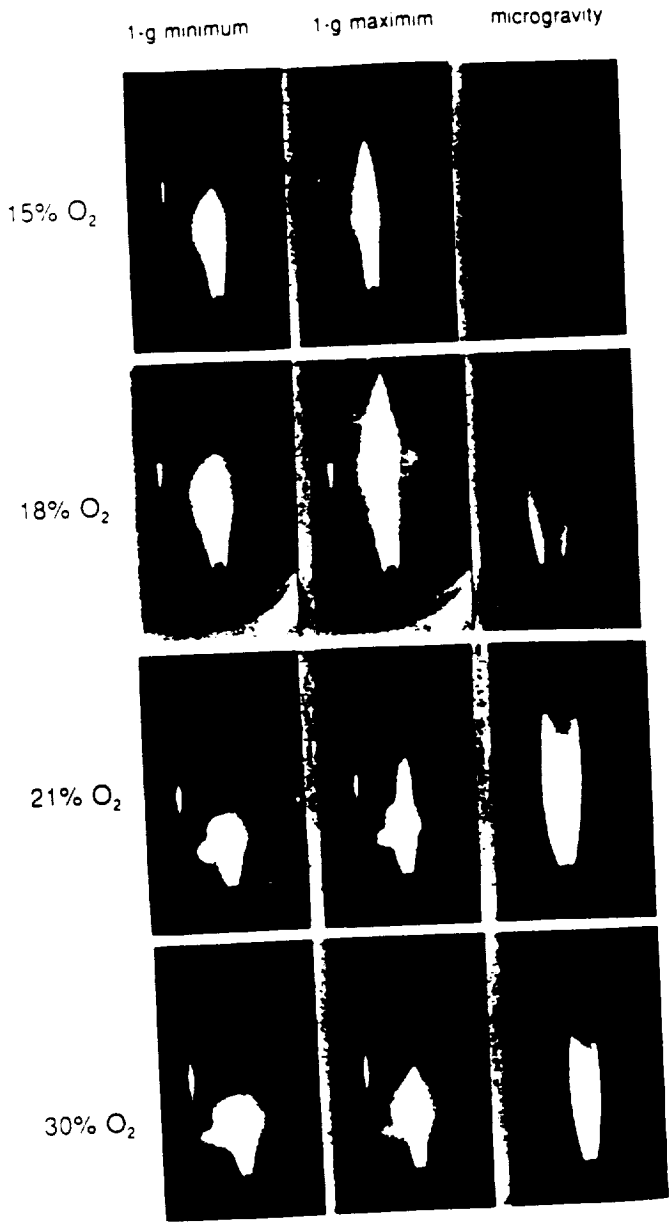

Fig. 2 Normal-gravity (both minimum and maximum heights of flicker) and microgravity flames of propane burning in different oxygen environments. Reproduction has slightly changed the intensity of the flames, and has reduced the visible length of the blue flame. These photographs are included to provide qualitative information on flame color and luminosity only.

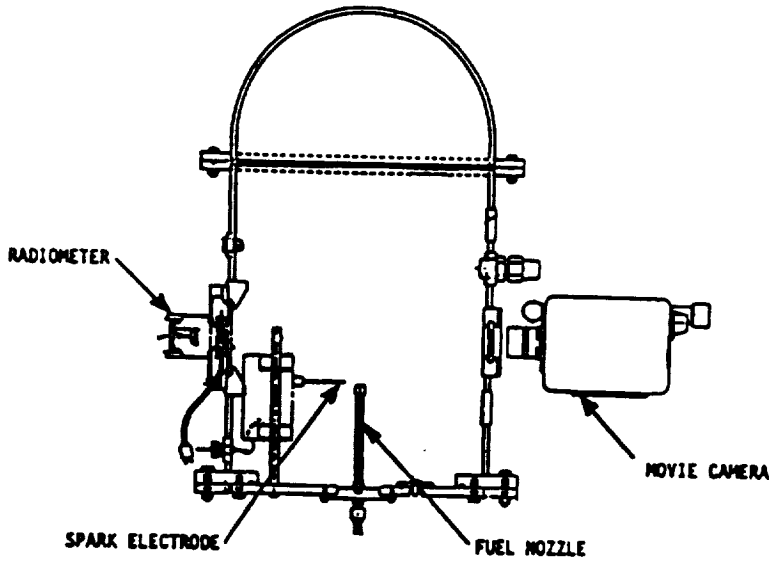

Fig. 1 Experiment package for the 5.18-second microgravity tests.

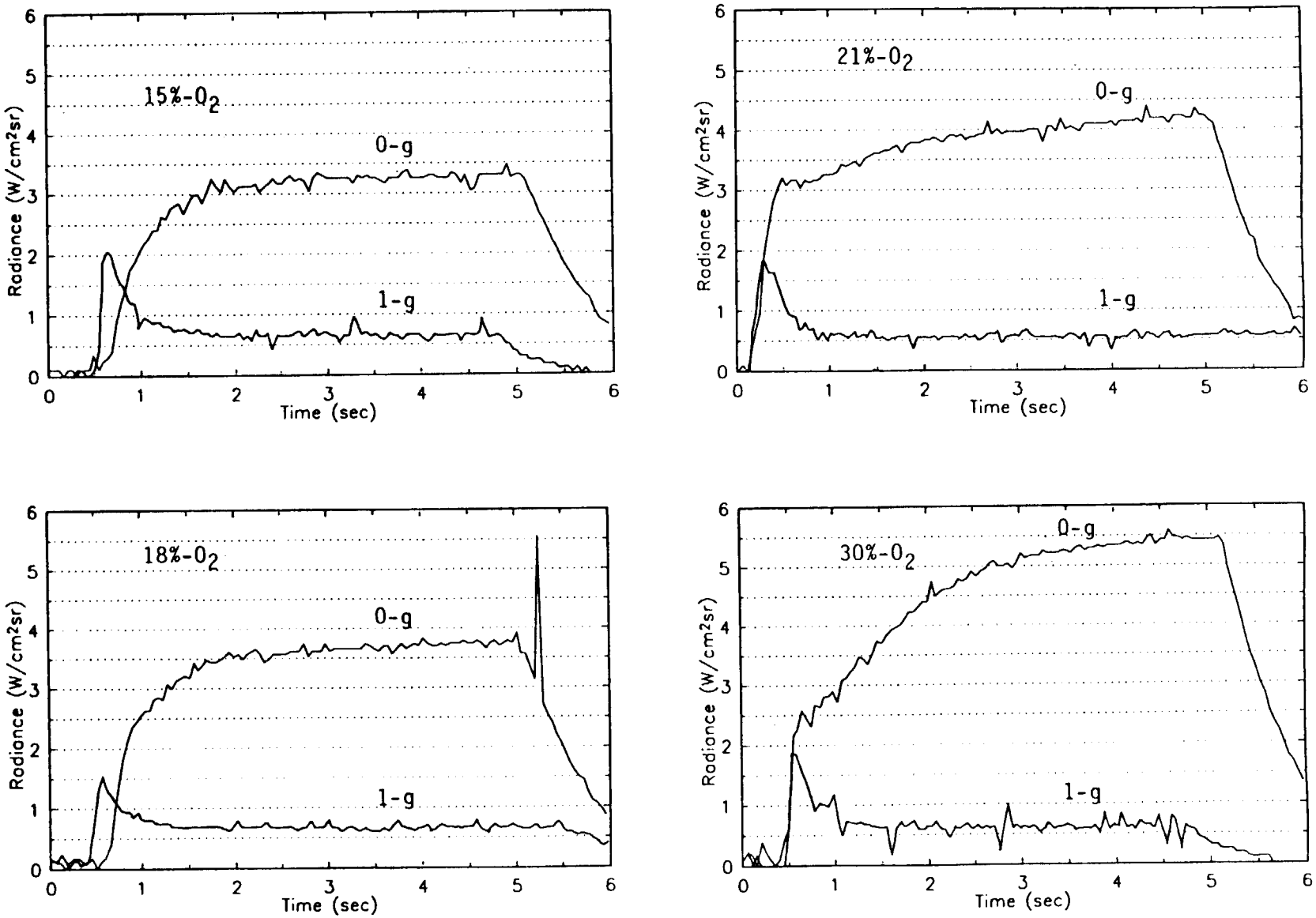

Fig. 3 Radiance vs. time for both normal-gravity and microgravity flames.

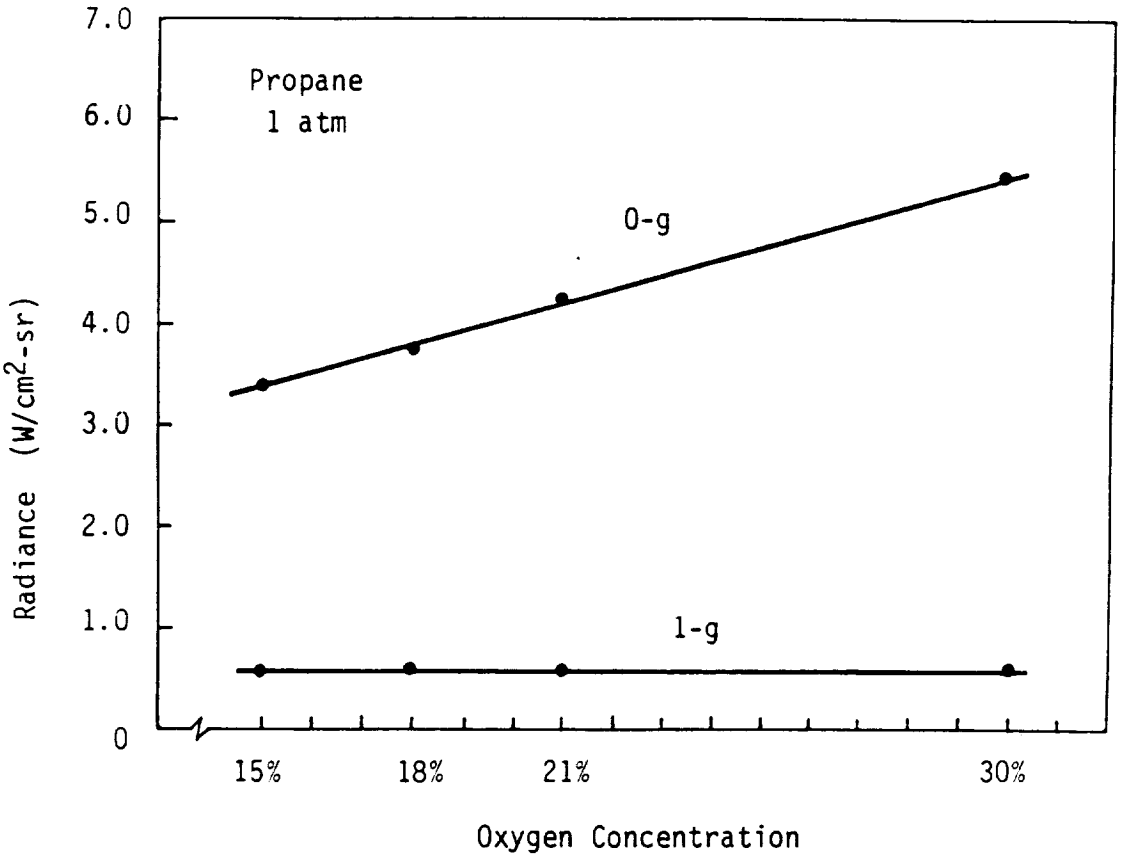

Fig. 4 Flame radiance (at approximately the last instant of the test) as a function of oxygen concentration.

Table 1 Normal-Gravity and Microgravity Data for Propane Flames Burning in Quiescent Oxidizing Environments at 1.0 Atmosphere.

$\%O_2$	Normal-Gravity Flames					Microgravity Flames				
	Avg. flame height (cm)	Max. flame dia. (cm)	Flame rad.(R), (W/cm^2-sr)	Rad. per unit flame area	dR/dt at t=4-5 sec.	Flame height (cm)	Max. flame dia. (cm)	Flame rad. (R) (W/cm^2-sr)	Rad. per unit flame area	dR/dt at t=4-5 sec.
15%	6.8	0.8	0.63	0.12	0	7.5	3.1	3.38	0.15	0.05
18%	8.8	0.9	0.65	0.08	0	9.4	2.7	3.74	0.15	0.11
21%	5.3	0.8	0.54	0.13	0	9.5	2.1	4.27	0.21	0.16
30%	4.4	0.6	0.65	0.25	0	7.6	1.5	5.43	0.48	0.18

Section 17

"PRELIMINARY OBSERVATIONS ON THE EFFECTS OF BUOYANCY ON TRANSITIONAL AND TURBULENT DIFFUSION FLAMES"

M. Y. Bahadori, D. F. Vaughan, D. P. Stocker, K. J. Weiland, and R. B. Edelman

Paper presented at the Central States Meeting of The Combustion Institute, Columbus, Ohio, April 1992

PRELIMINARY OBSERVATIONS ON THE EFFECTS OF BUOYANCY ON TRANSITIONAL AND TURBULENT DIFFUSION FLAMES*

M. Yousef Bahadori†
Science Applications International Corporation
Torrance, California

David F. Vaughan††, Dennis P. Stocker, and Karen J. Weiland
NASA Lewis Research Center
Cleveland, Ohio

and

Raymond B. Edelman§
Rockwell International Corporation, Rocketdyne Division
Canoga Park, California

Abstract

The investigation of gas jet diffusion flames of propane under both normal-gravity and microgravity conditions has been extended from the laminar region to the transition-to-turbulent and the fully developed turbulent regimes. Due to the significant reduction in the influence of buoyancy-generated turbulence in microgravity, flames burning in air at atmospheric pressure show different characteristics in microgravity compared to their normal-gravity counterparts. These characteristics include flame height, color, stand-off distance, luminosity, and sooting. Flame behavior as a function of jet Reynolds number for the three regimes of laminar, transitional, and turbulent is discussed. The results show that the microgravity flame height increases smoothly throughout the laminar region to the turbulent regime, and is longer at all flow rates than the normal-gravity flame.

---

* Presented at the 1992 Spring Technical Meeting of The Combustion Institute, Columbus, Ohio, April 26-28, 1992.

† Author and address for correspondence: M.Y. Bahadori, SAIC/NASA LeRC, MS 500-217, Cleveland, Ohio 44135.

†† Student presenter; Baldwin-Wallace College, Berea, Ohio.

§ Consultant

1. Introduction

A fundamental understanding of flame structure and characteristics under reduced-gravity conditions is essential to the problem of fire safety in spacecraft environments.[1] A major problem impeding our understanding of flame behavior in normal gravity is the masking effects of buoyancy, which results in significant differences between the structure of normal-gravity and microgravity flames.[2]

In recent studies of microgravity laminar diffusion flames, some unique and unexpected phenomena have been observed.[2-5] The results have shown that flame color, size, luminosity, sooting behavior, approach toward steady state and radiative loss, as well as the effects of pressure and oxygen concentration on these characteristics, are significantly different in microgravity compared to normal gravity.

No previous study exists on the influences of the removal of buoyancy on transitional and turbulent gas jet diffusion flames. The present work characterizes the different regimes of flame behavior under both normal-gravity and microgravity conditions. The available microgravity time and the experiment volume restrict the study to fairly small diffusion flames in the laminar, transitional and turbulent regimes.

2. Experimental

Diffusion flames of propane burning in quiescent air at atmospheric pressure were studied in the 2.2-Second Drop Tower of NASA Lewis Research Center. The combustion chamber was an open, rectangular (26 x 29 x 61 cm^3) container. The chamber and accessories where placed inside the (closed) drag shield. One side of the chamber was made of Lexan to provide photographic access. The other three (steel) sides were painted black to prevent the reflection of light from the walls. The vessel was covered by a finely woven copper screen to prevent flame-tip disturbance.

The fuel nozzle had a tip inner radius of 0.039 cm. A 4.4-cm elevated aluminum plate held the nozzle above the chamber floor. The plate, measuring 19 cm by 20 cm, acted as a flame holder by reducing the entrainment of the surrounding air. The nozzle, located at the center of the plate, protruded 2-3 mm above the plate to prevent water-vapor condensation.

Ignition was achieved using a hot-wire system. The ignitor was activated for up to 1 second. Once ignited, the hot wire was retracted from the flame. Ignition was achieved in normal gravity. Up to 4 seconds were allowed for the flame to establish itself and to film the normal-gravity flame prior to the release of the experiment into free fall. The fuel flow was maintained for the duration of the 2.2-second microgravity test.

A 16-mm Milliken movie camera recorded the normal-gravity and microgravity flames at a filming rate of 50 frames/second. Tungsten Eastman Ektachrome Video News films were used to record the flames.

The fuel was 99.9%-pure propane. The volume-flow rates were 100 to 1000 cm^3/min, corresponding to a cold-jet Reynolds number of 314-3140, based on the nozzle radius.

3. Results and Discussion

Figure 1 shows the variation of flame height with (cold jet) Reynolds number. A study of this diagram reveals some interesting and unexpected characteristics.

The normal-gravity flames of the laminar regime show a linear variation of height with Reynolds number, as is expected from the classical behavior.[6] These flames flicker due to the hydrodynamic instability, and the flicker range increases with increasing jet momentum. The laminar flames are generally yellow with a small blue base. As the jet momentum increases, the (average) flame height undergoes a transitional regime with a dip which is not a characteristic of typical transitional flame.[6] However, other studies (e.g., 7) have shown that relatively low-momentum flames exhibit this kind of behavior and, indeed, the flame height in the turbulent regime can be larger than that in the transitional regime.

In the transitional regime of normal-gravity flames, the flame starts to lift off, having a major blue-base section followed by a yellow brush which both flickers and wavers from side to side. This behavior persists throughout the turbulent regime, although the boundary of the break point shows the classical behavior. Blow-off occurs somewhere beyond Re = 3,000.

The microgravity flames, on the other hand, show a completely different behavior. In the laminar regime, the flame is flicker-free, much wider than the normal-gravity flame (up to four times larger in radius), and has an open tip with flame colors changing from blue at the base to yellow, then orange, then red, and finally dark red toward the flame tip. The flame color and shape indicate soot quenching and its subsequent escape through the tip, which resembles an underventilated-type behavior. The flame-tip opening in addition to the criteria for measuring the height of open-tip flames have been discussed in detail elsewhere.[4] However, as the jet momentum increases toward the transitional regime, the width of the flame tip decreases. In addition, the gap between microgravity and (average) normal-gravity flame heights increases with increasing Reynolds number.

The microgravity flames (at least for those particular Reynolds numbers of this study) show a monotonic flame-height variation, which means that the transition from the laminar region to the turbulent regime may occur quite smoothly, unlike the classical behavior for the normal-gravity flames. However, somewhere in the transition regime, the flame tip closes and large-scale, slow-moving structures develop which do not look like a brush-type behavior, as in the normal-gravity flame, but rather a wrinkled structure. The flame lifts off the nozzle tip, although the stand-off distance is almost half of that for the normal-gravity flame. Tip flicker was not observed for any of the microgravity flames. The flame maintains a constant length up to a Reynolds number of 2200, and then increases in length, which unfortunately falls out of the camera field of view. It is anticipated that the height will increase in this region with increasing Reynolds number. The microgravity flame height in the turbulent regime is almost twice that of the corresponding normal-gravity flame.

4. Conclusions

Diffusion flames of propane burning in air at atmospheric pressure have been studied under both normal-gravity and microgravity conditions. Laminar, transitional, and turbulent regimes have been investigated. The results show significant differences in the structure and characteristics of microgravity flames in the three regimes, compared to their normal-gravity counterparts. Work is underway to characterize the details of these regimes and to expand the database.

Acknowledgements

This work was supported by NASA Lewis Research Center under Contract NAS3-25982 with Science Applications International Corporation.

References

1. Sacksteder, K. R.: Twenty-Third Symposium (International) on Combustion, P. 1589, The Combustion Institute, 1990.

2. Edelman, R. B. and Bahadori, M. Y.: Acta Astronautica 13, 681 (1986); for previous studies of microgravity laminar diffusion flames, see references cited in this work.

3. Bahadori, M. Y., Stocker, D. P., and Edelman, R. B.: Effects of Pressure on Microgravity Hydrocarbon Diffusion Flames, Paper AIAA-90-0651, AIAA 28th Aerospace Sciences Meeting, Reno, Nevada, January 1990.

4. Bahadori, M. Y., Edelman, R. B., Stocker, D. P., and Olson, S. L.: AIAA J. 28, 236 (1990).

5. Bahadori, M. Y., Edelman, R. B., Stocker, D. P., Sotos, R. G., and Vaughan, D. F.: Effects of Oxygen Concentration on Radiative Loss From Normal-Gravity and Microgravity Methane Diffusion Flames, Paper AIAA-92-0243, AIAA 30th Aerospace Sciences Meeting, Reno, Nevada, January, 1992.

6. Hottel, H. C. and Hawthorne, W. R.: Third Symposium on Combustion, pp. 254-266, Williams and Wilkins Co., Baltimore, 1949.

7. Wohl, K., Gazley, C., and Kapp, N.: Third Symposium on Combustion, pp. 288-300, Williams and Wilkins Co., Baltimore, 1949.

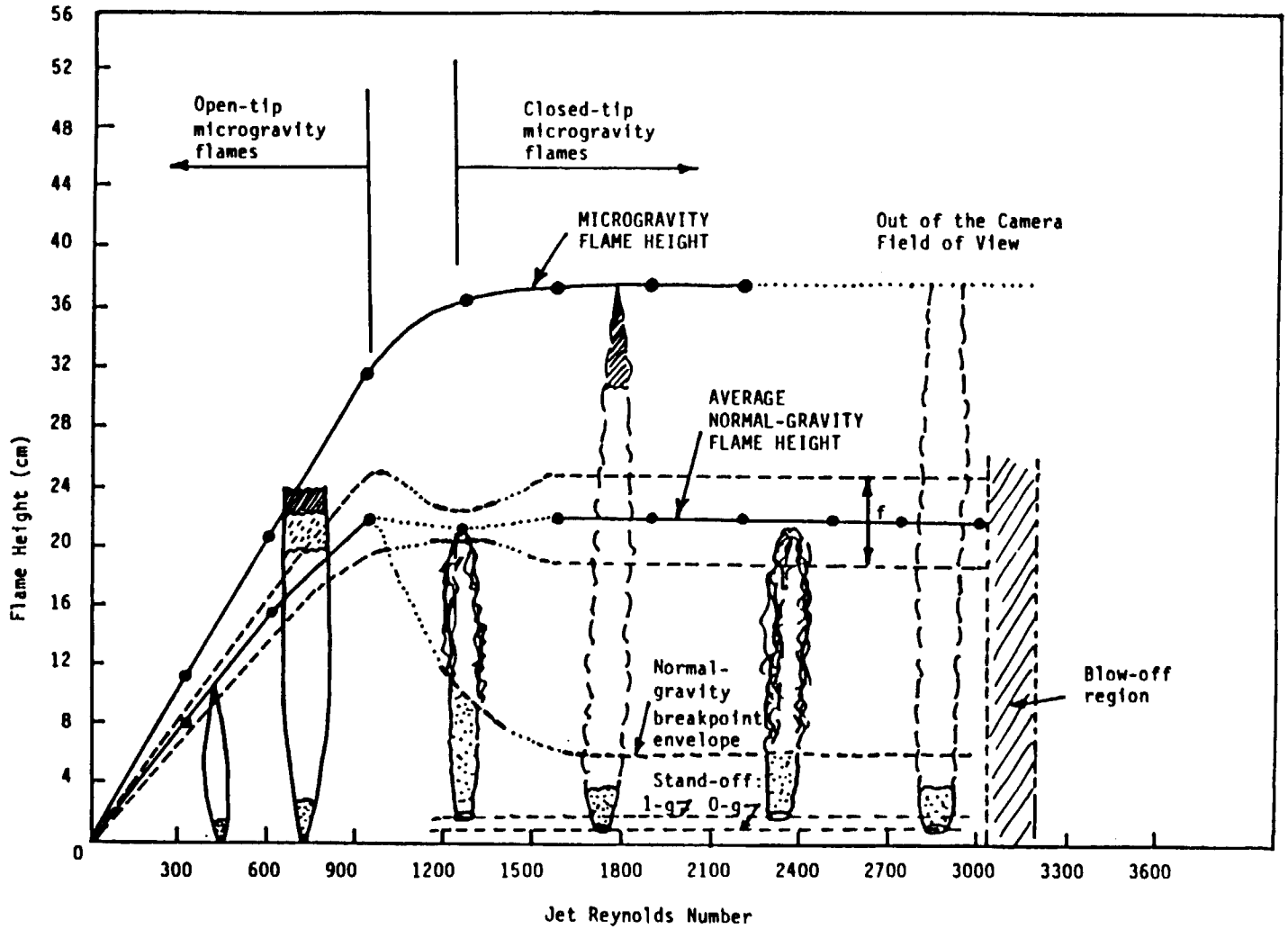

Fig. 1 Normal-gravity and microgravity flame heights of propane burning in quiescent air at 1 atm as a function of (cold-jet) Reynolds number. The colors indicated are as follows: ⬚ blue; ⬚ yellow/orange for microgravity, yellow for normal gravity; ⬚ orange, ⬚ red. The dotted lines in the normal-gravity plots indicate uncertainty in the trend which requires further investigation. The circles show the particular flames studied in this work; f is the flicker envelope for the normal-gravity flames.

Section 18

"EFFECTS OF BUOYANCY ON LAMINAR GAS-JET DIFFUSION FLAMES"

-Science Requirements Document-
(Space Experiment);

M. Y. Bahadori and R. B. Edelman

October 1991

EFFECTS OF BUOYANCY ON LAMINAR GAS JET DIFFUSION FLAMES

– Science Requirements Document –
(Space Experiment)

M. Yousef Bahadori and Raymond B. Edelman

SCIENCE APPLICATIONS INTERNATIONAL CORPORATION (SAIC)

Thermal Sciences Division
21151 Western Avenue
Torrance, California 90501

An Employee-Owned Company

Submitted to:

NASA LEWIS RESEARCH CENTER
Cleveland, Ohio 44135

October 18, 1991

SUMMARY

The proposed research is aimed toward the fundamental understanding of the behavior and characteristics of laminar gas-jet diffusion flames under microgravity conditions. By eliminating buoyancy, fundamental scientific information can be obtained in relation to the structure and physico-chemical aspects of flames in both normal-gravity and reduced-gravity environments.

The ground-based portion of the current program has resulted, to date, in some new and unique information, significantly enhancing our understanding of laminar diffusion flames in microgravity environments. However, unexpected characteristics have also been observed raising new questions on transport processes in diffusion flames in the absence of buoyancy. Observations and associated data show that earthbound facilities do not provide enough time to fully characterize the coupled physical and chemical processes which control the behavior of flames under microgravity conditions.

This document presents the science requirements for a highly productive program of space-based experiments for studying laminar diffusion flames. Critical, fundamental questions will be addressed through the efficient combination of longer microgravity test times, advanced diagnostics, and comprehensive numerical modeling.

TABLE OF CONTENTS

I. INTRODUCTION

Although diffusion flames have been the subject of research for many years they are not well understood and, while the effects of gravity on the burning process have been observed, the basic mechanisms responsible for these changes have yet to be determined. The goal of this research is to develop an improved understanding of gas jet diffusion flames. The laminar gas jet diffusion flame is selected for study because it embodies mechanisms important in all diffusion flames such as fires and practical combustion systems. Furthermore, due to its relative simplicity and ease of control, it lends itself to direct theoretical and experimental studies. However, existing theoretical models are deficient and improved models are required because they are essential to the interpretation of data, providing a means of theoretically isolating mechanisms influencing the observed behavior. The complexity of these mechanisms and their coupling establishes the requirement for data with which to verify assumptions inherent in the theoretical analyses. If gravity is significantly reduced, then its effect can be isolated, and the complication of buoyancy-induced convection would be removed from the problem. The combination of microgravity and normal-gravity data would provide the information, both theoretical and experimental, to improve our understanding of diffusion flames in general and the effects of gravity on the burning process in particular. Although earthbound experiments under reduced-gravity conditions have shown significant differences in flame behavior relative to normal-gravity conditions, the data is incomplete. This is mainly due to the limited available time in ground-based facilities, in addition to the limitations imposed by these facilities on the capability to conduct advanced diagnostics measurements. The existing data is confined to semi-quantitative visual observations on flames, and quantitative measurements (radiation, temperature, and species) from experiments currently being conducted in the 5.18-Second Zero-Gravity Facility and the upcoming KC-135 tests. This document describes the requirements of an experiment that if performed in space, would help to eliminate some major deficiencies in our understanding of gas jet diffusion flames.

II. BACKGROUND

The problem of fire safety has received the attention of researchers for many years which has resulted in a continuous effort to understand the complicated processes occurring in fires. Recently, interest in the fire problem has been expanded to include aerospace applications due to the concern over fires aboard spacecraft. The primary conclusion drawn from the existing base of information on fires is that a more fundamental understanding of diffusion flames is needed in order to predict their behavior and to control them. Although the significant effects of gravity on the burning process have been observed, the mechanisms responsible for these changes have yet to

be determined. A critical limitation of the existing earthbound experimental data is that only limited elapsed time is available to fully characterize the flame behavior under reduced-gravity conditions.

Diffusion flames involve convective and diffusive effects and fires are a complicated type of this class of combustion process. Regardless of the type of fuel involved (i.e., liquid, solid, or gaseous), the basic mechanisms which control the burning process are the same. These include the processes of mixing, radiation, chemical kinetics, soot formation, diffusion, and buoyancy-induced convection. The laminar gas-jet diffusion flame embodies these mechanisms (see Figure 1) while representing a basic element of more complex, convectively-induced turbulent flames (see Figure 2).

In order to understand the mechanisms controlling a fire, laboratory-scale turbulent gas-jet diffusion flames have been extensively studied. These small-scale flames provide important information in relation to the processes occurring in practical combustion systems as well. However, turbulent flames are not fully understood and their understanding requires more fundamental studies of laminar diffusion flames in which, under normal-gravity conditions, the complication of convection-induced turbulence is eliminated and the interplay of transport phenomena and chemical kinetics becomes more tractable. But even this basic, relatively simple flame is not completely characterized in relation to soot formation, radiation, diffusion, and kinetics. Therefore, gaining an understanding of laminar flames is essential to the understanding of fires in which the same basic phenomena occur. By working under microgravity conditions, the effects of buoyancy can be isolated and the results would form a basis to address, in logical order, the fundamental processes occurring in diffusion flames [1]. In the remainder of this section, we describe a cross-section of past experimental and theoretical efforts in relation to laminar diffusion flames under both normal-gravity and reduced-gravity conditions.

Laminar gas-jet diffusion flames have been a subject of extensive analytical, numerical, and experimental research since the appearance of the classical work of Burke and Schumann [2]. Most of the analytical studies to date deal with the mathematical representations of flame shapes based on the Burke-Schumann methodology which neglects some of the phenomena critical to understanding the structure of these flames. These include transient effects, soot formation, non-uniform flow parameters, variable transport properties, coupling between the conservation equations, and finite-rate chemical kinetics. In all of the analytical approaches, the effect of buoyancy had to be neglected in order to enable one to obtain a closed-form mathematical representation of flame shape, mass-fraction distribution and temperature distribution. Applications of this theory to laboratory-scale gas-jet diffusion flames [2-6] and to the flamelets of composite solid

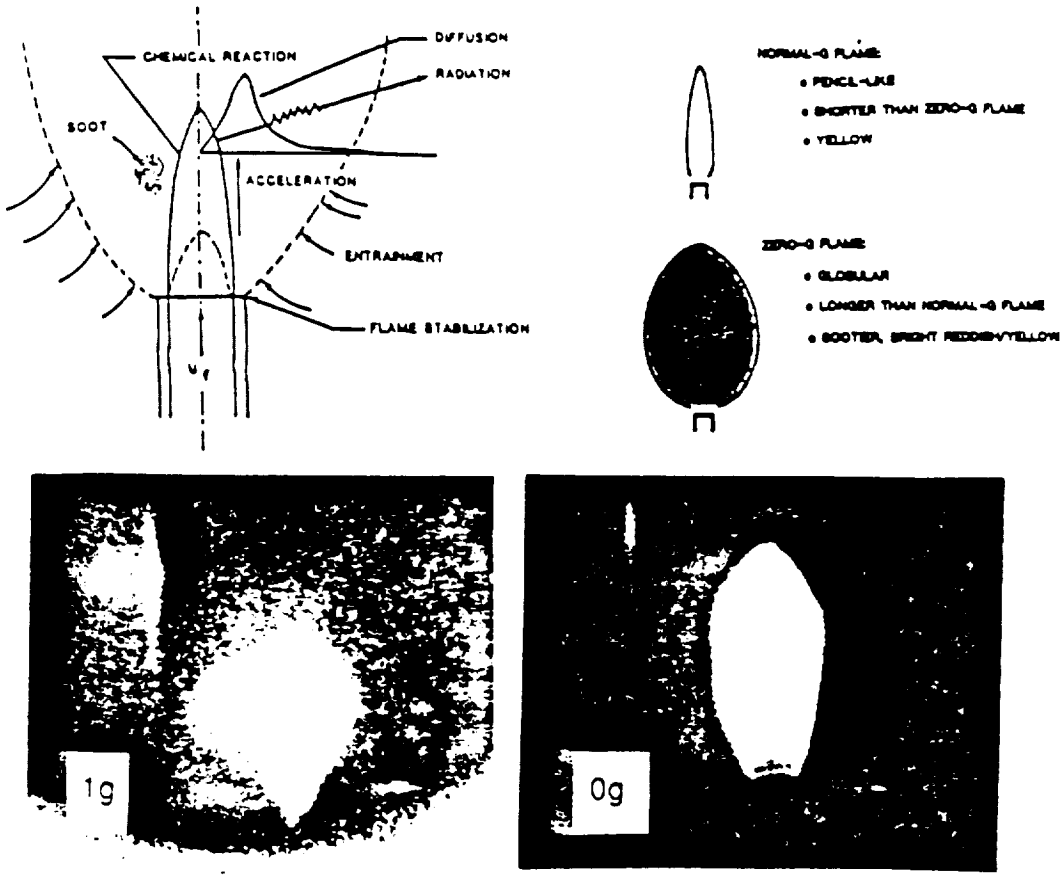

Fig. 1. Schematic diagram of a laminar gas-jet diffusion flame. The photograph shows a methane flame under both normal-gravity and microgravity conditions. The extensive yellow and red in the background for normal-gravity flame is reflection from the chamber wall. Reproduction has increased the color intensity.

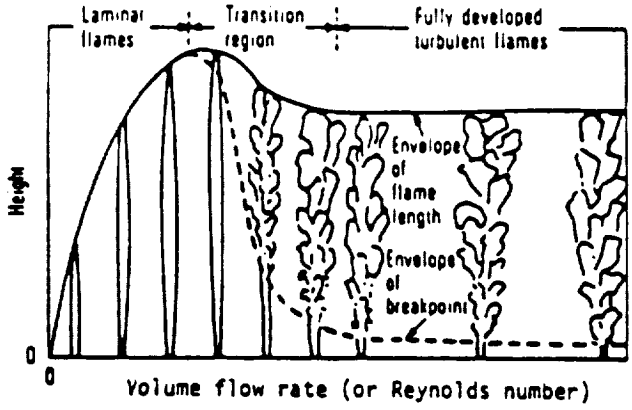

Fig. 2. Change in the flame height and behavior with increase in volume flow rate for a typical gas jet diffusion flame in normal gravity.

propellants [7] have shown satisfactory agreement between the theoretical and experimental flame characteristics. Table 1(a) describes a selected number of analytical works performed on laminar gas-jet diffusion flames. Few numerical investigations of these types of flames under normal-gravity and microgravity conditions have been attempted. The results of numerical calculations of the set of conservation equations for normal-gravity [8] and zero-gravity flames [9-12] have shown that improved understanding is needed in relation to the coupled physico-chemical phenomena occurring under these conditions. Table 1(b) shows a selected number of numerical modeling approaches. Experimental investigations of normal-gravity flames have provided a large amount of information which is not quite obtainable from the theoretical studies cited above, i.e., flame structure, soot mass fraction and number density, radiative characteristics, and temperature, species and velocity distributions; see, e.g., [8-13].

Efforts to isolate the buoyancy effects in laminar flames have been limited, to-date, to experiments in the 2.2-Second Drop Tower [9-11, 14-19] and 5.18-Second Zero-Gravity Facility of NASA-Lewis Research Center [20, 21], and accompanying numerical modeling [6, 9-11]. The 2.2-Second Drop-Tower experiments involve a self-contained gas-jet diffusion flame apparatus which is allowed to fall inside a falling drag shield. The apparatus is dropped (after establishing and recording the flame in normal gravity [9, 10, 14-17] or igniting the flame while in microgravity [11, 18, 19]) and the flame is observed throughout the duration of the fall. This provides time-resolved data on the development of the flame shape for the near-zero-gravity condition achieved during the drop. In the 5.18-Second Zero-Gravity Facility, the experiment package falls inside an evacuated tube, and the flame is ignited while the package is falling [20, 21].

Attempts have also been made to study the gas-jet diffusion flames under elevated-gravity conditions achieved in a centrifuge [22] and under negative-gravity conditions by inverting the flame using a downward-flow configuration [1, 17, 23]. Studies have been conducted on soot formation from laminar diffusion flames under normal-gravity conditions in the pressure range of 1.0-10 atm [e.g., 13]; there is no study to-date which quantitatively determines the effect of pressure on soot formation in the absence of buoyancy. Experimental studies have been underway on the behavior of Burke-Schumann type diffusion flames in microgravity environment [e.g., 24]. Results of selected experimental works on laminar flames are presented in Table 1(c). We see that while the effects of buoyancy are apparent in all of the studies presented in Tables 1(a)-1(c), it has not been strictly isolated (except for the flames of drop-tower experiments), and a large gap in the data base exists in this context.

Table 1(a). Selected Analytical Studies on Laminar Diffusion Flames.

AUTHOR(s)	METHOD	CHARACTERISTICS	DATA USED	DEFICIENCIES	COMMENTS
Burke and Schumann (1928); Ref. [2]	Analytical representations of the shapes of laminar, cylindrically-symmetric, co-axial gas-jet diffusion flames under steady-state conditions.	Assumptions of equal and constant velocities, transport coefficients, and physical properties of the two gas streams; flame-sheet approximation; Lewis number of unity (which decouples the energy and species-conservation equations); constant pressure (which eliminates the momentum equation); absence of buoyancy; no axial diffusion.	Methane, city gas, and CO flames are used. Air flow rate=6-42 ft^3/hr, fuel flow rate= 2-25 ft^3/hr. Inside radius= 1/4-5/16 in. Outside radius= 1/2-5/8 in.	No account of the formation of products of combustion; lack of finite-rate kinetics and soot-formation mechanism; no effects of radiation; no axial diffusion; assumption of decoupled conservation equations; no transient effects.	Theoretical flame heights are compared with the experimental results under normal-g; qualitative agreement is obtained between experiment and theory.
Astavin and Ryazantsev (1979); Ref. [3]	Same as Burke and Schmann (1928) but for fuel and oxidizer separated by a flow of an inert gas (a) from each other and (b) from the wall for both cylindrical and rectangular burners.	Same as Burke and Schumann (1928).	Parametric values of velocities, diffusion coefficients and tube diameters are used for methane/air flames.	Same as Burke and Schumann (1928).	Families of flame shapes and temperature contours are obtained. No comparison with data.
Penner, Bahadori and Kennedy (1984) Ref. [5]	Same as Burke and Schumann (1928).	Same as Burke and Schumann (1928) but for constant arbitrary flow velocities, transport parameters and physical properties in the presence of axial diffusion with unimolecular decomposition reactions of fuel and oxidizer.	The data of Burke and Schumann (1928) and Mitchell et al. (1980) are used.	Same as Burke and Schumann (1928) except for the effect of axial diffusion.	The results are in good agreement with experimental data.
Beckstead (1981); Ref. [7]	Analytical representation of the heights of laminar, cylindrically-symmetric flamelets of composite solid propellants under steady-state conditions.	Same as Burke and Schumann (1928) but in the presence of axial diffusion.	Typical coefficients of diffusion and velocities for evaporating solid propellant species are used.	Same as Burke and Schumann (1928) except for the effects of axial diffusion.	Flame stand-off distances are obtained. No data available.
Bahadori (1990); Ref. [6]	Analytical representation of the shapes of laminar, cylindrically-symmetric, transient, co-axial gas-jet diffusion flames.	Same as Burke and Schumann (1928) but in the presence of axial diffusion.	The data of Cochran (1972) and Cochran and Masica (1970) are used, e.g., nozzle radius=0.186 cm, methane velocity=25.8 cm/sec, etc.	Same as Burke and Schumann (1928) except for the effects of axial diffusion and transient phenomena.	Flame development with time is obtained. The results indicate that times greater than 5.0 sec are needed for flame to reach near-steady state under zero-g conditions.

Table 1(b). Selected Numerical Studies on Laminar Diffusion Flames.

AUTHOR(s)	METHOD	CHARACTERISTICS	DATA USED	DEFICIENCIES	COMMENTS
Mitchell, Sarofim and Clomburg (1980); Ref. [8]	Numerical solution of governing conservation equations for mass, momentum, species, and energy, using a global chemical reaction at the flame boundary with infinite rate. A steady-state normal-g methane/air flame was studied, which was laminar, confined, and axisymmetric.	Flame-sheet concept for locating the stoichiometric fuel-oxygen interface and hence, the points of heat release. Natural convection effects and variable thermodynamic and transport properties are allowed. Both axial and radial convection and diffusion are included.	Inner tube diameter=1.27 cm; outer tube diameter=5.18 cm, methane flow rate=5.7 cm^3/sec; air flow rate=187.7 cm^3/sec.	No detailed chemical kinetics, soot formation or radiation.	Temperatures, species concentrations and velocities are obtained. The results show the important effect of buoyancy, by which, the velocity increases by a factor of 40 inside an overventilated CH_4-air flame. Good comparison with experimental data is obtained.
Klajn and Oppenheim (1982); Ref. [12]	The numerical model treats the effects of exothermicity on the contours of gaseous, unconfined jet diffusion flames with negligible buoyancy effects.	Simplifying assumptions of flame-sheet approximation, Schmidt and Prandtl numbers of unity and constant specific heats. Solutions are obtained in closed algebraic form. Axial diffusion is not included.	Nondimensionalized values of diameters, stoichiometric ratios, velocities, etc. are used in a parametric form.	Lewis and Prandtl numbers of unity; infinite-rate global chemical reaction; no radiation or soot formation.	Fair agreement when compared with the experimental data under zero-g conditions of Cochran (1972) and Haggard and Cochran (1973).
Edelman, Fortune, Weilerstein, Cochran, and Haggard (1973) Ref. [10]	Numerical solution of conservation equations. It is shown that kinetic effects are of primary importance in flames under reduced gravity. Other controlling factors are axial diffusion, radiation and transient effects.	The model includes the coupled effects of inertia, viscosity, diffusion, gravity, and combustion in a boundary-layer type formulation. Axial and radial convection and radial diffusion are considered.	Comparison with drop-tower data of Cochran and Masica (1970) and Cochran (1972); see Table 1(c).	No detailed kinetics, soot formation, axial diffusion, and radiation.	Good agreement for normal-g flames and fair agreement for steady-state, low-Re, zero-g flames of NASA-Lewis drop-tower experiments.
Bahadori, Edelman, Stocker, and Olson (1990); Ref. [11]	The model of Edelman, et al. (1973).	Modified radiation model was used to accommodate the effects of gas-phase radiation.	Comparisons with drop-tower data of Cochran (1972) and Haggard and Cochran (1973), in addition to the new data. Also, comparisons with the predictions of Klajn and Oppenheim (1982).	Absence of radiation from soot; axial diffusion; soot processes.	Good agreement for zero gravity flames, and excellent agreement with the predictions of Klajn and Oppenheim (1982).

Table 1(c). Selected Experimental Studies on Laminar Diffusion Flames.

AUTHOR(s)	METHOD	CHARACTERISTICS	DATA USED	DEFICIENCIES	COMMENTS
Mitchell, Sarofim and Clomburg (1980); Ref. [8]	Confined, axisymmetric, laminar methane-air diffusion flames.	Distributions of temperature, velocity and species were measured. The effects of buoyancy have not been isolated.	Inner tube dia.= 1.27 cm; outer tube dia.=5.18 cm; methane flow rate= 5.7 cm^3/sec, air flow rate=187.7 cm^3/sec.	No kinetics, soot formation or radiation effects.	Importance of buoyancy is demonstrated, by which, the velocity increases by a factor of 40 inside an overventilated CH_4-air flame. The data are in good agreement with the results of modeling.
Flower and Bowman (1983) Ref. [13]	Structures of 2-D, laminar ethylene-air flames under normal-g and elevated-pressure conditions are studied.	Soot mass fraction and number density is obtained. No significant effect of pressure on the size of soot particles is observed.	Pressure range= 1.0 - 2.5 atm. A rectangular burner was used with air velocity = 22 cm/sec and fuel velocity= 7 cm/sec.	Only gas temperature and soot data are obtained.	Increase in soot yield (mass of soot/mass of fuel) as the pressure to the power 0.5 - 1.0 was observed. Maximum and integrated soot volume fractions increased as the pressure to a power between 1.5 - 2.0.
Cochran and Masica (1970) Ref. [14]	NASA/Lewis drop-tower experiments (see the text for details).	Flame behavior is observed during the 2.2-sec drop of the test chamber. Quiescent air for all of the drop-tower experiments except those of Haggard (1981) which were studied for inverted flames (under normal-g conditions) and zero-g flames in the presence of forced-air velocities; see the text for details.	CH_4/air flames; nozzle radius= 0.186 - 0.442 cm; methane flow rate= 1.2 - 5.3 cm^3/sec.	Only flame lengths and behaviors are observed. No measurements on quantitative data was possible due to the short periods of drop.	Sudden increase in gravity level resulted in immediate reduction in flame length followed by flame expanding away from the burner and final extinguishment.
Cochran (1972); Ref. [15]			CH_4/air flames; nozzle radius= 0.051 - 0.113 cm; fuel flow rate=0.7 - 12.2 cm^3/sec.		Steady-state, transient and extinguished flames existed in zero gravity. Flames were ~50% longer and wider in zero-g than in normal-g.

Table 1(c). Cont.

AUTHOR(s)	METHOD	CHARACTERISTICS	DATA USED	DEFICIENCIES	COMMENTS
Haggard and Cochran (1972); Ref. [16]			Ethylene and propylene diffusion flames; nozzle radius=0.051 - 0.083 cm; fuel flow rate=0.4 - 3.6 cm^3/sec.		Flame length is described in terms of flow parameters and fuel properties. Stable zero-g lengths were observed
Haggard (1981); Ref. [17]			CH_4/air flames, fuel-nozzle radius= 0.05 - 0.30 cm; coaxial, convergent air-nozzle radius= 1.4 cm at exit plane; fuel flow rate=1.55 - 10.3 cm^3/sec; air flow rate=0-597 cm^3/sec.		Experimental and computed flame lengths for normal-g have shown good agreement. Flame extinguishment upon entry into zero-g was studied. Relatively low forced-air velocities (≈10cm/sec) were sufficient to sustain combustion in zero gravity.
Altenkrich, Eichhorn, Hsu, Brancic, and Cerallos (1976); Ref. [22]	Gas-jet diffusion flames under elevated gravity conditions achieved in a centrifuge.	Hydrogen, methane, ethane and propane are used.	1.83-m diameter centrifuge; burner inside diameter= 0.05 - 0.21 cm; rotational speed= 200 rpm.	Only photographs are obtained and flame lengths are measured.	The results indicate that flame length and carbon luminosity decrease with increasing buoyancy. Also, flame lift-off and extinguishment were observed as the g-level increased.
Kimura and Ukawa (1961); Ref. [23]	Gas-jet diffusion flames under negative-g conditions by inverting the flame using a downward-flow configuration.	Data are obtained for both normal-g and inverted flames.	City gas flames are used. Fuel nozzle dia.=1.5, 3 and 6 mm; air duct dia.=52 and 98 mm; air flow rate ≤ 10 m/sec, fuel flow rate ≤ 40 m/sec.	Only flame lengths are observed.	Flame length is proportional to the fuel flow rate and inversely proportional to the diffusion coefficient.

Table 1(c). Cont.

AUTHOR(s)	METHOD	CHARACTERISTICS	DATA USED	DEFICIENCIES	COMMENTS
Edelman and Bahadori (1986); Ref. [1]	A downward-flow configuration is used to study coaxial gas-jet diffusion flames.	Temperature, flame shape, etc. are obtained. Stagnation points are predicted indicating that unattached recirculation zones exist above the centerline downstream of these flames.	Air inlet velocity =6.4 ft/sec; methane injection velocity=0.17 - 1.2 ft/sec; fuel-tube diameter=0.19 in.; duct diameter=6.0 in.	No quantitative information on soot, velocity, species, radiation, etc.	Importance of recirculation in inverted flames is demonstrated. The tip of the flame spread out and the flame was capped with a concave upward surface.
Stocker (1990); Ref. [24]	Co-axial jets of hydrocarbon fuels burning in air using a Burke-Schumann type configuration are studied in 2.2 seconds of microgravity.	Flames were ignited in microgravity. Both equal and non-equal reactant velocities are used for methane. Ethane and propane flames had non-equal fuel and air velocities.	Fuel-tube diameter =0.56 cm, outer dia. = 4.66 cm. Methane, ethane, and propane were used. Velocities up to 15 cm/s.	No quantitative information on soot, temperature, velocity distribution, radiation, etc.	Shape and size of flame is strongly influenced by gravity. Open tip was observed for ethane and propane flames.
Bahadori and Stocker (1989); Ref. [18]	2.2-sec. microgravity experiments conducted for methane and propane flames with O_2-N_2 . mixtures containing 18% to 30% oxygen in quiescent environments at 1 atm.	Flames were ignited in microgravity. Increase in oxygen concentration reduced the flame height. Underventilated behavior was observed for propane flames.	Nozzle radius = 0.048 and 0.074 cm. Flow rates = 1.75 and 5.25 cc/s for methane and 0.64 and 0.96 cc/s for propane.	No quantitative information on soot, radiation, temperature, etc.	Flames with 18% O_2 were entirely blue in microgravity but not in normal gravity.
Bahadori, Edelman, Stocker, and Olson (1990); Ref. [11]	Ignition and behavior of methane and propane flames burning in air are studied in 2.2 s of microgravity.	Flames were ignited in microgravity. Blue CH_4 flames were observed at low flow rates. Flame heights were in good agreement with predictions. Open tips were observed in micro-g.	Nozzle inside rad. = 0.051 and 0.0825 cm. Flow rate = 1.0-3.0 cc/s for methane and 0.5-1.5 cc/s for propane.	No quantitative measurement of temperature, radiation, etc.	Flames previously reported as extinguished were burning during the 2.0 s of micro-g due to improved photography.
Bahadori, Stocker, and Edelman (1990); Ref. [19]	Propane flames burning in quiescent air were studied in 2.2 sec. of microgravity at different pressures.	Flames were ignited in microgravity. Flames show non-monotonic height variation in microgravity.	P = 0.5, 1.0 and 1.5 atm. Fuel flow rate = 0.5 - 1.5 cc/s. Tube diameter = 0.15 cm.	No quantitative measurements of temperature, radiation, etc.	Observed open tip and soot escape. Sooting was increased with preasure increase.
Bahadori, Edelman, Sotos, and Stocker (1991); Ref. [20]	Methane and propane flames were studied in quiescent air at 1 atm pressure in 5.18-sec. of microgravity.	Radiation measurements using a thermopile detector. Flames were ignited in microgravity. 5 sec. was not sufficient for radiation to reach steady state.	Nozzle radius = 0.0825 cm. CH_4 flow rate = 1.0 - 3.0 cc/s; C_3H_8 flow rate = 0.5 - 1.5 cc/s.	No other quantitative measurement except flame radiation.	Radiance was up to 10 times larger in micro-g.
Bahadori, Edelman, Sotos, and Stocker (1992); Ref. [21]	Methane and propane flames studied in quiescent air at 1 atm in 5.18 sec of micro-g.	Flames were ignited in micro-g. Temperature measurements using a rake of 9 thermocouples.	Nozzle radius = 0.0825 cm. CH_4 flow rate = 1.0 - 3.0 cc/s; propane flow rate = 0.5 - 1.5 cc/s.	Only temperature data are reported.	Temperatures are lower compared to normal-g. 5 sec was not sufficient to reach steady state.

III. FUNDAMENTAL CHARACTERISTICS OF LAMINAR DIFFUSION FLAMES IN MICROGRAVITY

In this section, we present some of the important findings of the ground-based portion of the current program. Both experimental and theoretical aspects of this effort are described. The new findings, when analyzed and discussed, provide a set of objectives and associated justification for conducting a space-based experiment; these are presented in the later sections.

The experimental portion of the current ground-based program was designed to provide both qualitative and quantitative measurements in the chamber shown in Figure 3. These data are being obtained by the combined use of the 2.2-Second Drop Tower, 5.18-Second Zero-Gravity Facility and the KC-135 aircraft. To-date, quantitative data have been obtained during the approximately 5 seconds of low gravity in the form of temperature and radiation measurements. In addition, species concentrations will also be measured. Direct observations using cinematography have been obtained, revealing additional flame-visualization information in relation to flame color, luminosity, and dimensions.

The current theoretical work consists of the development and upgrading of comprehensive numerical models that are designed to predict flame characteristics, including temperature, velocity, and species fields, radiation from particulates and combustion products, and flame shapes for arbitrary gravity levels, in the presence of soot formation and oxidation, thermophoretic effects, finite-rate kinetics, and multi-component diffusion.

In the current study, the effects of pressure, oxygen concentration, fuel type, nozzle size, and fuel-flow rate (i.e., Reynolds number) have been examined. A comprehensive set of data (both qualitative and quantitative) have been obtained. Oxygen-nitrogen mixtures in the range of 15% to 50% oxygen at chamber pressures ranging from 0.5 atm to 1.5 atm have been used as the oxidizing environment. Both methane and propane flames have been studied in these quiescent environments under normal-gravity and microgravity (both 2.2-second and 5.18-second) conditions. Nozzle sizes of 0.051 to 0.0825 cm (inner radius) have been used. The fuel-flow rates (when converted to standard conditions of 1 atm and 298 K) were 0.5 - 1.5 cm^3/sec for propane and 1.0-3.0 cm^3/sec for methane.

Results of the research conducted to date under the current program have shown important, and in some cases unexpected phenomena. Some of these findings are presented below in the form of results, issues, and their impact on the direction of this research.

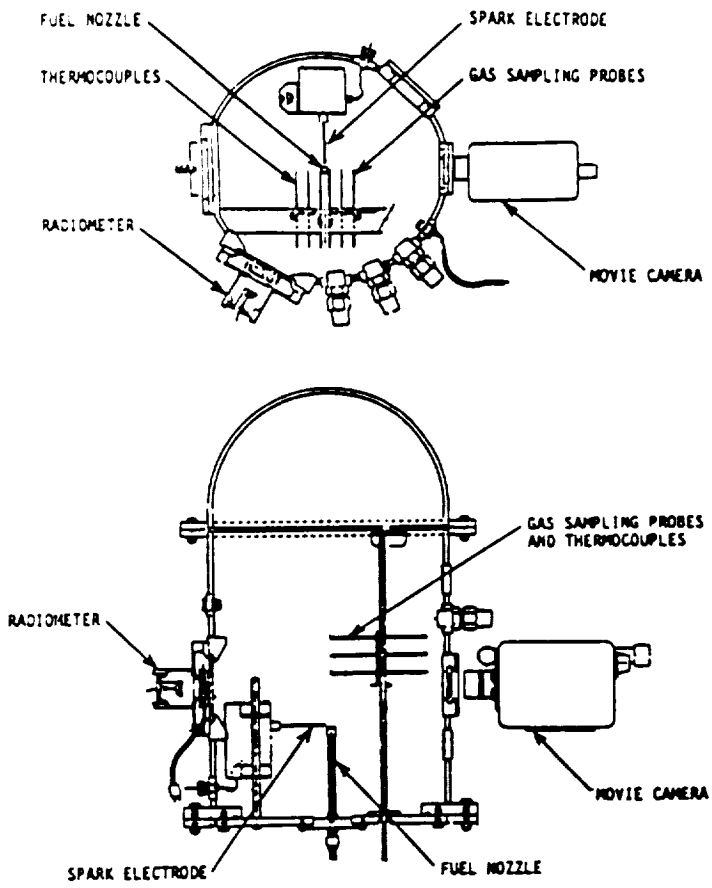

Fig. 3. Experiment package for the 5.18-Second Zero-Gravity Facility and KC-135 tests; current microgravity laminar diffusion-flame program.

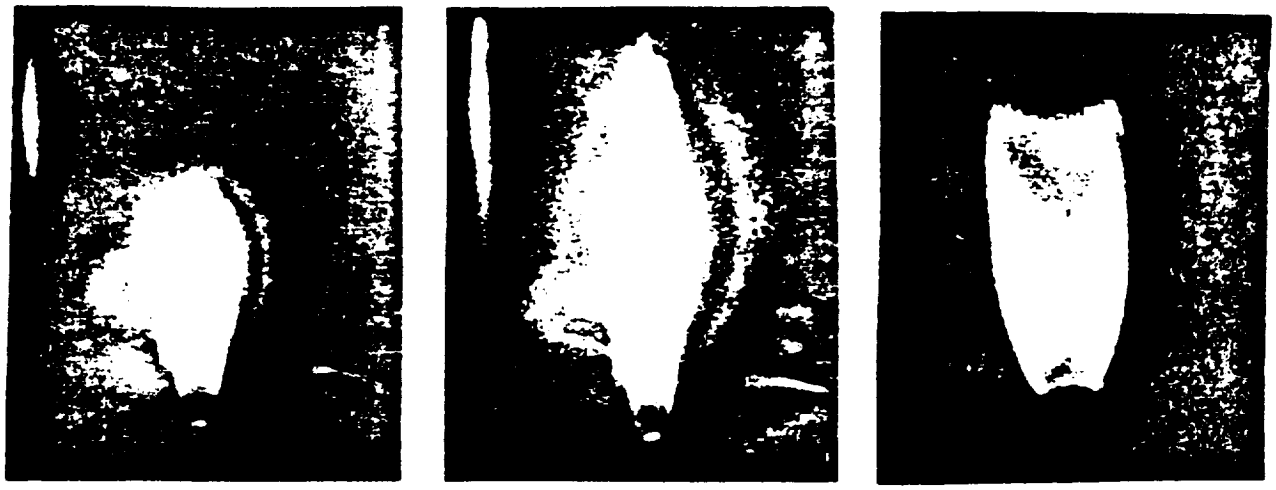

1-g minimum 1-g maximum Microgravity

Fig. 4. Normal-gravity (both minimum and maximum heights of flicker) and microgravity flames of propane burning in quiescent air at 1 atm; fuel-flow rate = 1.0 cm^3/sec. The extensive yellow and red in the background for normal-gravity flame is reflection from the chamber wall. Reproduction has increased the color intensity.

(a) Flame Characteristics

Laminar diffusion flames of hydrocarbons under microgravity conditions have shown distinct characteristics relative to normal-gravity flames [1]. Compared to the flames in normal-gravity environments, larger, sootier, and somewhat globular flames are observed in microgravity. This is due to the significant reduction in the buoyant force, which makes diffusion the dominant mechanism of transport. As a result, increased residence time, enhanced soot formation, radiation cooling due to the larger flame size, and the possible onset of a chemical-kinetics limitation on the heat-release process are apparently responsible for the very different characteristics of these flames compared to those in normal gravity. In normal-gravity environments, laminar diffusion flames of hydrocarbons flicker and are generally yellow, whereas their microgravity counterparts are flicker-free, with colors ranging from orange to red to entirely blue, depending on the oxidizer composition and pressure.

In gas-jet diffusion flames, the heat-release mechanism is not uniform throughout the flow field. Pyrolysis, producing soot and partially oxidized species, dominates in the near-jet region, while continued heating and increased residence time result in the tendency to burn off these species downstream. However, pyrolysis and soot formation reduce the temperature level in the flame and, with the aid of the increased residence time, sooting is enhanced. This, in turn, results in enhanced radiation, more cooling, and delayed soot burn-off downstream of the flame. This effect is much more pronounced in microgravity flames compared to those in normal gravity, due to the lack of buoyancy.

Figure 4 shows a typical normal-gravity and microgravity propane flame. The colors indicate the presence of particular species in hydrocarbon flames, e.g., blue-violet region (outer region at the base showing the spectrum of burning CO) and bluish-green region (showing C_2 and CH emissions, where C_2 bands appear green shaded toward violet and CH bands appear violet-blue). A highly luminous zone (bright yellow) indicates the thermal emission of burning carbon particles. This luminous zone becomes yellow, then orange, and then red and dark red toward the boundary of the visible region, as the temperature of the unburned soot decreases. The reddish-orange color of the flame is due to the soot at cooler temperatures than would be expected for typical burn-off conditions.

The color of the radiating soot, in conjunction with Wien's law, can be used as an indicator of the approximate local flame temperature. The cloud of burning soot particles is yellow, i.e., ~0.58-μm wavelength (1370 K<T< 1670 K, where 1670 K is the temperature of a white hot

body). As the temperature decreases, the soot particles become orange red (~1370 K, ~0.6 μm), then cherry red (~1170 K, 0.6-0.65 μm), and finally dull red (~970 K, 0.65-0.70 μm). These effects are shown clearly in Figure 4, which indicate cooling by pyrolysis and enhanced radiation due to increased soot formation.

Flame radiation is mainly due to the presence of soot particles, and the interaction between kinetics and radiation is directly influenced by soot generation and burn-off. These mechanisms are accentuated in the absence of buoyancy. The orange-reddish appearance of the microgravity flame in Figure 4 is an indication of pyrolysis in the hot fuel-rich portions of the flame which results in appreciable amounts of solid carbon. Studies of microgravity flames have shown that flame temperature is reduced due to the large globular flame surface and continuum radiation from soot. Thermal radiation can result in an energy loss of up to 40% of the heat input which augments the kinetic effects that can contribute to flame extinguishment [10]. The studies also suggest that pyrolysis and soot formation are of potential importance in terms of their effect upon the local molecular weight (buoyant force).

(b) Ignition, Flame Development, and Extinction

In previous studies [e.g., 14, 15], flames were ignited in normal gravity and then subjected to the microgravity condition. As a result, a transient period due to the sudden removal of the gravitational acceleration was imposed on the flame, which affected its characteristics and development toward steady state. Immediately after the release of the apparatus, the (steady-state, normal-gravity) flame height decreased and reached a minimum value in times on the order of 0.05 sec; see Figure 5(a). The flame height then continuously increased leading to either (reported) extinguishment, (apparent) steady state, or a transient situation where the flame needed more time to show its final behavior. The transitional behavior is due to the accumulation of hot products of combustion attendant with the sudden loss of buoyancy-driven convective flow. Such an occurrence was believed to lead to quenching in some cases or possibly a slow readjustment to a steady-state microgravity flame (see Figure 5).

The ignition approach previously used in the drop-tower experiments [14, 15] exposes an established normal-gravity flame to a sudden change in the gravity level. The reported microgravity flame behavior has been due to this step change in the gravity level. The normal-gravity ignition method also suggests that the microgravity flame behavior may be affected by the flickering normal-gravity flame at the instant the package is subjected to the microgravity condition. However, poor photography has resulted in erroneous conclusions on extinction of some of these

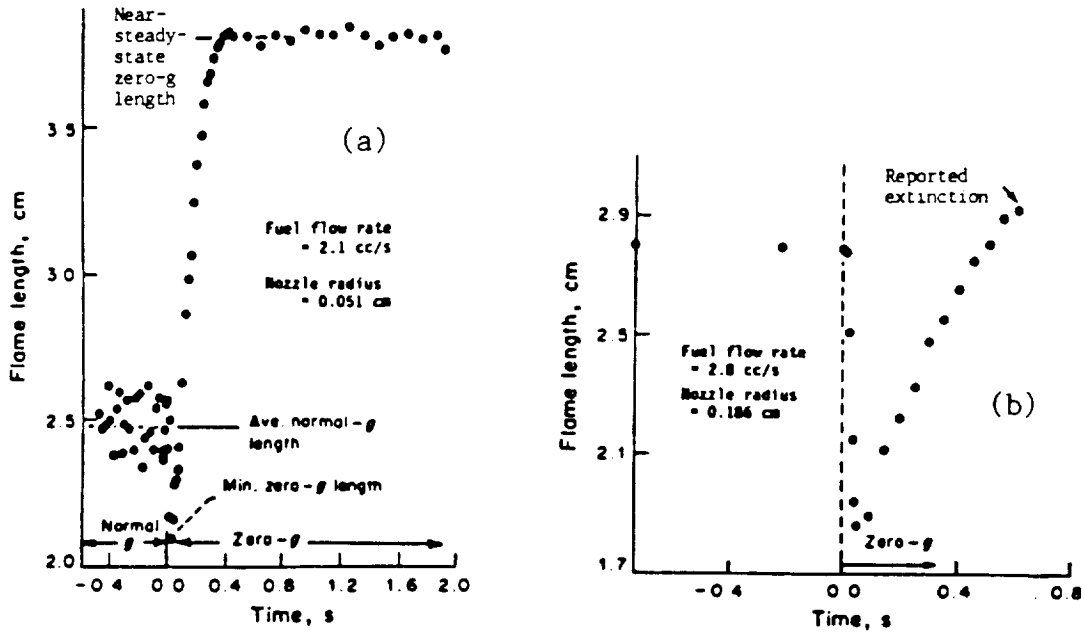

Fig. 5. Flame length as a function of time in microgravity for a methane-air diffusion flame that (a) reached near-steady-state, and (b) was reportedly extinguished; reproduced from [15] and [14], respectively.

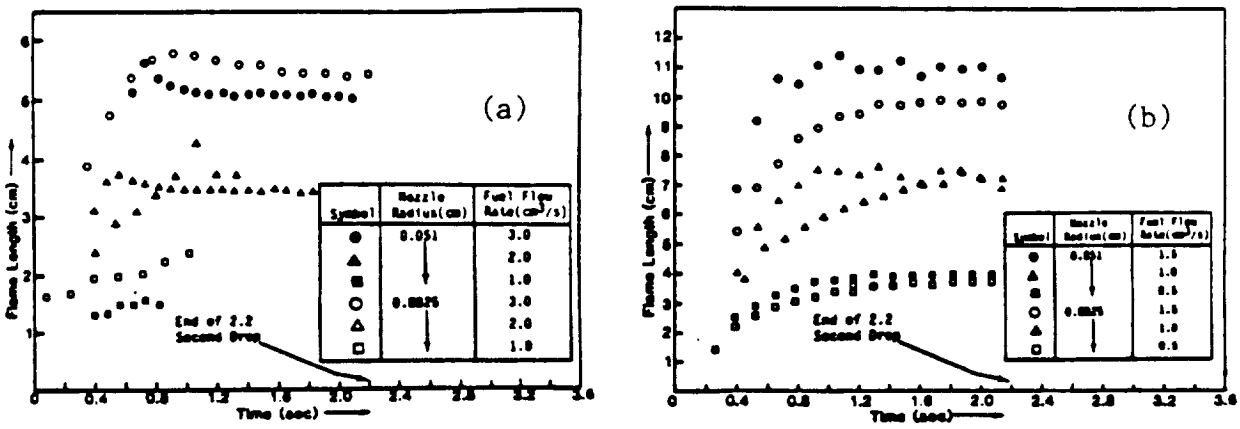

Fig. 6. Flame heights for (a) methane, and (b) propane, following ignition in microgravity. Note that extinction was not observed for these flames. Those which do not show a complete height development with time could not provide a conclusive result in relation to the flame height due to a very faint flame tip; reproduced from [11].

microgravity flames [14, 15]; see Figure 5(b). Recently, by improving the photographic technique, flames tested in the 5.18-Second Zero-Gravity Facility under identical conditions to those reported as extinguished, continued to burn throughout the available time of 5 seconds. As a matter of fact, none of the tests conducted to date under the current program have resulted in flame extinction in microgravity. In addition to the improved photography, these flames were ignited after the release of the package, therefore eliminating the complications arising from subjecting a normal-gravity flame to microgravity condition.

Figure 6 shows the behavior of a set of methane and propane flames following ignition in microgravity. The data have shown that most of the flames do not reach steady state in the 2.2 second available time. This prompted the use of the 5.18-Second Zero-Gravity Facility, the results of such tests will be discussed later.

Figure 7 shows a frame-by-frame analysis of a propane flame ignited in microgravity [11]. Frame number 35 shows the flame during rapid deceleration as the experiment package is brought to rest at the end of the drop. The high level of induced convection causes blowoff within <0.1 second. After the impact, re-ignition can be seen due to the spark pulses (in this case, the ignitor was active throughout the 3.0 seconds of experiment duration), resulting in normal-gravity behavior, i.e., flame flicker.

In order to theoretically study the development and behavior of a flame following ignition in microgravity, a model was developed in the course of the current program for transient, laminar jet diffusion flames in zero gravity [6]. The model includes axial diffusion, and the solution yields the development of the flame boundary from ignition toward steady state, and reduces smoothly to the classical solution of laminar diffusion flames as, independently, axial diffusion becomes negligible, and steady state is approached. Figure 8 compares the theory with results of the experimental work reported elsewhere [14, 15], and shows satisfactory agreement for the increase in flame height with time.

(c) Effects of Pressure and Oxygen Concentration

In order to study the effects of oxygen concentration and pressure on microgravity flames, tests have been conducted under various oxygen/pressure conditions. The results show that environmental conditions have a much more pronounced effect on flame characteristics, color, luminosity, and sooting behavior in microgravity compared to normal gravity. Sooting was eliminated in microgravity hydrocarbon flames at 18% O_2-0.5 atm, and the flames were entirely

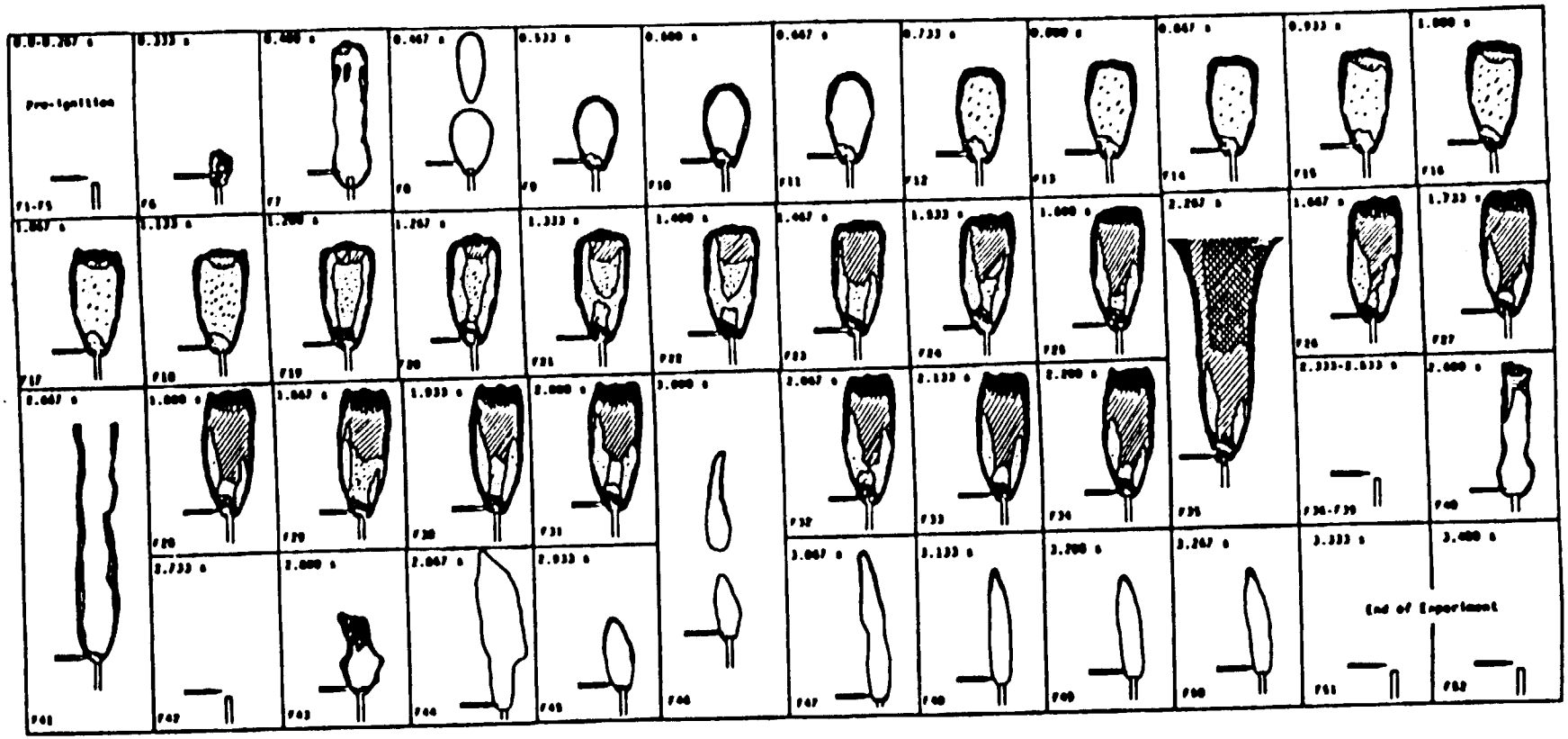

Fig. 7. Frame-by-frame analysis of a microgravity propane flame with nozzle radius = 0.0825 cm and volume flow rate = 1.0 cm^3/s. The different observed colors are as follows: ☐ Bright white; ▨ White with little yellow; ▨ White with more noticeable yellow; ▤ Blue; ▨ Dark blue; ▨ Violet-pink; ▨ Mixed blue/violet; ▨ Yellow; ▨ Orange; ■ Cherry red; ▨ Dull red, fainting; ▨ Color at the base, starting with dark at the bottom, becoming dark blue/pink, then pink/blue, then pink/orange, then orange/yellow, and then yellow/white toward the center of the flame; ✱ Bright white spark with bright blue at its boundary. Scale: ⊢ = 1 cm.

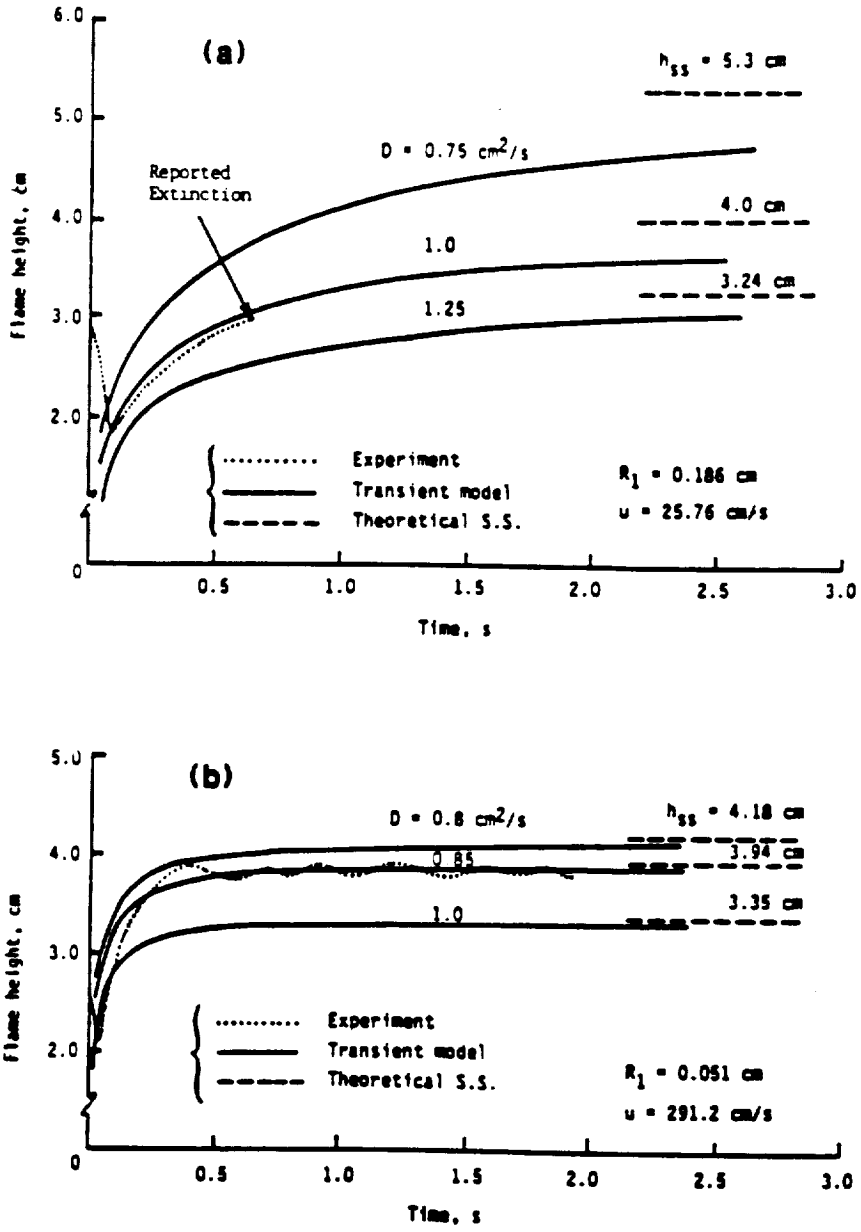

Fig. 8. Comparisons between the analytical [6] and experimental [14, 15] variations of flame height with time. The experimental work reports flame extinction (see a) at approximately 0.6 sec, and reaching an apparent steady state in 0.4 sec (see b). The binary diffusion coefficient of methane in nitrogen, D, has been used parametrically to show its effect. The values of 0.85 and 1.0 cm^2/s correspond, respectively, to temperatures of 650 and 750 K. Here, h_{ss} is the theoretical steady state-flame height, u is the gas velocity, and R_1 is the inner (nozzle) radius. Axial diffusion has been included in the analytical solution; reproduced from [6].

blue (see Figure 9), whereas their normal-gravity counterparts were yellow, luminous, and very similar to normal-gravity flames under atmospheric, or even high-pressure/high-oxygen-concentration conditions. This has a very important implication, namely, reduced radiation loss and reduced hazard of flame spread to surrounding combustible materials by reducing oxygen concentration and/or pressure in microgravity environments. In addition, there is a possibility that flammability limits may be quite different in microgravity and normal-gravity flames under these reduced oxygen-concentration and pressure conditions.

Figures 10 and 11 show, respectively, methane- and propane-flame heights as a function of oxygen concentration for different flow rates under both normal-gravity and microgravity conditions. The flames are taller and significantly wider in microgravity, the reason being that the accumulation of combustion products in the vicinity of the flame due to the absence of buoyant force (and hence, reduction in entrainment and mixing) makes diffusion the dominant mechanism of transport and results in longer residence time for fuel to burn. The normal-gravity heights are the averages of minimum and maximum flickering-flame height. In general, the lower the oxygen concentration, the taller the flame, regardless of gravity level. This is obvious since the residence time for burning the fuel is related to the level of oxygen in the environment.

Figure 10 shows that at some high-enough oxygen concentration, the normal-gravity and microgravity flame lengths may become equal. This indicates that oxygen may be so abundant that accumulation of the combustion products in the vicinity of the microgravity-flame front may have no effect on the diffusion of oxygen toward the flame. This phenomena has not been observed for propane flames (see Figure 11), probably due to massive sooting, tip opening, and quenching at the tip even at high oxygen concentrations.

Significant changes in flame color and luminosity occur in the absence of buoyancy for different oxygen levels. In microgravity, the oxygen concentration has a strong effect on methane flame heights, whereas color is more significantly changed in propane flames (see Figures 10 and 11). In addition, reduced buoyancy makes the flames wider compared to normal-gravity flames. This is due to the lack of entrainment, continuous release of products, and dominance of diffusion, which are responsible for the adjustment of the flame to the location of stoichiometry. However, in normal gravity, the buoyant force aids the arrival of oxygen to the flame front causing the flame to be pencil-like.

The various colors observed in microgravity have significant physical implications. In general, methane flames do not change drastically in color upon the removal of buoyancy, although

Fig. 9. Effects of pressure and oxygen concentration on microgravity laminar propane diffusion flames burning in quiescent oxygen-nitrogen environments. Here, the nozzle has a diameter of 0.15 cm, and the fuel flow rate corresponds to 1.0 cc/s under the standard conditions of 1 atm and 294 K; the cold jet Reynolds number based on the fuel properties and nozzle radius is 98. Silicon carbide fibers (15 μm in diameter) were stretched across some of the flames to identify the flame location and approximate level of temperature. Note that the normal-gravity counterparts of these flames were almost identical in color (i.e., were yellow), had a closed tip, and were flickering. The extensive red observed in the flame of 30% O_2-0.5 atm is reflection from the chamber wall. Reproduction has increased the color intensity for yellow and red, and has reduced the intensity for blue.

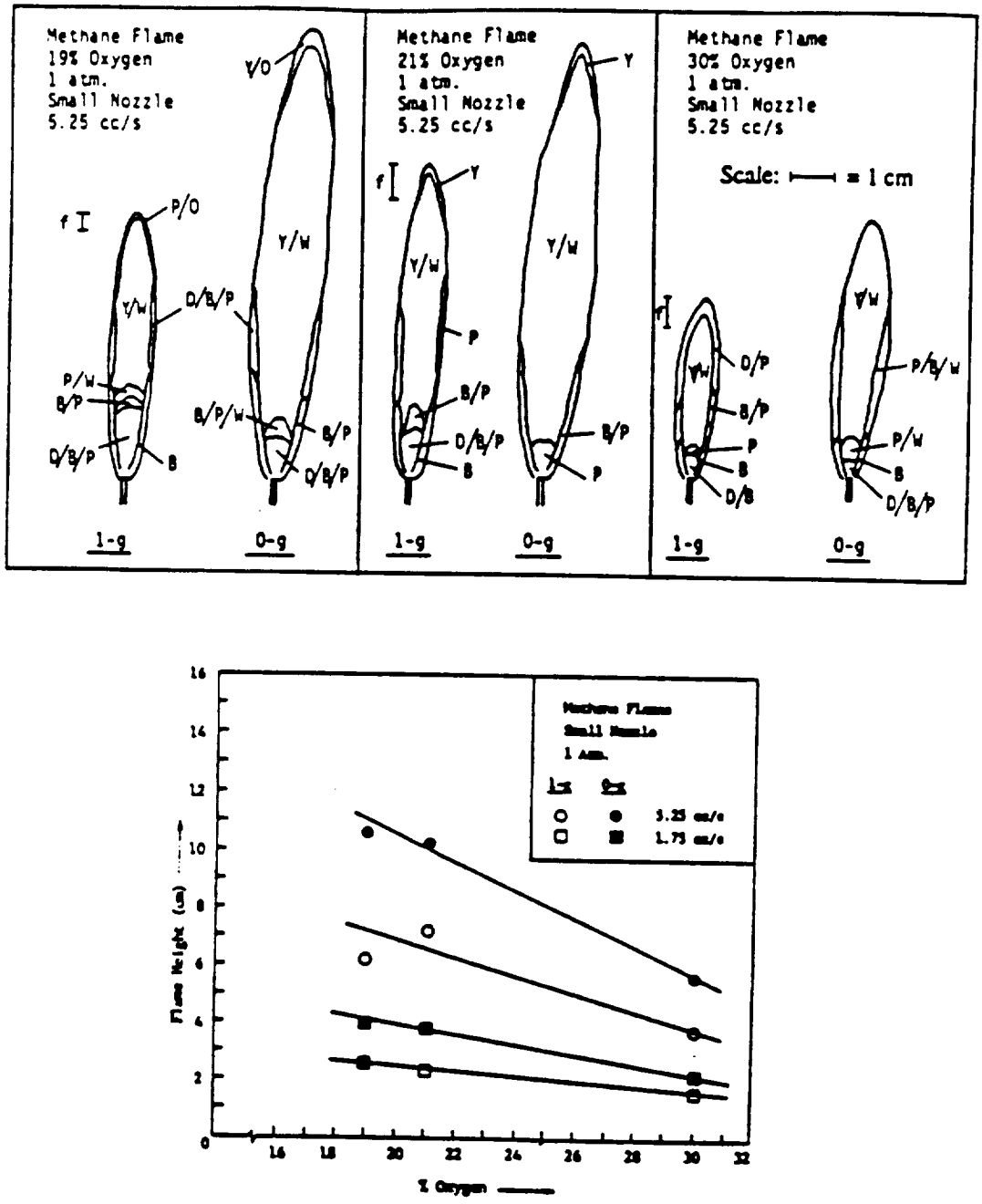

Fig. 10. Normal-gravity and microgravity flames of methane at 1 atm as a function of oxygen concentration. The nozzle had a tapered-tip radius of 0.048 cm. The various colors indicated in the diagram are as follows: B (blue), D (dark), O (orange), P (pink), R (red), W (white), and Y (yellow). The bars show the range of normal-gravity flame flicker (f); reproduced from [18].

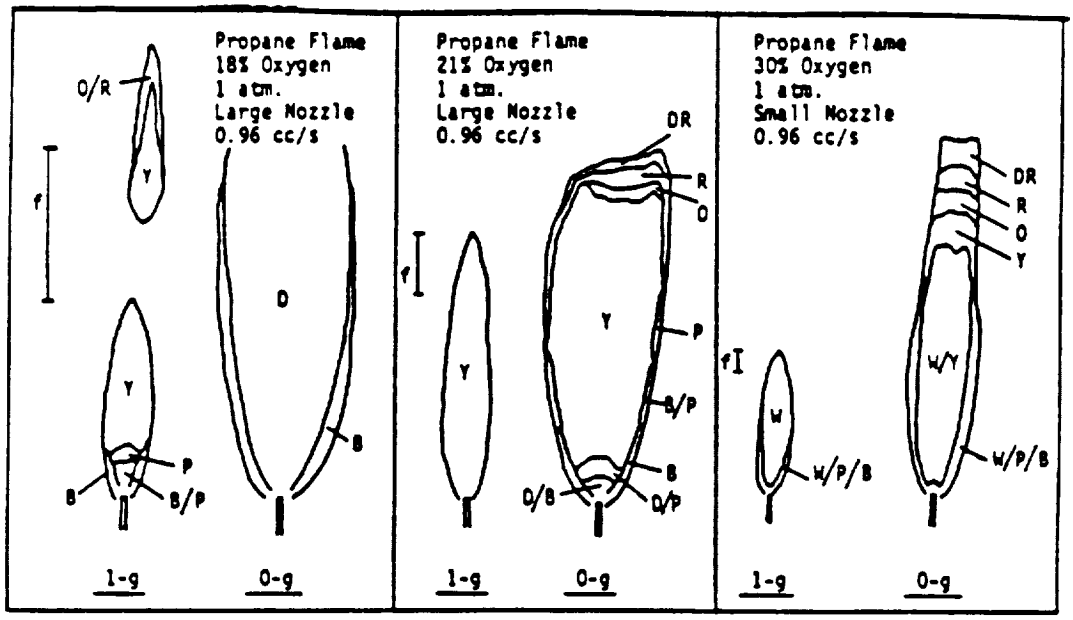

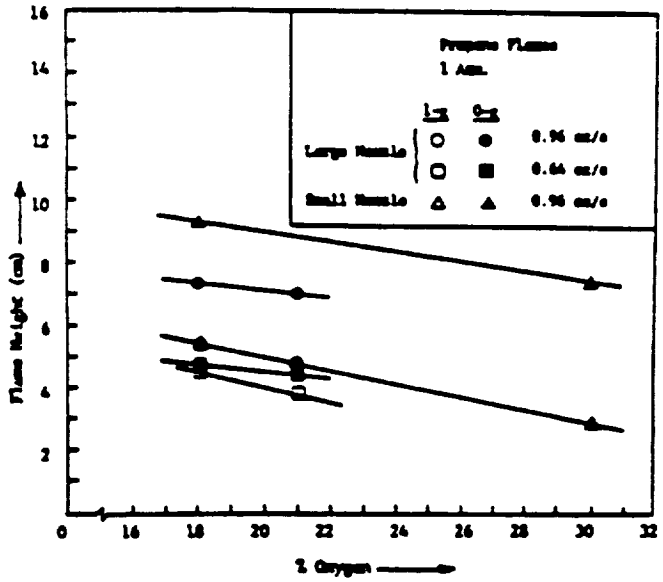

Fig. 11. Normal-gravity and microgravity flames of propane at 1 atm as a function of oxygen concentration. The nozzles had tapered-tip radii of 0.048 and 0.074 cm, respectively. The low-oxygen-concentration flame of propane in normal gravity shows pockets of flame leaving the flickering part. The various colors indicated in the diagram are as follows: B (blue), D (dark), O (orange), P (pink), R (red), W (white), Y (yellow), and DR (dark red). The bars show the range of normal-gravity flame flicker (f); reproduced from [18].

they become dimmer due to the larger flame surface, resulting in more radiative loss, and hence, cooler flames. However, the propane flames in microgravity change remarkably in both color and characteristics. Referring to Figure 9, the dim, large blue flame of propane at 18% oxygen concentration shows a cooler overall flame temperature with little or no soot formation. In addition, the intense yellow/ orange/red/dull red colors observed at higher oxygen concentrations show that extensive soot formation, burn-off and quenching occur with flames appearing underventilated even in the 30% - O_2 environment. Recent tests with 50% oxygen have still shown massive sooting with open tips (apparent underventilation), indicating that soot quenching may not be avoided in microgravity by merely increasing the oxygen level.

The unique underventilated behavior of microgravity propane flames shows that extensive soot formation due to pyrolysis, increased residence time, and radiation cooling is a characteristic of microgravity flames. Indeed, the films show that soot escapes through the tip of the flame. This tip-quenching is believed to be due to limited oxygen-fuel mixing, radiative loss from the hot combustion products and soot particles, and, possibly, unburned fuel escaping through the flame tip. The low-oxygen-concentration flames of propane (Figures 9 and 11) show that near-limit extinction may have been approached, and that the limit and mechanism may be different in microgravity compared to normal gravity. It seems that at low-enough oxygen concentrations, we may observe a flame of the same size but so cool and dim indicating that heat release due to reaction can no longer compete with heat loss, causing flame extinction in microgravity, but not in normal gravity.

The 18% - O_2, 1-atm flames of propane in Figures 9 and 11 look different, i.e., Figure 9 shows some red developing inside the flame. These tests were conducted in the 2.2-Second Drop Tower, and show a transient behavior in terms of a change in color but not shape and height. Recent 5.18-second microgravity tests of this flame have shown that during the first 2 seconds of microgravity, the flame is entirely blue. After 2 seconds, red (quenched soot emission) starts to develop inside the blue boundary, and increases in intensity throughout the rest of the drop period. This unusual behavior occurs slowly such that 5 seconds of microgravity is not sufficient to quantify the behavior of these low-oxygen-concentration and/or low-pressure flames. The increased residence time in microgravity flames affects the rate processes of soot formation, agglomeration, and burn-off, delaying the approach of the flame toward steady state. This subject will be discussed in more detail later.

In order to study the effects of pressure on microgravity flames, tests were conducted at different oxygen concentrations for the range of 0.5-1.5 atm in pressure. Propane flames burning

in air are shown in Figure 12 as a function of pressure. Observations on the color of microgravity flames show the strong effects of pressure on sooting, flame length, and flame diameter.

Microgravity flame heights are plotted as a function of both pressure and fuel Reynolds number in Figure 13. It appears from these data that the flame height correlates linearly with Reynolds number, but reaches an apparent minimum between 0.5 and 1.5 atm. The flame height in all of these tests was based on the location where red soot changes color into dull red, indicating local flame extinction (as can be seen in Figure 12). Experimental studies have shown that soot ceases to burn near 1300 K. The red to dull-red transition seems to roughly correspond to this temperature (as was discussed in Section III.a). It is believed that red/dull-red boundary gives a more accurate measure of flame height.

Figure 14 shows the soot quench region (defined as the length of the red zone at the flame tip), which increases with both pressure and fuel Reynolds number, indicating enhanced soot formation. This requires a longer residence time for soot to quench. The lowest Reynolds number at 0.5 atm shows no quench length since the flame tip is closed.

In Figure 15, the blue-base height (i.e., soot inception and agglomeration period prior to emission and burn-off) is plotted for both microgravity and normal-gravity flames as a function of fuel Reynolds number at different pressures. As the pressure increases, both normal-gravity and microgravity soot-inception heights decrease with little dependence on flow rate.

Figure 16 shows the microgravity flame-tip diameter vs. Reynolds number. Due to the uncertainty in the beginning of tip opening at 0.5 atm, no attempt has been made to connect the three data points. The 1.5-atm and 1.0-atm flames show an asymptotic type of convergence, indicating that beyond a certain Reynolds number, the flame tip has a fixed diameter. Therefore, regardless of pressure (and hence, availability of oxygen), jet momentum and fuel-mass flow rate dominate the flame adjustment to the location of stoichiometry.

These results show the unique characteristics of sooting microgravity flames. In general, for both normal-gravity and microgravity flames, the soot inception period and the regions of burning CO, C_2 emission and CH emission (blue region at the base) decrease as the pressure increases. This indicates that formation, burn-off and emission of soot is facilitated by pressure increase. Normal-gravity studies of hydrocarbon flames have shown that a pressure increase results in an increase in soot formation and a decrease in soot removal by oxidation. This agrees with the present observations of the normal-gravity flames, since brightness increases due to more

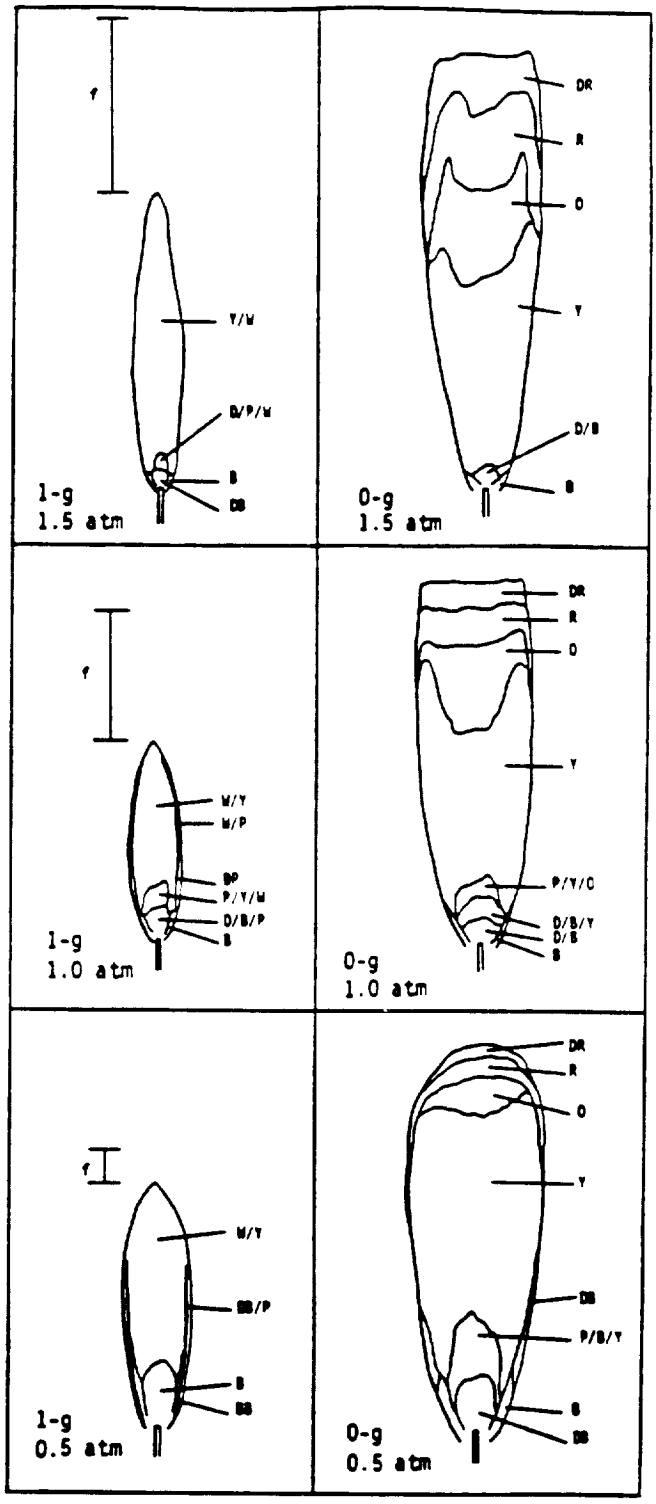

Fig. 12. Normal-gravity and microgravity flames of propane in air with nozzle diameter = 0.15 cm and fi Reynolds number = 98 (based on the nozzle radius). The various colors observed are as follows: B (blu BB (bright blue), D (dark), DB (dark blue), DP (dark pink), DR (dark red), O (orange), P (pink), R (re W (white), Y (yellow). The range of flicker (f) is also indicated for normal-gravity flames; scale: 1 cm, reproduced from [19].

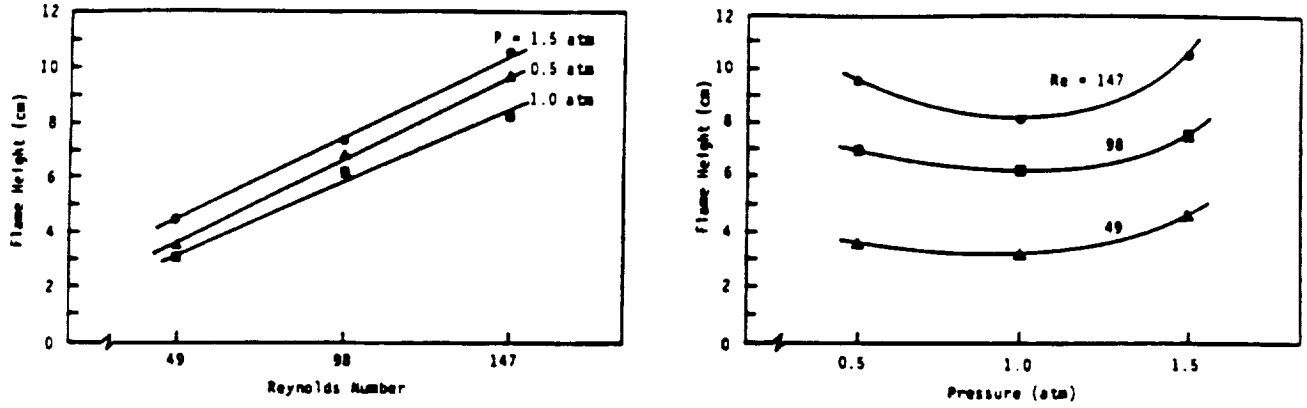

Fig. 13. Microgravity propane/air flame heights vs. pressure and fuel Reynolds number. The lines connect the data points; reproduced from [19].

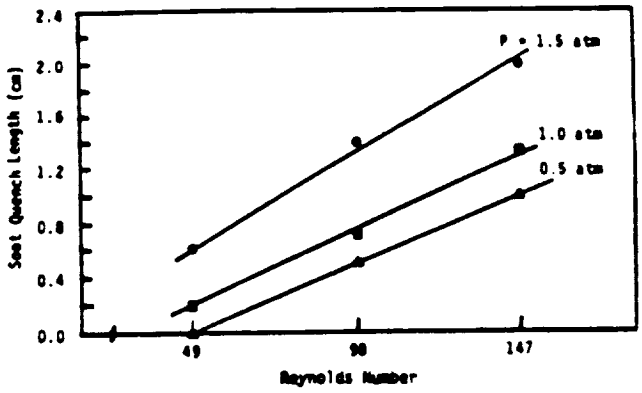

Fig. 14. Soot quench length (red region at the flame tip) vs. fuel Reynolds number as a function of pressure for microgravity propane-air flames. The lines connect the data points; reproduced from [19].

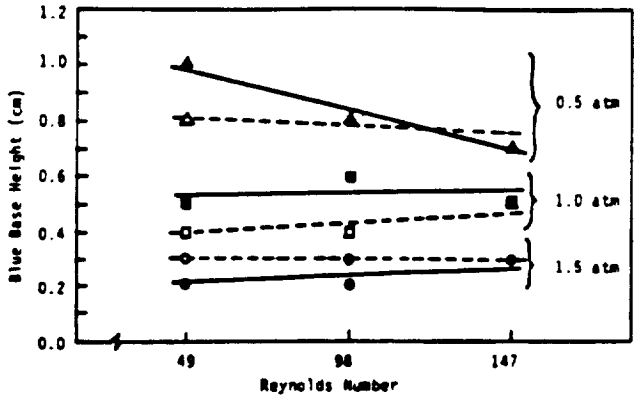

Fig. 15. Blue-base height vs. fuel Reynolds number at different pressures for normal-gravity flames (open symbols and dashed lines) and microgravity flames (closed symbols and solid lines). Whenever the normal-gravity and microgravity data coincide, only the microgravity symbol is used. The lines connect the data points; reproduced from [19].

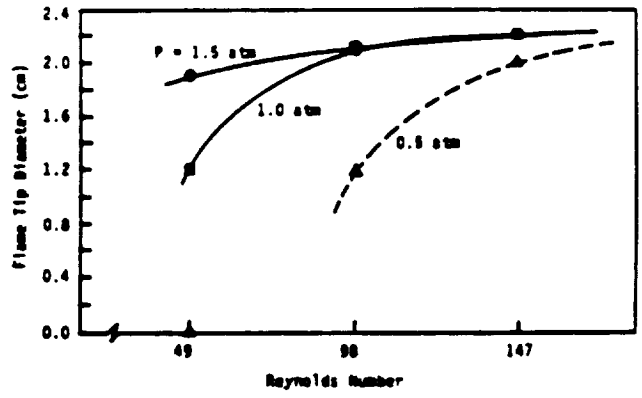

Fig. 16. Flame-tip diameter vs. fuel Reynolds number at different pressures for microgravity propane-air flames. The lines connect the data points. The broken line indicates uncertainty in connecting the data points due to the lack of information on Reynolds number at the onset of tip-opening; reproduced from [19].

soot, and hence, more emission in normal-gravity flames. In microgravity, as the pressure increases, the length of the yellow region decreases, but orange, red and dull red regions increase in length (see Figure 12), indicating that more soot has been formed.

The complex processes of fuel pyrolysis and soot formation, agglomeration and burn-off are all pressure-dependent. A pressure increase results in an increase in collision frequency of the particles, and hence, growth due to agglomeration. Also, collision frequency depends on the particle size, which is a determining factor in particle burn-off. But particle burn-off is oxygen-dependent. Therefore, there exist different, oxygen-dependent, competitive rates of fuel pyrolysis and particle agglomeration and burn-off, which suggest the importance of the relative effects of these rate processes. The competition between these rate processes may be responsible for the non-monotonic behavior of the flame height with pressure in both normal gravity [19] and microgravity (see Figure 13). It seems that there exists a pressure in the range 0.5 atm < P < 1.5 atm for any Reynolds number, at which the flame attains its minimum height due to the most efficient burning caused by the competing effects of oxygen availability, pressure, and the rate processes mentioned earlier. This phenomena is exacerbated by increasing Reynolds number. Hence, at low-enough Reynolds numbers, the flame heights may become equal regardless of pressure (see Figure 13).

(d) Radiation Measurements

Flame-radiation studies are being conducted in the 5.18-Second Zero-Gravity Facility for both methane and propane flames. In addition, normal-gravity counterparts of these flames are being studied simultaneously. Using a wide-view-angle, thermopile-detector radiometer, data is collected in terms of radiance (W/cm^2-sr). Figure 17 shows a typical set of data (in mV) for flame radiation in both normal-gravity and microgravity environments. The results have shown that radiative loss (in terms of radiance) is generally 6-10 times larger in microgravity. This is due to the larger flame size and extensive sooting. In addition, examination of the data shows that radiation does not reach steady state in 5 seconds of microgravity. This is apparently due to the accumulation and slow transport of combustion products in the vicinity of the flame. The luminous region does not appear to increase in size (from visualization). However, the diffusion of non-luminous hot gases in the surrounding causes the volume of the hot gas to increase, which is reflected through the continuous increase in radiation. This has a direct impact on the approach toward steady state in microgravity flames, indicating that reduced-gravity earthbound facilities do not provide enough time to obtain the true steady-state data.

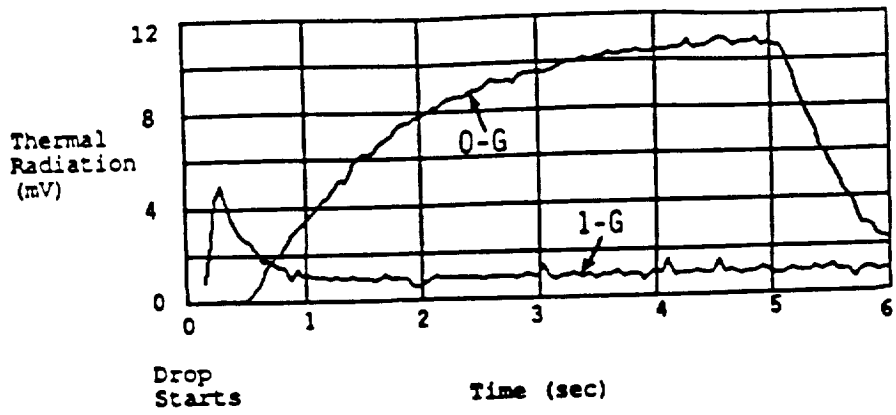

Fig. 17. Radiometer (thermopile detector) response from a propane flame burning in quiescent air at 1 atm under both normal-gravity and (5.18 sec.) microgravity conditions. The average radiance obtained from these tests (using the response between 4 sec. and 5 sec.) is 0.65 W/cm^2-sr for the normal-gravity flame and 5.32 W/cm^2-sr for the microgravity flame. Flame height = 5.0 cm (avg.) and 11.23 cm, and flame maximum diameter = 0.84 cm and 2.70 cm, for normal-gravity and microgravity flames, respectively; reproduced from [20]. Fuel-flow rate = 1.5 cm^3/s and nozzle radius = 0.0825 cm.

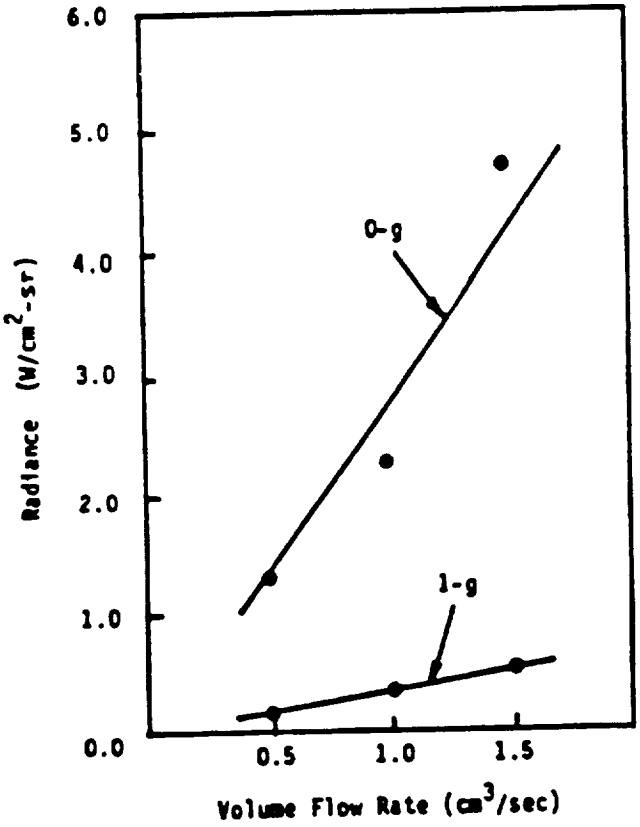

Fig. 18. Effect of fuel-flow rate on radiance from propane-air flames at 1 atm under both normal-gravity and microgravity conditions. The radiance data are the average values between 4.0 sec and 5.0 sec after ignition; reproduced from [20].

The data presented here is the first demonstration of flame-radiation measurement in microgravity environments. One important finding is that radiative loss may become a very crucial factor in radiative ignition in low-gravity environments, namely, a small fire may spread much more rapidly in microgravity because of the significantly higher levels of radiation. The data of Figure 18 support this argument. In normal gravity, a large fraction of heat release is removed rapidly via the convection of hot products of combustion, and therefore, does not contribute to the process of radiative loss from the flame zone. In microgravity, practically all of the released heat is accumulated around the flame through the combustion products, which causes radiative loss of up to an order of magnitude higher compared to normal gravity condition.

Pressure and oxygen concentration also show a very significant effect on radiative loss in microgravity. Figure 19 shows radiation from methane flames in both normal-gravity and microgravity environments under different conditions of pressure and oxygen content. The normal-gravity data show no sensitivity to the environmental condition, whereas radiation levels from microgravity flames are strongly affected by pressure and oxygen concentration. Figures 20 and 21 show these effects in more detail.

One interesting finding from the radiation data is that low-pressure/low-oxygen-concentration flames show near-steady-state radiation levels by the end of the available 5 seconds of microgravity, whereas high-pressure/high-oxygen-concentration flames show a continuous increase in radiative loss all the way to the end of the drop, indicating that 5 seconds of microgravity is not sufficient to obtain steady-state data in these flames. Figures 22 and 23 show the effects.

Figures 22 and 23 also show that the low-pressure/low-oxygen-concentration flames that are entirely blue (and therefore essentially soot-free), show appreciable amounts of radiation which would normally be associated with CO_2 and H_2O bands. Therefore, the radiation contribution from gas-phase combustion products is as important as that of soot in microgravity flames.

Figure 24 shows that even at 15% oxygen, a very faint, blue microgravity flame of methane still radiates appreciably. However, it is not obvious what longer test times would show for these very weak flames.

(e) Temperature Measurements

Quantitative data including the temperature field (using a fixed rake of nine thermocouples) have also been obtained in the 5.18-Second Zero-Gravity Facility for methane and propane

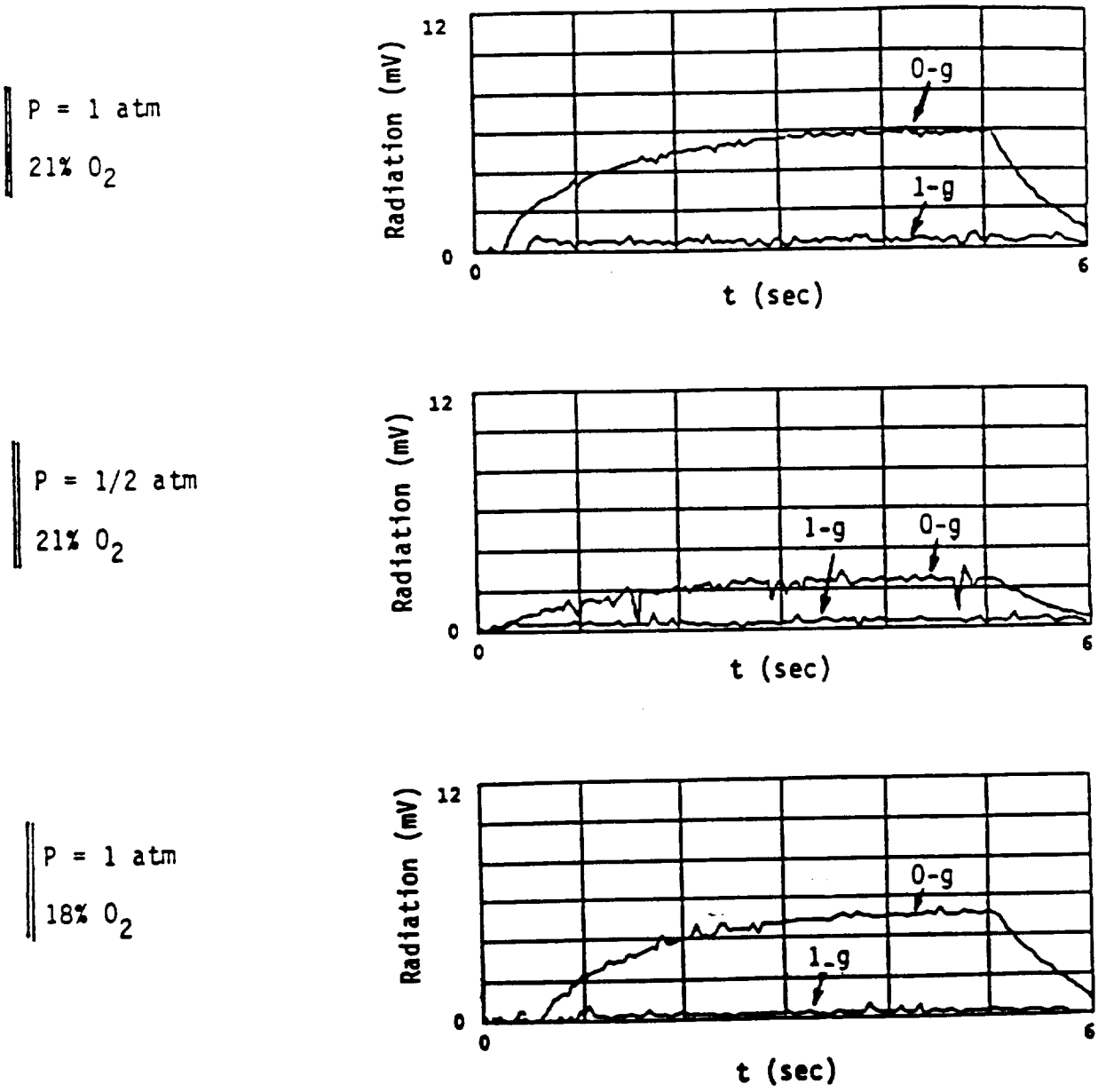

Fig. 19. Effects of pressure and oxygen concentration on radiative loss from methane flames under both normal-gravity and microgravity conditions. Here, fuel-flow rate = 3.0 cm^3/s, and nozzle radius = 0.0825 cm.

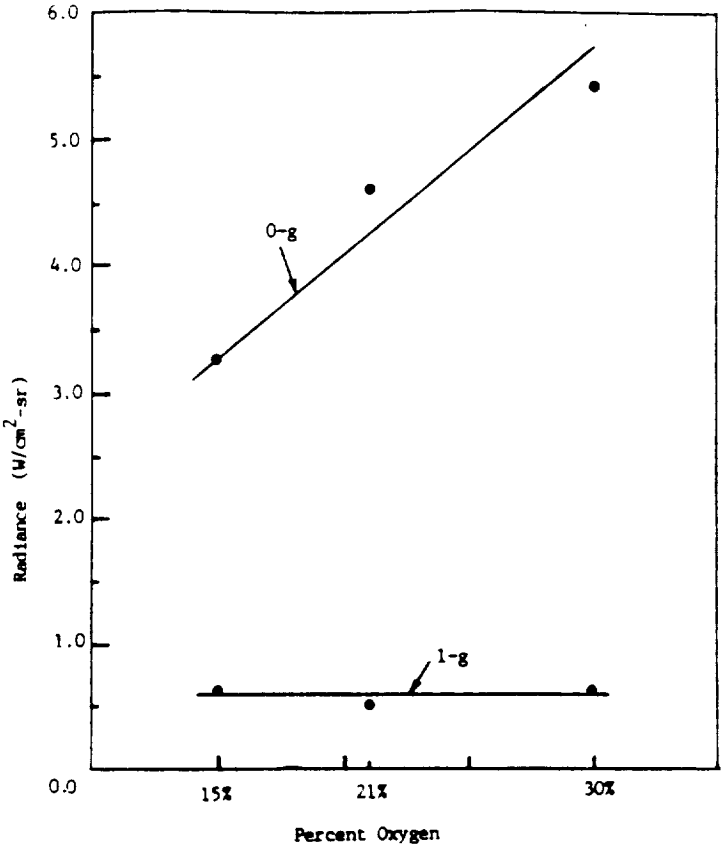

Fig. 20. Effects of oxygen concentration on radiative loss from propane flames. Here, P = 1 atm, fuel volume flow rate = 1.5 cm^3/sec, and nozzle radius = 0.0825 cm.

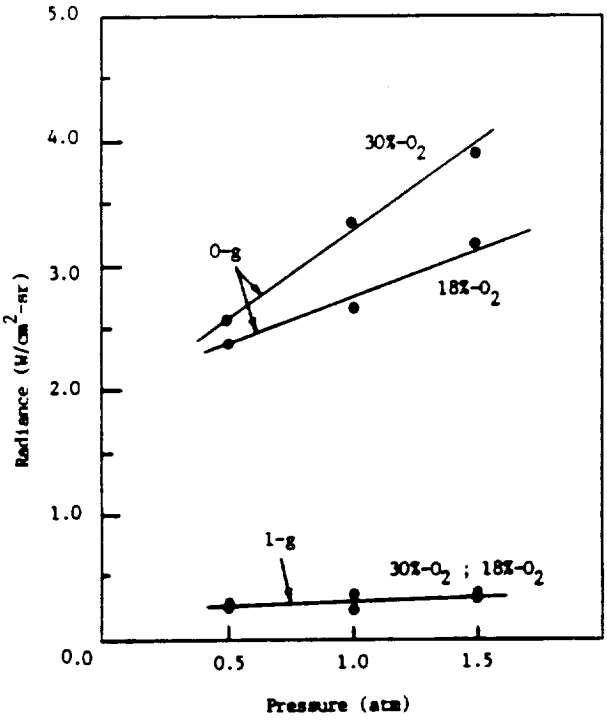

Fig. 21. Effects of oxygen concentration and pressure on radiative loss from methane flames at a fixed fuel mass flow rate corresponding to 3.0 cm^3/sec at 1 atm; nozzle radius = 0.0825 cm.

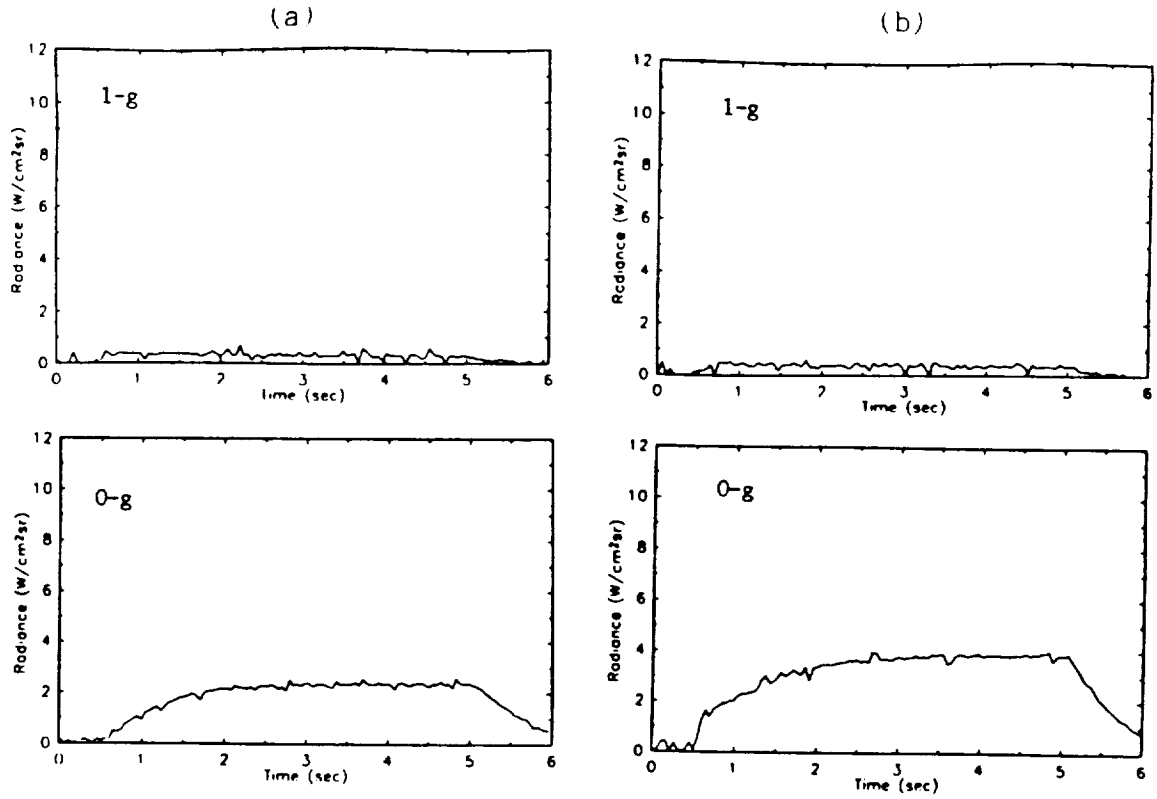

Fig. 22. Radiation from normal-gravity and microgravity flames of methane burning in (a) 0.5-atm, 18%-O_2, and (b) 1.5 atm, 30%-O_2 environments. The fuel mass-flow rate is fixed corresponding to 3.0 cm^3/sec under atmospheric condition; nozzle radius = 0.0825 cm.

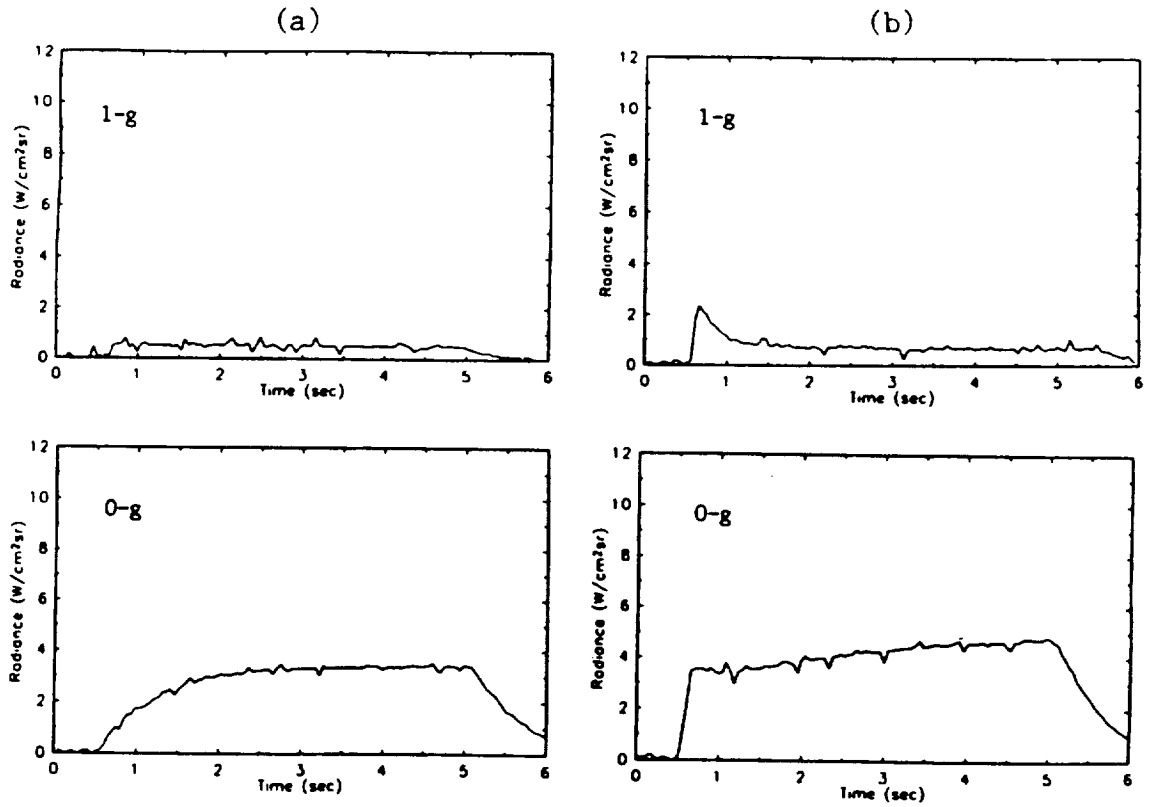

Fig. 23. Radiation from normal-gravity and microgravity propane flames in (a) 0.5-atm, 18%-O_2, and (b) 1.5 atm, 30%-O_2 environments. The fuel mass-flow rate is fixed corresponding to 1.5 cm^3/sec under atmospheric condition; nozzle radius = 0.0825 cm.

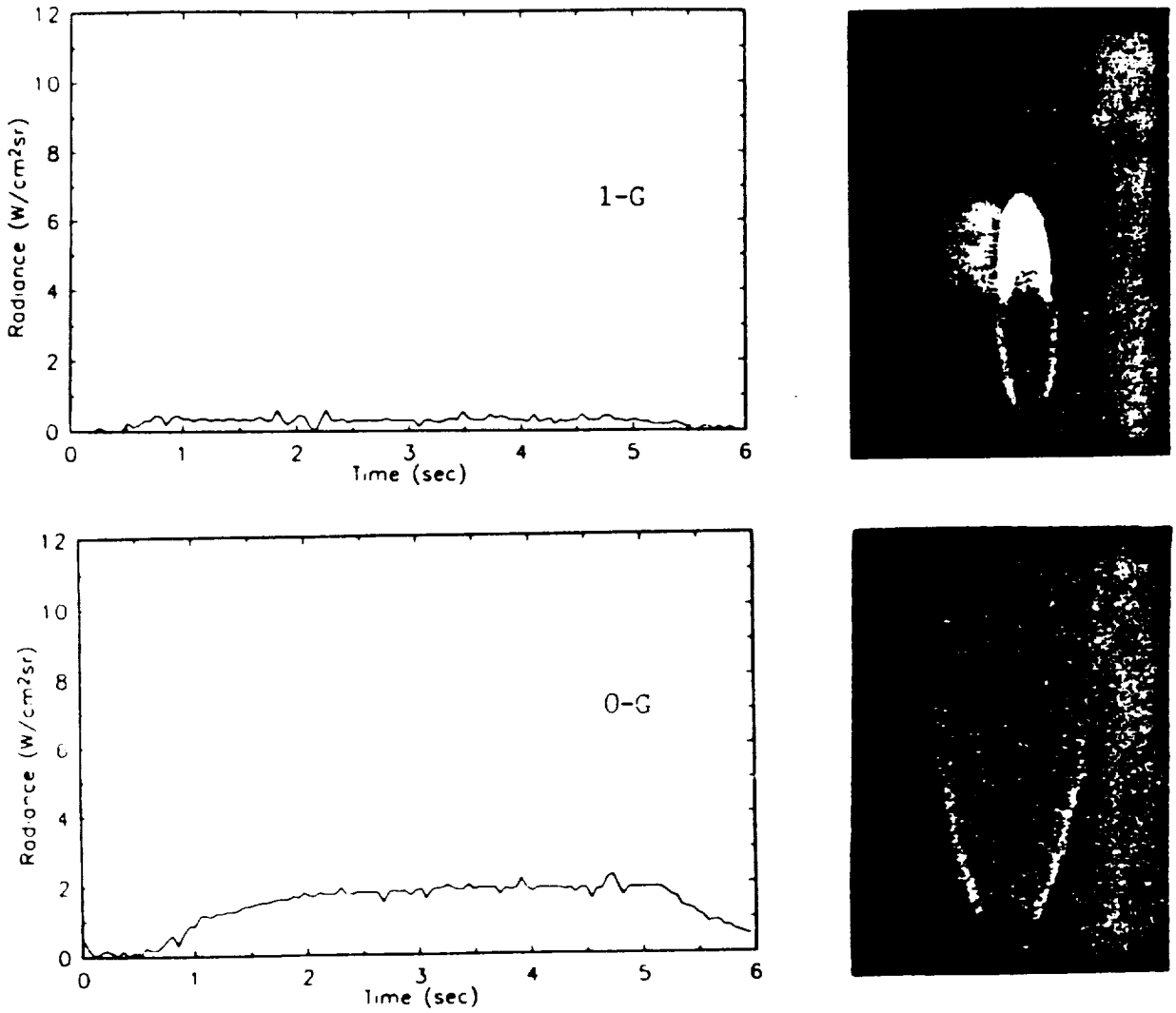

Fig. 24. Flame radiation for both normal-gravity and microgravity flames of methane (shown in the photographs) at 0.5 atm and 15% oxygen; nozzle radius = 0.0825 cm; mass-flow rate corresponds to 3.0 cm^3/sec under atmospheric condition. Reproduction has changed yellow to white, and has reduced the intensity and length of the blue flame.

diffusion flames burning in quiescent oxidizing environments of various pressure and oxygen concentrations.

Figure 25 shows the size, shape, and color of some of the flames studied in addition to the position of the thermocouple rake with respect to the flame. The microgravity flames shown in this figure correspond to the shapes and colors observed just prior to the deceleration of the package.

Figure 26 shows a typical set of temperature data for the propane flame burning in 19%-O_2/ 81%-N_2 environment at 1 atm, under both normal-gravity and microgravity conditions. The lowest row of thermocouples is 10 cm above the nozzle tip. An initial overshoot in temperature is observed in both cases due to the presence of excess fuel at ignition. This figure presents some useful information not only in relation to the temperature field, but also for other flame characteristics. The normal-gravity data show that the temperature drops quickly to the ambient somewhere between the radial locations of 0.75 and 2.75 cm. This is due to the effect of buoyant force which carries and removes the combustion products in a narrow column determined by the maximum flame radius. In addition, the strong buoyancy-driven portion of the flame causes the three thermocouples near the centerline to show roughly equal temperatures, which essentially reach steady state approximately 3 seconds after the start of the experiment.

The data presented in Figure 26 for microgravity flames show that far above and away from the flame, the gas is still experiencing a temperature rise due to the continuous release of the combustion products in the vicinity of the flame and their subsequent diffusion. This figure also shows that the gas temperature does not reach a steady value anywhere in the field during the 5 seconds of microgravity, again due to the continuous dilution and heating of the environment caused by the combustion products. In addition, large temperature gradients exist in the axial direction for the microgravity flame, and the variation of temperature in the radial direction is significant all the way to the far field.

Figure 27 shows the temperature data at $t \simeq 5$ seconds as a function of the axial location of the thermocouples for fixed radial locations. Both normal-gravity and microgravity data are shown in this figure. All of the normal-gravity data indicate that the second and third columns of thermocouples (see Figure 25) register a temperature of 300 K. The first column (closest to the centerline) shows a constant and small decrease in temperature with an increase in height for more diffuse flame due to the lower pressure. The microgravity flames A and B of Figure 27 show almost identical temperature distributions. Significant differences in temperature levels are

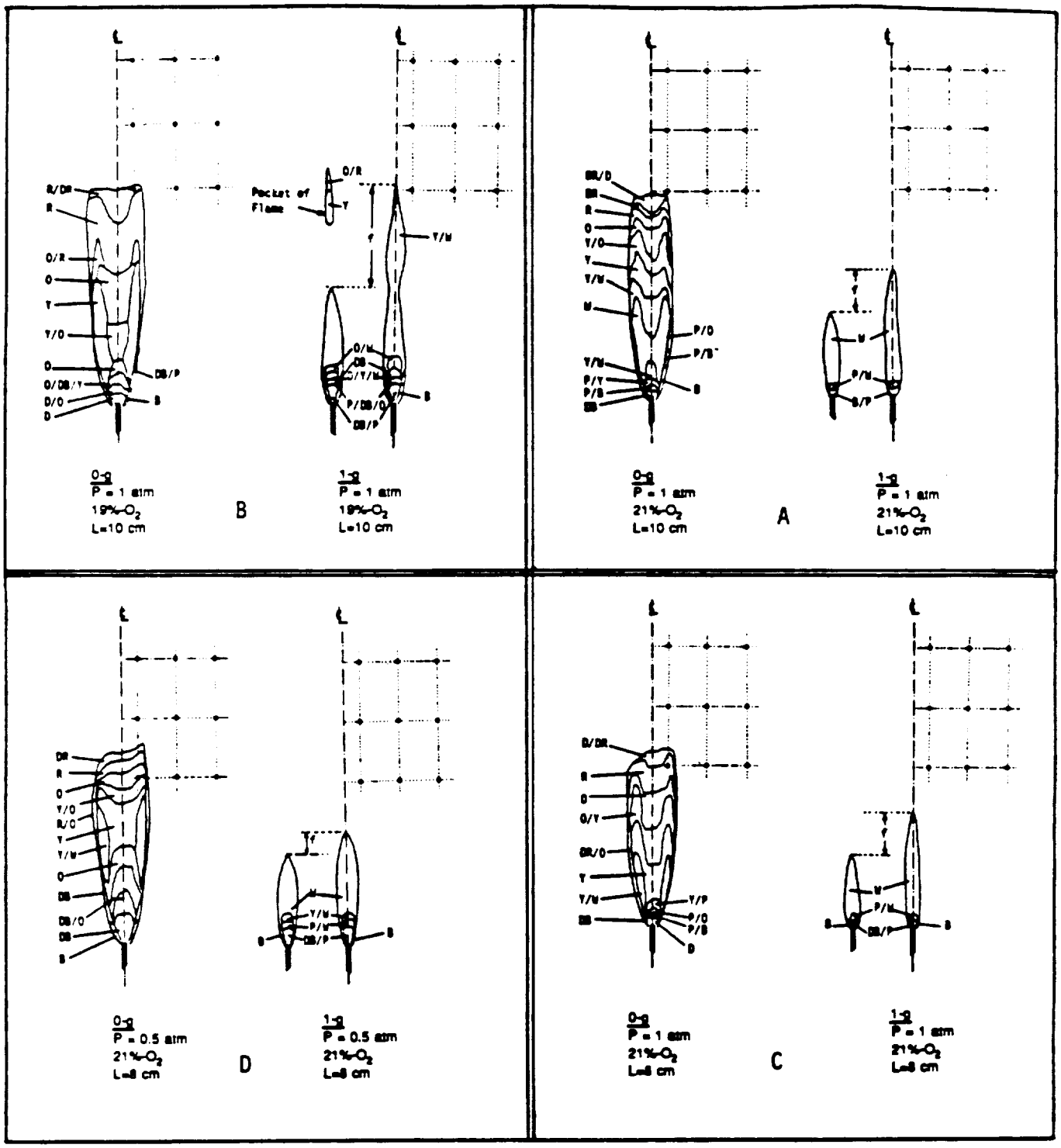

Fig. 25. Flames of propane at 1.5 cm^3/sec for both normal-gravity and microgravity conditions. The colors are as follows: B (blue), D (dark), DB (dark blue), DR (dull red), O (orange), P (pink), R (red), W (white), Y (yellow). The flicker range, f, is shown for the normal-gravity flames. L is the distance between the nozzle tip and the lowest row of thermocouples. The columns of thermocouples are, respectively, 0.75 cm away from the centerline, and then 2 cm apart. The rows of thermocouples are 3 cm apart. These diagrams are to scale; reproduced from [21].

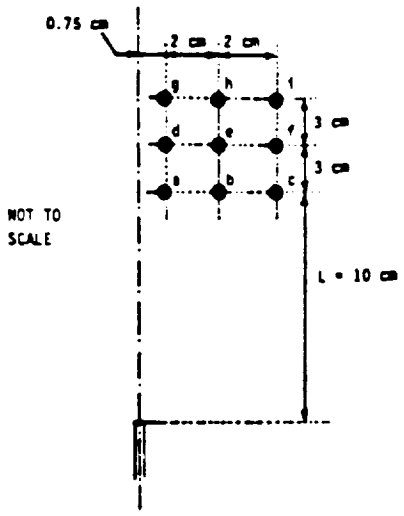

Propane - 19% O_2 Flame
Flow Rate = 1.5 cc/s
Nozzle Radius = 0.0825 cm
P = 1 atm

See Fig. 25(B).

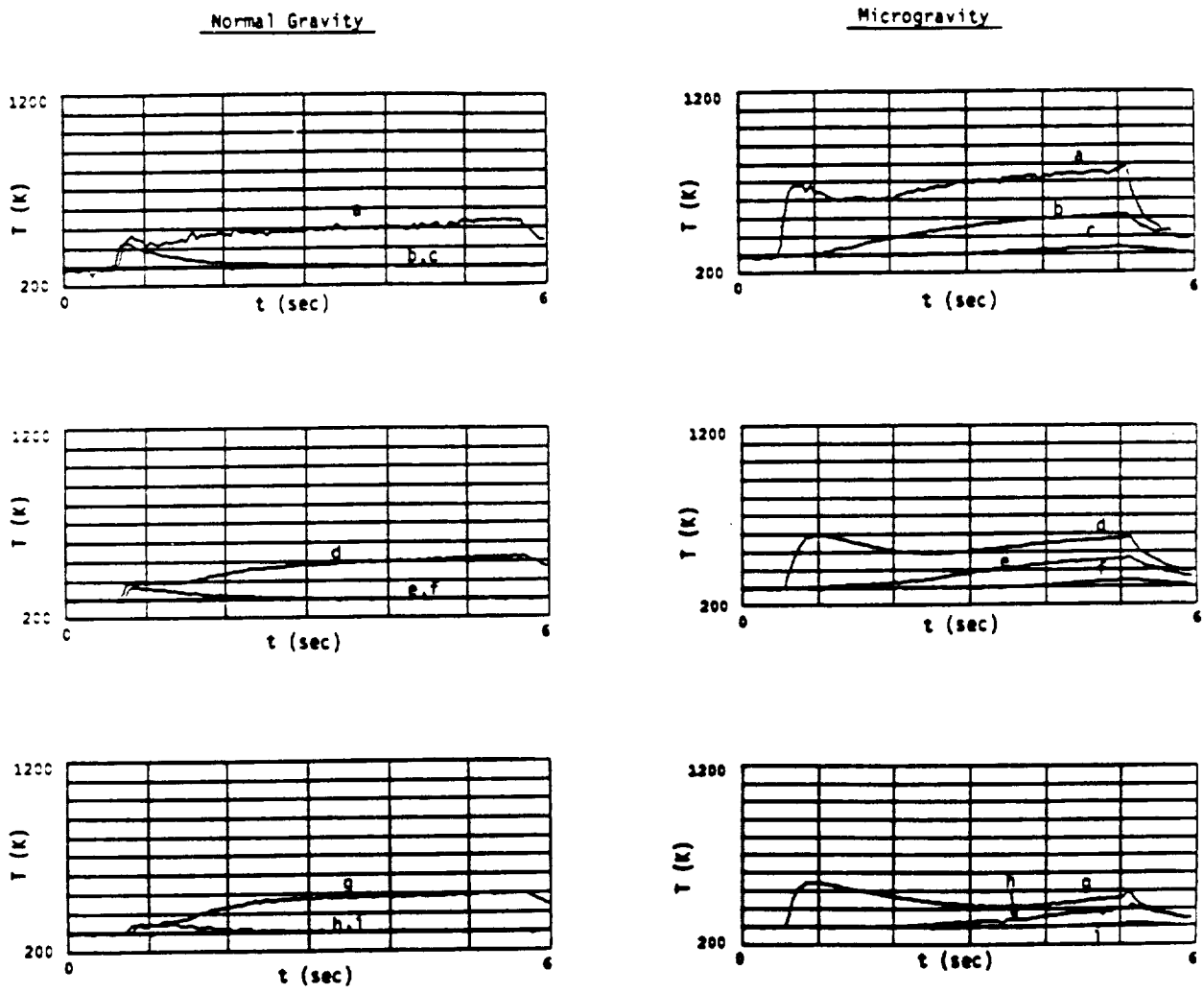

Fig. 26. Typical temperature data for a normal-gravity and microgravity flame; reproduced from [21].

observed between microgravity flames C and D, with the 0.5-atm flame being taller and wider. The combination of larger flame size and reduced pressure is responsible for this behavior.

Figure 28 shows the temperature data as a function of the radial location of the thermocouples for fixed axial locations in the microgravity flames. The normal-gravity data is not presented in this figure, since the temperature drops to ambient somewhere between the first two columns of thermocouples. Due to the uncertainty in the monotonic behavior of temperature between the first and second thermocouples of the lowest row, the plots have not been extended to the temperature at the first thermocouple. It is possible that there is a peak in temperature between the innermost thermocouples due to the presence of the flame zone, especially for flames C and D.

The temperature data, which like radiation-measurement results, are the first demonstration of the ability to map the far field in a microgravity combustion study, do not only provide quantitative data for comparison with the predictions, but also are a means of gaining insight into the characteristics of flames in addition to their behavior in microgravity environments. The data presented here show that 5 seconds of microgravity are not sufficient to obtain information on the flame structure, since the thermal field is continuously changing, at least in the available time of five seconds. In addition, the data suffers from the lack of capability to obtain a map of the near-field temperatures including the flame front. Longer test times provided by a space experiment would allow the complete mapping of the temperature field.

(f) Predictions

The mathematical model of [10] is under modification to obtain solutions for laminar jet diffusion flames. The approach involves a finite-difference solution of the partial differential equations for mass, momentum, elements, and energy, which are in their boundary-layer form. The effects included are diffusion, viscosity, inertia, kinetics, gravity, and radiation. The current chemistry assumed is that of shifting equilibrium.

In this axisymmetric, steady-state, vertical laminar-jet configuration, the fuel is injected at a finite velocity into the quiescent surroundings. The effects upon the velocity field are shear or molecular diffusion of momentum, pressure gradient, and gravity. The buoyant force is a combination of gravity and pressure gradient. In the vertical-jet problem, convection of energy, heat release rate, heat conduction, and the energy transported due to diffusion of species affect the temperature field through the velocity field and the concentration field. The concentration field is, in turn, affected by the convection of species through the flow and therefore by the velocity field.

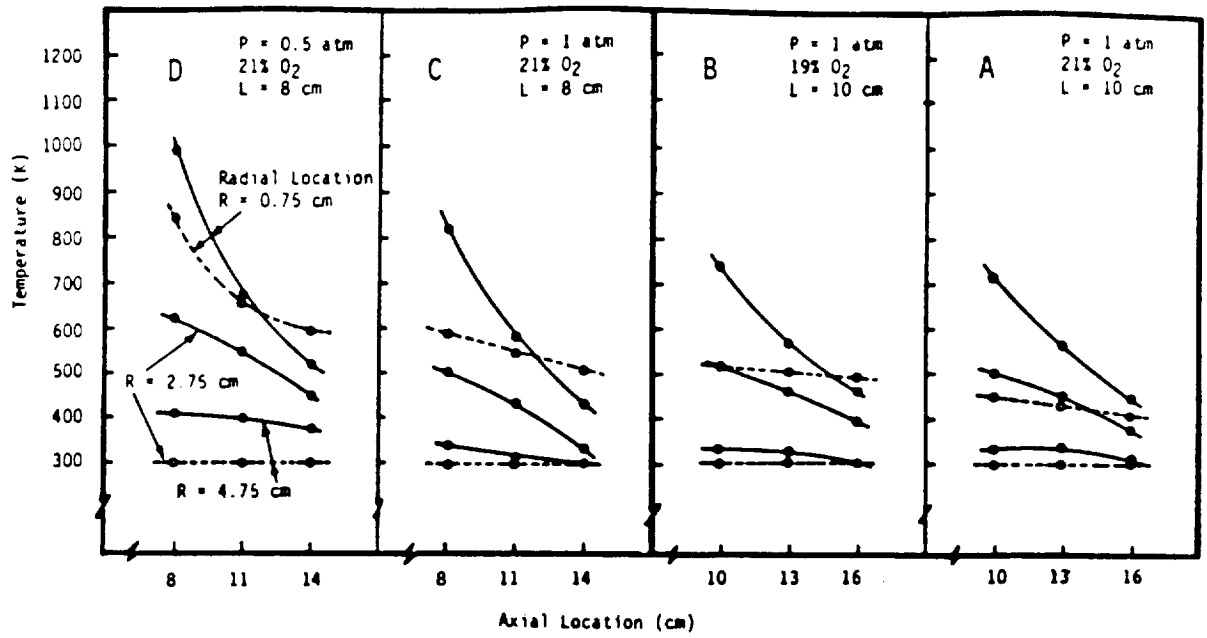

Fig. 27. Temperature plots as a function of the axial location of thermocouples for both normal-gravity (open symbols and dashed lines) and microgravity (closed symbols and solid lines) flames of propane with a volume flow rate of 1.5 cm^3/sec. L is the distance between the nozzle tip and the lowest row of thermocouples. The radial locations indicated in the diagram are applicable to all plots; reproduced from [21].

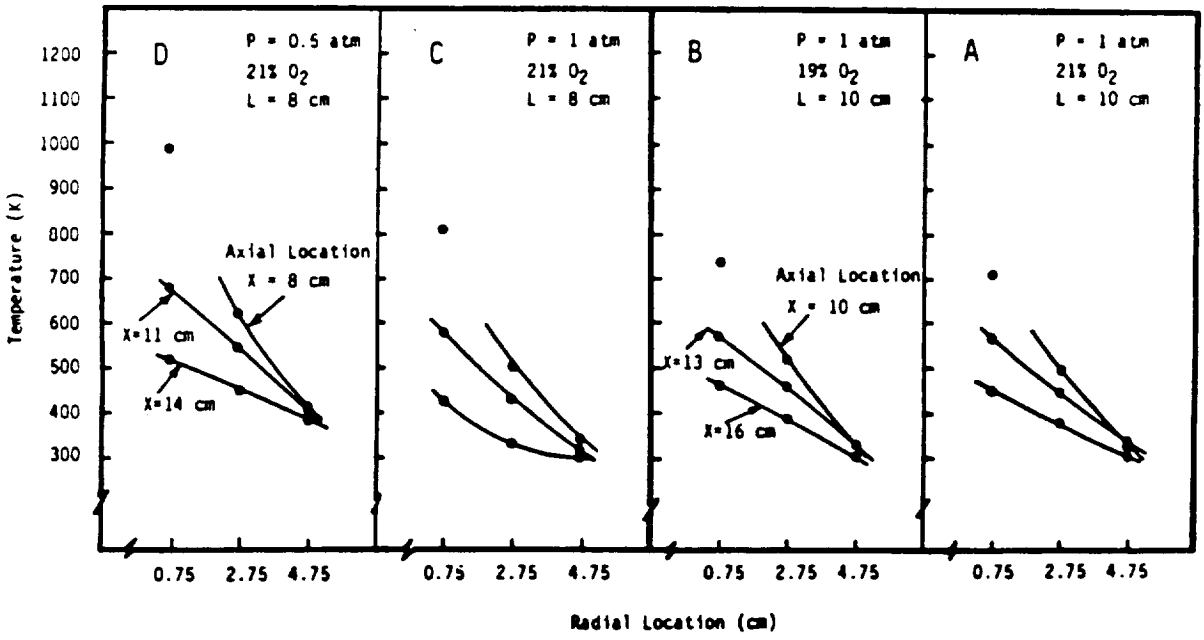

Fig. 28. Temperature plots as a function of the radial location of thermocouples for microgravity flames of propane with a volume flow rate of 1.5 cm^3/sec. L is the distance between the nozzle tip and the lowest row of thermocouples. The axial locations indicated in the diagram are applicable to those of the same family (i.e., same L). The incomplete plots indicate the presence of flame between the two columns of thermocouples; reproduced from [21].

Chemical production rate and diffusion are the mechanisms which directly cause changes in the species field. The diffusional gradients produce an air/fuel ratio distribution ranging from fuel rich to fuel lean in the mixing region. The surface upon which the equivalence ratio is unity is referred to as the "flame front", which corresponds to the maximum temperature. The assumptions made are: (a) diffusive processes are important only in the radial direction, (b) combustion is diffusion-controlled, and (c) flow is steady and axisymmetric. The equations of continuity, momentum, diffusion of elements, and energy are nondimensionalized with respect to the state of the flow at the maximum flame width point. The equations of state are used to complete the analysis, and radiation has recently been incorporated to include water and carbon-dioxide contributions via the approximation of optically thin medium.

The governing flow-field conservation equations are transformed into the von Mises plane, which eliminates the global continuity equation, and then solved numerically by employing an explicit finite-difference technique. The details of the flow field, i.e., velocity, temperature, and species fields along with the gross characteristics including combustion lengths and flow deflections are obtained by the solution of the system of conservation equations.

The model is currently being modified to incorporate the effects of: (a) soot formation and burn-off, (b) radiation from soot in addition to gas-phase radiation by incorporating the radiative-transfer equation in the formulation, (c) thermophoretic effects, which become significant in microgravity, (d) quasi-global kinetics, (e) multi-component diffusion in the presence of soot, and (f) elliptic effects due to the significance of axial diffusion in microgravity.

Experimental results have revealed the non-uniform heat-release mechanism throughout the flow field; partial combustion and soot formation dominate in the near-jet region, while the soot burn-off process is facilitated downstream due to increased residence time and continued heating. The kinetics of the combustion process under microgravity conditions significantly influence the accuracy of the predictions as can be seen in Figure 29, which shows the effect of heat release on flame shape and its comparison with the experimental data. The partial oxidation analysis shows smaller flame radii and shorter flame lengths. Further results are compared with the experimental data in Figure 30; they show substantially improved agreement with respect to the results obtained assuming complete combustion model. This confirms the potential role of chemical kinetics in microgravity flames.

Figures 31-33 show other examples of application of the model, where predicted micro-gravity flame heights are compared with experimental data [11]. A satisfactory trend in the

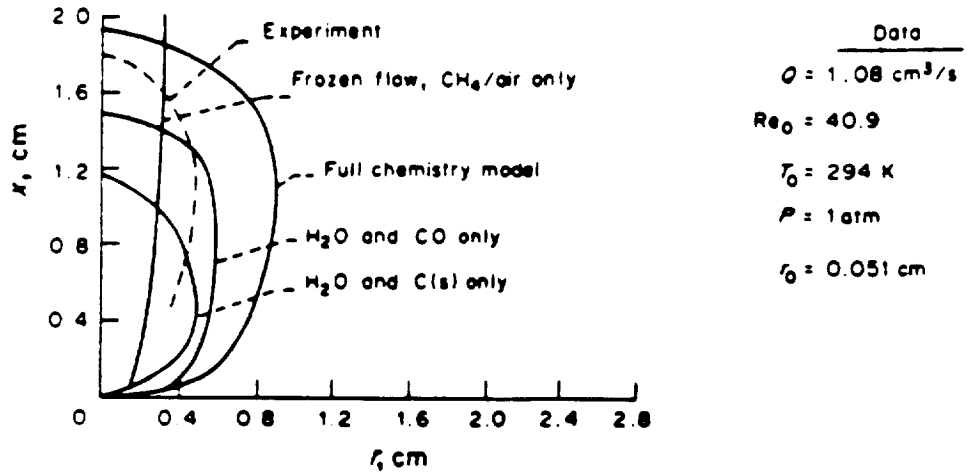

Fig. 29. Effect of chemistry model upon analytical prediction of a steady-state zero-gravity methane-air flame; reproduced from [10]. The experimental data were obtained from [15].

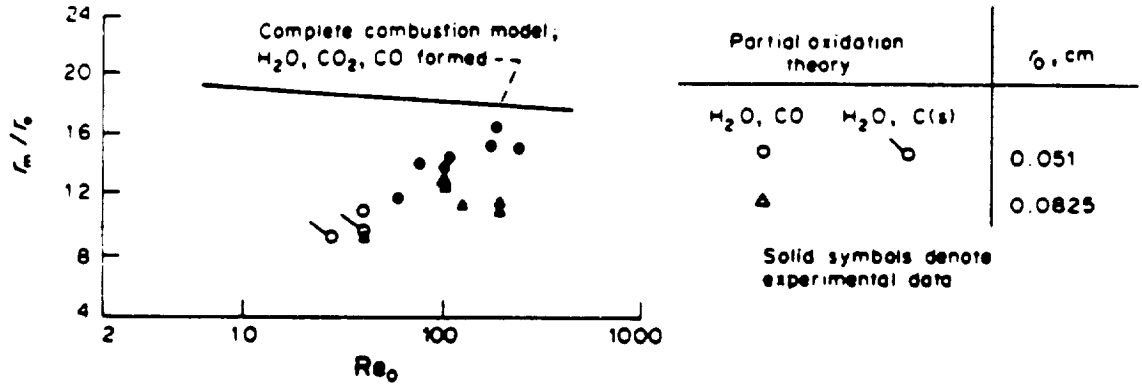

Fig. 30. Comparison of theoretical model with experimental zero-gravity flame widths in ambient methane-air flames, as a function of fuel Reynolds number; reproduced from [10]. The experimental data were obtained from [15].

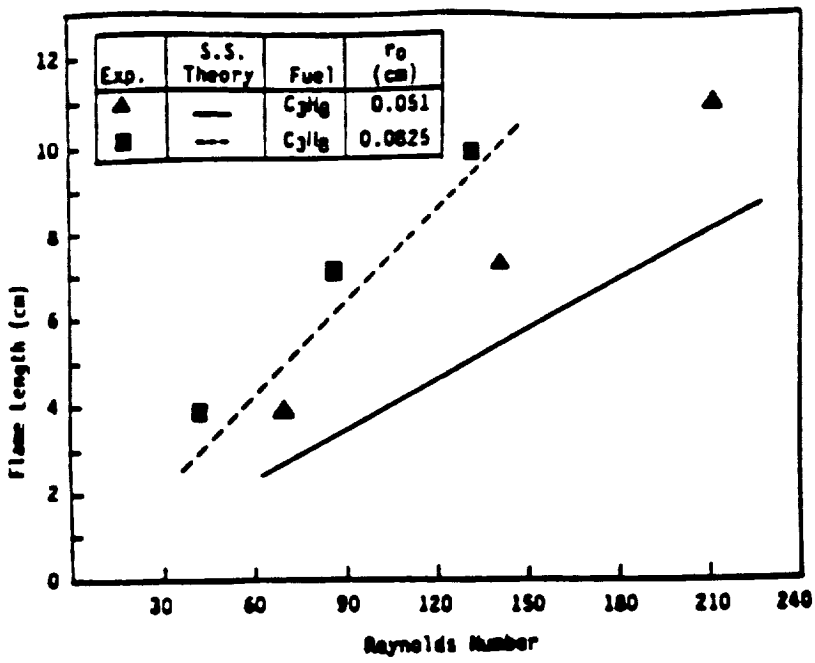

Fig. 31. Predicted and measured microgravity propane-air flame heights at 1 atm vs. jet Reynolds number; reproduced from [11].

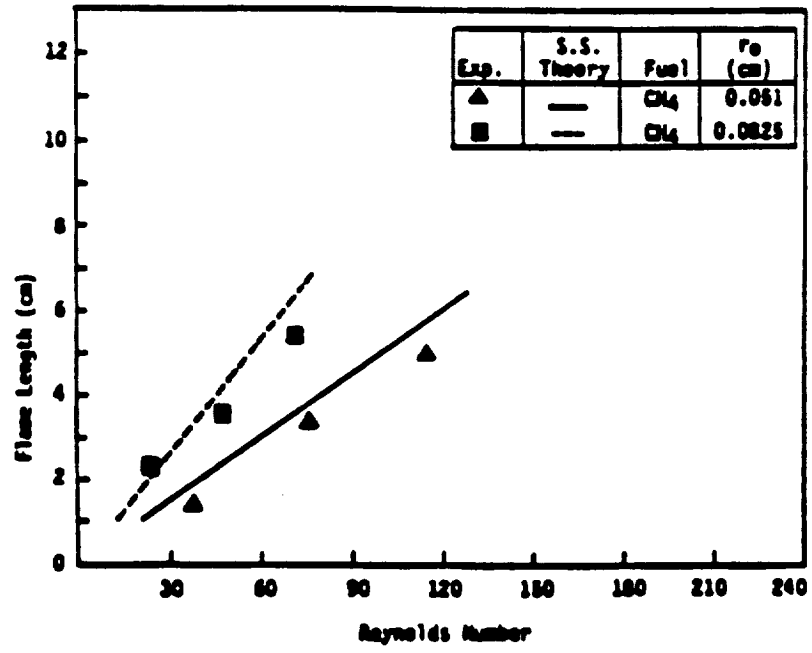

Fig. 32. Predicted and measured microgravity methane-air flame heights at 1 atm vs. jet Reynolds number; reproduced from [11].

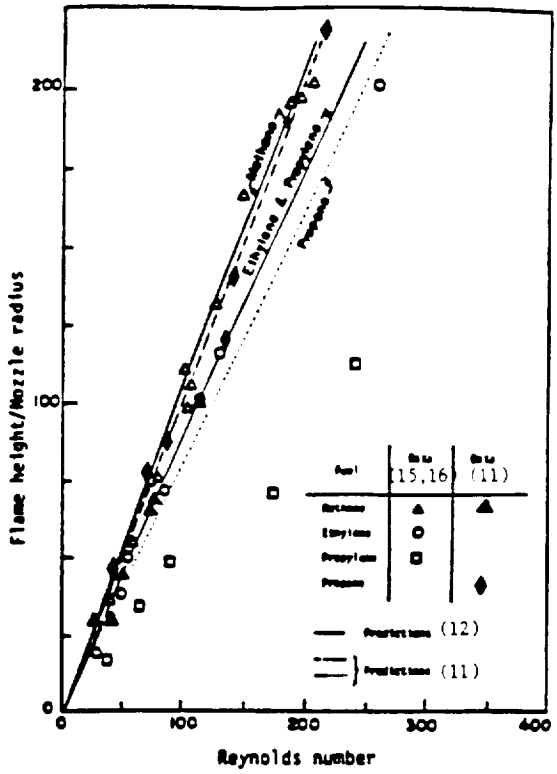

Fig. 33. Measured and predicted microgravity flame heights for different fuels burning in air at 1 atm; reproduced from [11].

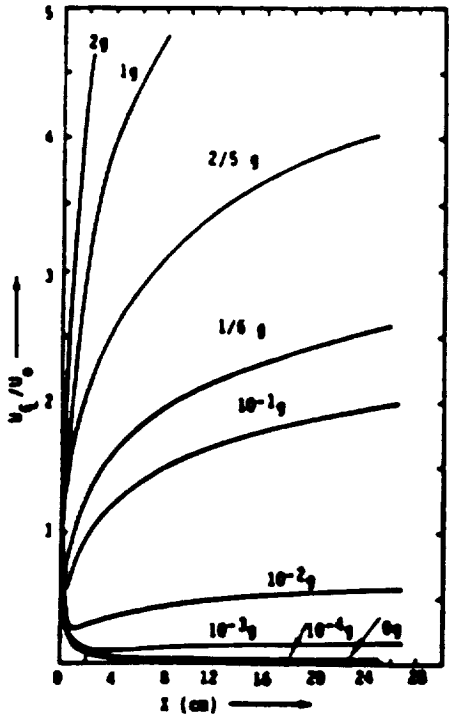

Fig. 34. Predicted non-dimensional centerline velocity (with respect to jet exit velocity) vs. axial distance along the jet as a function of gravitational level; methane-air flames, nozzle radius = 0.0825 cm, fuel-flow rate = 1.0 cc/sec, pressure = 1.0 atm, and jet exit velocity = 46.8 cm/sec; reproduced from [1].

behavior of the flames is demonstrated. However, the propane flames (Figure 31) are slightly longer and the methane flames (Figure 32) are shorter than the predicted flames. One explanation is the absence of soot and associated radiation in the model in contrast to the high concentrations of soot observed in most of the microgravity flames. In addition, the absence of elliptic effects (axial diffusion) and the relatively simple predictions for the molecular transport rates (i.e., species, momentum, and energy) may contribute to the differences between the predicted and measured flame heights.

Figure 33 shows a comparison between different theoretical and experimental results. The data points correspond to the steady-state flame heights of [11], [15], and [16]. The predictions are those presented in Figures 31 and 32 as well as the results of another theoretical modeling effort [12]. The two numerical models show a good agreement with each other and with the data. The propylene flame heights of the previous studies [15] do not agree with the predictions of [12]. This is surprising since propylene and propane are very close in chemical structure, and satisfactory agreement has been obtained for methane, ethylene, and propane. However, the present study does not deal with highly sooting fuels such as propylene and ethylene.

Application of this model to a family of methane flames under different gravitational levels shows the important role of convective effects (Figure 34). It can be seen that centerline velocity does not play a major role in diffusion flames under gravitational accelerations of $<10^{-3}$ g.

(g) Summary of Observations and Conclusions

- Flames in microgravity are taller, wider, sootier, and more diffuse than their normal-gravity counterparts.
- Low-pressure and/or low-oxygen-concentration flames in microgravity are entirely blue, unlike those in normal gravity.
- High-pressure and/or high-oxygen-concentration flames show massive sooting in microgravity.
- Flame-tip opening (underventilated-like behavior) has been observed in all of the microgravity propane flames studied to date.
- Most of the methane flames do not have open tips in microgravity.
- Radiative loss for all of the normal-gravity flames studied falls in the range of 0.0-1.0 W/cm^2-sr.

- Microgravity flames show a radiance of 6-10 times larger than those in normal gravity.
- Faint, blue flames of low-oxygen/low-pressure environments show appreciable amount of radiative loss compared to their normal-gravity counterparts.
- Pressure and oxygen concentration have a significant effect on radiation from microgravity flames, but not from normal-gravity flames.
- Radiation does reach near-steady state for low-oxygen/low-pressure flames in microgravity, however, other flames show a continuous rise in radiative loss during the 5 seconds of microgravity.
- Continuous change in color with time is observed for atmospheric-pressure, low-oxygen-concentration flames in microgravity; the color is blue at the beginning of the test followed by a steady buildup of red inside the flame up to the 5 seconds of the available test time.
- Appreciable temperature rise has been measured in the far-field of microgravity flames.
- Much steeper temperature gradients exist along the flame centerline in microgravity due to the lack of buoyancy.
- Temperature data do not show an approach toward steady state in 5 seconds of microgravity.

Of these observations, the most significant is the effects that pressure, oxygen concentration, and fuel type have on microgravity flames in contrast to the effects of these parameters on their normal-gravity counterparts, and that thermophoretic effects, diffusive processes, radiative loss, soot formation and oxidation, and gas-phase kinetics are critical to the description of these microgravity flames.

Based on this conclusion, the specific objectives for the continued work have been defined.

IV. OBJECTIVES

The overall objective of this program is to study the effects of pressure, oxygen concentration, and fuel type on the characteristics and structure of laminar gas-jet diffusion flames in the absence of buoyancy.

As described in detail in the previous section, the data from recent ground-based experiments have enhanced our understanding of laminar diffusion flames in microgravity

environments. However, unexpected characteristics have also been observed, raising new questions on transport processes in diffusion flames in the absence of buoyancy.

The questions that need to be answered are:

(a) What are the steady-state characteristics of the microgravity flame, and given enough time, do the weak flames extinguish by virtue of their size, radiative loss, and associated transport processes?

(b) Why does the removal of buoyancy result in underventilated-like behavior in some otherwise overventilated diffusion flames?

(c) Why does microgravity flame length vary nonmonotonically with pressure, and what are the roles of buoyancy and oxygen concentration in defining this behavior?

(d) Why are sooting characteristics sensitive to oxygen concentration in microgravity flames?

V. HYPOTHESES AND DATA REQUIREMENTS

This section discusses hypotheses for each of the questions raised in the prior objectives section, and identifies the data required to validate the hypotheses.

(a) What are the steady-state characteristics of the microgravity flame, and given enough time, do the weak flames extinguish by virtue of their size, radiative loss, and associated transport processes?

Hypothesis: The continuous release and slow transport of the combustion products creates a transient field in the vicinity of the flame during the early stages of burning (as is evident from the 5-second microgravity tests). However, a quasi-equilibrium state can be reached for both temperature and species fields, such that the flame approaches steady state, and the far field will not have an effect on the near-field (of the flame). This quasi-steady-state will persist for a period of time, and will then be followed by a transient state, in which oxygen arrival to the flame becomes more difficult, and the flame starts its transient approach toward extinction. On the other hand, for the weak microgravity flames of low-oxygen-concentration/low-pressure environments, there are two possibilities. The first is that radiative loss cannot compete with the heat release and consequent increase in temperature of the near-field region of the flame, again, resulting from the slow transport of the combustion products. In this case, given enough time, the flame may behave like the 18%-O_2,

1-atm flame (see Section III) resulting in the formation and subsequent glowing of soot, and leading to a bright, sooty flame. However, the second possibility is that the heat loss by radiation exceeds the heat input to the near-field, and the flame becomes incapable of sustaining combustion, undergoing a rather slow extinction process.

(b) Why does the removal of buoyancy result in underventilated-like behavior in some otherwise overventilated diffusion flames?

Hypothesis: The removal of buoyancy increases the residence time available for soot formation within the flame zone. This increased residence time augments the pyrolysis of the fuel, leading to increased soot nuclei and growth. Larger soot and more soot formation result in slower oxidation and persistence of the soot. All of the soot is formed within the flame, and these larger particles (unlike gas-phase species) virtually do not diffuse. But these particles being inside the flame, are forced to move toward the flame centerline through the process of thermophoresis which is caused by temperature gradient. As a result, the particles core up and stay within a column defined by the width of the flame at its open tip, impede oxygen transport to the center of the flame, and prevent the flame from closing on its axis. It is interesting to note that microgravity methane flames do not show this underventilated-like behavior, whereas all of the propane flames studied to date (except very small flames, ~1-2 cm in height) have open tips.

(c) Why does microgravity flame length vary nonmonotonically with pressure, and what are the roles of buoyancy and oxygen concentration in defining this behavior?

Hypothesis: The observed increase in length with pressure is due to increasing amounts of glowing and burning soot rather than a change in the gas-phase flame height. At low pressures, kinetics effects tend to lengthen the apparent gas-phase flame zone. As the pressure increases, reaction rate increases and flame length decreases. As the pressure is increased further, soot levels increase, and this heated, glowing and burning soot persists beyond the gas-phase flame front. This gives the indication (through direct photography) of an apparent longer flame. Although the normal-gravity counterparts of these flames show the same non-monotonic behavior for (the average between minimum and maximum flickering) flame height, no conclusive information can be obtained from these normal-gravity flames. The reason is the high degree of flicker, in addition to the (generally) continuous decrease in

maximum flame height with increase in pressure and the non-monotonic behavior of the minimum flame height as a function of pressure [19]. However, the microgravity flames are flicker-free, and provide the opportunity to substantiate the above hypothesis in relation to this non-monotonic flame-height behavior.

(d) Why are sooting characteristics sensitive to oxygen concentration in microgravity flames?

Hypothesis: The microgravity environment provides longer residence times, resulting in prolific sooting. Higher concentrations of oxygen facilitate the burning of soot, causing higher temperatures. On the other hand, lower oxygen concentrations produce relatively cooler flames, reduced pyrolysis and soot formation, and reduced heat and mass transfer. The competing effects of increased residence time and relative transport rates of mass and heat due to Schmidt-number and Lewis-number effects will enhance the influence of oxygen concentration on these processes.

To substantiate the hypotheses presented in this section, certain measurements are critical. These measurements are referred to as "required" measurements in the following discussion. In addition, there are measurements which greatly enhance the science return of this experiment, and each one helps in further validation of one or more of the hypotheses. These measurements are referred to as "desired" measurements.

The following measurements are "required" for this experiment:

(i) Temperature Field – Mapping of the temperature field is required for hypotheses (a), (b), (c), and (d). The temperature field must be defined because it is essential to fuel pyrolysis and thermophoretic transport of the soot particles. In addition, regions of soot quenching, exact flame location, far-field temperature map, and quantitative approach to steady-state flame characteristics will be obtained through temperature measurements. Also, understanding of the degree of completion of combustion and quantification of the radiative transfer of energy out of the flame will be accomplished by mapping the temperature field. When combined with the "desired" measurements for species field and soot size and concentration, the temperature field provides a map of effective emissivities and absorptivities which are essential to the modeling of radiative transfer. The mapping of temperature field also provides a means of validating the theoretical model.

(ii) Flame Visualization (Cinematography) – Visualization via cinematography is essential to monitor the behavior, color, luminosity, tip characteristics, development, and approach to steady state for all of the flames, regardless of the nature of the hypothesis presented in this section.

(iii) Radiation Measurement – Flame radiation is an integral part of the measurements. It provides quantitative information on the flame development and approach toward steady state in addition to the variation of the thermal field with time. Through simultaneous measurements of overall radiation, and CO_2, H_20, and soot radiation, a complete breakdown of contribution of gas-phase combustion products and particulates to radiative transfer can be obtained. This measurement is required for all of the hypotheses (a)-(d). In addition, radiation data help in developing the radiation submodel and validating the numerical model for flame characteristics.

(iv) Pressure Measurement – Measurement of pressure is needed to monitor any pressure rise that may occur due to the burning process, and to obtain estimates of the overall heat-release rate. This measurement is required for all of the hypotheses (a)-(d).

The following measurements are "desired" since they enhance the data and help in further substantiation of the hypotheses. In addition, they provide unique data in characterizing the structure of microgravity diffusion flames.

(v) Acceleration Data – Measurements of acceleration are desired to obtain the flame response to any residual acceleration or g-jitter effects during the experiment. These data will be used as input to the theoretical model for the prediction of flame characteristics. The acceleration data are equally important for hypotheses (a)-(d). In addition, theoretical analyses have shown that acceleration levels less than 10^{-3} g do not significantly affect the flame behavior. To validate these findings, acceleration measurements are desired.

(vi) Species Field – Measurements of the gas-phase species are desired to provide distributions of major combustion products, oxidizer, and any unburned hydrocarbon. This is important especially for hypotheses (b) and (c), since it not only provides information on the distribution of combustion products, but helps to delineate the characteristics of the underventilated-type behavior (hypothesis b). In addition, the

influence of oxygen concentration on the burning process in microgravity will be quantified through the measurement of distributions of oxidizer and gas-phase combustion products (hypothesis d).

(vii) Infrared Imaging for Species – This measurement is desired because a complete map of CO_2 and/or H_2O throughout the test period will be obtained. It not only identifies the flame location (locus of maximum products concentration) for hypotheses (a) to (d), but quantifies the development and transport of the field of products, thereby helping in validation of hypothesis (a). The issue of masking of the flame tip by soot will be addressed. In addition, for blue flames, the question of open or closed tip (given enough time for the flame to develop) will be answered.

(viii) Density-Gradient Field Imaging – This measurement technique is desired since a map of density gradient (and therefore, location of the flame) and qualitative field of temperature will be obtained. In addition, the flame response to disturbances caused by intrusive probes will be identified. It also provides a map of any large-scale structures which cannot be obtained through direct visualization. This method provides information for hypotheses (a) to (d).

(ix) Velocity Field – This measurement is desired since it provides a map of the gas-phase velocity, helps to quantify the convective effects due to the initial jet momentum, and defines the nature of any stagnation region at the flame tip that may be contributing to soot accumulation and underventilated-type behavior. It is most important for hypotheses (a), (b), and (d). Model validation will benefit from velocity-field measurement.

(x) Soot Size – This desired measurement provides the soot size at various locations in the flame. It helps in validation of hypotheses (a), (c), and (d). It provides information on soot processes (formation, agglomeration, burn-off) and thermophoretic effects, in addition to soot build-up at the flame tip.

(xi) Soot Concentration – This method is desired to obtain the field of soot concentration, to quantify the thermophoretic process, and to obtain information on the build-up and coring effect of soot (as described before). It helps to validate hypotheses (a) to (d). The data will also be used to improve the soot-processes and radiation submodels in the numerical model.

In the next section, justification for a space experiment is presented.

VI. JUSTIFICATION FOR LONGER-DURATION EXPERIMENTS

Observations, measurements, and theoretical analyses show that five seconds is not sufficient to quantify the steady-state characteristics of microgravity laminar diffusion flames. Specifically:

(1) Observations on the flame behavior show that although flame shape appears to reach near-steady-state, flame color continuously changes throughout the five seconds of available time. This indicates a continuous change in transport and chemical processes.

(2) Temperature data show a continuous increase in the five seconds of microgravity, and that even the far field is being affected by the temperature rise, indicating a continuous release and show transport of the combustion products in the vicinity of the flame.

(3) Radiation data show that although very weak (i.e., blue) flames show an approach toward steady state for radiative transfer in the five seconds of microgravity, brighter and sootier flames show a continuous increase in radiation loss, needing more time to reach steady state.

(4) The results of a transient, analytical model for laminar diffusion flames in microgravity show that the flames need more than five seconds to reach near-steady-state. This is in direct agreement with the radiation and temperature data, and even with observations through visualization.

In addition to the need for longer test times based on the results obtained to date from the 5-second tests and analyses, longer-duration experiments are needed for each objective of the program presented in Section IV, as shown below.

(i) In relation to Objective (a), i.e., the question of steady-state characteristics and the behavior of weak flames in microgravity, five seconds is not sufficient to allow the bright flames to approach steady-state, or the weak flames to show either steady-state approach or extinction process.

(ii) In relation to Objective (b), i.e., the underventilated behavior of microgravity flames, it is possible that soot formation and subsequent quenching and accumulation at the

tip of the flame will ultimately result in extinction. This process may happen if soot stays at the tip, does not diffuse away from the flame, and results in reducing the flame height. In this case, the flame may get shorter in time until abundance of soot causes flame extinction. This requires longer microgravity test times. In addition, it is possible that some of the flames which had a closed tip in the 5-second tests may open given longer test times.

(iii) In relation to Objective (c), i.e., the nonmonotonic behavior of micro-g flame height with pressure, it is conceivable that at longer times, this behavior may correct itself due to the interplay between the soot formation and accumulation, and the build-up and transport of gas-phase products. Longer times may result in abundance of soot at the tip of the flame, changing the nonmonotonic behavior.

(iv) In relation to Objective (d), i.e., the sensitivity of sooting characteristics to oxygen concentration in microgravity flames, as the products of combustion continuously diffuse toward the far field, the effect of oxygen partial pressure may become less significant in the near-field, resulting in a different behavior of the flame compared to what has been observed in five seconds of microgravity.

In the course of the current program, observations from the 2.2-second tests have led to the conclusion that 5-second microgravity tests should be conducted. However, measurements and observations from the 5-second tests have shown that still longer test times are needed. The results of theoretical modeling (see Figure 34), a separate analysis for the g-jitter effects on laminar flames, and recent tests of both bolted-down ($\sim 10^{-2}$ g) and free-float ($\sim 10^{-3}$ g) configurations of the frame for this experiment in the KC-135 aircraft, all point out to the fact that g-jitter and g levels in the aircraft will probably affect the flame, and that available times are not sufficient to characterize the flame. In the immediate future, we are planning to conduct tests in the KC-135, but based on the g-jitter analyses, the results are uncertain. The true understanding of the behavior and structure of these flames needs a combined set of advanced diagnostics for an extended period of time (of the order of 1-2 minutes). Regardless of whether these diagnostics can be used in the available earthbound facilities, the time constraint does not allow achieving the objectives of this program and substantiating the associated hypotheses.

VII. IDENTIFICATION OF EXPERIMENTS

A total program of space-based experiments for laminar gas-jet diffusion flames is given in Table 2. The parameters that will be varied are the type of fuel, chamber pressure, and chamber oxidizer (i.e., O_2/N_2 ratio). The number of tests in the matrix will provide a highly productive experimental program. The fundamental effects to be studied are: transient behavior, steady-state flame structure, kinetics effects, soot processes, radiation, and the influences of fuel reactivity and environmental conditions.

Hydrocarbons (methane and propane) are selected as fuels because of the available background and theory. Methane is selected because of the base of data that already exists. Propane is selected to examine a heavier-than-air fuel, and because it is a representative of a wide range of higher-molecular-weight hydrocarbons. With these fuels, the effects of reactivity, molecular weight, stoichiometry, and diffusivity on the flame structure and behavior, kinetics, sooting characteristics, heat release, and radiative transfer will be studied.

The effects of pressure and oxygen concentration on flames will be studied for a range of pressures (0.5, 1.0, and 1.5 atm) and oxygen-nitrogen mixtures (15%, 21%, and 30% O_2). Air at 1.0 atm will be the baseline oxidizing environment. Reduced pressure and/or oxygen concentration will be used to approach the near-limit behavior, and to enhance the kinetics effects, vary the partial pressure of oxygen, and reduce sooting and radiative loss. High pressure and/or high-oxygen-concentration will enhance sooting and subsequent burnoff, in addition to increasing the radiative loss and combustion intensity. The combination of various pressures and oxygen levels will provide a complete set of data for the effects of environmental conditions on the behavior and characteristics of flames in microgravity.

As described in Section V, certain diagnostics are necessary to provide the data. Of critical importance are the temperature map, visualization via cinematography, flame radiation (both overall radiation and CO_2, H_2O, and soot radiation), and chamber pressure. These are identified in Table 3 as the "required" diagnostics. In addition to these essential diagnostics, the following are highly desired because they significantly enhance the database and provide important information on flame characteristics: visualization (both Schlieren and infrared imaging of H_2O and/or CO_2 fields), species field, velocity field, acceleration data, soot samples (via thermophoretic sampling), and soot concentration (via light absorption/extinction method). These diagnostics are identified in Table 3 as "desired." Table 3 also provides the rationale for these diagnostics and application of

Table 2. Test Matrix.

OPERATING CONDITIONS	NO. OF EXPERIMENTS	SPECIFICS AND REQUIREMENTS
Fuel	2	Methane and Propane.
Fuel Flow Rate	1	xed but different mass flow rate for .fferent fuels. When converted to atmospheric condition, 1.0 cm^3/sec for propane and 2.0 cm^3/sec for methane.
Nozzle Radius	1	Tapered-tip nozzle. Inner radius = 0.0825 cm.
Oxidizer	3	Oxygen/nitrogen mixtures; O_2/N_2 volume ratio = 0.15/0.85, 0.21/0.79, and 0.30/0.70.
Chamber Pressure	3	P = 0.5, 1.0, and 1.5 atm.

Total No. of Flames = 18

Table 3. Diagnostics Requirements.

VARIABLE	RECOMMENDED DIAGNOSTICS	RATIONALE/APPLICATIONS TO MODEL DEVELOPMENT	NOTE
Flame Structure and Visualization	Schlieren system	To obtain qualitative field of density gradient.	D
	Cinematography (using movie camera or video camera)	Obtaining time-resolved visualization data on ignition, flame development, color, luminosity, sooting, and quenching. Flame shapes can be compared directly with model predictions.	R
Temperature	Array of thermocouples	Obtaining temperature distributions in the flow field. They can be compared directly with the model predictions of the thermal field.	R
Combustion and Fuel Decomposition Products	Array of gas sampling probes and sample bottles	Obtaining species distributions which can be compared with the model prediction of the species field.	D
Chamber Pressure	Pressure transducer	Monitoring any increase in chamber pressure due to the burning process, which yields estimates of the overall heat release rate.	R
Gas Velocity	Single-component laser Doppler velocimetry (LDV), or particle image velocimetry (PIV)	Centerline and radial velocities can be obtained. Velocity measurements will be compared directly with the model predictions of the flow field.	PIV: D or LDV: D
Flame Radiation	Radiometry	Isolation of thermal radiation will determine the effect of radiation on reduction in temperature within the flame. Total infrared radiation, in addition to isolated radiation from soot, CO_2, and H_2O can be measured. Model predictions and results of sampling for gas-phase species, combined with measured radiation, provide the contributions from soot and gas-phase species.	R
Gravitational Acceleration	Accelerometer	Measurement of gravitational acceleration enables us to interpret the data that could be affected by gravitational levels greater than 10^{-5} g. Provides direct comparisons with model predictions on flame characteristics and behavior as a function of gravitational level.	D
Species Imaging	Infrared imaging	To map species field using appropriate optical filters with infrared camera. Particularly useful for H_2O and/or CO_2 fields.	D
Soot Volume Fraction and Size	Light absorption	This is a convenient non-intrusive method to infer soot volume fraction and number density (knowing soot size). When combined with radiation data, species measurements, and model predictions, provides information on the characteristics and influence of soot in microgravity.	D
	Thermophoretic Sampling	Soot can be collected and size distribution can be obtained. However, collected soot needs to be removed from the chamber after the test or a series of tests.	D

R: Required. D: Desired.

the data to model development and validation. For any flame of the test matrix of Table 2, the "required" diagnostics are essential, and the "desired" diagnostics provide significant data.

VIII. APPARATUS, CONDITIONS, AND EXPERIMENT TIMELINE

Experimental conditions, components of apparatus, ranges, requirements, and specifications are presented in Table 4 (Experiment Requirements) and Table 5 (Measurement Requirements). The existing chamber for the ground-based microgravity tests is shown in Figure 3, which may be used as a guide in designing the new chamber. Assuming that all of the diagnostics methods presented in Table 3 are incorporated in the chamber, Table 6 presents a very preliminary experiment timeline to obtain a comprehensive set of data on each flame of the test matrix.

IX. RELATIONSHIP BETWEEN DATA AND MODELING

The numerical model described in Section III (f) is in the parabolic form of the partial differential equations for mass, momentum, elements, and energy. The effects included are diffusion, viscosity, inertia, kinetics, gravity, and radiation, with a shifting-equilibrium chemistry model.

The model is currently being modified to incorporate the effects of: (a) soot formation and burn-off, (b) radiation from soot in addition to gas-phase radiation by incorporating the radiative-transfer equation in the formulation, (c) thermophoretic effects, which become significant in microgravity, (d) quasi-global kinetics, (e) multi-component diffusion in the presence of soot, and (f) elliptic effects due to the significance of axial diffusion in microgravity.

The relationship between data and modeling is presented in Table 3 and in the next section on data analysis.

X. DATA ANALYSIS

The films from standard flame imaging will be developed and analyzed using a motion-picture analyzer. Flame development, height, radius, shape, and color will be obtained as a function of time. The data will provide information on the overall characteristics of flames. Comparisons of flame shapes and dimensions will be made with the predicted results. Observations on color and luminosity will provide information on particulate formation, various species, and approach toward steady state.

Table 4. Experiment Requirements.

COMPONENT	GENERAL REQUIREMENTS	MINIMUM REQUIREMENTS
Experiment Chamber	Closed, cylindrical chamber. Minimum height/diameter = 1.5. Wall reflectivity less than 0.05. Burned gas recirculation should be minimized at the top of the chamber. Recommend mounting a mesh at a TBD location near the chamber top. Chamber should be sealed during the test.	Minimum volume = 0.035 m^3 (critical); 0.050 m^3 (desired).
Chamber Environment	Initial conditions are as follows. Oxidizer: 15% to 30% (by volume) of oxygen in nitrogen. Pressure: 0.5 to 1.5 atm. Before each test, the gas temperature should be 295 +/- 5 K (measurement accuracy is +/- 10 K), pressure should be P +/- 0.02P atm, and oxygen concentration should be x% +/- 0.5% on a volume basis (e.g., for the 15% case, between 14.5% and 15.5%). However, these values must be accurately known before each test (accuracy: +/- 0.05 %).	Oxidizer: 15% to 30% of oxygen in nitrogen. Pressure: 0.5 to 1.5 atm.
Nozzle	Tapered-tip, stainless-steel nozzle along the centerline of the cylindrical chamber. Minimum distance from wall = 20 cm. Protruding 15 +/- 2 cm inside the chamber. Minimum distance from nozzle exit to top of the chamber = 35 cm. The last 4 cm (at least) of the nozzle tube (including the tip section) must have a constant inner radius. Maximum wall thickness is 1 mm for the last 4.0 cm of nozzle length. Details of the tip including tapering angle TBD.	Inner radius = 0.0825 cm.
Fuel	High-quality, commercially available, minimum purity 99.9%-pure fuel. Methane and propane. Fuel mass-flow rate should remain within the tolerance throughout the burn.	Methane and propane. Single mass-flow rate for each fuel in the whole matrix. Volume flow rate when converted to atmospheric condition (1 atm) is 1.0 cc/sec for propane and 2.0 cc/sec for methane, tolerance: +/- 1%.
Combustion Time	The last 10 seconds of the test must have no probes inside the flame (minimum 4 cm away from the nozzle centerline).	Experiment time: 30 - 60 sec, depending on carrier, chamber volume, extent of diagnostics, and particular flame.
Ignitor	Ignitor must be in excess of 1200 K before the fuel flow starts. Retracting, nichrome, hot-wire ignitor is recommended. Must be at least 4.0 cm away from the nozzle axis when not inside the flame. Ignition occurs immediately following the start of fuel flow. Ignitor should remain in the flame for approximately 2.0 sec after ignition, and then removed in less than 2.0 sec without extinguishing the flame.	Same as General Requirements.
Illumination	Illumination prior to test is desired to be able to locate the nozzle and probes on the film. It must be turned off before ignition.	Same as General Requirements.
Allowable Acceleration Levels	Accelerations less than or equal to 10^{-4} g are desirable. Frequency should be above 10 Hz.	Same as General Requirements.

Table 5. Measurement Requirements.

MEASUREMENT	GENERAL REQUIREMENTS	MINIMUM REQUIREMENTS
Acceleration	Acceleration (3 axes) should be recorded continuously during the experiment. Data collection rate: minimum of 30/sec-axis. Accelerometer in the vicinity of the chamber. Range of measurement: 10E-5 to 10E-2 g. One axis aligned with the nozzle. Frequency range of interest: 0 - 25 Hz.	Same as General Requirements.
Chamber Pressure	Chamber pressure should be monitored throughout the conduct of the experiment at one location on the chamber wall. Measurement precision: 1%. Measurement rate: 1/sec. Reading: 0.05 to 3.0 atm.	Same as General Requirements.
Overall Chamber Temperature	The overall gas-phase temperature should be monitored during and between tests. Range: 270 - 1500 K. Collection rate: 10/sec. Accuracy: +/- 10 K. Recommend a thermocouple located along the nozzle centerline, inside the chamber, and 5 - 10 cm away from the chamber top. Screen (mesh) is between thermocouple and chamber top.	Same as General Requirements.
Flame Radiation	Radiation should be measured throughout the test. Require measurements of the entire range 0.3 to 9.0 micrometers, with at least 95% of incident radiation being recorded. In addition, two discrete bands in the IR range (TBD) should be measured. Field of view at the plane passing through the nozzle centerline: circle of 20 cm in radius. Must be able to see 5 cm below the nozzle tip. Data collection rate: 20/sec. Precision: 1%. Four wide-view-angle, thermopile-detector radiometers are recommended: one for overall radiation (entire wavelength range), one for a water vapor band (IR) TBD, one for a CO_2 band (IR) TBD, and one for soot (IR) TBD.	Same as General Requirements.
Soot Size	Soot samples must be collected from at least four points in the flame covering a region 2 cm horizontal (from the nozzle axis) and 15 cm vertical (along the nozzle axis). Collection duration: less than 30 msec at a specified time toward the end of the test. If a flame-perturbing mechanism is used, it should be at least 6 cm away from nozzle centerline when not in the flame. A retracting, thermophoretic-sampling mechanism is recommended. The collection mechanism should have at least four arms and at least two grids per arm. Mechanism activation: going in the flame, up to the nozzle centerline, and out of the flame in no more than 30 msec. Note that samples must be removed from the chamber at the end of the test (Phase II) and after return to Earth (Phase I). Locations, specifics, and mechanism TBD.	For a selected number of tests (TBD).
Soot Volume Fraction	Measurement of soot volume fraction in a 10-cm-diameter field and centered 10 cm above the nozzle tip at the centerline of the nozzle. Light absorption/extinction method is recommended. A beam of light, passing through the flame at a specified time, and collected with a detector. Requires (preferably) a monochromatic beam. Specifics TBD. Detector collection rate: 20/sec. Detector specifics: TBD.	Same as General Requirements.
Gas-Phase Temperature Field	Radial temperature distributions at 6-8 TBD axial locations must be measured. Upper limit: 1800 K. Sampling rate: 10/sec. Measurement accuracy: +/- 10 K. Measurements at TBD locations in a plane passing through the nozzle axis. Region of interest is 5 cm horizontally outward from the nozzle axis and 20 cm vertical (along nozzle axis). It is recommended to use a rake of 6-8 thermocouples on a single line parallel to the nozzle axis which can be moved in the radial direction (to 4-5 cm from the axis) at a controlled rate (1-2 mm/sec). Separation between thermocouples: TBD (2-4 cm). Tolerance on the location of the TC tip is +/- 0.5 mm. Type, wire diameter, and bead size: TBD. It is preferred to move the rake in a direction perpendicular to the thermocouple axis; if not possible, then along the axis. There are other possibilities, e.g., turning the mechanism along an arc going in the flame and continuing out of the flame. Controlling factors for the selection of mechanism are: experiment duration, minimum flame perturbation, rate of movement of the mechanism, and local flame quenching by thermocouple arms.	Same as General Requirements.

Table 5. Cont.

MEASUREMENT	GENERAL REQUIREMENTS	MINIMUM REQUIREMENTS
Concentration of Species	Concentration measurements of CO_2, H_2O, CO, H_2, O_2, N_2, formaldehyde, unburned hydrocarbons, etc. Will analyze the samples after tests are done. Location: TBD; separation: TBD. Rake of gas-sampling probes and associated sample bottles are recommended. Quenching quartz microprobes. At a specified time, and preferably, for a specified period during the test, they will remove gas samples from the flow field by suction into vacuum teflon-lined sampling bottles of approximately 10 cc in volume. A rake of 3x3 is recommended. Region of interest is 5 cm radially outward from, and 20 cm vertical along, the nozzle axis. One extreme column to withdraw samples at the centerline. Separations and locations TBD. Should not affect or interfere with temperature measurement. Probes inside the flame for a specified time only.	As a minimum, three sampling probes: one at 3 cm away from the nozzle centerline and 5 cm above the nozzle tip; one above and one below the flame tip (locations TBD) at the centerline. All three measurements simultaneously at a specified time.
Velocity Measurement	Gas-phase velocity measurement in and around the flame. Range of velocities: 0.1 to 500 cm/sec. Point measurements are preferred if velocity can be measured at several (TBD) points; otherwise, field measurements. Point measurements: axial velocities at TBD locations in the flame region in a plane passing through the nozzle axis. Field measurements: 2-D velocity vector field, in a plane passing through the nozzle axis. The entire region of interest is 15 cm horizontal by 25 cm vertical, starting at 0.2 - 0.4 cm above the nozzle tip. Spatial resolution: 1 mm. Measurement accuracy: +/- 5% of reading. Sampling rate: 30/sec.	Same as General Requirements. Single-componenet laser Doppler velocimetry (LDV) is recommended if point measurements; particle image velocimetry (PIV) if field measurements.
Flame Imaging (Standard)	Side view of the flame to be imaged in color. Field of view: 15 cm horizontal by 25 cm vertical (must see 2 cm of the nozzle tip). A timing system should be provided to record accurate time intervals on the film (approx. 0.1 sec). If a mirror is used, should not produce double-imaging on the film. Framing rate of 30 fps is desired. Camera should see the perturbation of the flame by thermocouples and sampling probes (approx. 90 degrees to probe arms). Resolution: 0.5 mm.	Same as General Requirements.
Infrared Imaging for Species	Water vapor and/or carbon-dioxide imaging. Field of view: 20 cm horizontal by 30 cm vertical. View must see 2 cm of the nozzle tip. Focus on nozzle axis. Resolution: 0.5 mm. Imaging throughout the test. Depth of field: 2-4 cm. Infrared camera is recommended. Filters (wavelengths of interest to be specified) are needed to identify the CO_2 and H_2O fields. Framing rate: 30 fps.	Same as General Requirements.
Density-Gradient Field Imaging	Imaging of density gradient to see the entire flame and region above it. Minimum field of view is a circle 15 cm in diameter, and centered on the flame axis; center of the circle is 7.0 cm from the nozzle tip. Desired resolution: 0.5 mm. Schlieren system is recommended. Frame rate: 30 fps. Either color or B/W; color preferred.	Same as General Requirements.

Table 6. Preliminary Timeline for Each Test.
(Times are in Seconds)

t < 0 :	Thermocouples are at nozzle centerline. Ignitor is above the nozzle tip.
t = 0 :	Start recording: accelerometer, movie camera, thermocouples, pressure transducer, infrared camera, radiometers. Ignitor heat-up starts. Fuel-flow starts.
t = 1-2:	Ignitor is moved away from nozzle centerline.
t = 10:	Thermocouple rake starts to move away (rate: 1.5 mm/sec). Light absorption/extinction starts.
t = 30:	Light absorption/extinction stops. Schlieren starts. Soot-sampling mechanism starts to move toward the flame.
t = 34:	Soot-sampling mechanism stops near the flame (at least 5-6 cm away from nozzle centerline).
t = 35:	Soot sampling is conducted.
t = 36:	Soot-sampling mechanism starts to move toward its rest position. Gas-sampling mechanism starts to move toward and into the flame.
t = 40:	Thermocouple rake stops moving. Soot-sampling mechanism arrives at its rest position. Gas-sampling probes are now inside the flame. Gas sampling starts.
t = 42:	Gas sampling stops. Gas-sampling probes start to move out of the flame and toward their rest position.
t = 46:	Sampling probes get to their rest position. Schlieren system stops.
t = 55:	Particle-Image Velocimetry (PIV) system is activated.
t = 65:	Fuel flow stops.
t = 70:	PIV system is turned off. Infrared and cinematography cameras stop. Thermocouples, accelerometer, radiometers, and pressure transducer stop recording. Experiment is ended.

Acceleration data will be reduced to obtain the flame behavior as a function of any small variations in gravity level. These data combined with the results of film analysis will provide information on the response of the flame to any g-jitter effects. These acceleration data will be used as input to the computer programs for prediction of flame characteristics.

The gas samples withdrawn from various locations inside and outside the flame will be analyzed. Concentrations of O_2, CO, CO_2, N_2, H_2, and unburned hydrocarbons will be obtained, which provide species distributions. The data will be compared with the predicted values of species field, and will specifically provide information on any potential escape of unburned fuel through the tip of the open flames.

Radiation data will be analyzed to obtain heat loss as a function of time. Any approach toward steady state will be compared with the results of flame visualization data. The measured overall radiative loss combined with the data from discrete-radiation measurements on CO_2, H_2O, and soot will provide a complete breakdown of radiation contribution from these stable products and from particulates. The radiation model in the numerical code will be validated using these measurements.

The data from temperature-field measurements will provide the distribution of temperature in both axial and radial directions. In addition, flame temperature and location, far-field temperature as a function of time, and the overall gas-phase temperature will be obtained. These data will help quantify tip-quenching due to the presence of soot. When combined with the radiation data, species measurements, and the predicted species field, the temperature data will provide a complete map of effective emissivities and absorptivities.

The chamber-pressure data will be used to deduce the overall heat-release rate and combustion efficiency.

The data from velocity measurements will be analyzed, and a complete map of the velocity field will be constructed. The tip-opening phenomena in microgravity flames will be better understood through the mapping of velocity field at the flame tip. These data together with the theoretical model will quantify the thermophoretic effects.

The collected soot samples will be analyzed to obtain soot size and overall soot distribution in the flame. Once the soot size and soot concentration are measured, the input from soot contribution in the submodels for radiation and soot formation/agglomeration/burn-off will be quantified.

The data from concentration measurements for soot will be analyzed to construct a map of soot concentration, and to better characterize the effects of thermophoresis, soot blockage and coring effects, and soot quenching, which contribute to flame extinction at the tip. When combined with the soot-collection data, a complete set of information on soot size, number density, and concentration will be obtained.

The infrared-imaging data for CO_2 and/or H_2O will provide the local relative intensities of contributions from stable combustion products. The field of products will be monitored throughout the test which will help to define the location of the flame and the extent of the field during the experiment.

The films of the density-gradient field imaging will be analyzed to obtain information on flame structure, the fields of temperature and density, and help to define the perturbations caused by the presence of probes in the flame.

Theoretical predictions will be used to support the analysis and interpretation of the database developed from these experiments. The results of individual measurements, when combined, provide both quantitative and qualitative information to validate and improve the theoretical analyses.

REFERENCES

1. Edelman, R. B. and Bahadori, M. Y. (1986) Effects of buoyancy on gas jet diffusion flames: Experiment and theory. Acta Astronautica 13, No. 11/12, 681-688.

2. Burke, S. P. and Schumann, T. E. W. (1928) Diffusion flames. Ind. Eng. Chem. 20, 998-1004.

3. Astavin, V. S. and Ryazantsev, Yu. S. (1979) Temperature and concentration distribution in the reaction region of parallel flows of unmixed reactants. Fluid Dynamics 14, 274-279; Translated from Izvestiya Akademii Nauk SSSR - Mekhanika Zhidkosti i Gaza 14, 139-146.

4. Bahadori, M. Y., Li, C-P., and Penner, S. S. (1986) Two adjacent, coupled laminar diffusion flames With cylindrical symmetry. Progress in Astronautics and Aeronautics, Vol. 105 – Dynamics of Reactive Systems, Part I: Flames and Configurations (J. R. Bowen, J.-C. Leyer and R. I. Soloukhin, Eds.). pp. 192-207. American Institute of Aeronautics and Astronautics, New York.

5. Penner, S. S., Bahadori, M. Y., and Kennedy, E. M. (1984) Laminar diffusion flames with cylindrical symmetry, arbitrary values of diffusion coefficients and inlet velocities, and chemical reactions in the approach streams. Progress in Astronautics and Aeronautics, Vol. 95 – Dynamics of Flames and Reactive Systems (J. R. Bowen, N. Manson, A. K. Oppenheim, and R. I. Soloukhin, Eds.). pp. 261-292. American Institute of Aeronautics and Astronautics, New York.

6. Bahadori, M. Y. (1990) An analytical solution for transient, cylindrically symmetric laminar diffusion flames in the absence of buoyancy. Spring Technical Meeting (Central States Section) of The Combustion Institute, Cincinnati, Ohio.

7. Beckstead, M. W. (1981) A model for solid propellant combustion. Eighteenth Symposium (International) on Combustion, pp. 175-185. The Combustion Institute, Pittsburgh, PA; see also Derr, R. L., Beckstead, M. W., and Cohen, N. S. (1969) Combustion tailoring criteria for solid propellants. AFRPL-TR-69-190 (835-F), Redlands, CA.

8. Mitchell, R. E., Sarofim, A. F., and Clomburg, L. A. (1980) Experimental and numerical investigation of confined laminar diffusion flames. Combust. Flame 37, 227-244.

9. Edelman, R. B., Fortune, 0., and Weilerstein, G. (1973) Analytical study of gravity effects on laminar diffusion flames. NASA CR-120921, 136 pp.

10. Edelman R. B., Fortune, O. F., Weilerstein, G., Cochran, T. H., and Haggard, JR., J. B. (1973) An analytical and experimental investigation of gravity effects upon laminar gas jet diffusion flames. Fourteenth Symposium (International) on Combustion, pp. 399-412. The Combustion Institute, Pittsburgh, PA.

11. Bahadori, M. Y., Edelman, R. B., Stocker, D. P., and Olson, S. L. (1990) Ignition and behavior of laminar gas-jet diffusion flames in microgravity. AIAA J. 28, 236-244.

12. Klajn, M. and Oppenheim, A.K. (1982) Influence of exothermicity on the shape of a diffusion flame. Nineteenth Symposium (International) on Combustion, pp. 223-235. The Combustion Institute, Pittsburgh, PA.

13. Flower, W. L. and Bowman, C. T. (1983) Measurements of the structure of sooting laminar diffusion flames at variable pressure. Report SAND83-8776, Sandia National Laboratories, Livermore, CA 94550; paper Western States Section of the Combustion Institute, WSS/CI 83-56.

14. Cochran, T. H. and Masica, W. J. (1970) Effects of gravity on laminar gas jet diffusion flames. NASA TN D-5872.

15. Cochran, T. H. (1972) Experimental investigation of laminar gas jet diffusion flames in zero gravity. NASA TN D-6523, 26 pp.

16. Haggard, J. B. and Cochran, T. H. (1973) Hydrogen and hydrocarbon diffusion flames in a weightless environment. NASA TN D-7165, 28 pp.

17. Haggard, J. B. (1981) Forced and natural convection in laminar jet diffusion flames. NASA Technical Paper No. 1841. 21 pp.

18. Bahadori, M. Y. and Stocker, D. P. (1989) Oxygen-concentration effects on microgravity laminar methane and propane diffusion flames. Fall Technical Meeting (Eastern Section) of The Combustion Institute, Albany, New York.

19. Bahadori, M. Y., Stocker, D. P., and Edelman, R. B. (1990) Effects of pressure on microgravity hydrocarbon diffusion flames. Paper AIAA 90-0651, AIAA 28th Aerospace Sciences Meeting, Reno, Nevada.

20. Bahadori, M. Y., Edelman, R. B., Sotos, R. G., and Stocker, D. P. (1991) Radiation from gas-jet diffusion flames in microgravity environments. Paper AIAA 91-0719, AIAA 29th Aerospace Sciences Meeting, Reno, Nevada.

21. Bahadori, M. Y., Edelman, R. B., Sotos, R. G., and Stocker, D. P. (1990) Measurements of temperature for microgravity laminar diffusion flames. Fall Technical Meeting (Eastern Section) of The Combustion Institute, Orlando, Florida.

22. Altenkirch, R. A., Eichhorn, R., Hsu, N. N., Brancic, A. B., and Cerallos, N. E. (1976) Characteristics of laminar gas jet diffusion flames under the influence of elevated gravity. Sixteenth Symposium (International) on Combustion, pp. 1165-1174. The Combustion Institute, Pittsburgh, PA.

23. Kimura, I. and Ukawa, H. (1961) A study of the combustion of laminar fuel jets. Japan Society of Mechanical Engineers 27, 736-746; translated as NASA Technical Translation, NASA TT F-13, 459, February 1971.

24. Stocker, D.P. (1990) Size and shape of laminar Burke-Schumann diffusion flames in microgravity. Spring Technical Meeting (Central States Section) of The Combustion Institute, Cincinnati, Ohio.

Section 19

"EFFECTS OF BUOYANCY ON GAS-JET DIFFUSION FLAMES"

-Concept Design-
(Space Experiment)

M. Y. Bahadori and R. B. Edelman

December 1991

Effects of Buoyancy on Laminar Gas-Jet Diffusion Flames

(Space Experiment)

- Science Requirements and Concept Design -
Contract NAS3-22822

M. Yousef Bahadori and Raymond B. Edelman

Science Applications International Corporation
Thermal Sciences Division
21151 Western Avenue, Torrance, California 90501

Presented at:

NASA Lewis Research Center
Space Experiments Division
Cleveland, OH 44135

December 11, 1991

SAIC. Science Applications International Corporation

Introduction and Background

SAIC. Science Applications International Corporation

Laminar Gas-Jet Diffusion Flames

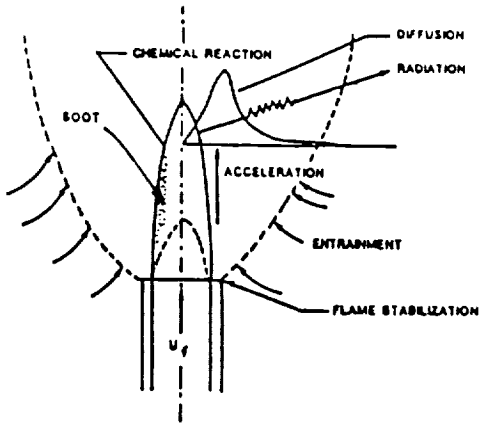

1-g 0-g

- Jet diffusion flames embody nearly all the mechanisms found in natural fires relevant to fire safety and to controlled combustion processes
- Simple, basic, and easy to control
- Need better understanding
- A step toward understanding the more complex turbulent diffusion flame

SAIC.
Science Applications International Corporation

Laminar Gas-Jet Diffusion Flames (Cont.)

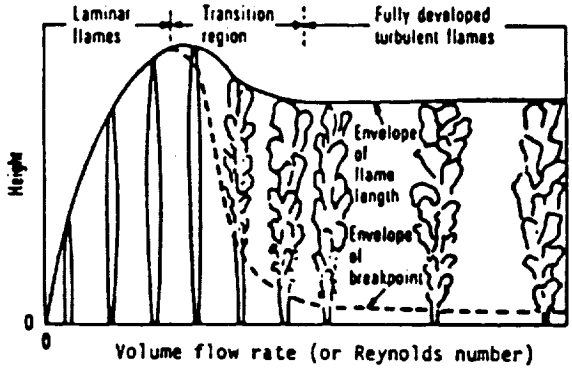

- **Understanding laminar flames is basic to the physics of the broader, more general turbulent combustion process**
- **The transition process to turbulent flames is governed, in part, by the characteristics of laminar flames**
- **Laminar flames are inherent in the detailed structure of turbulent flames from the molecular point of view**

SAIC.
Science Applications International Corporation

Approach

- Isolate the effects of buoyancy by eliminating gravity
- Experimental (2.2-sec. tower, 5.18-sec. facility, KC-135 aircraft, and space experiment)
- Theoretical (analytical and numerical modeling)

Results applicable to the fundamental understanding of combustion in space and earth environments

SAIC. Science Applications International Corporation

*Previous Research - 2.2-Second Drop-Tower Experiments**

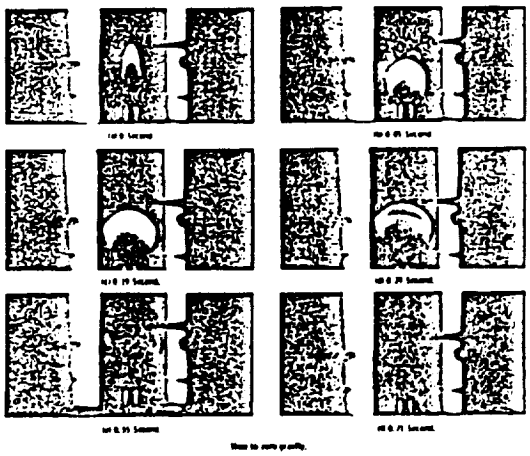

Extinguished microgravity methane diffusion flame
Nozzle radius = 0.186 cm
Flow rate = 2.8 cm^3/sec
Flow velocity = 25.44 cm/sec
Reynolds no. = 28.4

- Hydrocarbon flames were ignited in normal gravity and then subjected to microgravity condition
  - Some flames extinguished
  - Some were in transition between extinguishment and steady-state (lack of enough time)
  - Others reached (an apparent) steady-state with flame-height fluctuations

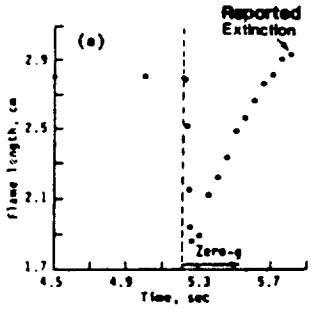

* Cochran, Masica, Haggard, Edelman (1970-1974).

SAIC. Science Applications International Corporation

Previous Research - Theoretical Analysis

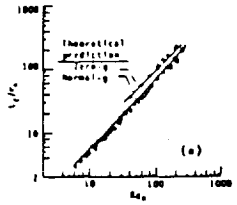

Experimental data[e,f]

Normal-g	r_0 (cm)
○	0.051
△	0.0825
□	0.113
◇	0.186
◈	0.318
▽	0.442

Solid symbols denote zero-g

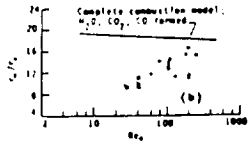

Partial oxidation theory	r_0 (cm)
H_2O, CO H_2O, C(s)	
○ ◔	0.051
△	0.0825

Solid symbols denote experimental data[e]

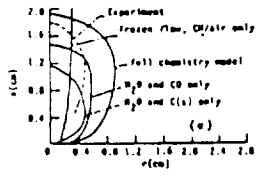

Data[e]
Q = 1.08 cm³/sec
Re_0 = 40.9
T_0 = 294 K
P = 1 atm
r_0 = 0.051 cm

[e] Cochran (1972)
[f] Cochran and Masica (1970)

ANALYSIS

Used

- Steady flow
- Axisymmetric, 2-D conservation equations for mass, momentum, and energy
- Parabolic form of governing equations
- Infinitely fast reactions with shifting equilibrium chemistry, in addition to partial oxidation
- Multicomponent diffusion

Required

- Kinetic effects in the presence of soot processes
- Flame radiation
- Transient effects, ignition, and extinction
- Axial diffusion

SAIC Science Applications International Corporation

Current Ground-Based Program

- 2.2-Second Drop-Tower Tests
- 5.18-Second Microgravity Tests
- KC-135 Tests
- Theoretical Analyses

SAIC Science Applications International Corporation

Background Summary

- Buoyancy significantly alters the flame structure
- Pressure and oxygen concentration have a more dramatic effect in microgravity than in normal gravity
- Prolific sooting results from absence of buoyancy, and is strongly pressure- and oxygen-dependent
- Radiation and temperature data show that longer test times are needed to substantiate the observed behavior of these flames at steady-state
- Chemical kinetics - radiation - transient interactions are important in reduced-gravity environments
- Extinction limits may be different in microgravity and normal gravity

SAIC. Science Applications International Corporation

Transition from Ground-Based to Space Program

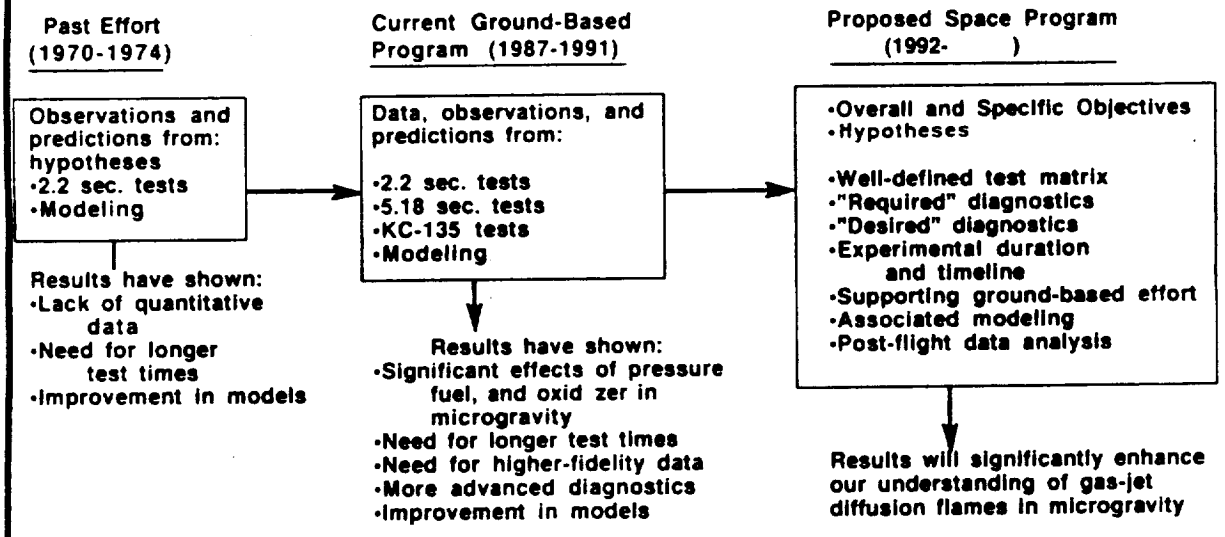

SAIC. Science Applications International Corporation

Is Space Necessary?

Requirement	Criticality
G-level has to be $<10^{-3}$	Critical
Time Requirement: ·Achieve steady state (>5sec.) ·Obtain quantitative data (conventional or advanced diagnostics ~60sec.)	Critical
Quantitative data via advanced diagnostics	Desirable

SAIC. Science Applications International Corporation

Current Ground-Based Program

SAIC. Science Applications International Corporation

Current Ground-Based Program - 2.2-Second Drop-Tower Experiments

- Approximately 100 tests were conducted
- Flames were ignited in microgravity (using a newly developed spark ignitor)
- Flame extinction was not observed (unlike previous works), once the flames were ignited in low-g and the photographic technique was improved
- Studied methane and propane flames under various environmental conditions of pressure (0.5-1.5 atm) and oxygen concentration (18%-50%O_2)
- Defined and revised the test matrix for the 5.18-second microgravity experiments, based on findings from the 2.2-second tests
- Observed some new and unique characteristics of microgravity flames (e.g., transient effects, blue flames, prolific sooting, tip-opening)
- Representative results will follow

SAIC. Science Applications International Corporation

Current Program - 5.18 Second Microgravity Tests

- Approximately 45 successful tests were conducted
- Flames were ignited in microgravity (originally with a spark ignitor, and later with a more reliable, retracting hot-wire ignitor)
- Studied methane and propane flames in different pressure (0.5-1.5 atm) and oxygen-concentration (15%-30% O_2) environments
- Employed flame visualization using movie camera
- Measured flame radiation
- Obtained temperature distributions at various locations
- .Observed new and unexpected phenomena

- Defined the test matrix for KC-135 experiments
- Species distributions via gas sampling will be obtained
- Representative results will follow

SAIC. Science Applications International Corporation

Current Ground-Based Program - KC-135 Tests

- Testing has begun (first week of flights: visualization only, oxidyzing environment: air at 1 atm)
- Test matrix is selected based on 5.18-second microgravity results
- Flame visualization via video camera and movie camera
- Chamber pressure has been recorded
- Temperature distributions will be obtained
- Flame radiation will be measured
- Acceleration data will be recorded and compared with flame behavior
- Both attached (~10^{-2}g) and free-float (~10^{-3}g) tests

Results from the first flight will follow

SAIC
Science Applications International Corporation

Ground-Based Test Matrix - Current Program

5.18-Second Microgravity Tests

Fuel	CH_4 and C_3H_8	2
Oxidizer	18% O_2, 21% O_2, and 30% O_2 in N_2	3
Nozzle radius	0.0825 cm	1
Fuel flow rate	Methane: 1.0, 2.0, and 3.0 cc/s Propane: 0.5, 1.0, and 1.5 cc/s	3
Pressure	0.5, 1.0, and 1.5 atm	3
	Total:	54

KC-135 Tests

Fuel	CH_4 and C_3H_8	2
Oxidizer	15% O_2, 21% O_2, and 30% O_2 in N_2	3
Nozzle radius	0.0825 cm	1
Fuel flow rate	Methane: 2.0 cc/s; propane: 1.0 cc/s	1
Pressure	0.5, 1.0, and 1.5 atm	3
	Total:	18

SAIC
Science Applications International Corporation

Hardware - 5.18-Second and KC-135 Tests

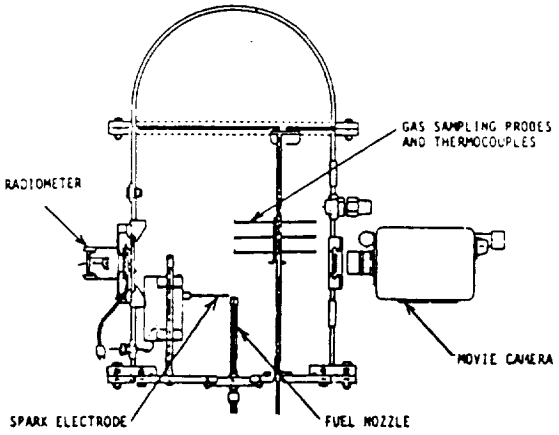

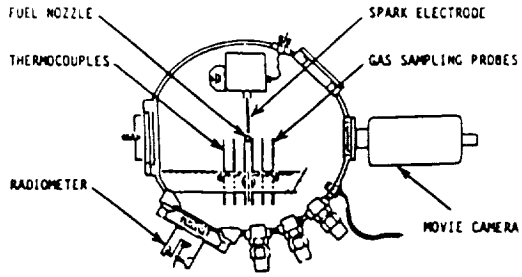

- Radiometer
- Rake of 9 thermocouples
- Rake of 9 sampling probes
- Pressure transducer
- Movie camera and video camera
- Accelerometer

SAIC.
Science Applications International Corporation

Observations from Current Ground-Based Gas-Jet Experiments

Under reduced-gravity conditions, flames exhibit distinctive characteristics relative to normal-gravity flames

- Flame flicker disappears
- Flames become taller and wider
- Take much longer time to reach steady-state
- Drastically change in color and luminosity
- Removal of buoyancy results in prolific sooting
- Tip-opening and soot escape is observed for higher hydrocarbons
- Show significant radiative loss
- Results have helped to clarify what was previously believed to be quenching of gas-jet diffusion flames in microgravity

SAIC.
Science Applications International Corporation

Results from Current Ground-Based Program

SAIC. Science Applications International Corporation

Ignition Behavior and Flame Development

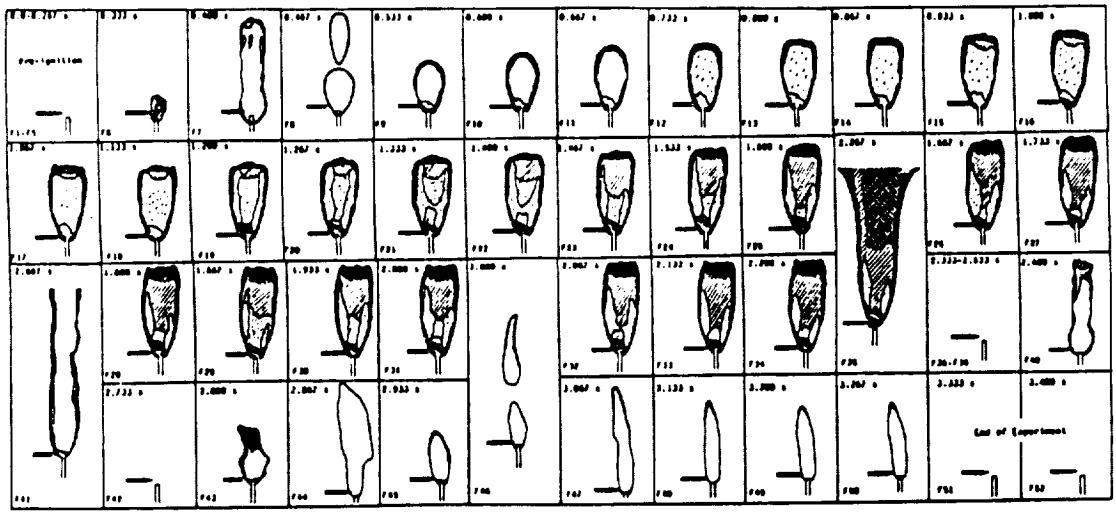

Frame-by-frame analysis of a microgravity propane flame with nozzle radius = 0.0825 cm and volume flow rate = 1.0 cm^3/s. The different observed colors are as follows: □Bright white; ▨White with little yellow; ▨White with more noticeable yellow; ▨Blue; ■Dark blue; ▨Violet-pink; ▨Mixed blue/violet; ▨Yellow; ▨ Orange; ■ Cherry red; ■Dull red, fainting; ▨Color at the base, starting with dark at the bottom, becoming dark blue/pink, then pink/blue, then pink/orange, then orange/yellow, and then yellow/white toward the center of the flame; ■Bright white spark with bright blue at its boundary. Scale: ⊢ ≡ 1 cm.

* Reproduced from Bahadori, et al., 1990 [7]

SAIC. Science Applications International Corporation

Effects of Oxygen Concentration*

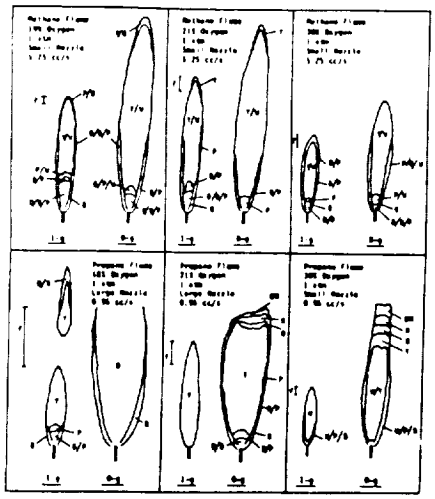

Normal-gravity and microgravity laminar diffusion flames of methane and propane, burning in quiescent environments at 1 atm with different oxygen-nitrogen mixtures. The two nozzles have a tapered-tip radius of 0.048 and 0.074 cm. The various colors indicated in the diagram are as follows: B (blue), D (dark), O (orange), P (pink), R (red), W (white), Y (yellow), and DR (dull red). The bars show the range of normal-gravity flame flicker (f). The coloring may be slightly off due to the force-processing of films for low-oxygen and 21%-O_2 environments. The films for the flames in 30%-O_2 environments were not force-processed. The low-oxygen-concentration flame of propane in normal gravity shows pockets of flame leaving the flickering part. Scale: ⟵ = 1 cm.

- Most of the low-O_2 flames are blue and cool
  - Apparently soot-free
  - Contrary to what was expected
  - May be able to control the soot process by the environment
- Open tip (underventilated-type behavior) is attributed to:
  - Enhanced radiative loss due to larger flame size
  - Extensive soot and cooling at the tip
  - Thermophoretic effects, which become more important in microgravity
- Even at 50% O_2 , open tip and massive soot escape through the tip were observed in microgravity
  - Soot quenching may not be avoided in microgravity by merely increasing the oxygen level

* Reproduced from Bahadori and Stocker, 1989 [4]

SAIC. Science Applications International Corporation

Effects of Oxygen Concentration (Cont.)*

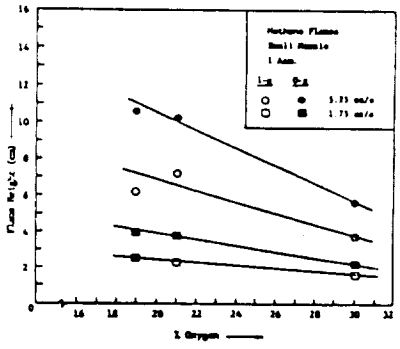

Methane

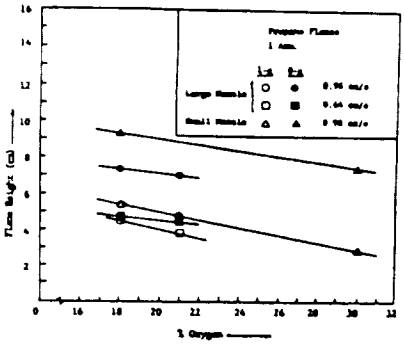

Propane

- **The difference between normal-gravity flame heights decreases as oxygen concentration increases**
  - **However, color, luminosity, and soot formation are different**
- **Quantitative data is helping to characterize these processes including extinction limits in terms of oxygen concentration**

*** Reproduced from Bahadori and Stocker, 1989 (4)**

SAIC. Science Applications International Corporation

Effects of Pressure*

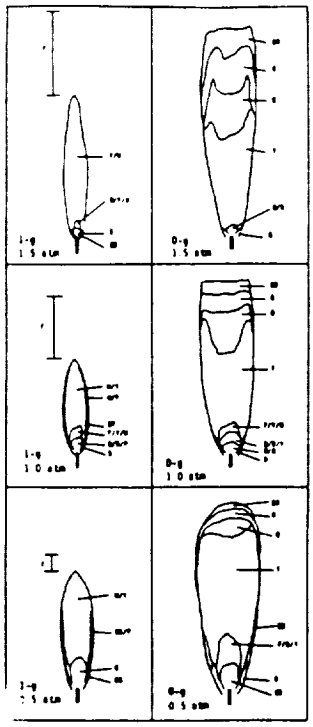

- Increase in pressure has a significant effect on tip opening and increased soot in microgravity
- Flame radius decreases with increase in pressure
- Blue-base region (soot inception zone) decreases in length with increase in pressure
- At low pressures, less-efficient burning and broader flame zone exist due to the kinetics effects

Normal-gravity and microgravity flames of propane in air with nozzle diameter = 0.15 cm and fuel Reynolds number = 98 (based on the nozzle radius). The various colors observed are as follows: B (blue), BB (bright blue), D (dark), DB (dark blue), DP (dark pink), DR (dark red), O (orange), P (pink), R (red), W (white), and Y (yellow). The range of flicker (f) is also indicated for normal-gravity flames; scale: —— = 1 cm; reproduced from [8].

* Reproduced from Bahadori, et al., 1990 [5]

SAIC. Science Applications International Corporation

Effects of Pressure (Cont.)*

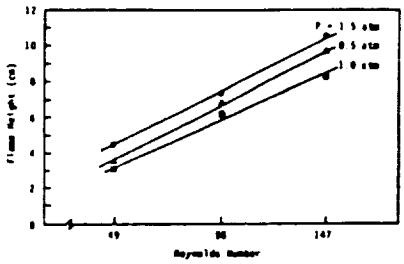

Microgravity flame height vs. fuel Reynolds number for different pressures. The lines connect the data points. Note that the flame height is largest at 1.5 atm and smallest at 1.0 atm.

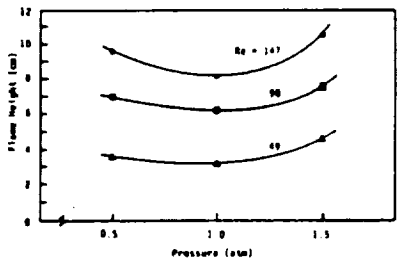

Microgravity flame height vs. pressure for different fuel Reynolds number. The lines connect the data points. Note that at each Reynolds number, there exists a pressure between 0.5 and 1.0 atm at which the flame is shortest.

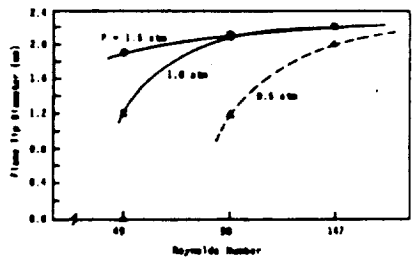

Flame-tip diameter vs. fuel Reynolds Number at different pressures for microgravity flames. The broken line indicates uncertainty in connecting the data points due to the lack of information on the smallest Reynolds number for which the tip opens.

- For the range of pressures studied, there exists an intermediate pressure at which flame height is minimized
  - Competition between the different pressure-dependent gas-phase combustion rates and soot processes may be responsible for this non-monotonic behavior
- Flame-tip diameter has an asymptotic type of convergence with increasing Reynolds number
  - Regardless of pressure (and hence, availability of oxygen), flame tip has a fixed diameter beyond a certain Reynolds number

* Reproduced from Bahadori, et al., 1990 [5]

SAIC. Science Applications International Corporation

*Effects of Pressure (Cont.)**

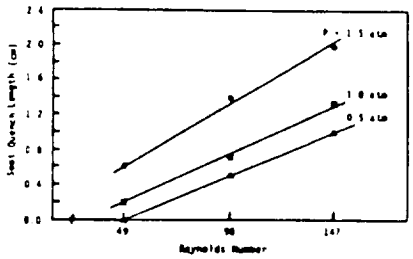

Soot quench length (red region at the flame tip) vs. fuel Reynolds number as a function of pressure. The solid lines connect the data points.

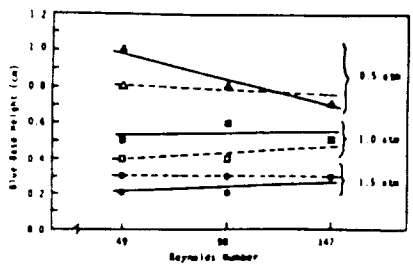

Blue-base height vs. fuel Reynolds number at different pressures for normal-gravity flames (open symbols and dashed lines) and microgravity flames (closed symbols and solid lines). Whenever the normal-gravity and microgravity data coincide, only the microgravity symbol is used. The lines connect the data points.

- Soot quench length (at the tip) increases with both pressure and Reynolds number, indicating enhanced soot formation
- As pressure increases, both microgravity and normal-gravity soot-inception regions (i.e., blue-base region) decrease in length with little dependence on flow rate

* Reproduced from Bahadori, et al., 1990 [5]

SAIC. Science Applications International Corporation

Flame Radiation - Comparison Between Normal Gravity and Microgravity

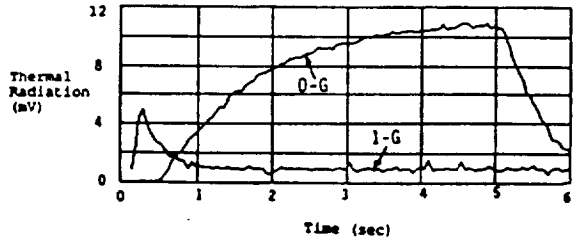

Propane flames burning in quiescent air at 1 atm; nozzle radius = 0.0825 cm; fuel-flow rate = 1.5 cm^3/sec; recent 5.18-second microgravity tests

- Radiative loss is constant for normal-gravity flames throughout the test; this is largely due to
  - Instantaneous removal of the hot combustion products under the influence of buoyancy
  - Immediate flame establishment following ignition
- In 5-second microgravity environments, a continuous development of the flame is observed
  - Radiation increases continuously; more than 5 seconds is needed to reach steady-state (verified both visually by examining the films and through radiation data)
  - This is due to the continuous accumulation and slow transport of the combustion products in the vicinity of the flame

SAIC. Science Applications International Corporation

Flame Radiation - Effects of Pressure

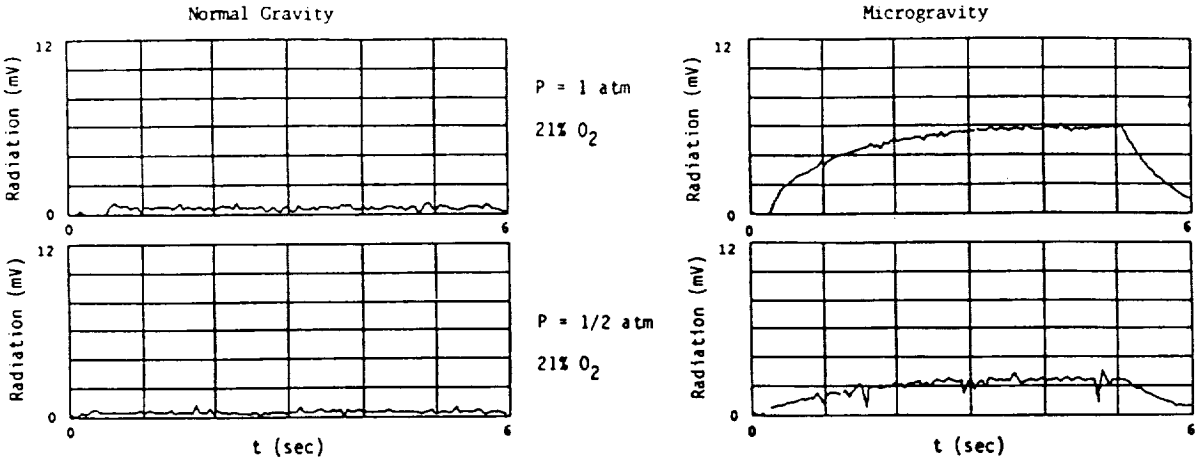

Methane flames burning in quiescent air; nozzle radius = 0.0825 cm; fuel-flow rate = 3.0 cm^3/sec; recent 5.18-second microgravity tests

- Pressure has a significant effect on radiative loss in microgravity
- Normal-gravity flames do not show this magnitude of difference

SAIC. Science Applications International Corporation

Flame Radiation - Effects of Oxygen Concentration

Propane
1.0 atm

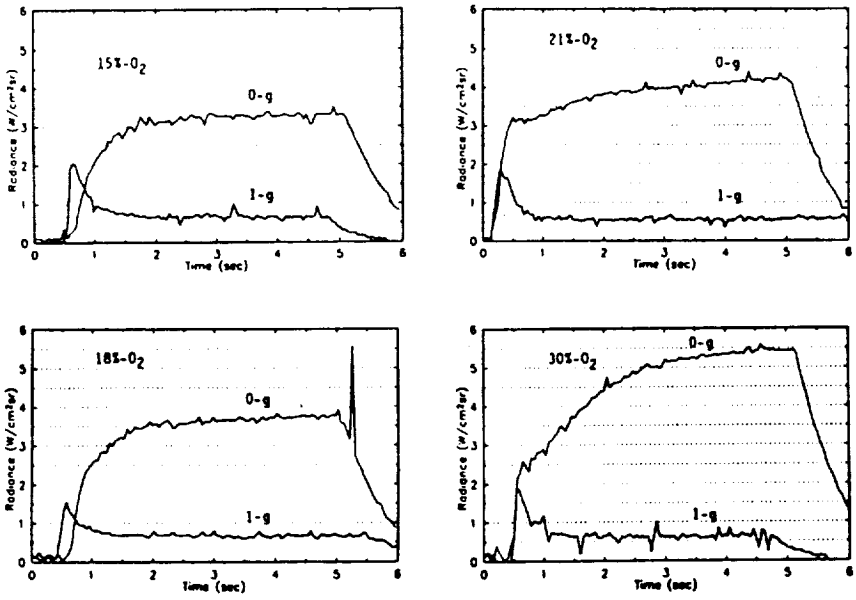

- Oxygen concentration has a significant effect on radiative loss in microgravity
- Normal-gravity flames do not show this effect due to the presence of buoyancy

SAIC. Science Applications International Corporation

*Flame Radiation - Effects of Fuel-Flow Rate**

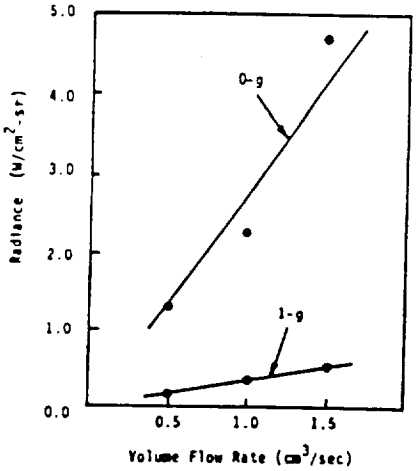

Radiance as a function of fuel volume-flow rate for propane flames burning in quiescent air at 1 atm. The radiance data are the average values between 4.0-sec. and 5.0-sec. after ignition in the 5.18-Second Zero Gravity Facility

- Fuel flow rate has a much more pronounced effect on the level of radiation from microgravity flames compared to those in normal gravity
- Radiance varies almost linearly with flow rate under both microgravity and normal-gravity conditions, but radiation in microgravity can be up to 10 times larger than in normal gravity
- In addition to larger flame size and extensive soot formation, CO_2 and H_2O appear to contribute dramatically to radiative loss from microgravity flame due to the accumulation and slow transport of these products
- The data suggests that radiative ignition of nearby materials may be promoted in low-gravity environments due to the increased radiative loss from fires

* Reproduced from Bahadori, et al., 1991 [10]

SAIC. Science Applications International Corporation

Temperature Measurement - Normal-Gravity Tests

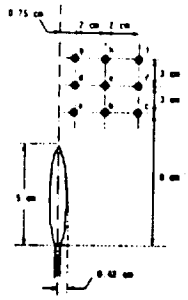

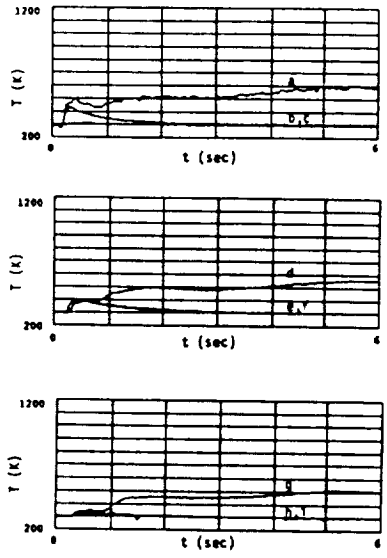

Temperature measurements for a normal-gravity propane-air flame at 1 atm. Note that regardless of pressure or oxygen concentration, thermocouples b, c, e, f, h, and i do not show a temperature rise in normal gravity. This flickering flame had on (average) height of 5.0 cm, and a maximum diameter of 0.84 cm, reproduced from [10]. Here, fuel-flow rate = 1.5 cm³/s, and nozzle radius = 0.0825 cm.

- The middle- and outer-columns of thermocouples do not register any temperature rise due to the pencil-like character of the flame
- The three centerline thermocouples show almost the same temperature levels due to the presence of buoyancy

SAIC. Science Applications International Corporation

Temperature Measurement - Microgravity Tests

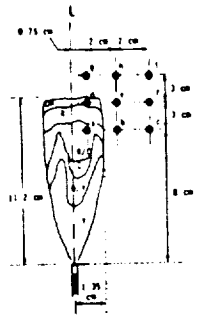

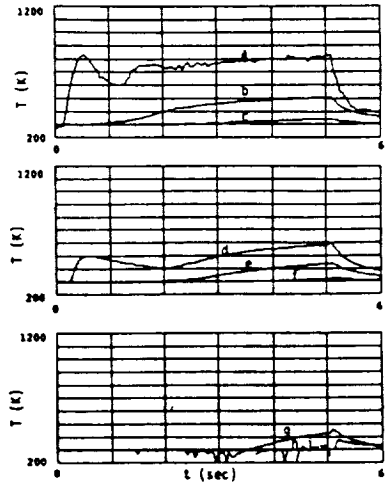

Temperature measurements for a (5.18-sec) microgravity propane-air flame at 1 atm. Thermocouple h was not functioning properly during this drop. reproduced from [10]. The initial overshoot is due to the ignition process, i.e., due to the release of fuel prior to the activation of the spark ignitor. Here, fuel flow rate = 1.5 cm^3/s, and nozzle radius = 0.0825 cm.

- Data show the existence of taller and wider flames in microgravity
- Steep temperature gradients exist in the axial direction
- Far field shows temperature rise
- 5 seconds of microgravity is not sufficient to obtain information on steady-state behavior, since the field is continuously changing due to the release and slow transport of combustion products

SAIC. Science Applications International Corporation

Overriding Observation

- Quantitative measurements show that steady-state has not been achieved in the ground-based experiments
  - The applicability of the previously cited observations hinges on this issue
  - Results to-date have clearly demonstrated the significance of quantitative data which can be augmented with the time available in a space experiment

SAIC. Science Applications International Corporation

Theoretical Analyses

SAIC. Science Applications International Corporation

Theoretical Methods for Gas-Jet Diffusion Flames

- To-date
  - Model for filling process in evacuated bottles (for sampling)
  - G-jitter analysis for acceptable g-levels
  - Transient, elliptic analytical model for flame development
  - Parabolic, steady-state numerical model
    - Radiation from CO_2 and H_2O
    - Inverted-flame (negative-g) studies
    - Detailed transport processes
    - Multicomponent diffusion
- In progress
  - Parabolic, steady-state numerical model
    - Detailed radiation (absorption/emission) model
    - Quasiglobal kinetics
    - Soot processes and thermophoresis
    - Radiation from soot
    - Detailed kinetics
- Planned
  - Elliptic, 2-D, steady-state numerical model
    - Submodels developed from application of parabolic model
  - Transient, 2-D, Navier-Stokes model
  - Analytical modeling

SAIC. Science Applications International Corporation

Predictions - Theoretical and Experimental Flame Heights

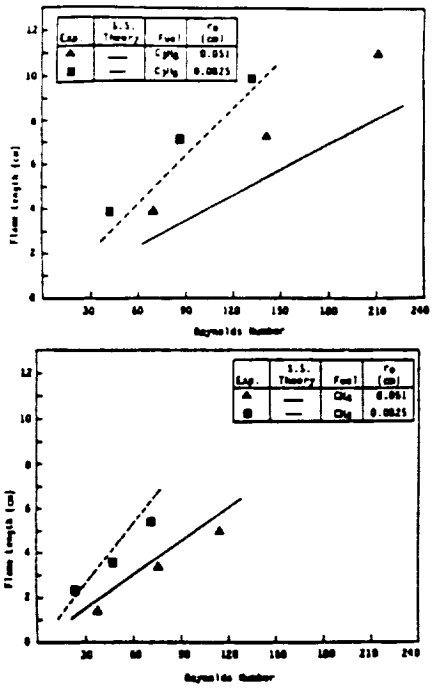

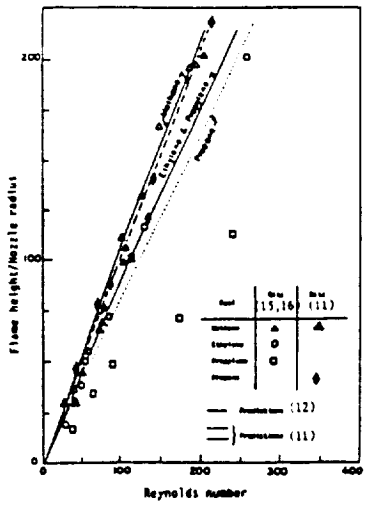

SAIC
Science Applications International Corporation

Transient Analytical Model

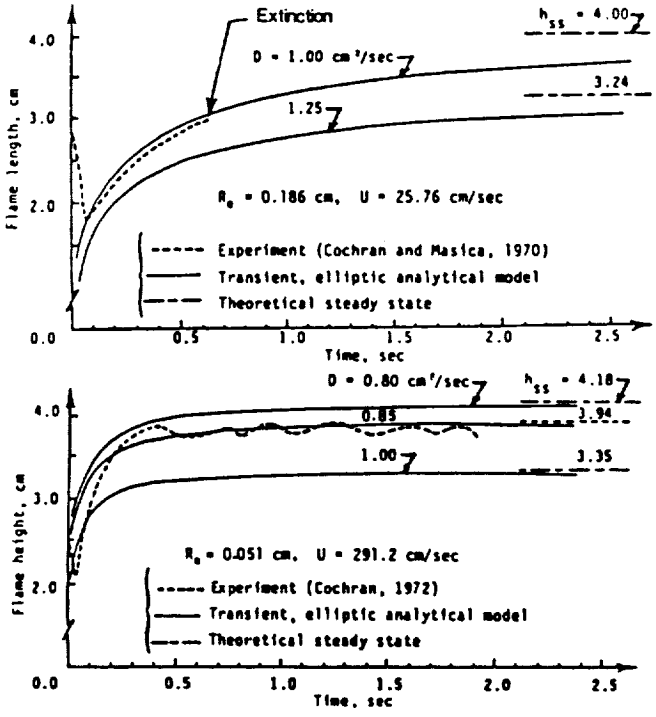

D = binary diffusion coefficent of methane in nitrogen.

The values of D=1.0 and 0.85 cm^2/sec correspond to T=750 and 650k, respectively.

SAIC
Science Applications International Corporation

Open Issues

- Non-steady-state
- Effects of P
- Effects of O_2
- Fuel type
- Analysis and theoretical methods

SAIC. Science Applications International Corporation

Proposed Program

SAIC. Science Applications International Corporation

Program Objectives

- Specific Objectives

  The questions that need to be answered are:

  (a) What are the steady-state characteristics of the microgravity flame, and given enough time, do the weak flames extinguish by virtue of their size, radiative loss, and associated transport processes?

  (b) Why does the removal of buoyancy result in the underventilated-like behavior in some otherwise overventilated diffusion flames?

  (c) Why does microgravity flame length vary non-monotonically with pressure, and what are the roles of buoyancy and oxygen concentration in defining this behavior?

  (d) Why are the sooting characteristics sensitive to oxygen concentration in microgravity flames?

SAIC. Science Applications International Corporation

Program Objectives- Specific Objective (a)

What are the steady-state characteristics of the microgravity flame, and given enough time, do the weak flames extinguish by virtue of their size, radiative loss, and associated transport processes?

- Continuous release and slow transport of products creates a transient field in the early stages of burning.
- A quasi-equilibrium state can be reached for both temperature and species fields.
- The flame approaches steady state, and the far-field will not have an effect on the near-field.
- This quasi-steady-state persists for a period of time, and will then be followed by a transient approach toward extinction due to depletion of oxygen.
- Which one of the following processes occurs in longer test times?
  - Radiative loss can not compete with the heat release, leading to bright, sooty flames.
  - Radiative loss exceeds the heat input, leading to extinction.

Originally blue, weak flame

- $Q_{rad.} < Q_{release}$ — Brighter, sootier flame, ultimately reaching steady state
- $Q_{rad.} > Q_{release}$ — Slow extinction process

SAIC. Science Applications International Corporation

Program Objectives- Specific Objective (b)

Why does the removal of buoyancy result in underventilated-like behavior in some otherwise overventilated diffusion flames?

- Removal of buoyancy increases the residence time for soot formation.
- Fuel pyrolysis is therefore augmented, leading to increased soot nuclei and growth.
- Larger soot and more soot formation result in slower oxidation and persistence of the soot.
- Soot is formed within the flame and unlike gas-phase species, virtually does not diffuse.
- Thermophoresis, caused by temperature gradient, forces the soot toward the flame centerline.
- As a result, the particles core up and stay within a column at the tip of the flame.
- The tip opens, oxygen transport is impeded from reaching the center, and the flame is prevented from closing on the axis.
- What happens to this core of soot in longer test times?

SAIC. Science Applications International Corporation

Program Objectives - Specific Objectives (c)

Why does microgravity flame length vary non-monotonically with pressure, and what are the roles of buoyancy and oxygen concentrations in defining this behavior?

- Observed increase in length with pressure is due to increasing amounts of soot rather than a change in the gas-phase flame height.
- At low-P, kinetic effects lengthen the gas-phase flame height.
- As the pressure increases, reaction rate increases and flame length decreases.
- As the pressure increases further, soot levels increase, and persist beyond the gas-phase flame front.
- This gives an indication (through visualization) of an apparently longer flame.
- Does this non-monotonic behavior tend to correct itself in longer test times, or is the effect aggrevated?

SAIC. Science Applications International Corporation

Program Objectives - Specific Objectives (d)

Why are sooting characteristics sensitive to oxygen concentration in microgravity flames?

- Microgravity environment provides longer residence times.
- This results in prolific sooting.
- Higher O_2 concentrations facilitate the soot oxidation, causing higher temperatures.
- Lower oxygen concentrations produce cooler flames, reduced pyrolysis and soot formation, and reduced heat and mass transfer.
- The competing effects of increased residence time with Lewis-number and Schmidt-number effects need to be clarified through longer test times.

SAIC. Science Applications International Corporation

Program Objectives (Cont.)

The overall and specific objectives of the program will be achieved through the following measurements and associated modeling:

- Measurements (R: Required; D: Desired):
  - Temperature field (R)
  - Flame visualization (R)
  - Flame radiation (R)
  - Chamber pressure (R)
  - Acceleration (D)
  - Gas-phase species concentrations (D)
  - Infrared imaging for species (D)
  - Density-gradient field imaging (D)
  - Velocity field (D)
  - Soot size and distribution (D)
  - Soot volume fraction and number density (D)
- Modeling that includes:
  - Multicomponent diffusion
  - Thermophoretic effects
  - Kinetics
  - Soot formation and particulate radiation
  - Axial diffusion effects
  - Transient effects

SAIC. Science Applications International Corporation

Justification for Space Experiment

- Flame shape and color change continuously in 5 seconds of available time
- Temperature data show a continuous increase in the 5 seconds of microgravity
- Sooty flames show a continuous increase in radiation loss
- Analytical predictions consistent with these observations
- G-levels less than 10^{-3} are needed
- The following (based on objectives of the program) need longer duration experiments
  - Steady-state characteristics
  - Weak-flame behavior
  - Underventilated-like phenomena
  - Non-monotonic flame-height variation with pressure
  - Effects of oxygen on the sensitivity of sooting characteristics

SAIC. Science Applications International Corporation

Concept Design

SAIC. Science Applications International Corporation

Experimental Options

All objectives require: Temperature field, Flame visualization, Radiation, and Pressure measurements

Objective	Desired Measurements						
	Accel.	Species field	Infrared imaging	Density-gradient field	Velocity field	Soot size	Soot conc.
(a) Steady state characteristics. Given enough time, do the weak flames extinguish?	X	X	X	X	X	X	X
(b) Underventilated-like behavior in otherwise overventilated flame due to removal of buoyancy.	X	X	X	X	X		X
(c) Nonmonotonic behavior of microgravity flame-length with pressure. Roles of buoyancy and %O2 in defining this behavior.	X	X	X	X		X	X
(d) Sensitivity of sooting characteristics to Oxygen in microgravity flames.	X	X	X	X	X	X	X

SAIC
Science Applications International Corporation

Concept Design - Middeck

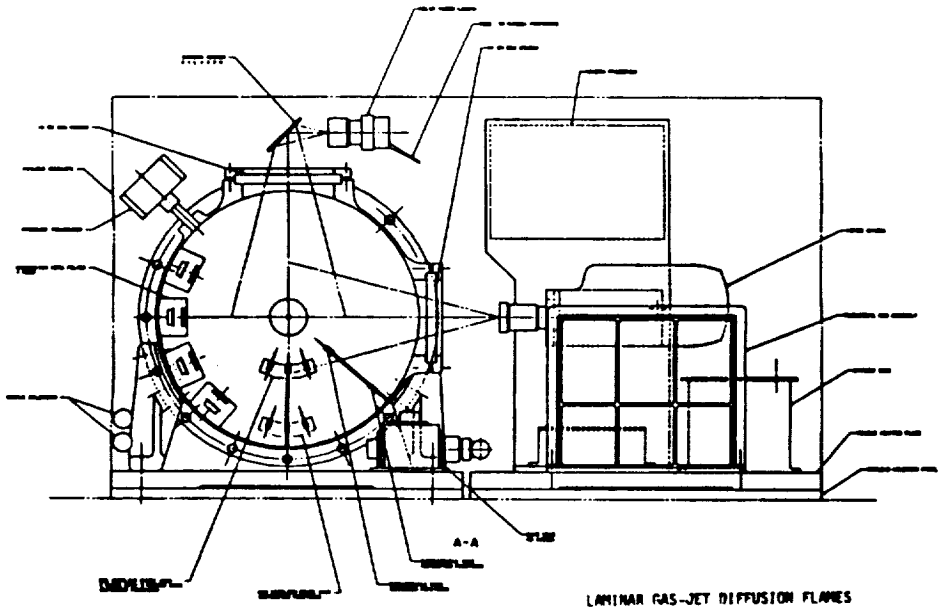

LAMINAR GAS-JET DIFFUSION FLAMES

SAIC
Science Applications International Corporation

Concept Design - CEM

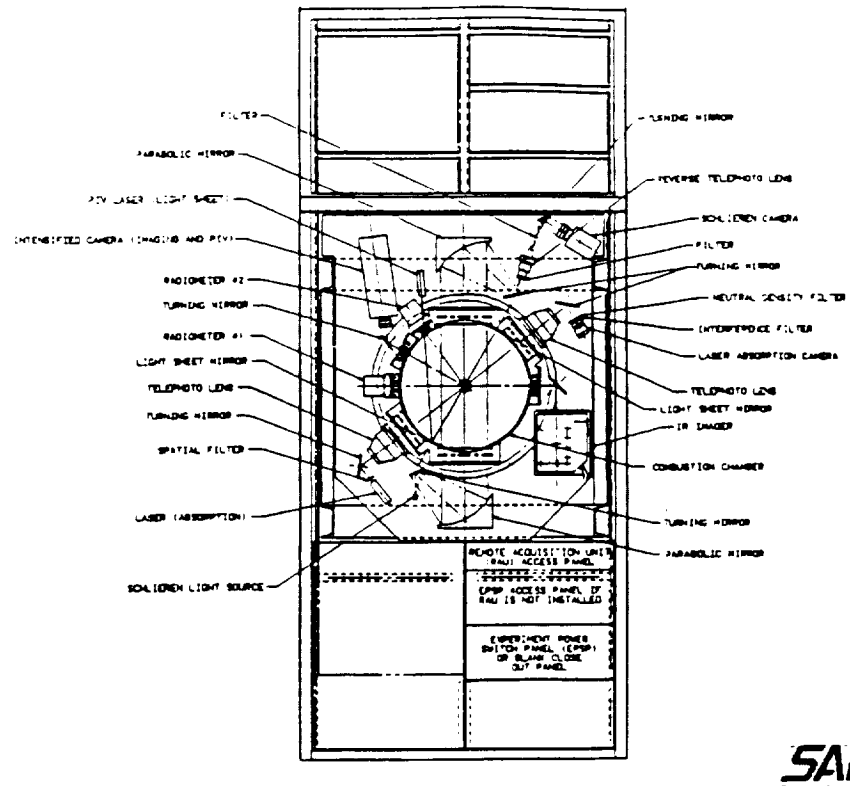

SAIC
Science Applications International Corporation

Test Matrix for Space Experiment

Operating Conditions	No. of Experiments	Note
Fuel	2	Methane; propane
Fuel-flow rate	1	Fixed mass-flow rate. When converted to atmospheric condition, 1.0 cm^3/sec for propane and 2.0 cm^3/sec for methane
Nozzle radius	1	Tapered-tip nozzle; inner radius = 0.0825 cm
Oxidizer	3	Oxygen/nitrogen mixtures; O_2/N_2 = 0.15/0.85, 0.21/0.79, and 0.30/0.70
Chamber pressure	3	P = 0.5, 1.0, and 1.5 atm
Total no. of flames	18	

* Limited to one Reynolds number for each fuel.

SAIC
Science Applications International Corporation

Diagnostics Requirements

Variable	Diagnostics	Rationale/Applications to Model Development	Required	Desired
Flame Structure	Video camera	Enables the experimenter to monitor the flame behavior during the experiment	✓	
	Cinematography (using movie camera)	Obtain time-resolved visualization data on ignition, flame development, color, luminosity, sooting, and quenching. Flame shapes can be compared directly with model predictions		
	Schlieren camera	To obtain qualitative temperature/density field		✓
Temperature	Array of thermocouples	Obtaining temperature distributions in the flow field. They can be compared directly with the model predictions of the thermal field.	✓	
Combustion and fuel decomposition products	Row of gas sampling probes (3) and array of probes (3 x 3)	Obtaining species distributions which can be compared with the model predictions of the species field. Unburned hydrocarbons are extremely important		✓
Chamber pressure	Pressure transducer	Monitoring any increase in chamber pressure due to the burning process, which yields estimates of the overall heat release rate; also used for safety detection	✓	
Gas velocity	Single-component laser-doppler velocimetry (LDV), or particle-image velocimetry (PIV)	Centerline and radial velocities can be obtained using traversing mechanisms; LDV needs seeding. Compact lasers are becoming available. Velocity measurements will be compared directly with the model predictions of the flow field		✓

SAIC. Science Applications International Corporation

Diagnostics Requirements (Cont.)

Variable	Diagnostics	Rationale/Applications to Model Development	Required	Desired
Flame radiation	Radiometry	Isolation of thermal radiation, and determination of the effect of radiation on reduction in temperature within the flame. Potential exists for determination of soot concentration. Predictions can be directly compared with measurements	✓	
Gravitational acceleration	Accelerometer	Measurements of acceleration enables us to interpret the data that could be affected by low gravitational levels		✓
Specific species	Light-intensified array camera	To identify species using appropriate optical filters; particularly useful for H_2O, CO_2, and CO fields in non-sooting (blue) flames, as well as sooty flames		✓
Soot number density and size	Light absorption/ extinction	A convenient, non-intrusive method to infer soot number density; when combined with radiation and species measurements, provides information on soot behavior and characteristics		✓
	Thermophoretic sampling	Soot can be collected and size distribution can be obtained. Collected soot needs to be removed from the chamber after Shuttle landing (in middeck), and after test is done (in Spacelab)		✓

SAIC. Science Applications International Corporation

REPORT DOCUMENTATION PAGE

Form Approved
OMB No. 0704-0188

1. AGENCY USE ONLY (Leave blank)	2. REPORT DATE	3. REPORT TYPE AND DATES COVERED
	August 1992	Final Contractor Report

4. TITLE AND SUBTITLE

Effects of Buoyancy on Gas Jet Diffusion Flames

5. FUNDING NUMBERS

WU-694-03-0A
C-NAS3-22822

6. AUTHOR(S)

M. Yousef Bahadori and Raymond B. Edelman

7. PERFORMING ORGANIZATION NAME(S) AND ADDRESS(ES)

Science Applications International Corporation
Thermal Sciences Division
21151 Western Avenue
Torrance, California 90501-1724

8. PERFORMING ORGANIZATION REPORT NUMBER

E-7720

9. SPONSORING/MONITORING AGENCY NAMES(S) AND ADDRESS(ES)

National Aeronautics and Space Administration
Lewis Research Center
Cleveland, Ohio 44135-3191

10. SPONSORING/MONITORING AGENCY REPORT NUMBER

NASA CR-191109

11. SUPPLEMENTARY NOTES

Project Manager, D. Stocker, Space Experiments Division, (216) 433-2166.

12a. DISTRIBUTION/AVAILABILITY STATEMENT

Unclassified - Unlimited
Subject Category 29

12b. DISTRIBUTION CODE

13. ABSTRACT ***(Maximum 200 words)***

The objective of this effort was to gain a better understanding of the fundamental phenomena involved in laminar gas jet diffusion flames in the absence of buoyancy by studying the transient phenomena of ignition and flame development, (quasi-) steady-state flame characteristics, soot effects, radiation, and, if any, extinction phenomena. This involved measurements of flame size and development, as well as temperature and radiation. Additionally, flame behavior, color and luminosity were observed and recorded. The tests quantified the effects of Reynolds number, nozzle size, fuel reactivity and type, oxygen concentration, and pressure on flame characteristics. Analytical and numerical modeling efforts were also performed. Methane and propane flames were studied in the 2.2-Second Drop Tower and the 5.18-Second Zero-Gravity Facility of the NASA Lewis Research Center. In addition, a preliminary series of tests were conducted in the KC-135 research aircraft. Both microgravity and normal-gravity flames were studied in this program. The results have provided unique and new information on the behavior and characteristics of gas jet diffusion flames in microgravity environments.

14. SUBJECT TERMS	15. NUMBER OF PAGES
Microgravity combustion; Laminar flames; Diffusion flames	200
	16. PRICE CODE A09

17. SECURITY CLASSIFICATION OF REPORT	18. SECURITY CLASSIFICATION OF THIS PAGE	19. SECURITY CLASSIFICATION OF ABSTRACT	20. LIMITATION OF ABSTRACT
Unclassified	Unclassified	Unclassified	

Case File Document Withdrawal

DOCUMENT NUMBER / N93-31031

DATE OUT	WITHDRAWN BY: (SIGNATURE)	DATE RETURNED	DATE OUT	WITHDRAWN BY: (SIGNATURE)	DATE RETURNED	DATE OUT	WITHDRAWN BY: (SIGNATURE)	DATE RETURNED
9-20	RETD							

FACILITY FORM NO. 441 REV. DEC. 1963

Case File Document Withdrawal

DOCUMENT NUMBER /

DATE OUT	WITHDRAWN BY: (SIGNATURE)	DATE RETURNED	DATE OUT	WITHDRAWN BY: (SIGNATURE)	DATE RETURNED	DATE OUT	WITHDRAWN BY: (SIGNATURE)	DATE RETURNED

FACILITY FORM NO. 441 REV. DEC. 1963